MAX PLANCK INSTITUTE
OF MOLECULAR PHYSIOLOGY

technische universität
dortmund

CHEMICAL GENOMICS CENTRE
OF THE MAX PLANCK SOCIETY

Modification of Peptides for Improved Membrane Permeability and Side Chain Diversity

Dissertation
For achievement of the academic degree of
Doctor of natural sciences
(Dr. rer. nat.)

Submitted to

Faculty of Chemistry and Chemical Biology

Technical University Dortmund

By
M. Sc. Oweta Joseph Noah Openy
Born on 04.12.1988
In Apac, Uganda

Dortmund, 2023

The work described in this thesis was performed between January 2019 and April 2023 under the supervision of Prof. Dr. Dr. h.c. Herbert Waldmann and Dr. Peter ‘t Hart at the Chemical Genomics Centre of the Max Planck Institute of Molecular Physiology in Dortmund and the Faculty of Chemistry and Chemical Biology at Technical University Dortmund.

First Examiner: Prof. Dr. Dr. h.c. Herbert Waldmann

Second Examiner: Prof. Dr. Andreas Brunschweiger

Bang Onwala, Agulo kede Acen

The results presented in this thesis contributed to the following publication.

J. Openy, G. Amrahova, J.-Y. Chang, A. Noisier, P. ‘t Hart, Chem. – Eur. J. 2022, 28, e202201121.

Results displayed in this dissertation can be found in the following master thesis:

S. V. Ces, “ Improving Macrocycle Cell Permeability by Introducing Intramolecular Hydrogen Bond Forming Fragments,” Masters Thesis, Universiteit van Amsterdam, 2022.

Acknowledgments

The four-year journey abroad in pursuing a Dr. rer. nat. has been incredibly enriching on both academic and personal fronts. It would not have been possible without the support and encouragement of people around me at the CGC, MPI, and back home. Therefore, I am grateful to everyone who contributed to this phase of my life in various ways.

I want to begin by thanking Prof. Dr. Dr. h.c. Herbert Waldmann for establishing the CGC and in collaboration with industry partners who funded my Project. In addition, I am grateful for the opportunity to carry out my research project in Department IV of the MPI, wherein I had access to first-in-class scientific equipment. At the CGC and MPI-Dortmund, I was in a productive multidisciplinary academic environment that nurtured my intellectual growth in a socially conducive atmosphere.

Secondly, I am grateful to Dr. Peter ‘t Hart for entrusting me to work on these challenging but exciting projects in this period marked by productive scientific discussions and encouragement. As my MSc. mentor and doctoral supervisor, I am very fortunate to experience first-hand the co-existence of good social relationships and outstanding science, something that I wish upon anyone dedicating almost half a decade to their doctoral studies. Even with the unexpected global pandemic, my life at the CGC was serene mainly because of your tremendous empathy for the group members, which enabled me to be resilient despite the ever-changing circumstances.

I am also grateful to Prof. Dr. Andreas Brunschweiger for accepting to be my thesis’s second examiner, especially given that you are transitioning from TU Dortmund to Julius-Maximilians-Universität Würzburg.

From our collaborators in AstraZeneca, Gothenburg, I would like to thank Dr. Anaïs F. M. Noisier and Dr. Laurent Knerr for their scientific input in the projects reported in this thesis. Furthermore, from the former AstraZeneca satellite unit in Dortmund, I am grateful to Dr. Hélène Adihou for the supportive scientific discussions as I ventured into peptide chemistry.

Within the Hart Lab at the CGC, I would like to thank Stefan Schmeing for constructive discussions on my projects and for aiding me in navigating through the necessary bureaucracies and social life in the City of Dortmund. Similarly, I would like to thank Jessica Nowacki for her steadfast advocacy for a vibrant social environment at the CGC. I also enjoyed collaborating with her on the SICLOPPS project, whereby we had fruitful exchanges of fundamental principles of chemistry and biology.

I would also like to thank Dr. Adrian Krzyzanowski for the discussions on peptide chemistry and collaboration on the LSD1 project I participated in while at the MPI. I am grateful to Jen-yao Chang for being an excellent lab and office colleague with whom we initially explored the Katritzky salt project. Furthermore, I would like to thank Sabela Vega Ces for her hard work and motivation that gave the Chameleonic peptide project a vital boost. Additionally, I thank Dr. Sunit Pal for sharing his knowledge of peptide macrocycles. To Gulshan Amrahova and Dr. Laura Pasoda, thank you for sharing your lab space with me at the MPI as I carried out experiments and for your contributions to my project during group meetings.

From the CGC lab, I would first like to thank Dr. Pascal Hommen and Dr. Jimin Hwang, with whom we shared the incredibly challenging group job of maintaining the LCMS systems. I am also indebted to Stavroula Petrolia for sharing her cell culture expertise. Furthermore, I would like to thank Lydia Borgelt, Dr. Fubao Huang, Oguz Hastürk, Amrutha Krishnan, Mao Jiang, and all the members of the CGC for being such a great scientific network at the CGC.

From the MPI and TU Dortmund, I would like to thank Dr. Petra Janning and Jens Warmers for their assistance with operating and maintaining the LCMS systems. I also would like to thank apl. Prof. Dr. Wolf Hiller and Benjamin Kissel for performing NMR experiments reported in this thesis.

Finally, I would like to thank my parents and siblings for their unwavering support for my academic goals and numerous phone calls during my stay abroad. Your support kept me going even when I was miles away from home. I want to express my deepest gratitude to my partner, Jana Augustin, for her support, compassion, and empathy throughout this academic journey. Little Ava and I are lucky to have you in our lives.

Table of Contents

Abstract

Advances in drug discovery have led to the rapid discovery of potent hit peptides, which are privileged scaffolds for targeting protein-protein interactions (PPI) or protein-nucleic acid interaction sites that are typically large featureless hydrophobic interfaces. Typically falling in the "beyond- rule-of-five" (bRo5) chemical space and primarily composed of canonical amino acids, hit peptides are commonly faced with poor pharmacokinetics and membrane permeability.

In Chapter 2, we aimed to improve peptide membrane permeability by incorporating (hetero)aromatic linkers in the peptide backbone. Sanguinamide A (**1**), a membrane-permeable cyclic peptide of marine origin with a reasonable reported oral bioavailability (F = 7 ± 4%) and featuring a thiazole ring in its backbone, was selected as a model peptide. Its cysteine-containing homodetic peptide analogue was designed as a negative control, while the *tert*-butylglycine-containing analogue, Danamide F (**2**, F = 51 ± 9%), was our positive control. A compound library consisting of pyridine, pyridine N-oxide, and 3-amino benzoic acid linkers was followed by a membrane permeability screen using IAM chromatography. Pyridine-containing analogue **21** had an IAM score comparable to Sanguinamide A indicting good membrane permeability. Furthermore, variable temperature ^{1}H-NMR studies showed that amides in the backbone of **21** might form a hydrogen bond HB network different from Sanguinamide A but dynamically to enable chameleonicity.

In Chapter 3, we aimed at peptide late-stage functionalization to introduce unnatural amino acids (UAAs) using Katritzky salts. In this method, lysine residues were converted to Katritzky salts, followed by photochemical Giese reactions under mild conditions. The method was compatible with all canonical amino acids and commercially available resins and linkers save for the 2-chloritrityl chloride resin. A broad substrate scope was reported, and the utility of the method was demonstrated through the selective modification of one of two lysine residues of the histone 3 tail peptide (residues 1 – 10), one of two ornithine residues of the cyclic antibiotic peptide Gramicidin S, and modification of the longer p53 (15 – 29) peptide.

Zusammenfassung

Fortschritte in der Arzneimittelforschung haben zur raschen Entdeckung potenter Hit-Peptide geführt, die bevorzugte Gerüste für die gezielte Beeinflussung von Protein-Protein-Wechselwirkungen (PPI) oder Protein-Nukleinsäure-Wechselwirkungsstellen darstellen, bei denen es sich in der Regel um große, funktionslose hydrophobe Schnittstellen handelt. Hit-Peptide, die typischerweise in den chemischen Raum der "beyond- rule-of-five" (bRo5) fallen und hauptsächlich aus kanonischen Aminosäuren bestehen, haben in der Regel eine schlechte Pharmakokinetik und Membranpermeabilität.

In Kapitel 2 haben wir versucht, die Membranpermeabilität von Peptiden durch den Einbau von (hetero)aromatischen Linkern in das Peptidgerüst zu verbessern. Als Modellpeptid wurde Sanguinamid A (**1**) ausgewählt, ein membrandurchlässiges zyklisches Peptid marinen Ursprungs mit einer angemessenen berichteten oralen Bioverfügbarkeit (F = 7 ± 4 %), das einen Thiazolring in seinem Rückgrat aufweist. Sein cysteinhaltiges homodetisches Peptidanalogon wurde als Negativkontrolle entwickelt, während das tert-Butylglycin-haltige Analogon, Danamid F (**2**, F = 51 ± 9%), unsere Positivkontrolle war. Auf eine Verbindungsbibliothek, die aus Pyridin, Pyridin-N-Oxid und 3-Aminobenzoesäure-Linkern bestand, folgte ein Screening der Membranpermeabilität mittels IAM-Chromatographie. Das Pyridin-haltige Analogon **21** wies einen mit Sanguinamid A vergleichbaren IAM-Wert auf, was auf eine gute Membranpermeabilität hindeutet. Darüber hinaus zeigten ^{1}H-NMR-Studien bei variabler Temperatur, dass die Amide im Rückgrat von **21** ein Wasserstoffbrückenbindungs-HB-Netzwerk bilden könnten, das sich von dem von Sanguinamid A unterscheidet, aber dynamisch ist, um Chamäleonität zu ermöglichen.

In Kapitel 3 befassten wir uns mit der späten Funktionalisierung von Peptiden, um unnatürliche Aminosäuren (UAAs) mit Hilfe von Katritzky-Salzen einzuführen. Bei dieser Methode wurden Lysinreste in Katritzky-Salze umgewandelt, gefolgt von photochemischen Giese-Reaktionen unter milden Bedingungen. Die Methode war mit allen kanonischen Aminosäuren und handelsüblichen Harzen und Linkern kompatibel, mit Ausnahme des 2-Chlornitrit-Chlorid-Harzes. Es wurde über einen breiten Substratbereich berichtet, und die Nützlichkeit der Methode wurde durch die selektive Modifizierung eines von zwei Lysinresten des Histon-3-Schwanzpeptids (Reste 1-10), eines von zwei Ornithinresten des zyklischen antibiotischen Peptids Gramicidin S und die Modifizierung des längeren p53-Peptids (15-29) nachgewiesen.

1.0. Introduction

1.1. Background

Peptides predominantly exist in nature as macromolecules comprised of canonical amino acid building blocks and, less frequently, non-canonical structural motifs that lead to their increased structural and functional complexity.[1] The latter may result from non-ribosomal synthesis or post-translational modifications that are tuned mainly to suit their biological activities.[3] With limited structural roles in comparison to their larger protein counterparts, peptides are reportedly functionally relevant in several biological systems.

Naturally occurring peptides have a diverse range of homeostatic and host defense functions. In homeostasis, peptides partake in signal transduction as neuropeptides and hormones, involved in the modulation of neurotransmission at synapses[4]. Over 5000 neuropeptides are currently reported with a range of 3 – 100 amino acid residues in length[5]. Peptide hormones are important components in the regulation of metabolism and are typically derived from the cleavage of N-terminal sequences of secretory pre-proteins.[6] Insulin, Glucagon-like peptide 1 (GLP-1), and glucagon are typical examples of peptides that regulate glucose metabolism[7]. Furthermore, peptide growth factors also regulate several aspects of the cell cycle, including tissue, organ, and embryonic development.[8] For example, the epidermal growth factor (EGF) is a 53 amino acid residue ligand for the EGFR tyrosine kinase receptor, whose overexpression in tumor cell lines is associated with poor prognosis[9].

Further beyond homeostasis, antimicrobial peptides (AMPs) of ribosomal or non-ribosomal origin are known to play host defense functions across all three domains of life[10]. Bacteriocins, for example, are antimicrobial polypeptides of ribosomal origin that commonly possess bacteriostatic or bactericidal properties against other strains or species of bacteria[11]. Besides anti-bacterial properties, this structurally diverse group of peptides often possesses a broad repertoire of functions, including anti-tumour activities[12]. Notably, there are several AMPs at several stages of clinical trials, mostly as antimicrobial agents for topical, oral, and intravenous administration[13].

Nonribosomal peptides (NRPs) also nearly exclusively exist as a part of the metabolite repertoire of bacteria and fungi, with rarely exempt examples of a few higher-order organisms, including *Drosophila melanogaster*[14]. Synthesized by enzyme complexes known as non-ribosomal peptide synthetases (NRPSs), these peptides typically contain non-canonical structural motifs, including D-configured amino acids, N-methylations, halogenated amino acids, reduced C-termini to alcohols or aldehydes, peptides conjugated with lipids at the termini or heterocyclic backbones.[15]

Heterocyclic fragments in peptide backbones are an example of commonly encountered products of Non-Ribosomal Peptide Synthetases (NRPSs) or hybrids with polyketide synthase (PK), also known as PK–NRP hybrids.[16] The fragments are commonly derived from non-ribosomal amino acid modifications. In the NRPS assembly line, for example, a cyclization domain (Cy) catalyzes a nucleophilic attack by the side chain of serine or cysteine residues resulting in the formation of a heterocyclic moiety. The intermediate products' dehydration followed by oxidation catalyzed by an oxidation (Ox) domain to form oxazoles or thiazoles, respectively (Scheme 1A).[17]

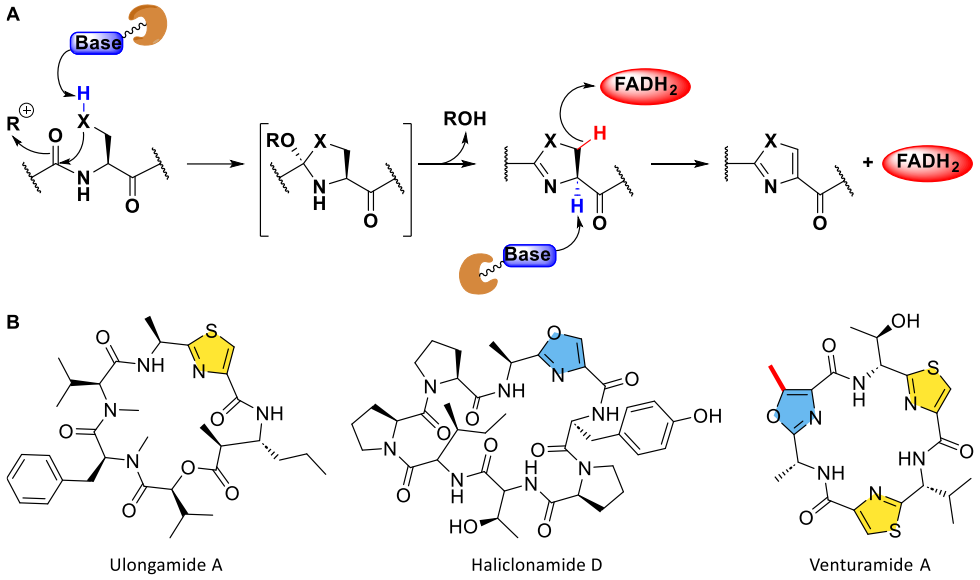

Scheme 1. A: Cyclisation of amino acid side chains by NRPSs. B. Examples of naturally occurring cyclic peptides containing heterocyclic fragments derived from NRPS modifications. Figure adapted from Dowling and co-workers[18]

Incorporating heterocycles in peptides has been shown to improve stability against proteases by masking side chains as recognition motifs, improving membrane permeability and their specificity for target proteins through conformational restrictions on the peptide backbone.[19] Examples of peptides with heterocyclic fragments in their backbone include the thiazole-containing ulongamide A, haliclonamide D and Venturamide A with oxazole and methyloxazole moieties and derived from cyanobacteria and marine sponges (scheme 1B).[20–22] Other heterocyclic moieties can be derived from other amino acids beyond serine, threonine, and cysteine. The amatoxin, α-amanitin, for example, is a potent cyclic peptide isolated from the death cap mushroom in which cyclization occurs as a result of condensation between tryptophan and cysteine to form an indole-derived cross bridge.[23]

Additionally, structural diversity accrued from NRPs has inspired peptidic therapeutic natural products. Examples of clinically relevant antibiotic peptides include gramicidin S, N-methylated peptides, such as the immunosuppressant cyclosporine A, and heterocyclic-backbone modified antibacterial peptide bacitracin, as notable.[24] Nonetheless, despite their broadly characterized

pharmacological and toxicological properties, NRPs are structurally complex compounds with barely understood modalities of their host-related functions that comprise virulence and tolerance to stress factors like reactive oxygen species.[25]

The existence of peptides across all three domains of life highlights their potential diversity, thereby presenting their potential for developing contemporary, relevant therapeutics (Figure 1A).[27] Existing under extreme environmental conditions, peptides from archaea include Acyl homoserine lactones (acyl-HSLs) and Diketopiperazines (DKPs), which are known disruptors of quorum sensing in microbial populations. These metabolites have been postulated as potential therapeutics for inhibiting biofilm formation or water treatment.[28] In higher-order organisms, peptides have been isolated in venomous organisms, including insects, reptiles, and the duck-billed platypus as the only known venomous mammal. Owing to their neuroactive nature, these peptides have the potential for the development of ion channel modulators.[29] There are several characterized structurally diverse peptides derived from marine organisms. Owing to the complex marine ecosystem and biodiversity, the peptides have a wide array of reported bioactivities, some of which are unrelated to their functions in their primary sources.[30] Despite the diversity of peptides in regard to their structure, bioactivity, and source, major bottlenecks in their discovery still need to be addressed during their extraction, characterization, and challenging chemical synthesis (Figure 1B).[31]

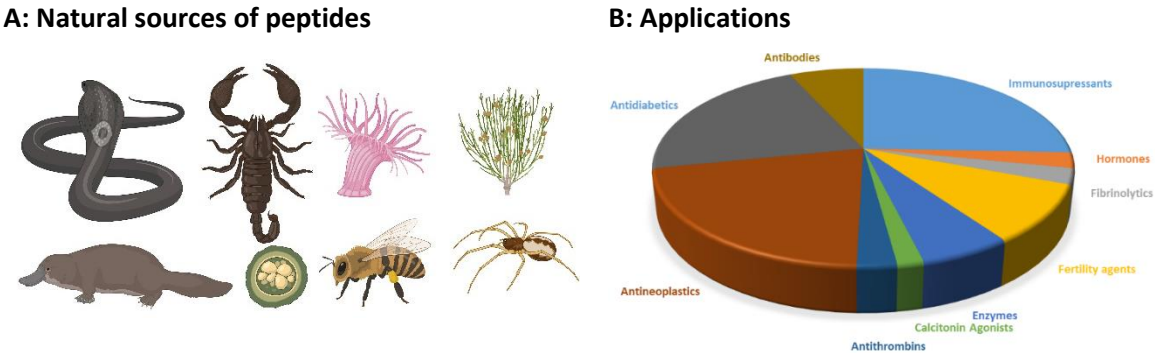

Figure 1. A: A representation of sources of bioactive peptides covering species from all three domains of life, including single-celled organisms, marine life, plants, and poisonous animals. **B:** The application of currently approved peptides for clinical use reflects the diversity of their function and potential as therapeutics. Based on the Figure by Sikora and co-workers.[26]

1.2. Peptides as therapeutics

As macromolecules, peptides are privileged scaffolds for binding at large protein surfaces. Consequently, they are investigated for their ability to inhibit protein-protein interactions (PPI) or protein-nucleic acid interactions, which play a crucial role in regulating cellular functions, including signal transduction and epigenetic control.[32] Dysregulation of PPIs has therefore been implicated in

several pathologies, including cancers and metabolic disorders, making them attractive targets in drug development.[33] Several approaches have been used to explore the chemical space of PPI inhibitors, including using small molecule modulators of proteins that bind at allosteric pockets and subsequently disrupt the recognition characteristics of proteins.[34]

The interface of a typical PPI is often a large hydrophobic shallow space that can be unsuitable for orthosteric modulation using small molecules owing to the lack of suitable binding pockets.[35] Peptides, on the hand, are capable of mimicking a fragment of a binding partner with a potentially higher affinity such that the PPI is disrupted. This is possible if a peptide sequence contains several hotspot residues, also known as a hotspot cluster which is energetically important for anchoring a protein to another macromolecule. To be considered a hotspot residue, an alanine mutation should lead to a reduction of the binding free energy difference between the wild type and mutant of more than 2.0 kcal/mol. [36]

The first clinically approved peptide therapeutics were extracts of endogenous bioactive hormones, starting with insulin obtained from bovine fetal pancreas and used for treating type II diabetes mellitus in the late 1920s.[37] The rapid approval of insulin for clinical use led to a series of fast-paced advancements in peptide drug discovery (Figure 2). The first notable development was a method for sequencing amino acids reported by Sanger and Tuppy about 30 years later, also commonly known as Sangers method, that proceeded via cleavage of N-terminal amino acid residues. This was a fundamental step to understanding sequence dependence as a factor contributing to the biological activity of peptides.[38]

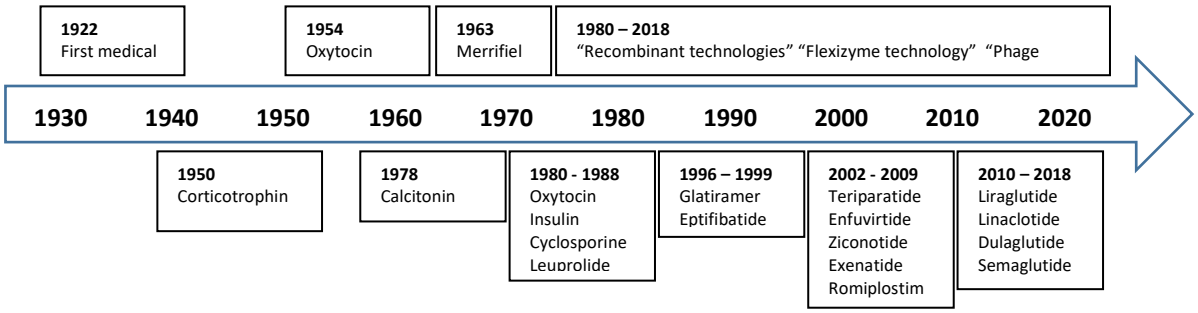

Figure 2. Advances followed the discovery of insulin in techniques for the discovery of peptide therapeutics, which in turn led to an increase in the number of approved peptide-based therapies.

Sanger’s method consequently stimulated the development of several peptide sequencing methodologies. Shortly after the sequencing of insulin, for instance, Vigneaud and co-workers reported the sequence of oxytocin using Sanger’s method. Subsequently, they followed up their efforts by describing its total synthesis in solution.[39,40] After that, the sequence of the decapeptide angiotensin from bovine renal extract was determined, and in a similar manner, its truncated

octapeptide analog was synthesized by Schwarz and co-workers aimed at demonstrating that the shorter sequence is sufficient for its vasoconstrictive properties.[41] Likewise, the 19-mer and 23-mer polypeptide analogues of adrenocorticotropic hormone (ACTH) were synthesized, further highlighting the biological activities of peptide fragments of ACTH instead of the full-length wild-type variants.[42,43] The current state-of-the-art technologies for peptide sequencing uses liquid chromatography (LC) coupled to multiple-stage mass spectrometry (LC/MS^n), which is additionally capable of quantification even when used for the analysis of complex mixtures of peptides and proteins.[44]

In parallel with the development of sequencing methodologies, there was increasing scientific interest in mutant derivatives of biologically active peptides. However, this progress was hampered by challenges faced during the chemical synthesis of peptides that exclusively took place in solution.[45] Each step in peptide coupling was laborious, marked by rather tedious aqueous work-ups, deprotection, and purification procedures.[46] Purification was notoriously challenging because of racemization as a result of the predominant use of carbodiimide coupling reagents.[47] The use of triethylamine (Et_3N) for the formation of free bases of peptide products was also reported as contributing factor to racemization. Additionally, the iterative process of peptide synthesis was prone to the formation of higher-order peptide side products from the slight excess of reagents used in the reaction.[48] Likewise, as the sequences increased in length, the peptides tended to aggregate, significantly hampering subsequent elongation efforts. Merrifield developed a method for synthesizing linear peptides on chemically inert solid polystyrene support to address several of these challenges. This method did not require intermediate purification and circumvented the challenge of aggregation of longer peptide sequences.[49] Furthermore, solid phase peptide chemistry (SPPS) enabled the use of large excesses of reagents and the use of better-suited protic polar solvents like N,N-Dimethylformamide (DMF) for coupling.[50]

The advent of SPPS fostered increased research momentum in the development of peptide therapeutics. The application of SPPS was further improved by the introduction of automation and the development of several protecting groups that could be cleaved under mild conditions.[51] The introduction of Fmoc/tBu chemistry for SPPS was another key step for progress in the synthesis of peptides. It replaced the Boc/Bzl strategy in which the final deprotection of side chain protecting groups and cleavage from the resin was carried out using HF, which is highly toxic[52]. In the current strategy, base labile fluorenylmethyloxycarbonyl (Fmoc) to protect the α-amino group and acid labile side chain protecting groups with synthesis proceeding in C-to-N terminal direction are used. Cleavage of peptides from the solid support uses milder TFA or weaker acidic conditions.[53] Other improvements currently applied in peptide synthesis include microwave (MW)-assisted peptide

synthesis as well as the use of induction heating aimed at reducing reaction time and increasing purity[54]. Furthermore, advancements were also made in the purification of peptides considering an evolution from cation exchange chromatography used in the 1950s to the state-of-the-art preparatory reverse-phase high-pressure liquid chromatography coupled with mass spectrometry (RP-LCMS).[55]

Early strategies for the development of peptides as therapeutics also got improved over time, marked by amino acid substitutions as a means to enhance the biological activity of endogenous human signaling peptides. As exemplified by vasopressin, whose analogue featured a β-mercaptopropionic acid substitution of cysteine at the first position and L-Arginine at position eight substituted with D-arginine and with clinical relevance.[56] Sources of bioactive peptides have been remarkably diversified over time. A noteworthy example is the discovery of cyclosporine A which was isolated from the fungus *Cylindrocarpon lucidum* and is currently used in the clinic as an immunosuppressant to prevent graft rejection, whose discovery sparked a renewed interest in microbes as sources of bioactive peptides.[57]

Recent advancements in genomic technologies have resulted in a marked understanding of the mechanisms of disease and, consequently, an exponential increase in the number of drug targets. Therefore, technologies, including peptide-based library screening techniques, have been developed to cope by enabling a rapid and robust modality for the discovery of novel high-affinity binders.[58] Split and pool techniques are an example of an established chemical peptide library strategy designed to generate randomized peptide sequences from which high-affinity binders can be identified for specific targets and subsequently optimized.[59] Additionally, biological peptide libraries utilize microorganisms to generate peptide libraries and can be broadly categorized into *in vitro* and in-vivo systems, with examples of the latter including phage display, mRNA display, and split-intein circular ligation of peptides and protein (SICLOPPS).[60,61]

1.3. Chemical instability of peptides

Beyond challenges in pharmacokinetics and pharmacodynamics, peptide compounds are also prone to chemical and physical instability. Cysteine is commonly prone to oxidation and desulfurization. The reversible oxidation of cysteine under physiological conditions results in the formation of disulphide bond formation and performs a vital signaling function in vivo. Conversely, the formation of cystic acid during peptide synthesis and storage also poses a challenge for peptide compounds.[62] Cysteine is also prone to β-elimination under mild conditions during trypsin digestion to form dehydroalanine and in the presence of phosphines at elevated temperatures to generate an alanine residue and thereby altering the peptide sequence with a possibility for loss of biological activity.[63] This setback may be

encountered during the synthesis of cyclic peptides containing cysteine residues upon treatment with a TCEP-containing buffer using the MeDbz method.[64]

Secondly, the racemization of peptides leads to the formation of diastereoisomers that have different polarities and, thereby, are distinguishable by LCMS. Since stereochemistry is often an important binding site recognition factor, racemization may alter the peptide's biological activity with the possibility of adverse effects or none at all.[65] Synthetically, racemization commonly occurs during peptide macrocyclization as well as solid phase synthesis of linear peptides, especially for epimerisation-prone amino acid residues like phenylglycine.[66,67]

Finally, concerns regarding the physical stability of peptides revolve around the aggregation and precipitation of peptide compounds, which is an essential factor that is taken into consideration when designing the delivery systems of pharmaceuticals. Aggregation, for example, is a phenomenon dependent on multiple factors, including peptide sequence, pH, and concentration.[68] Occurring in solution or on surfaces (adsorption) and stabilized by hydrophobic interactions, hydrogen bonding, π–π stacking, aggregates pose concerns as biologically inactive substances or potentially immunogenic or toxic species.[69]

In summary, the challenges faced by peptides as therapeutic compounds are countless. Still, they mainly arise from their structural features that affect their potential for formulation, drug delivery, membrane permeability, and metabolism.

1.4. Drawbacks to peptide drug development

Drawbacks to the development of peptides as therapeutics can generally be viewed from pharmacodynamic or pharmacokinetic perspectives. Upon administration, peptide therapeutics are prone to a rapid first-pass effect in addition to susceptibility to plasma and renal clearance.[70] Initially, peptides in blood are prone to hydrolysis by serum peptidases which are not only numerous but also recognize several individual peptide side chains as well as combinations.[71] In the liver, membrane-permeable peptides are reportedly more susceptible to degradation by hepatocyte hydrolases, while their counterparts with reduced permeability are more prone to degradation via cytochrome P450 enzymes.[72] Non-enzymatic renal clearance of peptides arises from their relatively low molecular weight compared to proteins (<30 kDa), such that they have a high susceptibility to glomerular filtration, further aggravated by the presence of naturally hydrophilic side chains.[73]

Peptides that successfully evade the aforementioned pharmacokinetic barriers are typically faced with the inability to cross plasma membranes into the cytosol passively and perhaps other organelles

in which their targets may be located. This may result from possible violations of Lipinski's rule of five (Ro5) for determining drug-like compounds as well as predicting membrane permeability.[74] The Ro5 defines parameters such as the number of hydrogen bond donors – (HBAs ≤10), hydrogen bond acceptors – (HBDs≤5), molecular weight (MW≤500), and a calculated octanol-water partition coefficient (clog P≤5). The analysis was based on a data set consisting of small molecules whose binding mode typically involves pockets in target proteins (Figure 3A) and falls within the rule of five. Larger molecules, including peptides, are less frequent in the drug chemical space and are prone to violations of the Ro5 despite their advantages at targeting proteins and other macromolecular structures that cannot be targeted by small molecules (Figure 3B & 3C).

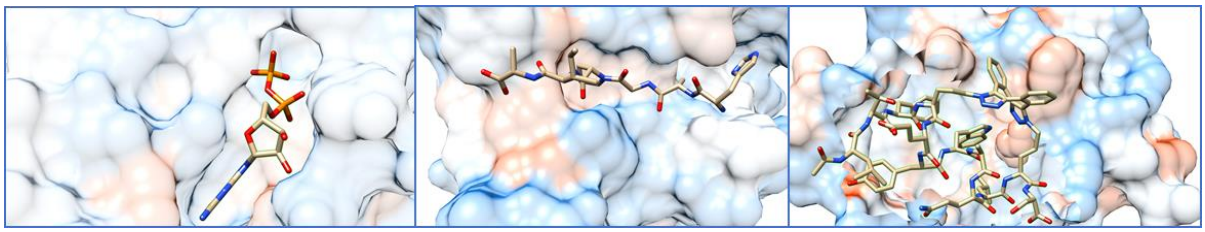

A. Strict Rule of 5	***B. Extended rule of 5***	***C. Beyond* Rule of 5**
MW <500 Da, cLogP 0-5, HBD ≤5, HBA ≤10	*MW 500-700 Da, cLogP 0-7.5, HBD ≤5, HBA ≤10, PSA ≤200 Å^2, NRoTB ≤20*	*MW >500 and at least one of MW 700-3000 Da, cLogP < or >7.5, HBD >5, HBA >10, PSA > PSA ≤200 Å^2, NRoTB >20*
Internal and pocket shapes	*Groove, tunnel, and pocket shapes*	*Flat and groove shapes*
Small: ~285 – 575 Å^3	*Large: ~440 – 760 Å^3*	*Large : ~415 – 820 Å^3*
GPCRS, ion channels, nuclear hormone receptors.	*Protease/Hydrolase, kinase, transferase, structural and molecular glues.*	*Protease/Hydrolase, transferase, isomerases, structural and molecular glues.*

Figure 3. A representation of the Lipinski rule of five and an illustration of the corresponding binding modes of molecules in the different chemical spaces to their targets. Based on the figures by Matsson and co-workers & Doak and co-workers.[79,80]

Notably, a large number of HBDs and HBAs arise from the amide groups on the peptide backbone and some polar amino acid sidechains as well and thereby leading to a high propensity for violating this particular rule of the Ro5. Extensive hydrogen bonding with water creates strong solute-solvent bonding, thereby increasing the penalty for solute release and affecting the availability of the peptide to the cell membrane.[75] Furthermore, widespread hydrogen bonding with the hydrophilic head of phospholipids also impedes further solute dissolution into the lipid bilayer.[76]

Similarly, as a further consequence of numerous backbone and side chain functionalities, peptides are also prone to also having large polar surface areas (PSA) that impede their release and solubilization in the lipid bilayer of the cell membrane during passive transport.[77] Additionally, with a recommendation of a molecular weight of <500, peptides are usually macromolecules with higher molecular weights and thereby prone to a further violation of this Ro5, considering the reported range of molecule sizes of 1000 $Å^3$ (approximately 1000 Da) as the limit for passive permeability.[78]

Many peptide drug candidates typically contain canonical amino acid side chains. They are consequently susceptible to degradation by endopeptidases that typically perform housekeeping functions, including the maturation of higher molecular weight pre-hormones to peptide hormones.[81] The mutual recognition motifs, in this case, are single or multiple amino acid side chains, for example, serine residues in the case of serine proteases and lysine and arginine-specific proteinases; that ultimately cleave peptide therapeutics along the backbone leading to loss of activity.[82] Peptide bonds may also be hydrolyzed at the amino terminus or the carboxylic acid terminus of the peptide by exopeptidases. By utilizing individual terminal amino acids as recognition motifs, exopeptidases are capable of truncating linear peptides and thereby affecting their biological activity. For example, the transmembrane exopeptidase CD26/DPP4 is expressed on the surface of cells and is involved in the adaptive immunity. It recognizes and cleaves N-terminal(or penultimate) proline/alanine residues of chemokines in vivo, thereby modulating their receptor activity.[83]

The Ro5 has had some extensions made in the recent past. One attempt to improve the Ro5 analysis by Ghose and colleagues incorporates analysis of the number of heavy atoms, with a proposed optimal range of 20 – 70, and diversity of functional groups beyond the scope of peptide backbones and side chains that generally places peptides in a disadvantaged position as potential therapeutics.[84] Veber's rule points out the need for a limited number of rotatable bonds to ≤10 as a predictor for good oral bioavailability irrespective of molecular weight based on a compound's reduced flexibility.[77] A valine tripeptide of 315 Da already meets this limit, yet peptide therapeutics are typically much larger macromolecules with an average molecular weight range of 500 – 5000 Da.[85]

Other descriptors have been developed to rationalize the activity of compounds that violate the Lipinski Ro5 based on the type of interactions that the ligands have with their targets. Several small molecule therapeutic compounds reportedly fall within the Ro5 chemical space and are dependent on classical pocket binding to modulate target activity of well-established targets (Figure 3A).[86] Compounds that have molecule weights in the range of 500 – 700 Da are considered as part of the extended rule of five (eRo5) chemical space, comprising of compounds like peptides that are capable of targeting large hydrophobic spaces that do not contain any features suitable for interactions by Ro5

compounds. Mainly falling in this category, peptides are, therefore, less prone to prioritization as drug development candidates compared to their small molecule counterparts in drug discovery programs.[79]

Furthermore, it is also common for peptides to fall in the beyond rule of five (bRo5) space, which is defined on the basis of having a molecular weight range of 700 - 3000 Da and, additionally, fulfilling at least one of the following criteria: a cLogP that is less than zero or greater than 7.5, more than 5 HBDs, more than 10 HBAs, a polar surface greater than 200 $Å^2$ or having more than 20 rotatable bonds.[79] This chemical space is not only limited to peptides but also frequently includes biologics, natural products, and PROTACs that are often used to address challenging targets in drug discovery.[87]

Unlike eRo5 compounds that are capable of binding to both flat surfaces and pockets, the bRo5 compounds almost exclusively bind at flat featureless surfaces and grooves and interact with interface residues of PPIs[88]. As a result of their large molecular weights, molecules falling within the bRo5 chemical space often have poor oral bioavailability, just as eRo5 compounds.[89] Nonetheless, some have been approved for clinical use. A notable example of peptides approved for clinical use is the natural product Actinomycin D, containing two cyclic pentapeptides bridged by a phenoxazinone linker in its structure and used as a cytotoxic drug that suppresses transcription by intercalating DNA.[90] Its Ro5 violations include having a molecular weight of 1255 Da, 6 HBDs, 28 HBAs, and a tPSA of 360 $Å^2$.

1.5. Improving the therapeutic properties of peptides

Despite the challenges faced by peptides, numerous strategies have been employed by synthetic chemists to improve their drug-like properties. From the viewpoint of a drug discovery pipeline, these chemical techniques for the rational design of peptides can be applied along each stage of peptide drug discovery towards clinical applications (Figure 4).[91]

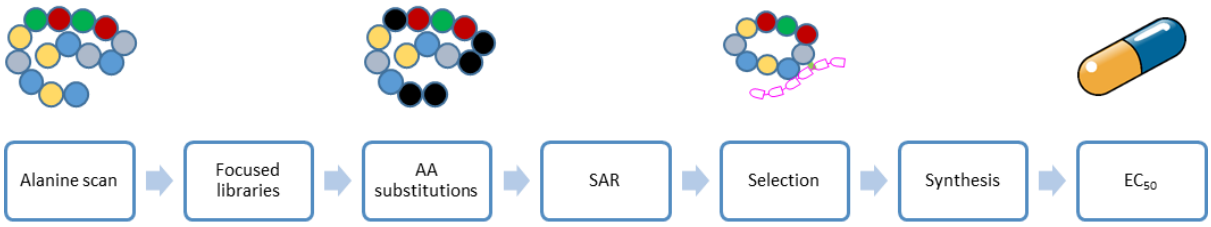

Figure 4. Optimization of peptide-based therapeutic compounds in drug discovery towards clinical applications. Figure adapted from Hoffmann and Fosgerau.[92]

Upon hit identification, peptides typically undergo optimization. However, key themes that are usually encountered during the development of peptide therapeutics are the incorporation of unnatural amino acids in the peptide, cyclization, and improving membrane permeability of peptides.[92]

1.5.1. Incorporating unnatural amino acids

Alanine scans on a hit peptide sequence are usually the first step to determine which residues are important for binding. Therefore, the low-impact residues can be substituted by unnatural amino acids.[93] Otherwise, residues may also be deleted from the sequence if deemed unnecessary or otherwise mutated to improve the biological activities of the hit. It is, however, increasingly common that the UUAs are incorporated into peptide sequences during hit optimization.[94]

Typically not found in natural polypeptides, unnatural amino acids may occur as analogues of canonical amino acids, e.g., hydroxyproline (Hyp), or otherwise as surrogates that are significantly different from canonical amino acids, e.g., 1,2,3,4-Tetrahydroisoquinoline-3-carboxylic acid (Tic).[95] Their incorporation into peptides is a renowned avenue for improving affinity for targets by adjusting hydrophobicity, charge, secondary structure and peptide flexibility to enhance ligand binding and modulation of protein activity.[96] Garnirelix is an example of a linear octapeptide antagonist of gonadotropin-releasing hormone (GnRH) currently in clinical use for assisted reproduction. Peptide optimization was mainly reliant on using unnatural amino acids to inhibit the PPI between GnRH and its receptor.[97] A key innovation in its development was incorporating D-Pal [3-(3-pyridyl)alanine] residues in its sequence to overcome histamine release stimulated by the lead analogues.[98] In this way, UUAs were simultaneously used to increase potency and reduce adverse effects.

The side chains of UAAs have been shown to improve the membrane permeability of peptides. Pipecolinic acid, for example, was serendipitously discovered to enhance membrane permeability of fluorescently labeled linear peptides by Verhelst and co-workers without any clear rationale at the time.[99] However, it could be inferred from later studies that the presence of this moiety on the peptide backbone may have contributed to the adoption of a secondary structure more suited for membrane permeability and, additionally, the occlusion of a backbone amide.[100] Furthermore, the presence of HBAs in the side chains of UAAs has been demonstrated as a contributing factor for the stabilization of peptide secondary structure and improvement of membrane permeability.[101]

A substitution of a canonical amino acid for a UUA also potentially enables the evasion of proteases by peptides in order to enhance their metabolic stability.[102] D-enantiomeric peptides, for example, are widely commercially available tools that have an altered side chain orientation such that their side chains are not recognizable by protease binding sites and often have improved metabolic stability.[103]

However, this is not an infallible approach, given that affinity for the ligand bind site may also reduce dramatically from incorporating UUAs owing to the same change in side chain orientation. As a remedy, an approach known as retro-inverso isomerization is used to overcome this shortfall, in which the peptide sequence is reversed. Consequently, the D-amino acid is presented with a similar topology at the target binding site as the native peptide to form a retro-inverso peptide.[104] By a similar mechanism, UUAs have been used to reduce the immunogenicity of peptides by way of evading recognition by antibodies.[102] Kapoerchan and co-workers, for example, synthesized a library of peptidic human leukocyte antigen blockers (HLABs) and used azidoproline to reduce T-cell response to the highly promiscuous peptide sequences.[105]

1.5.2. Peptide cyclization

Commonly encountered in nature and chemical synthesis, cyclization serves as an overarching tool for optimizing both the metabolic properties and biological activity of peptides. As such, it often complements other peptide modifications during hit optimization efforts.[29] Cyclization may promote proteolytic resistance to peptidases through the evasion of exopeptidases, particularly if performed via the peptide termini. Additionally, by changing the backbone conformation and masking side chains of peptides, amino acid side chains may not be recognized by endopeptidases as well.[106] The absence of termini has also been argued as a possible explanation for the often observed improvement in cyclic peptides' membrane permeability compared to their linear counterparts.[107]

The general approaches to cyclization include head-to-tail cyclization, side chain-to-terminus, and side chain-to-side chain cyclization (Figure 5).[106] Two important considerations for a successful cyclization are macrocycle ring size and peptide pre-conformation prior to cyclization. Smaller ring sizes tend to be difficult to cyclise owing to lowered proximities of functional groups participating in cyclization. Successful attempts at the synthesis of 3 – 5mer long cyclic peptides often necessitated the use of backbone tuning techniques for favorable pre-conformations, including N-methylation, the use of pseudo-prolines, or the addition of chaotropic salts to the reaction solvent lest only oligomeric structures are synthesized.[67] Pseudo-prolines can also enable the formation of cis peptide bonds that tend to be favorable for improving the proximities of functional groups. A combination of these approaches was successfully used for the synthesis of a cyclotripeptide.[108]

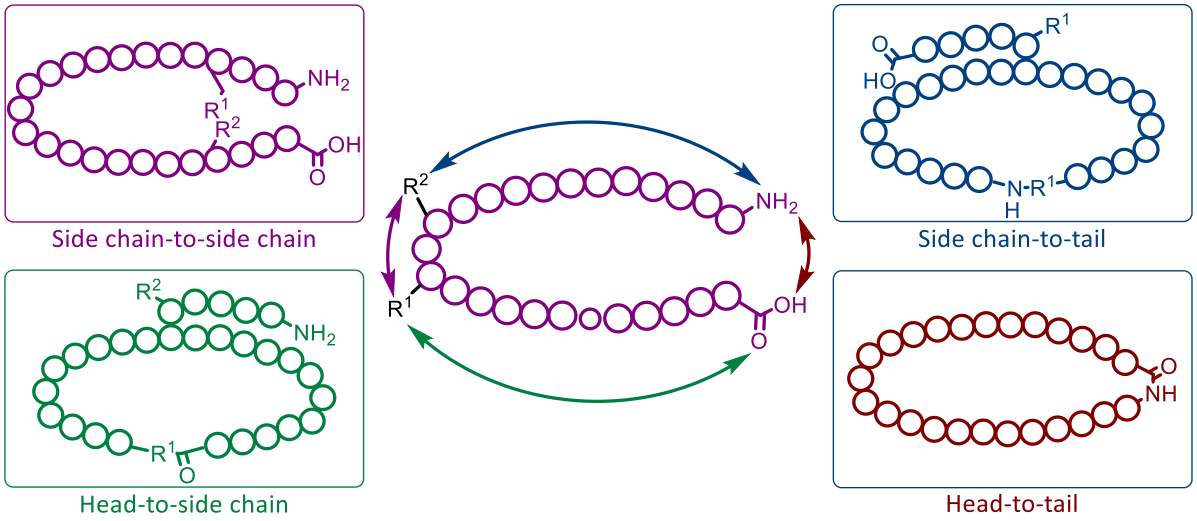

Figure 5. Modalities for peptide cyclization. Figure adapted from Yudin and white[109]

Solution phase head-to-tail cyclization is a common method used for the synthesis of cyclic peptides. Herein, a very dilute solution of the linear precursor is treated with a base and coupling reagent, and the reaction typically takes about 12 hours or more.[110] However, it is also possible to perform on resin cyclization as a method to introduce a pseudo-dilution effect and reduce the chance of oligomerization. In this case, the peptide is anchored on the solid support using an amino acid side chain.[111] On-resin approaches also allow for the use of higher equivalents of reagents since any unreacted reagent as well as side products in solution, can be easily washed off.[49]

Other methods of cyclization that do not rely on the formation of traditional amide bonds have been reported. A common strategy utilizes cysteine thiols. In nature, thiols in close proximity are oxidized to form disulphide bonds that stabilize the tertiary structure of proteins and peptides.[112] Insulin, for example, contains two peptide chains that are linked by two disulphide bonds which are critical for its proper function.[113] However, the use of disulphide bonds has been widely applied for the synthesis of cyclic peptides, requiring only two cysteine residues in the peptide sequence as a means for attaining conformational stability and resistance to proteases. The approach may be extended to use benzylic bromide linkers to optimize ligand binding at hydrophobic regions of proteins or, in the case of most PPI interfaces.[114]

From more recent advancements, a cysteine residue containing an S-*p*-methoxybenzyl Cysteine sulfoxide protecting group has also been recently utilized to form a thioether bond via S-arylation to achieve a tryptathionine bond that is commonly encountered in nature.[115] The reaction used guanidine as an S-p-methoxybenzyl cation trap under acidic conditions necessary for the activation of the sulphoxide.[116] A second approach uses click chemistry for the cyclization of peptides via both the

peptide termini and side chains. This method has been demonstrated to be useful for the synthesis of cyclic cell-penetrating peptides by Feni and Neundorf.[117]

Several transitional metal-catalyzed peptide cyclization techniques have been developed as well. The ruthenium-catalyzed ring-closing metathesis (RCM), for example, is commonly used to introduce hydrocarbon staples that typically tend to stabilize peptide α-helical structures and has been shown to improve the membrane permeability of peptides. [118] ATSP-7041 is a 16-mer stapled peptide mainly composed of biogenic amino acids that is undergoing clinical trials for the treatment of p53-positive tumors. The cell-permeable peptide is a PPI dual inhibitor of the interaction between P53 and both MDM2 and MDMX.[119]

Finally, photo-redox mediated peptide cyclizations are gaining traction owing to their ability to avoid the introduction of polar elements in the peptide backbones just as the RCM approach. Molander and co-workers recently generated alaninyl radicals from an activated N-Hydroxyphthalimide ester on a peptide side chain using blue light followed by the formation of new $C(sp^3)$–$C(sp^3)$ via a single electron transfer in order to afford cyclic analogues of Atosiban, an oxytocin antagonist.[120]

Peptide therapeutics may acquire improved affinities for their biological targets through cyclization resulting from their enhanced conformational rigidity. The resulting decrease in their entropic penalty enables more efficient binding to their targets, which is achieved by eliminating multitudes of potential conformations that a peptide can assume and presenting a closely optimal one for binding ab initio.[121] Elimination of other conformations also enhances the selectivity of the cyclic peptides and reduces the chance of off-target effects. These conformations are further potentially stabilized as a result of the spatial arrangement of intramolecular hydrogen bonding elements arising from cyclization.[122]

Some cyclic peptides of large ring sizes have been observed to have excellent membrane permeability despite their violation of the Ro5 parameters. Cyclization may improve the permeability of peptides across biological membranes by enabling their behavior as molecular chameleons.[123] The term “molecular chameleon” was first coined by Carrupt and co-workers after the unexpected observation of morphine-6-glucoronide (M6G)’s tenfold potency relative to morphine, albeit its high polarity and remarkable CNS activity, a property almost exclusively attributed to lipophilic molecules. They postulated that the membrane permeability of the polar molecule through the blood-brain barrier and plasma half-life alike were facilitated by an equilibrium shift to its folded (closed) conformer from an extended (open and polar) conformer in response to solvation environmental polarity.[124] In the same manner, cyclic peptides can utilize a change in their solvent polarity to alter their own hydrogen bond patterns in order to attain open or closed conformations. This conformational heterogeneity

reduces the penalty for dissolution of the peptide as it transitions across the cell membrane by exposing polar functionalities or hydrophobic side chains as required for solvation.[125] This effect is largely possible due to the constrained nature of the peptide, which is imparted by cyclization such that there is a reduction of the energy barrier for adapting to its environment relative to their linear counterparts.[126]

Additionally, cyclic peptides can potentially mimic protein secondary structures, including α-helices and the β-sheets, especially when stabilized by hydrocarbon staples.[127] These structural motifs are also thought to contribute to the membrane permeability of peptides by mechanisms used by membrane-active peptides, such as disruption of lipid packing, translocation, or formation of inverted micelles.[128] Moreover, the (pseudo)secondary protein structures arising from cyclization may mimic secondary structures of proteins to enable protein-protein interaction inhibition by the peptide.[129] Some secondary structure mimics arising from cyclization assume supramolecular architectures in order to enact their biological activities. Gramicidins, for example, are cyclic peptides with cytotoxic and antibiotic activities that adopt a unique β-helix-like conformation capable of dimerizing within the membrane and consequently disrupting the bacterial cell membrane.[130]

Cyclic peptides have been traditionally developed using the structure-guided design approach whereby the crystal structure of a protein is used to design an oligopeptide mimic that is capable of either stabilizing or disrupting an interaction with binding partners or directly modulating the target proteins' activity.[131] However, high-throughput screens for cyclic peptides have enabled faster identification of hits against specific targets. Examples of these platforms include phage display, SICLOPPS mRNA display, and *in silico* techniques.[85] Phage display technologies, for instance, have benefited from a number of cyclization strategies and their ability to incorporate unnatural amino acids to enable screens for chemically diverse cyclic peptides.[132] Recently, linear peptides displayed on phage were treated with dichloropentadione (DPD) and functionalized with hydrazine derivatives. This enabled enrichment of hits with nanomolar affinities for carbonic anhydrase bearing benzene sulphonamide pharmacophores.[133] SICLOPPS is another notable screening platform that uses self-excising protein domains (inteins) flanking the termini of a peptide from a randomized library, such that upon translation, a *cis*-intein is formed that facilitates the cyclization of the peptide.[134] Tavassoli and co-workers identified a high-affinity inhibitor of hypoxia-inducible factor-1 (HIF-1) heterodimerization for their potential as a cancer therapeutics and with marked selectivity for the HIF-1α/HIF-1β PPI.[135] Other cyclic peptide screening methods include in-silico approaches and mRNA display.

Cyclization of peptides is, therefore, an invaluable tool for the optimization of peptide therapeutics that has driven advances in synthetic methodologies for peptide synthesis and enabled a number of peptides to progress to different stages of clinical trials with over 20 FDA approvals in the past two decades.[126]

1.5.3. Improving membrane permeability of peptides

1.5.3.1. Cell-penetrating peptides

Despite the aforementioned advances in the design of peptides as therapeutics, poor membrane permeability hinders peptides from reaching their intracellular targets, as a result of which they modulate biological activity.[136] One common approach for improving the passive membrane permeability of peptides is through the use of cell-penetrating peptide (CPP) sequences. The earliest CPP sequence to be used was discovered from the 86-mer HIV trans-activator protein TAT, a known regulatory protein considered essential for viral replication and containing a highly basic lysine and arginine-rich sequence.[137] The first proposed mechanism by which the polybasic sequence delivers its protein cargo was based on the principle of "scrape-loading," in which the cell membranes are transiently disrupted to allow cytosolic delivery of macromolecules.[138]

Further mechanistic insights show that the highly positively charged sequence adheres strongly to the membrane, following a strong association with the negatively charged phospholipid layer of the membrane.[139] Thereafter, the peptide is internalized and captured into a vesicle by any of the cell membrane's natural recycling pathways, including endocytosis and pinocytosis.[140] It is essential that the CPP binds long enough for the particular section of the membrane to get turned over. Essentially, with a turnover estimated at approximately 2% - 5% per minute, it is highly likely for the membrane-bound CPP and cargo to be delivered into the cell.[141]

Cell-penetrating peptides are predominantly polybasic sequences, but their sequences are not limited to the HIV-1 Tat (48–60) analogues. Other sequences have been identified from alternative nucleic acid-binding proteins and proteins that interact with highly negatively charged proteins like heparin. The lysine-rich C-terminus of the heparin-binding domain (HBD) of heparin-binding endothelial growth factor (HB-EGF) was used to design a cationic CPP with a similar mechanism of action as the arginine-rich rich HIV-1 Tat (48–60) peptide.[142] Furthermore, a hydrophobic CPP was designed based on the sequence of the mammalian proline-rich antimicrobial peptide (PrAMPs) Bac7. The CPP is reportedly capable of conformational changes, including adopting a helical formation in order to traverse the cell membrane. Notably, one of the sequences has only two arginine residues that were arguably not sufficient to fit the cationic peptide mechanism of membrane permeation.[143]

In its first application for intracellular cargo delivery as a CPP from HIV-1 Tat (48–60), the peptide was used for the delivery of a number of heterologous proteins, highlighting its robustness for applications beyond peptide therapeutics to larger macromolecules. Additionally, the polybasic sequence allowed for substrate conjugation using various approaches, including maleimide and iodoacetamide-based substrate conjugation.[139] More recent advances have led to a diverse structural repertoire of arginine-rich sequences based on HIV-1 Tat (48–60), including cyclization and incorporation of unnatural amino acids for the stability of the CPP and design of β-hairpin arginine-rich peptides as CPPs for cytosolic stability.[144] The recent development of a tumor-homing polybasic sequence has led to the first reported development of a bi-functional CPP conjugated to a pro-apoptotic peptide and led to the successful targeting of malignant hepatocytes, in an elegant highlight of the utility of CPPs for intracellular peptide delivery.[145] Furthermore, a number of peptide-based therapeutics conjugated to CPPs are currently in various phases of clinical trials, including ATX-101, a PCNA interacting peptide in phase I/II for the treatment of advanced solid tumors, and PEP-010, caspase 9 – PP2A PPI in Phase Ia/Ib for the treatment of metastatic solid tumors.[144]

There are several drawbacks to the usage of CPPs for the intracellular delivery of therapeutic peptides, with instability in the digestive tract as a factor that affects their use for oral delivery of therapeutics.[146] Even after parenteral administration and upon internalization into the cell, CPPs are prone to endosomal entrapment, hampering their ability to release their cargo into the cytosol and access their targets.[147] This has necessitated the application of endosomolytic strategies for the release of the cargo once inside the cytosol. Unfortunately, endosomolytic peptides typically derived from venom extracts are prone to having cytotoxic effects, especially at concentrations required for cargo delivery.[148,149]

The polybasic nature of the CPPs has generated discussions about their potential toxicity, particularly their potential to complex the highly negatively charged nucleic acids.[150] However, this is potentially only true for cationic polymers with much larger molecular weights of up to 10 kDa, and no evidence of cytotoxicity from polybasic CPPs has been reported.[148] Nonetheless, as derivatives of antimicrobial proteins, they pose a potential risk of immunogenicity.

Cell-penetrating peptides do not show a cellular specificity that would effectively require increased cargo doses which is, unfortunately, also a predisposing factor to toxicity.[151] Additionally, the therapeutic peptide cargo of CPPs in endosomes may be subject to hydrolases that could degrade the peptide or protein cargo, leading to a loss in activity. The first peptide therapeutic using a CPP as a peptide therapeutic failed at phase IIb of clinical trials as a result of the very slow release of the cargo

– cyclosporine A along with a rapid renal clearance; leading to suboptimal plasma concentrations for therapy.[152]

1.5.3.2. N-methylation

Currently, N-methylation is a valuable technique in the chemist's toolbox, which is primarily used to improve membrane permeability. In its early development, N-methylation was investigated as a means to control the conformation of peptides by influencing the peptide backbone and hydrogen bonding patterns.[153] At the early stages of peptide chemistry, the incorporation of N-methyl phenylalanine led to a serendipitous observation of the improved analgesic activity of encephalin. This observation was alluded to the N-methylated peptide's enhanced ability to evade proteolysis, increasing its plasma half-life.[154] Likewise, Mazur and co-workers later applied it to improve the biological activity of bradykinin.[155] However, early progress in N-methylation was mainly hindered by their synthetic drawbacks, viz. coupling sterically hindered secondary amine moieties of N^{α}-methylamino acids residues during peptide synthesis. The commercial availability of N^{α}-methylamino building acid blocks was limited as well.[156]

Inspired by the high oral bioavailability of the extensively N-methylated cyclic peptide cyclosporine and the development of synthetic methods for N-methylation on solid phase, Biron and co-workers first reported the application of peptide N-methylation in improving membrane permeability. A library of somatostatin analogues was synthesized, and a panel of membrane permeability assays was used to successfully demonstrate improved transcellular transport of N-methylated somatostatin analogues.[157]

This observation may result from a decrease in the number of hydrogen bond donors in a peptide. It's well established that a cell's milieu is typically aqueous, and the availability of a molecule at the membrane surface for possible permeation is determined by the molecule's penalty for leaving the aqueous phase. This availability is influenced by nature and the number of hydrogen bonds formed between the dissolved molecule and water.[158] Since the HBD – water bond energies are reportedly higher than their HBA – water counterparts, decreasing the number of HBDs may result in a marked reduction in the peptide's penalty for leaving the aqueous environment outside the cell membrane.[159] By generating a tertiary N^{α}-amine functionality on the peptide backbone, N-methylation, therefore, effectively reduces the number of hydrogen bond donors present in the peptide and potentially improves its ability to leave the cellular milieu and access the cell membrane surface for possible permeation.[75]

However, the design of membrane-permeable peptides through backbone modifications poses the possibility of altering biological activity through modification of the molecule's pharmacophore and could be a major setback in the development of peptide therapeutics.[160] Furthermore, random changes in the availability of hydrogen bond donors may instead lead to loss of membrane permeability via disruptions of hydrogen bonds necessary for the stabilization of a peptide's secondary structure, which could aid in the process of traversing the lipid by a layer of the cell membrane.[161]

Moreover, an increase in the hydrophobicity of peptide therapeutics has also been reported to have a bidirectional effect on the permeability of peptides, depending on their polarity. N-methylation of peptides with a low clogP has been shown to improve their permeability, while a decrease in permeability would ensue for lipophilic peptides, owing to a reduction of the peptide's lipophilic permeability efficiency, with the latter attributed to a reduction in aqueous solubility.[162]

An increase in molecular weight has been noted as an inherent factor that hampers membrane permeability of bRo5 molecules with a proposed limit at 1000 Da above which, the feasibility of optimization for druggability is drastically hampered irrespective of log P – a phenomenon coined the molecular weight penalty.[158] Adding multiple methyl groups on the backbone of an eRo5 peptide molecule in attempt to improve its membrane permeability effectively increases its molecular weight. This may result in a decrease in the efficiency of diffusion across the membrane, leading to the sequestration of compounds inside the membrane since the molecular weight and diffusion coefficient of a compound is inversely (logarithmically) related.[163] However, the correlation between MW and sequestration may also be confounded by the unstirred water layer (UWL) phenomenon of the PAMPA assay that has been shown to lower the observed permeability of the hydrophobic compounds used in the study by Pye and co-workers who proposed the MW limit.[164]

N-Methylation may further hinder the ability of peptides to cyclise during chemical synthesis because successful cyclization of peptides is majorly dependent on the pre-conformation of the linear precursors. Consequently, modifying the peptide backbone may lead to a pre-conformation that is unsuitable for cyclization.[165] By creating new HBAs and changing the overall relative positions of HBAs and pre-existing HBDs, N-methylation has the potential to influence the structural configuration of a molecule.[166] The reportedly low cyclic peptide library synthesis success rate of 3% by Biron and co-workers was attributed to N-methylated analogues that failed to adopt the native peptide's optimal pre-conformation for cyclization.[167] Therefore despite the potential to improve membrane permeability, optimization of a hit N-methylated cyclic peptide therapeutic may fail due to the backbone modification. Secondly, N-Methylated peptides have been reported to be unstable under TFA conditions which are commonly used for cleaving peptides off the resin. The acid lability is

dependent on the side chain and typically occurs on the amide bond adjacent to the C-terminus of the N^{α}-methylamino acid residue as a result of the formation of an oxalone intermediate during cleaving with TFA.[168]

Current alternatives for masking HBDs on the peptide backbone include the use of cycloalanine and peptoids (Figure 6). The cycloalanine building block was developed as a means to mask HBDs with an unnatural building block just as N-methylation but without the need for using highly activated acylating agents to overcome the challenges posed by the sterically hindered less nucleophilic secondary amine intermediate formed during peptide synthesis.[169] The cycloalanine moiety may, however, potentially decrease the bRo5 peptide's lipophilic permeability efficiency more than the less bulky n-methyl moiety. The second notable alternative for masking a peptide's HBDs is the use of peptoids which are oligomers of N-substituted glycine residues.[170] These macromolecules are reportedly resistant to proteases and have a marked reduction in immunogenicity, especially if they are analogues of antimicrobial peptides (AMPs).[171] Peptoids may affect the secondary conformation of a peptide in the same manner as N-methylated peptides, and the loss of chiral centers in the peptoid backbone may, additionally, affect the affinity of the modified peptide.[172]

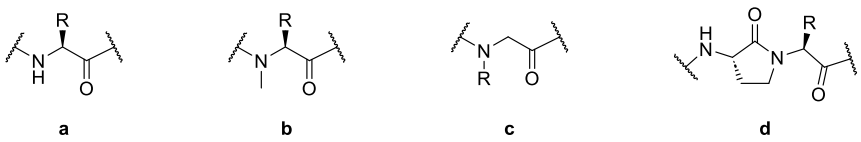

Figure 6. Peptide backbone modifications that mask amide nitrogen HBDs in bid to improve membrane permeability: **a.** Unmodified peptide bond; **b**. N-methylation; **c** peptoid and **d**: cycloalanine. Figure adapted from Lamers[173]

In summary, backbone nitrogen modifications as an approach to improving the membrane permeability of peptides pose a challenge of robustness for application on molecules with varying lipophilicities and molecular weights, given that there are no hard and fast rules based on these parameters. Furthermore, the choice of location for the N-methylation of peptides is yet another challenge, given the potential to disrupt the molecule's pharmacophore by a change in the backbone configuration and uncertainty on successful peptide cyclization based on the backbone alteration.[174]

As an illustration, Lokey and co-workers synthesized a library of 1152 cyclic peptides inspired by the backbone of guangomide A and consisting of N-methylated peptides variants of peptides at different positions. From their report, improving membrane permeability as a result of N-methylation was an inundating task further complicated by the dependence of the technique on side chain orientation and intramolecular hydrogen bonds, which made it rather unpredictable.[175]

1.5.3.3. Heterocyclic fragments

Heterocyclic fragments in peptide backbones are commonly encountered as surrogate UUAs because they have garnered research interest in their potential for improving passive cellular uptake and bioactivity.[176] A repertoire of these heterocyclic moieties is commonly encountered in nature and includes thiazoles, oxazoles, indoles, imidazoles, and pyridines, which are derived from modifications of amino acids.[177] Earlier studies on the heterocycles focused on their biosynthetic origin, their contribution to observed bioactivities, and in relation to their influence on peptide conformations.[178]

However, advances in synthetic and analytical techniques led to increased interest in heterocyclic fragments as tools for improving cellular uptake, for example, the early observation of improved cellular uptake of triazole fragments as dipeptide surrogates.[179] Conformational control by the heterocycles was later postulated to result in a network of intramolecular hydrogen bonds that modulate the interactions between the macrocycles and solvation environment and, thereby, facilitate their availability to interact with the cell membrane.[180] In contrast to covalently constrained structures, the hydrogen bonding networks in which heterocycles partake usually maintain a degree of flexibility that enables the molecules to alter their exposed polarity and, as such, improve solubility and membrane permeability in a phenomenon known as molecular chamelonicity (Figure 7A).[181]

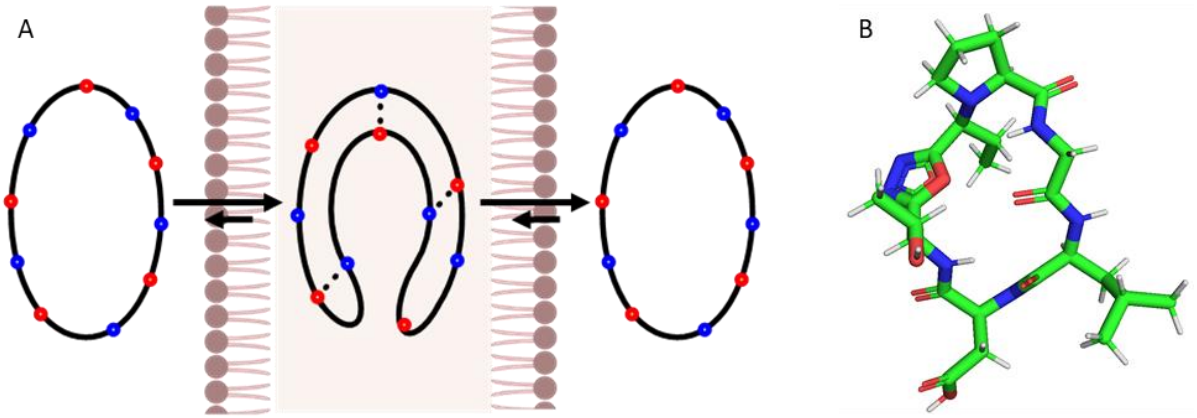

Figure 7. A; Conformational changes by molecular chameleons which facilitate their uptake may utilize hydrogen bonding networks for transient structural stabilization. **B**; An oxadiazole-containing peptide in a β-sheet conformation. Figures adapted from Whitty and co-workers[182] & Yudin and Saunders[183]

In addition, heteroatoms in the macrocycles avail additional HBAs that are deemed favorable for drug-like activity and participate in the hydrogen bond network involved in the peptide's conformational control.[181] Furthermore, the typically aromatic moieties subtly increase the lipophilicity of the peptides and act in tandem with peptide side chains to improve the interaction of the peptides with

the lipid bilayer while avoiding a high hydrophobic penalty and consequently reduced solubility, which would have been accrued from much more elaborate lipophilic moieties [184].

From their study of a select library of 24 compounds of molecular weights ranging from 100 – 2000 Da, Kihlberg and co-workers further pointed out the importance of conformational flexibility as contributed by the number of rotatable bonds, the presence of flexibly attached aromatic systems for dynamic shielding of PSA and ability to form IMHBs for successful cellular uptake mediated by chameleonic behavior.[185] In a more specific study on a library of more than 200 macrocycles in the eRo5 and bRo5 chemical space, the team pointed out the superiority of nitrogen HBAs over oxygen HBAs; furthermore, among heterocyclic fragments, phenyl, pyridyl, and oxazoles fragment were privileged motifs for enhanced cellular uptake while sulphonamides, ureas, and primary amines were deemed detrimental for the passive membrane permeability of macrocycles.[186]

In their seminal work, therefore, Yudin and co-workers developed a method for the incorporation of an oxadiazole ring into the backbone of peptides with simultaneous cyclization to augment chameleonic behavior and foster membrane permeability (Figure 7B). PAMPA assays were used to compare the membrane permeabilities of the oxadiazole-containing peptide with the homodetic analogue, and the observations were further corroborated with data from variable temperature NMR (VTNMRs), which showed a hydrogen bonding network, in which the heterocyclic fragment contributed an HBA.[122] In a follow-up of their work, the team designed an oxadiazole fragment in close proximity to a reduced amide bond, also known as a reduced amide bond/heterocycle (RAH) motif, which was designed to be a beta-turn-inducing element in peptide macrocycles as a design tool the control of the conformation of peptides conformations.[187] In a follow-up investigation, multiple heterocyclic fragments were determined to proportionately improve membrane permeability in comparison to a single one via a combination of enhanced dynamic lipophilicity as well as conformational control. Notably, the heterocyclic fragments were sequentially introduced into a model peptide of known poor cellular uptake in order to avoid passive permeability endowed by naturally occurring peptide sequences.[183]

1.5.3.4. Peptide drug delivery systems

Recently, various systems for the delivery of peptides have been investigated. These include peptides with multiple domains, such as the Feldan shuttle technology, which uses a CPP (PTD4) fused to an endosomal leakage domain (ELD) peptide, the antimicrobial peptide CM18, and a histidine-rich domain that further promotes endosomal release via the proton sponge effect.[188] While ELDs are incapable of delivering macromolecular cargo into a cell, they lyse endosomes to enable endosomal

escape.[189] The Feldan shuttle peptide is advantageous since it only needs to be co-incubated with the cargo macromolecule and does not require conjugation to the peptide cargo like conventional CPPs.[190]

Vallis and co-workers have also reported the design of trimeric cyclic tat peptides that showed a marked improvement in the cytosolic delivery of macromolecular cargo. They reported improved efficiency at endosomal delivery and escape. Owing to the cyclic nature of the TAT subunits, the peptide was shown to have better proteolytic stability than the linear counterpart.[191] Inasmuch as this approach did not require conjugation to cargo, the delivery system may face challenges in robustness with regard to different types of cargo. For example, its dependence on a charge for cargo uptake which could be disadvantageous for neutral peptides, as shown by the team.[192]

Secondly, Sun and co-workers recently reported using a pH and redox-responsive conjugated peptide that forms coacervates from liquid-liquid phase separation (LLPS); and are capable of recruiting macromolecules, including peptides within the phase-separated liquid droplets followed by rapid intracellular cargo delivery.[193] This delivery system was motivated by histidine-rich beak proteins isolated from the Humboldt squid beak, resulting in the development of a peptide capable of direct cytosolic delivery of macromolecular cargo while bypassing the endosomal-mediated pathway of conventional delivery systems.[194]

1.5.3.5. Techniques for studying passive membrane permeability

Early studies used physicochemical metrics to predict membrane permeability, including octanol-water partition (log *P*). [195] Unfortunately, it may not be a close reflection of the membrane environment but may serve as a quick screen for compounds based on Lipinski's Ro5.[74] The solubility of a compound was also used to predict its oral druggability with a similar justification since it can be used to predict the ability of the compound to access the GIT mucosa cell membranes for subsequent passive permeability, mainly if the solubility experiments are performed at the stomach's acidic pH (1.5 – 3.5).[196]

The Parallel Artificial Membrane Permeability Assay (PAMPA), for example, is a technique that is used to estimate the rate at which a molecule passively traverses the cell membrane by using an artificial membrane that is affixed between two buffer wells and, therefore, excluding observations from active transport making the assay uniquely suited to study chameleonic peptides (Figure 8).[197] Occasionally, anionic lipids like lecithin may be added into the buffer to improve the mimicry of the cell membrane's hydrophobic bilayer, particularly that of the blood-brain barrier, hence potentially extending its application in the screening peptides which modulate targets in the central nervous systems.[198]

However, this technique has setbacks, including an unstirred water layer (UWL) close to the artificial membrane, potentially leading to much lower membrane permeability observations than its actual rate.[199]

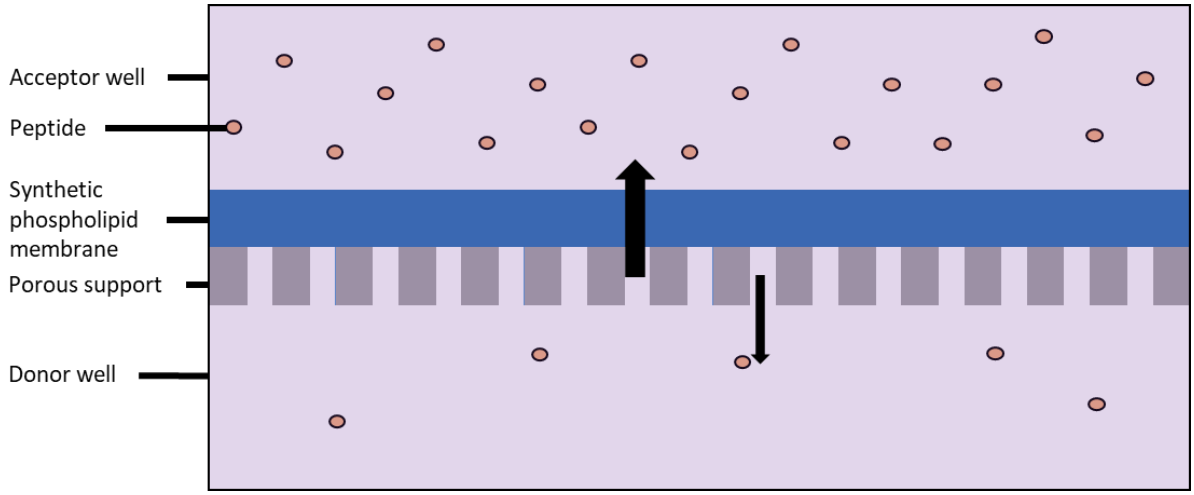

Figure 8. An illustration of a PAMPA model wherein in the rate of permeation of a peptide across an artificial membrane is quantified using LCMS. Figure adapted from Yu and co-workers.[200]

PAMPA may also not be best suited for predicting membrane permeability across the gastrointestinal tract's endothelial layer owing to efflux pumps that may completely offset the internalization of orally administered compounds.[201] A secondary screen that uses an immobilized layer of colorectal adenocarcinoma-2 (Caco-2) cells, a cell culture–based mimic of the (gastrointestinal) GIT wall, may give much more reliable correlations of chameleonic peptide's oral druggability based on their ability to passively traverse the GIT with susceptibility to bidirectional efflux pumps.[202] However, the Caco-2 assay is not ideal for screening large compound libraries because of the slow cell growth rate and the variability in the expression of transporters and efflux pumps vary across cell batches.[203] An alternative tool commonly used for screening membrane permeability employs the faster-growing Madin-Darby canine kidney (MDCK) cells since it can be established much faster than Caco-2 assays.[204]

A recent innovation for the high throughput screening of membrane permeability of compounds is the LCMS-based immobilized artificial membrane (IAM) technique (Figure 9).[205] The screen obtains a compound’s chromatographic hydrophobicity index (CHI IAM) using its retention time in an analytical column packed with particles that are decorated with a monolayer of phospholipids. The CHI IAM value of the compound as an indicator of its passive membrane permeability is determined against a calibrated gradient of retention times of a set of standard compounds.

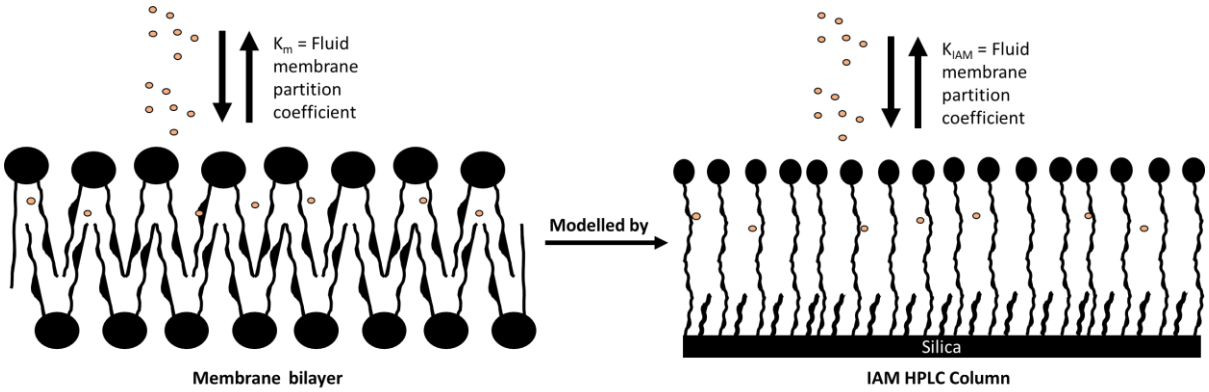

Figure 9. A schematic representation of the membrane lipid bilayer and the stationary phase of the IAM column. Figure adapted from Tsantili-Kakoulidou*[206]*

This technique is remarkably advantageous owing to the low amount of material required for screening, the potential for automation via LCMS, and, consequently, high throughput. Furthermore, a noteworthy series of studies by Barbarto and co-workers found linear relationships between the chromatographic hydrophobic indices from IAM measurements (CHI-IAM), a factor derived from a compounds phospholipid affinity, and membrane permeability screens from PAMPA as well as Caco-2 assays. [207,208] Valko and co-workers also demonstrated a linear relationship between neutral compounds' octanol/water lipophilicity measurements and CHI IAM measurements.[209] Furthermore, investigations by Bienert and co-workers also showed that IAM chromatography is well-suited for predicting the interaction of peptides with lipid membranes.[210]

However, caution has to be made with cationic compounds, which tend to have strong electrostatic interactions with the immobilized negatively charged phospholipids, giving indications of false high membrane permeability.[211] An inadvertent application of this weakness of CHI IAM measurements is its potential application as a screen for potential Drug-induced phospholipidosis (DIPL) by compounds.[212] Nonetheless, this application warrants caution when dealing with compounds conjugated with cationic cell-penetrating sequences and, more importantly, ionizable heterocyclic fragments during investigations of their chameleonic properties.[213]

It is, however, desirable to discriminate between passive membrane permeability arising from chameleonicity derived from alternating patterns of hydrogen bond networks and alternative mechanisms.[214] And as such, variable temperature NMR (VT-NMR) studies in different solvents, for example, have been employed for ascertaining the pattern of hydrogen bond networks in cyclic chameleonic peptides.[215] In these experiments, analyses are commonly performed in $CDCl_3$ to mimic the hydrophobic lipid environment of the lipid bilayer and DMSO-d_6 as a mimic of the aqueous cellular internal and external milieu.[181]

Little or no change in the shift of amide backbone protons with increasing temperature, quantified by temperature coefficients, is used to determine which protons are involved in intramolecular hydrogen bonding and, perhaps, indicating the existence of a molecular chameleon.[181] The VT-NMR experiments may be complemented with D_2O exchange experiments and solvent titration experiments that may be used to confirm which backbone protons are contributing to the chameleonic behavior of a peptide via their participation in an interchangeable network of intramolecular hydrogen bonds.[216]

A recent advancement in evaluating the chameleonic properties of compounds features a high throughput chromatographic technique based on supercritical fluid chromatography (SFC), which was developed as an efficient means for probing changes in IMHBs and utilized super supercritical CO_2 as a non-polar eluent in a normal phase column in the same manner that the technique is routinely used for the separation of chiral compounds of low molecular weight.[217]

Shapiro and co-workers used a correlation between the retention times of a data set of compounds and their topological surface areas to obtain a calibration curve for estimating experimental polar surface area (EPSA) and thereby predicting variations in IMHBs during the HPLC analysis.[218] In a follow-up of their invention, the team reported their observation of IMHB changes in a model peptide. Subsequently, it used a series of strategically N-methylated peptides as a proof of concept for applying EPSA to design cyclic peptides with passive membrane permeability based on their chameleonic properties.[219]

Techniques that enable the ability to observe changes in the IMHBs in cyclic peptides can potentially be combined with in silico approaches for ab initio design of molecular chameleons, exemplified by the work by Baker and co-workers who designed chameleonic peptides from a virtual library of cyclic peptides of various residue lengths with the aid of NMR experiments to study IMHBs and Caco-2 experiments to affirm their membrane permeability via changes in their IMHB networks.[160]

1.6. Late-stage functionalization of peptides

Upon lead identification, it is often desirable to modify the resulting complex molecules to develop a library of analogs with improved metabolic or therapeutic profiles, necessitating chemo- and regioselective transformations, also referred to as late-stage functionalization (LSF). These transformations are usually performed without the need for protecting groups.[220] Ideally, LSF methodologies should be able to tolerate all the functional groups present in the lead molecule and should also be feasible for the introduction of typically smaller substituents on the substrate molecule, as is often the case for lead optimization (Figure 10).[221]

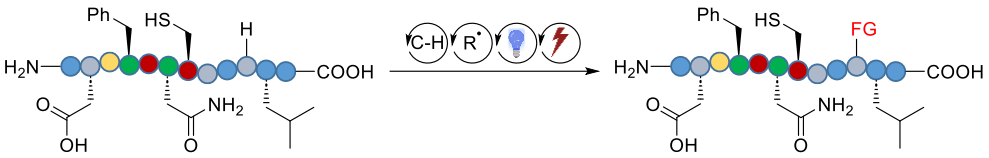

Challenges

Multiple C-H bonds **Stereogenic centers**

Multiple reactive sites **Metal binding inhibition**

Side chain Functional groups

Key features

Position selectivity **Chemoselectivity**

No racemization **Bioorthogonal**

Catalytic efficiency **Step economy**

Figure 10: Late-stage functionalization of peptides utilizes several methodologies to optimize complex peptide substrate through the introduction of new functional groups, albeit with several challenges. Figure based on the minireview by Wang and co-workers.[225]

The application of LSF in peptide drug development poses a multifactorial challenge. Amino acid side chains have multiple functional groups, and as such, a single peptide may simultaneously possess several functional groups, including nucleophilic side chains like amines and thiols, acidic as well as aromatic functional groups, and several chiral centers.[222] Furthermore, resin, solvent, reagent, and side chain protecting group compatibility during solution and SPPS are vital factors to be taken into account during the development of new LSF methodologies.[223] Therefore, the complexity of peptides and their current synthetic strategies make LSF an attractive approach for application in peptide optimization, taking into account the multistep synthesis of amino acid building blocks, which is further complicated by stereoisomeric intermediates.[224]

Contemporary peptide LSF efforts demonstrate the utility of various methodologies initially developed for small-molecule LSF as well as opportunities accrued from the diversity in amino acid side chains and resulting peptide backbone modifications (Scheme 2). These methodologies have enabled access to highly coveted non-canonical amino acid side chains with improved atom and step economy.[226] Early LSF efforts on peptides relied on a combination of side chain functional groups and their orthogonal protecting groups, consequently increasing the molecular complexity of substrates and often necessitating harsh reaction conditions.[227]

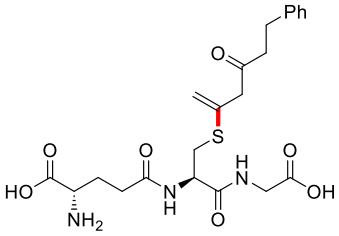

Glutathione modification, Abbas et al.
Orthogonal allenamide handles

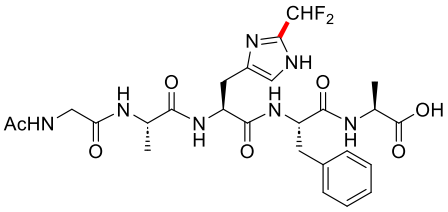

Unprotected peptides at histidine, Noisier et. al
C–H functionalization

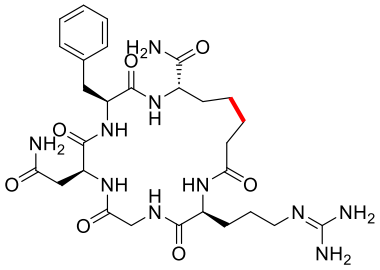

Cyclo-RGDf Peptides Chenoweth et.al
NHPI mediated decarboxylative lakylation

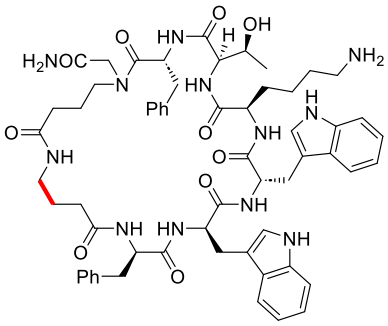

Somatostatin Analogue, **COR-005**
photoredox catalysis

Scheme 2. Examples of contemporary late-stage peptide modification strategies include the use of allenamide handles for labeling peptides and proteins, modification of histidine, and radical-mediated peptide cyclization.

Initially focused on bioconjugation, the methodologies relied on nucleophilic substitution of leaving groups or addition to Michael acceptors to lysine and cysteine residues of peptides.[228] Abbas and co-workers, for example, developed the selective modification of cysteine residues on fully deprotected peptides and proteins using allenamides. Their strategy relied on a combination of reduced reactivity of allenamide substrates and relatively strong nucleophilicity of thiols.[229] As such, their strategy was reportedly superior to other non-selective substrates such as α-halo acyl and maleimide substrates since it proved to be irreversible and not prone to cross-reactivity with other nucleophilic side chains of residues such as histidine and lysine.[230]

In the recent past, transition metal-catalyzed C-H activation LSF methodologies were used for modifications of aromatic moieties on peptide side chains of phenylalanine, tyrosine, and tryptophan. Noisier and co-workers, for example, reported a palladium-catalyzed late-state stage stapling of tetra-peptides enabled by C(sp^2)–H and C(sp^3)–H functionalization via a pivaloyl-protected alanine residue and phenylalanine using an iodide substituent as a directing group on the latter on solid support.[231]

Photoredox-mediated peptide modifications have recently gained momentum in LSF methodology development. These approaches typically proceed through radical-based mechanisms initiated by a single electron transfer (SET) after irradiation with visible light and with or without the need for photocatalysts. Consequently, they have enabled access to several unnatural amino acids with

complex chemotypes.[232] A notable example was reported by McCarver and co-workers, who reported head-to-tail peptide macrocyclization using blue light. Their method used Ir[dF(CF_3)ppy]$_2$(dtbbpy) as a photoredox catalyst, an activated ester at the C-terminus to generate a free radical upon SET and an acrylic acid residue at the N-terminus. As such, macrocyclization was achieved through a key C−C bond.[233]

2. Improving the Chameleonic Properties of Cyclic Peptides Using Small-Molecule Fragments

2.1. Introduction to Chapter II

Several platforms have been developed to efficiently discover macrocyclic peptides, which often exhibit a high level of specificity for their target proteins.[134] However, since most libraries generate peptides from canonical amino acids, they usually face challenges accrued from their physicochemical properties that lead to barriers in their GIT and metabolic stability following their oral administration and subsequent cell membrane permeability.[234] While the former may be circumvented using parental administration, improving membrane permeability while maintaining bioactivity is a challenge that usually prompts post-discovery peptide optimization.[235]

Incorporating non-peptidic fragments in the backbone of cyclic peptides can improve their biological activities (Figures 1A and 1B).[236] For instance, using aminobenzoic acid as aromatic linkers in the backbone of peptides is one approach to using turn-inducing non-peptidic motifs that are suitable for stabilizing their secondary structures via intramolecular hydrogen bonding (IMHB) networks.[237] Moreover, the phenyl ring in these fragments has been described as an isosteric moiety suitable for substituting dipeptide bonds.[238] Additionally, to foster membrane permeability, the aromatic moieties do not only shield polar functionalities on the peptide backbone in concert with hydrophobic side chains but also act as lead moieties for making contact with the lipid bilayer as the peptide traverses the cell membrane.[239]

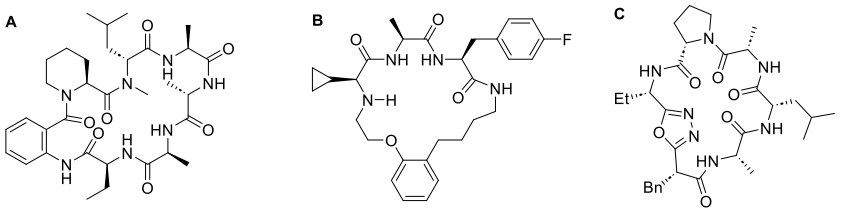

Figure 1. Examples of peptides containing (hetero)aromatic linkers include **A**. The anti-parasitic peptide **PF1171** contains an anthranilic acid fragment. **B**: Phenol-containing peptide from Tranzyme. **C**: Oxadiazole grafted cyclic peptide from Yudin and co-workers. Figure adapted from Sciammetta and co-workers.

Yudin and co-workers, for example, expanded this repertoire of cyclic aromatic spacers beyond the phenyl linker to oxadiazoles such that, in addition to promoting the formation of intermolecular hydrogen bonds, the moieties also participated in the IMHB networks (Figure 1C).[187] Such heterocycles are, however, not unique to synthetic cyclic peptides. Indeed, they are commonly encountered in naturally occurring peptides, wherein the (hetero)aromatic moieties improve

membrane permeability by participating in the IMHBs while shielding polar groups on the peptide backbone and masking amino acid side chains towards increased protease stability.[21] Their relatively small sizes, in particular, make these small aromatic linkers attractive modalities for improving the membrane permeability of peptides owing to a reduced possibility of replacing several amino acids and effectively altering the pharmacophore of the peptide.[240]

Modifying biologically active homodetic peptides with heterocyclic spacers is a desirable approach for improving their passive membrane permeability by enhancing chameleonic behavior, but not without challenges. One major setback is the reduced versatility of their incorporation into peptides since they typically require synthetic handles. For example, introducing the oxadiazole linker into cyclic peptides is possible through a multicomponent reaction dependent on a free carboxylic acid and amine from the peptide. As such, it is potentially limited in its application to head-to-tail cyclization or via the side chain of select amino acids. [122] Furthermore, modification of peptide backbones using oxa- and thiazoles linkers is not only synthetically challenging but restricted to homodetic peptide sequences that contain cysteine or serine/threonine residues if effective mimicry of the parent peptide is to be maintained.[241] Incorporating structurally elaborate fragments may introduce undesired off-target effects owing to their potentially inherent bioactivities, bearing in mind that even thiazoles, for instance, are essential pharmacophores in several clinically approved therapeutics with a wide array of biological activates and therefore suggesting a multitude of binding sites in the cell.[242]

Choosing a model peptide for evaluating the effectiveness of the heterocyclic fragments for improving a peptide's chameleonic properties requires careful consideration, mainly because it needs to be guaranteed that observations are solely derived from the systematic replacement of heterocyclic fragments in a model peptide.[243] This may be further complicated if the model peptide is derived from nature since the homodetic peptide sequences may have been pre-tuned for their intended biological activity and membrane permeability.[183] Nonetheless, additional experimental evidence may aid in ascertaining the extent of this confounding factor, including in vitro screening techniques.[244]

2.2. Selection and synthesis of model peptides

This project aimed to introduce pyridine fragments into a peptide to promote IMHBs and, therefore, chameleonic behavior. It was envisioned that the pyridine linker would contribute to the hydrophobicity of the peptide backbone and potentially partake in the IMHB network of the peptide via the nitrogen heteroatom.[245] Furthermore, a phenyl linker was also considered a suitable control since it lacks HBA but maintains the ability to influence the peptide backbone.[237] A pyridine N-oxide

linker was available as an intermediate compound in the synthetic scheme of the pyridine linker. It was therefore included as a control with increased polarity while contributing an HBA.[246]

Selection of a model peptide was, therefore, initially undertaken during project inception. As such, considerations for a rational model system were made, such as a head-to-tail cyclized peptide with a modified backbone, preferably with a (hetero)aromatic fragment to guide substitutions with linkers that could potentially participate in IMHB networks as well as their controls. A model peptide with a known membrane permeability from literature was also deemed desirable, but bioactivity was not necessary, as is the case for multiple reported model systems.[247]

Not surprisingly, given the vast repertoire of membrane-permeable cyclic peptides of marine origin, the cyclic peptide Sanguinamide A (**1)** with a thiazole residue in its backbone and isolated from the sea slug *Hexabranchus sanguineous,* commonly known as the Spanish dancer was deemed a fitting model peptide (Figure 2).[22]

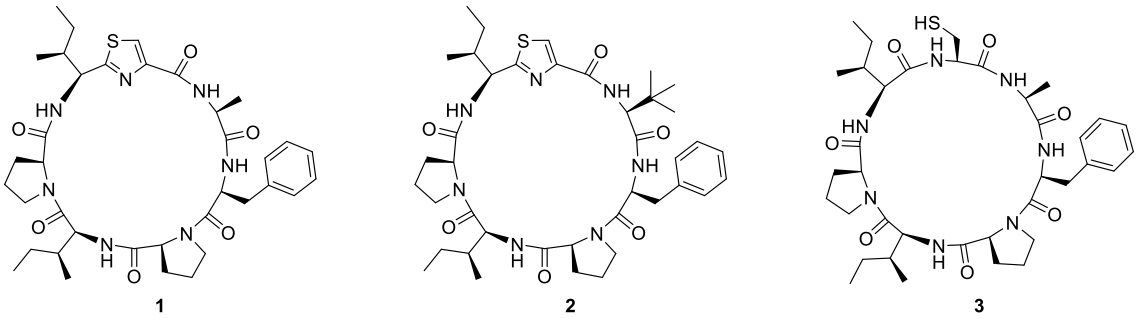

Figure 2. The thiazole-containing peptide, Sanguinamide A (**1),** was selected as the model system. At the same time, its analogue, Danamide F (**2),** in which alanine in **1** is substituted for *tert*-butylglycine, was used as the positive control. The homodetic peptide **3** was designed as a potential negative control.

Sanguinamide A is a hexameric peptide isolated from *H. sanguineous* and contains six natural amino acids and a thiazole moiety fused with an isoleucine residue (IleThz).[248] This fragment's position was envisioned for substitution with aromatic linkers during library synthesis. Unlike its analogue, Sanguinamide B, isolated from H. sanguineous and with antibacterial properties, it has no reported biological activity.[249] Nonetheless, the peptide fitted well with our desired model system because it has good oral bioavailability (F = 7 ± 4%) and falls in the eRo5 (MW = 722) chemical space. [250]

Nielsen and co-workers conducted extensive NMR studies on Sanguinamide A and reported its chameleonic behavior as a factor arising from forming IMHBs between two amide protons from IleThz and Ile residues, respectively, in DMSO-d_6 as a mimic of an aqueous solvent environment (Figure 3). The ensuing conformation shielded the polar peptide backbone by using the side chains of the two isoleucine residues and Ala.[181]

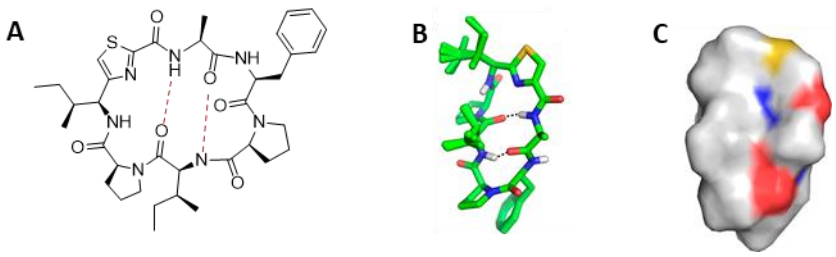

Figure 3. A & **B**. Sanguinamide A shields its polar backbone via an IMHB network in polar environments. The dashed red lines represent hydrogen bonds. The model peptide exposes its hydrophobic side chains and enables subsequent interactions with the cell membrane's lipid bilayer. **C**. The region shaded in grey represents the hydrophobic surface area impregnated by polar groups (oxygen, red; nitrogen, red). Figure adapted from Nielsen and co-workers.[181]

Furthermore, in subsequent experiments, they showed that substituting Ala for *tert*-butylglycin (Tle) in Danamide F (**2**) resulted in an increased shielding of the polar backbone by the bulkier side chain and improved membrane permeability observed by LCMS PAMPA and a remarkable increase in its oral bioavailability (F = 51±9%, Figure 2).[161] Additionally, the contribution of the IMHB networks towards membrane permeability was demonstrated via the peptide's marked reduction in membrane permeability upon N-methylation, which is one of the critical weaknesses arising from using N-methylation to improve membrane permeability.[251]

Therefore, compound **2** was selected as a positive control compound for analysis of our analogues. Furthermore, given the possibility of the nature-derived peptide's potential inherent membrane permeability, the homodetic analogue of Sanguinamide A, **3** (Figure 2), devoid of the thiazole modification but with cysteine in its sequence, was deemed appropriate as a negative control, wherein the IleThz was substituted with an Ile-Cys dipeptide.[183] As such, desirable subtle changes in the peptide would be achieved, including increased rotatable bonds and loss of the heteroaromatic fragment on the peptide backbone.

The synthesis of IleThz **4** was performed according to the procedure reported by Nielsen and co-workers, in which a Boc-protected IleThz moiety was derived from Boc-Ile-OH via a thioamide intermediate followed by Hantzsch thiazole synthesis to afford the thiazole dipeptide analogue **4** after ester hydrolysis and purification by flash chromatography (Scheme 1).[181]

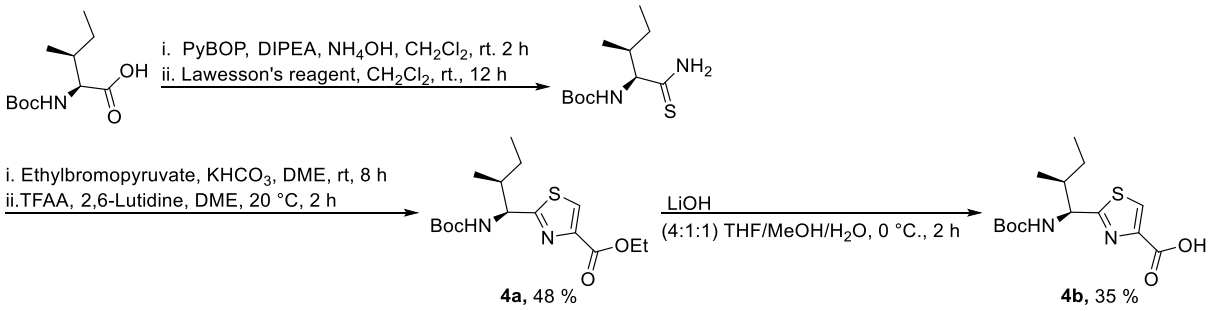

Scheme 1. Synthesis of the Boc-protected isoleucine-derived thiazole dipeptide analogue **4** using a modified Hantzsch ester synthesis.

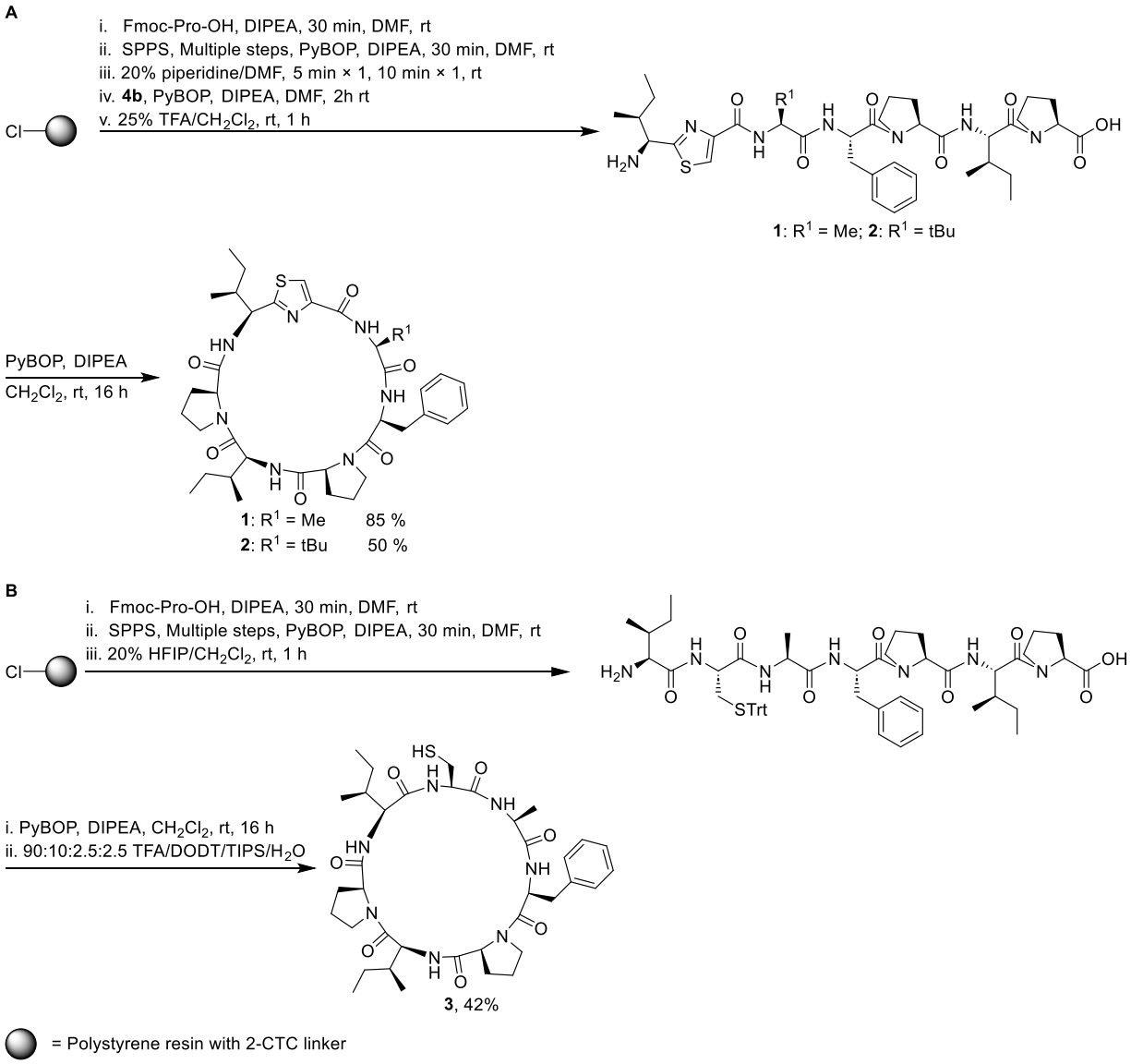

Scheme 2. A: Synthesis of the model peptidic compound Sanguinamide A (**1)** and positive control reference compound, Danamide F (**2**). **B**. Synthesis of the cyclic control peptide with a homodetic backbone.

In parallel, an Fmoc-protected linear pentapeptide was synthesized via SPPS on polystyrene resin (PS) resin with a 2-chlorotrityl (2-CTC) resin linker that was previously activated with $SOCl_2$ in the presence

of DMAP as a base before coupling of the first amino acid (Scheme 2A).[252] The linear precursor peptide was deprotected, and **4b** was coupled to the N-terminus on solid phase, followed by cleavage under TFA conditions and further purified by reverse phase preparatory HPLC. Next, cyclization was performed at a 0.5 mM concentration using HATU as an activating reagent and DIPEA as the base.[110] Synthesis of positive control peptide **2** proceeded similarly but with Fmoc-Tle-OH instead of Fmoc-Ala-OH.

The synthesis of the negative control peptide **3** was carried out using SPPS (Scheme 2B) of the respective linear precursor followed by cleavage off the 2-CTC resin with 20 % HFIP in CH_3Cl_2, a solution acidic enough to cleave the peptide off the solid support, but capable of maintaining protecting groups of nucleophilic amino acid side chains.[253] The linear peptide was then purified using RP preparatory HPLC and cyclized in the same manner as in Scheme 1, followed by global cleavage with a TFA cocktail.

2.3. Synthesis of Sanguinamide A Analogues

The strategy for library synthesis was adapted from that of **1,** in which a dipeptide with a (hetero)aromatic linker would be coupled to the linear peptide on solid phase, followed by cleavage and cyclization. With interest in developing a small library for evaluating the effects of (hetero)aromatic linkers with HBAs for enhancing the chameleonic properties of cyclic peptides, it was envisioned that the ideal linkers should be hydrophobic to partake in shielding the peptide backbone and have functional carboxylic acid and amine functional groups to aid in their incorporation in the cyclic peptide. Pyridine **5** was therefore considered an ideal model linker owing to its small size and the presence of a nitrogen atom as a potential HBA (Figure 4). Additionally, pyridines are part of the repertoire of aromatic linkers found in pyridine-based macrocyclic peptides (pyritides).[254]

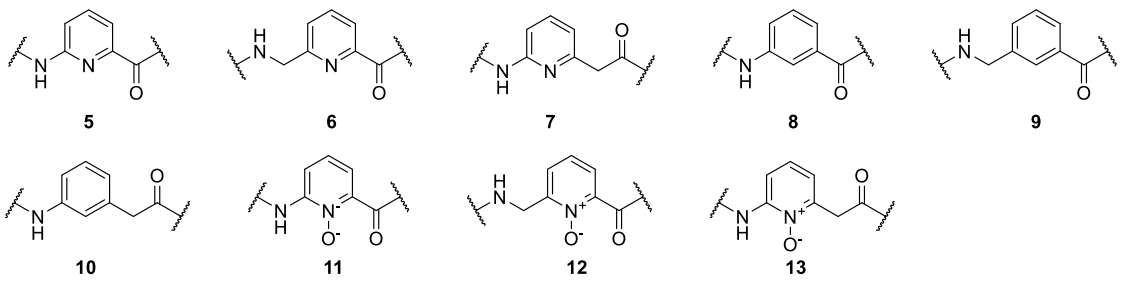

Figure 4. Aromatic linkers for evaluating the impact of small molecule fragments with HBAs on improving the chameleonic properties of cyclic peptides.

Furthermore, the number of rotatable bonds in a cyclic peptide may influence its physicochemical properties with a bi-directional potential to enhance its propensity for conformational changes required for chameleonicity or otherwise, impart a penalty for the establishment of stable IMHBs as

are necessary for membrane permeability.[77] As such, a set of two control pyridine linkers with one methyl group at each of the amine **6** and carboxylic acid **7** functional groups were designed as controls to study the effect of an additional rotatable bond count (RBC) on the ability of a heteroaromatic linker to enhance chameleonicity of cyclic peptides.

As controls for the contribution of the HBA heteroatoms to chameleonicity, phenyl linkers **8** – **10** were designed, which maintain similar conformational constraints on the peptide backbone.[255] Furthermore, their hydrophobic nature could potentially lead to a shielding effect of the peptide backbone. These subtle differences could potentially highlight whether increased membrane permeability is dependent on just hydrophobicity or new IMHBs only possible from heteroaromatic linkers. The more polar linkers **11** – **13** were included in the library to evaluate any penalty for increased PSA to chameleonic behavior and passive membrane permeability in addition to their potential for contributing an HBA in the peptide backbone.

2.3.1. Synthesis of analogues of cyclic peptide 1 with 6-amino-2- picolinic acid (6-Apa) derived linkers

An initial attempt at the solution-phase coupling of the methyl ester **15** from commercially available **14** under standard conditions for peptide synthesis with PyBOP as a coupling reagent, suited for activation of challenging amino acid residues over an extended period of 16 h, was futile, likely owing to the poor nucleophilicity of the amine (Scheme 3A).[256] An alternative uranium-type coupling reagent, COMU, was not successful either.[257] A further attempt by activating Boc-Ile-OH by generating an acyl chloride using $SOCl_2$ was also unsuccessful.[257] Moreover, a mixed anhydride approach was also used to activate the Boc-Ile-OH substrate using $SOCl_2$ in the presence of MeOH, but in vain. Furthermore, our attempt to generate an acid fluoride in situ from Boc-Ile-OH using TFFH also failed to afford the desired dipeptide.[258]

It was subsequently strategized that increasing the nucleophilicity of the 6-Apa amine was likely necessary for efficient peptide coupling. As such, the pyridine N-oxide (PNO) derivative of 6-Apa was adjudged as a suitable substrate since the reactivity of amines of PNOs has been previously successfully demonstrated.[259] Therefore, N-oxide **16** was prepared from **15** using mCPBA, followed by successful coupling to Boc-Ile-OH and affording dipeptide **17** under mild conditions previously reported by Liu and co-workers.[260] Subsequently, the 6-Apa containing dipeptide **18** was obtained from the reduction of N-oxide **17** under similarly mild conditions and using the oxophilic diboron reagent, bis(pinacolato) diboron (B_2Pin_2).[261]

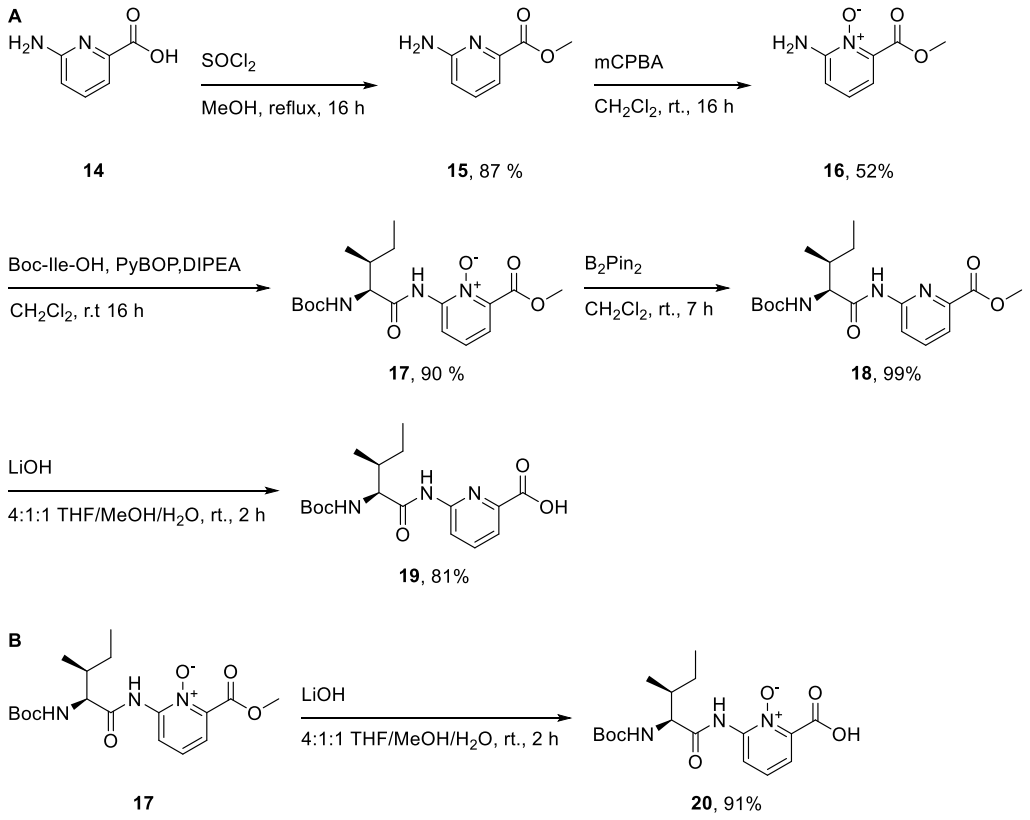

Scheme 3. A: Synthesis of dipeptide **19** containing a pyridine moiety. **B:** The corresponding PNO containing **20** was derived from intermediate **17**.

It was envisioned that dipeptide **19** would be suitable for incorporation into the cyclic peptide analogue of **1** in the same fashion as reported by Nielsen and co-workers. It was therefore obtained from **18** following ester hydrolysis (Scheme 3A).[181] Additionally, intermediate **17** was used to obtain dipeptide **20** for incorporating a PNO linker in a cyclic peptide analogue of **1** to evaluate the effect of increased polarity on the chameleonic properties while potentially maintaining an HBA in the linker (Scheme 3B).

Therefore, compound **19** was used to synthesize peptide **21** with a pyridine linker substituting cysteine in the sequence of homodetic cyclic peptide **3**. The more polar analogue **22** was subsequently obtained using the same strategy but using the PNO-containing dipeptide **20** (Scheme 4).

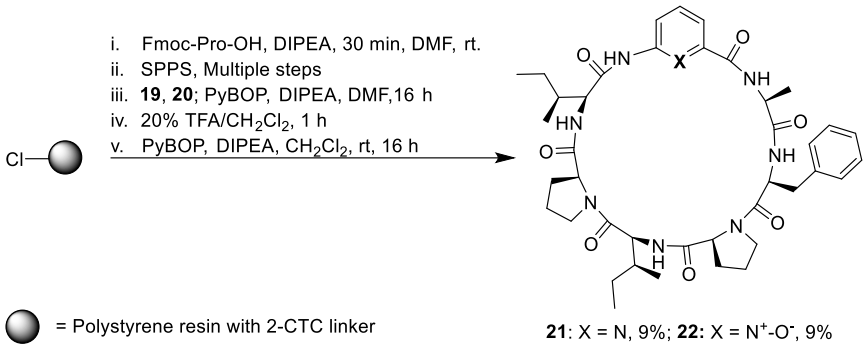

Scheme 4. Synthesis of analogues of **1** using dipeptides containing a 6-APA linker **21** and corresponding PNO **22.**

2.3.2. Synthesis of analogues of cyclic peptide 1 with 6-(aminomethyl)picolinic acid derived linkers

It was anticipated that 6-(aminomethyl)picolinic acid, with a methylene spacer between the amine and the pyridine moiety, would enable less delocalization of electrons on the N-atom towards the heterocycle.[262] It was also previously reported that 6-(aminomethyl)picolinic acid could partake in peptide coupling using conditions applicable to those used for canonical amino acids.[263] Consequently, it was expected that peptide coupling to Boc-Ile-OH would proceed without needing an N-oxide modification, and an N-oxide could be conveniently derivatized at a later stage of the synthetic scheme relative to that of 6-Apa.

Therefore the methyl diester of commercially available dicarboxylic acid **23** was prepared using methanol and thionyl chloride (Scheme 5A).[264] After that, di-ester **24** was reduced using $NaBH_4$ to afford a mono-alcohol intermediate. The reaction time was optimized from reported conditions in literature to avoid the formation of the di-alcohol side product.[265] The methyl chloride functionality in **25** was obtained from the mono-alcohol by treatment of **24** with $SOCl_2$. Subsequently, azide **26** was prepared by azidation, followed by a hydrogenation reaction using Pd/C under acidic conditions to afford the methylamine intermediate that could be efficiently coupled to Boc-Ile-OH to afford ester **27**.[266] The desired dipeptide **28** was then obtained following ester hydrolysis to prepare it for incorporation during SPPS. [181]

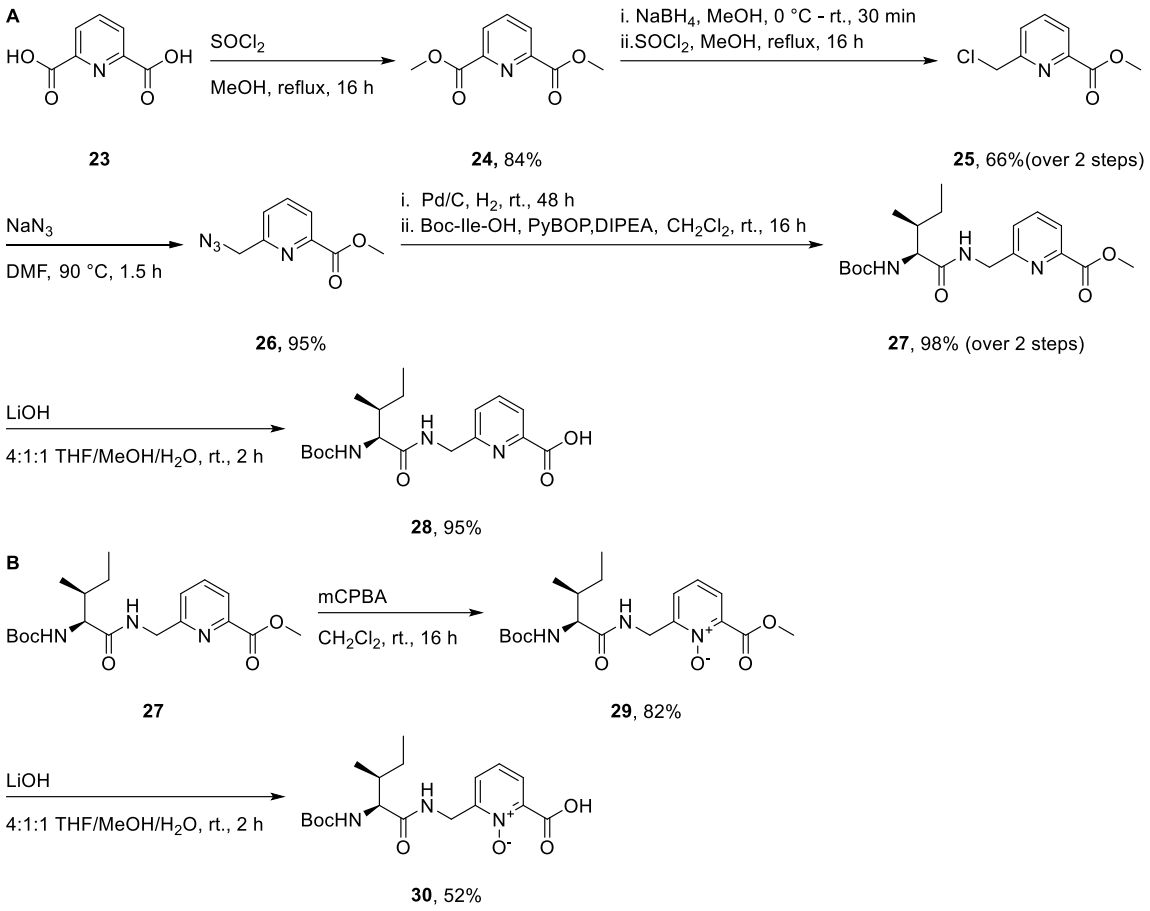

Scheme 5. A: Synthesis of dipeptide **26,** an extra rotatable bond compared to 6-Apa derived dipeptide **20. B:** Synthesis of PNO-containing dipeptide **30** derived from intermediate **27.**

A portion of intermediate **27** was oxidized and saponified to afford the dipeptide **30** with the more polar PNO linker (Scheme 5B).[260] Corresponding analogues of **1** were synthesized using the dipeptide with aromatic linkers **28** and **30** (Scheme 6)

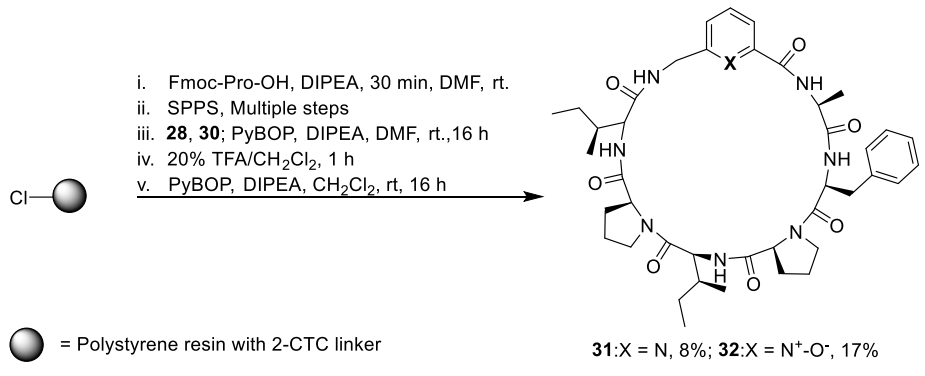

Scheme 6. Synthesis of cyclic peptide analogues of **1** derived from 6-(aminomethyl)picolinic acid and containing a pyridine linker **31** and PNO linker **32**.

2.3.3. Synthesis of Sanguinamide A analogues with 2-(6-aminopyridin-2-yl)acetic acid and corresponding PNO aromatic linkers

Prior experience with 6-Apa led to the assumption that 2-(6-aminopyridin-2-yl)acetic acid would be insufficiently nucleophilic for coupling to Boc-Ile-OH and require the formation of a PNO intermediate before coupling to Boc-Ile-OH under standard peptide coupling conditions.[267] Therefore, a synthetic route similar to that of compounds 19 and 20 was designed, which started with Boc-protection of commercially available picoline **33** to enable the subsequent benzylic lithiation of **34,** followed by quenching with diethyl carbonate to afford ester **35** (Scheme 7A).[268] After that, the pyridine was oxidized using mCPBA to give PNO **36**.[260]

Maintaining the Boc-protecting group at this step enabled a higher yield during flash column chromatography than the PNO with an unprotected amine that required purification under basic conditions.[269] Additionally, the subsequent steps could be performed in a one-pot approach with simple evaporation of volatiles after Boc deprotection followed by peptide coupling for improved yields of dipeptide PNO **37**.[270] After that, reduction with B_2Pin_2 and ester hydrolysis under basic conditions gave the final desired dipeptide **39** with a linker derived from 2-(6-aminopyridin-2-yl)acetic acid. Moreover, the PNO-containing analogue **40** was also prepared via ester hydrolysis of intermediate **37** (Scheme 7B).[181]

Initial attempts at coupling dipeptides **39** and **40** to the precursor linear peptide on solid phase failed. It was assumed that the pyridine and PNO-containing linkers may have formed intermolecular hydrogen bonds, so the coupling reagent could not activate the stabilized structure (Scheme 7C).[271]

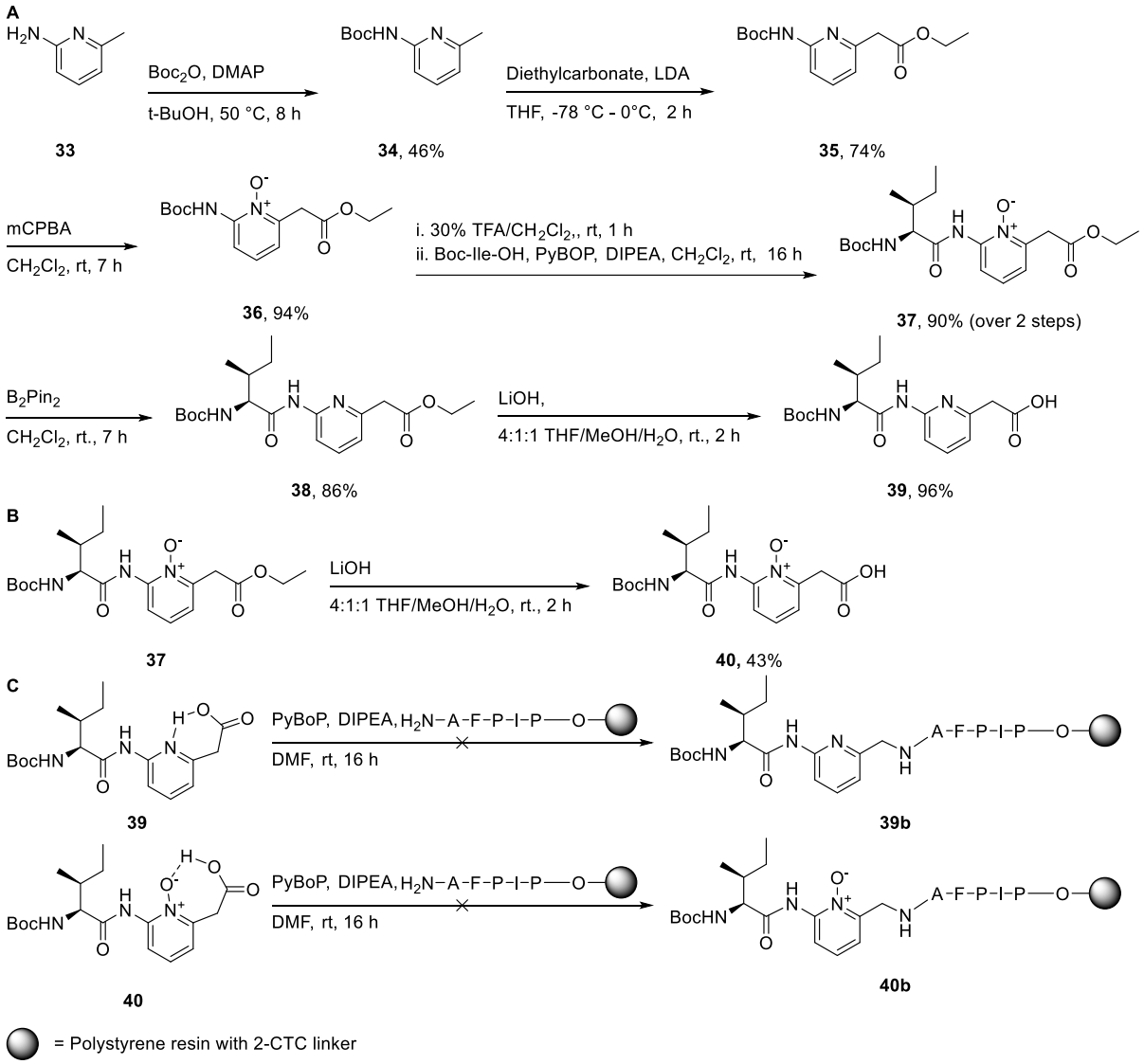

Scheme 7. A: Synthesis of dipeptide **39** containing a pyridine moiety and a methylene spacer between the acid and aromatic ring. **B**: The corresponding PNO containing analogue **40** was derived from intermediate **37**. **C**: Coupling **39** and **40** to a linear pentapeptide on solid phase failed under mild conditions.

2.3.4. Synthesis of cyclic peptide analogues of Sanguinamide A containing a phenyl spacer.

We also needed to synthesize peptides with control linkers to study whether the heteroaromatic linkers in the analogues of 1 could promote passive uptake via promoting chameleonic properties via IMHB formation.[122] Therefore, phenyl linkers were envisioned as suitable since they mimic the pyridines in structure but can't form the IMHB.[238]

Upon heating the reaction using microwave irradiation for 1 h, the desired linear precursor peptides were observed by LCMS. After that, the precursor was cleaved off solid support using TFA and further cyclized to afford analogues **41** and **42** (Scheme 8).

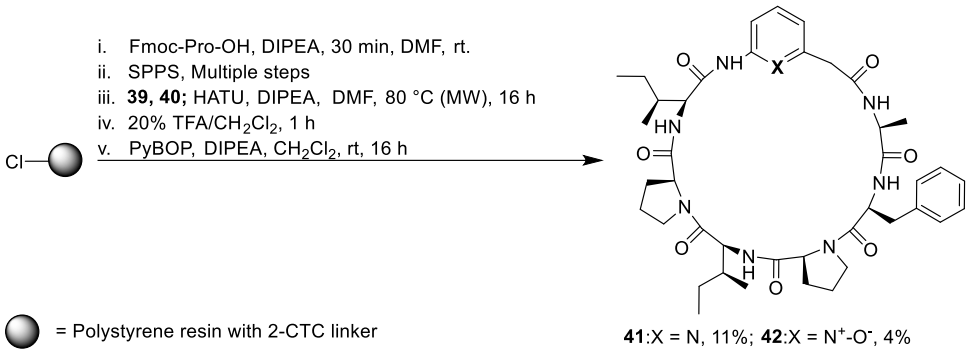

Scheme 8. Synthesis of cyclic peptide analogues of Sanguinamide A containing 2-(6-aminopyridin-2-yl)acetic acid **41** and **42**.

Furthermore, being the least polar relative to the pyridine and PNO surrogate linkers, it was expected that any penalty from polarity on membrane permeability could be correlated to the different degrees of polarities between the pyridines, PNOs, and aromatic linkers.[219]

Therefore, considering the decreased delocalization of electrons of aromatic amines relative to pyridines and, consequently, increased nucleophilicities, it was anticipated that Fmoc-protected building blocks could be synthesized before incorporation into the linear peptide on solid phase. This could be followed by coupling Boc-protected isoleucine to the linear intermediate, avoiding solution-phase dipeptide synthesis.[272]

Amine **44** was first derived from the nitrile reduction of commercially 3-cyanobenzoic acid **43 (**Scheme 9A).[273] The rest of the starting materials for Fmoc-protection, **45** and **46,** were commercially available. After that, the free amines of **44** – **46** were protected using Fmoc-OSu and $NaHCO_3$ at a pH of 8 to afford corresponding Fmoc-protected building blocks **47** – **49** (Scheme 9B).[274]

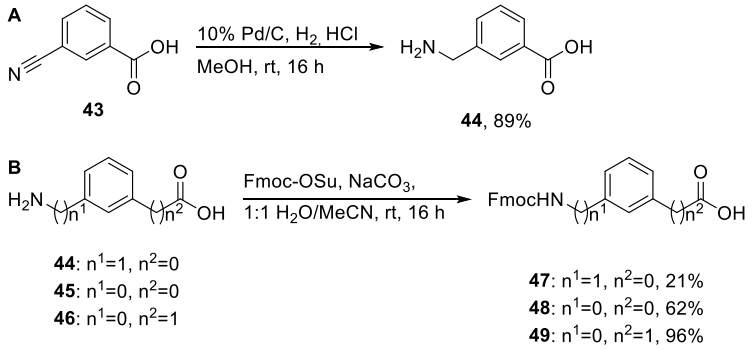

Scheme 9. A: Nitrile reduction to afford intermediate **30**. **B**: Synthesis of Fmoc-protected phenyl linkers 47- 49 for incorporation into the sequence of Sanguinamide A.

Compounds **47**- **48** were then successfully coupled to a linear peptide on solid phase at room temperature (Scheme 10A). At the same time, the coupling of **49** to the linear peptide was performed at 80 °C under microwave irradiation (Scheme 10B). The resulting linear peptides were coupled to Boc-

Ile-OH after Fmoc-deprotection, followed by cleavage off resin and cyclization to afford analogues **50** – **52**.

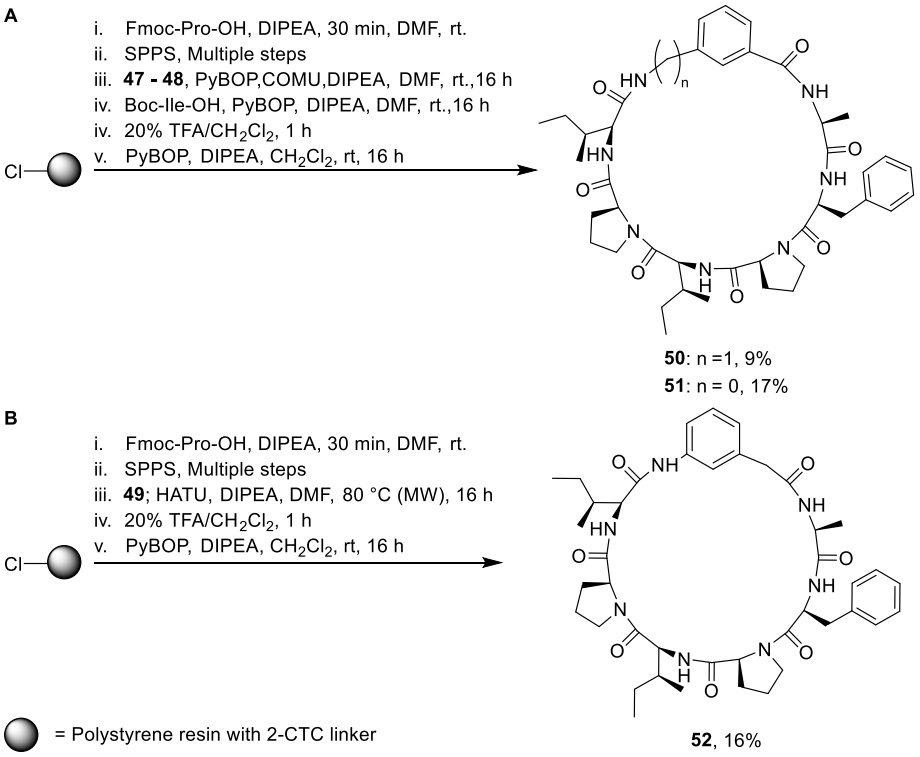

Scheme 10. Synthesis of cyclic peptide analogues of Sanguinamide A containing phenyl linkers. **A**: synthesis of **50** and **51** was carried out at room temperature. **B**: Synthesis of **52** required heating during the coupling of **49** to the linear peptide.

2.4. IAM Chromatographic Analysis

All peptides were analyzed by IAM chromatography, a high throughput method to evaluate membrane permeability. Additionally, cyclosporine A (**CSA**) was included as a peptidic control with a reported high oral bioavailability and for comparison with other peptides (Figure 5).[123]

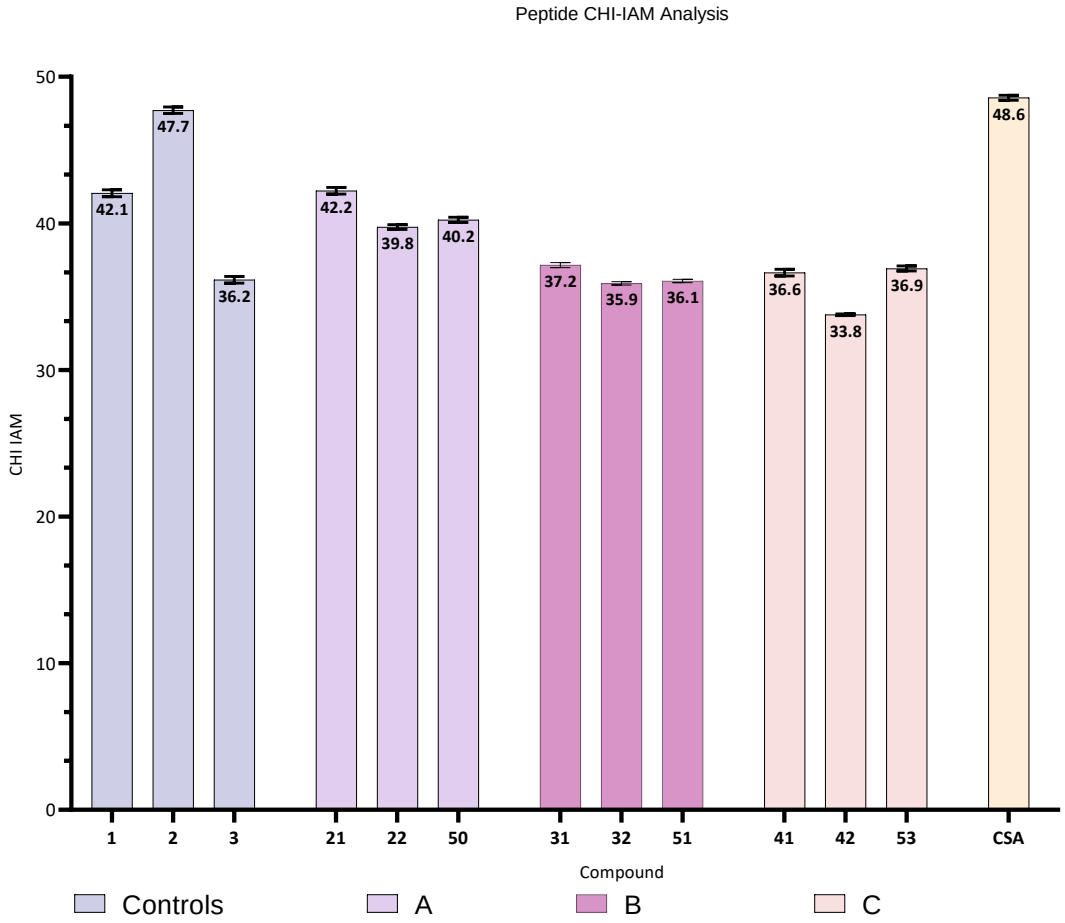

Figure 5. Measured CHI IAM values of peptides grouped into Sangunamide and Control peptides; A: peptides with a 6-Apa linker and derivatives, which also had the highest overall CHI-IAM values and in comparison to other linker analogues with extra methylene groups, B and C. All data was obtained in duplicate.

Overall, **CSA** (F = 21%, CHI IAM = 48.6) and **2** (F = 51%, CHI IAM = 47.7) had the highest measured IAM chromatography retention times, which was consistent with their high reported oral bioavailability (table 1). In comparison, model peptide **1** had a lower CHI IAM score of 42.1 and an F of 7% (table 1).[250] Furthermore, the CHI IAM values for **1** and **2** corroborate with Nielsen and co-workers' experientially determined bioavailability of the rationally designed cyclic peptide **2** towards improved membrane permeability, which was augmented from **1** by using a more hydrophobic Tle residue side chain mutation from alanine.[275]

Table 1. Measured CHI IAM values for control and study peptides and relevant parameters for an indication of their conformity to the Lipinsky Ro5.

Peptide	Controls				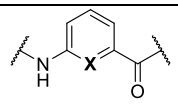			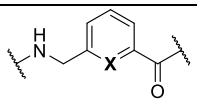			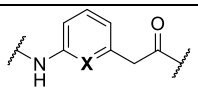		
	1	**2**	**3**	**CSA**	**21**	**22**	**50**	**31**	**32**	**51**	**41**	**42**	**52**
CHI IAM	42.1	47.7	36.2	48.6	42.2	39.8	40.2	37.2	35.9	36.1	36.6	33.8	36.9
SD	0.2	0.2	0.1	0.2	0.2	0.1	0.1	0.1	0.1	0.1	0.2	<0.1	0.1
MW	722	764	743	1202	759	775	758	773	789	772	773	789	772
cLogP	5.4	6.8	5.8	14.4	6	4	6	5	3	6	5	3	6
tPSA*	169	169	186	279	198	221	186	198	221	186	198	221	186
NAtMC**	21	21	21	33	23	23	23	24	24	24	24	24	24

* The tPSA value was calculated and not experimentally determined. ** NAtMC denotes the number of atoms in the macrocycle. X = N or N^{+}-O^{-}.

As further expected, the control peptide **3** (CHI IAM = 36.2), devoid of either a (hetero)aromatic linker or a non-canonical side chain modification, was found to have the lowest CHI IAM score and, therefore, supporting the notion that peptide backbone and side chain modifications are worthwhile approaches for improving membrane permeability.[22]

The group of model peptide **1** analogues with the least number of atoms in the macrocycle (NAtMC = 23) and featuring a 3-Apa linker **21** (CHI IAM = 42.2), PNO **22** (CHI IAM = 39.8) as well 3-amino benzoate (3-Abz)-containing **50** (CHI IAM = 40.2) were the most privileged. Peptides with larger macrocycle sizes had a generally low CHI IAM score. (Figure 5, group A).

The CHI-IAM score of **21** (CHI IAM = 42.2, PSA = 198) is similar to that of control peptide **1** (CHI IAM = 42.1, PSA = 159) despite having a larger PSA relative to that of the control as well as a larger macrocycle size. In a similar manner, **22** (CHI IAM = 39.8, PSA = 221) with a much higher PSA also maintains a CHI IAM score significantly higher than that of the negative control peptide **3** (CHI IAM = 36.2, PSA = 186), suggesting that the N-oxide may partake of IMHBs thereby improving its CHI IAM score despite a higher polarity. The reduced CHI IAM score of compound **50** (CHI IAM = 40.2) with a phenyl linker and relative to **21** (CHI IAM = 42.2, PSA = 198) is suggestive of the contribution of the HBA in the linker **21** towards a high CHI IAM score.

Larger macrocycles had comparatively lower CHI IAM scores and therefore suggesting a lower membrane permeability as a result (Figure 5, groups B and C). For example, an extra methyl group at both the amine and carboxyl functionalities proximate to the pyridine linker in analogues **31** (CHI IAM = 37.2) and **41** (CHI IAM = 36.6) led to an almost equal reduction of their CHI IAM values relative to

that of **21** (CHI IAM = 42.2). This observation suggests a similar penalty to membrane permeability and consistent with that postulated in Veber's rule.[77] Furthermore, their corresponding PNO-containing linkers in **32** (CHI IAM = 35.9) and **42**(CHI IAM = 33.8) had even lower CHI IAM scores resulting from additional penalties from their high polarity relative to the pyridine-containing peptides **31** and **41**. Following the same trend, a similar observation can be made for the phenyl linker containing peptide **52** (CHI IAM = 36.9) relative to **41** (CHI IAM = 36.6).

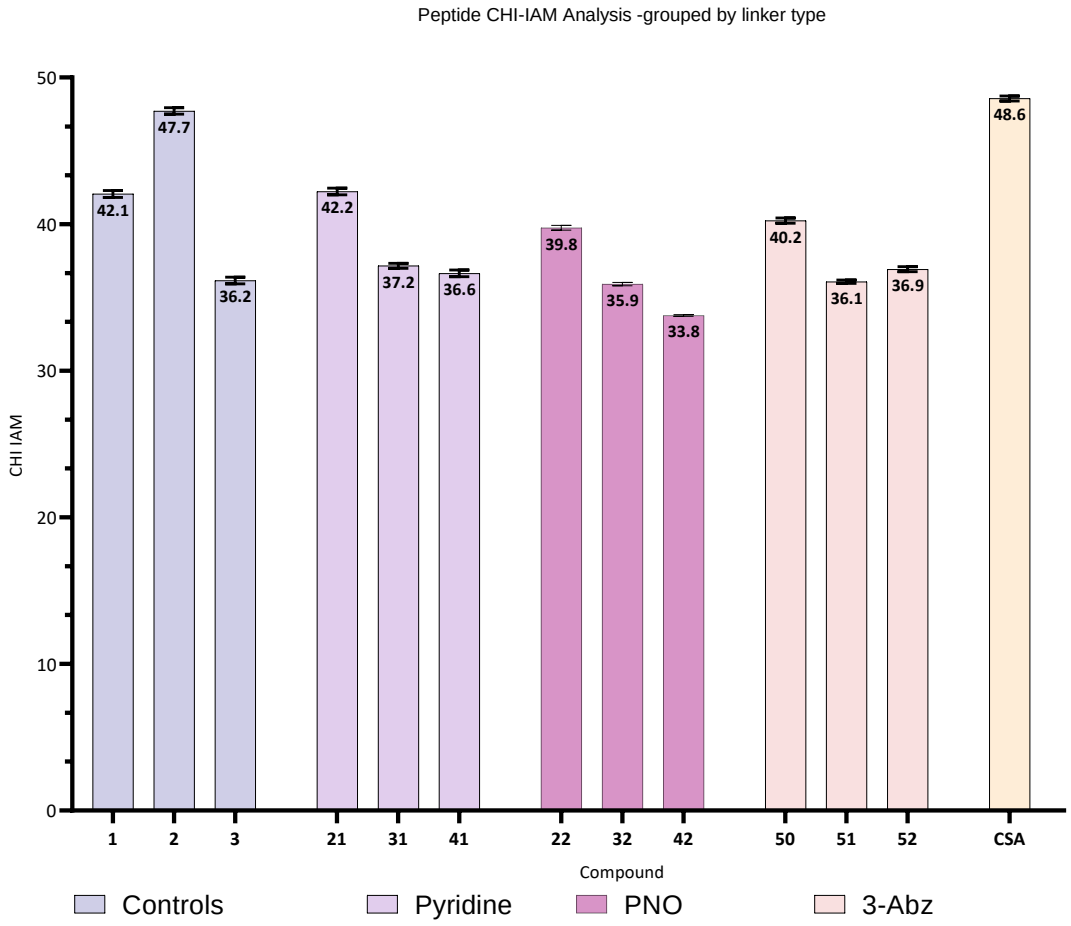

Figure 6. Sanguinamide A analogues grouped by the nature of HBA, i.e., pyridines, PNO, or none (3-Abz).

No difference between CHI IAM scores of peptides with PNO or 3-Abz linkers could be observed when grouped based on the nature of the HBA (Figure 6). Only pyridine linkers appear to have been privileged motifs for improving membrane permeability. This observation likely arose from their lower polarity relative to PNOs and potentially participating in HB formation with the nitrogen heteroatom, unlike 3-Abz linkers. (Figure 6).

Using an HBA-containing heteroaromatic linker seemed to improve the chameleonic properties of the peptides, as indicated by their higher CHI-IAM score compared to their benzene or PNO equivalents.

Increasing the polarity of the aromatic linker contributes to a reduction in the CHI-IAM score, indicating a reduced membrane permeability.

2.5. VT-NMR analysis of select peptides

Variable temperature NMR (VT-NMR) experiments have been used to characterize the nature of IMHBs in peptide **1**[181]. We used the same technique to evaluate the nature of IMHB networks formed by our Sanguinamide A analogues with various non-peptidic linkers. It was expected that the method would give insights into the conformational behavior of the synthesized peptides and possible correlation with chameleonic behavior.[276] Discerning the strength of an HB is a judicious task. As such, backbone amides showing an NMR chemical shift temperature coefficient ($\Delta\delta_{NH}/\Delta T$) of a relatively high magnitude (i.e., $\Delta\delta_{NH}/\Delta T > 4.0$ ppb/K) were considered solvent exposed. In contrast, moderately lower volumes of $\Delta\delta_{NH}/\Delta T$ (2 ppb/K < $\Delta\delta_{NH}/\Delta T \leq 4.0$ ppb/K) have been proposed to participate in weak HBs, while lower magnitudes ($\Delta\delta_{NH}/\Delta T \leq 2.0$ ppb/K) were considered to participate in a strong HB.[277]

2.5.1. Sanguinamide A (1)

Notably, membrane permeable peptide **1** appeared to form an IMHB network in DMSO-d_6, consistent with the report by Nielsen and co-workers. Further confirming the hypothesis that membrane permeability comes from increased inherent hydrophobicity from a shielded polar backbone (Figure 7).[181]

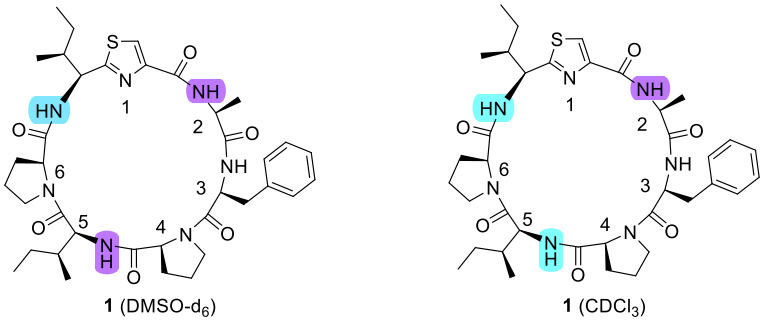

Figure 7. The structures of model peptide **1** and its corresponding amide HB patterns in DMSO-d_6 and $CDCl_3$, whereby strong bonds are highlighted in purple and weak ones in cyan.

The temperature coefficients of Phe-3 ($\Delta\delta_{NH}/\Delta T$ = -4.3 ppb/K) and IleThz-1($\Delta\delta_{NH}/\Delta T$ = -4.0 ppb/K) had the largest magnitudes were suggestive that their amides were solvent exposed. Ala-2 ($\Delta\delta_{NH}/\Delta T$ = 0.0 ppb/K) and Ile-5 ($\Delta\delta_{NH}/\Delta T$ = -1.6 ppb/K) had the lowest ΔδNH/ΔT values and may have participated in strong HBs.[277] Although the absolute values differed from those reported by Nielsen et al. (Ala-2

$\Delta\delta_{NH}/\Delta T$ = 0.5 ppb/K and Ile-5 $\Delta\delta_{NH}/\Delta T$ = -1.5 ppb/K), the amides found to be involved in strong hydrogen bonds corresponded (Figure 7).

Table 2. Calculated backbone amide variable temperature coefficients (ppb/K) for compound **1** in DMSO-d_6 and $CDCl_3$

Residue	IleThz 1	Ala 2	Phe 3	Ile 5
$\Delta\delta_{NH}/\Delta T$ - DMSO-d_6 (ppb/K)	-4.0	0.0	-4.3	-1.6
$\Delta\delta_{NH}/\Delta T$ – $CDCl_3$ (ppb/K)	-3.4	0.0	-10.3	-3.2

To estimate the nature of HBs formed by **1** in the cell membrane's lipid bilayer and in extension to reported analyses, a similar VT-NMR experiment was performed using $CDCl_3$ as a solvent whose dielectric constant (ϵ=4.8) is close to that of the lipid bilayer of the membrane (ϵ=3.0).[278] In this case, the model peptide **1** seemed to form three HBs, a strong one formed by the amide of Ala-2 ($\Delta\delta_{NH}/\Delta T$ = 0.0 ppb/K) and two weak bonds formed by Ile 5 ($\Delta\delta_{NH}/\Delta T$ = -3.2 ppb/K) and IleThz 1($\Delta\delta_{NH}/\Delta T$ = -3.4 ppb/K). Therefore, the HB pattern of the amide backbone of **1** varies in different solvents.

2.5.2. Analogue 21 with a pyridine linker

Analysis of the pyridine-containing peptide **21** was first performed in DMSO-d_6, and it demonstrated a possibly different HB pattern from compound **1** (Figure 8). In comparison to the model peptide **1**, two amides of Pyr-1 ($\Delta\delta_{NH}/\Delta T$ = -1.5) and Phe-3 ($\Delta\delta_{NH}/\Delta T$ = -1.7) participated in strong HBs in addition to those formed by Ala-2 ($\Delta\delta_{NH}/\Delta T$ = -0.5) and Ile-5 ($\Delta\delta_{NH}/\Delta T$ = -1.7) (table 3). However, Ile-7 ($\Delta\delta_{NH}/\Delta T$ = -6.6) of **21** was solvent exposed, unlike that of IleThz-1 ($\Delta\delta_{NH}/\Delta T$ = -6.6) of **1,** in a similar position, where it participated in a weak HB.

However, on analysis in **21** in $CDCl_3$, a change in the HB network was observed (Figure 8) relative to the model peptide **1** in $CDCl_3$ and **21** in DMSO-d_6. Compared to model peptide **1** in $CDCl_3$, there was an overall increase in backbone amides participating in HBs. Two additional strong HBs were formed by Pyr-1 ($\Delta\delta_{NH}/\Delta T$ = -1.0) and Ile-7 ($\Delta\delta_{NH}/\Delta T$ = -0.0), of which the latter participated in a weak HB in compound **1**. Ala-2 ($\Delta\delta_{NH}/\Delta T$ = -0.6) and Ile-5 ($\Delta\delta_{NH}/\Delta T$ = -4.0) participated in weak and strong HBs, respectively, in a similar manner as those of the model peptide **1.** The HB pattern of **21** in $CDCl_3$ and DMSO-d_6 was almost identical with Ile-5 ($\Delta\delta_{NH}/\Delta T$ = -4.0) in $CDCl_3$ participating in a weak HB as opposed to a strong HB in DMSO-d_6 (Ile-7, $\Delta\delta_{NH}/\Delta T$ = -1.7).

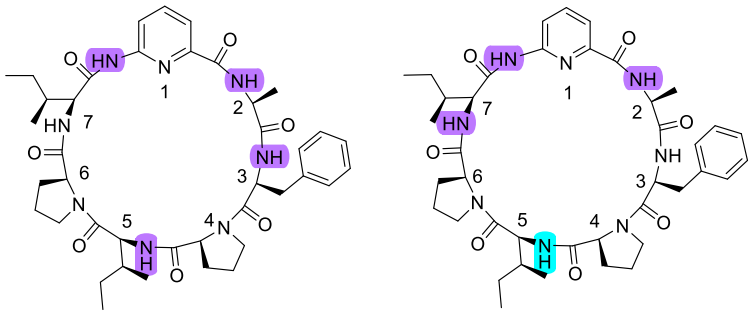

Figure 8. The structures of the pyridine-containing compound **21** and its corresponding HB patterns in DMSO-d_6 and $CDCl_3$, whereby strong bonds are highlighted in purple and weak ones in cyan.

Table 3. Calculated backbone amide variable temperature coefficients (ppb/K) for compound **21** in DMSO-d_6 and $CDCl_3$

Residue	**Pyr-1**	**Ala-2**	**Phe-3**	**Ile-5**	**Ile 7**
$\Delta\delta_{NH}/\Delta T$ - DMSO-d_6 (ppb/K)	-1.5	-0.5	-1.7	-1.7	-6.6
$\Delta\delta_{NH}/\Delta T$ – $CDCl_3$ (ppb/K)	-1.0	-0.6	-10.4	-4.0	0.0

2.5.3. Analogue 22 with a PNO linker

The observations from VT-NMR experiments for PNO-containing peptide **22** in DMSO-d_6 showed more HBs formed by the backbone amides relative to the model peptide **1,** arising from an additional amide from PNO-1 ($\Delta\delta_{NH}/\Delta T$ = 1.3) with a low-temperature coefficient (Figure 9 and table 4). The rest of the backbone amides had temperature coefficients similar to the model peptide **1** and may have participated in HBs identical to compound **1**.

In $CDCl_3$, Ile-7 ($\Delta\delta_{NH}/\Delta T$ = -0.6) may have formed a strong HB in **22,** making it the only residue to contrast to the similarly positioned IleThz-1 ($\Delta\delta_{NH}/\Delta T$ = 3.9) that may have formed a weak HB in compound **1**. The amide of PNO-1 ($\Delta\delta_{NH}/\Delta T$ = 0.0) had a consistently low-temperature coefficient in both solvents.

Furthermore, the HB pattern for **22** was largely similar between both solvents and only differed in the magnitudes of temperature coefficients of Ile-7 and Ile-5. In $CDCl_3$, Ile-7 ($\Delta\delta_{NH}/\Delta T$ = 0.6) had a low-temperature coefficient as opposed to a moderate one in DMSO-d_6 (Ile-7: $\Delta\delta_{NH}/\Delta T$ = -3.6), while Ile-5 ($\Delta\delta_{NH}/\Delta T$ = -2.6) has a moderate temperature coefficient as opposed to a lower score in DMSO-d_6 (Ile-5: $\Delta\delta_{NH}/\Delta T$ = -1.5).

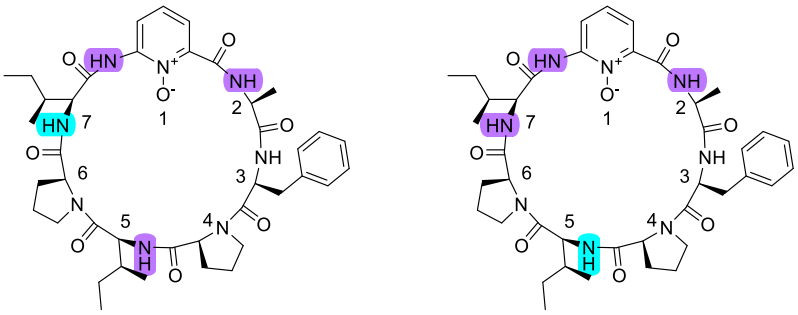

Figure 9. The structures of the PNO-containing analogue of Sanguinamide A **22** and its corresponding amide IMHB patterns in DMSO-d_6 and $CDCl_3$, whereby strong bonds are highlighted in purple and weak ones in cyan.

Table 4. Calculated backbone amide variable temperature coefficients (ppb/K) for compound **22** in DMSO-d_6 and $CDCl_3$

Residue	PNO-1	Ala-2	Phe-3	Ile 5	Ile 7
T_{coeff} **(DMSO-D_6)**	1.3	-0.3	-4.2	-1.5	-3.6
T_{coeff} **($CDCl_3$)**	0.0	-1.0	-6.4	-2.6	0.6

While both **22** and **21** maintained the same number of amide protons potentially participating in HBs across the two solvents, the pyridine-containing peptide **22** had a variation in the position of residues potentially participating in HBs, unlike **21,** in which only Phe-3 was exclusively solvent exposed in both DMSO-d_6 and $CDCl_3$.

2.5.4. Analogue 50 with a 3-Abz linker

Overall, peptide **50** in DMSO-d_6 had a remarkable structural similarity to **21** with a pyridine linker. In DMSO-d_6, one difference in temperature coefficients was observed in the moderately lower shift of Phe-3 ($\Delta\delta_{NH}/\Delta T$ = -3.7) in compound **50** (Figure 10 and Table 5). Compared with Phe-3 ($\Delta\delta_{NH}/\Delta T$ = -1.7) of compound **21**, a lower shift was observed, suggesting a reduction in the HB strength of the compounds in DMSO-d_6.

In $CDCl_3$, compound **50** also had an identical pattern of amino acid residues with temperature coefficients suggestive of HB formation comparable to **21**. Ala-2 ($\Delta\delta_{NH}/\Delta T$ = -3.8), for instance, had a higher temperature coefficient relative to that of **21** (Ala-2: ($\Delta\delta_{NH}/\Delta T$ = -0.6). Additionally, Ile-5 ($\Delta\delta_{NH}/\Delta T$ = -0.0) of **50** had a lower temperature coefficient relative to Ile-5 ($\Delta\delta_{NH}/\Delta T$ = -4.0) of **21**.

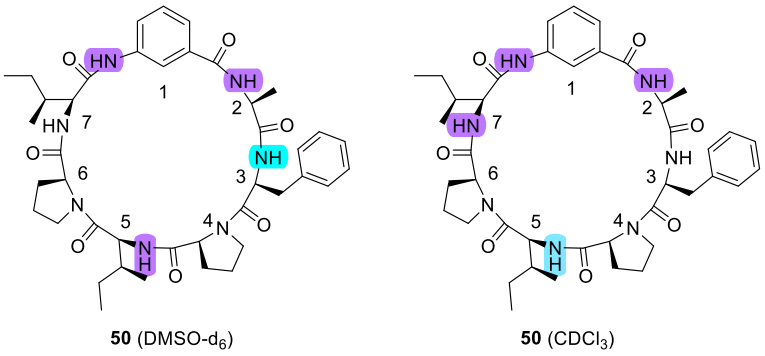

Figure 10. The structures of the 3-Abz-containing analogue **50** and its corresponding amide HB patterns in DMSO-d_6 and $CDCl_3$, whereby strong bonds are highlighted in purple and weak ones in cyan.

Table 5. Calculated backbone amide variable temperature coefficients (ppb/K) for compound **50** in DMSO-d_6 and $CDCl_3$

Residue	3-Abz-1	Ala-2	Phe-3	Ile 5	Ile 7
T_{coeff} (DMSO-D_6)	-1.8	-0.5	-3.7	-1.7	-6.5
T_{coeff} ($CDCl_3$)	-0.6	0	-11.4	-3.8	0

2.6. Summary and conclusions

VT-NMR experimental results showed HB formation consistent with the IMHB network in Sanguinamide A (**1**), similar to Nielsen and co-workers' reported network in DMSO-d_6. However, an additional HB was formed by a backbone amide in chloroform, suggesting a closed conformation aimed at occluding the backbone amide.[181]

Compound **21,** with a pyridine linker, had a different pattern regarding HB strength and position in DMSO-d_6 and $CDCl_3$ solvent environments. The observations suggest a novel IMHB network different from the secondary structures adopted by model peptide **1** in the two solvent environments**.** Therefore, the VTNMR observation agrees with the high CHI IAM measurement observed in **21** (CHI IAM = 42.2, PSA = 198). The CHI IAM score was close to model peptide **1** (CHI IAM = 42.1, PSA = 169). This observation suggests an enhancement in chameleonic behavior from incorporating a pyridine into the sequence of Sanguinamide A despite an increase in PSA introduced by the pyridine linker**.**[125]

However, the PNO containing peptide **22** (CHI IAM = 39.8, PSA = 221) had a lower CHI IAM score than model peptide **1**. Including the linker may have led to a very high PSA and possibly a penalty for membrane permeability.[279] Furthermore, VTNMR observations for compound **22** showed a remarkably similar number of HB forming residues and HB strengths in both DMSO-d_6 and $CDCl_3$, suggesting an inability of the peptide to alter its conformation in different solvent environments.

Therefore, the observation of a low CHI IAM corroborates with the high PSA and potential lack of chameleonicity of compound **22.**

VTNMR observations also suggested that compounds **50** and **21** had identical residues participating in HBs, in both DMSO-d_6 and $CDCl_3$. It is possible that compound **50** can also change its conformations in different solvents, just as previously proposed for **21**. However, the pattern of HB strengths differed between both peptides despite having identical residues participating in HB formation. Moreover, compound **21** had a higher CHI IAM score than **50** (CHI IAM = 40.2, PSA = 186), suggesting the conformations adapted by the **21** as more suitable for membrane permeability and highlighting the contribution of a single C to N change in the linker.

Introducing an additional methylene linker in the peptide sequences markedly reduced the CHI IAM scores for the rest of the peptides. A substantial backbone restriction may have occurred by incorporating 6-Apa and 3-Abz fragments into the backbone, enabling chameleonic behavior.[280] However, further conformational studies are required to confirm this assertion.[160]

3. Solid-Phase Peptide Late Stage Functionalisation (LSF) Using Katritzky Salts via Deaminative C-C Bond Formation

3.1. Introduction to Chapter III

Late-stage functionalization (LSF) enables rapid access to diverse libraries of peptides in a chemo and regio-selective manner.[221] It can potentially be used to modify peptides towards functionalities beyond the capability of the 20 canonical amino acids.[281]. As such, LSF methodologies have been a valuable source of tool compounds for manipulating and studying biological systems.[282] Drug discovery programs further employ LSF methodologies to optimize lead compounds by accessing and screening a library of peptides containing UAAs, which are privileged moieties for improving biological activity and metabolic stability.[4, 5] Peptide LSF is a more efficient approach for derivatizing these UAA motifs than synthesizing individual amino acid building blocks for later application in solid phase peptide synthesis (SPPS).[285]

Additionally, peptide LSF can take advantage of canonical amino acids as a pool of commercially available chiral substrates that have already been pre-organized regarding their stereochemistry and positions in a peptide sequence for biological activity.[286] For example, one early LSF method used bromophenyl alanine residues incorporated in a peptide sequence as handles for the derivatization of Biphenyl alanine (Bip) via Suzuki–Miyaura cross-coupling with boronic acids to access analogues of the antiretroviral drug Saquinavir and on solid phase (Scheme 1).[287]

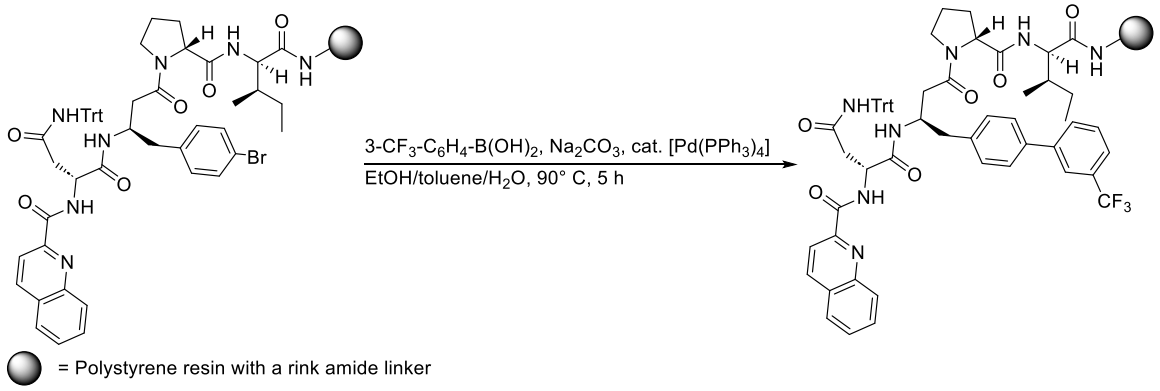

Scheme 1. Suzuki cross-coupling with a tetrapeptide on solid phase. Figure adapted from Limbach and co-workers.[287]

Early LSF methodologies primarily relied on transition metal-catalyzed C-H functionalization reactions that were mainly developed for small molecules. As such, subsequent efforts at their application to peptides faced solvent incompatibility, harsh reaction conditions, and long reaction times, amongst

other setbacks.[10, 11] Another key challenge was the limited application of C-H functionalization methodologies to the formation of new C(sp^2)–C(sp^3) bonds mainly derived from pre-activated (hetero)aryl C(sp^2)–H and C(sp^3)–H bonds, with the latter frequently proximal to electron withdrawing groups for acidity.[290] Consequently, initial exploratory efforts on C(sp^3)–H activation methodologies were limited to regions close to the peptide backbone because they utilized proximal carbonyl groups for activation and excluded their application from the more populous distal C(sp^3)–H bonds.[291]

Though less explored, other C(sp^2)–H functionalization methodologies also aimed at modifying histidine, tryptophan, tyrosine, and phenylalanine and were dependent on transitional metal catalysis, including arylations, borylations, and halogenation reactions.[292] They aimed to tune the amino acids' aromatic moieties for optimal biological activity since they contribute to ligand-target binding in drug development.[293] Despite their abundance in proteins and peptides, C-H bonds are largely inert and considerably less attractive substrates for peptide LSF.[294]

Carbon–nitrogen (C-N) bonds may be as inert as C-H bonds. Even so, they are as common in peptides and proteins just as carboxylic acids.[295] They are generally encountered as nitrogen-containing functional groups on the peptide backbone and side chains of canonical and non-canonical amino acids. Moreover, they constitute side chain amine functionalities at different lengths from the peptide backbone in amino acids such as lysine, ornithine, aminobutyric acid, and diamino propionic acid.[296] The diversity of C-N bonds at side chains is not limited to free amines but also guanidinium, indole, and imidazole-containing residues, *viz.* arginine, tryptophan, and histidine, respectively.[297] Several protecting groups orthogonal to Fmoc have been developed for free amines of peptide residues and include the acid-sensitive groups like Boc, trityl, and Pbf protecting groups as well as the Alloc and IvDde protecting groups that require palladium catalysis and hydrazine conditions for deprotection; subsequently enabling both modulated lability during SPPS.[298]

Therefore, the ubiquity and diversity of C-N bonds drove research efforts at activating C-N bonds and aimed at enabling transition-metal catalyzed cross-coupling reactions to access new C-C bonds, which are deemed attractive transformations in drug development.[299]

Early methodologies for activating C–N bonds were only based on electronic and azaheterocyclic ring strain to overcome their high dissociation energy of $DH_{298}(CH_3N)$ = 122.4 ± 0.07 kcal mol^{-1}).[300] Aryl, benzylic and allylic amines were commonly used in addition to the less widely encountered strained activated C-N bonds of azirines[301]. Notably, most of the reported transition-metal catalyzed cross-coupling reactions were from C(sp^2)–N and, to a lesser extent, C(sp^3)–N bonds.

Brown and Keith first reported redox-active N-substituted pyridinium salts (Katritzky salts) for activating C(sp^2)–N bonds in a Suzuki-Miyaura cross-coupling with boronic acids. Their method, however, required the use of activated alkyl amines that would have limited application in peptide LSF, especially for the modification of side chains.[302] Nonetheless, it was a tangent from conventional applications of Katritzky salts that were mainly used as bench-stable reagents for the derivatization of functional groups like esters and alcohols from primary amines via nucleophilic substitution reactions; wherein pyridine acted as a leaving group from N-substituted pyridinium salts.[303]

Watson and co-workers later reported a radical-mediated palladium-catalyzed deaminative cross-coupling reaction with Katritzky salts to afford new C(sp^3)– C(sp^2) bonds from unactivated alkyl groups, thereby setting precedence for a series of subsequent LSF methodology studies on Katritzky salts (scheme 2A). In their scope studies, the team synthesized analogues of proline, isoleucine, and lysine to demonstrate the method's utility for obtaining unnatural amino acids. The latter was obtained directly from a lysine-derived Katritzky salt.[304]

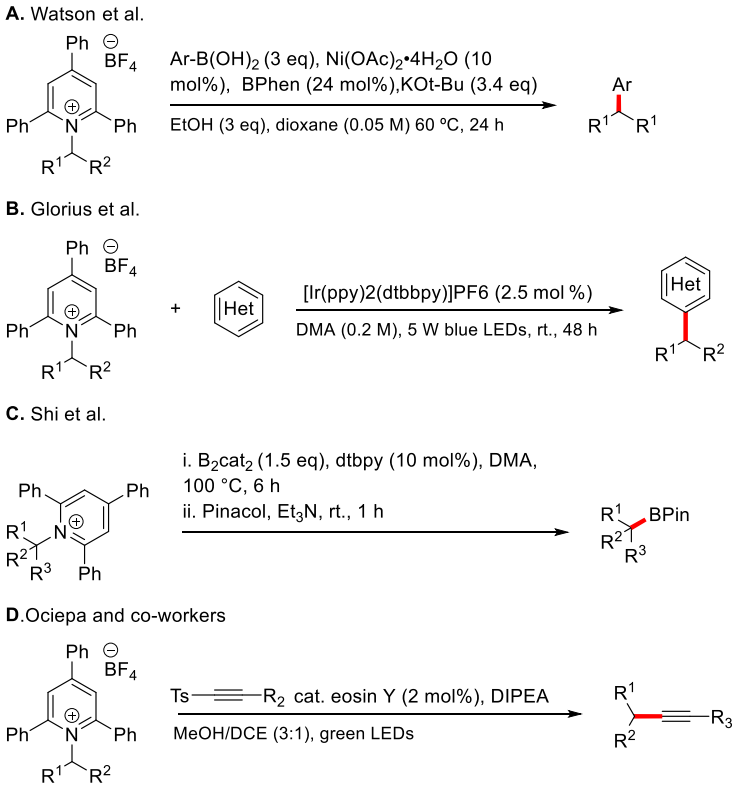

Scheme 2. Overview of early methodologies that used Katritzky salts for the modification of alkyl amines.

A further repertoire of transitional metals and reactions alike were investigated, including deaminative Minisci-type reactions using [Ir(ppy)$_2$(dtbbpy)]PF$_6$ as a photocatalyst and under visible light conditions and to afford new C(sp^3)–C(sp^2) bonds by Glorius and co-workers(Scheme 2B). This method was successfully used to synthesize indole and amino acid analogues derived from an alanine-

based Katritzky salt.[305] After that, Hu and co-workers reported a bis(catecholato) diboron-based deaminative borylation of primary amines in the presence of a Lewis base (scheme 2C).[306] Later, C(sp^3)– C(sp) bonds were derivatized via a deaminative alkynylation of Katritzky salts by Ociepa and co-workers (scheme 2D).[307]

Accentuating the advantages of SPPS and progressing beyond the synthesis of individual amino acids, a nickel-catalyzed LSF of a complex peptide was reported by Baran and co-workers for the generation of new C(sp^3)– C(sp^3) bonds from redox-active esters. The methodology used organo-Zinc reagents and on solid phase using, polystyrene (PS) resin with a Rink amide linker as solid support (Scheme 3A).[308]

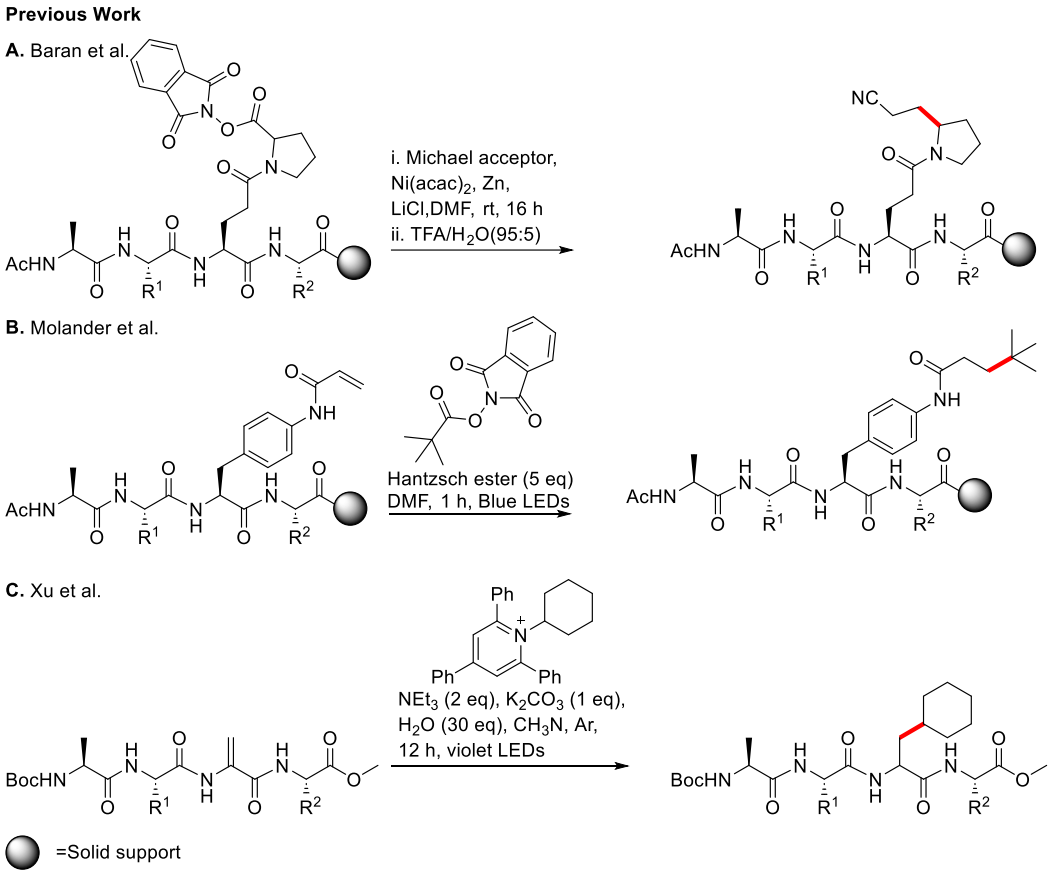

Scheme 3. Overview of key methodologies for peptide LSF. Scheme based on a report by 't Hart and Co-workers.*[309]*

Later on, Molander and co-workers also reported using Hantzsch esters to form an EDA with a redox-active ester subjected to homolytic cleavage under irradiation by blue LEDs on solid phase and at room temperature (Scheme 3B). The resulting open-shell species was amenable to a Giese-type reaction.[310]

Furthermore, LSF efforts in peptides using Katritzky salts were also reported, with early examples featuring dipeptides and using a number of modalities for modification.[311] However, the first methodology purposively developed for LSF in more complex peptides using Katritzky salts was

reported by Wang and co-workers. The group reported a catalyst-free and radical-based C(sp^3)-H alkylation of glycine in polypeptides under visible light conditions and using DBU for the formation of an electron donor-acceptor (EDA) with a Katritzky salt before a single electron transfer (SET) preceding homolytic cleavage and radical generation. The reaction was carried out in solution phase following the cleavage of peptide precursors from solid phase, albeit with poor diastereoselectivity. [312]

Subsequently, Baran and co-workers reported the compatibility of Katritzky salts with SPPS for peptide LSF. They used an alkyl radical generated from Nickel-Catalysed decarboxylation of the redox active ester for macrocyclization of a resin-bound linear tetra-peptide with an N-terminal acrylic acid residue as Michael acceptor in a Giese addition reaction.[313] In another study, Watson and co-workers reported that a Nickel catalyzed cross-coupling of Aryl-bromides with Katritzky salts for peptide LSF to forge new C(sp^3)–C(sp^2) bonds, also on solid support. Their approach used DMA as a solvent compatible with SPPS, albeit with a low yield and necessitating the use of TBAI for phase transfer and reaction employing Zinc powder as a reductant.[314]

Some photochemistry-based methods for peptide LSF with Katritzky salts also used conditions devoid of catalysts. For example, highlights in using EDA complexes for radical generation include Wang and co-workers' reported use of ionic compounds to promote the homolytic cleavage of Katritzky salts under visible light conditions (scheme 3C). They further demonstrated the utility of the resulting radical in a Giese-type reaction for the dipeptide model peptide LSF and, subsequently, peptide macrocyclization. Unfortunately, the reaction was performed in solution phase and necessitated the aqueous conditions for the dissolution of the salts, which was not attractive for SPPS.[315].

3.2. Results and Discussion

3.2.1. Late-Stage Nickel Catalysed Cross Electrophile Peptide Functionalisation

We envisioned performing late-stage derivatization of phenylalanine analogues through deaminative reductive nickel-catalyzed cross-coupling of Katritzky salts and aryl bromides on solid phase based on the method reported by Martin and co-workers.[316] They proposed a rational mechanism to proceed via a sequential reduction pathway instead of the kinetically disfavoured radical chain pathway.[317] Ergo, the catalytic cycle is initiated with the reduction of the catalyst from Ni(II) to active Ni(0) by reductants like Zn or Mn, followed by oxidative addition into the C(sp^2)-Br bond forming an Ar-Ni(II)Br intermediate. The catalyst is subsequently reduced to Ar-Ni(I), which further undergoes oxidative addition to an open shell species generated from the reduction of the Katritzky salt, followed by a final reductive elimination to afford the product and regenerate Ni(I) (Figure 1).[318]

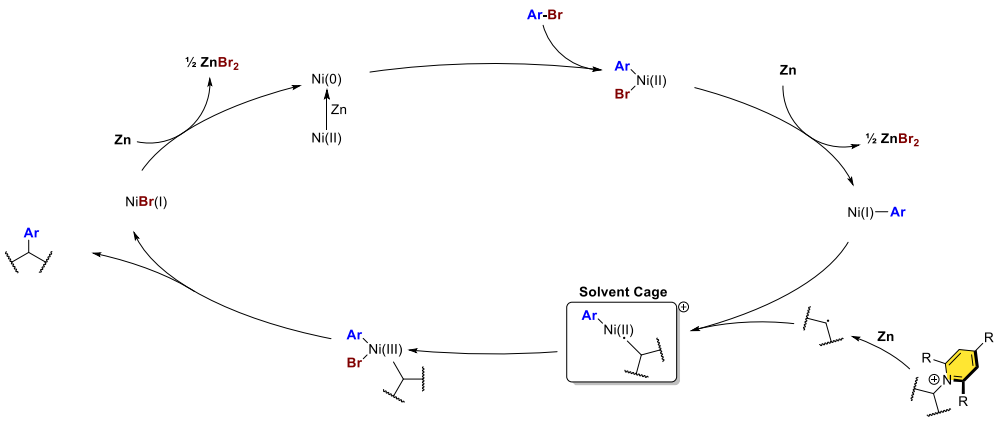

Figure 1. Proposed sequential reduction mechanism for nickel-catalyzed deaminative electrophile cross-coupling between a Katritzky salt and an aryl bromide using Zn as a reductant. Figure adapted from Pan and co-workers.*[318]*

Therefore, with peptide LSF in mind, a linear tripeptide **1** was synthesized using PS resin with a Rink amide linker as the solid support, followed by capping and alloc deprotection (Scheme 4).[319] The corresponding Katritzky salt was obtained upon a reaction between the resulting free lysine side chain with commercially sourced 2,4,6-triphenyl substituted pyrylium salt under microwave irradiation to afford **2**, determined by LCMS following test cleavage of an aliquot of the peptidyl resin. [320] Attempts to obtain compound **3** under reported literature conditions were relatively futile as only trace conversion was observed by HPLC (table 1, entry 1).

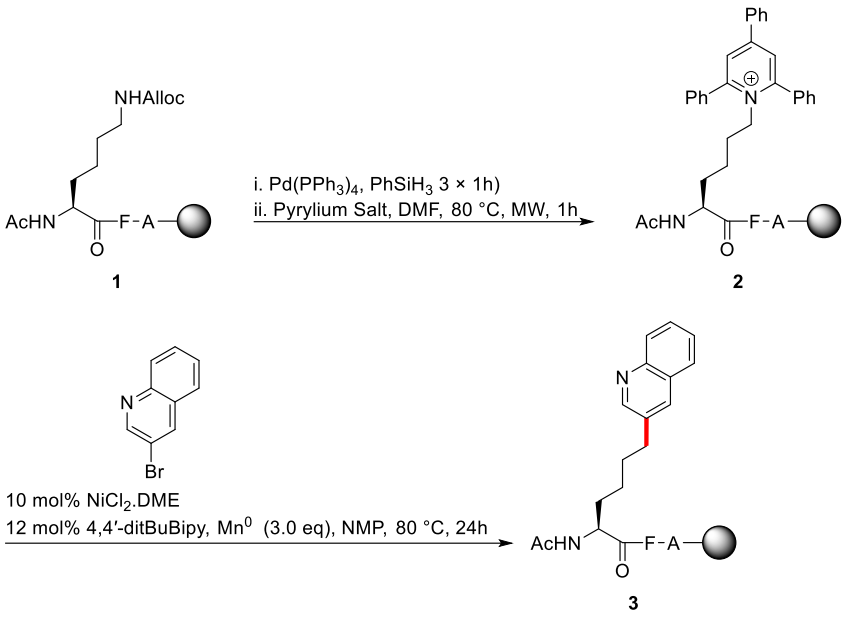

Scheme 4. Workflow for exploratory Nickel catalyzed deamination using Katritzky salts and 3-bromo quinoline as substrate.

Initial optimization attempts for peptide LSF began with the substitution of $NiBr_2$.DME for $NiCl_2$.DME and increasing both the catalyst and ligand loading (table 1, entries 2 – 4). After that, **L1** (4,4'-ditBuBipy) was substituted with **L2** (4,4'-diOMeBipy) as an electron-rich ligand to screen electronic and steric effects for improved conversion to no avail (table 1, entry 5).[321] The ligand loading was increased to 60 mol % from 12 mol% (table 1, entry 6). In these cases, only trace conversion was observed by LC-MS. Watson and co-workers had previously used $NiCl_2$ and **L2** to optimize a similar reductive cross-Electrophile coupling reaction.[321]

After that, optimization efforts were followed by including $MgCl_2$ and LiCl as additives (table 1, entries 7 – 8). Subsequently, Zn was used as a reductant instead of Mn without any additive (table 1, entry 9). Successive reactions were also performed with $MgCl_2$ and LiCl while using Zn as an additive (table 1, entries 10 – 11). This was based on the report by Watson and co-workers, who suggested that such additives may activate the reductant surface or potentially accelerate the regeneration of Ni(i) in the catalytic cycle. However, no conversion was observed by LC-MS in all these cases.[316] 3-Bromo quinoline was then substituted as a test substrate for 4-bromoanisole to aid the quantification of HPLC conversion due to its improved UV absorption (Scheme 4).[321] In this case, only a 5 % conversion was observed (table 1, entry 12).

Table 1. Screening of conditions for Nickel catalyzed cross-coupling for late-stage functionalization on solid phase.

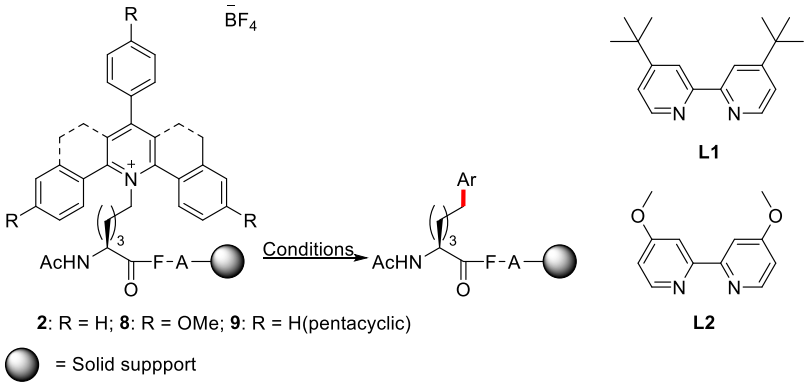

No.	Cat.	Ligand	Pyridinium salt	Substrate	Reductant	Add.	Conversion
1	$NiBr_2$.DME (10 mol %)	**L1** (12 mol %)	**2**	*p*-Bromoanisole	Mn	-	trace
2	$NiCl_2$.DME (10 mol %)	**L1** (12 mol %)	**2**	*p*-Bromoanisole	Mn	-	trace
3	$NiCl_2$.DME (50 mol %)	**L1** (12 mol %)	**2**	*p*-Bromoanisole	Mn	-	trace
4	$NiCl_2$.DME (50 mol %)	**L1** (60mol %)	**2**	*p*-Bromoanisole	Mn	-	trace
5	$NiCl_2$.DME (50 mol %)	**L2** (12 mol %)	**2**	*p*-Bromoanisole	Mn	-	trace
6	$NiCl_2$.DME (50 mol %)	**L2** (60mol %)	**2**	*p*-Bromoanisole	Mn	-	trace
7	$NiCl_2$.DME (50 mol %)	**L2** (60mol %)	**2**	*p*-Bromoanisole	Mn	$MgCl_2$	0
8	$NiCl_2$.DME (50 mol %)	**L2** (60mol %)	**2**	*p*-Bromoanisole	Mn	$LiCl_2$	0
9	$NiCl_2$.DME (50 mol %)	**L2** (60mol %)	**2**	*p*-Bromoanisole	Zn	-	0
10	$NiCl_2$.DME (50 mol %)	**L2** (60mol %)	**2**	*p*-Bromoanisole	Zn	$MgCl_2$	0
11	$NiCl_2$.DME (50 mol %)	**L2** (60mol %)	**2**	*p*-Bromoanisole	Zn	$LiCl_2$	0
12	$NiCl_2$.DME (50 mol %)	**L2** (60mol %)	**2**	3-bromo quinoline	Mn	$MgCl_2$	5%
13	$NiCl_2$.DME (50 mol %)	**L2** (60mol %)	**8**	3-bromo quinoline	Mn	$MgCl_2$	5%
14	$NiCl_2$.DME (50 mol %)	**L2** (60mol %)	**9**	3-bromo quinoline	Mn	$MgCl_2$	5%

15	$NiCl_2$.DME (50 mol %)	**L2** (60mol %)	**8**	3-bromo quinoline	TTF	$MgCl_2$	0
16	$NiCl_2$.DME (50 mol %)	**L2** (60mol %)	**8**	3-bromo quinoline	$PhSiH_3$	$MgCl_2$	0
17	$NiCl_2$.DME (50 mol %)	**L2** (60mol %)	**8**	3-bromo quinoline	$EtSiH_3$	$MgCl_2$	0
18[a]	$NiCl_2$.DME (50 mol %)	**L2** (60mol %)	**8**	3-bromo quinoline	Mn	$MgCl_2$	9

[a] The reaction was carried out in solution phase.

Changing the electronics of the Katritzky salts was also reported to aid the generation of open-shell species after SET, especially for primary alkyl Katritzky salts that were deemed less reactive.[322] As such, p-anisaldehyde **4** was used to prepare pyrylium **5** (scheme 5A). Subsequently, a linear model peptide with *p*-methoxyphenyl substituted Katritzky salt **8** was synthesized, bearing in mind lysine's primary alkyl amine side chain, for improved reactivity (table 1).[316] Cornelia and co-workers also reported the activation and subsequent homolytic cleavage of a C(sp^3)–NH_2 bonds by using a tethered pyridinium salt **7** to overcome the high bond dissociation energy of their primary aryl amine substrates and carry out radical C-N borylation.[323] After that, linear peptide **9** was synthesized on solid phase from pyrylium salt **7**.

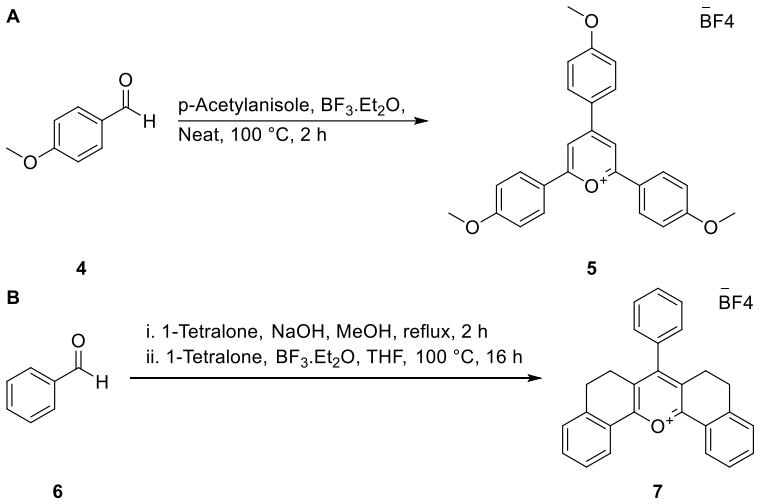

Scheme 5. A: Synthesis of p-methoxyphenyl substituted pyrylium salt **5. B** Synthesis of tethered pyrylium salt **7**.

Therefore, the corresponding pyrylium salt **9** was synthesized, followed by Katritzky salt synthesis (Scheme 5B). An attempt was then made to use the strained pyridinium salt to improve the substrate's reactivity, but with no improvement in conversion, leading to a conclusion that the challenge did not solely arise from the pyridinium salt used in the reaction (table 1, entries 13 – 14). The observed trace

conversion when using Zn and Mn as reductants led to the conclusion that the heterogeneous nature of the reaction was disadvantageous for phase transfer.[324]

A panel of organic reductants was then screened, including Tetrathiafulvalene (TTF), Phenylsilane ($PhSiH_3$), and triethylsilane ($EtSiH_3$) were also explored in vain, perhaps owing to a lower reduction potential in comparison to the metal reductants (table 1, entries 15 – 17). An attempt at a solution phase reaction using the model peptide following TFA cleavage only gave a 9% HPLC conversion (table 1, entry 18).

Other screens included changing the resin from polystyrene (rink amide-AM) to PEG-based H-Rink amide ChemMatrix® resin, expecting increased resin swelling to improve phase transfer. Unfortunately, larger solvent volumes were needed for sufficient resin suspension, leading to larger reagent dilutions.[325] Furthermore, the reaction temperature increased to 80 °C, but no screens improved the reaction yield. Only the solution phase reaction showed a slight improvement in conversion at 9%. With little or no conversion under different conditions, the reaction was deemed unfavorable for peptide LSF on solid phase.

3.2.2. Late-Stage Functionalisation of Peptides via Deaminative Photochemical C(sp3)-C(sp3) Bond Formation Using Katritzky Salts on Solid Phase.

3.2.2.1. Initial exploration

Aggarwal and co-workers described a deaminative Giese-type functionalization of primary amines via Katritzky salts under irradiation with Blue LEDs (420 nm). According to the proposed mechanism, the electron-deficient Katritzky salt **8** forms an EDA complex with a Hantzsch ester **9** in the presence of Et_3N, leading to a red shift of the complex (Scheme 6). Upon irradiation, a photoelectron transfer to the Hantzsch ester results in the formation of a Katritzky salt radical **10** and a dihydropyridine radical cation **11** followed by C(Sp^3)-N homolysis at the pyridinium to afford a free C(Sp^3) radical intermediate **12**. In the presence of a Michael acceptor and following the subsequent addition reaction, the radical intermediate **14** partakes in a hydrogen atom transfer from **9** or **11** to afford the final product **15**.[326]

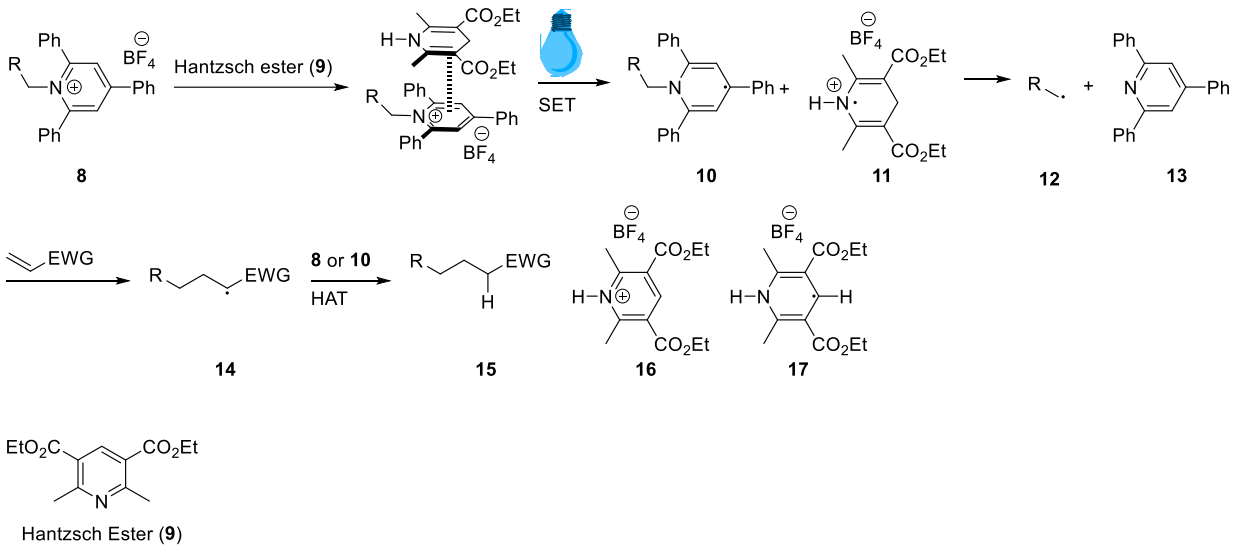

Scheme 6. Proposed mechanism for deaminative Giese-type functionalization of primary amines via Katritzky salts. The Giese-type reactions use Katritzky salts and Hantzsch esters in an EDA to generate open-shell species upon irradiation with blue light. Figure adapted from Aggarwal and co-workers.[326]

The initial exploratory reaction was performed in solution and using the model tripeptide with a 2,4,6-trimethoxyphenyl substituted Katritzky salt to afford compound **18** after TFA cleavage (Scheme 7). Compound **19** was obtained in a 22% isolated yield following preparatory HPLC purification. In this test reaction, methyl acrylate was used as a Michael acceptor, and the molar equivalent of Et_3N was doubled compared to that used in the report by Aggarwal and co-workers.

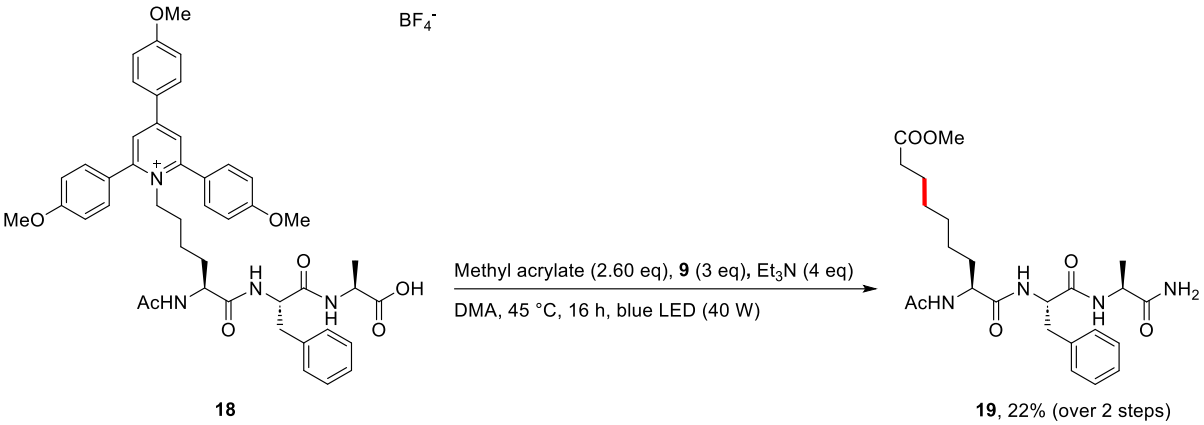

Scheme 7. Initial exploration of the peptide LSF with Katritzky salts in solution phase using methyl acrylate as the Michael acceptor.

Encouraged by these results, it was first deemed best to determine the resin loading based on the isolated yield of an aliquot of the Katritzky salt before the Giese-type reaction. Additionally, the sequence of the model pyridinium peptide **18** was altered such that phenylalanine was substituted with tryptophan in that of peptidyl resin **20** to facilitate the detection of any unreacted precursor peptide by thin-layer chromatography (Scheme 8). The change was aimed at enabling efficient purification by flash column chromatography with UV detection.[327]

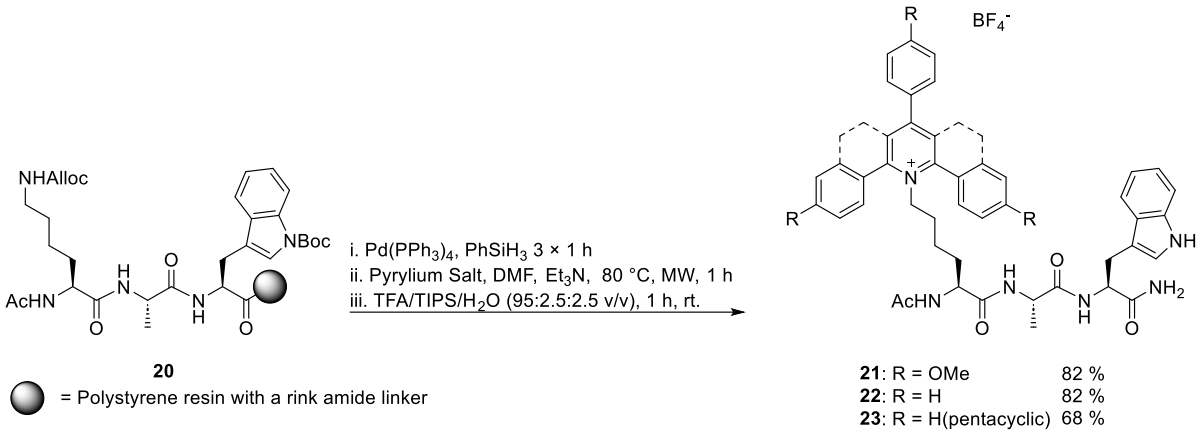

Scheme 8. Synthesis of Katritzky salt precursors for peptide LSF.

Moreover, a more stringent wash protocol after alloc deprotection was adopted. It used a solution of pyridine hydrochloride in MeOH/CH_2Cl_2 as an additional wash step aimed at removing any residual $Pd(PPh_3)_4$.[328] Consequently, an HCl salt was generated from the deprotected lysine leading to a complete failure of the Katritzky salt synthesis. Therefore, excess Et_3N (pK_a = 10) was added to the reaction mixture to generate a free base from lysine and facilitate a nucleophilic substitution for the generation the pyridinium.[329]

Subsequently, an aliquot of a batch of the synthesized peptidic pyridinium salt **20** was cleaved off solid support under TFA conditions and purified by silica flash column chromatography with an 82% isolated yield, affirming the modified protocol's high efficiency. The same protocol was used to synthesize alternative pyridinium salts **22** and **23** from their respective pyrylium salts.

A test reaction was then performed with the model peptidyl resin **24** and twice the equivalents of methyl acrylate and Et_3N to obtain an isolated yield of 25% after TFA cleave and purification by preparatory HPLC (Table 2, entry 1).

Table 2. Optimization of the reaction conditions for Giese-type reactions with Katritzky salts on solid phase.

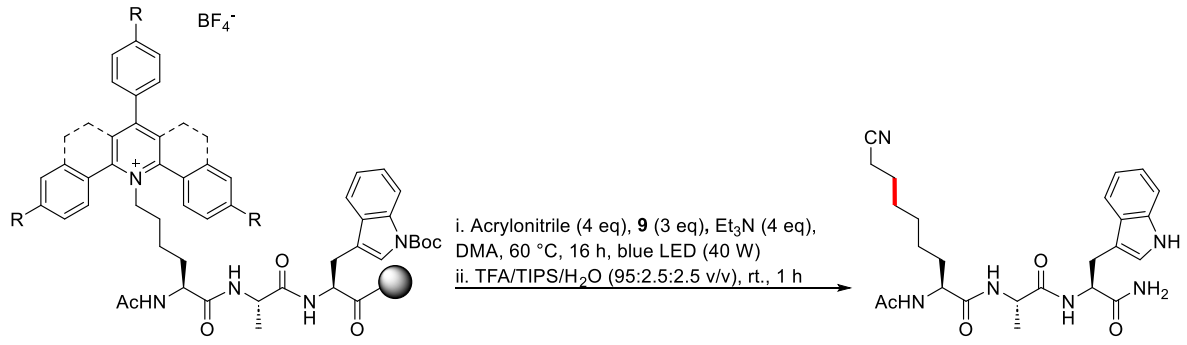

= Solid support

Entry	Starting Material	Deviation from optimized conditions	Yield [a] (%)	Conversion (%)
1	**24**	Methyl acrylate substrate	25	-
2	**24**	45 °C	19	-
3	**24**	Methyl acrylate substrate	52	-
4	**24**	-	59	-
5	**25**	-	6	-
6	**26**	-	13	-
7	**24**	1 h	-	0
8	**24**	2 h	-	0
9	**24**	4 h	-	14
10	**24**	20 h	-	88
11	**24**	No Et_3N	0	-
12	**24**	No **9**	0	-
13	**24**	No blue LED	0	-
14	**24**	rt.	0	-
15	**24**	Precaution-free set up	26	-

3.2.2.2. Optimization of reaction conditions

With a model peptidyl pyridinium **24** at hand, the ambient reaction temperature solely generated by a Kessil® LED lamp (40 Watt, 420 nm) was probed, considering the subtle differences in the modified reaction setup and the one reported by Aggarwal and co-workers (Figure 2a).[326] An ambient temperature of 45 °C was recorded after 16 h, which was divergent from the 60°C that was supposedly optimized for primary alkyl pyridinium salts in accordance to literature (table 2, entry 2). The relatively low yield of 19% from the Giese reaction prompted the need to increase the temperature to drive the reaction to completion.[330]

Therefore, a vial containing the reaction mixture was affixed in a glass beaker sealed off with aluminium foil and subsequently immersed in an oil bath at 100 °C (Figure 2b). An ambient temperature of 60 °C was recorded upon irradiation with blue light. The setup also gave the advantage of performing multiple reactions in vials affixed to a beaker using a single lamp in one instance and the opportunity to vary the reaction temperature using an oil bath.

Figure 2. The reaction setup was based on one reportedly optimized for primary alkyl pyridinium salts (**a**) to enable increased temperature using an oil bath and could accommodate multiple vials (**b**).

Furthermore, considering the need for excess equivalents of reagents and high concentrations as useful approaches for driving reactions performed on solid support to completion, the equivalents of the base and Michael acceptor were increased.[331] Hence, with four equivalents of both Et_3N and methyl acrylate as Michael acceptor, the reaction was performed over 16 h, followed by TFA cleavage and purification by reverse phase preparatory HPLC to obtain compound **27** an isolated yield of 52%, which was deemed sufficient for the model peptide LSF on solid phase (table 2, entry 3). A subsequent reaction was performed under the same condition but using acrylonitrile as substrate instead of methyl acrylate to give a satisfactory isolated yield of 59% (table 2, entry 4). Thus, acrylonitrile was used for further exploratory reactions as Michael acceptor.

To facilitate easy incorporation of pyridinium salts into SPPS, an Fmoc-protected amino acid building block **29** with a Katritzky salt at the Nϵ of lysine was synthesized (Scheme 9). However, any attempts at coupling an amino acid after Fmoc deprotection of the linear peptide were futile. Pyridinium salts have been previously shown to be compatible with Fmoc deprotection conditions.[332] However, their compatibility with amino acid coupling conditions is problematic since they possess a bulky group that may sterically occlude the Nα of lysine. Moreover, the SPPS compatibility experiment was specifically designed to include the coupling of beta-branched Valine after the Katritzky salt building block.

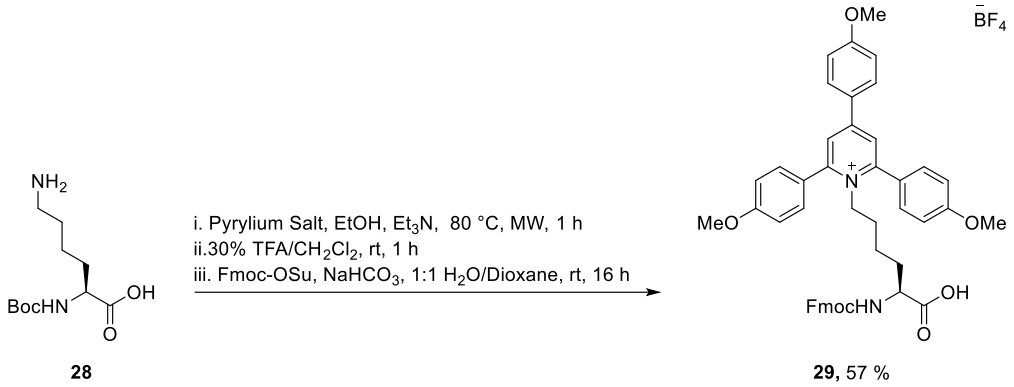

28 **29,** 57 %

Scheme 9. Synthesis of Katritzky salt building block **29** to pyridinium salt to determine compatibility with SPPS.

Reactions with different pyridinium salts were then probed using acrylonitrile as the substrate. Katritzky salt **24** had the highest yield compared to **25** and **26** (table 2, entries 5 – 6). Salt **25** may have been less reactive and reluctant to generate a free radical.[316] Salt **26** may have been too reactive and possibly formed side products that ultimately affected the conversion of the pyridinium salt substrate to the product.[323] The *p*-methoxy phenyl substituted salt **24** was deemed the best suited for the LSF method, and further experiments were continued with it as starting material.

To evaluate the progress of the reaction, samples were taken at various time points. A 14% conversion was observed after 4 hours and 88% after 20 hours (table 2, entries 7 - 10). Unfortunately, the UV absorbance of **24** is much higher than that of product **27,** which only contains tryptophan making the observed conversions rather unreliable.[333]

The importance of base in the reaction was then probed. According to the proposed mechanism by Aggarwal and co-workers, Et_3N contributed to a significant red shift in a ternary EDA complex that increased the efficiency of homolytic cleavage for generating free radicals.[326] Therefore, pyridinium salts **31** - **32** were prepared from Boc-Lysine-OH and the corresponding pyrylium salts (Scheme 10).

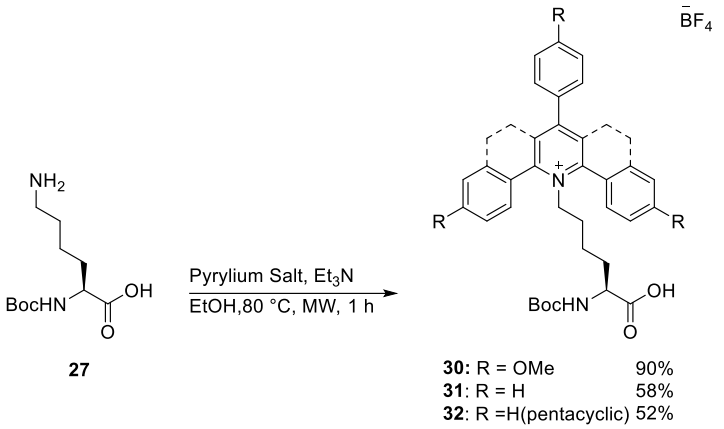

Scheme 10. Synthesis of pyridinium salts 29 – 30 for Spectroscopic studies

On performing spectroscopic experiments, a major redshift was only noted when the Hantzsch ester and pyridinium salts were in solution and barely any observable influence addition of base (Figure 3). However, upon performing the reaction devoid of the base, no conversion was observed by HPLC (table 2, entry 11).

Further analysis of the experimental conditions included carrying out reactions devoid of Hantzsch ester, light, and at room temperature, which all resulted in trace conversions of Katritzky salts to the product as observed by HPLC (table 2, entries 12 – 14). Reducing the Michael acceptor to 2.6 equivalents also led to a proportionate loss in the product yield. Furthermore, a carefree setup was performed wherein the reaction vials were not dried, and neither was the solvent purged nor was the reaction stirred under Argon atmosphere. Consequently, a conversion of 26% was observed, validating the need for precautionary steps undertaken during reaction setup to ensure a moisture-free reaction setup under argon (table 2, entry 15).

A

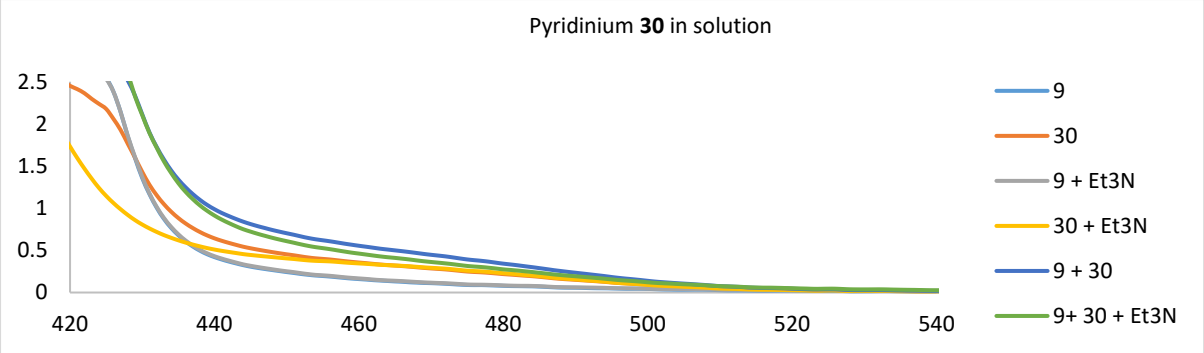

B

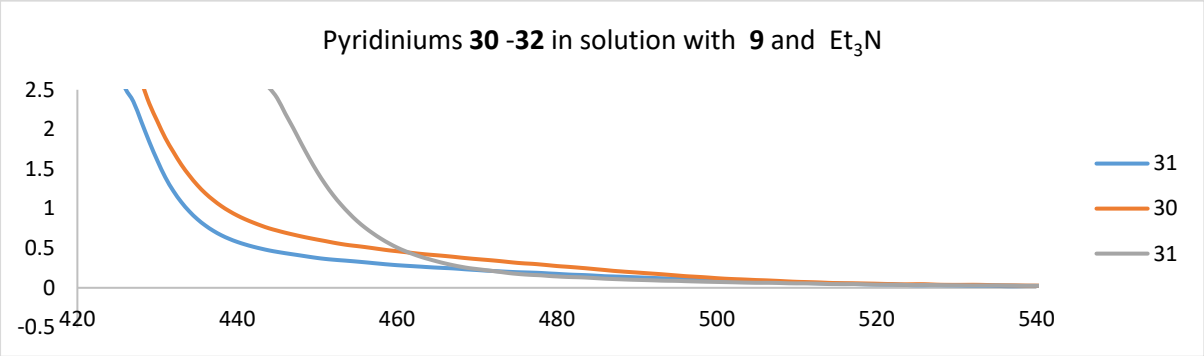

Figure 3. A: Spectroscopic studies on the effect of the base on absorbance for inducing a bathochromic shift of individual EDA complex partners of pyridinium **30,** including Hantzsch Ester **9**, trimethylamine (Et_3N) in solution. **B:** Pyridiniums **30** – **32** in solution with Hantzsch ester **9** and Et_3N.

3.2.2.3. Substrate scope studies

With an optimized protocol, the Michael acceptor substrate scope of the reaction was explored (Scheme 11). Of the successful examples, 2-pyridine **33** and pyrazine **34** had excellent yields compared to 4-pyridine **35**. Additionally, biphenyl **36** had a high yield, while styrene **37** did not react.

Compared to the test substrate used for model peptide **27**, the more sterically hindered nitriles **38** and **39** were not tolerated in the reaction. Similarly, analogues of initially explored ester **40** with methyl substitutions at the β-position were less tolerated and gave a very meager yield of **41**, while more hindered analogue **42** completely failed to afford any product. However, a methyl group at the alpha position was well tolerated for **43** while the phenyl substituent in **44** gave excellent yield superseding that of ester **40**. Other successful esters with good yields included the benzyl ester 45 and the diester 46.

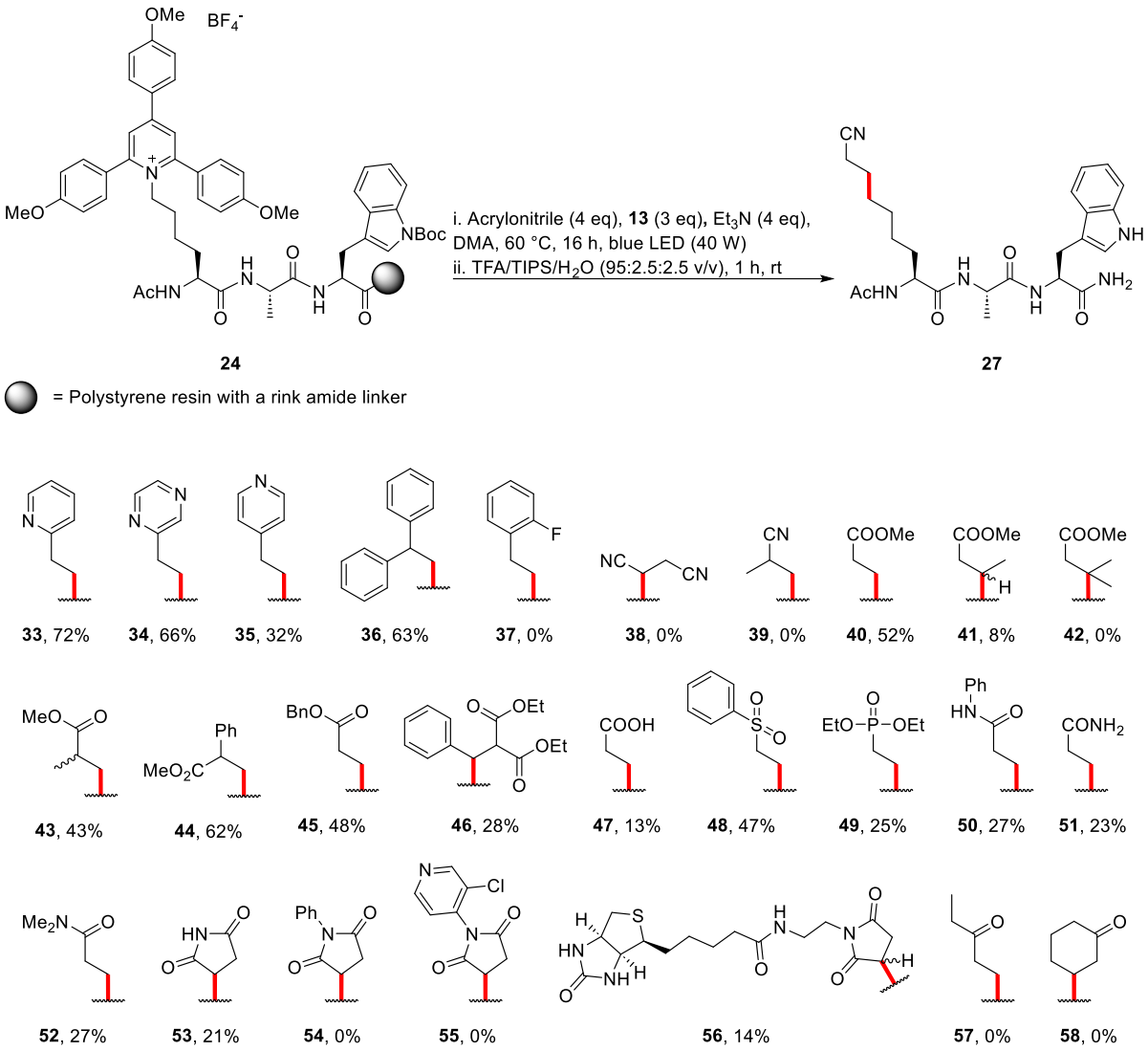

Scheme 11. The substrate scope of Michael acceptors was studied using the modified optimized conditions for the Giese-type reactions.

The acid functionalized **47** was derivatized from a tBu-protected substrate during global deprotection under TFA conditions. Other substrates containing heavy atoms other than carbon were tolerated, including sulfur in **48** and phosphorous in **49**. Amides were also taken in the scope (**50** – **52**). The acid functionalized **47** and the amides are also analogues of biogenic amino acids that could be directly derivatized with the LSF method. Having successfully obtained maleimide analogue **52** and despite the failure of **54** and **55**, biotinylated **56,** commonly used as a probe for investigating biochemical processes, was synthesized. Ketone substrates, however, did not react in the scope studies (**57** & **58**).

Given variations in the yields of similarly functionalized substrates, attempts were made to optimize reaction conditions further to rescue low-yielding and failed reactions. Compound **47** was selected, and a review of its crude HPLC chromatogram after global cleavage revealed three significant peaks of interest corresponding to the desired product and side products (Figure 4).

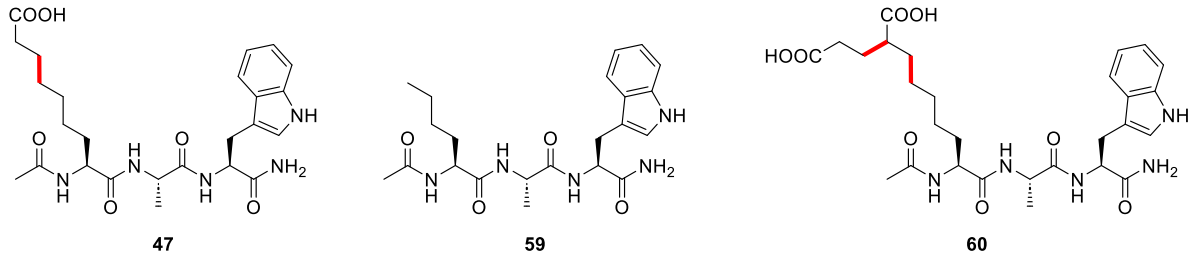

Figure 4. Side product profile observed from HPLC analysis of crude peptide after cleavage of **47** from resin.

The first peak had a mass corresponding to the product ($[M+H]^+$ = 502). In contrast, the second peak had a mass corresponding to a deaminated side product **59** generated from the peptidyl pyridinium salt that underwent pre-mature HAT following homolytic cleavage ($[M+H]^+$ = 430). The third peak, however, had multiple masses under it with increasing orders of substrate mass, suggesting multiple Michael acceptors partook in a cascade of Giese-type reactions prior to the final HAT. For example, **60** ($[M+H]^+$ = 574) may have been formed after a successive reaction with two Michael acceptors.

Subsequent efforts were then aimed at minimizing the formation of **59** by increasing the amount of the Michael acceptor to 8 molar equivalents. It was reasoned that such an increase in concentration would increase the propensity for the radical formed from C-N homolysis to form product **47**. Unfortunately, only an increase in the peak area for **60** was observed relative to **47** and **59**.

After that, as previously employed by Knowles and co-workers, an attempt was made to use 2,4,6-triisopropylbenzenethiol (TRIP thiol) as a catalyst to expedite the final HAT step of the proposed mechanism (Scheme 6).[334] Similarly, the equivalents of Hantzsch ester were also increased since its radical cation was proposed to partake of the final HAT in the reaction mechanism. Unfortunately, no significant increase in yield was observed, and as such, it was concluded that the low yield is substrate specific.

3.2.2.4. Scope of alternative Katritzky salt substrates.

Following an extensive study on the Michael acceptor scope, alternative Katritzky salts other than those derived from the Nε of the lysine side chain were considered for substrate analysis. Therefore, unnatural amino acid analogues of lysine bearing different side chain lengths were first considered for pyridinium salt synthesis. Consequently, three Katritzky salt substrates for the Giese reaction were synthesized using mutated sequences of the model peptide containing shorter side chains lengths, including Dap (n = 1 carbon), Dab (n = 2 carbons), and ornithine (n = 3 carbons) (scheme 12, compounds **61** - **63**). [335] A clear pattern of decreasing yield with side chain length was observed, which could be alluded to increasing steric constraints for a reaction between the free amines closer to the peptide backbone with bulky pyrylium salts (Scheme 12).[336]

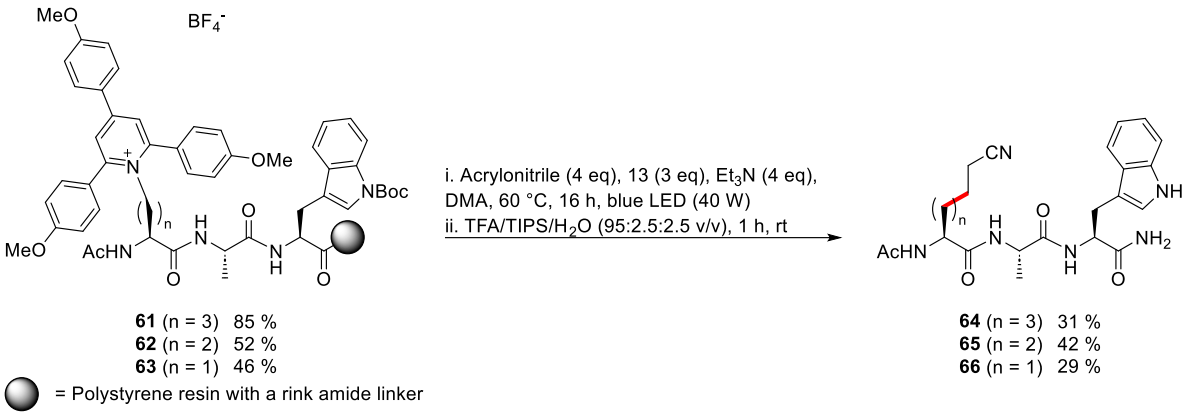

Scheme 12. Lysine analogue side-chain length screen for compatibility with Katritzky salt LSF. Yields of **61**– **63** were determined from cleaved aliquots of peptidyl resin.

After the Giese reaction with acrylonitrile as the Michael acceptor substrate, all desired products were obtained, but there was no perceivable trend between side chain length and yield (**64** - **66**). Furthermore, there seemed to be no loss of the chirality in **66** since only one diastereomer was observed by NMR analysis.

Secondly, a modification of the peptide backbone amine via C-N homolysis was considered, as inspired by the previously reported application of LSF at the termini for cyclization.[315] Additionally, it was foreseen as an opportunity to showcase the derivatization of non-amino acid fragments at the termini of peptides beyond acetyl groups for potentially improved biological activities.[85] As such, a linear peptidyl resin 67 was synthesized with an N-terminal glycine that was subsequently subjected to Katritzky salt synthesis to afford 68 in good yield (Scheme 13). Glycine's suitability at the N-terminus was anticipated owing to its potential for avoiding steric hindrance, diastereomer synthesis, and the generation of a reasonably nucleophilic radical suitable for the Giese reaction, as would not have been the case for other canonical amino acids with side chains.[337]

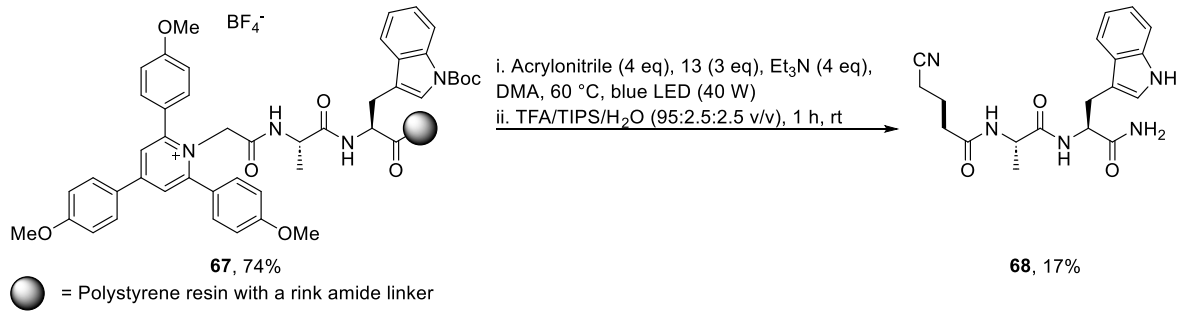

Scheme 13. Modifying a tripeptide backbone using a Katritzky salt derived from a deprotected N-terminal glycine residue. The yield of **67** was determined from the cleaved aliquots of the peptidyl resin.

3.2.2.5. Amino acid compatibility studies

It was further deemed prudent to examine the compatibility of the LSF methodology with all 20 canonical amino acids and their commonly used orthogonal protecting groups on SPPS.[338] As such, a library of 5 hexapeptides with randomized sequences was designed, with each containing an alloc protected lysine for late-stage modification on solid phase using PS resin with a Rink amide (AM) linker as solid support (table 3). The linear peptides were acetylated, followed by selective alloc deprotection and subsequent synthesis of the Katritzky salt using optimized conditions.

Table 3. Amino acid sequences and protecting groups used in the amino acid compatibility experiments.

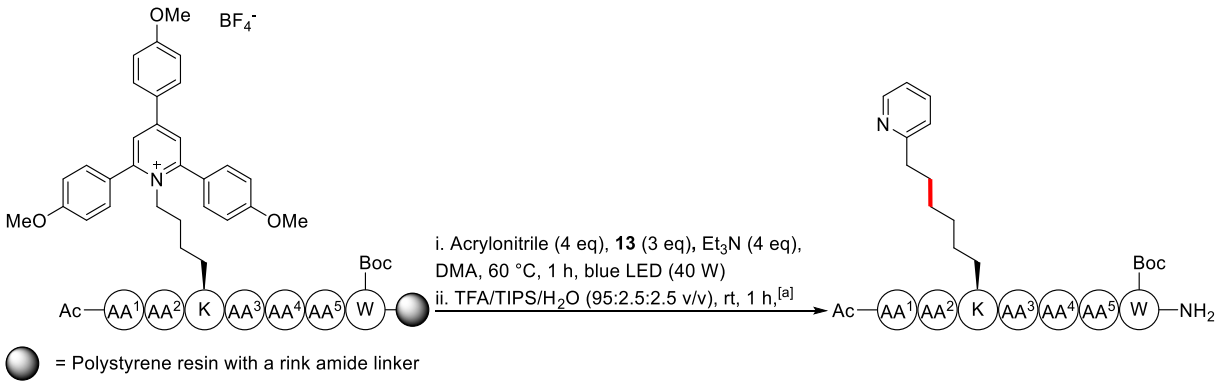

Compound	AA[1]	AA[2]	AA[3]	AA[4]	AA[5]
69	His(Trt)	Gly	Ala	Asp(tBu)	4
70	Val	Thr(tBu)	Arg(Pbf)	Met	13
71	Ile	Gln(Trt)	Pro	Phe	8
72	Tyr(tBu)	Ser(tBu)	Gly	Leu	13
73	Asn(Trt)	Cys(Trt)	Lys(Boc)	Glu(tBu)	9

[a] 2,2 –diethanethiol (DODT) was added to the deprotection cocktail for peptides containing cysteine and methionine residues.

The resulting pyridinium peptidyl resins were then subjected to the Giese-type reaction, global cleavage, ether precipitation, and final purification by reverse phase preparatory HPLC (**69 - 73**). In these reactions, 2-vinylpyridine was used as the Michael acceptor, and the yields observed were not based on resin loading but instead calculated over the entire synthesis starting from resin loading.

All canonical amino acids were compatible with Katritzky salt formation and the photochemical Giese reaction. Likewise, all the side chain protecting groups were compatible with the reaction conditions. However, substrate 2-vinylpyridine, which had a high yield from the scope experiments, tended to form side products from oligomerization, which was complicated purification and lowered the yields.

As anticipated, peptide **69** with histidine in its sequence had the lowest yield, considering that histidine has been investigated for its ability to partake of nucleophilic radical-mediated reactions at an elevated temperature of 70 °C – conditions which were similar to those of the Giese type reaction.[339] Furthermore, it was interesting that the residues containing thiols, especially methionine, were stable to the radical-mediated reaction, given their propensity to partake in such.[340]

3.2.2.6. Resin compatibility studies

All previous reactions were carried out using PS resin with a Rink amide linker as solid support. However, its common practice to use other resins in SPPS, particularly to overcome challenges associated with long or difficult sequences.[341] For example, polyethylene glycol (PEG) based resins are commonly used in such situations owing to their higher swelling properties that facilitate improved reagent diffusion.[53] Alternatively, PS resins with hydroxymethyl linkers and 2-CTC linkers may be used to synthesize peptides with free carboxyl groups at their termini.[342]

Therefore, a panel of resins and their respective linkers was screened for suitability as solid support during Katritzky salt synthesis and the subsequent Giese-type reaction (table 4). The resin loading was determined from that of a cleaved aliquot of the pyridinium salt, just as in the scope experiments.

The PS resin with a rink amide linker had the highest overall yield for pyridinium salt **24** and Giese product **33** (table 4 entry 1)**.** Changing the linker of PS resin to the hydroxymethyl moiety of the Wang resin resulted in a yield decline for both pyridinium salt **74** and subsequent product **75** (table 4, entry 2)**.** Pyridinium salt synthesis using a 4-(4-Hydroxymethyl-3-methoxyphenoxy)-butyric acid (HMPB) linker was satisfactory for **76**, albeit lower comparable yields of **77** and **78** in comparison to **33** (table 4, entries 3 – 4)**.** The yield was still low even when **78** was synthesized using acrylonitrile as an alternate substrate. Notably, only the 2-CTC linker on PS resin used for **79** was incompatible with solid-phase Katritzky salt synthesis (table 4 entry 5).

Upon changing the polymer support to PEG but maintaining the privileged rink amide linker, a marked reduction in the yield of Katritzky salt **80** was observed, with the resulting product **81** having the lowest yield of all compatible resins. This observation corresponds with the low concentration of reagents accrued from the larger volume of DMA required to adequately suspend the PEG-based resin, owing to its high swelling properties compared to PS.[343]

In order to take advantage of PEG resin swelling for improved diffusion, it may be worthwhile to perform future reactions using higher reagent equivalents to counterbalance the lower yields arising

from increased dilution, but this would likely result in the formation of Giese products with oligomerized Michael acceptors as previously observed.[344]

Table 4. Resin compatibility using different polymers and linkers for the synthesis of Katritzky salts and subsequent Giese products. The Michael acceptor substrate was 2-vinyl pyridine.

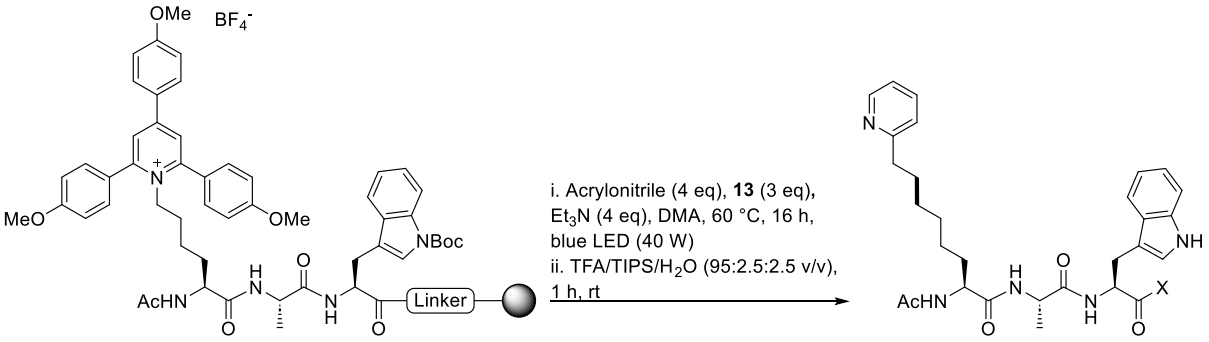

Linkers

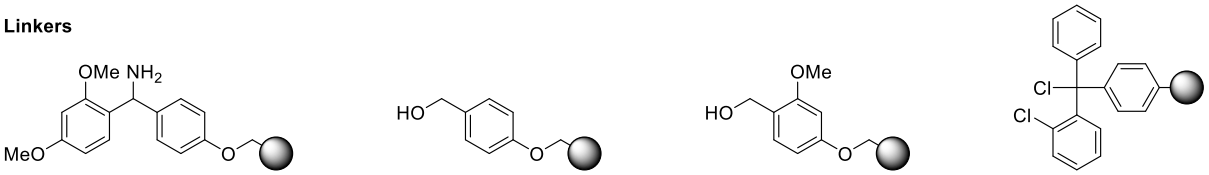

a: Rink amide **b**: Wang **c**: HMPB **d**: 2-CTC

Entry	Resin	Linker	Loading [mmol/g]	Kat. salt	Yield [%]	Giese product	Yield [%]
1	PS	**a**	0.63	**24**	82	**33**	72
2	PS	**b**	0.45	**74**	49	**75**	21
3	PS	**c**	0.50	**76**	70	**77**	32
4	PS	**c**	0.50	**76**	70	**78**(Acrylonitrile substrate)	29
5	PS	**d**	0.79	**79**	0	-	-
6	PEG	**a**	0.4	**80**	53	**81**	5

3.2.2.7. Modification of biologically relevant model peptides

Having interrogated conditions for optimal solid phase deaminative peptide LSF on solid phase, including the scope of tolerated Michael acceptors and solid support compatibly, a demonstration of methodical utility was subsequently performed. This was performed in the context of longer linear peptides that potentially pose synthetic challenges based on their structural complexity.[49]

The first model peptide was the histone 3 tail peptide (residues 1 – 10) **82** (scheme 14A). It has been extensively utilized as a tool compound for investigating epigenetic control mediated by gene repression due to variations in histone H3 lysine K4 (H3K4) methylation states.[345,346] Peptide p53 (15

– 29) **86** is a 15-mer oligopeptide inhibitor derived from the N-terminal transactivation domain of the tumor suppressor protein p53, which inhibits the PPI between p53 and the oncoprotein Mdm2(Scheme 14B).[347]

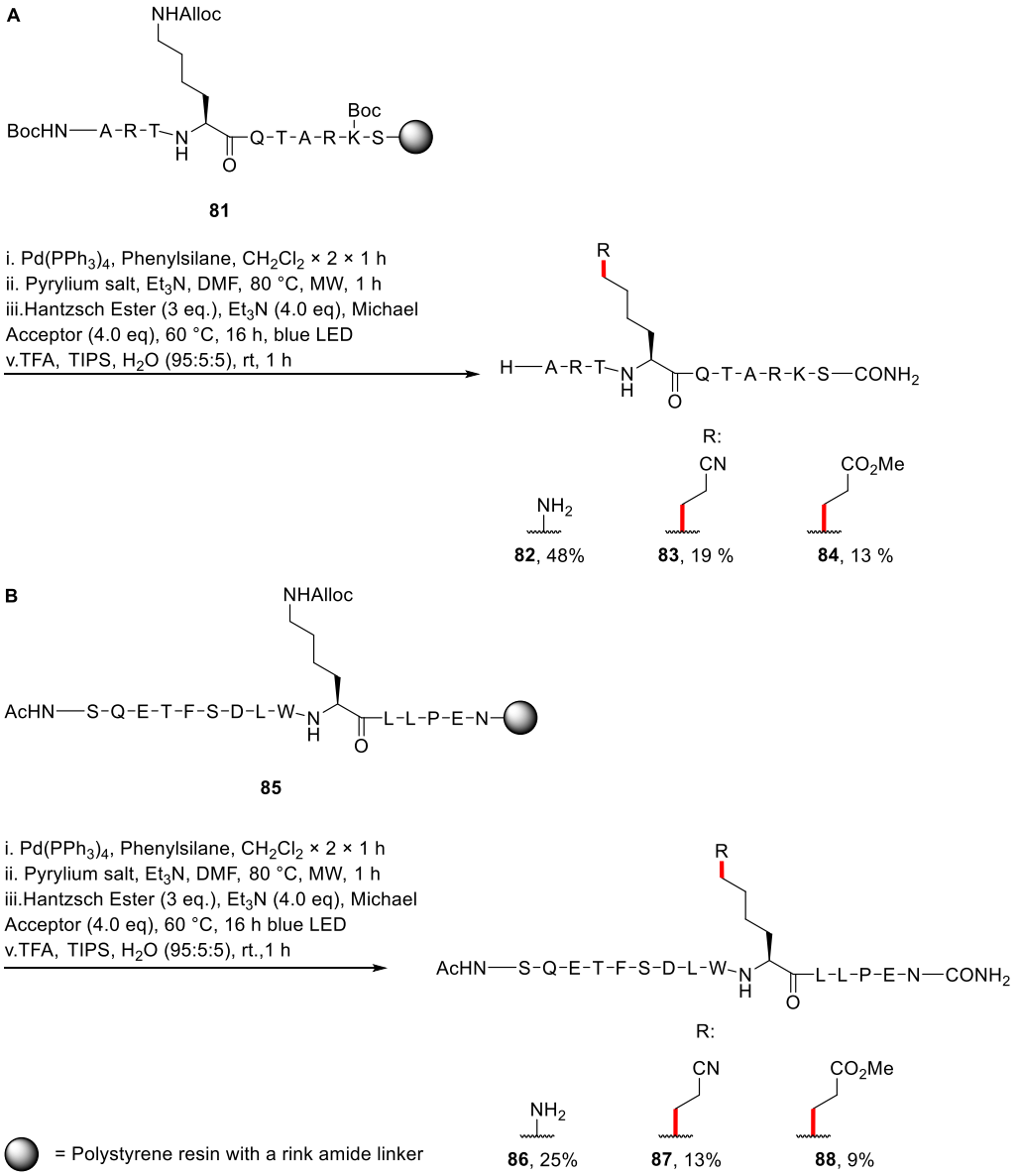

Scheme 14. LSF of linear peptides. **A**: For the modification of H3 (1 – 10) peptide **82**, the Giese reaction was performed at K4 with acrylonitrile and methyl acrylate as substrates to afford **83** and **84,** respectively; **B**: Likewise, modification of p53 (15 – 29) **86** was performed to afford analogues **87** and **88**.

Both peptides were synthesized on a 300 µmole scale and using PS rink amide resin as solid support. Two batches of 100 µmol could be used for diversification into Giese products via Katritzky salt synthesis. The other 100 µmole batch was used to synthesize unmodified linear peptides for a yield comparison.

The linear precursor of the H3 peptide **81** was first synthesized on solid phase with an N-terminal Boc-protected alanine residue as well as Alloc and Boc-protecting groups on the two lysine residues at positions 4 and 9, respectively. Following selective deprotection of the Alloc group at K4, the peptidyl resin was split into three batches. The first two batches underwent Katritzky salt synthesis at K4, followed by a Giese reaction with acrylonitrile **83** and methyl acrylate **84**, respectively. After that, all batches underwent global cleavage under TFA conditions and preparatory HPLC purification.[348] The unmodified H3 peptide **82** was obtained in a yield of 48%, and modified analogues in yields of 13% and 19% for **83** and **84,** respectively.

Similarly, the synthesis of **86** and analogs **87** and **88** was relatively more straightforward without the need for two orthogonal protecting groups. Alloc deprotection and Katritzky salt synthesis were performed at K9 of the linear N-terminal acetylated peptidyl resin batches designated for late-stage derivatization, followed by Giese reactions to afford **87** and **88** after global cleavage. Peptide **86** was obtained in a yield of 25% after Alloc deprotection, while respective Giese reaction products **87** and **88** were obtained in yields of 13% and 9%.

The cyclic symmetric peptide antibiotic gramicidin S was finally selected to showcase LSF using the developed method based on the protocol reported by Ulrich and co-workers, who had previously optimized the starting amino acid residue to aid efficient cyclization (Scheme 15).[165] A linear precursor **88** with Alloc and IvDde protecting groups on one of each of the Ornithine residues was synthesized on PS resin with a hydroxymethyl Wang linker as solid support and with a Boc-protected proline at the N-terminus. The Giese-type reaction was then carried out following selective Alloc deprotection and successive Katritzky salt synthesis to afford two analogues of Gramicidin S in yields of 7% and 8% after cyclization (**89** & **90**).

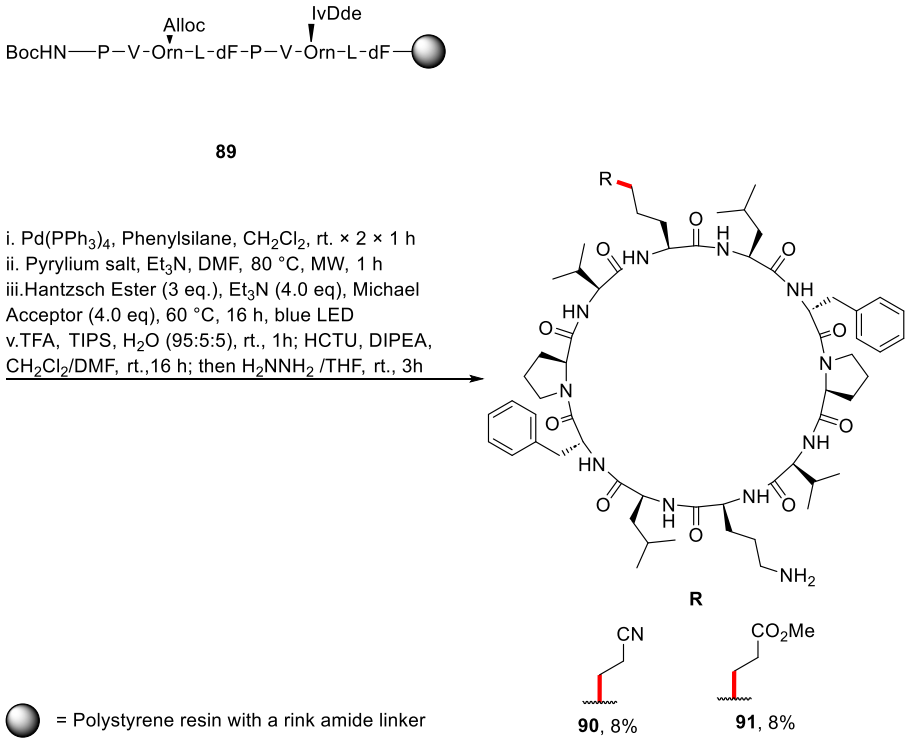

Scheme 15. Synthesis of Gramicidin S analogues by selectively functionalizing one ornithine residue with a Katritzky salt followed by LSF with acrylonitrile and methyl acrylate.

Finally, analysis of **91** ($[M+H]^+$ = 1212) by tandem mass spectrometry (MS/MS) demonstrated a notably symmetrical fragmentation pattern, amongst others, that occurred between proline and phenylalanine residues, thereby confirming the presence of a modified ornithine residue in **91** (Figure 5). Collision-induced dissociation (CID) is predominant at the amide bond of proline residues owing to its ring strain.[349] Therefore, fragments containing an unmodified ornithine residue **92** ($[M+H]^+$ = 571) and modified ornithine residue **93** ($[M+H]^+$ = 642) were observed, confirming the presence of a selectively modified residue in the Gramicidin S analogue. A mass of 1098.23 Da corresponded to fragment **94**, which was only devoid of a single proline residue, was also observed.

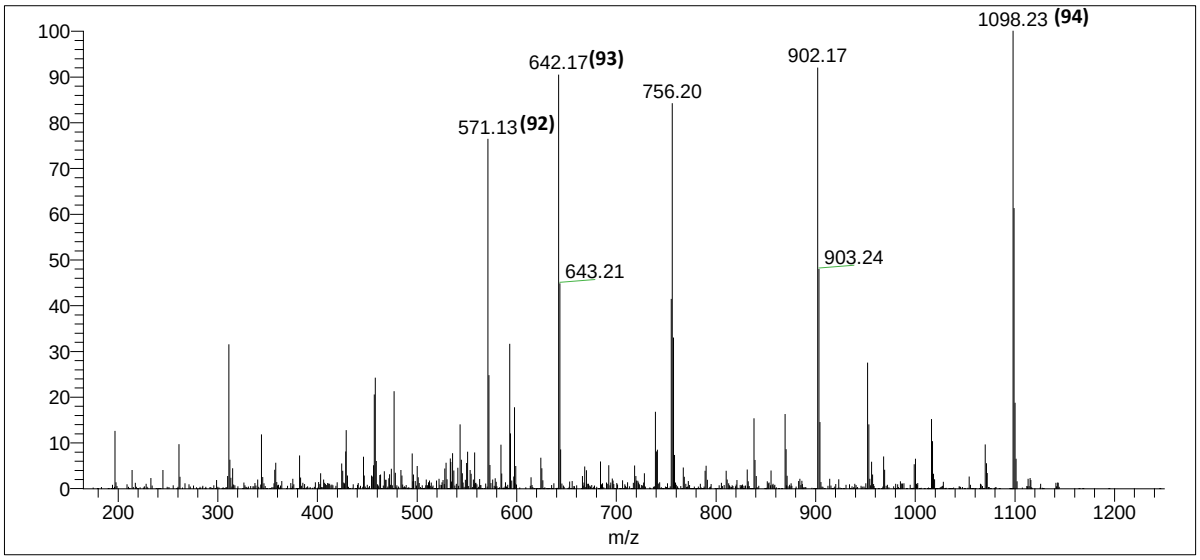

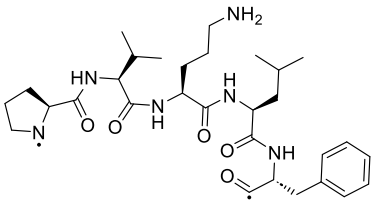

92. Exact Mass: 570.35

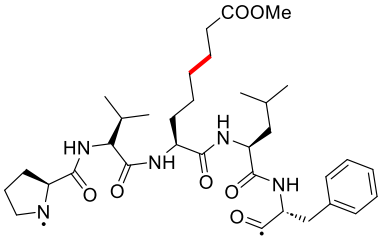

93.Exact Mass: 641.38

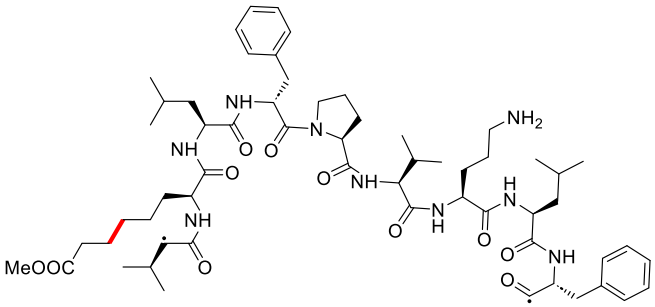

94. Exact Mass: 1099.67

Figure 5. Mass spectrometry analysis of Gramicidin s analogue **90** as evidence that a single modified ornithine residue had been modified on analysis of fragments generated from CID.

3.3. Summary and Conclusion

Initial attempts at deaminative $C(sp^3)$ -$C(sp^2)$ bond formation using nickel as a catalyst were futile owing to the incompatibility of SPPS with solid reductants, such that there was barely any reagent contact by diffusion to enable the catalytic cycle. A series of organic reductants were subsequently used, albeit only with trace conversions, perhaps because of their inadequately low reduction potentials, despite the fact that the use of more reactive *p*-methoxyphenyl substituted Katritzky salt as a peptidyl substrate.

Upon shifting to a photochemical approach for radical generation aimed at deaminative $C(sp^3)$-$C(sp^3)$ bond formation, an initial suboptimal conversion was observed in solution phase. Subsequently, with optimization of the reaction setup and substrate tripeptide sequence while utilizing SPPS, a satisfactory substrate conversion was observed by LCMS, and thereafter, a Michael acceptor scope study was performed. High isolated yields were obtained for pyrazine **33**, biphenyl **35**, and 4-pyridine **34** substrates**.** Having observed moderate toleration of maleimide **52**, biotin-conjugated maleimide **55** was synthesized, given its importance as a probe for studying protein interactions in biological systems. Ketones and styrenes failed under optimized reaction conditions. The major side products formed during the scope experiments were **58** obtained after a pre-mature HAT and **59** from oligomerization.

The *p*-methoxyphenyl substituted Katritzky salt **53**, derived from lysine, gave the highest yield during both pyridinium synthesis and the Giese reaction, compared to lysine derivatives of shorter side chain lengths and alternative pyridinium salts. All canonical amino acids were compatible with the reaction conditions, while the 2-CTC linker on PS resin was the only incompatible solid support encountered.

Analogues **75**, **79**, and antibiotic **83** were also successfully synthesized to showcase their methodological utility for modifying more complex biologically relevant peptides. Their overall yields were lower than the unmodified compounds, which is justifiable by the additional reactions compared to the unmodified peptides.

In conclusion, a photocatalyst-free method for late-stage deamination and subsequent formation of $C(sp^3)$-$C(sp^3)$ bonds was developed to modify lysine residues on solid phase using Katritzky salts. The method was amenable to peptides containing all canonical amino acids and with a broad substrate scope, albeit incompatibility with only a 2-CTC linker on PS resin. The utility was demonstrated by late-stage diversification of complex substrates with the potential for incorporating UAAs for tuning the biological and physicochemical properties of peptides.

4. Experimental

4.1. General Information

4.1.1. General remarks

All solvents and reagents were of analytical grade and obtained from commercial sources unless stated otherwise. During the setup of photochemistry reactions, anhydrous DMA was sparged with argon prior to use and reactions were carried out in flamed dried 7 mL vials under argon atmosphere.

Manual solid phase peptide synthesis was carried out on a promega® vacuum manifold while automatic solid phase synthesis was carried using a Syro I ® peptide synthesizer. A CEM Discover® SP reactor was used to carry out microwave-based synthesis in 10 ml glass vials fitted with ActiVent™ caps.

Silica flash chromatography was carried out on a Büchi Pure C-850 Flash Prep using a flash column (RediSep®, 24g). Thin layer chromatography was performed using silica gel coated aluminium plates (Merk 60 F254) and visualized under UV irradiation at 254nm. Analytical UHPLC was performed using 2.1 mm x 50 mm, 1.8 µm Zorbax Eclipse C18 Rapid Resolution columns equipped on either an Agilent 1290 or Agilent 1260 Infinity system. Analytical LCMS was performed using an Agilent 1260 Infinity system equipped with a 2.1 mm x 150 mm, 2.7 µm InfinityLab Poroshell 120 EC-C18 column. Preparatory HPLC purification was carried out using 125 mm x 21 mm, 5 µm, Macherey-Nagel C18 Gravity columns (Macherey-Nagel GmbH & Co. KG, Germany) on a Büchi Pure C-850 Flash Prep for tripeptides or an Infinity II LC-MS system (Agilent Technologies, USA) for longer peptides. High resolution mass spectra were recorded on an LTQ Orbitrap in tandem with an HPLC-System fitted with a 50 mm x 1 mm, 1.9 µm Hypersyl GOLD using electrospray ionization method.

Nuclear magnetic resonance (NMR) spectra were recorded using Bruker DRX500 (500 MHz), and Bruker DRX700 spectrometers and chemical shifts are reported with reference to deuterated solvent peaks.

4.1.2. General synthetic methods

a. General method for linear peptide synthesis

Solid phase peptide synthesis was carried out using the Fmoc strategy on Rink Amide AM resin (loading ca. 0.7 mmol/g, 100 – 200 mesh) unless stated otherwise. Fmoc protected amino acids (4.00 eq) were coupled using PyBOP (4.00 eq) and DIPEA (8.00 eq) in DMF (0.02 mL/µmol) for 30 minutes at room temperature. Deprotection of the Fmoc protecting group was carried out using a 20% solution of

piperidine in DMF (0.02 mL/µmol) for 5 minutes followed by addition of fresh reagents and further reaction for 10 minutes. Additional deprotection solution was added if necessary to completely suspend the resin. Linear peptides were N-terminally acetylated using DIPEA (10.0 eq) and Ac_2O (10.0 eq) in DMF (0.02 mL/µmol) over 30 minutes. In between steps the resin was washed with DMF (2.00 mL × 4 × 1 min). In all cases, additional DMF was added if necessary to completely suspend the resin.

b. General method for Alloc deprotection

The linear peptide (100 µmol) was suspended in anhydrous CH_2Cl_2 (2.00 mL) followed by the addition of phenylsilane (308 µl; 2.48 mmol; 24.8 eq) and $Pd[(C_6H_5)_3P]_4$ (28.8 mg, 0.025 mmol, 0.25 eq) and the suspension was shaken for 1 h followed by removal of the liquid and the addition of fresh reagents. After 1 h, the peptidyl resin was washed with CH_2Cl_2 (2.00 mL × 4 × 1 min), DMF (2.00 mL × 4 × 1 min), 0.5% diethyldithiocarbamate in DMF (2.00 mL × 4 × 1 min), 11.5% pyridine hydrochloride in 5% MeOH/ CH_2Cl_2 (2.00 mL × 5 × 5 min), CH_2Cl_2 (2.00 mL × 4 × 1 min) and DMF (2.00 mL × 4 × 1 min). In all cases, additional solvents were added if necessary to completely suspend the resin.

c. General method for peptide Katritzky salt formation

A 10 mL microwave vial containing dry peptidyl resin (300 µmol) was charged with a solution of pyrylium salt (1.50 eq) and TEA (4.00 eq) in DMF (4.00 mL) and the reaction mixture was heated for 1 h at 80 °C under microwave irradiation. Additional DMF was added if necessary to completely suspend the resin. The peptidyl resin was washed with DMF (2.00 mL × 4 × 1 min), CH_2Cl_2 DMF (2.00 mL × 4 × 1 min), and Et_2O (2.00 mL × 1 × 1 min) then dried under high vacuum.

d. General method for peptide Giese reaction

A flame dried reaction vial with a magnetic stirring bar under argon atmosphere was charged with peptidyl resin (100 µmol) and sealed. The vial was then charged with a solution of Hantzsch ester (76.0 mg; 300 µmol; 3.00 eq) in DMA (400 µl) followed by three evacuation-backfill cycles with argon and thereafter, charged with a solution of Michael acceptor (4.00 eq) and TEA (4.00 eq) in DMA (300 µl). Additional DMA was added if necessary to completely suspend the resin. The vial was affixed in a 100 mL beaker that was then sealed with aluminum foil. The beaker was placed in an oil bath with the temperature set to 100 °C followed by irradiation with blue LEDs. The combined heat of the lamp and oil bath maintain an internal temperature of 65 °C in the beaker (see Fig. 2). After 16 h, the peptidyl resin was washed with DMF (2.00 mL × 4 × 1 min) and CH_2Cl_2 (2.00 mL × 4 × 1 min).

e. General method for cleavage and deprotection of short peptides

Peptidyl resin (100 µmol) was cleaved with TFA/TIPS/H_2O (95/2.5/2.5 v/v, 4.00 mL) for 1 h. The solution was collected and excess TFA was removed under a stream of argon followed by co-evaporation with $CHCl_3$ (50 mL × 3).

f. General method for cleavage and deprotection of long peptides

Peptidyl resin was cleaved with TFA/TIPS/H_2O (95/2.5/2.5 v/v, 4.00 mL) for 1 h followed by precipitation in cold Et_2O (100 mL) and centrifugation. The supernatant was removed, and the pellet resuspended in cold Et_2O (100 mL followed by centrifugation. This procedure was repeated twice. The resulting pellet was dissolved in H_2O/MeCN (1:1, 2.5 mL) and lyophilized.

g. General method for cleavage and deprotection of long peptides with sulfur-containing amino acid residues

Similar to procedure f, however the cleavage cocktail was TFA/ODT/TIPS/H_2O (90/2.5/2.5/5 v/v, 4.00 mL)

h. General method for attachment of first amino acid to hydroxymethyl based resins (300 µmol)

Wang or HMPB resins in a 50 mL flask were swollen by suspending in CH_2Cl_2 (3.00 ml) and stirred for 20 minutes. The Fmoc protected amino acid (10.00 eq) was dissolved in anhydrous CH_2Cl_2 (25.0 mL) and the solution was cooled to 0 °C followed by the addition of DIC (5.00 eq) and DMF as needed to aid complete dissolution. The solution was stirred for 10 minutes and added to the resin followed by the addition of DMAP (0.50 eq). The resulting suspension was stirred for 1 h, washed with DMF (3.00 mL × 1 min × 4) followed by CH_2Cl_2 (3.00 mL × 1 min × 4) and dried with Et_2O (1.00 mL × 1 min). The resin was dried in vacuo for 18 h followed by loading determination by Fmoc release and spectrophotometric quantification.

i. General method for 2-CTC resin reactivation

To a cooled suspension of 2-CTC resin (2.00 g, 1.5 mmol) in CH_2Cl_2 (20.0 ml) in a 50 ml round bottomed flask was added pyridine (0.580 ml, 7.20 mmol, 2.40 eq.) followed by the dropwise addition of thionyl chloride (0.261 ml, 3.60 mmol, 1.20 eq.). The suspension temperature was allowed to rise to room temperature and then refluxed for 2 h. The suspension was filtered in a fitted syringe reactor and the residue washed with CH_2Cl_2 (3.00 mL × 1 min × 4) and dried in vacuo.

j. General method for attachment of first amino acid to 2CTC resin

Dry peptidyl resin (3.00 mmol) was swollen in CH_2Cl_2 (10 mL) for 20 minutes in 20 ml fritted syringe reactor. The solvent was drained and a solution of Fmoc-Proline-OH (4.05 g, 12.00 mmol, 4.0 eq.) and DIPEA (4.18 ml, 24.0 mmol, 8.00 eq.) in anhydrous CH_2Cl_2 (10.0 ml) was drawn into the syringe and

shaken. After 1 h, the resin was washed with CH_2Cl_2 (10.0 mL × 1 min × 4), CH_2Cl_2 (10.0 mL × 1 min × 4).

k. General method for ester hydrolysis.

To a solution ester (1.00 eq) added a 0.5 M solution of LiOH in THF:MeOH:H_2O (4:1:1; 30 mL) in an ice bath. The reaction temperature was allowed to rise to room temperature while stirring. After 2 h, the excess solvent was removed in vacuo, and the reaction pH was lowered to 5 using 0.1 M HCl followed by extraction with CH_2Cl_2 (3 × 30 mL). The combined organic layers was dried over $MgSO_4$, filtered and dried over high vacuum to afford the title compound.

l. General method for N-oxide synthesis

m-Chloroperoxybenzoic acid (1.01 eq) was added to a solution of pyridine (1.00 eq) in a minimum amount of CH_2Cl_2 required for dissolution at 0 °C. The reaction temperature was allowed to rise to room temperature and the solution was stirred overnight. The solution was purified by silica column chromatography (0–15% CH_2Cl_2/MeOH) afford the title compounds.

m. General method for for Fmoc protection.

To a solution of benzoic acid (1.00 eq) and $NaHCO_3$ (2.00 eq) in a minimum amount of water required for complete dissolution and cooled in an ice bath, was added a solution of Fmoc-OSu (1.2 eq) in MeCN dropwise while stirring. After 20 min, the ice bath was removed, and additional MeCN was added if precipitation was observed. After 4 h, the reaction was extracted with EtOAc (30 mL × 3). The combined organic phase was extracted with a saturated solution of $NaHCO_3$ (30 mL × 1). The combined aqueous layer was acidified with 2M HCl to a pH range of 1 – 3; extracted with EtOAc (30 mL × 3), washed with saturated $NaHCO_3$ and brine. The combined organic layer was dried over $MgSO_4$, filtered and concentrated in vacuo to afford the title compounds.

4.1.3. Purification methods

Method A

Peptides were purified by silica flash chromatography (1 – 30% methanol in CH_2Cl_2) on a Büchi Pure C-850 Flash Prep using a flash column (RediSep®, 24g).

Method B

Peptides were purified by preparative HPLC on a Büchi Pure C-850 Flash Prep system equipped with a 125 mm x 21 mm, 5 µm, Macherey-Nagel C18 Gravity column, eluting at 20 mL/min with a binary mixture of MeCN and H_2O with both containing 0.1% TFA using a gradient of 0% - 95% MeCN over 60 min.

Method C

Peptides were purified by preparative HPLC on a Büchi Pure C-850 Flash Prep system equipped with a 50 mm x 10 mm, 5 µm, Macherey-Nagel C18 Gravity column, eluting at 6 mL/min , eluting with a binary mixture of MeCN and H_2O with both containing 0.1% TFA using a gradient of 5% - 95% MeCN over 60 min.

Method D

Peptides were purified on an Infinity II LC-MS system (Agilent Technologies, USA) with the rest of the method similar to method B.

Method E

Peptides were purified on an Infinity II LC-MS system (Agilent Technologies, USA), eluting with a binary mixture of MeOH and H_2O with both containing 0.1% TFA using a gradient of 0% - 55% MeOH over 55 min.

4.2. Improving the Chameleonic Properties of Cyclic Peptides Using Small-Molecule Fragments

4.2.1. Linker fragment synthesis

4.2.1.1. Synthesis of Boc-Ile(Thz)-OH

Ethyl 2-((1S,2S)-1-((tert-butoxycarbonyl)amino)-2-methylbutyl)thiazole-4-carboxylate (4a).

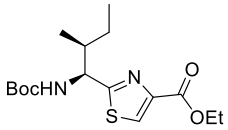

Synthesis was performed in accordance to the method described by Nielsen and co-workers.[181] PyBOP (12.0 g, 23.2 mmol, 1.05 eq.) and DIPEA (4.07 mL, 23.4 mmol, 1.06 eq) were added to a solution of Boc-Ile-OH (5.10 g, 22.1 mmol, 1.00 eq) in CH_2Cl_2 (100 mL) while stirring. After 20 min, aqueous ammonia 28% (15.7 mL, 110 mmol, 5.00 eq) was added, and the reaction mixture was stirred for 2 h. The reaction mixture was filtered, and the resulting filtrate was concentrated in vacuo. The residue was suspended in EtOAc (200 mL), filtered, and washed with saturated $NaHCO_3$ (3 × 100 mL) and brine (100 mL) and then dried over $MgSO_4$. Lawesson's reagent (6.24 g, 15.4 mmol, 0.70 eq) was then added to a solution of the resulting amide in CH_2Cl_3 (100 mL) while stirring at rt. After 12 h, the suspension was filtered through a plug of celite, and the filtrate was concentrated in vacuo. The resulting residue was dissolved in EtOAc (200 mL), washed with saturated $NaHCO_3$ (3 × 100 mL) and brine (100 mL), then dried over $MgSO_4$, filtered, and concentrated in vacuo to afford Boc-isoleucine thioamide as a yellow solid.

$KHCO_3$ (1.50 g, 15.0 mmol, 1.54 eq) was charged in an oven-dried round-bottomed flask containing a solution of Boc-isoleucine thioamide (2.40 g, 9.70 mmol, 1.00 eq) in anh. DME (25) under argon atmosphere at −40 °C followed by the dropwise addition of a solution of 2-ethyl-bromo pyruvate (1.62 mL, 12.9 mmol, 1.33 eq) in anh. DME (20 mL) while stirring. The reaction temperature was then raised to −20 °C. After 6 h, the reaction mixture was filtered, and the filtrate was concentrated in vacuo. Subsequently, to a cooled solution of the resulting residue in anh. DME (25 mL) in a round-bottomed flask at −40 °C under argon atmosphere was added to a solution of trifluoroacetic anhydride (4.32 mL, 31.1 mmol, 3.21 eq) and 2,6-lutidine (9.00 mL, 77.5 mmol, 8.00 eq) in anh. DME (10 mL) dropwise. The reaction temperature was then raised to −20 °C and stirred for 1 h. The solvent was then removed in vacuo, and the resulting residue dissolved in EtOAc (250 mL), washed with H_2O (50 mL), 20% citric acid (aq) (3 × 50 mL), and brine (50 mL). The organic layer was then dried over $MgSO_4$, filtered, and

concentrated in vacuo. The crude mixture was purified by silica column chromatography (0 – 30% EtOAc/petroleum ether) to afford the title compound. Yield: 3.91 g (10.6 mmol, 48%) as a yellow solid. **^{1}H NMR (600 MHz, DMSO-d_6) δ** 8.41 (s, 1H), 7.73 (d, *J* = 8.4 Hz, 1H), 4.65 (t, *J* = 7.7 Hz, 1H), 4.29 (dtt, *J* = 10.8, 7.1, 3.8 Hz, 2H), 1.99 – 1.88 (m, 1H), 1.55 – 1.42 (m, 1H), 1.38 (s, 9H), 1.30 (t, *J* = 7.1 Hz, 3H), 1.28 – 1.19 (m, 1H), 0.84 – 0.79 (m, 3H), 0.77 (d, *J* = 6.8 Hz, 3H). **^{13}C NMR (151 MHz, DMSO) δ** 174.66, 160.70, 155.65, 145.48, 128.74, 78.39, 60.61, 57.36, 38.32, 28.11, 24.50, 15.52, 14.14, 11.28. **HRMS (ESI)**: *m/z* calculated for $C_{16}H_{26}N_2O_4S$ $[M+H]^+$ = 343.1692, measured = 343.1686.

2-((1S,2S)-1-((Tert-butoxycarbonyl)amino)-2-methylbutyl)thiazole-4-carboxylic acid (4b).

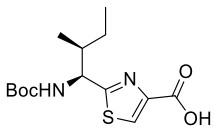

Synthesis was performed in accordance to the general synthetic method **k** for ester hydrolysis from **4a** (1.50 g, 15.0 mmol, 1.54 eq) Yellow solid. Yield: 220 mg (0.56 mmol, 35%) **^{1}H NMR (600 MHz, DMSO-d_6) δ** 12.97 (s, 1H), 8.33 (s, 1H), 7.71 (d, *J* = 8.4 Hz, 1H), 4.65 (t, *J* = 7.7 Hz, 1H), 2.03 – 1.79 (m, 1H), 1.65 – 1.43 (m, 1H), 1.38 (s, 9H), 1.31 – 1.20 (m, 1H), 0.83 (t, *J* = 7.2 Hz, 3H), 0.78 (d, *J* = 6.8 Hz, 3H).**^{13}C NMR (151 MHz, DMSO) δ** 174.24, 162.05, 155.39, 146.60, 128.22, 57.31, 38.35, 28.10, 24.51, 15.51, 10.93. **HRMS (ESI)**: *m/z* calculated for $C_{14}H_{22}N_2O_4S$ $[M+H]^+$ = 315.1379, measured = 315.1374.

4.2.1.2. Synthesis of dipeptides with pyridine and PNO fragments derived from 6-aminopicolinic acid

Methyl 6-aminopicolinate (15).

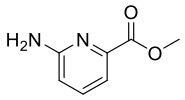

$SOCl_2$ (5.25 mL, 72.4 mmol, 2.00 eq) was added dropwise to a suspension of 6-aminopicolinic acid (5.00 g, 36.2 mmol, 1.00 eq) in MeOH (100 ml) at 0 °C and the reaction was heated at reflux to form a solution which was stirred overnight. The solution was allowed to cool to room temperature, and the excess solvent was removed under reduced pressure. The residue was dissolved in CH_2Cl_2 and washed with $NaHCO_3$. The aqueous layer was extracted with CH_2Cl_2 (30 ml × 2). The combined organic layer was dried over $MgSO_4$, filtered, and concentrated under reduced pressure to afford the title compound. Yield: 4.79 g (31.5 µmol, 87%) as a white solid. **^{1}H NMR (400 MHz, DMSO-d_6)** δ 7.51 (t, 1H), 7.33 – 7.13 (m, 1H), 6.65 (d, *J* = 8.3 Hz, 1H), 6.28 (s, 2H), 3.79 (d, *J* = 0.6 Hz, 3H). **^{13}C NMR (101 MHz, DMSO-d_6)** δ 159.68, 145.70, 137.66, 113.18, 112.20, 51.85. **HRMS (ESI)**: *m/z* calculated for $C_7H_8N_2O_2$ $[M+H]^+$ = 153.0664, measured = 153.0658.

2-Amino-6-(methoxycarbonyl)pyridine 1-oxide (16).

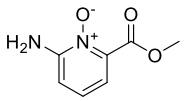

Synthesized according to the general synthetic method **I** for N-oxide synthesis using *m*-Chloroperoxybenzoic acid (5.48 g, 31.73 mmol, 1.01 eq), **27** (4.78 g, 31.42 mmol, 1.00 eq). Yield: 2.77 g (16.5 mmol, 52%) as a white solid. **^{1}H NMR (400 MHz, DMSO-d_6)** δ 7.28 (dd, *J* = 8.5, 7.5 Hz, 1H), 6.98 (dd, *J* = 8.5, 1.7 Hz, 1H), 6.86 (dd, *J* = 7.5, 1.8 Hz, 1H), 3.85 (d, *J* = 0.6 Hz, 3H). **^{13}C NMR (101 MHz, DMSO-d_6) δ** 162.28, 151.32, 139.63, 128.51, 111.29, 111.16, 52.84. **HRMS (ESI)**: *m/z* calculated for $C_7H_9N_2O_3$ $[M+H]^+$ = 169.0613 , measured = 169.0608.

2-((2S,3S)-2-((tert-butoxycarbonyl)amino)-3-methylpentanamido)-6-(methoxycarbonyl)pyridine 1-oxide (17).

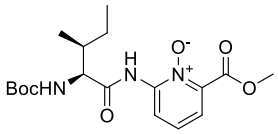

DIPEA (11.1 mL g, 64.23mmol, 4.00 eq) was added dropwise to a solution of **16** (2.70 g, 16.06 mmol, 1.00 eq), and PyBOP (16.7 g, 32.11 mmol, 2.00 eq) in CH_2Cl_2 (100 mL) at 0 °C. The reaction mixture was allowed to warm up to room temperature while stirring. After 16 h, the crude mixture was washed with $NaHCO_3$ and brine and then dried over $MgSO_4$. The solvent was removed under reduced pressure, and the crude mixture was purified by silica column chromatography (0 – 30% EtOAc/petroleum ether) afford the title compound. Yield: 5.52 g (14.7 mmol, 90%) as a white solid. **^{1}H NMR (500 MHz, DMSO-d_6)** δ 10.79 (s, 1H), 8.32 (d, *J* = 8.3 Hz, 1H), 7.98 (t, *J* = 8.0 Hz, 1H), 7.78 (dd, *J* = 7.6, 0.9 Hz, 1H), 7.01 (d, *J* = 8.6 Hz, 1H), 4.13 (t, *J* = 8.1 Hz, 1H), 3.88 (s, 3H), 1.85 – 1.73 (m, 1H), 1.54 – 1.43 (m, 1H), 1.37 (s, 9H), 1.29 (s, 1H), 1.15 (dt, *J* = 13.3, 8.1 Hz, 1H), 0.86 (d, *J* = 6.9 Hz, 3H), 0.82 (t, *J* = 7.4 Hz, 3H). **^{13}C NMR (126 MHz, DMSO)** δ 164.85, 155.48, 151.81, 145.81, 139.71, 120.47, 117.40, 78.10, 59.37, 52.40, 36.22, 28.21, 24.51, 15.33, 10.86.**HRMS (ESI)**: *m/z* calculated for $C_{18}H_{28}N_3O_6$ $[M+H]^+$ = 382.1978, measured = 382.1966.

Methyl 6-((2S,3S)-2-((tert-butoxycarbonyl)amino)-3-methylpentanamido)picolinate (18).

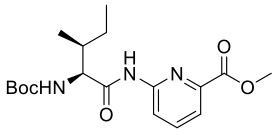

Bis(pinacolato)diboron (2.50 g, 9.83mmol, 1.50 eq) was added to a cooled solution of **17** (2.50 g, 6.55 mmol, 1.00 eq) in CH_2Cl_2 (100 mL) at 0 °C while stirring. After 7 h, the excess solvent was removed in vacuo, and the residue was dissolved in EtOAc, washed with brine then dried over $MgSO_4$. The solvent was removed under reduced pressure, and the crude mixture was purified by silica column chromatography (0–30% EtOAc/petroleum ether) afford the title compound. Yield: 2.39 g (6.54 mmol, 99%) as a white solid. **^{1}H NMR (500 MHz, DMSO-d_6)** δ 10.76 (s, 1H), 8.32 (d, *J* = 8.3 Hz, 1H), 7.98 (t, *J* = 8.0 Hz, 1H), 7.78 (dd, *J* = 7.6, 0.9 Hz, 1H), 6.98 (d, *J* = 8.6 Hz, 1H), 4.13 (t, *J* = 8.3 Hz, 1H), 3.88 (s, 3H), 1.77 (q, *J* = 7.9 Hz, 1H), 1.56 – 1.42 (m, 1H), 1.37 (s, 9H), 1.19 – 1.13 (m, 1H), 0.86 (d, *J* = 6.8 Hz, 3H), 0.82 (t, *J* = 7.4 Hz, 3H). **^{13}C NMR (126 MHz, DMSO)** δ 172.88, 165.29, 155.92, 152.25, 146.28, 140.12, 120.90, 117.85, 81.83, 78.57, 73.98, 59.84, 52.82, 36.70, 28.65, 25.41, 24.95, 15.77, 11.29. **HRMS (ESI)**: *m/z* calculated for $C_{18}H_{27}N_3O_5$ $[M+H]^+$ = 366.2023, measured = 366.2024.

6-((2S,3S)-2-((Tert-butoxycarbonyl)amino)-3-methylpentanamido)picolinic acid (19).

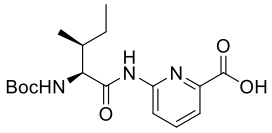

Synthesis was performed in accordance to the general synthetic method **k** for ester hydrolysis from **18** (2.390 g, 6.54 mmol, 1.00 eq), 1.54 eq). Yield: 1.94 g (5.52 mmol, 84%) as a white solid. **^{1}H NMR (500 MHz, DMSO-d_6)** δ 13.26 (s, 1H), 10.71 (s, 1H), 8.28 (d, *J* = 8.3 Hz, 1H), 7.95 (t, *J* = 7.9 Hz, 1H), 7.75 (d, *J* = 7.4 Hz, 1H), 7.01 (d, *J* = 8.5 Hz, 1H), 4.12 (t, *J* = 8.3 Hz, 1H), 1.77 (p, *J* = 7.9, 6.8 Hz, 1H), 1.56 – 1.41 (m, 1H), 1.37 (s, 9H), 1.23 – 1.12 (m, 1H), 0.86 (d, *J* = 6.8 Hz, 3H), 0.81 (t, *J* = 7.4 Hz, 3H). **^{13}C NMR (126 MHz, DMSO)** δ 172.28, 165.80, 155.39, 151.54, 146.87, 139.41, 120.26, 116.86, 78.02, 59.29, 36.11, 28.09, 24.41, 15.22, 10.74. **HRMS (ESI)**: *m/z* calculated for $C_{17}H_{26}N_3O_5$ $[M+H]^+$ = 352.1872, measured = 352.1865.

2-((2S,3S)-2-((Tert-butoxycarbonyl)amino)-3-methylpentanamido)-6-carboxypyridine 1-oxide (20).

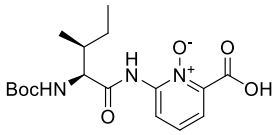

Compound **17** (3.20 g, 8.39 mmol, 1.00 eq) was added to a 0.5M solution of LiOH in THF: MeOH: H_2O (4: 1: 1; 30 mL) in an ice bath. The reaction temperature was allowed to rise to room temperature while stirring. After 2 h, the excess solvent was removed in vacuo, and the reaction pH was lowered to 5 using 0.1M HCl followed by extraction with CH_2Cl_2 (3 × 30 mL). The combined organic layer was dried over $MgSO_4$, filtered, and dried over high vacuum to afford the title compound. Yield: 2.80 g (7.62 mmol, 91%) as a white solid. **^{1}H NMR (500 MHz, DMSO-d_6)** δ 10.74 (s, 1H), 8.61 (dd, *J* = 8.7, 1.9 Hz, 1H), 7.99 (dd, *J* = 7.9, 1.9 Hz, 1H), 7.87 (t, *J* = 8.2 Hz, 1H), 7.44 (d, *J* = 7.6 Hz, 1H), 4.31 (t, *J* = 7.4 Hz, 1H), 1.87 (dtt, *J* = 14.6, 11.0, 5.4 Hz, 1H), 1.57 – 1.42 (m, 1H), 1.39 (s, 9H), 1.36 – 1.18 (m, 1H), 0.89 (d, *J* = 6.8 Hz, 1H), 0.82 (t, *J* = 7.4 Hz, 3H). **^{13}C NMR (126 MHz, DMSO)** δ 172.97, 161.29, 156.33, 143.01, 135.50, 132.94, 122.26, 119.43, 79.11, 60.40, 36.30, 28.62, 24.81, 15.78, 11.51. **HRMS (ESI)**: *m/z* calculated for $C_{17}H_{25}N_3O_6$ $[M+H]^+$ = 368.1822, measured = 368.1816.

4.2.1.3. Synthesis of analogues of cyclic peptide 1 with 6-(aminomethyl)picolinic acid derived linkers

Dimethyl pyridine-2,6-dicarboxylate (24).

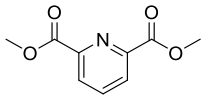

Thionyl chloride (5.52 mL, 76.1 mmol, 1.20 eq) was added dropwise to a suspension of isophthalic acid (10.6 g, 63.4 mmol, 1.00 eq) in MeOH (100 mL) at 0 °C and the reaction temperature was heated at reflux while stirring. After 16 h, the excess solvent was removed in vacuo. The residue was dissolved in CH_2Cl_2 (50 mL), washed with $NaHCO_3$ and brine, then dried over $MgSO_4$, followed by concentration in vacuo. The product was used in the subsequent step without any further purification. Yield: 10.4 g (53.3 mmol, 84%) as a white solid. **^{1}H NMR (500 MHz, DMSO-d_6)** δ 8.78 – 8.71 (m, 2H), 8.65 (dd, *J* = 8.4, 7.1 Hz, 1H), 4.40 (s, 6H). **^{13}C NMR (126 MHz, DMSO)** δ 215.89, 175.44, 158.95, 149.15, 138.27, 62.59. **HRMS (ESI)**: *m/z* calculated for $C_9H_9NO_4$ $[M+H]^+$ = 196.0610, measured = 196.0604.

Methyl 6-(chloromethyl)picolinate (25).

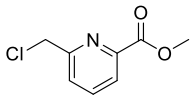

Sodium borohydride (2.71 g, 71.7 mmol, 1.40 eq) was added portion wise to a solution of **24** (10.0 g, 51.2 mmol, 1.00 eq) in MeOH (100 mL) in a flame-dried round-bottomed flask under argon atmosphere at 0 °C. The ice bath was removed, and the temperature was allowed to rise. After 30 minutes following observation of effervescence, the reaction pH was lowered to 6 by dropwise addition of 0.1 M HCl and the excess MeOH was removed under reduced pressure. The resulting aqueous solution was extracted with CH_2Cl_2 (50 mL × 3), and the combined organic layer was dried over $MgSO_4$, followed by concentration in vacuo. The intermediate was suspended in MeOH (100 mL) at 0 °C followed by dropwise addition of $SOCl_2$ (5.52 mL, 76.1 mmol, 1.20 eq). The reaction mixture was heated at reflux and stirred overnight. The excess solvent was removed in vacuo, and the residue was dissolved in CH_2Cl_2 (50 mL), washed with $NaHCO_3$ and brine, then dried over $MgSO_4$, followed by concentration in vacuo. The crude product was purified by silica column chromatography (0 – 30% EtOAc/Petroleum ether) to afford the title compound. Yield: 6.30 g (33.9 mmol, 66 %) as a white solid. **^{1}H NMR (500 MHz, DMSO-*d*$_6$)** δ 8.03 – 7.98 (m, 1H), 7.92 (dd, *J* = 7.8, 1.1 Hz, 1H), 7.73 (dd, *J* = 7.8, 1.1 Hz, 1H), 4.61 (s, 2H), 3.87 (s, 3H). **^{13}C NMR (126 MHz, DMSO)** δ = 165.23, 162.55, 146.32, 138.21, 123.95, 123.09, 63.89, 52.41. **HRMS (ESI)**: *m/z* calculated for $C_8H_8ClNO_2$ $[M+H]^+$ = 186.0316, measured = 186.0316.

Methyl 6-(azidomethyl)picolinate (26).

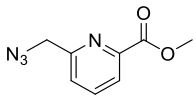

To a solution of **25** (6.6 g, 35.5 mmol, 1.00 eq) in DMF (50 mL) in an oven-dried flask under argon atmosphere was added NaN_3 (2.18 g, 42.7 mmol, 1.20 eq) portion wise while stirring and the reaction temperature was raised to 90 °C. After 16 h, the reaction was quenched by adding H_2O (20 mL) and stirred for a further 10 min. The excess DMF was removed under high vacuum, and the crude product was dissolved in CH_2Cl_2 (50 mL), washed with brine and dried over $MgSO_4$, and concentrated in vacuo followed by purification by silica column chromatography (0 – 30% EtOAc/Petroleum ether) to afford the title compound. Yield: 6.50 g (33.8 mmol, 95 %) as a white solid. **^{1}H NMR (700 MHz, DMSO-*d*$_6$)** δ 8.04 (t, *J* = 7.7 Hz, 1H), 8.01 (dd, *J* = 7.8, 1.3 Hz, 1H), 7.69 (dd, *J* = 7.5, 1.3 Hz, 1H), 4.63 (s, 2H), 3.89 (s,

3H). **^{13}C NMR (176 MHz, DMSO)** δ = 165.00, 156.27, 147.31, 138.73, 125.93, 124.09, 54.17, 52.52. HRMS (ESI): *m/z* calculated for $C_8H_8N_4O_2$ $[M+H]^+$ = 193.0720, measured = 193.0718.

Methyl 6-(((2S,3S)-2-((tert-butoxycarbonyl)amino)-3-methylpentanamido)methyl)picolinate (27).

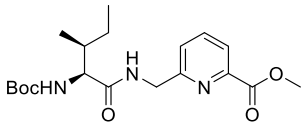

A 100 mL round-bottomed flask under argon atmosphere was charged with 10% Pd/C (3.60 g, 3.38 mmol, 0.10 eq), followed by three evacuation and argon refill cycles. The catalyst was then suspended in MeOH (30 ml) and charged with a solution of **26** (6.50 g, 33.8 mmol, 1.00 eq) in a minimum amount of MeOH required for complete dissolution, followed by three evacuation and H_2 refill cycles. The reaction mixture was charged with 36% HCl (8.70 mL, 101 mmol, 3.00 eq) while stirring under H_2, then checked by LCMS. After 48 h, the suspension was filtered using a bed of celite, concentrated in vacuo, and the intermediate was dissolved in CH_2Cl_2 (100 mL). The flask was then charged with Boc-Ile-OH (11.7 g, 50.6 mmol, 1.50 eq), PyBOP (26.4 g, 50.74 mmol, 1.50 eq) and DIPEA (17.7 ml, 101 mmol, 3.00 eq). Extra CH_2Cl_2 was added as necessary for complete dissolution while stirring. After 16h, the organic phase was washed with citric acid, saturated $NaHCO_3$, and brine, then dried over $MgSO_4$ and concentrated in vacuo. The crude product was purified by silica column chromatography (0 – 30% EtOAc in petroleum ether). Yield: 5.63 g (1.48 mmol, 41%) as an off-white solid. **^{1}H NMR (500 MHz, DMSO-d_6)** δ 8.59 (t, *J* = 6.0 Hz, 1H), 7.92 (d, *J* = 4.4 Hz, 2H), 7.55 (t, *J* = 4.5 Hz, 1H), 6.83 (d, *J* = 8.6 Hz, 1H), 4.42 (t, *J* = 5.7 Hz, 1H), 3.88 (s, 3H), 1.79 – 1.61 (m, 1H), 1.47 – 1.41 (m, 1H), 1.40 (s, 9H), 1.22 – 1.03 (m, 1H), 0.82 (dd, *J* = 8.3, 6.7 Hz, 6H). **^{13}C NMR (126 MHz, DMSO)** δ 172.49, 165.69, 159.94, 156.03, 147.23, 138.36, 124.95, 123.60, 78.51, 59.53, 52.84, 44.51, 36.46, 28.66, 25.01, 15.93, 11.38. **HRMS (ESI)**: *m/z* calculated for $C_{19}H_{29}N_3O_5$ $[M+H]^+$ = 380.2185, measured = 380.2177.

6-(((2S,3S)-2-((Tert-butoxycarbonyl)amino)-3-methylpentanamido)methyl)picolinic acid (28).

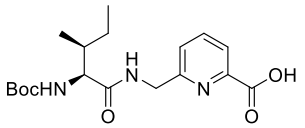

Synthesized according to the general synthetic method **k** for methyl ester hydrolysis from **27** (2.40 g, 6.32 mmol, 1.00 eq) was added to a 0.5M solution of LiOH in THF: MeOH: H_2O (4:1:1; 30 mL). Yield: 2.20 g (6.04 mmol, 95%). **^{1}H NMR (500 MHz, DMSO-d_6)** δ 8.96 (s, 1H), 8.11 – 7.78 (m, 2H), 7.46 (dd, *J* = 7.1, 1.6 Hz, 1H), 7.17 (s, 1H), 4.52 – 4.28 (m, 2H), 3.82 (t, *J* = 8.3 Hz, 1H), 1.78 – 1.67 (m, 1H), 1.51 – 1.40 (m, 1H), 1.34 (s, 9H), 1.19 – 1.04 (m, 1H), 0.79 (dd, *J* = 8.7, 6.6 Hz, 6H). **^{13}C NMR (126 MHz, DMSO)**

δ = 173.57, 172.12, 166.82, 155.68, 137.95, 137.91, 123.79, 123.79, 122.52, 122.52, 77.92, 28.18, 24.67, 15.51, 10.93. **HRMS (ESI)**: *m/z* calculated for $C_{19}H_{29}N_3O_6$ $[M+H]^+$ = 396.2135, measured = 366.2026.

2-(((2S,3S)-2-((Tert-butoxycarbonyl)amino)-3-methylpentanamido)methyl)-6-(methoxycarbonyl)pyridine 1-oxide (29).

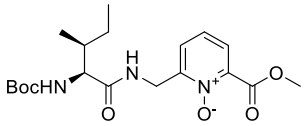

Synthesized according to the general synthetic method **l** for N-oxide synthesis using *m*-Chloroperoxybenzoic acid (0.510 g, 2.96 mmol, 1.02 eq), **27** (1.10 g, 2.90 mmol, 1.00 eq). Yield: 0.945 g (2.39 mmol, 82%) as a white solid. **^{1}H NMR (500 MHz, DMSO-d_6)** δ 8.54 (t, *J* = 6.0 Hz, 1H), 7.63 (dd, *J* = 7.8, 2.0 Hz, 1H), 7.50 (d, *J* = 5.9 Hz, 1H), 7.37 (t, *J* = 7.9 Hz, 1H), 7.00 (d, *J* = 8.1 Hz, 1H), 4.41 (dd, *J* = 17.6, 6.2 Hz, 1H), 4.29 (dd, *J* = 17.7, 5.8 Hz, 1H), 3.87 (s, 3H), 3.81 (t, *J* = 8.0 Hz, 1H), 1.77 – 1.67 (m, 1H), 1.55 – 1.41 (m, 1H), 1.40 (s, 9H), 1.20 – 1.06 (m, 1H), 0.82 (t, *J* = 7.2 Hz, 6H). **^{13}C NMR (126 MHz, DMSO)** δ = 172.59, 162.33, 155.81, 149.27, 141.61, 124.85, 124.71, 123.43, 78.20, 59.28, 53.00, 37.92, 35.57, 29.61, 28.20, 24.96, 24.68, 15.48, 10.87. **HRMS (ESI)**: *m/z* calculated for $C_{19}H_{29}N_3O_6$ $[M+H]^+$ = 396.2135, measured = 396.2129.

2-(((2S,3S)-2-((tert-butoxycarbonyl)amino)-3-methylpentanamido)methyl)-6-carboxypyridine 1-oxide (30).

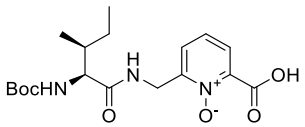

Synthesized according to the general synthetic method **k** for methyl ester hydrolysis from **29** (0.900 g, 2.28 mmol, 1.00 eq). Yield: 0.451 mg (1.18 mmol, 52%) as a white solid. **^{1}H NMR (500 MHz, DMSO-d_6)** δ 12.91 (s, 1H), 8.46 (t, J = 6.0 Hz, 1H), 7.80 (dt, J = 7.7, 1.5 Hz, 1H), 7.49 (d, J = 7.6 Hz, 1H), 7.41 (t, J = 7.6 Hz, 1H), 6.74 (d, J = 8.9 Hz, 1H), 4.48 – 4.22 (m, 2H), 3.82 (t, J = 8.2 Hz, 1H), 1.73 – 1.63 (m, 1H), 1.37 (s, 9H), 1.08 (dtd, J = 13.4, 8.6, 8.1, 5.7 Hz, 1H), 0.79 (t, J = 7.5 Hz, 6H). **^{13}C NMR (126 MHz, DMSO)** δ = 172.11, 167.74, 155.87, 140.50, 132.17, 128.88, 128.67, 128.19, 78.44, 59.36, 42.19, 28.64, 24.90, 15.91, 11.41. **HRMS (ESI)**: *m/z* calculated for $C_{18}H_{27}N_3O_6$ $[M+H]^+$ = 382.1973, measured = 382.1973.

4.2.1.4. Synthesis of Sanguinamide A analogues with 2-(6-aminopyridin-2-yl)acetic acid and corresponding PNO aromatic linkers

Tert-butyl (6-methylpyridin-2-yl)carbamate (34).

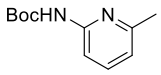

N,N-Dimethylpyridin-4-amine (5.65 g, 46.2 mmol, 1.00 eq) was added to a solution of 6-methylpyridin-2-amine (5.00 g, 46.2 mmol, 1.00 eq) and Boc_2O in t-BuOH (50 mL) at rt. while stirring, and the reaction temperature was raised to 50 °C. After 16 h, the reaction temperature was lowered to room temperature and the solvent was removed under reduced pressure. The residue was dissolved in EtOAc (50 mL) and washed with a saturated solution of $NaHCO_3$ and brine. The organic layer was dried over $MgSO_4$ and concentrated in vacuo. The crude oil was purified by silica column chromatography (0 – 5% EtOAc/Petroleum ether) to afford the title compound. Yield: 4.47 g (21.5 mmol, 46%) as a white solid. **^{1}H NMR (500 MHz, DMSO-d_6)** δ 9.57 (s, 1H), 7.82 – 7.13 (m, 2H), 7.07 – 6.70 (m, 1H), 2.35 (s, 3H), 1.45 (s, 9H). **^{13}C NMR (126 MHz, DMSO)** δ 156.30, 152.78, 151.80, 138.20, 117.50, 109.29, 79.36, 28.03, 23.65. **HRMS (ESI)**: *m/z* calculated for $C_{11}H_{16}N_2O_2$ $[M+H]^+$ = 209.1285, measured = 209.1285.

Ethyl 2-(6-((tert-butoxycarbonyl)amino)pyridin-2-yl)acetate (35).

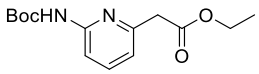

LDA (2M, 23.6mL, 47.3 mmol, 4.00 eq) was added dropwise to a cooled solution of **34 (**2.50 g, 11.8 mmol, 1.00 eq**)** in anh. THF (20 mL) at -78 °C while stirring. After 30 min, diethyl carbonate (2.86 ml, 23.6 mmol, 2.00 eq) was added dropwise and stirred for a further 10 minutes. The temperature was raised to 0 °C. After 2 h, the reaction was quenched with saturated NH_4Cl solution and extracted with EtOAc (30 mL × 3), and the combined organic layer was dried over MgSO4 and concentrated in vacuo to give the crude product as a yellow oil which was purified by silica column chromatography (0–30% EtOAc/petroleum ether) afford the title compound. Yield: 2.50 g (8.78 mmol, 74 %) as a yellow oil.**^{1}H NMR (500 MHz, DMSO-d_6)** δ 9.71 (s, 1H), 7.91 – 7.50 (m, 2H), 6.97 (dd, *J* = 4.8, 3.5 Hz, 1H), 4.07 (q, *J* = 7.1 Hz, 2H), 3.71 (s, 2H), 1.45 (s, 9H), 1.17 (t, *J* = 7.1 Hz, 3H). **^{13}C NMR (126 MHz, DMSO)** δ 170.28, 152.97, 152.80, 152.02, 138.54, 118.35, 110.68, 79.45, 60.36, 42.87, 28.02, 14.09.**HRMS (ESI)**: *m/z* calculated for $C_{14}H_{20}N_2O_4$ $[M+H]^+$ = 281.1496, measured = 281.1495.

2-((tert-butoxycarbonyl)amino)-6-(2-ethoxy-2-oxoethyl)pyridine 1-oxide (36).

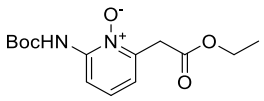

*m*CPBA (1.82 g, 10.53 mmol, 1.00 eq) was added to a solution of **35** (2.46 g, 8.78 mmol, 1.00 eq) in a minimum amount of CH_2Cl_2 required for dissolution in an ice bath. The reaction temperature was allowed to rise to room temperature. After 7 h, excess CH_2Cl_2 was blown off under a stream of argon and the solution was purified by silica column chromatography (0 – 30% EtOAc/petroleum ether) afford the title compound. Yield: 2.44 g (8.23 mmol, 94%) as a yellow oil.**^{1}H NMR (500 MHz, DMSO-*d*$_6$)** δ 9.34 (s, 1H), 7.96 (dd, *J* = 8.5, 1.9 Hz, 1H), 7.41 (t, *J* = 8.1 Hz, 1H), 7.24 (dd, *J* = 7.8, 1.9 Hz, 1H), 4.07 (q, *J* = 7.0 Hz, 2H), 3.89 (s, 2H), 1.50 (s, 9H), 1.17 (t, *J* = 7.1 Hz, 3H).**^{13}C NMR (126 MHz, DMSO)** δ 168.86, 151.52, 144.20, 143.83, 127.08, 120.13, 111.91, 82.19, 60.87, 37.34, 28.18, 14.53. **HRMS (ESI)**: *m/z* calculated for $C_{14}H_{20}N_2O_5$ $[M+H]^+$ = 297.1445, measured = 297.1446.

2-((2S,3S)-2-((Tert-butoxycarbonyl)amino)-3-methylpentanamido)-6-(2-ethoxy-2-oxoethyl)pyridine 1-oxide (37).

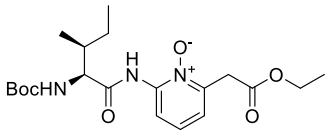

A round-bottomed flask containing **36** (2.44 g, 8.23 mmol, 1.00 eq) in an ice bath was charged with 30% TFA/CH_2Cl_2 (30 ml, 119.34 mmol, 15.0 eq) dropwise. The reaction temperature was allowed to rise to room temperature while stirring. After 1 h, the volatiles were removed under a stream of argon and subsequently in vacuo. The residue was dissolved in CH_2Cl_2 (30 mL), and the flask was placed in an ice bath followed by the addition of DIPEA (8.60 mL, 49.4 mmol, 6.00 eq), Boc-Ile-OH (3.81 g, 16.46 mmol, 2.00 eq), and PyBOP (8.57 g, 16.46 mmol, 2.00 eq) while stirring and the reaction temperature was allowed to rise to room temperature. After 16 h, the solution was washed with NaHCO3, NH_4Cl, and brine. The organic phase was dried over $MgSO_4$, and concentrated in vacuo to give the crude product as a yellow oil which was purified by silica column chromatography (0 – 30% EtOAc/petroleum ether) to afford the title compound. Yield: 3.03 g (7.41 mmol, 90%) as a yellow oil.**^{1}H NMR (500 MHz, DMSO-*d*$_6$)** δ 10.61 (s, 1H), 8.27 (dd, *J* = 8.5, 1.9 Hz, 1H), 7.54 (d, *J* = 7.6 Hz, 1H), 7.41 (t, *J* = 8.1 Hz, 1H), 7.29 (dd, *J* = 7.8, 1.9 Hz, 1H), 4.16 – 4.00 (m, 3H), 3.89 (s, 2H), 1.54 – 1.40 (m, 1H), 1.38 (s, 9H), 1.33 – 1.24 (m, 1H), 1.22 (ddd, *J* = 13.7, 6.8, 2.5 Hz, 1H), 1.16 (t, *J* = 7.1 Hz, 3H), 0.87 (d, *J* = 6.9 Hz, 3H), 0.82 (t, *J* = 7.4 Hz, 3H). **^{13}C NMR (126 MHz, DMSO)** δ 172.17, 168.86, 156.32, 144.36, 143.42, 126.87, 121.15,

113.26, 79.09, 60.84, 37.43, 36.32, 28.67, 28.62, 24.97, 15.88, 14.56, 14.51, 11.73, 11.62.**HRMS (ESI)**: *m/z* calculated for $C_{20}H_{31}N_3O_6$ $[M+H]^+$ = 410.2291, measured = 410.2283.

Ethyl 2-(6-((2S,3S)-2-((tert-butoxycarbonyl)amino)-3-methylpentanamido)pyridin-2-yl)acetate (38).

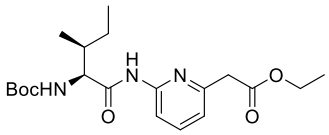

Synthesized according to the method for compound **18** using **37** (3.25 g, 7.93 mmol, 1.00 eq)**,** Bis(pinacolato)diboron (3.02 g, 11.9 mmol, 1.50 eq). Yield: 2.70 g (6.85 mmol, 86%) as a yellow oil. **^{1}H NMR (500 MHz, DMSO-d_6)** δ 10.37 (s, 1H), 7.98 (d, *J* = 8.4 Hz, 1H), 7.74 (t, *J* = 7.9 Hz, 1H), 7.07 (dd, *J* = 7.5, 0.8 Hz, 1H), 6.98 (d, *J* = 8.6 Hz, 1H), 4.09 (qd, *J* = 7.1, 1.3 Hz, 3H), 3.76 (s, 2H), 1.85 – 1.63 (m, 1H), 1.55 – 1.41 (m, 1H), 1.37 (s, 9H), 1.33 – 1.23 (m, 1H), 1.17 (d, *J* = 6.4 Hz, 3H), 0.84 (d, *J* = 6.8 Hz, 3H), 0.81 (t, *J* = 7.4 Hz, 3H). **^{13}C NMR (126 MHz, DMSO)** δ 172.40, 170.69, 155.91, 153.66, 151.74, 139.35, 120.06, 112.20, 83.32, 78.53, 60.86, 43.27, 36.69, 28.65, 25.30, 24.96, 15.78, 14.54, 11.32. **HRMS (ESI)**: *m/z* calculated for $C_{20}H_{31}N_3O_5$ $[M+H]^+$ = 394.2336, measured = 394.2334.

Ethyl 2-(6-((2S,3S)-2-((tert-butoxycarbonyl)amino)-3-methylpentanamido)pyridin-2-yl)acetate (**39**).

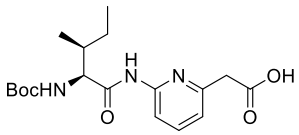

Synthesized according to the general synthetic method **k** for ester hydrolysis from **38** (2.90 g, 6.84 mmol, 1.00 eq). Yield: 2.40 g (6.57 mmol, 96%) as a white solid. **^{1}H NMR (700 MHz, DMSO-d_6)** δ 10.31 (s, 1H), 7.88 (d, *J* = 8.3 Hz, 1H), 7.68 (t, *J* = 7.9 Hz, 1H), 7.01 – 6.93 (m, 2H), 4.11 – 4.04 (m, 1H), 3.69 (s, 2H), 1.76 (d, *J* = 8.3 Hz, 1H), 1.56 – 1.42 (m, 1H), 1.38 (s, 9H), 1.15 (dt, *J* = 15.0, 7.7 Hz, 1H), 0.85 (d, *J* = 6.8 Hz, 3H), 0.82 (t, *J* = 7.4 Hz, 3H). **^{13}C NMR (176 MHz, DMSO)** δ = 172.18, 156.86, 155.89, 151.39, 139.21, 119.22, 110.92, 78.55, 59.94, 43.50, 36.76, 28.66, 24.98, 15.79, 11.35. **HRMS (ESI)**: *m/z* calculated for $C_{18}H_{27}N_3O_5$ $[M+H]^+$ = 366.2029, measured = 366.2023.

2-((2S,3S)-2-((Tert-butoxycarbonyl)amino)-3-methylpentanamido)-6-(carboxymethyl)pyridine 1-oxide (40).

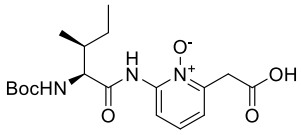

Synthesized according to the general synthetic method **k** for ester hydrolysis from **37** (3.24 g, 7.93 mmol, 1.00 eq) in 4:1:1 and 0.5M solution of LiOH in THF: MeOH: H_2O (4:1:1; 50 mL). Yield: 1.31 g (3.42 mmol, 43%) as a white solid. ^{1}H NMR (500 MHz, DMSO-d_6) δ 12.53 (s, 1H), 10.63 (s, 1H), 8.25 (dd, *J* = 8.4, 1.9 Hz, 1H), 7.54 (d, *J* = 7.8 Hz, 1H), 7.40 (t, *J* = 8.1 Hz, 1H), 7.28 (dd, *J* = 7.9, 1.9 Hz, 1H), 4.11 (t, *J* = 7.3 Hz, 1H), 3.83 (s, 2H), 1.96 – 1.82 (m, 1H), 1.50 – 1.40 (m, 1H), 1.38 (s, 9H), 1.31 – 1.16 (m, 1H), 0.87 (d, *J* = 6.8 Hz, 3H), 0.85 – 0.79 (m, 3H). ^{13}C NMR (126 MHz, DMSO) δ = 173.61, 171.68, 169.87, 155.72, 144.37, 126.41, 120.71, 112.66, 78.00, 58.12, 37.09, 35.91, 28.24, 24.52, 15.46, 11.18. **HRMS (ESI)**: *m/z* calculated for $C_{18}H_{27}N_3O_6$ $[M+H]^+$ = 382.1978, measured = 382.1973.

4.2.1.5. Synthesis of cyclic peptide analogues of Sanguinamide A containing a phenyl spacer.

3-(Aminomethyl)benzoic acid (44).

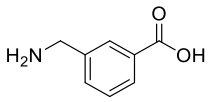

A 100 mL round-bottomed flask under argon atmosphere was charged with 10% Pd/C (0.72 g, 0.68 mmol, 0.10 eq) followed by three evacuation and argon refill cycles. The catalyst was then suspended in MeOH (30 mL) and charged with a solution of 3-cyanobenzoic acid (1.00 g, 6.80 mmol, 1.00 eq) in a minimum amount of MeOH required for complete dissolution followed by three evacuation and H_2 refill cycles. The reaction mixture was charged with 37% HCl (2.00 mL, 20.4 mmol, 3.00 eq) while stirring under H_2. After 16 h, the suspension was filtered using a bed a celite concentrated in vacuo. The intermediate was purified by reverse phase flash column chromatography (0 – 30% MeOH with both eluents containing 0.1% TFA). Yield: 5.36 g (6.05 mmol, 42%) as a white solid**. ^{1}H NMR (700 MHz, DMSO-d_6)** δ 13.10 (s, 1H), 8.55 (s, 2H), 8.09 (s, 1H), 7.93 (d, *J* = 7.8 Hz, 1H), 7.76 (d, *J* = 7.7 Hz, 2H), 7.54 (t, *J* = 7.7 Hz, 1H), 4.09 (s, 2H). **^{1}H NMR (700 MHz, DMSO-d_6)** δ 13.10 (s, 1H), 8.55 (s, 2H), 8.09 (s, 1H), 7.93 (d, *J* = 7.8 Hz, 1H), 7.76 (d, *J* = 7.7 Hz, 2H), 7.54 (t, *J* = 7.7 Hz, 1H), 4.09 (s, 2H). **HRMS (ESI)**: *m/z* calculated for $C_8H_9NO_2$ $[M+H]^+$ = 152.0712, measured = 152.0703.

3-(((((9H-Fluoren-9-yl)methoxy)carbonyl)amino)methyl)benzoic acid (47).

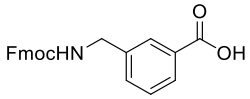

Prepared using the general synthetic method **m** for Fmoc-protection from **44** (0.985 mg, 6.65 mmol, 1.00 eq), Fmoc-OSu (2.64 g, 7.82 mmol, 1.20 eq) and $NaHCO_3$ (1.10 g, 13.0 mmol, 2.00 eq). Yield: 500 mg (13.4 mmol, 21%) as a white solid. **^{1}H NMR (500 MHz, DMSO-d_6)** δ 12.95 (s, 1H), 8.02 – 7.79 (m, 5H), 7.70 (d, *J* = 7.5 Hz, 2H), 7.49 – 7.27 (m, 6H), 4.34 (d, *J* = 7.0 Hz, 2H), 4.29 – 4.08 (m, 3H). **^{13}C NMR (126 MHz, DMSO)** δ = 167.74, 156.82, 144.33, 141.22, 140.81, 132.06, 131.25, 129.05, 128.34, 128.27, 128.09, 127.54, 125.63, 120.60, 65.92, 47.21, 43.95. **HRMS** (ESI): *m/z* calculated for $C_{23}H_{19}NO_4$ $[M+H]^+$ = 374.1387 measured = 374.1387.

3-((((9H-Fluoren-9-yl)methoxy)carbonyl)amino)benzoic acid (48).

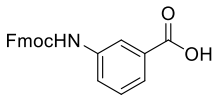

Prepared using the general synthetic method m for Fmoc-protection from 3-aminobenzoic acid (2.00 g, 14.6 mmol, 1.00 eq), $NaHCO_3$ (2.45 g, 29.16 mmol, 2.00 eq) Fmoc-OSu (5.90 g, 17.5 mmol, 1.20 eq). Yield: 3.23 g (8.98 mmol, 62%) as a white solid**. ^{1}H NMR (700 MHz, DMSO-d_6)** δ 12.93 (s, 1H), 9.91 (s, 1H), 8.13 (s, 1H), 7.94 – 7.88 (m, 2H), 7.76 (d, J = 7.5 Hz, 2H), 7.68 (s, 1H), 7.57 (dt, J = 7.7, 1.3 Hz, 1H), 7.43 (t, J = 7.5 Hz, 2H), 7.40 (t, 1H), 7.36 (td, J = 7.4, 1.1 Hz, 2H), 4.50 (d, J = 6.8 Hz, 2H), 4.32 (t, J = 6.7 Hz, 1H). **^{13}C NMR (176 MHz, DMSO)** δ 167.61, 153.89, 153.81, 144.21, 141.28, 139.80, 131.79, 129.48, 128.18, 127.61, 125.62, 123.79, 122.85, 120.68, 119.44, 66.16, 47.07. **LRMS** (ESI): *m/z* calculated for $C_{22}H_{17}NO_4$ $[M+Na]^+$ = Exact Mass: 382.1050, measured = 382.00

2-(3-((((9H-fluoren-9-yl)methoxy)carbonyl)amino)phenyl)acetic acid (49).

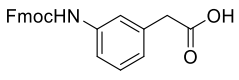

Prepared using the general synthetic method **m** for Fmoc-protection from 2-(3-aminophenyl)acetic acid (570 mg, 3.77 mmol, 1.00 eq), Fmoc-OSu (4.53 g, 4.52 mmol, 1.20 eq) and $NaHCO_3$ (634 mg, 7.54 mmol, 2.00 eq). Yield: 1.35 g (6.62 mmol, 96%) as a white solid. **^{1}H NMR (700 MHz, DMSO-d_6)** δ 9.71 (s, 1H), 7.90 (d, *J* = 7.5 Hz, 2H), 7.75 (d, *J* = 7.5 Hz, 2H), 7.43 (t, *J* = 7.4 Hz, 2H), 7.39 (s, 1H), 7.35 (td, *J* = 7.4, 1.1 Hz, 3H), 7.20 (t, *J* = 8.0 Hz, 1H), 6.88 (d, *J* = 7.5 Hz, 1H), 4.45 (d, *J* = 6.9 Hz, 2H), 4.30 (t, *J* = 6.8 Hz, 1H), 3.49 (s, 2H). **^{13}C NMR (176 MHz, DMSO)** δ 172.65, 153.48, 143.84, 140.86, 139.05, 135.62,

128.71, 127.79, 127.22, 125.23, 123.68, 120.25, 119.24, 118.17, 116.75, 65.67, 46.68.**HRMS (ESI)**: *m/z* calculated for $C_{23}H_{19}NO_4$ $[M+H]^+$ = 374.1387, measured = 374.1386.

4.2.2. Cyclic peptide synthesis

NH_2-Thz(Ile)-Ala-Phe-Pro-Ile-Pro-Rink (E1).

Polystyrene resin with a 2-CTC linker (1.88 g, loading 1.6 mmol/g) was activated according to the general synthetic method **i**, and then loaded with Fmoc-Pro-OH (4.05 g, 12.0 mmol, 4.00 eq.) and DIPEA (4.180 mL, 24.0 mmol, 8.00 eq) in anh. CH_2Cl_2 (10 mL) and according to general synthetic method **j** on a 3.00 mmol scale and shaken for 2 h. The aminoacyl resin was then washed with CH_2Cl_2 (10 mL × 4 × 30 s). The resin was shaken in CH_2Cl_2 /MeOH/ DIPEA (80:15:15, 10 mL). After 30 min, the capped aminoacyl resin was washed with DMF (10 mL × 4 × 30 s), CH_2Cl_2 (10 mL × 4 × 30 s), Et_2O (10 mL × 1 × 1 min) and dried under high vacuum followed by spectroscopic quantification of the actual resin loading by Fmoc release. Synthesis of linear NH_2-Thz(Ile)-Ala-Phe-Pro-Ile-Pro-OH (**E1**) on solid phase was performed according to general synthetic method **a** ending with Fmoc deprotection.

Compound 1.

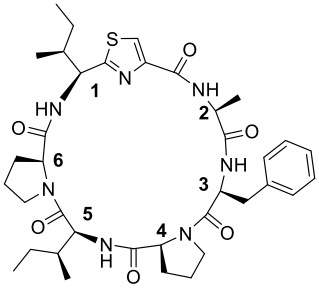

Synthesized according to the method reported by Nielsen and co-workers.[181] A 100 µmol aliquot of peptidyl resin **E1** was shaken with a solution of 4b (43.0 mg, 0.20 mmol, 2.00 eq.), DIPEA (70.0 µL, 402 µmol, 4.02 eq) and PyBOP (104 mg, 200 µmol, 2.00 eq) in DMF (2.00 mL) at room temperature for 16 h. The peptidyl resin was washed with DMF (2.00 mL × 4 × 1 min), CH_2Cl_2 (2.00 mL × 4 × 1 min), and Et_2O (2.00 mL × 1 × 1 min), and then dried under high vacuum. The peptide was cleaved off resin by shaking with a solution of (1:4: TFA: CH_2Cl_2, 4.00 mL) over one hour at room temperature.

The volatiles were removed in vacuo and the residue was dissolved in CH_2Cl_2 (200 mL) followed by the addition of DIPEA (140.0 µL, 804 mmol, 8.04 eq), and PyBOP (104 mg, 200 µmol, 2.00 eq) while stirring. After 16 h, the solvent was removed in vacuo and the residue was dissolved in H_2O/MeCN (1:1, 2.50 mL) and then lyophilized.

The peptide was purified on an Infinity II LC-MS system (Agilent Technologies, USA) equipped with a 125 mm x 21 mm, 5 µm, Macherey-Nagel C18 Gravity column, eluting at 20 mL/min with a binary mixture of MeCN and H_2O with both containing 0.1% TFA using a gradient of 15% - 95% MeCN over 60 min. Yield: 62.0 mg (85.9 µmol, 86%). **HRMS ESI** m/z calculated for $C_{37}H_{51}N_7O_6S$ $[M+H]^+$: 722.3694, measured: 722.3691.

Compound **1** Assigned ^1H and ^{13}C NMR signals in DMSO-d_6

Entry	**Residue**	**Atom**	**δ ^{13}C (ppm)**	**δ ^1H (ppm), mult. (*J* in Hz)**
1.	Ile-1	NH		8.50 (d, *J* = 7.6 Hz, 1H)
2.		αCH	55.04	5.06 (dd, *J* = 7.4, 6.3 Hz, 1H)
3.		βCH	40.40	1.7101
4.		γ1CH_2	24.98	1.11 – 1.03 (m, 1H), 1.42 – 1.35 (m, 1H)
5.		γ2CH_3	14.71	0.69 (d, *J* = 6.8 Hz, 3H)
6.		δCH_3	10.20	0.81 (t, *J* = 7.4 Hz, 3H)
7.	Thz	C=O	159.36	
8.		C2	168.25	
9.		CH(3)	124.21	8.27 (s, 1H)
10.		C4	147.82	
11.	Ala-2	NH	-	8.01 (d, *J* = 7.0 Hz, 1H)
12.		C=O	170.57	-
13.		αCH	48.08	4.65 (p, *J* = 6.5 Hz, 1H)
14.		βCH_3	18.14	1.28 (d, *J* = 6.5 Hz, 3H)
15.	Phe-3	NH	-	9.05 (d, *J* = 1.6 Hz, 1H)
16.		C=O	169.05	-
17.		αCH	53.61	4.15 – 4.10 (m, 1H)
18.		βCH_2	36.79	2.86 – 2.79 (m, 1H), 3.04 (dd, *J* = 12.7, 5.3 Hz, 1H)
19.		γC	135.58	-
20.		δCH_2	129.42	7.26 (t, *J* = 7.3 Hz, 2H)
21.		εCH_2	128.49	7.25 – 7.14 (m, 2H)
22.		ζCH	127.07	7.26 (t, *J* = 7.3 Hz, 1H)
23.	Pro-4	N	-	-
24.		C=O	170.29	-
25.		αCH	59.98	3.42 (under D_2O, 1H)
26.		βCH_2	21.40	1.62 – 1.54 (m, 2H), 1.36 – 1.30 (m, 1H)
27.		γCH_2	29.41	1.98 – 1.93 (m, 1H), 0.66 (dd, *J* = 13.7, 6.1 Hz, 1H)
28.		δCH_2	45.50	3.17 (t, *J* = 9.8 Hz, 1H), 3.35 – 3.28 (m, 1H)
29.	Ile-5	NH	-	9.19 (d, *J* = 8.2 Hz, 2H)
30.		C=O	173.30	-
31.		αCH	55.21	4.28 (t, 1H)

32.		βCH	35.20	2.25 – 2.12 (m, 1H)
33.		γ1CH2	24.50	1.33 – 1.22 (m, 1H), 1.58 (ddt, *J* = 13.3, 10.4, 5.0 Hz, 1H)
34.		γ2CH3	14.86	0.84 (t, *J* = 7.4 Hz, 3H)
35.		δCH3	11.22	0.9388
36.	Pro-6	N	-	-
37.		C=O	169.98	-
38.		αCH	60.31	4.54 (d, *J* = 7.0 Hz, 1H)
39.		βCH_2	25.74	2.38 (dt, *J* = 11.9, 6.3 Hz, 1H), 1.68 – 1.62 (m, 1H)
40.		γCH_2	24.50	1.79 – 1.71 (m, 1H), 1.91 (dd, *J* = 11.9, 6.4 Hz, 1H)
41.		δCH_2	47.57	3.64 (t, *J* = 8.0 Hz, 1H), 3.83 – 3.72 (m, 1H)

Compound **1** VTNMR stacked spectra (DMSO-d_6).

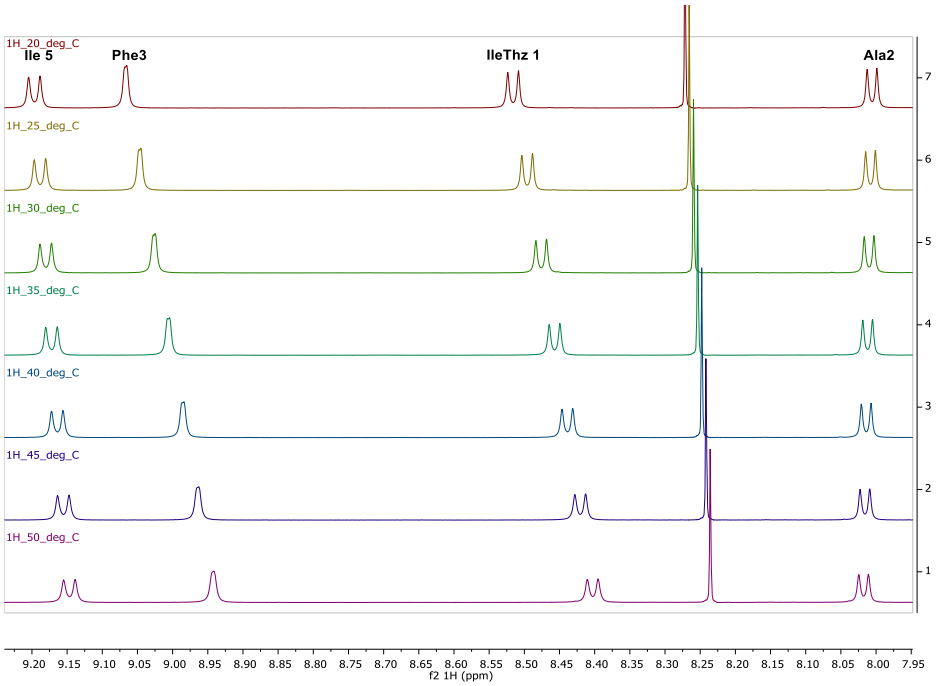

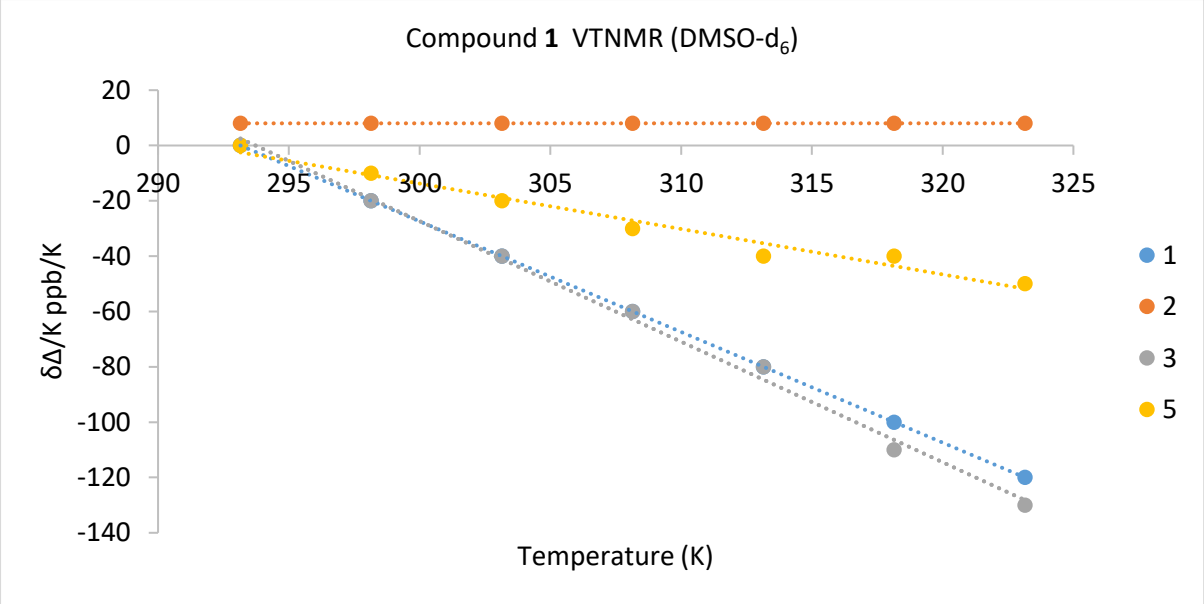

Residue	IleThz-1	Ala-2	Phe-3	Ile-5
$\Delta\delta_{NH}/\Delta T$ (ppb/K)	-4.0	0	-4.3	-1.6

Compound **1** Assigned ^{1}H and ^{13}C NMR signals in $CDCl_3$.

Entry	Residue	Atom	δ ^{13}C (ppm)	δ ^{1}H (ppm), mult. (*J* in Hz)
1.	Ile-1	NH	-	8.70 (d, *J* = 7.4 Hz, 1H)
2.		αCH	55.31	5.02 (t, 1H)
3.		βCH	24.80	1.78 – 1.74 (m, 1H)
4.		γ1CH_2	24.00	1.14 – 1.01 (m, 1H), 1.27 – 1.16 (m, 1H)
5.		γ2CH_3	14.06	0.70 (d, *J* = 6.7 Hz, 3H)
6.		δCH_3	9.38	0.88 – 0.82 (m, 6H)
7.	Thz	C=O	159.47	-
8.		C2	147.47	-
9.		CH(3)	122.18	7.94 (s, 1H)
10.		C4	167.21	-
11.	Ala-2	NH	-	4.71 (p, 1H)
12.		C=O	170.22	-
13.		αCH	48.18	4.71 (p, 1H)
14.		βCH_3	16.96	1.40 (d, *J* = 6.5 Hz, 3H)
15.	Phe-3	NH	-	6.65 (s, 1H)
16.		C=O	170.22	-
17.		αCH	53.54	4.19 – 4.14 (m, 1H)
18.		βCH_2	36.84	2.99 – 2.94 (m, 1H), 3.04 (t, 2H)
19.		γC	133.49	-
20.		δCH_2	128.40	7.10 (d, *J* = 6.7 Hz, 2H)
21.		εCH_2	128.09	7.22 (t, *J* = 7.0 Hz, 2H)

22.		ζCH	126.79	7.21 – 7.17 (m, 1H)
23.	Pro-4	N	-	-
24.		C=O	170.22	-
25.		αCH	59.90	3.34 (d, *J* = 7.8 Hz, 1H)
26.		βCH_2	24.80	1.67 – 1.54 (m, 2H), 1.79 – 1.69 (m, 2H)
27.		γCH_2	29.49	2.04 (s, 1H), 0.88 – 0.82 (m, 7H)
28.		δCH_2	45.45	3.42 – 3.37 (m, 1H), 3.50 – 3.43 (m, 1H)
29.	Ile-5	NH	-	9.17 (d, *J* = 7.5 Hz, 1H)
30.		C=O	173.42	-
31.		αCH	55.45	4.23 – 4.18 (m, 1H)
32.		βCH	34.55	2.25 – 2.17 (m, 1H)
33.		$\gamma 1CH_2$	24.48	1.67 – 1.54 (m, 2H), 1.78 – 1.74 (m, 1H)
34.		$\gamma 2CH_3$	14.17	0.95 (d, *J* = 6.9 Hz, 1H)
35.		δCH_3	10.53	0.88 – 0.82 (m, 6H)
36.	Pro-6	N	-	-
37.		C=O	169.73	-
38.		αCH	60.03	4.63 – 4.59 (m, 1H)
39.		βCH_2	24.88	2.67 – 2.57 (m, 3H)
40.		γCH_2	24.80	1.90 – 1.81 (m, 1H), 1.99 – 1.93 (m, 1H)
41.		δCH_2	47.33	3.55 (t, *J* = 7.9 Hz, 1H), 3.92 (td, *J* = 10.1, 6.7 Hz, 1H)

Compound **1** VTNMR stacked spectra ($CDCl_3$).

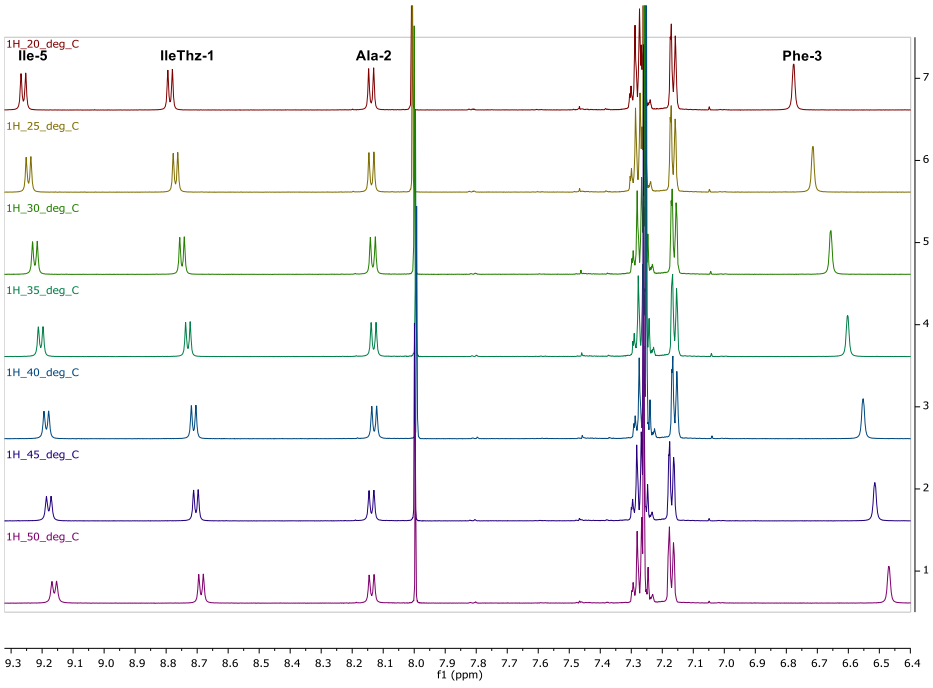

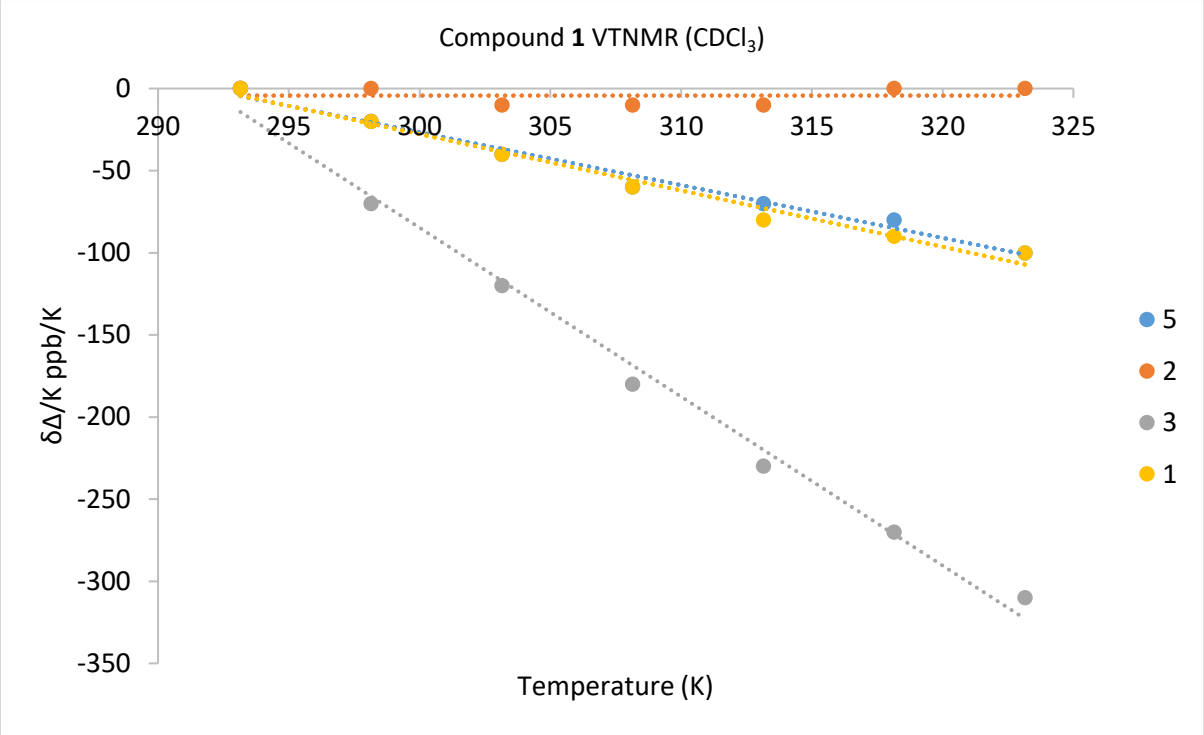

Residue	IleThz-1	Ala-2	Phe-3	Ile-5
$\Delta\delta_{NH}/\Delta T$ (ppb/K)	-3.4	0	-10.3	-3.2

Compound **1** LC Trace

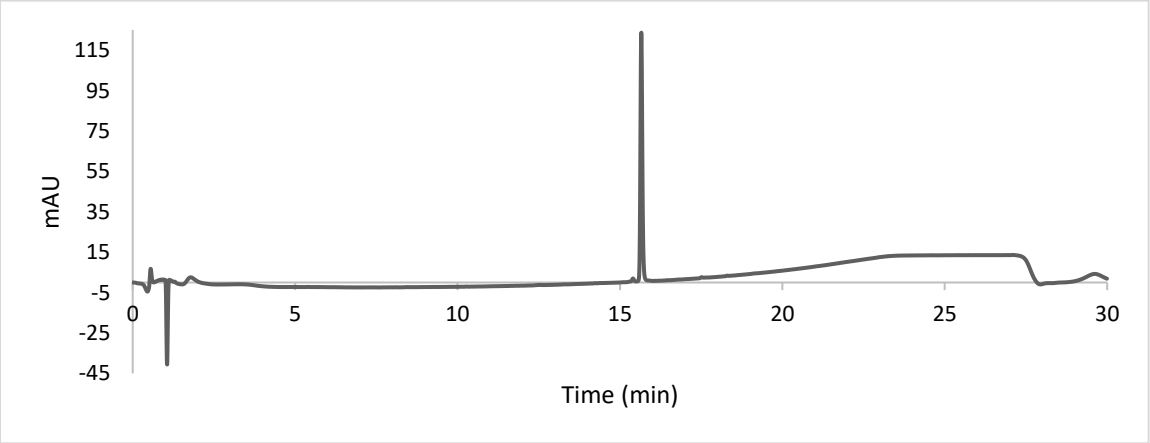

Compound **2**.

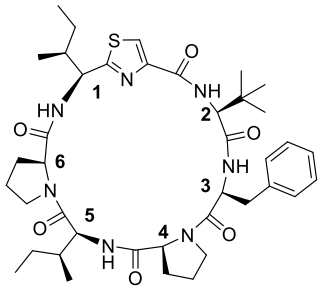

Synthesized according to the method described for compound **1** on a 300 µmol scale using **4b**. Yield: 61.5 mg (80.5 µmol, 28%). **HRMS ESI** m/z calculated for $C_{40}H_{57}N_7O_6S$ $[M+H]^+$: 764.4164, measured: 764.4161.

Compound **2** Assigned ^1H and ^{13}C NMR signals in $CDCl_3$.

	Residue	**Atom**	**δ ^{13}C (ppm)**	**δ ^1H (ppm), mult. (*J* in Hz)**
1.	Ile-1	NH	-	6.67 (d, *J* = 9.1 Hz, 1H)
2.		αCH	53.85	5.51 (dd, *J* = 9.1, 4.5 Hz, 1H)
3.		βCH	40.25	2.05
4.		γ1CH_2	27.48	1.50, 1.22 – 1.14 (m, 1H)
5.		γ2CH_3	14.63	0.94 (d, *J* = 6.7 Hz, 3H)
6.		δCH_3	12.04	1.01
7.	Thz	C=O	171.04	-
8.		C2	150.23	-
9.		CH(3)	123.95	8.07 (s, 1H)
10.		C4	161.84	-
11.	Tle-2	NH	-	7.76 (d, *J* = 9.5 Hz, 1H)
12.		C=O	170.27	-
13.		αCH	60.00	4.55 (d, *J* = 9.5 Hz, 1H)
14.		βC	36.23	-
15.		γ(I-III)CH_3	26.63	1.07 (s, 9H)
16.	Phe-3	NH	-	6.47 (d, 1H)
17.		C=O	169.84	-
18.		αCH	54.42	4.42 – 4.28 (m, 1H)
19.		βCH_2	38.02	3.09 – 3.00 (m, 1H), 2.94 (dd, *J* = 12.3, 4.8 Hz, 1H)
20.		γC	134.95	-
21.		δCH_2	129.58	7.27
22.		εCH_2	129.18	7.26
23.		ζCH	127.85	7.25
24.	Pro-4	N	-	-

25.		C=O	171.30	-
26.		αCH	61.41	3.58 – 3.51 (m, 1H)
27.		βCH_2	21.56	1.70 – 1.59 (m, 1H), 1.47 – 1.40 (m, 1H)
28.		γCH_2	29.49	2.07, 0.59 – 0.42 (m, 1H)
29.		δCH_2	45.84	3.52 – 3.48 (m, 1H)
30.	Ile5	NH	-	9.37 (d, *J* = 8.0 Hz, 1H)
31.		C=O	171.94	-
32.		αCH	56.36	4.20 (dd, *J* = 10.4, 8.0 Hz, 1H)
33.		βCH	35.82	2.30 – 2.23 (m, 1H)
34.		$\gamma 1CH_2$	25.28	1.49, 1.22 – 1.14 (m, 1H)
35.		$\gamma 2CH_3$	14.90	1.00
36.		δCH_3	10.00	0.78 (t, J = 7.4 Hz, 3H)
37.	Pro-6	N	-	-
38.		C=O	172.28	-
39.		αCH	61.66	4.16 (t, *J* = 7.3 Hz, 1H)
40.		βCH_2	29.86	2.17 – 2.14 (m, 1H), 2.14 – 2.09 (m, 1H)
41.		γCH_2	25.59	2.19, 1.99 – 1.92 (m, 1H)
42.		δCH_2	48.20	4.12 – 4.07 (m, 1H), 3.69 – 3.63 (m, 1H)

Compound **2** LC Trace

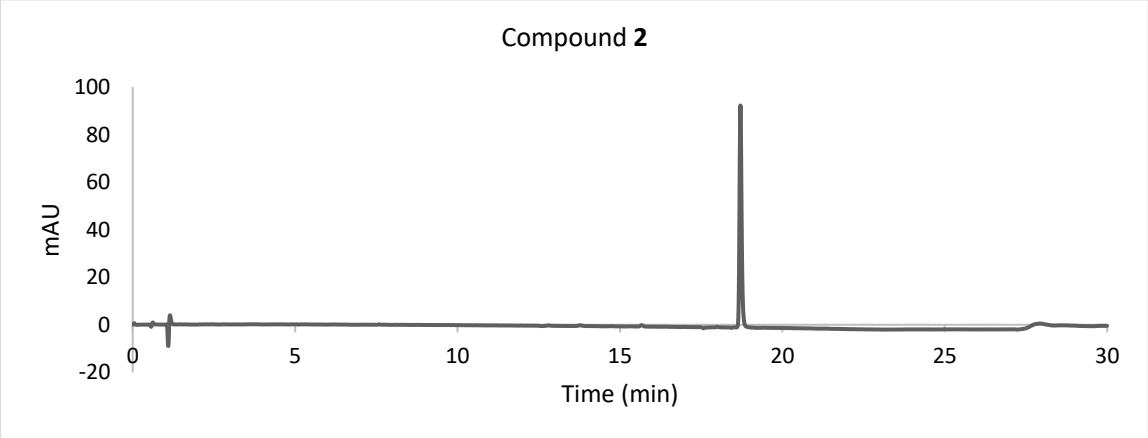

Compound **3.**

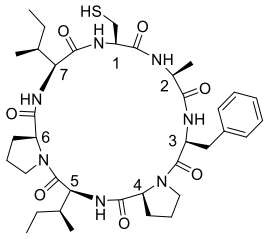

Resin reactivation was performed according to the general synthetic method **i** followed by attachment of the first amino acid according to the general synthetic method **h**. Next, linear peptide synthesis on a 300 µmol scale was performed until the final Fmoc deprotection in accordance to the general synthetic method **a**, to afford the linear heptapeptide NH_2-Ile-Cys-Ala-Phe-Pro-Ile-Pro-OH, on resin. Peptide cleavage was performed by shaking a suspension of the peptidyl resin in HFIP/CH_2Cl_2 (1/4 v/v, 6.00 mL) for 1 h, followed by filtration and concentration under reduced pressure. The resulting oil was suspended in CH_2Cl_2 (600 mL), followed by the addition of PyBOP (2.00 eq) and DIPEA (4.00 eq), and stirred overnight. The reaction mixture was then concentrated in vacuo, and global cleavage was performed according to the general synthetic method **G** followed by precipitation in cold Et_2O (100 mL) and centrifugation. The supernatant was removed, and the pellet was suspended in cold Et_2O (100 mL followed by centrifugation. This procedure was repeated twice, and the pellet was dried under a stream of inert gas, dissolved in H_2O/MeCN (1:1, 2.50 mL) then lyophilized. Purification was performed by preparatory HPLC using the general purification method **D**. Yield: 33.0 mg (0.05 mmol, 42%) **HRMS (ESI)**: *m/z* calculated for $C_{37}H_{55}N_7O_7S$ $[M+H]^+$ = 742.3956, measured = 742.3955.

Compound **3** Assigned ^1H and ^{13}C NMR signals in DMSO-d_6.

	Residue	**Atom**	**δ ^{13}C (ppm)**	**δ ^1H (ppm), mult. (*J* in Hz)**
1.	Cys-1	NH	-	7.59 (d, *J* = 9.0 Hz, 1H)
2.		αCH	56.16	4.36
3.		βCH_2	25.87	2.71 – 2.62 (m, 2H)
4.		γCH_2	39.86	2.42 – 2.36 (m, 1H)
5.	Ala-2	NH	-	7.40 (d, *J* = 5.7 Hz, 1H)
6.		αCH	50.11	4.11
7.		βCH_3	17.23	1.34
8.	Phe-3	NH	-	8.70 (d, *J* = 7.4 Hz, 1H)
9.		αCH	53.31	4.08
10.		βCH_3	37.61	2.99, 2.80
11.		δCH_2	129.19	7.18.
12.		εCH_2	128.44	7.32.
13.		ζCH	127.64	7.27

14.	Pro-4	N	-	-
15.		αCH	60.34	3.35
16.		βCH_2	21.60	1.64, 1.30
17.		γCH_2	29.85	1.90, 0.86
18.		δCH_2	45.83	3.27, 3.17
19.	Ile-5	NH	-	8.56 (d, *J* = 8.6 Hz, 1H)
20.		αCH	54.64	4.33
21.		βCH	34.82	2.05
22.		γ1CH2	24.79	1.44, 1.11.
23.		γ2CH3	15.85	0.91
24.		δCH3	10.89	0.82
25.	Pro-6	N	-	-
26.		αCH	61.61	4.00
27.		βCH_2	24.64	2.15, 1.82.
28.		γCH_2	29.15	2.15, 1.82
29.		δCH_2	47.63	4.00, 3.65.
30.	Ile-7	NH	-	8.06 (d, *J* = 6.6 Hz, 1H)
31.		αCH	59.46	3.65
32.		βCH	34.79	2.11
33.		$\gamma 1CH_2$	23.98	1.54, 1.04.
34.		$\gamma 2CH_3$	14.99	0.88
35.		δCH_3	10.40	0.80

Compound **3** LC Trace

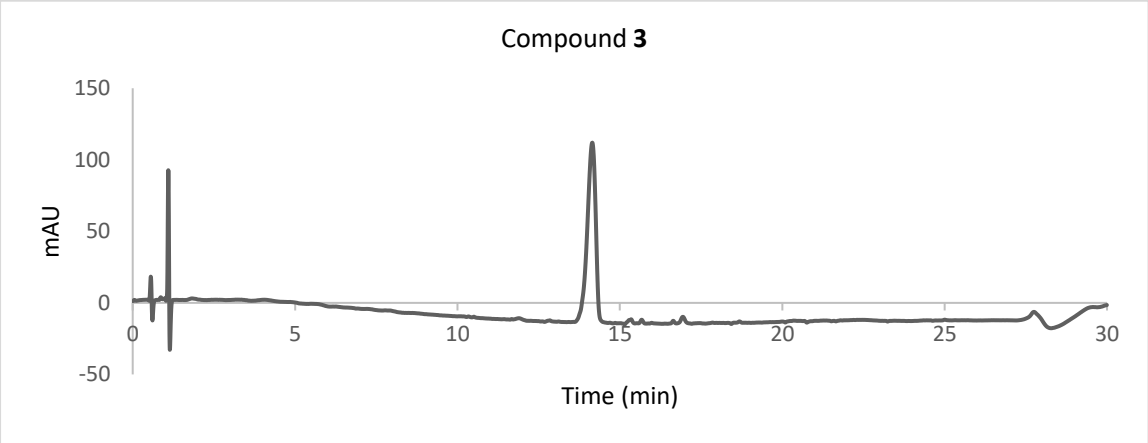

Compound **21**.

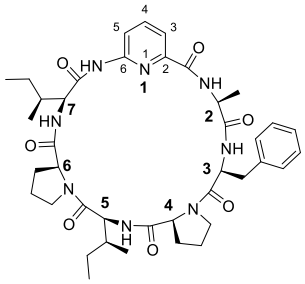

A 300 µmol aliquot of peptidyl resin **E1** was shaken with a solution of **19** (202 mg, 0.60 mmol, 2.00 eq.), DIPEA (210 µL, 1.21 mmol, 4.02 eq) and PyBOP (312 mg, 600 µmol, 2.00 eq) in DMF (6.00 mL) at room temperature for 16 h. The peptidyl resin was washed with DMF (8.00 mL × 4 × 1 min), CH_2Cl_2 (8.00 mL × 4 × 1 min), and Et_2O (8.00 mL × 1 × 1 min), then dried under high vacuum. The peptide was cleaved off resin by shaking with a solution of (1:4: TFA: CH_2Cl_2, 8.00 mL). The volatiles were removed in vacuo and the residue was dissolved in CH_2Cl_2 (600 mL) followed by the addition of DIPEA (520.0 µL, 2.99 mmol, 10.0 eq) and PyBOP (312 mg, 600 µmol, 2.00 eq) while stirring. After 16h, the solvent was removed in vacuo and the residue was dissolved in H_2O/MeCN (1:1, 2.50 mL) and then lyophilized. Purification was then performed using the general method for purification **D**. Yield: 20.2 mg (27.61 µmol 9%) **HRMS (ESI)**: *m/z* calculated for $C_{40}H_{54}N_8O_7$ $[M+H]^+$ = 759.4188, measured = 759.4201

Compound **21** Assigned ^1H and ^{13}C NMR signals in DMSO-d_6.

	Residue	**Atom**	**δ ^{13}C (ppm)**	**δ ^1H (ppm), mult. (*J* in Hz)**
1.	Pyridine-1	NH	-	9.14 (s, 1H)
2.		C=O	162.27	-
3.		C(2)	150.23	-
4.		CH(3)	116.11	8.44 (d, *J* = 8.4 Hz, 1H)
5.		CH(4)	139.93	7.99 (t, *J* = 8.0 Hz, 1H)
6.		CH(5)	117.49	7.79 (d, *J* = 7.4 Hz, 1H)
7.		C(6)	147.49	-
8.	Ala-2	NH	-	8.49 (d, *J* = 6.7 Hz, 1H)
9.		C=O	171.71	-
10.		αCH	47.72	4.60 (p, *J* = 6.6 Hz, 3H)
11.		βCH_3	18.99	1.31 (d, *J* = 6.6 Hz, 3H)
12.	Phe-3	NH	-	7.04 (d, *J* = 5.2 Hz, 1H)
13.		C=O	171.70	-
14.		αCH	52.63	4.67 – 4.62 (m, 1H)
15.		βCH_2	37.00	3.05 – 3.01 (m, 1H), 2.88 – 2.80 (m, 1H)
16.		γC	135.72	-

17.		δCH_2	129.33	7.27
18.		εCH_2	128.49	7.31
19.		ζCH	126.97	7.26
20.	Pro-4	N	-	-
21.		C=O	169.37	-
22.		αCH	60.13	4.02 (d, *J* = 6.8 Hz, 1H)
23.		βCH_2	21.10	1.49, 1.36.
24.		γCH_2	36.95	2.01 – 1.97 (m, 1H), 0.29 – 0.16 (m, 1H)
25.		δCH_2	44.44	3.41, 2.95 – 2.90 (m, 1H)
26.	Ile-5	NH	-	9.35 (d, *J* = 8.6 Hz, 1H)
27.		C=O	173.78	-
28.		αCH	54.90	4.34 (t, *J* = 9.4 Hz, 1H)
29.		βCH	34.09	2.39 – 2.29 (m, 1H)
30.		$\gamma 1CH_2$	24.45	1.96 – 1.90 (m, 1H), 1.42 – 1.39 (m, 1H)
31.		$\gamma 2CH_3$	15.89	0.92 (d, *J* = 6.8 Hz, 3H)
32.		δCH_3	9.90	0.73 (t, *J* = 7.5 Hz, 3H)
33.	Pro-6	N	-	-
34.		C=O	172.10	-
35.		αCH	61.82	4.10
36.		βCH_2	24.45	1.94, 1.84
37.		γCH_2	29.26	2.22 – 2.11 (m, 1H), 1.84
38.		δCH_2	47.50	4.12, 3.96 – 3.90 (m, 1H)
39.	Ile-7	NH	-	7.04 (d, *J* = 5.2 Hz, 1H)
40.		C=O	170.47	-
41.		αCH	59.48	4.09
42.		βCH	35.55	2.07 – 2.02 (m, 1H)
43.		$\gamma 1CH_2$	25.15	1.44 – 1.42 (m, 1H), 1.32
44.		$\gamma 2CH_3$	15.37	0.90 (d, *J* = 6.9 Hz, 3H)
45.		δCH_3	11.85	0.87 (t, *J* = 7.4 Hz, 3H)

Compound **21** VTNMR stacked spectra in DMSO-d_6.

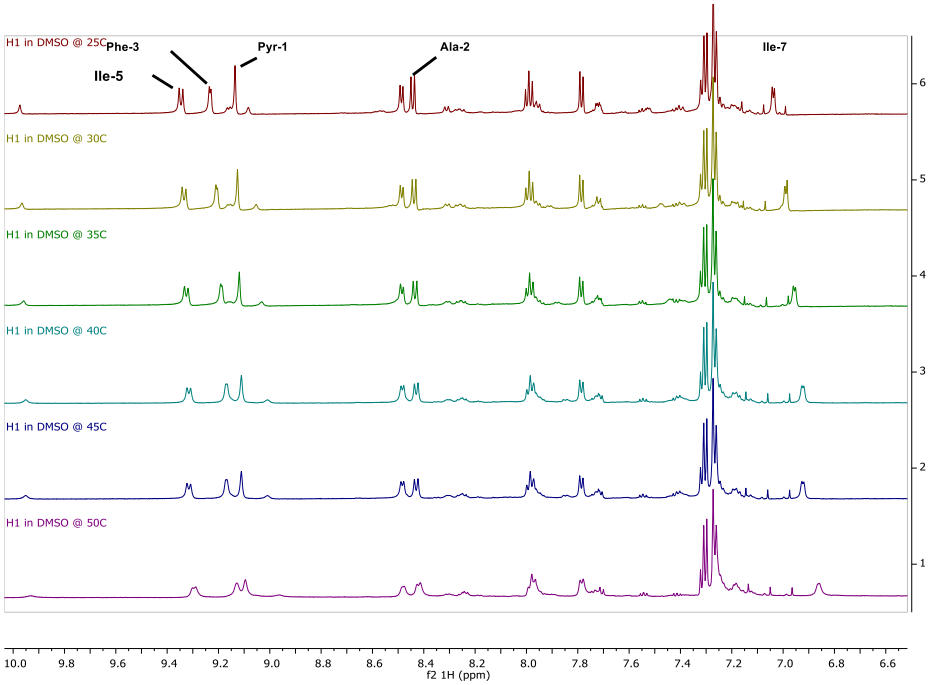

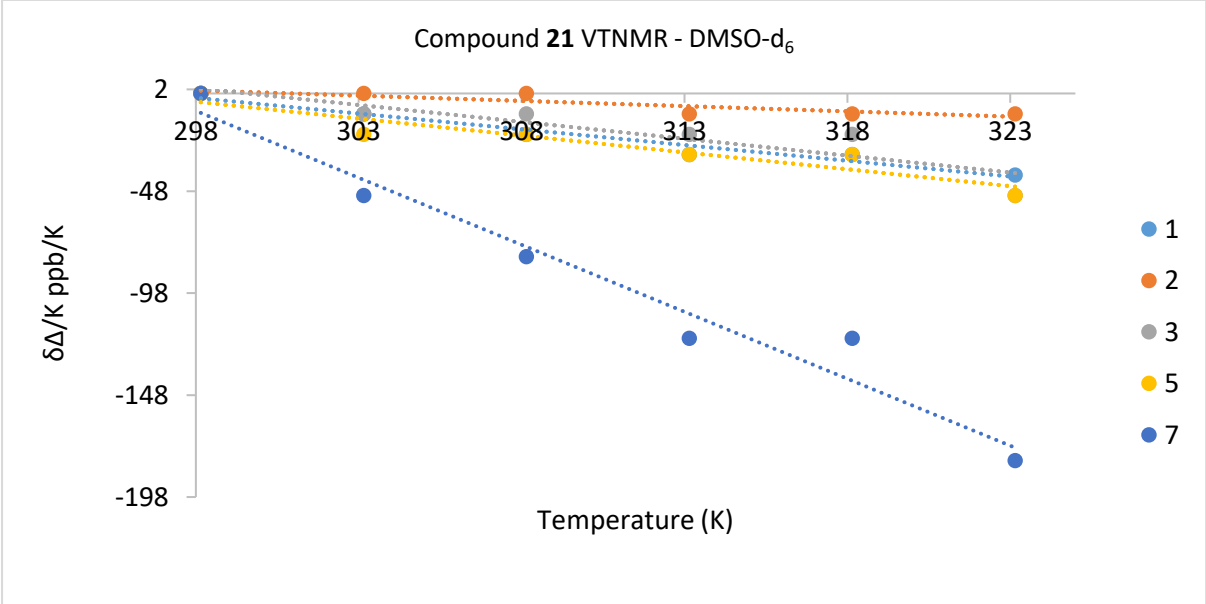

Residue	**Pyr-1**	**Ala-2**	**Phe-3**	**Ile-5**	**Ile 7**
$\Delta\delta_{NH}/\Delta T$ - DMSO-d_6 (ppb/K)	-1.5	-0.5	-1.7	-1.7	-6.6

Compound 21 Assigned ^{1}H and ^{13}C NMR signals in $CDCl_3$.

	Residue	**Atom**	**δ ^{13}C (ppm)**	**δ ^{1}H (ppm), mult. (*J* in Hz)**
1.	Pyridine-1	NH	-	8.87 (s, 1H)
2.		C=O	163.79	-
3.		C(2)	150.40	-

4.		CH(3)	118.64	8.46 (dd, *J* = 8.3, 1.0 Hz, 1H)
5.		CH(4)	139.69	7.83 (t, 1H)
6.		CH(5)	117.78	7.90 (dd, *J* = 7.5, 1.0 Hz, 1H)
7.		C(6)	140.71	-
8.	Ala-2	NH	-	8.58 (d, *J* = 7.8 Hz, 1H)
9.		C=O	172.91	-
10.		αCH	48.82	4.86 (p, *J* = 6.9 Hz, 1H)
11.		βCH_3	19.27	1.47 (d, *J* = 6.7 Hz, 3H)
12.	Phe-3	NH	-	7.34 – 7.24 (m, 4H)
13.		C=O	171.52	-
14.		αCH	54.08	4.60 – 4.52 (m, 3H)
15.		βCH_2	38.07	3.14 – 3.01 (m, 2H)
16.		γC	134.85	-
17.		δCH_2	129.53	7.21 – 7.15 (m, 2H)
18.		εCH_2	129.35	7.34 – 7.24 (m, 4H)
19.		ζCH	128.00	7.34 – 7.24 (m, 4H)
20.	Pro-4	N	-	-
21.		C=O	170.66	-
22.		αCH	61.44	3.72 (t, *J* = 6.5 Hz, 1H)
23.		βCH_2	25.38	1.96 – 1.87 (m, 1H), 2.07 2.11 – 2.03 (m, 1H)
24.		γCH_2	28.79	0.54 – 0.41 (m, 1H), 2.18 – 2.13 (m, 1H)
25.		δCH_2	45.71	3.27 – 3.17 (m, 1H), 3.68 – 3.57 (m, 1H)
26.	Ile-5	NH	-	9.49 (d, *J* = 7.7 Hz, 1H)
27.		C=O	172.91	-
28.		αCH	56.42	4.36 (dd, *J* = 10.7, 7.7 Hz, 1H)
29.		βCH	34.87	2.56 – 2.45 (m, 1H)
30.		γ1CH2	25.25	1.28 – 1.16 (m, 1H) , 1.61 – 1.49 (m, 2H)
31.		γ2CH3	16.50	1.02 (d, *J* = 6.8 Hz, 3H)
32.		δCH3	12.01	0.91 (t, *J* = 7.3 Hz, 3H)
33.	Pro-6	N	-	-
34.		C=O	173.70	-
35.		αCH	62.48	4.60 – 4.52 (m, 3H)
36.		βCH_2	29.77	2.20,2.23
37.		γCH_2	25.04	2.06, 1.96 – 1.87 (m, 1H)
38.		δCH_2	48.81	4.45 – 4.39 (m, 1H), 3.78 – 3.74 (m, 1H),
39.	Ile-7	NH	-	6.43 (d, *J* = 8.4 Hz, 1H)
40.		C=O	170.40	-
41.		αCH	59.18	4.60 – 4.52 (m, 3H)
42.		βCH	36.03	2.29 – 2.19 (m, 1H)
43.		γ1CH2	25.04	1.56, 1.26 – 1.16 (m, 1H)
44.		γ2CH3	16.50	0.97 (d, *J* = 6.8 Hz, 3H)

45.		δCH3	10.21	0.86 (t, *J* = 7.5 Hz, 3H)

Compound **21** VTNMR stacked spectra in $CDCl_3$

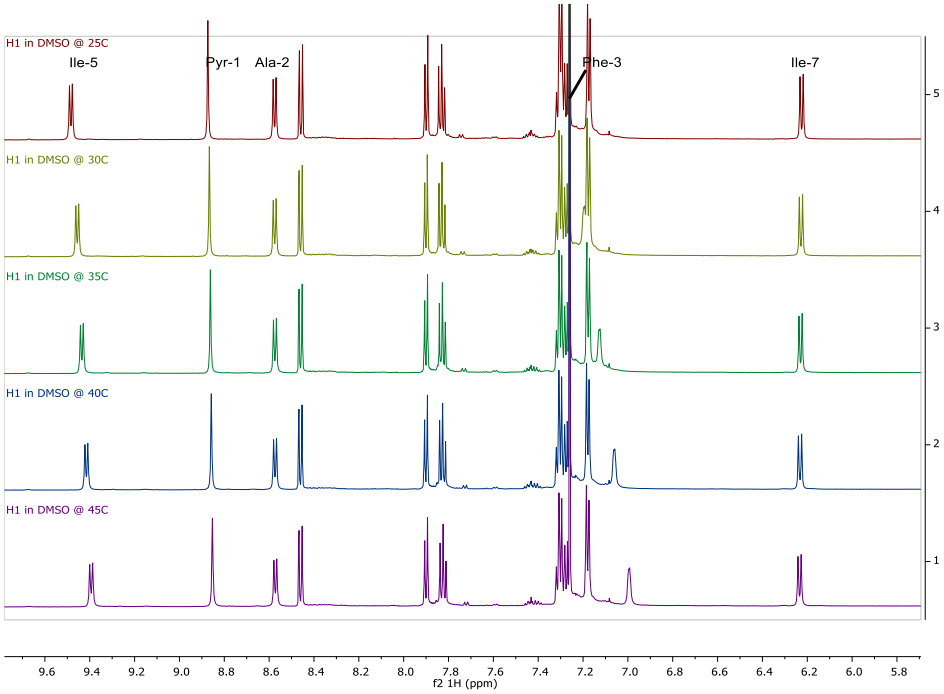

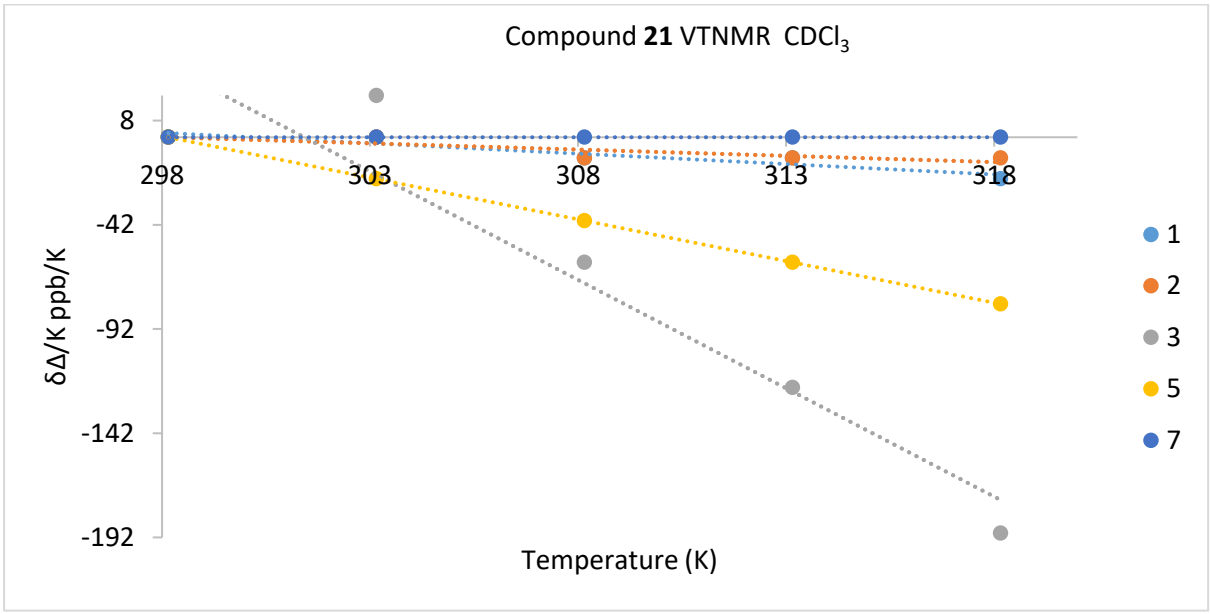

Residue	**Pyr-1**	**Ala-2**	**Phe-3**	**Ile-5**	**Ile 7**
$\Delta\delta_{NH}/\Delta T$ - DMSO-d_6 (ppb/K)	-1.0	-0.6	-10.4	-4.0	0.0

Compound **21** LC Trace

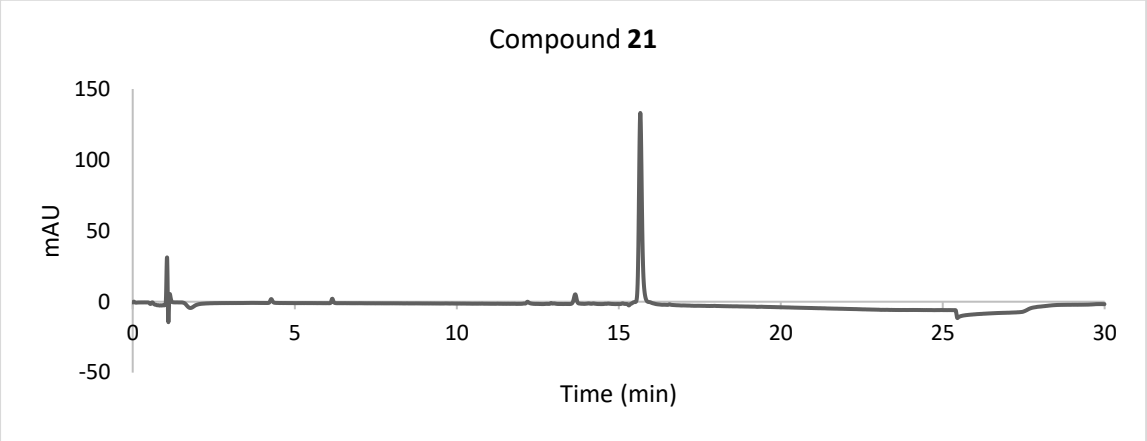

Compound **22**.

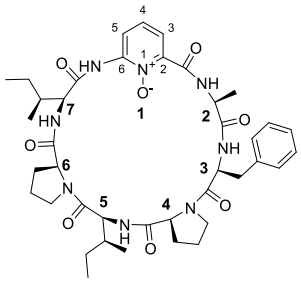

Synthesized according to the method described for compound **21** on a 300 µmol scale using **20** (121 mg, 0.60 mmol, 2.00 eq). Yield: 20.7 mg (26.7 µmol, 9%) **HRMS (ESI)**: *m/z* calculated for $C_{40}H_{54}N_8O_8$ $[M+H]^+$ = 775.4137, measured = 775.4135.

Compound **22** Assigned ^1H and ^{13}C NMR signals in DMSO-d_6.

	Residue	**Atom**	**δ ^{13}C (ppm)**	**δ ^1H (ppm), mult. (*J* in Hz)**
1.	PNO-1	NH	-	10.35 (s, 1H)
2.		C=O	169.84	-
3.		C(2)	143.33	-
4.		CH(3)	115.50	8.52 (dd, *J* = 8.4, 2.0 Hz, 1H)
5.		CH(4)	128.13	7.63 (t, *J* = 8.3 Hz, 1H)
6.		CH(5)	120.37	7.96 (dd, *J* = 8.1, 2.0 Hz, 1H)
7.		C(6)	137.88	-
8.	Ala-2	NH	-	11.81 (d, *J* = 6.9 Hz, 1H)
9.		C=O	171.23	-
10.		αCH	48.26	4.74 – 4.67 (m, 1H)
11.		βCH_3	18.35	1.32 (d, *J* = 6.6 Hz, 3H)
12.	Phe-3	NH	-	9.17 (d, *J* = 2.8 Hz, 1H)

13.		C=O	169.78	-
14.		αCH	53.42	4.33 – 4.22 (m, 1H)
15.		βCH_2	36.50	3.03, 2.93 – 2.77 (m, 1H)
16.		γC	135.54	-
17.		δCH_2	129.43	7.26 – 7.22 (m, 2H)
18.		εCH_2	128.51	7.26 – 7.22 (m, 2H)
19.		ζCH	127.21	7.29 – 7.26 (m, 1H)
20.	Pro-4	N	-	-
21.		C=O	174.21	-
22.		αCH	60.25	3.60 (d, *J* = 7.2 Hz, 1H)
23.		βCH_2	24.69	1.58 – 1.52 (m, 1H), 1.30 – 1.25 (m, 1H
24.		γCH_2	28.19	1.97, 0.55 – 0.39 (m, 1H)
25.		δCH_2	44.86	3.43 – 3.29 (m, 1H), 3.05
26.	Ile-5	NH	-	9.15 (d, *J* = 6.7 Hz, 1H)
27.		αCH	56.08	4.04
28.		βCH	34.27	2.49
29.		γ1CH2	24.93	1.60, 1.22
30.		γ2CH3	15.49	1.06 (d, *J* = 6.8 Hz, 3H)
31.		δCH3	10.31	0.83 (t, *J* = 7.4 Hz, 3H)
32.	Pro-6	N	-	-
33.		C=O	174.21	-
34.		αCH	61.33	4.18 (dd, *J* = 8.6, 5.7 Hz, 1H)
35.		βCH_2	24.68	1.96, 1.87
36.		γCH_2	29.36	2.11,1.86
37.		δCH_2	47.58	4.02, 3.89 – 3.80 (m, 1H)
38.	Ile-7	NH	-	6.83 (d, *J* = 4.7 Hz, 1H)
39.		αCH	60.35	4.10
40.		βCH	35.43	2.08
41.		γ1CH2	25.08	1.42, 1.46 – 1.38 (m, 1H)
42.		γ2CH3	15.33	0.89 (d, *J* = 6.8 Hz, 3H)
43.		δCH3	11.38	0.88 (t, 3H)

Compound **22** VTNMR stacked spectra in DMSO-d_6

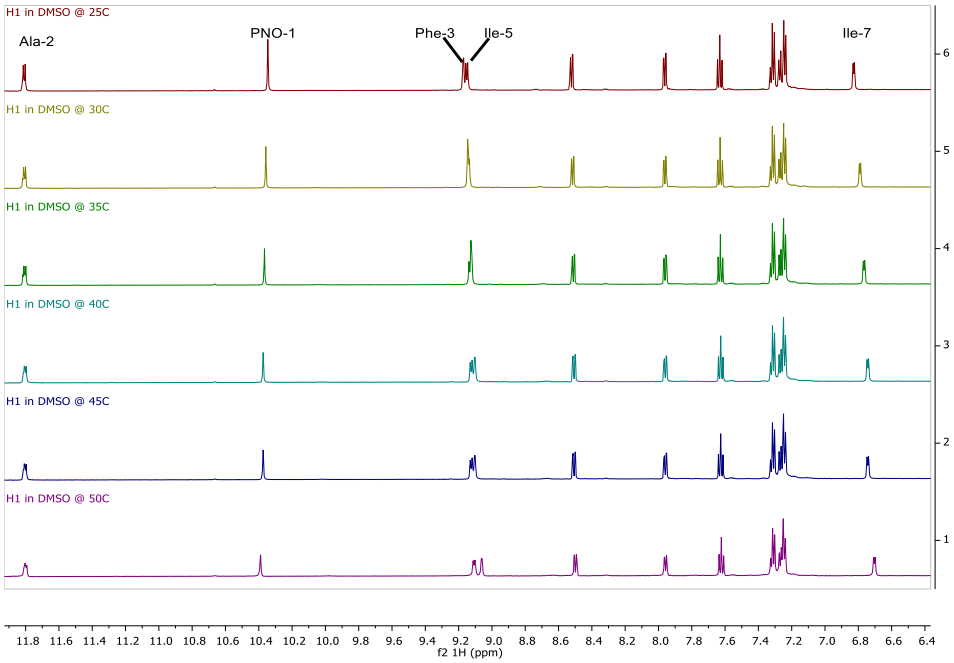

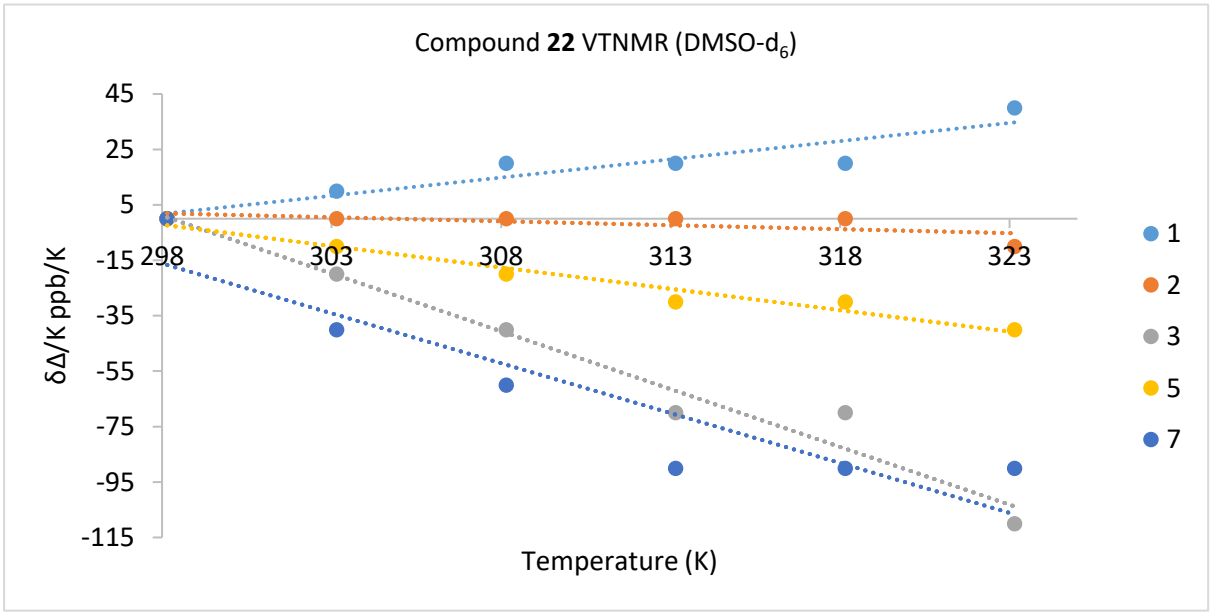

Residue	PNO-1	Ala-2	Phe-3	Ile-5	Ile 7
$\Delta\delta_{NH}/\Delta T$ - DMSO-d_6 (ppb/K)	1.3	-0.3	-4.2	-1.5	-3.6

Compound **22** Assigned ^{1}H and ^{13}C NMR signals in $CDCl_3$

	Residue	**Atom**	**δ ^{13}C (ppm)**	**δ ^{1}H (ppm), mult. (*J* in Hz)**
1.	PNO-1	NH	-	10.65 (s, 1H)
2.		C=O	159.38	-
3.		C(2)	144.02	-
4.		CH(3)	116.47	8.54 (dd, *J* = 8.4, 2.0 Hz, 1H)
5.		CH(4)	127.93	7.44 (t, *J* = 8.2 Hz, 1H)
6.		CH(5)	121.45	8.03 (dd, *J* = 8.1, 2.0 Hz, 1H)
7.		C(6)	138.48	-
8.	Ala-2	NH	-	12.26 (d, *J* = 6.7 Hz, 1H)
9.		C=O	172.32	-
10.		αCH	59.73	4.67 – 4.63 (m, 1H)
11.		βCH_3	18.83	1.52 (d, *J* = 6.6 Hz, 3H)
12.	Phe-3	NH	-	6.48 (d, *J* = 3.4 Hz, 1H)
13.		C=O	170.06	-
14.		αCH	54.34	4.53 – 4.48 (m, 1H)
15.		βCH_2	38.06	3.11 – 2.98 (m, 2H)
16.		γC	134.62	-
17.		δCH_2	129.57	7.30 (dd, *J* = 8.1, 6.5 Hz, 2H)
18.		εCH_2	129.39	7.28 – 7.25 (m, 3H)
19.		ζCH	127.93	7.28 – 7.25 (m, 3H)
20.	Pro-4	N	-	-
21.		C=O	171.28	-
22.		αCH	61.40	3.65 – 3.63 (m, 1H)
23.		βCH_2	29.92	2.17 – 2.12 (m, 2H)
24.		γCH_2	29.42	0.69 – 0.45 (m, 1H), 2.32 – 2.20 (m, 2H)
25.		δCH_2	45.92	3.33 – 3.28 (m, 1H), 3.63 – 3.58 (m, 1H)
26.	Ile-5	NH	-	9.23 (d, *J* = 6.6 Hz, 1H)j
27.		C=O	173.84	-
28.		αCH	57.08	4.16 (dd, *J* = 10.6, 6.6 Hz, 1H)
29.		βCH	35.03	2.72 – 2.56 (m, 1H)
30.		γ1CH2	26.01	1.73 – 1.64 (m, 2H), 1.32 – 1.23 (m, 1H)
31.		γ2CH3	16.62	1.12 (d, *J* = 6.8 Hz, 3H)
32.		δCH3	12.04	0.91 (td, *J* = 7.4, 2.9 Hz, 6H)
33.	Pro-6	N	-	-
34.		C=O	173.07	-
35.		αCH	61.90	4.75 – 4.71 (m, 1H)
36.		βCH_2	21.78	1.73 – 1.64 (m, 2H), 1.50 – 1.45 (m, 1H)
37.		γCH_2	25.56	1.97 – 1.83 (m, 1H), 2.12 – 2.07 (m, 1H)
38.		δCH_2	48.61	4.23 – 4.18 (m, 1H), 3.75 – 3.69 (m, 1H)

39.	Ile-7	NH	-	6.43 (d, *J* = 8.4 Hz, 1H)
40.		C=O	170.37	-
41.		αCH	50.19	4.69 (t, *J* = 6.6 Hz, 1H)
42.		βCH	36.78	2.32 – 2.20 (m, 2H)
43.		γ1CH2	25.16	1.08 – 1.00 (m, 1H), 1.43 – 1.34 (m, 1H)
44.		γ2CH3	16.36	0.98 (d, *J* = 6.9 Hz, 3H)
45.		δCH3	10.46	0.91 (td, *J* = 7.4, 2.9 Hz, 6H)

Compound **22** VTNMR stacked spectra in $CDCl_3$.

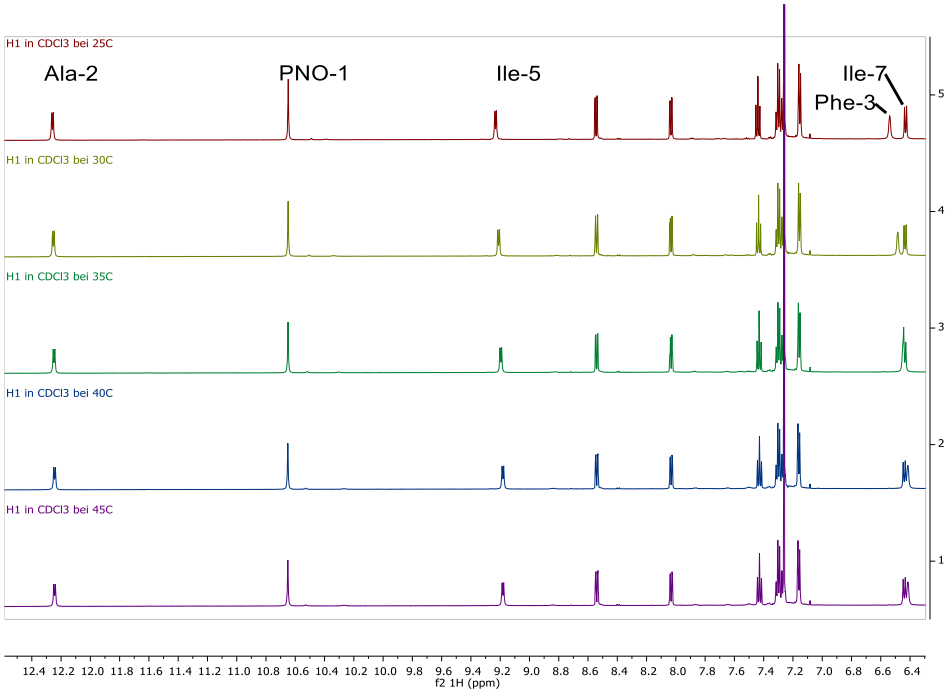

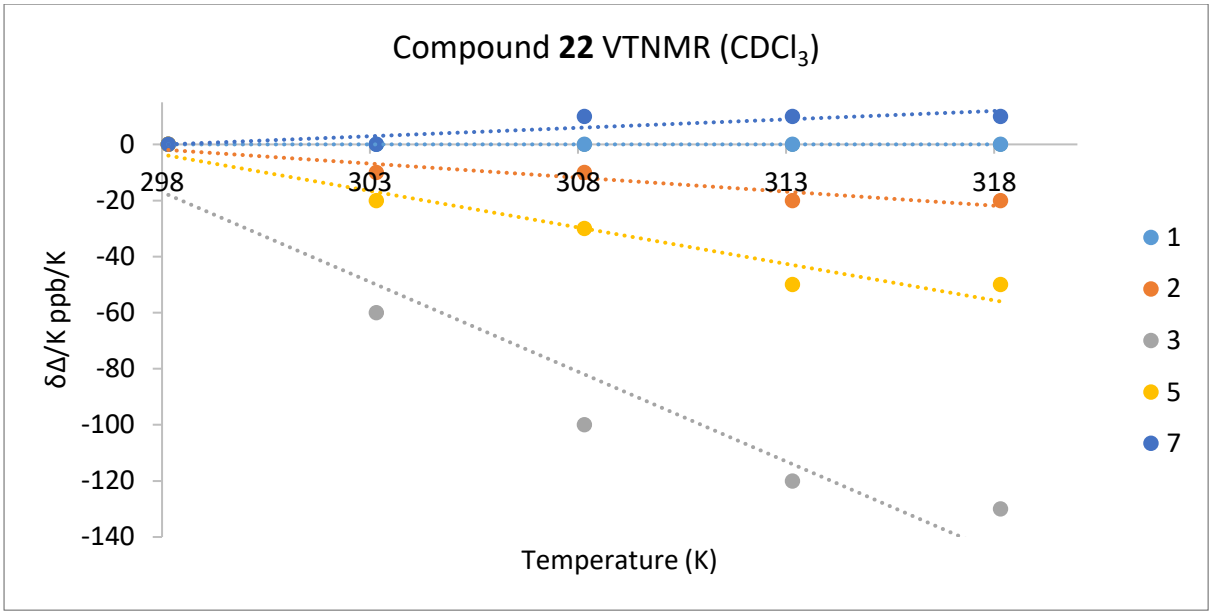

Residue	PNO-1	Ala-2	Phe-3	Ile-5	Ile 7
$\Delta\delta_{NH}/\Delta T$ - $CDCl_3$ (ppb/K)	0	-1	-6.4	-2.6	0.6

Compound **22** LC Trace.

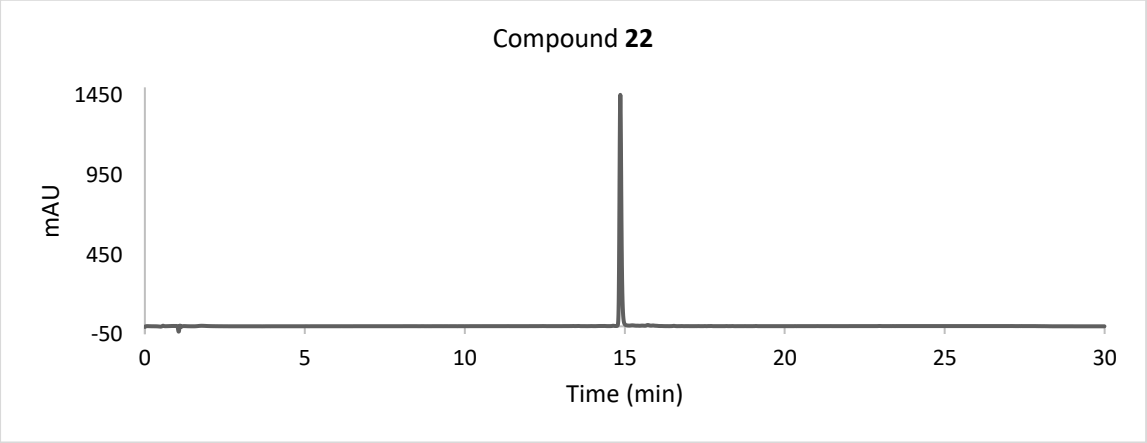

Compound **50**.

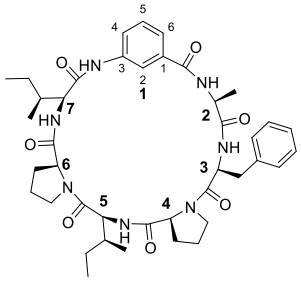

A 300 µmol aliquot of peptidyl resin **E1** was shaken at rt. with a solution of **48** (283 mg, 600 µmol, 2.00 eq), DIPEA (210 µL, 1.20 mmol, 4.00 eq), PyBOP (312 mg, 600 µmol, 2.00 eq) and COMU (128 mg, 300 µmol, 1.0 eq) in DMF (6.00 mL). The peptidyl resin was then washed with DMF (6.00 mL × 2 × 1 min) followed by Fmoc deprotection by shaking with a solution of Piperidine/DMF (1:4, 6.00 mL × 5 min). The deprotection solution was drained, and the peptidyl resin was shaken with a fresh solution of Piperidine/DMF (1:4, 6.00 mL × 10 min). The peptidyl resin was then washed with DMF (6.00 mL × 4 × 1 min) then suspended in a solution of Boc-Ile-OH (278 mg, 1.20 mmol, 4.00 eq), DIPEA (420 µL, 2.41 mmol, 8.04 eq) and PyBOP (624 mg, 1.20 mmol, 4.00 eq) in DMF (6.00 mL) and shaken for 16 h. The peptidyl resin was then washed with DMF (6.00 mL × 2 × 1 min), CH_2Cl_2 (6.00 mL × 2 × 1 min) and Et_2O (6.00 mL × 1 × 1 min), and then dried under high vacuum.

The peptide was cleaved off resin by shaking with a solution of (1:4: TFA: CH_2Cl_2, 6.00 mL). The volatiles were removed in vacuo and the residue was dissolved in CH_2Cl_2 (600 mL) followed by the addition of DIPEA (520 µL, 2.99 mmol, 10.0 eq), and PyBOP (312 mg, 600 µmol, 2.00 eq) while stirring. After 16 h, the solvent was removed in vacuo and the residue was dissolved in H_2O/MeCN (1:1, 2.50 mL) then lyophilized. Purification was then performed using the general method for purification **D**. Yield: 19.6 mg (25.9 µmol, 9%) **HRMS (ESI)**: *m/z* calculated for $C_{41}H_{55}N_7O_7$ $[M+H]^+$ = 758.4236, measured = 758.4235.

Compound **50** Assigned ^1H and ^{13}C NMR signals in DMSO-d_6

Entry	Residue	Atom	δ ^{13}C (ppm)	δ ^1H (ppm), mult. (*J* in Hz)
1.	Phenyl-1	NH	-	9.14 (s, 1H)
2.		C=O	162.33	-
3.		C (1)	150.29	-
4.		CH(2)	128.35	7.27
5.		C(3)	147.56	-
6.		CH(4)	117.55	7.84 – 7.73 (m, 1H)
7.		CH(5)	139.99	7.99 (t, *J* = 8.0 Hz, 1H)

8.		CH(6)	116.17	8.44 (d, *J* = 8.4 Hz, 1H)
9.	Ala-2	NH	-	8.49 (d, *J* = 6.7 Hz, 1H)
10.		C=O	171.57	-
11.		αCH	47.66	1.31 (d, *J* = 6.6 Hz, 3H)
12.		βCH_3	19.05	1.49 (d, *J* = 6.7 Hz, 3H)
13.	Phe-3	NH	-	9.23 (d, *J* = 4.2 Hz, 1H)
14.		C=O	169.39	-
15.		αCH	52.60	4.67 – 4.62 (m, 1H)
16.		βCH_2	37.06	3.06 – 3.00 (m, 2H), 2.88 – 2.82 (m, 1H)
17.		γC	135.78	-
18.		δCH_2	129.35	7.28
19.		εCH_2	128.42	7.31
20.		ζCH	126.84	7.27
21.	Pro-4	N	-	-
22.		C=O	170.53	-
23.		αCH	60.25	4.02 (d, *J* = 6.7 Hz, 1H)
24.		βCH_2	21.18	1.49, 1.37
25.		γCH_2	27.03	2.02 – 1.96 (m, 1H), 0.24 (s, 1H)
26.		δCH_2	44.51	3.41 (dt, *J* = 11.8, 8.7 Hz, 1H), 2.92 (td, *J* = 10.3, 9.8, 5.5 Hz, 1H)
27.	Ile-5	NH	-	9.35 (d, *J* = 8.6 Hz, 1H)
28.		C=O	172.38	-
29.		αCH	54.97	4.35 (t, *J* = 9.4 Hz, 1H)
30.		βCH	34.16	2.36 (d, *J* = 7.1 Hz, 1H)
31.		γ1CH2	25.22	1.42, 1.33
32.		γ2CH3	15.96	0.92 (d, *J* = 6.8 Hz, 3H)
33.		δCH3	9.97	0.73 (t, *J* = 7.4 Hz, 3H)
34.	Pro-6	N	-	-
35.		αCH	61.88	4.10
36.		βCH_2	24.52	1.97 – 1.90 (m, 1H), 1.85
37.		γCH_2	29.43	2.28 – 2.10 (m, 1H), 1.85
38.		δCH_2	47.66	4.12, 3.96 – 3.86 (m, 1H)
39.	Ile-7	NH	-	7.04 (d, *J* = 5.2 Hz, 1H)
40.		αCH	59.55	4.10
41.		βCH	35.62	2.08 – 2.02 (m, 1H)
42.		γ1CH2	23.87	1.42, 1.06 (p, *J* = 14.2, 7.5 Hz, 1H)
43.		γ2CH3	15.44	0.90 (d, *J* = 6.9 Hz, 3H)
44.		δCH3	11.91	0.87 (t, *J* = 7.4 Hz, 3H)
45.	Unassigned	^{13}C NMR (151 MHz, DMSO) δ = 171.15, 169.39.		

Compound **50** VTNMR stacked spectra in DMSO-d_6.

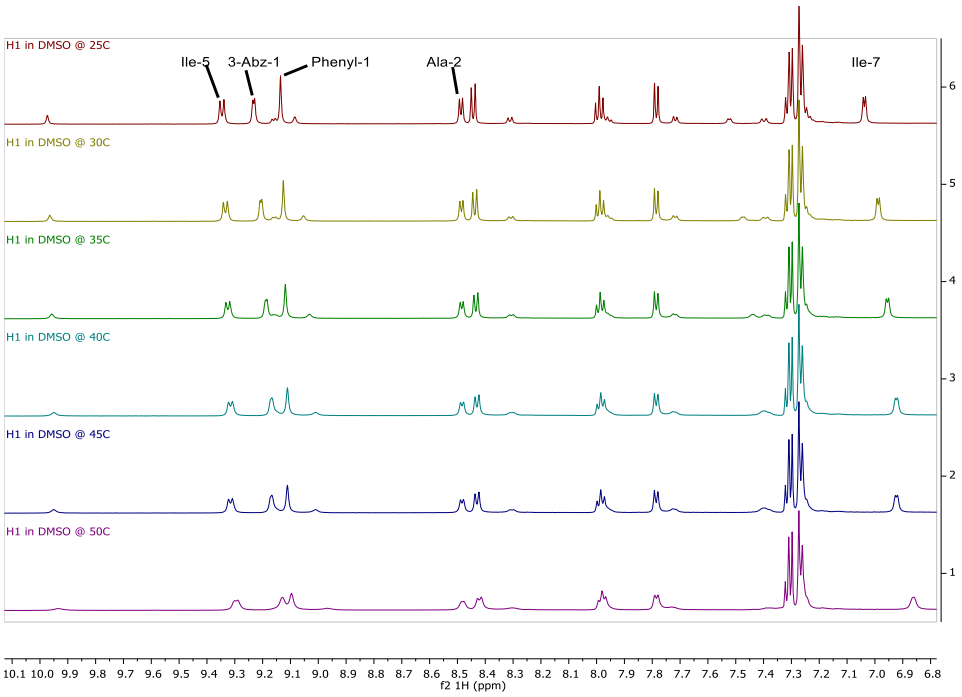

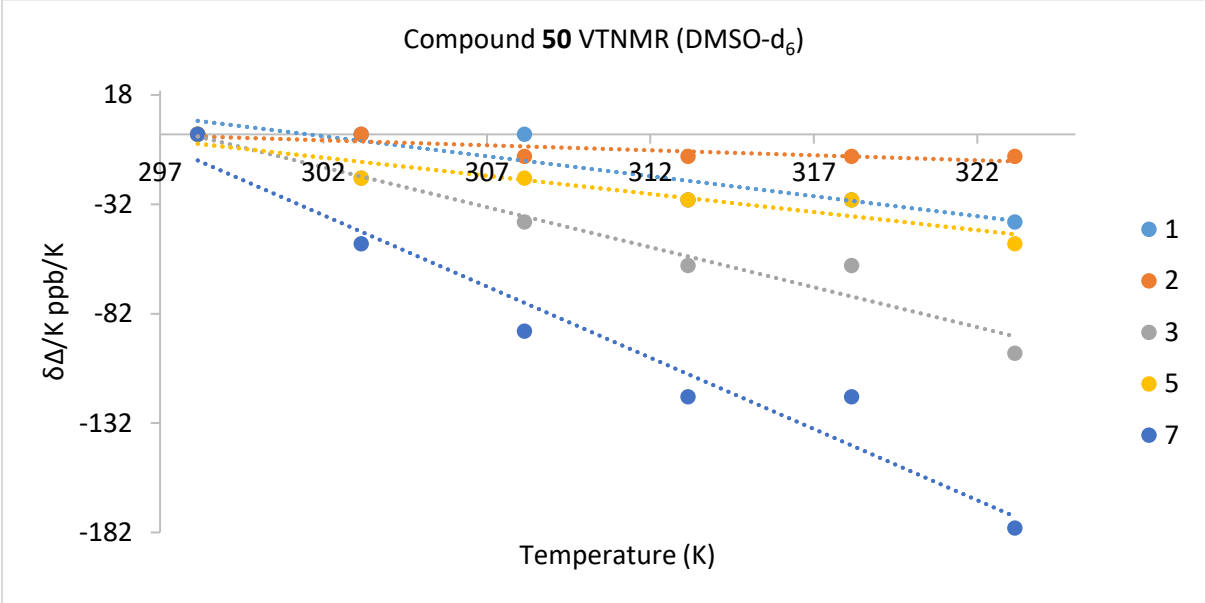

Residue	**3-Abz-1**	**Ala-2**	**Phe-3**	**Ile-5**	**Ile 7**
$\Delta\delta_{NH}/\Delta T$ - DMSO-d_6 (ppb/K)	-1.8	-0.5	-3.7	-1.7	-6.5

Compound **50** Assigned ^{1}H and ^{13}C NMR signals in $CDCl_3$

Entry	**Residue**	**Atom**	**δ ^{13}C (ppm)**	**δ ^{1}H (ppm), mult. (*J* in Hz)**
1.	Phenyl-1	NH	-	8.88 (s, 1H)
2.		C=O	163.61	-
3.		C (1)	150.24	-
4.		CH(2)	127.87	7.27 – 7.25 (m, 2H)

5.		C(3)	147.57	-
6.		CH(4)	118.47	7.90 (dd, *J* = 7.5, 1.0 Hz, 1H)j
7.		CH(5)	139.54	7.83 (t, *J* = 7.9 Hz, 1H)
8.		CH(6)	117.62	8.46 (dd, *J* = 8.4, 1.0 Hz, 1H)
9.	Ala-2	NH	-	8.57 (d, *J* = 7.9 Hz, 1H)
10.		C=O	172.75	-
11.		αCH	48.69	4.89 – 4.79 (m, 1H)
12.		βCH_3	19.14	1.49 (d, *J* = 6.7 Hz, 3H)
13.	Phe-3	NH	-	7.12 (d, *J* = 3.8 Hz, 1H
14.		C=O	170.01	-
15.		αCH	53.90	4.60 – 4.52 (m, 3H)
16.		βCH_2	37.97	3.07 – 3.02 (m, 1H), 3.12 – 3.07 (m, 1H)
17.		γC	134.64	-
18.		δCH_2	129.36	7.18 (d, *J* = 6.7 Hz, 2H)
19.		εCH_2	129.21	7.31 (t, *J* = 7.2 Hz, 2H)
20.		ζCH	117.62	7.27 – 7.25 (m, 2H)
21.	Pro-4	N	-	-
22.		C=O	170.29	-
23.		αCH	61.27	3.73 – 3.70 (m, 1H)
24.		βCH_2	21.59	1.54 – 1.50 (m, 1H), 1.71 – 1.63 (m, 1H)
25.		γCH_2	28.67	0.54 – 0.43 (m, 1H), 2.18 – 2.13 (m, 1H)
26.		δCH_2	45.55	3.26 – 3.18 (m, 1H), 3.67 – 3.57 (m, 1H)
27.	Ile-5	NH	-	9.47 (d, *J* = 7.7 Hz, 1H)
28.		C=O	173.54	-
29.		αCH	56.26	4.36 (dd, *J* = 10.7, 7.8 Hz, 1H)
30.		βCH	34.72	2.59 – 2.43 (m, 1H)
31.		γ1CH2	25.22	1.26 – 1.17 (m, 1H), 1.60 – 1.54 (m, 1H)
32.		γ2CH3	16.35	1.02 (d, *J* = 6.8 Hz, 3H)
33.		δCH3	11.87	0.91 (t, *J* = 7.3 Hz, 3H)
34.	Pro-6	N	-	-
35.		C=O	172.75	-
36.		αCH	62.33	4.60 – 4.52 (m, 3H)
37.		βCH_2	29.61	2.28 – 2.19 (m, 2H)
38.		γCH_2	25.09	1.95 – 1.86 (m, 1H), 2.10 – 2.03 (m, 1H)
39.		δCH_2	48.65	3.78 – 3.73 (m, 1H), 4.45 – 4.39 (m, 1H)
40.	Ile-7	NH	-	6.23 (d, *J* = 8.6 Hz, 1H)
41.		C=O	170.29	-
42.		αCH	59.01	4.60 – 4.52 (m, 3H)
43.		βCH	35.87	2.28 – 2.19 (m, 2H)
44.		γ1CH2	24.89	1.07 – 1.04 (m, 1H), 1.43 – 1.36 (m, 1H)
45.		γ2CH3	16.35	0.98 (d, *J* = 6.8 Hz, 3H)

46.		δCH3	10.06	0.86 (t, *J* = 7.4 Hz, 3H)

Compound **50** VTNMR stacked spectra in $CDCl_3$.

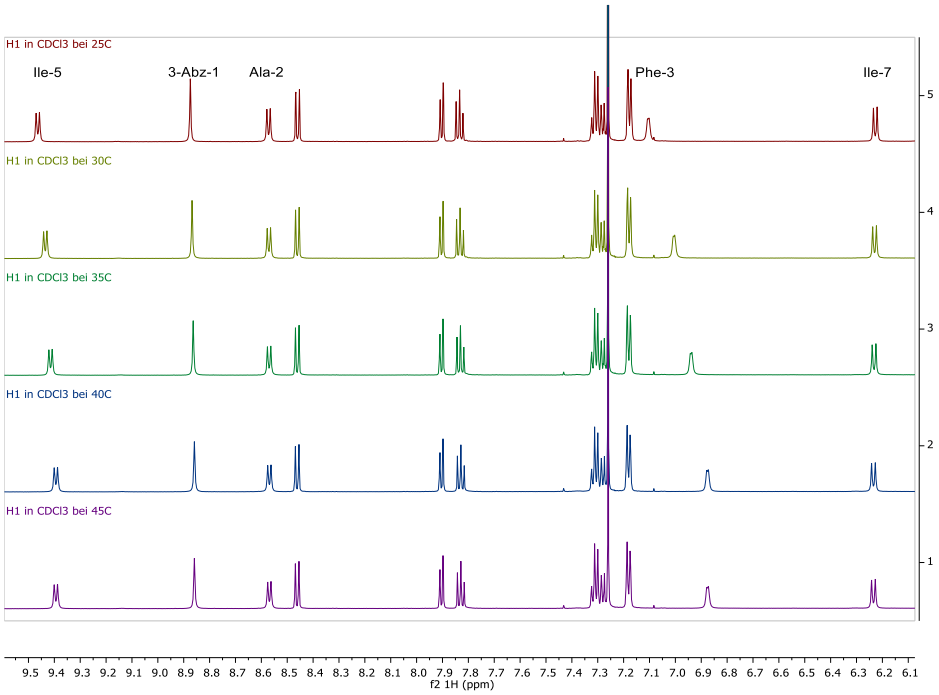

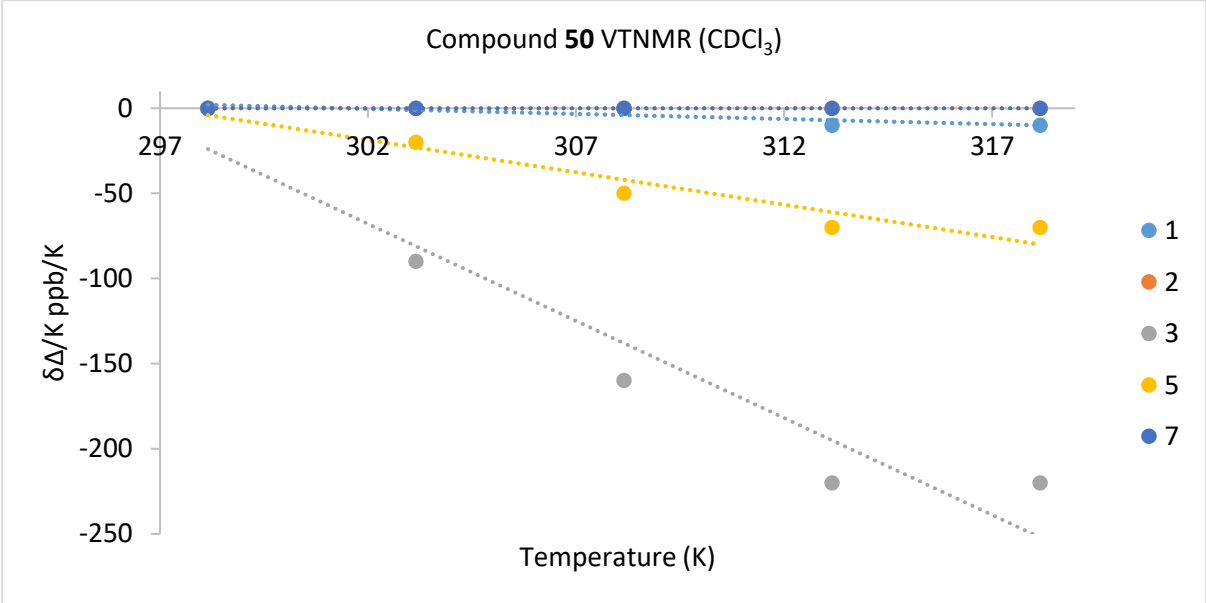

Residue	**3-Abz-1**	**Ala-2**	**Phe-3**	**Ile-5**	**Ile 7**
$\Delta\delta_{NH}/\Delta T$ – $CDCl_3$ (ppb/K)	-0.6	0	-11.4	-.38	0

Compound **50** LC Trace

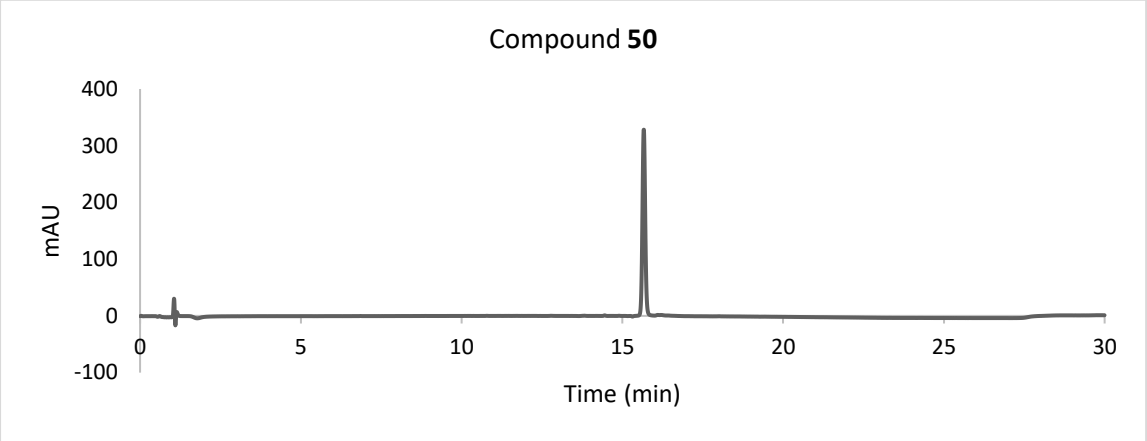

Compound **31**.

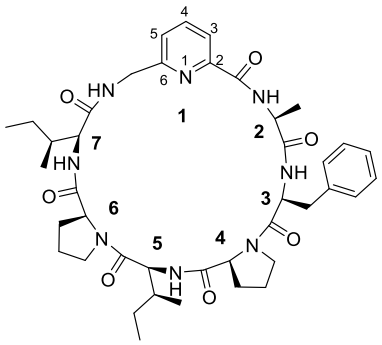

Synthesized according to the method described for compound **21** on a 300 µmol scale using **28**. Yield: 18.6 mg (24.0 µmol, 8%) **HRMS ESI** m/z calculated for $C_{41}H_{56}N_8O_7$ $[M+H]^+$: 773.4345, measured: 773.4344.

Compound **31** Assigned ^1H and ^{13}C NMR signals in $CDCl_3$.

Entry	Residue	Atom	δ ^{13}C (ppm)	δ ^1H (ppm), mult. (*J* in Hz)
1.	Pyridinyl Linker-1	NH	-	7.07 – 7.03 (m, 1H)
2.		C=O	163.79	-
3.		C(2)	155.78	-
4.		CH(3)	121.64	8.14 (d, J = 7.6 Hz, 1H)
5.		CH(4)	138.43	7.87 (t, J = 7.8 Hz, 2H)
6.		CH(5)	125.19	7.41 (d, 1H)
7.		C(6)	148.86	-
8.		CH_2	43.71	4.98 (dd, *J* = 16.7, 7.1 Hz, 1H), 4.37 (dd, *J* = 16.8, 3.5 Hz, 1H)
9.	Ala-2	NH	-	8.22 (d, *J* = 8.0 Hz, 1H)
10.		αCH	48.64	4.79 (p, 1H)

11.		βCH_3	16.31	1.50 (d, *J* = 7.0 Hz, 3H)
12.	Phe-3	NH	-	7.29 (d, J = 3.4 Hz, 1H)
13.		αCH	54.15	4.22 – 4.17 (m, 1H)
14.		βCH_2	43.71	4.38 (d, *J* = 3.5 Hz, 1H), 4.38 (d, *J* = 3.5 Hz, 1H)
15.		γC	135.11	-
16.		δCH_2	129.52	7.31 (d, J = 6.9 Hz, 1H)
17.		εCH_2	129.52	7.16 (d, J = 6.7 Hz, 1H)
18.		ζCH	128.81	7.24
19.	Pro-4	N	-	-
20.		αCH	61.07	3.53 – 3.45 (m, 1H)
21.		βCH_2	22.18	1.72, 1.51
22.		γCH_2	30.95	1.10, 2.07
23.		δCH_2	46.69	3.50 – 3.46 (m, 2H)
24.	Ile-5	NH	-	8.68 (d, *J* = 8.0 Hz, 1H)
25.		αCH	56.08	4.32 (dd, *J* = 10.7, 8.1 Hz, 1H)
26.		βCH	35.28	2.18
27.		γ1CH2	25.13	1.58, 1.16.
28.		γ2CH3	15.97	0.94 (d, J = 6.9 Hz, 3H)
29.		δCH3	12.06	0.91
30.	Pro-6	N	-	-
31.		αCH	61.14	4.71 – 4.65 (m, 1H)
32.		βCH_2	21.78	2.55 – 2.40 (m, 1H), 1.86 – 1.77 (m, 1H)
33.		γCH_2	25.23	2.00, 1.91,
34.		δCH_2	48.64	4.10 – 4.04 (m, 1H),3.66 – 3.55 (m, 1H)
35.	Ile-7	NH	-	7.86
36.		αCH	58.30	4.60(dd, J = 9.4, 3.6 Hz, 1H)
37.		βCH	36.41	2.15
38.		γ1CH2	24.68	1.49 – 1.39 (m, 1H), 1.10
39.		γ2CH3	15.56	0.92 (d, J = 6.5 Hz, 5H)
40.		δCH3	10.27	0.86 (t, *J* = 7.4 Hz, 3H)
41.	Unassigned carbonyl shifts	^{13}C NMR (176 MHz, $CDCl_3$) δ 174.10, 171.95, 171.61, 171.39, 171.18, 170.37		

Compound **31** HPLC trace

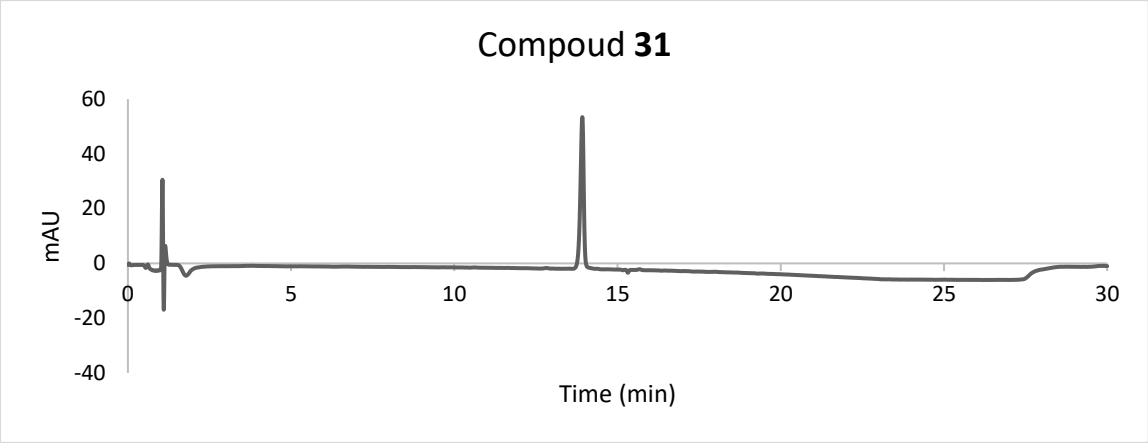

Compound **32.**

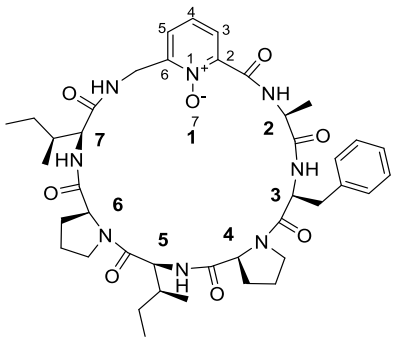

Synthesized according to the method described for compound **21** on a 300 µmol scale using **30**. Yield: 40.4 mg (51.2 µmol, 17%) **HRMS ESI** m/z calculated for $C_{41}H_{56}N_8O_8$ $[M+H]^+$: 789.4294, measured: 789.4293.

Compound **32** Assigned ^1H and ^{13}C NMR signals in DMSO-d_6.

Entry	Residue	Atom	δ ^{13}C (ppm)	δ ^1H (ppm), mult. (*J* in Hz)
1.	PNO Linker-1	NH	-	7.99 (dd, *J* = 8.6, 3.4 Hz, 1H)
2.		C=O	163.79	-
3.		C(2)	158.12	-
4.		CH(3)	128.96	8.19 (dd, J = 8.1, 2.2 Hz, 1H)
5.		CH(4)	128.40	7.55 (t, J = 7.9 Hz, 1H)
6.		CH(5)	125.19	7.71 (dd, *J* = 7.7, 2.2 Hz, 1H)
7.		C(6)	148.12	-
8.		CH_2	39.18	4.68 (dd, *J* = 14.1, 8.7 Hz, 1H), 4.30 (dd, *J* = 14.1, 3.3 Hz, 1H)
9.	Ala-2	NH	-	11.56 (d, *J* = 8.3 Hz, 1H)
10.		αCH	47.75	4.73 (p, 1H)

11.		βCH_3	19.67	1.35 (d, *J* = 6.8 Hz, 3H)
12.	Phe-3	NH	-	8.58 (d, *J* = 5.7 Hz, 1H)
13.		αCH	53.94	4.15 – 4.11 (m, 1H)
14.		βCH_2	35.53	3.12 – 3.02 (m, 1H), 2.88 – 2.78 (m, 1H)
15.		γC	137.15	-
16.		δCH_2	128.96	7.37 – 7.27 (m, 3H)
17.		εCH_2	128.40	7.37 – 7.27 (m, 3H)
18.		ζCH	126.79	7.27 – 7.21 (m, 1H)
19.	Pro-4	N	-	-
20.		αCH	60.61	4.21 – 4.17 (m, 1H)
21.		βCH_2	31.33	2.01, 1.70
22.		24.65	26.43	1.08, 1.41
23.		δCH_2	46.91	3.50 – 3.44 (m, 1H), 3.41 – 3.34 (m, 2H)
24.	Ile-5	NH	-	8.13 (d, *J* = 9.0 Hz, 1H)
25.		αCH	54.83	4.44 (t, 1H)
26.		βCH	34.72	2.26 – 2.17 (m, 1H)
27.		γ1CH2	24.20	1.46, 1.08
28.		γ2CH3	15.68	0.87 (d, *J* = 6.6 Hz, 3H)
29.		δCH3	11.45	0.87
30.	Pro-6	N	-	-
31.		αCH	60.67	4.55 (dd, *J* = 8.4, 3.1 Hz, 1H)
32.		βCH2	21.72	1.74, 1.62
33.		γCH2	26.43	1.15 – 1.11 (m, 1H), 1.62
34.		δCH_2	47.34	3.55 – 3.50 (m, 1H), 3.41 – 3.34 (m, 2H)
35.	Ile-7	NH	-	7.84 (d, *J* = 7.4 Hz, 1H)
36.		αCH	59.06	3.77 (t, *J* = 7.4, 5.5 Hz, 1H)
37.		βCH	35.51	1.81 – 1.74 (m, 1H)
38.		γ1CH2	24.08	1.41, 1.07
39.		γ2CH3	15.62	0.84
40.		δCH3	10.52	0.83
41.	Unassigned C=O shifts	**^{13}C NMR (176 MHz, DMSO)** δ 171.63, 171.57, 170.76, 170.68, 170.06		

Compound **32** HPLC trace.

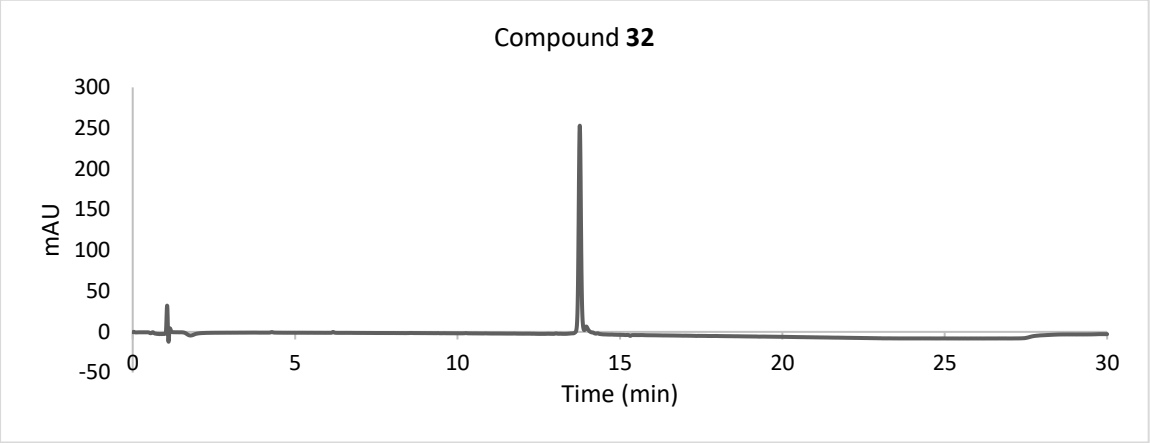

Compound **51**.

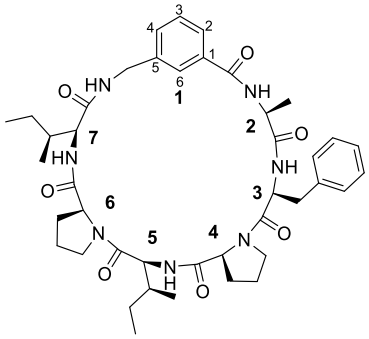

Synthesized according to the method described for compound **50** on a 300 µmol scale using **47**. Yield: 40.4 mg (52.34 mmol, 17%) **HRMS ESI** m/z calculated for $C_{41}H_{56}N_8O_8$ $[M+H]^+$: 789.4294, measured: 789.4293.

Compound **51** Assigned ^1H and ^{13}C NMR signals in DMSO-d_6.

Entry	Residue	Atom	δ ^{13}C (ppm)	δ ^1H (ppm), mult. (*J* in Hz)
1.	Phenyl linker-1	NH	-	8.19 (t, *J* = 6.3 Hz, 1H)
2.		C=O	165.41	-
3.		C(1)	139.63	-
4.		CH(2)	125.84	7.69
5.		CH(3)	127.72	7.39
6.		CH(4)	129.99	7.44
7.		C(5)	139.52	-
8.		CH(6)	125.33	7.91
9.		CH_2	41.40	4.36 – 4.31 (m, 1H), 4.22 – 4.16 (m, 2H)
10.	Ala-2	NH	-	7.73 – 7.70 (m, 1H)
11.		αCH	48.30	4.52

12.		βCH_3	18.71	1.37
13.	Phe-3	NH	-	8.68 (d, *J* = 4.4 Hz, 1H)
14.		αCH	53.96	4.14
15.		βCH_2	36.65	2.96, 2.93
16.		γC	136.41	-
17.		δCH_2	127.48	7.28
18.		εCH_2	129.17	7.26
19.		ζCH	129.10	7.22
20.	Pro-4	N	-	-
21.		αCH	61.06	4.07 – 4.03 (m, 1H)
22.		βCH_2	30.92	1.74, 1.41
23.		γCH2	29.50	2.02, 1.23
24.		δCH_2	47.10	3.66, 3.27
25.	Ile-5	NH	-	8.55 (d, *J* = 8.7 Hz, 1H)
26.		αCH	54.89	4.39 (t, *J* = 9.0 Hz, 1H)
27.		βCH	35.70	1.74
28.		γ1CH2	24.89	1.90, 1.38
29.		γ2CH3	15.11	0.81
30.		δCH3	10.99	0.82
31.	Pro-6	N	-	-
32.		αCH	61.02	4.72
33.		βCH2	26.80	2.27, 2.12
34.		γCH2	24.73	1.93,1.16
35.		δCH_2	47.54	3.74, 3.59
36.	Ile-7	NH	-	7.22
37.		αCH	54.26	4.52
38.		βCH	34.81	1.87
39.		γ1CH2	24.88	1.97, 1.90
40.		γ2CH3	15.47	0.72
41.		δCH3	10.78	0.75
42.	Unassigned Carbonyl C=O	**^{13}C NMR (176 MHz, DMSO)** δ 172.64, 171.23, 170.77, 170.30, 170.22, 169.50		

Compound **51** HPLC trace.

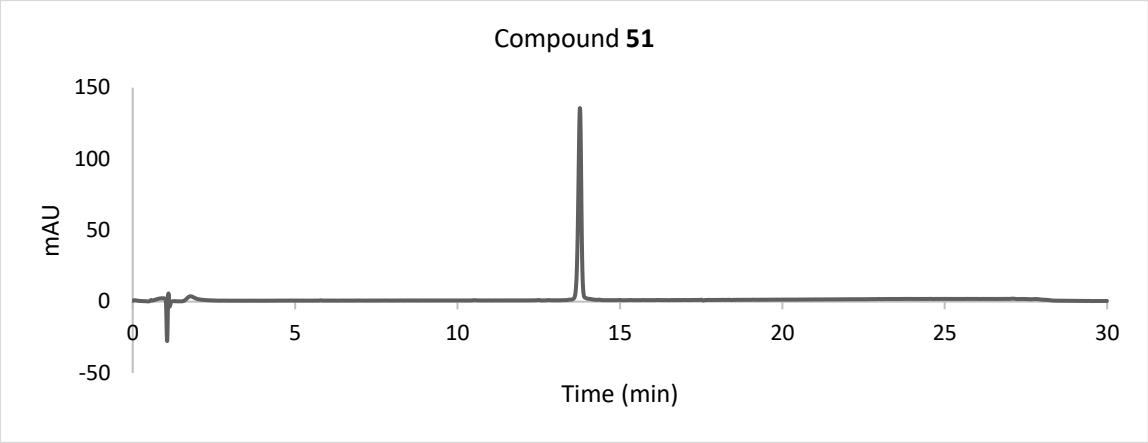

Compound **41**.

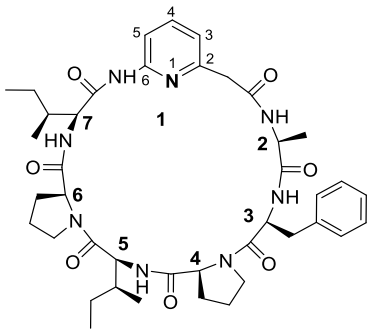

A 200 µmol aliquot of peptidyl resin **E1** was suspended in a solution of **39** (281 mg, 0.80 mmol, 4.00 eq.), DIPEA (350 µL, 2.01 mmol, 10.1 eq) and HATU (304 mg, 0.80 mmol, 4.00 eq) in DMF (4.00 mL). The suspension was heated at 80 °C under microwave irradiation for 1 h. The peptidyl resin was washed with DMF (4.00 mL × 4 × 1 min), CH_2Cl_2 (4.00 mL × 4 × 1 min) and Et_2O (4.00 mL × 1 × 1 min) then dried under high vacuum. The peptide was cleaved off resin by shaking with a solution of (1:4: TFA: CH_2Cl_2, 4.00 mL). The volatiles were removed in vacuo and the residue was dissolved in CH_2Cl_2 (400 mL) followed by the addition of DIPEA (350 µL, 2.01 mmol, 10.1 eq) and PyBOP (208 mg, 400 µmol, 2.00 eq) while stirring. After 16 h, the solvent was removed in vacuo and the residue was dissolved in H_2O/MeCN (1:1, 2.50 mL) then lyophilized. Purification was then performed using the general method for purification **D**. Yield: 17.6 mg (22.8 µmol, 11%) **HRMS ESI** m/z calculated for $C_{41}H_{56}N_8O_7$ $[M+H]^+$: 773.4345, measured: 773.4344.

Compound **41** Assigned ^1H and ^{13}C NMR signals in $CDCl_3$.

	Residue	**Atom**	**δ ^{13}C (ppm)**	**δ ^1H (ppm), mult. (*J* in Hz)**
1.	Pyridine linker-1	NH	-	11.86
2.		CH(3)	121.70	7.41

3.		CH(4)	129.58	7.54
4.		CH(5)	145.55	8.12
5.		CH_2	40.54	4.10, 3.68
6.	Ala-2	NH	-	8.55
7.		αCH	60.17	4.86
8.		βCH_3	16.24	1.3
9.	Phe-3	NH	-	7.22
10.		αCH	52.26	4.68
11.		βCH_2	39.65	3.15, 3.02
12.		γC	137.15	-
13.		δCH_2	128.63	7.26
14.		εCH_2	129.42	7.21
15.		ζCH	127.27	7.21
16.	Pro-4	N	-	-
17.		αCH	61.63	3.43
18.		βCH_2	29.89	2.07, 1.73
19.		γCH_2	30.64	2.09, 1.01
20.		δCH_2	47.27	3.27, 2.73
21.	Ile-5	NH	-	8.78
22.		αCH	53.87	4.35
23.		βCH	37.43	1.96
24.		$\gamma 1CH_2$	24.98	1.55, 1.19
25.		$\gamma 2CH_3$	16.24	0.90
26.		δCH_3	11.55	0.87
27.	Pro-6	N	-	-
28.		αCH	61.13	4.57
29.		βCH_2	32.47	2.40, 2.33
30.		γCH_2	22.36	2.01, 1.74
31.		δCH_2	45.35	4.03, 3.54
32.	Ile-7	NH	-	6.42
33.		αCH	53.95	4.48
34.		βCH	38.25	1.71
35.		$\gamma 1CH_2$	23.75	1.51, 1.02
36.		$\gamma 2CH_3$	15.67	0.87
37.		δCH_3	10.85	0.88

Compound **41** HPLC trace.

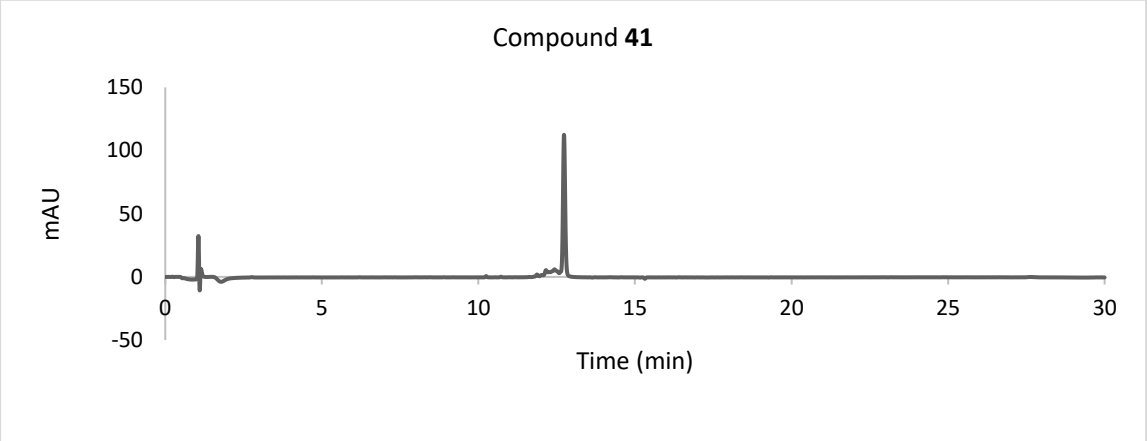

Compound **42**

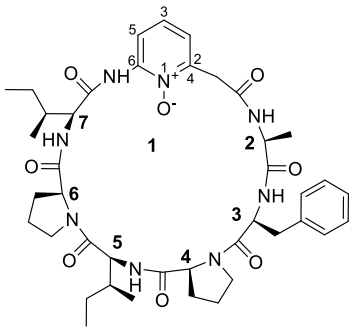

Synthesized according to the method described for compound **41** on a 200 µmol scale using **40**. Yield: 5.44 mg (6.90 µmol, 3%) **HRMS ESI** m/z calculated for $C_{41}H_{56}N_8O_8$ $[M+H]^+$: 789.4294, measured: 789.4292.

Compound **42** Assigned ^1H and ^{13}C NMR signals in $CDCl_3$.

Entry	Residue	Atom	δ ^{13}C (ppm)	δ ^1H (ppm), mult. (*J* in Hz)
1.	PNO linker-1	NH	-	10.84 (s, 1H)
2.		C=O		-
3.		C(2)	144.28	-
4.		CH(3)	120.37	7.13
5.		CH(4)	113.70	8.35
6.		CH(5)	114.20	8.42
7.		C(6)	144.14	
8.		CH_2	40.72	4.35, 4.04
9.	Ala-2	NH	-	9.34
10.		αCH	48.21	4.63 (p, *J* = 7.4 Hz, 1H)
11.		βCH_3	17.76	1.15 (d, *J* = 6.8 Hz, 3H)

12.	Phe-3	NH	-	6.41
13.		αCH	53.64	4.43 – 4.39 (m, 1H)
14.		βCH_2	39.69	3.24, 3.00
15.		γC	134.91	-
16.		δCH_2	129.20	7.31
17.		εCH_2	129.61	7.20
18.		ζCH	127.86	7.16
19.	Pro-4	N	-	-
20.		αCH	61.17	3.60 – 3.57 (m, 1H)
21.		βCH_2	22.09	1.72, 1.52
22.		γCH_2	30.72	2.09, 1.02
23.		δCH_2	46.56	3.60 – 3.57 (m, 1H), 3.46 – 3.36 (m, 1H)
24.	Ile-5	NH	-	8.47 (d, *J* = 7.7 Hz, 1H
25.		αCH	56.10	4.36
26.		βCH	35.34	2.20
27.		$\gamma 1CH_2$	24.73	1.57, 1.15
28.		$\gamma 2CH_3$	16.14	0.94 (d, *J* = 6.8 Hz, 3H)
29.		δCH_3	11.94	0.88 (t, *J* = 7.3 Hz, 3H)
30.	Pro-6	N	-	-
31.		αCH	61.40	4.98 – 4.90 (m, 1H)
32.		βCH_2	48.14	3.62, 3.55
33.		γCH_2	25.21	2.07, 1.97
34.		δCH_2	48.49	4.18, 3.79
35.	Ile-7	NH	-	7.65 (d, *J* = 9.3 Hz, 1H)
36.		αCH	59.20	4.75 (dd, *J* = 9.3, 4.0 Hz, 1H)
37.		βCH	35.34	2.22
38.		$\gamma 1CH_2$	25.20	2.14, 1.85
39.		$\gamma 2CH_3$	15.89	0.91 (d, *J* = 6.9 Hz, 3H)
40.		δCH_3	10.25	0.86 (d, *J* = 7.2 Hz, 5H)
41.	Unassigned C=O region	^{13}C NMR (176 MHz, $CDCl_3$) δ = 173.94, 172.25, 171.74, 171.29, 170.47, 170.37, 168.49		

Compound **42** HPLC trace

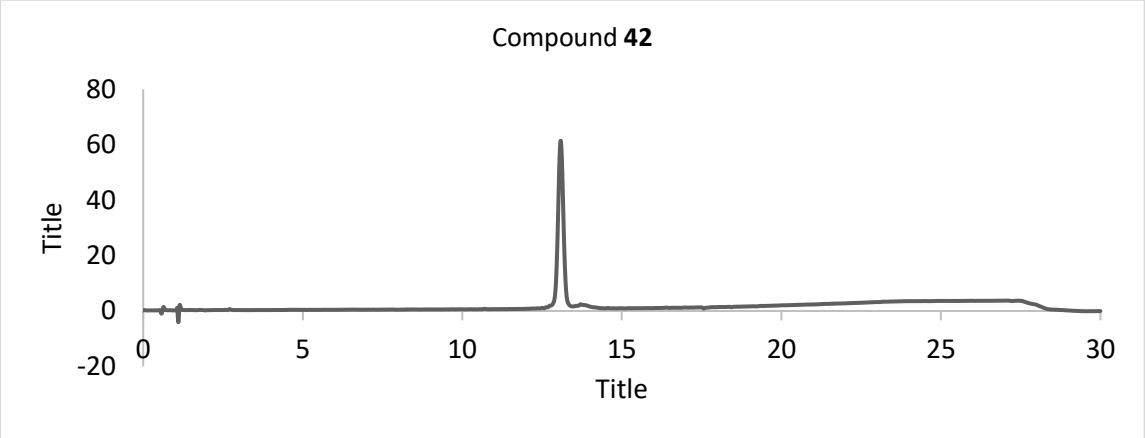

Compound **52**.

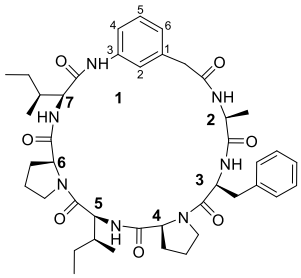

A 200 µmol aliquot of peptidyl resin **E1** was suspended in a solution of **49** (280 mg, 0.80 mmol, 4.00 eq.), DIPEA (304 µL, 0.80 mmol, 4.00 eq) and HATU (304 mg, 0.80 mmol, 4.00 eq) in DMF (4.00 mL). The suspension was heated at 80 °C under microwave irradiation for 1 h. The peptidyl resin was washed with DMF (4.00 mL × 4 × 1 min), then suspended in a solution of Boc-Ile-OH (185 mg, 0.80 mmol, 4.00 eq), DIPEA (280 µL, 1.61 mmol, 8.04 eq) and PyBOP (416 mg, 0.80 mmol, 4.00 eq) in DMF (4.00 mL) and shaken for 16 h. The peptidyl resin was then washed with DMF (4.00 mL × 2 × 1 min), CH_2Cl_2 (4.00 mL × 2 × 1 min) and Et_2O (4.00 mL × 1 × 1 min) then dried under high vacuum.

The peptide was cleaved off resin by shaking with a solution of (1:4: TFA: CH_2Cl_2, 4.00 mL). The volatiles were removed in vacuo and the residue was dissolved in CH_2Cl_2 (200 mL) followed by the addition of DIPEA (350 µL, 2.01 mmol, 10.1 eq), and PyBOP (208 mg, 0.40 mmol, 2.00 eq) while stirring. After 16 h, the solvent was removed in vacuo and the residue was dissolved in H_2O/MeCN (1:1, 2.50 mL) then lyophilized. Purification was then performed using the general method for purification **D**. Yield: 24.0 mg (31.1 µmol, 16%) **HRMS ESI** m/z calculated for $C_{42}H_{57}N_7O_7$ $[M+H]^+$: 772.4392, measured: 772.4391.

Compound **52** Assigned ^{1}H and ^{13}C NMR signals in $CDCl_3$

Entry	Residue	Atom	δ ^{13}C (ppm)	δ ^{1}H (ppm), mult. (*J* in Hz)
1.	Phenyl linker-1	NH	-	8.36
2.		CH(2)	121.38	7.41
3.		CH(4)	120.69	8.01
4.		CH(5)	130.23	7.40
5.		CH(6)	121.40	6.93
6.		CH_2	48.60	4.45, 3.69.
7.	Ala-2	NH	-	5.62 (d, *J* = 8.1 Hz, 1H)
8.		αCH	47.66	4.55
9.		βCH_3	16.50	1.15
10.	Phe-3	NH	-	7.20 (d, *J* = 7.5 Hz, 1H)
11.		αCH	51.94	4.75
12.		βCH_2	39.93	2.92, 2.71
13.		δCH_2	128.27	7.27
14.		εCH_2	129.07	7.30
15.		ζCH	129.22	7.13
16.	Pro-4	N	-	-
17.		αCH	60.73	3.59
18.		βCH_2	22.12	1.64, 1.40
19.		γCH_2	29.28	2.13, 0.65.
20.		δCH_2	45.85	3.56, 3.22
21.	Ile-5	NH	-	9.03 (d, *J* = 6.5 Hz, 1H)
22.		αCH	56.77	4.12
23.		βCH	34.34	2.04
24.		$\gamma 1CH_2$	25.08	1.51, 1.10
25.		$\gamma 2CH_3$	16.27	0.96
26.		δCH_3	12.08	0.95
27.	Pro-6	N	-	-
28.		αCH	62.32	4.57
29.		βCH_2	29.26	2.29, 2.13
30.		γCH_2	25.27	2.02, 1.95
31.		δCH_2	48.57	3.82, 3.69
32.	Ile-7	NH	-	6.14 (d, *J* = 9.7 Hz, 1H)
33.		αCH	58.06	4.57
34.		βCH	35.07	2.45
35.		$\gamma 1CH_2$	24.68	1.39, 0.91
36.		$\gamma 2CH_3$	15.79	0.87 (d, *J* = 6.8 Hz, 3H)
37.		δCH_3	10.06	0.78 (t, *J* = 7.4 Hz, 3H)

Compound **52** LC trace

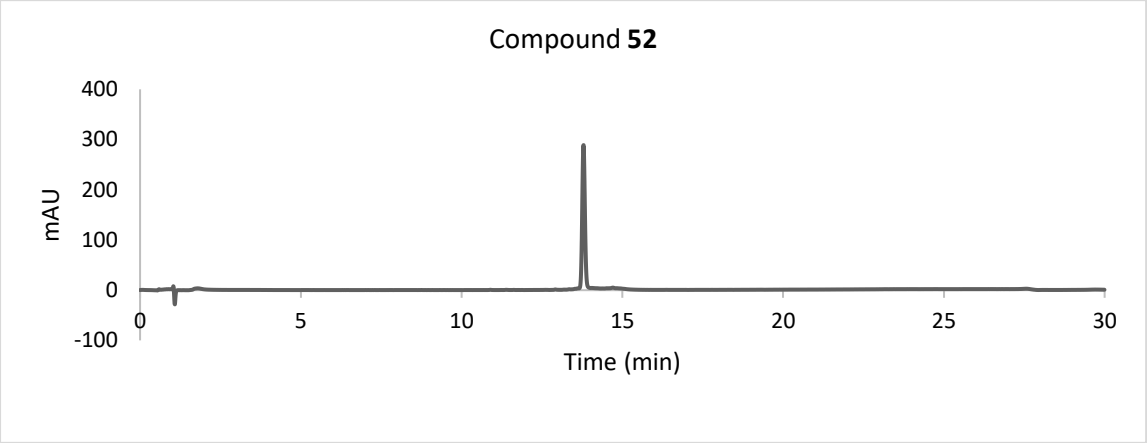

4.3. Solid-Phase Peptide Late Stage Functionalisation (LSF) Using Katritzky Salts via Deaminative C-C Bond Formation

4.3.1. Reagent and amino acid building block synthesis.

2,4,6-Tris(4-methoxyphenyl)pyrylium tetra fluoroborate (5).

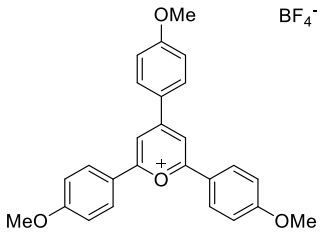

Synthesized according to the method described in literature.[350] A round bottomed flask was charged with p-anisaldehyde (4.00 mL, 32.9 mmol, 1.00 eq) and p-acetylanisole (10.0 g, 66.6 mmol, 2.02 eq). The reaction mixture was cooled to 0 °C followed by the dropwise addition of $BF_3.Et_2O$ (5.00 mL, 40.51 mmol, 1.23 eq) and the reaction temperature was raised to 100 while stirring. After 2 h, the reaction mixture was allowed to cool to room temperature and the resulting crude suspension was diluted with acetone (131 mL) and Et_2O (160 mL) and filtered to obtain an orange-brown solid, which was washed with warm acetone and dried under vacuum to give the title compound. Yield: 3.38 g (6.94 mmol, 21%) as an orange solid.**^{1}H NMR (500 MHz, DMSO-*d*$_6$)**: δ 8.70 (s, 2H), 8.54 (d, *J* = 9.0 Hz, 2H), 8.42 (d, *J* = 9.0 Hz, 4H), 7.23 (d, *J* = 9.1 Hz, 6H), 3.96 (s, 3H), 3.94 (s, 6H). **^{13}C NMR (126 MHz, DMSO)**: δ 167.83, 165.27, 164.51, 161.83, 132.43, 130.68, 124.51, 121.44, 115.35, 110.80, 56.15, 56.03. **HRMS (ESI)**: *m/z* calculated for $C_{26}H_{23}O_4^+$ $[M]^+$ = 399.1591, measured = 399.1580.

7-phenyl-5,6,8,9-tetrahydrodibenzo[c,h]xanthen-14-ium tetra fluoroborate (7).

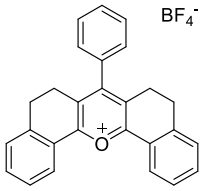

Synthesized according to the method described in literature.[351]

To a bottomed flask containing 3,4-dihydronaphthalen-1(2H)-one (4.00 mL, 32.9 mmol, 1.00 eq) was added benzaldehyde (4.00 mL, 32.9 mmol, 1.00 eq) and methanol (10 mL). The reaction mixture was cooled to 0 °C follwed by the addition of NaOH (5%, 5 eq.). The ice bath was removed and the reaction mixture was stirred at room temperature. The reaction progress was checked by LCMS and upon completion, the methanol was evaporated and the mixture extracted with EtOAc (30 mL × 3), and the

combined organic layers were evaporated in vacuo. An oven dried round bottomed flask was then charged with a solution of the an aliquot of the residue (1.76 g, 7.50 mmol, 1.00 eq) and α-tetralone (0.988 mL, 7.50 mmol, 1.00 eq) in anh. THF (3.80 mL). The resulting solution was cooled in an icebath followed by the dropwise addition of tetrafluoroboric acid diethyl ether complex (1.4 mL, 11.3 mmol, 1.50 eq) while stirring. The reaction temperature was then raised to 85 °C. After 16 h, the reaction mixture was allowed to cool down to room temperture, filtered and the filtrate was washed with Et_2O (50 mL × 3,) and dried under high vacuum to afford the title compound. Yield: 1.82 g (4.06 mmol, 55%) as a yellow solid. **^{1}H NMR (500 MHz, DMSO-d_6)**: δ 8.44 (dd, *J* = 7.9, 1.3 Hz, 2H), 7.76 (td, *J* = 7.5, 1.3 Hz, 2H), 7.73 – 7.60 (m, 5H), 7.55 (d, *J* = 7.6 Hz, 2H), 7.49 – 7.45 (m, 2H), 3.06 (t, *J* = 7.6 Hz, 4H), 2.95 – 2.84 (m, 4H). **^{13}C NMR (126 MHz, DMSO)**: δ 165.08, 164.34, 141.51, 135.28, 132.57, 130.53, 130.16, 129.33, 129.09, 128.45, 127.46, 126.31, 125.71, 25.66, 24.14. **HRMS (ESI)**: *m/z* calculated for $C_{27}H_{21}O^+$ $[M]^+$= 361.1587, measured = 361.1582.

Diethyl 2,6-dimethyl-1,4-dihydropyridine-3,5-dicarboxylate (9).

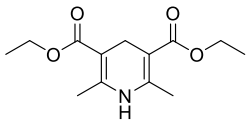

Synthesized according to the method described in literature.[352] A round bottomed flask containing a mixture of ethyl acetoacetate (3.00 mL, 23.72 mmol, 1.00 eq.), ammonium acetate (1.37 g, 17.79 mmol, 0.75 eq.) and formaldehyde (37%, 0.900 mL, 12.09 mmol, 0.510 eq.) was heated to 60°C while stirring. After 16h, the reaction mixture was suspended in a Et_2O/acetone (1:2, 200 mL) filtered and washed with acetone. The residue was dried under vacuum to afford the title compound as a yellow solid. Yield: 2.13 g (8.40 mmol, 69%) as a yellow solid. **^{1}H NMR (700 MHz, DMSO-d_6)**: δ 8.27 (s, 1H), 4.05 (q, *J* = 7.1 Hz, 4H), 3.11 (s, 2H), 2.11 (s, 6H), 1.19 (t, *J* = 7.1 Hz, 6 H**). ^{13}C NMR (176 MHz, DMSO)**: δ 167.03, 146.46, 96.95, 58.84, 24.64, 17.86, 14.34. **HRMS (ESI)**: *m/z* calculated for $C_{13}H_{19}NO_4$ = 253.1314, measured = 253.1262.

(S)-1-(5-((((9H-fluoren-9-yl)methoxy)carbonyl)amino)-5-carboxypentyl)-2,4,6-tris(4-methoxyphenyl)pyridin-1-ium tetra fluoroborate (28).

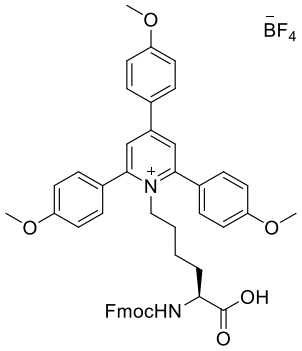

A solution of Boc-Lys-OH (1.55 g, 6.30 mmol, 1.00 eq), Pyrylium **5** (2.98 g, 6.00 mmol, 0.95 eq.) and Trimethylamine (3.34 ml, 24.00 mmol, 3.8 eq.) in EtOH (7 mL) was stirred under microwave irradiation at 80 °C for 1 h. Upon cooling, the resulting yellow solution was transferred to a 100 ml round bottomed flask and the excess solvent was removed in vacuo. LCMS of the crude material showed full conversion. The crude material was treated with 30% TFA/ CH_2Cl_2 (30 mL) and the resulting dark red solution was stirred at room temperature. After 2 h, the excess TFA was blown off under argon followed concentration in vacuo to afford the free amine as a brick red oil. LCMS showed full conversion of the crude material.

A round bottomed flask containing the amine was then charged with saturated $NaHCO_3$ (30 ml) and solution of Fmoc-OSu (2.159 g, 6.4 mmol, 31.02 eq) in dioxane (30 mL) and the pH was adjusted to 8 using saturated $NaHCO_3$. The resulting suspension was stirred at room temperature for 16 h. LCMS analysis of the crude showed full conversion. The reaction mixture was acidified to a pH <3 followed by extraction with CH_2Cl_2 (30 ml × 4). The combined organic fractions were dried over $MgSO_4$, filtered and concentrated in vacuo to obtain the crude product as an orange powder. The crude pyridinium was purified by silica column chromatography (0–10% MeOH in CH_2Cl_2) to afford the amino acid building block as a yellow powder. Yield: 3.2 g (3.84 mmol, 61%) as a yellow solid. **^{1}H NMR (600 MHz, DMSO-d_6) δ** 8.27 (s, 2H), 8.23 (d, *J* = 9.0 Hz, 2H), 7.88 (t, 2H), 7.77 (d, *J* = 8.7 Hz, 4H), 7.64 (t, 2H), 7.45 – 7.36 (m, 2H), 7.32 – 7.25 (m, 2H), 7.21 (d, *J* = 8.8 Hz, 4H), 7.10 (d, *J* = 9.0 Hz, 3H), 4.38 – 4.28 (m, 2H), 4.23 (dd, *J* = 9.2, 5.9 Hz, 1H), 4.20 – 4.11 (m, 1H), 3.86 (s, 3H), 3.85 (s, 6H), 1.39 – 1.26 (m, 2H), 1.26 – 1.18 (m, 1H), 1.17 – 1.07 (m, 1H), 0.77 (p, *J* = 7.7 Hz, 2H). **^{13}C NMR (151 MHz, DMSO) δ** 162.82, 160.98, 155.85, 155.74, 153.11, 143.85, 143.73, 140.71, 140.69, 130.96, 130.56, 128.93, 127.62, 127.60, 127.30, 127.02, 127.00, 125.41, 125.18, 125.12, 124.57, 121.39, 120.13, 120.10, 120.04, 115.02, 114.46, 65.39, 55.67, 55.52, 54.06, 53.62, 46.66, 30.70, 30.04, 28.30, 21.97.**HRMS ESI** m/z calculated for: $C_{47}H_{45}N_2O_7^+$ $[M]^+$: 749.3221, measured: 749.3221.

Compound **29**.

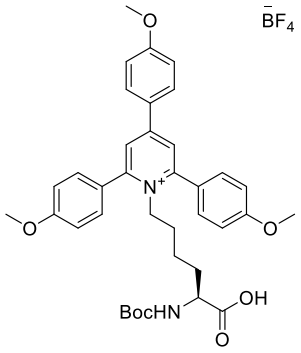

A solution of Boc-Ile-OH (0.369 g, 1.50 mmol, 1.00 eq), **2** (0.720 g, 1.48 mmol, 0.99 eq) and Et_3N (0.900 µL, 6.46mmol, 4.31 eq) in EtOH (7 mL) was heated at 80 °C under microwave irradiation for 1 h. The solvent was removed in vacuo followed by purification by silica column chromatography (0–10% MeOH in CH_2Cl_2) to afford the amino acid building block as a yellow powder. Yield: 968 mg (1.35 mmol, 90%) as a yellow solid. **^{1}H NMR (500 MHz, DMSO-d_6)** δ 12.39 (s, 1H), 8.30 (s, 2H), 8.28 – 8.23 (m, 2H), 7.79 – 7.73 (m, 4H), 7.24 – 7.18 (m, 4H), 7.17 – 7.10 (m, 2H), 6.88 (d, *J* = 8.0 Hz, 1H), 4.33 (tq, *J* = 11.9, 6.1, 5.6 Hz, 2H), 3.88 (s, 6H), 3.87 (s, 3H), 3.56 (ddd, *J* = 9.8, 8.0, 4.8 Hz, 1H), 1.32 (s, 11H), 1.19 – 1.00 (m, 2H), 0.78 (p, *J* = 7.5 Hz, 2H). **^{13}C NMR (126 MHz, DMSO)** δ = 173.85, 162.87, 161.00, 155.84, 155.50, 130.98, 130.63, 125.44, 125.14, 124.59, 115.06, 114.47, 77.97, 55.72, 55.57, 28.17, 22.12. . **HRMS ESI** m/z calculated for $C_{37}H_{43}N_2O_7^+$ $[M]^+$: 627.3065, measured: 627.3068.

Compound **30**.

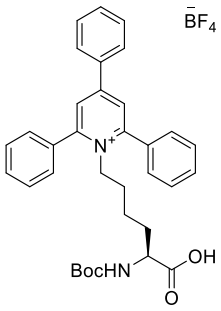

Synthesized according to the method for compound **29** using of Boc-Ile-OH (0.369 g, 1.50 mmol, 1.00 eq), 2,4,6-triphenylpyrylium tetrafluoroborate (0.574 g, 1.45 mmol, 0.98 eq) and Et_3N (0.900 µL, 6.46mmol, 4.31 eq). Yield: 546 mg (0.87 mmol, 58%) as a yellow solid. **^{1}H NMR (500 MHz, DMSO-d_6)** δ 12.37 (s, 1H), 8.48 (s, 2H), 8.29 – 8.23 (m, 2H), 7.86 – 7.80 (m, 4H), 7.71 – 7.68 (m, 6H), 7.66 – 7.64 (m, 1H), 7.61 (dd, *J* = 8.3, 6.5 Hz, 2H), 6.87 (d, *J* = 7.9 Hz, 1H), 4.39 – 4.07 (m, 2H), 3.53 (ddd, *J* = 9.6, 7.9, 4.8 Hz, 1H), 1.33 (s, 12H), 1.13 – 0.95 (m, 2H), 0.75 (p, *J* = 7.5 Hz, 2H**). ^{13}C NMR (126 MHz, DMSO)** δ = 155.97, 133.01, 130.92, 129.61, 129.20, 129.08, 128.72, 126.06, 55.98, 54.15, 29.32, 28.18, 21.87. **HRMS ESI** m/z calculated for $C_{34}H_{37}N_2O_4^+$ $[M]^+$: 537.2748, measured: 537.2747.

Compound **31**.

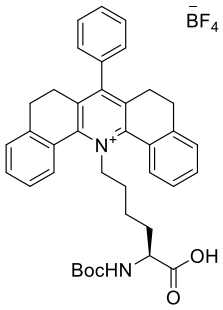

Synthesized according to the method for compound **29** using of Boc-Ile-OH (0.369 g, 1.50 mmol, 1.00 eq), **7** (0.663 g, 1.48 mmol, 0.99 eq) and Et_3N (0.900 µL, 6.46mmol, 4.31 eq). Yield: 530 mg (0.78 mmol, 52%) as a yellow solid. ^{1}H NMR (500 MHz, DMSO-d_6) δ 12.43 (s, 1H), 8.54 – 8.46 (m, 2H), 7.69 (t, *J* = 6.6 Hz, 1H), 7.66 – 7.53 (m, 9H), 7.30 (d, *J* = 5.9 Hz, 1H), 6.94 (d, *J* = 8.1 Hz, 1H), 5.35 (dt, *J* = 14.3, 6.0 Hz, 1H), 5.23 (dt, *J* = 13.9, 6.5 Hz, 1H), 3.60 (td, *J* = 8.4, 4.9 Hz, 1H), 2.98 – 2.76 (m, 4H), 2.69 (d, *J* = 16.1 Hz, 2H), 2.47 – 2.34 (m, 2H), 1.34 (s, 9H), 1.21 (dtd, *J* = 19.0, 11.7, 9.4, 5.8 Hz, 4H), 0.70 – 0.52 (m, 2H). ^{13}C NMR (126 MHz, DMSO) δ = 173.73, 158.05, 157.78, 155.52, 154.69, 141.29, 134.96, 132.61, 129.28, 128.58, 128.26, 127.76, 127.45, 77.99, 64.25, 52.99, 29.73, 29.03, 28.18, 27.08, 26.04, 21.73. **HRMS ESI** m/z calculated for $C_{38}H_{41}N_2O_4^+$ $[M]^+$: 589.3061, measured: 589.3060

4.3.2. Peptide synthesis

Compound **18**.

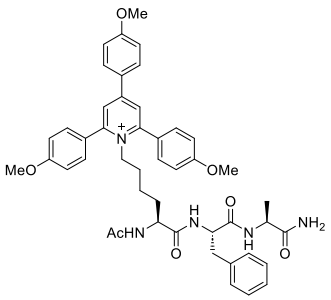

The N-terminal acetylated peptide with an alloc-protected lysine residue was synthesized according to the general methods **2a** a 200 µmol scale. Thereafter, the linear peptide was suspended in anhydrous CH_2Cl_2 (400 µL) followed by the addition of phenylsilane 616 µl; 4.96 mmol; 24.8 eq) and $Pd[(C_6H_5)_3P]_4$ (56.7 mg, 50 µmmol, 0.25 eq) and the suspension was shaken for 1 h followed by removal of the liquid and the addition of fresh reagents. After 1 h, the peptidyl resin was washed with CH_2Cl_2 (400 µL × 4 × 1 min), DMF (400 µL × 4 × 1 min), 0.5% diethyldithiocarbamate in DMF (400 µL × 5 × 5 min), CH_2Cl_2 (400 µL × 4 × 1 min) and DMF (400 µL × 4 × 1 min) and Et_2O (2.00 mL × 1 × 1 min) then

dried under high vacuum. A 10 mL microwave vial containing the peptidyl resin was charged with a solution of pyrylium salt **5** (1.50 eq) in DMF (3.00 mL) and the reaction mixture was heated for 1 h at 80 °C under microwave irradiation. The peptidyl resin was washed with DMF (2.00 mL × 4 × 1 min), CH_2Cl_2 DMF (2.00 mL × 4 × 1 min), and Et_2O (2.00 mL × 1 × 1 min) then dried under high vacuum. The peptidyl resin was cleaved according to general method **2e** and purified by general purification method **C**. Yield: 83.9 mg (107 µmol, 53%). **^{1}H NMR (700 MHz, DMSO-d_6)** δ 8.28 (s, 2H), 8.25 (d, *J* = 9.0 Hz, 2H), 7.86 (d, *J* = 7.5 Hz, 1H), 7.79 – 7.73 (m, 6H), 7.22 (d, *J* = 8.8 Hz, 5H), 7.19 – 7.10 (m, 7H), 6.99 (d, *J* = 2.1 Hz, 1H), 4.41 (ddd, *J* = 9.4, 8.1, 4.6 Hz, 1H), 4.33 – 4.26 (m, 2H), 4.14 (p, *J* = 7.3 Hz, 2H), 3.88 (s, 6H), 3.87 (s, 3H), 3.00 (dd, *J* = 14.0, 4.6 Hz, 1H), 2.73 (dd, *J* = 13.9, 9.4 Hz, 1H), 1.91 (s, 3H), 1.24 (h, *J* = 7.3 Hz, 3H), 1.17 (d, *J* = 7.1 Hz, 3H), 1.06 (td, *J* = 7.9, 7.0, 5.0 Hz, 1H), 0.94 (ddt, *J* = 13.6, 8.4, 4.7 Hz, 1H), 0.66 – 0.52 (m, 2H). **^{13}C NMR (176 MHz, DMSO)** δ = 173.84, 171.14, 170.20, 169.23, 162.79, 160.92, 155.80, 153.06, 137.56, 130.90, 130.51, 129.09, 127.84, 126.09, 125.34, 125.04, 124.48, 114.98, 114.40, 55.61, 55.48, 54.02, 53.44, 52.01, 47.98, 39.92, 39.78, 39.66, 39.54, 39.42, 39.31, 39.19, 39.07, 36.93, 28.33, 21.65, 20.97, 18.17. **HRMS ESI** m/z calculated for $C_{46}H_{52}N_5O_7^+$ $[M]^+$: 786.3861, measured: 786.3861.

Compound **19**.

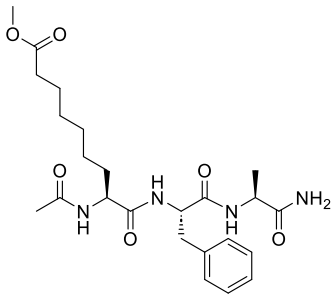

A flame dried reaction vial with a magnetic stirring bar under argon atmosphere was charged with compound **18** (75.0 mg, 1.00 mmol, 1.00 eq) and sealed. The vial was then charged with a solution of Hantzsch ester (75.0 mg; 0.30 mmol; 3.00 eq) in DMA (400 µl) followed by three evacuation-backfill cycles with argon and thereafter, charged with a solution of methyl acrylate (24.0 µL, 0.26 mmol, 2.60 eq) and TEA (56 µL, 0.40 mmol eq) in DMA (300 µl). The vial was irradiated with blue LEDs while stirring. The heat generated by the lamp maintained an ambient temperature of 45 °C. After 16 h, the reaction mixture was purified according to the general purification method **B**. Yield: 10.2 mg (21.4 µmol, 22%). ^{1}H NMR (700 MHz, DMSO-d_6) δ 7.93 (dd, *J* = 7.9, 3.3 Hz, 2H), 7.86 (d, *J* = 7.5 Hz, 1H), 7.23 (h, *J* = 6.0 Hz, 4H), 7.17 (td, *J* = 6.5, 2.1 Hz, 1H), 7.14 – 7.11 (m, 1H), 7.01 – 6.98 (m, 1H), 4.47 (ddd, *J* = 9.5, 8.1, 4.6 Hz, 1H), 4.16 (p, *J* = 7.1 Hz, 1H), 4.10 (td, *J* = 8.1, 5.6 Hz, 1H), 3.58 (s, 3H), 3.05 (dd, *J* = 14.0, 4.6 Hz, 1H), 2.80 (dd, *J* = 14.0, 9.5 Hz, 1H), 2.28 (t, *J* = 7.4 Hz, 2H), 1.81 (s, 3H), 1.49 (dq, *J* = 14.8, 7.5,

6.5 Hz, 3H), 1.39 (tdt, *J* = 12.8, 9.8, 4.2 Hz, 1H), 1.27 – 1.21 (m, 1H), 1.22 – 1.15 (m, 9H). ^{13}C NMR (176 MHz, DMSO) δ = 173.92, 173.37, 171.82, 170.38, 169.42, 137.80, 129.18, 127.98, 126.19, 53.67, 52.83, 51.16, 48.07, 33.24, 31.75, 30.35, 28.42, 28.29, 25.01, 24.37, 22.47, 22.08, 18.25. **HRMS ESI** m/z calculated for $C_{24}H_{36}N_4O_6$ [M+Na]$^+$: 499.2527, measured: 499.2522.

Compound **21**.

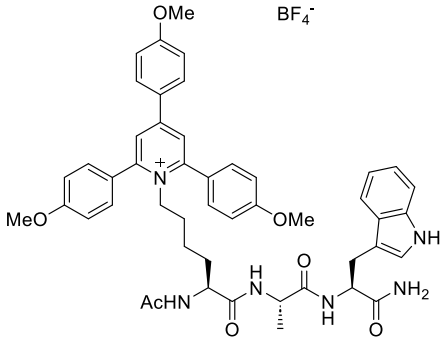

Peptide was synthesized according to the general methods **2a**, **2b**, **2c** on a 300 µmol scale and a 100 µmol aliquot was cleaved according to general method **2e** and purified by general purification method **A**. Yield: 67.4 mg (81.9 µmol, 82%). Synthesized according to the method described for **18.** Yield: 73.9 mg (81.0 µmol, 81%). **^{1}H NMR (700 MHz, DMSO-*d*$_6$)** δ 10.78 (d, *J* = 2.4 Hz, 1H), 8.29 (s, 2H), 8.25 (d, *J* = 9.1 Hz, 2H), 7.89 (d, *J* = 7.0 Hz, 1H), 7.81 (d, *J* = 7.9 Hz, 1H), 7.76 (d, *J* = 8.7 Hz, 4H), 7.69 (d, *J* = 8.0 Hz, 1H), 7.55 (d, *J* = 7.9 Hz, 1H), 7.30 – 7.25 (m, 2H), 7.20 (d, *J* = 8.8 Hz, 4H),7.13 (d, *J* = 9.0 Hz, 2H), 7.09 (d, *J* = 2.3 Hz, 1H), 7.04 – 7.00 (m, 2H), 6.96 – 6.91 (m, 1H), 4.38 (td, *J* = 7.8, 5.8 Hz, 2H), 4.34 (t, *J* = 7.6 Hz, 2H), 4.12 (p, *J* = 7.1 Hz, 1H), 3.97 – 3.93 (m, 1H), 3.87 (s, 3H), 3.86 (s, 6H), 3.08 (dd, *J* = 14.7, 5.5 Hz, 1H), 2.96 (dd, *J* = 14.7, 7.7 Hz, 1H), 1.74 (s, 3H), 1.33 – 1.20 (m, 2H), 1.17 – 1.12 (m, 1H), 1.10 (d, *J* = 7.1 Hz, 3H), 1.01 – 0.94 (m, 1H), 0.77 – 0.63 (m, 2H). **^{13}C NMR (176 MHz, DMSO)** δ 173.00, 171.62, 169.27, 162.79, 160.91, 155.84, 153.06, 135.91, 130.93, 130.52, 127.33, 125.35, 125.04, 124.47, 123.41, 120.69, 118.34, 118.10, 114.97, 109.88, 55.62, 54.11, 53.16, 51.88, 48.33, 30.71, 28.31, 27.49, 22.30, 21.79, 17.69.**HRMS ESI** m/z calculated for $C_{48}H_{53}N_6O_7^+$ [M]$^+$: 825.3970, measured: 825.3929.

Compound **22**.

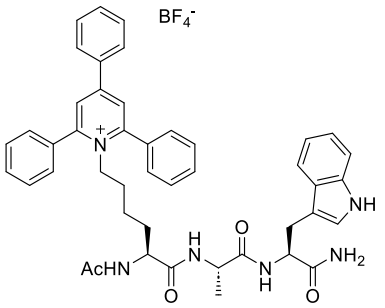

Synthesized according to the method described for **21.** Yield: 67.4 mg (81.9 µmol, 82%). **^{1}H NMR (700 MHz, DMSO-*d*$_6$)** δ 10.79 (d, *J* = 2.4 Hz, 1H), 8.46 (s, 2H), 8.25 (d, *J* = 7.4 Hz, 2H), 7.87 (d, *J* = 7.0 Hz, 1H), 7.84 – 7.80 (m, 4H), 7.79 (d, *J* = 7.9 Hz, 1H), 7.72 (d, *J* = 8.0 Hz, 1H), 7.69 – 7.64 (m, 8H), 7.61 (t, *J* = 7.6 Hz, 3H), 7.56(d, 1H), 7.31 – 7.27 (m, 2H), 7.10 (d, *J* = 2.3 Hz, 1H), 7.02 (m, *J* = 7.1 Hz, 2H), 6.94 (t, *J* = 7.2 Hz, 1H), 4.39 (m, *J* = 7.8, 5.6 Hz, 1H), 4.29 (t, *J* = 7.9 Hz, 2H), 4.13 (p, *J* = 7.1 Hz, 1H), 3.94 – 3.90 (m, 1H), 3.10 (dd, *J* = 14.7, 5.5 Hz, 1H), 2.97 (dd, *J* = 14.7, 7.7 Hz, 1H), 1.75 (s, 3H), 1.46 – 1.26 (m, 2H), 1.11 (d, *J* = 7.1 Hz, 3H), 1.09 – 1.02 (m, 1H), 0.98 – 0.89 (m, 1H), 0.78 – 0.64 (m, 2H). **^{13}C NMR (176 MHz, DMSO)** δ 173.01, 171.64, 171.15, 169.26, 155.95, 154.04, 135.92, 133.04, 132.88, 132.30, 130.82, 129.50, 129.11, 128.98, 128.61, 127.34, 125.97, 123.45, 120.70, 118.36, 118.12, 109.89, 54.23, 53.20, 51.89, 48.32, 39.95, 39.81, 39.70, 39.58, 39.46, 39.34, 39.22, 39.10, 30.53, 28.46, 27.51, 22.35, 21.82, 17.78. **HRMS ESI** m/z calculated for $C_{45}H_{47}N_6O_4^+$ $[M]^+$: 735.3653, measured: 735.3662.

Compound **23**.

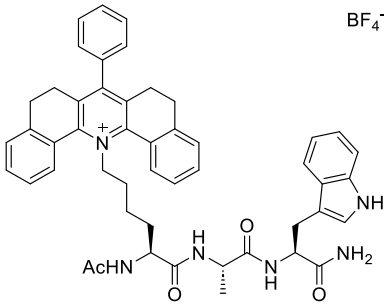

Synthesized according to the method described for **21.** Yield: 59.9 mg (68.5 µmol, 68%). **^{1}H NMR (700 MHz, DMSO-*d*$_6$)** δ 10.76 (d, *J* = 2.4 Hz, 1H), 8.51 – 8.46 (m, 2H), 7.91 (d, *J* = 7.0 Hz, 1H), 7.86 (d, *J* = 7.9 Hz, 1H), 7.69 (s, 1H), 7.67 (d, *J* = 8.0 Hz, 1H), 7.63 – 7.47 (m, 10H), 7.29 (s, 1H), 7.27 – 7.22 (m, 2H), 7.07 (d, *J* = 2.3 Hz, 1H), 7.04 – 6.97 (m, 2H), 6.92 (t, 1H), 5.35 – 5.28 (m, 1H), 5.26 – 5.18 (m, 1H), 4.39 – 4.33 (m, 1H), 4.12 (p, *J* = 7.0 Hz, 1H), 3.98 – 3.92 (m, 1H), 3.07 (dd, *J* = 14.7, 5.4 Hz, 1H), 2.94 (dd, *J* = 14.7, 7.8 Hz, 1H), 2.90 – 2.76 (m, 4H), 2.74 – 2.63 (m, 2H), 2.45 – 2.30 (m, 2H), 1.74 (s, 3H), 1.22 – 1.12 (m, 3H), 1.11 (d, *J* = 7.1 Hz, 3H), 1.06 – 0.98 (m, 1H), 0.64 – 0.49 (m, 2H). **^{13}C NMR (176 MHz, DMSO)** δ

173.03, 171.54, 171.24, 169.22, 157.90, 157.72, 154.49, 152.46, 152.33, 141.25, 141.21, 137.17, 137.02, 135.90, 134.82, 132.52, 129.47, 129.23, 129.01, 128.48, 128.19, 127.95, 127.72, 127.35, 127.31, 123.42, 120.68, 118.36, 118.10, 111.08, 109.84, 64.20, 53.08, 51.87, 48.34, 30.93, 29.01, 27.48, 26.99, 26.98, 26.02, 25.94, 22.35, 21.57, 17.75. **HRMS ESI** m/z calculated for $C_{49}H_{51}N_6O_4^+$ $[M]^+$: 787.3966, measured: 787.3976

Compound **27**.

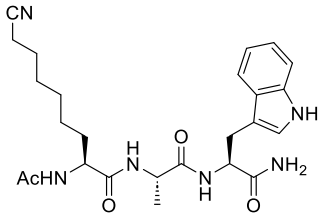

Peptide was synthesized from Katritzky salt **21** according to the general method **2d** on a 82 µmol scale based on resin loading, and then cleaved and deprotected according to general method **2e.** The crude peptide was then purified by general purification method **B**. Yield: 23.0 mg (47.7 µmol, 59%). **^{1}H NMR (600 MHz, DMSO-d_6)** δ 10.79 (d, *J* = 2.4 Hz, 1H), 8.07 (d, *J* = 7.0 Hz, 1H), 7.99 (d, *J* = 7.7 Hz, 1H), 7.71 (d, *J* = 8.0 Hz, 1H), 7.56 (dd, *J* = 7.9, 1.1 Hz, 1H), 7.31 (d, *J* = 8.2 Hz, 1H), 7.28 (s, 1H), 7.11 (d, *J* = 2.3 Hz, 1H), 7.08 – 7.02 (m, 1H), 6.99 – 6.92 (m, 1H), 4.51 – 4.33 (m, 1H), 4.30 – 4.09 (m, 2H), 3.11 (dd, *J* = 14.7, 5.5 Hz, 1H), 2.99 (dd, *J* = 14.7, 7.7 Hz, 1H), 2.42 (t, *J* = 7.1 Hz, 2H), 1.84 (s, 3H), 1.60 – 1.53 (m, 1H), 1.52 – 1.48 (m, 2H), 1.47 – 1.37 (m, 1H), 1.35 – 1.19 (m, 6H), 1.16 (d, *J* = 7.1 Hz, 3H). **^{13}C NMR (151 MHz, DMSO)** δ 135.99, 127.42, 123.46, 120.79, 120.73, 118.43, 118.20, 111.21, 109.98, 53.19, 27.57, 25.02, 24.63, 22.50, 17.74, 16.05. **HRMS ESI** m/z calculated for $C_{25}H_{34}N_6O_4$ $[M+H]^+$: 483.2720, measured: 483.2706.

Compound **33**.

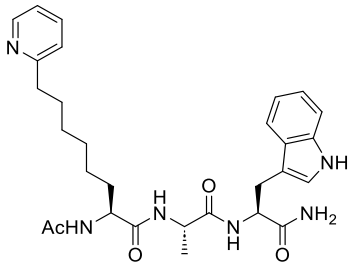

Synthesized according to the method described for **27**. Yield: 30.7 mg (57.4 µmol, 72%). **^{1}H NMR (600 MHz, DMSO-d_6)** δ 10.79 (d, *J* = 2.4 Hz, 1H), 8.74 (d, *J* = 4.1 Hz, 1H), 8.34 (t, *J* = 8.0 Hz, 1H), 8.06 (d, *J* = 7.0 Hz, 1H), 8.00 (d, *J* = 7.7 Hz, 1H), 7.81 (d, *J* = 8.0 Hz, 1H), 7.76 (t, *J* = 6.7 Hz, 1H), 7.73 (d, *J* = 8.0 Hz, 1H), 7.56 (d, *J* = 7.9 Hz, 1H), 7.30 (d, *J* = 8.1 Hz, 1H), 7.29 (s, 1H), 7.11 (d, *J* = 2.3 Hz, 1H), 7.06 – 7.00 (m,

2H), 6.98 – 6.89 (m, 1H), 4.42 – 4.36 (m, 1H), 4.28 – 4.12 (m, 2H), 3.10 (dd, *J* = 14.7, 5.5 Hz, 1H), 2.98 (dd, *J* = 14.7, 7.7 Hz, 1H), 2.90 (t, *J* = 7.8 Hz, 2H), 1.84 (s, 3H), 1.72 – 1.61 (m, 2H), 1.61 – 1.51 (m, 1H), 1.48 – 1.39 (m, 1H), 1.29 – 1.20 (m, 6H), 1.16 (d, *J* = 7.1 Hz, 3H). **^{13}C NMR (151 MHz, DMSO)** δ 173.03, 171.79, 171.74, 169.39, 157.83, 144.36, 142.74, 135.91, 127.33, 126.04, 123.89, 123.41, 120.71, 118.35, 118.12, 111.14, 109.90, 53.19, 52.50, 48.39, 33.44, 31.71, 28.52, 28.19, 27.49, 25.01, 22.43, 17.68. **HRMS ESI** m/z calculated for $C_{29}H_{38}N_6O_4$ $[M+H]^+$: 535.3033, measured: 535.3028.

Compound **34**.

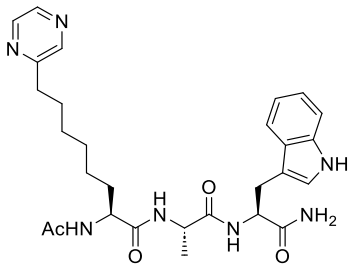

Synthesized according to the method described for **27**. Yield: 15.3 mg (28.6 µmol, 66%). **^{1}H NMR (700 MHz, DMSO-d_6)** δ 10.78 (d, *J* = 2.5 Hz, 1H), 8.54 – 8.51 (m, 2H), 8.45 – 8.43 (m, 1H), 8.06 (d, *J* = 7.0 Hz, 1H), 7.98 (d, *J* = 7.7 Hz, 1H), 7.70 (d, *J* = 8.0 Hz, 1H), 7.56 (d, *J* = 7.9 Hz, 1H), 7.30 (d, *J* = 8.0 Hz, 1H), 7.27 (s, 1H), 7.11 (d, *J* = 2.4 Hz, 1H), 7.06 – 7.01 (m, 2H), 6.97 – 6.94 (m, 1H), 4.44 – 4.32 (m, 1H), 4.27 – 4.09 (m, 2H), 3.11 (dd, *J* = 14.8, 5.3 Hz, 1H), 2.98 (dd, *J* = 14.8, 7.8 Hz, 1H), 2.79 – 2.62 (m, 2H), 1.84 (s, 3H), 1.69 – 1.61 (m, 2H), 1.59 – 1.52 (m, 1H), 1.48 – 1.40 (m, 1H), 1.32 – 1.20 (m, 6H), 1.16 (d, *J* = 7.1 Hz, 3H). **^{13}C NMR (176 MHz, DMSO)** δ 173.03, 171.88, 171.71, 169.42, 158.27, 158.06, 157.27, 144.28, 143.92, 143.87, 142.11, 135.92, 127.35, 123.37, 120.70, 118.35, 118.12, 111.13, 109.92, 53.14, 52.61, 48.43, 34.34, 31.72, 28.58, 28.42, 28.41, 27.49, 25.14, 22.42, 17.64. **HRMS ESI** m/z calculated for $C_{28}H_{37}N_7O_4$ $[M+H]^+$: 536.2985, measured: 536.2979.

Compound **35**.

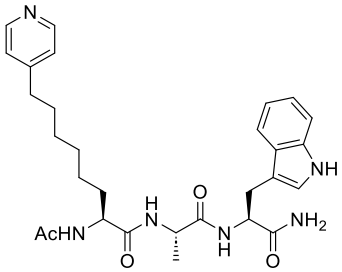

Synthesized according to the method described for **27**. Yield: 13.3 mg (24.9 µmol, 32%). **^{1}H NMR (600 MHz, DMSO-d_6)** δ 10.78 (d, *J* = 2.5 Hz, 1H), 8.68 (d, *J* = 6.5 Hz, 2H), 8.06 (d, *J* = 7.1 Hz, 1H), 7.98 (d, *J* = 7.7 Hz, 1H), 7.75 – 7.69 (m, 3H), 7.56 (d, *J* = 7.9 Hz, 1H), 7.30 (d, *J* = 8.1 Hz, 1H), 7.28 (s, 1H), 7.11 (d, *J* = 2.4 Hz, 1H), 7.06 – 7.01 (m, 2H), 6.95 (t, *J* = 7.4 Hz, 1H), 4.44 – 4.35 (m, 1H), 4.29 – 4.12 (m, 2H), 3.10

(dd, *J* = 14.7, 5.6 Hz, 1H), 2.98 (dd, *J* = 14.7, 7.7 Hz, 1H), 2.74 (t, *J* = 7.7 Hz, 2H), 1.83 (s, 3H), 1.64 – 1.52 (m, 3H), 1.48 – 1.40 (m, 1H), 1.27 – 1.21 (m, 6H), 1.16 (d, *J* = 7.1 Hz, 3H). **^{13}C NMR (151 MHz, DMSO)** δ 173.12, 171.90, 171.83, 169.49, 157.94, 143.40, 136.01, 127.43, 126.07, 123.49, 120.81, 118.44, 118.22, 111.24, 109.99, 53.28, 52.60, 48.49, 34.76, 31.82, 29.25, 28.34, 27.59, 25.09, 22.51, 17.74. **HRMS ESI** m/z calculated for $C_{29}H_{38}N_6O_4$ $[M+H]^+$: 535.2955, measured: 535.3000.

Compound **36**.

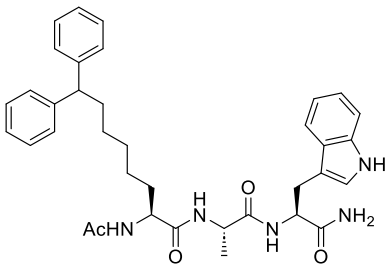

Synthesized according to the method described for **27**. Yield: 30.1 mg (49.3 µmol, 63%). **^{1}H NMR (600 MHz, DMSO-d_6)** δ 10.79 (d, *J* = 2.4 Hz, 1H), 8.04 (d, *J* = 7.0 Hz, 1H), 7.97 (d, *J* = 7.6 Hz, 1H), 7.71 (d, *J* = 8.0 Hz, 1H), 7.56 (d, *J* = 7.9 Hz, 1H), 7.31 (d, *J* = 8.1 Hz, 1H), 7.28 – 7.22 (m, 8H), 7.16 – 7.09 (m, 3H), 7.06 – 7.01 (m, 2H), 6.97 – 6.92 (m, 1H), 4.47 – 4.35 (m, 1H), 4.21 – 4.07 (m, 2H), 3.85 (t, *J* = 7.9 Hz, 1H), 3.11 (dd, *J* = 14.7, 5.5 Hz, 1H), 2.98 (dd, *J* = 14.7, 7.7 Hz, 1H), 1.96 (q, *J* = 7.8 Hz, 2H), 1.82 (s, 3H), 1.56 – 1.48 (m, 1H), 1.46 – 1.37 (m, 1H), 1.28 – 1.17 (m, 4H), 1.18 – 1.03 (m, 5H). **^{13}C NMR (151 MHz, DMSO)** δ 172.85, 171.71, 171.53, 169.28, 145.04, 145.02, 135.74, 128.08, 127.28, 127.16, 125.65, 123.19, 120.54, 118.17, 117.96, 110.96, 109.74, 52.98, 52.45, 50.24, 48.22, 34.45, 31.53, 28.36, 27.30, 27.17, 24.98, 22.22, 17.42. **HRMS ESI** m/z calculated for $C_{36}H_{43}N_5O_4$ $[M+H]^+$: 610.3393, measured: 610.3383.

Compound **40**.

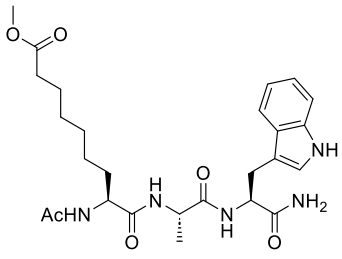

Synthesized according to the method described for **27**. Yield: 21.6 mg (41.9 µmol, 52%). **^{1}H NMR (700 MHz, DMSO-d_6)** δ 10.78 (d, *J* = 2.4 Hz, 1H), 8.05 (d, *J* = 7.0 Hz, 1H), 7.98 (d, *J* = 7.7 Hz, 1H), 7.70 (d, *J* = 8.0 Hz, 1H), 7.56 (d, *J* = 7.9 Hz, 1H), 7.31 (d, *J* = 8.1 Hz, 1H), 7.26 (s, 1H), 7.11 (d, *J* = 2.3 Hz, 1H), 7.06 – 7.02 (m, 2H), 6.98 – 6.93 (m, 1H), 4.45 – 4.37 (m, 1H), 4.25 – 4.13 (m, 2H), 3.56 (s, 3H), 3.11 (dd, *J* = 14.7, 5.5 Hz, 1H), 2.98 (dd, *J* = 14.7, 7.7 Hz, 1H), 2.25 (t, *J* = 7.4 Hz, 2H), 1.84 (s, 3H), 1.60 – 1.52 (m,

1H), 1.47 (q, *J* = 7.3 Hz, 2H), 1.45 – 1.39 (m, 1H), 1.35 – 1.18 (m, 6H), 1.16 (d, *J* = 7.1 Hz, 3H). **^{13}C NMR (176 MHz, DMSO)** δ 173.37, 173.09, 171.94, 171.77, 169.48, 135.99, 127.41, 123.43, 120.77, 118.41, 118.18, 111.19, 109.98, 53.19, 52.67, 51.14, 48.49, 33.22, 31.76, 28.37, 28.32, 27.55, 25.15, 24.36, 22.48, 17.71. **HRMS ESI** m/z calculated for $C_{26}H_{37}N_5O_6$ $[M+H]^+$: 516.2822, measured 516.2809.

Compound **41**.

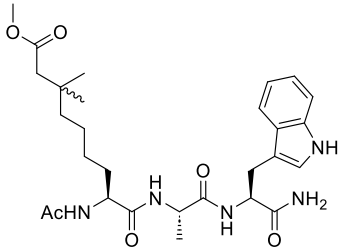

Synthesized according to the method described for **27**. Yield: 3.2 mg (6.0 µmol, 8%). **^{1}H NMR (600 MHz, DMSO-d_6)** δ 10.78 (d, *J* = 2.5 Hz, 1H), 8.05 (d, *J* = 7.0 Hz, 1H), 7.99 (d, *J* = 7.7 Hz, 1H), 7.71 (d, *J* = 8.0 Hz, 1H), 7.56 (d, *J* = 7.9 Hz, 1H), 7.30 (d, *J* = 8.1 Hz, 1H), 7.27 (s, 1H), 7.11 (d, *J* = 2.3 Hz, 1H), 7.07 – 7.01 (m, 2H), 6.98 – 6.91 (m, 1H), 4.49 – 4.36 (m, 1H), 4.23 – 4.07 (m, 2H), 3.57 (s, 3H), 3.11 (dd, *J* = 14.7, 5.5 Hz, 1H), 2.98 (dd, *J* = 14.7, 7.7 Hz, 1H), 2.26 (ddd, *J* = 15.0, 5.9, 2.0 Hz, 1H), 2.06 (ddd, *J* = 15.0, 8.2, 4.1 Hz, 1H), 1.84 (s, 3H), 1.82 – 1.76 (m, 1H), 1.59 – 1.51 (m, 1H), 1.48 – 1.39 (m, 1H), 1.29 – 1.18 (m, 5H), 1.16 (d, *J* = 7.1 Hz, 3H), 1.12 – 1.03 (m, 1H), 0.84 (d, *J* = 5.7 Hz, 3H). **^{13}C NMR (151 MHz, DMSO)** δ 173.09, 172.83, 171.94, 171.78, 169.49, 135.99, 127.41, 123.44, 120.78, 118.42, 118.19, 111.20, 109.99, 53.20, 52.65, 51.11, 48.49, 40.83, 35.88, 31.81, 29.73, 27.56, 26.04, 25.49, 22.49, 17.73. **HRMS ESI** m/z calculated for $C_{27}H_{39}N_5O_6$ $[M+H]^+$: 530.2979, measured 530.2973.

Compound **43**.

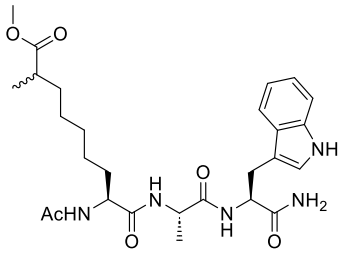

Synthesized according to the method described for **27**. Yield: 15.8 mg (29.8 µmol, 43%). **^{1}H NMR (700 MHz, DMSO-d_6)** δ 10.78 (d, *J* = 2.4 Hz, 1H), 8.05 (d, *J* = 5.8 Hz, 1H), 7.98 (d, *J* = 7.7 Hz, 1H), 7.70 (d, *J* = 8.0 Hz, 1H), 7.56 (d, *J* = 7.9 Hz, 1H), 7.31 (d, *J* = 8.1 Hz, 1H), 7.26 (s, 1H), 7.11 (d, *J* = 2.3 Hz, 1H), 7.08 – 7.01 (m, 2H), 6.98 – 6.89 (m, 1H), 4.52 – 4.33 (m, 1H), 4.25 – 4.12 (m, 2H), 3.57 (s, 3H), 3.11 (dd, *J* = 14.7, 5.5 Hz, 1H), 2.99 (dd, *J* = 14.7, 7.7 Hz, 1H), 2.38 (h, *J* = 7.0 Hz, 1H), 1.84 (s, 3H), 1.60 – 1.47 (m, 2H), 1.47 – 1.40 (m, 1H), 1.35 – 1.30 (m, 1H), 1.28 – 1.17 (m, 6H), 1.16 (d, *J* = 7.2 Hz, 3H), 1.04 (d, *J* =

7.0 Hz, 3H). **^{13}C NMR (176 MHz, DMSO)** δ 176.30, 173.10, 171.95, 171.78, 169.51, 136.00, 127.42, 123.44, 120.78, 118.41, 118.19, 111.20, 109.99, 53.22, 52.70, 51.25, 48.51, 38.55, 33.21, 31.76, 28.63, 27.55, 26.48, 25.19, 22.49, 17.71, 16.85. **HRMS ESI** m/z calculated for $C_{27}H_{39}N_5O_6$ $[M+H]^+$: 530.2979, measured 530.2958.

Compound **44**.

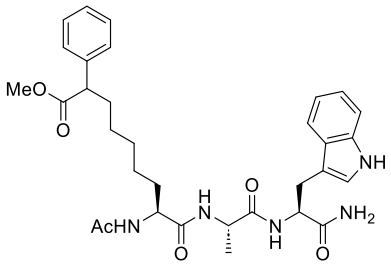

Synthesized according to the method described for **27**. Yield: 28.4 mg (48.0 µmol, 62%). **^{1}H NMR (700 MHz, Methanol-d_4)** δ 10.78 (d, *J* = 2.3 Hz, 1H), 8.03 (d, *J* = 6.5 Hz, 1H), 7.97 (dd, *J* = 7.7, 2.6 Hz, 1H), 7.70 (dd, *J* = 8.1, 2.0 Hz, 1H), 7.56 (d, *J* = 7.9 Hz, 1H), 7.34 – 7.28 (m, 3H), 7.27 – 7.22 (m, 4H), 7.11 (d, *J* = 2.3 Hz, 1H), 7.06 – 7.01 (m, 2H), 6.96 (td, *J* = 7.3, 6.8, 1.0 Hz, 1H), 4.47 – 4.31 (m, 1H), 4.25 – 4.03 (m, 2H), 3.60 – 3.54 (m, 4H), 3.11 (dd, *J* = 14.7, 5.5 Hz, 1H), 2.98 (dd, *J* = 14.7, 7.8 Hz, 1H), 2.00 – 1.88 (m, 1H), 1.83 (s, 3H), 1.69 – 1.58 (m, 1H), 1.56 – 1.48 (m, 1H), 1.44 – 1.36 (m, 1H), 1.31 – 0.98 (m, 9H). **^{13}C NMR (176 MHz, MeOD)** δ 173.84, 173.10, 171.93, 171.92, 171.76, 169.49, 139.17, 135.99, 128.54, 127.70, 127.41, 127.05, 123.43, 120.77, 118.41, 118.18, 111.19, 109.99, 53.20, 52.67, 52.66, 51.68, 50.40, 50.38, 48.49, 32.95, 31.72, 28.43, 27.54, 26.80, 25.16, 25.13, 22.48, 17.70. **HRMS ESI** m/z calculated for $C_{32}H_{41}N_5O_6$ $[M+H]^+$: 592.3135, measured: 592.3110.

Compound **45**.

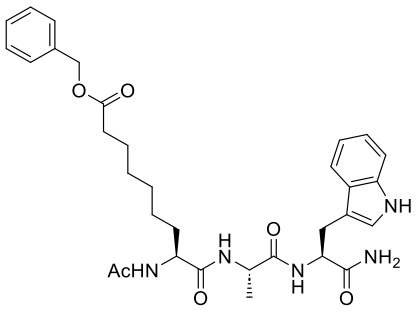

Synthesized according to the method described for **27**. Yield: 21.9 mg (37.0 µmol, 48%). **^{1}H NMR (600 MHz, DMSO-d_6)** δ 10.78 (d, *J* = 2.4 Hz, 1H), 8.06 (d, *J* = 7.0 Hz, 1H), 7.99 (d, *J* = 7.7 Hz, 1H), 7.71 (d, *J* = 8.0 Hz, 1H), 7.56 (d, *J* = 7.8 Hz, 1H), 7.39 – 7.29 (m, 6H), 7.27 (s, 1H), 7.11 (d, *J* = 2.3 Hz, 1H), 7.07 – 7.01 (m, 2H), 6.95 (ddd, *J* = 8.0, 7.0, 1.0 Hz, 1H), 5.07 (s, 2H), 4.46 – 4.36 (m, 1H), 4.33 – 4.12 (m, 2H), 3.25

– 3.07 (m, 1H), 3.03 – 2.93 (m, 1H), 2.31 (t, *J* = 7.4 Hz, 2H), 1.84 (s, 3H), 1.66 – 1.47 (m, 3H), 1.47 – 1.38 (m, 1H), 1.30 – 1.18 (m, 6H), 1.16 (d, *J* = 7.1 Hz, 3H). **^{13}C NMR (151 MHz, DMSO)** δ 173.11, 172.80, 171.95, 171.79, 169.49, 136.30, 135.99, 128.43, 127.98, 127.92, 127.42, 123.44, 120.78, 118.42, 118.19, 111.20, 109.99, 65.28, 53.20, 52.67, 48.50, 33.42, 31.78, 28.39, 28.32, 27.57, 25.19, 24.42, 22.50, 17.73. **HRMS ESI** m/z calculated for $C_{32}H_{41}N_5O_6$ $[M+H]^+$: 592.3135, measured 592.3120.

Compound **46**.

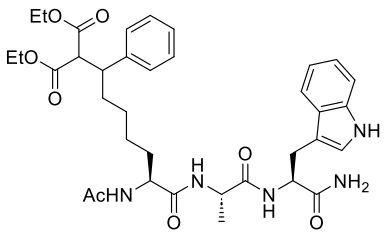

Synthesized according to the method described for **27**. Yield: 14.7 mg (21.7 µmol, 28%). **^{1}H NMR (600 MHz, DMSO-d_6)** δ 10.77 (d, *J* = 2.4 Hz, 1H), 8.00 – 7.92 (m, 2H), 7.70 (dd, *J* = 11.7, 8.0 Hz, 1H), 7.55 (dd, *J* = 7.9, 1.2 Hz, 1H), 7.29 (dd, *J* = 8.1, 1.0 Hz, 1H), 7.27 – 7.14 (m, 3H), 7.12 – 7.08 (m, 1H), 7.07 – 7.00 (m, 2H), 6.99 – 6.92 (m, 1H), 4.45 – 4.33 (m, 1H), 4.22 – 4.11 (m, 2H), 3.80 – 3.69 (m, 6H), 3.10 (ddd, *J* = 14.6, 5.6, 2.2 Hz, 1H), 2.96 (dd, *J* = 14.7, 7.9 Hz, 1H), 1.84 – 1.76 (m, 3H), 1.66 – 1.52 (m, 2H), 1.50 – 1.37 (m, 1H), 1.38 – 1.27 (m, 1H), 1.28 – 1.06 (m, 8H), 1.02 – 0.92 (m, 1H), 0.94 – 0.84 (m, 1H), 0.81 (t, *J* = 7.1 Hz, 3H). **^{13}C NMR (151 MHz, DMSO)** δ 173.15, 171.79, 170.07, 169.55, 167.97, 167.33, 136.00, 129.39, 128.34, 128.09, 127.40, 126.68, 123.45, 120.79, 118.42, 118.21, 111.21, 110.02, 61.10, 60.49, 55.35, 55.11, 53.26, 52.73, 48.51, 45.04, 44.97, 33.72, 33.28, 31.66, 31.59, 27.50, 26.49, 26.40, 25.25, 25.15, 22.48, 17.72, 17.71, 13.93, 13.50. **HRMS ESI** m/z calculated $C_{36}H_{47}N_5O_8$ $[M+H]^+$: 678.3503, measured: 678.3483.

Compound **47**.

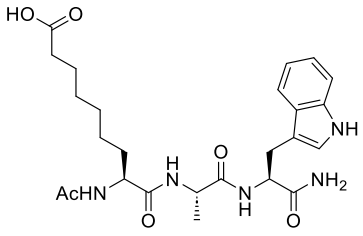

Synthesized according to the method described for **27**. Yield: 5.2 mg (10.4 µmol, 13%). **^{1}H NMR (600 MHz, DMSO-d_6)** δ 10.78 (d, *J* = 2.4 Hz, 1H), 8.05 (d, *J* = 7.0 Hz, 1H), 7.99 (d, *J* = 7.7 Hz, 1H), 7.70 (d, *J* = 8.0 Hz, 1H), 7.56 (d, *J* = 7.9 Hz, 1H), 7.31 (d, *J* = 8.1 Hz, 1H), 7.27 (s, 1H), 7.11 (d, *J* = 2.3 Hz, 1H), 7.07 – 7.02 (m, 2H), 6.97 – 6.93 (m, 1H), 4.43 – 4.35 (m, 1H), 4.25 – 4.09 (m, 2H), 3.11 (dd, *J* = 14.7, 5.4 Hz,

1H), 2.98 (dd, *J* = 14.7, 7.8 Hz, 1H), 2.16 (t, *J* = 7.4 Hz, 2H), 1.84 (s, 3H), 1.60 – 1.51 (m, 1H), 1.49 – 1.41 (m, 3H), 1.26 – 1.19 (m, 6H), 1.16 (d, *J* = 7.1 Hz, 3H). **^{13}C NMR (151 MHz, DMSO)** δ 174.51, 173.12, 171.97, 171.79, 169.51, 135.99, 127.41, 123.44, 120.79, 118.42, 118.20, 111.20, 109.99, 53.19, 52.70, 48.51, 33.62, 31.78, 28.47, 28.45, 27.55, 25.23, 24.45, 22.50, 17.73. **HRMS ESI** m/z calculated for $C_{25}H_{35}N_5O_6$ $[M+Na]^+$: 524.2485, measured 524.2473.

Compound **48**.

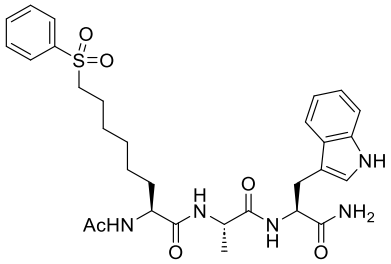

Synthesized according to the method described for **27**. Yield: 22.2 mg (37.1 µmol, 46%). **^{1}H NMR (600 MHz, DMSO-d_6)** δ 10.78 (d, *J* = 2.4 Hz, 1H), 8.05 (d, *J* = 7.0 Hz, 1H), 7.97 (d, *J* = 7.7 Hz, 1H), 7.88 (d, *J* = 7.3 Hz, 2H), 7.74 (t, *J* = 7.5 Hz, 1H), 7.69 (d, *J* = 8.0 Hz, 1H), 7.65 (t, *J* = 7.8 Hz, 2H), 7.55 (d, *J* = 7.9 Hz, 1H), 7.30 (d, *J* = 8.0 Hz, 1H), 7.27 (s, 1H), 7.11 (d, *J* = 2.3 Hz, 1H), 7.06 – 7.00 (m, 2H), 6.97 – 6.90 (m, 1H), 4.50 – 4.36 (m, 1H), 4.24 – 4.10 (m, 2H), 3.24 (t, 2H), 3.10 (dd, *J* = 14.7, 5.5 Hz, 1H), 2.98 (dd, *J* = 14.7, 7.7 Hz, 1H), 1.83 (s, 3H), 1.55 – 1.45 (m, 3H), 1.42 – 1.36 (m, 1H), 1.26 – 1.21 (m, 2H), 1.15 (d, *J* = 7.1 Hz, 7H). **^{13}C NMR (151 MHz, DMSO)** δ 173.03, 171.82, 171.69, 169.37, 139.02, 135.91, 133.66, 129.36, 127.53, 127.33, 123.37, 120.71, 118.35, 118.11, 111.12, 109.89, 54.41, 53.09, 52.44, 48.41, 31.62, 28.04, 27.49, 27.20, 24.91, 22.41, 22.16, 17.64. **HRMS ESI** m/z calculated for: $C_{30}H_{39}N_5O_6S$ $[M+H]^+$: 598.2699, measured: 598.2691.

Compound **49**.

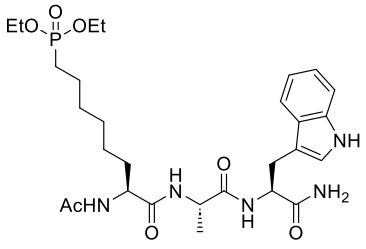

Synthesized according to the method described for **27**. Yield: 11.7 mg (19.7 µmol, 25%). **^{1}H NMR (600 MHz, DMSO-d_6)** δ 10.79 (d, *J* = 2.5 Hz, 1H), 8.07 (d, *J* = 7.0 Hz, 1H), 7.99 (d, *J* = 7.7 Hz, 1H), 7.70 (d, *J* = 8.0 Hz, 1H), 7.55 (d, *J* = 1.1 Hz, 1H), 7.31 (d, *J* = 8.1 Hz, 1H), 7.28 (s, 1H), 7.11 (d, *J* = 2.4 Hz, 1H), 7.08 – 7.02 (m, 2H), 6.98 – 6.86 (m, 1H), 4.48 – 4.32 (m, 1H), 4.25 – 4.12 (m, 2H), 4.04 – 3.88 (m, 4H), 3.11

(dd, *J* = 14.7, 5.4 Hz, 1H), 2.98 (dd, *J* = 14.7, 7.7 Hz, 1H), 1.84 (s, 3H), 1.69 – 1.61 (m, 2H), 1.59 – 1.51 (m, 1H), 1.47 – 1.37 (m, 3H), 1.34 – 1.27 (m, 2H), 1.21 (t, *J* = 7.0 Hz, 10H), 1.16 (d, *J* = 7.1 Hz, 3H). **^{13}C NMR (151 MHz, DMSO)** δ 173.11, 171.94, 171.78, 169.46, 135.99, 127.42, 123.44, 120.78, 118.42, 118.19, 111.20, 109.98, 60.76, 60.71, 53.18, 52.60, 48.50, 31.79, 29.70, 29.59, 28.22, 27.57, 25.10, 24.87, 23.95, 22.49, 22.01, 21.98, 17.73, 16.33, 16.29. **HRMS ESI** m/z calculated for $C_{28}H_{44}N_5O_7P$ $[M+H]^+$: 594.3057, measured: 594.3053.

Compound **50**.

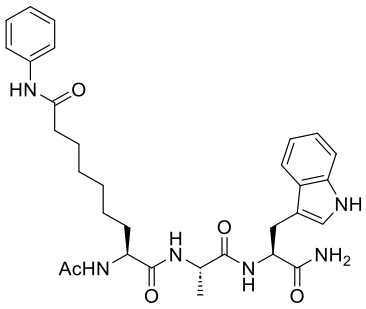

Synthesized according to the method described for **27**. Yield: 12.6 mg (21.9 µmol, 27%). **^{1}H NMR (600 MHz, DMSO-d_6)** δ 10.78 (d, *J* = 2.5 Hz, 1H), 9.83 (s, 1H), 8.05 (d, *J* = 7.0 Hz, 1H), 8.00 (d, *J* = 7.7 Hz, 1H), 7.71 (d, *J* = 8.0 Hz, 1H), 7.61 – 7.53 (m, 3H), 7.37 – 7.22 (m, 4H), 7.11 (d, *J* = 2.3 Hz, 1H), 7.07 – 6.98 (m, 3H), 6.98 – 6.93 (m, 1H), 4.48 – 4.31 (m, 1H), 4.25 – 4.11 (m, 2H), 3.12 (dd, *J* = 14.7, 5.4 Hz, 1H), 2.99 (dd, *J* = 14.7, 7.8 Hz, 1H), 2.27 (t, *J* = 7.5 Hz, 2H), 1.84 (s, 3H), 1.68 – 1.52 (m, 3H), 1.50 – 1.42 (m, 1H), 1.36 – 1.21 (m, 6H), 1.16 (d, *J* = 7.1 Hz, 3H). **^{13}C NMR (151 MHz, DMSO)** δ 173.14, 171.99, 171.82, 171.27, 169.55, 139.35, 135.99, 128.64, 127.42, 123.46, 122.91, 120.80, 119.02, 118.43, 118.21, 111.22, 110.00, 53.22, 52.73, 48.53, 36.41, 31.81, 28.61, 28.57, 27.55, 25.28, 25.11, 22.51, 17.75. **HRMS ESI** m/z calculated for $C_{31}H_{40}N_6O_5$ $[M+H]^+$: 577.3138, measured 577.3121.

Compound **51.**

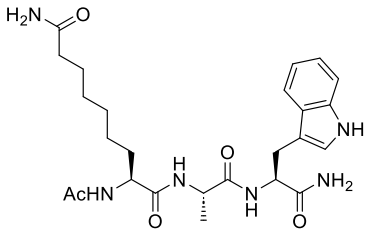

Synthesized according to the method described for **27**. Yield: 9.0 mg (18.0 µmol, 23%). **^{1}H NMR (600 MHz, DMSO-d_6)** δ 10.79 (d, *J* = 2.4 Hz, 1H), 8.05 (d, *J* = 7.0 Hz, 1H), 7.99 (d, *J* = 7.7 Hz, 1H), 7.71 (d, *J* = 8.0 Hz, 1H), 7.56 (d, *J* = 7.9 Hz, 1H), 7.31 (d, *J* = 8.1 Hz, 1H), 7.28 (s, 0H), 7.20 (s, 1H), 7.11 (d, *J* = 2.3 Hz, 1H), 7.07 – 7.01 (m, 2H), 6.96 (ddd, *J* = 8.0, 6.9, 1.1 Hz, 1H), 6.67 (s, 1H), 4.45 – 4.35 (m, 1H), 4.28 –

4.08 (m, 2H), 3.11 (dd, *J* = 14.7, 5.4 Hz, 1H), 2.98 (dd, *J* = 14.7, 7.8 Hz, 1H), 2.00 (t, *J* = 7.5 Hz, 2H), 1.84 (s, 3H), 1.66 – 1.50 (m, 1H), 1.49 – 1.39 (m, 3H), 1.33 – 1.17 (m, 6H), 1.16 (d, *J* = 7.2 Hz, 3H). **^{13}C NMR (151 MHz, DMSO)** δ 174.36, 173.13, 171.98, 171.81, 169.53, 135.99, 127.42, 123.45, 120.80, 118.43, 118.21, 111.22, 110.00, 53.21, 52.72, 48.53, 35.11, 31.81, 28.62, 28.55, 27.54, 25.28, 25.08, 22.51, 17.75. **HRMS ESI** m/z calculated for $C_{25}H_{36}N_6O_5$ $[M+H]^+$: 501.2825, measured 501.2815.

Compound **52**

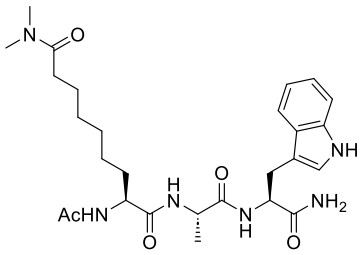

Synthesized according to the method described for **27**. Yield: 11.0 mg (20.8 µmol, 27%). **^{1}H NMR (600 MHz, DMSO-d_6)** δ 10.79 (d, *J* = 2.4 Hz, 1H), 8.07 (d, *J* = 7.0 Hz, 1H), 8.00 (d, *J* = 7.7 Hz, 1H), 7.71 (d, *J* = 8.0 Hz, 1H), 7.56 (d, *J* = 8.1 Hz, 1H), 7.31 – 7.29 (m, 1H), 7.27 (s, 1H), 7.11 (d, *J* = 2.3 Hz, 1H), 7.08 – 7.01 (m, 2H), 6.99 – 6.93 (m, 1H), 4.49 – 4.36 (m, 1H), 4.23 – 4.09 (m, 2H), 3.76 – 3.69 (m, 6H), 3.21 – 3.08 (m, 1H), 3.04 – 2.95 (m, 1H), 2.31 (t, *J* = 7.4 Hz, 2H), 1.84 (s, 3H), 1.60 – 1.38 (m, 4H), 1.32 – 1.17 (m, 6H), 1.16 (d, *J* = 7.1 Hz, 3H). **^{13}C NMR (151 MHz, DMSO)** δ 173.15, 172.82, 171.99, 171.82, 169.55, 136.01, 127.43, 123.47, 120.80, 118.43, 118.21, 111.23, 110.00, 55.36, 55.12, 53.23, 52.71, 48.54, 33.43, 31.78, 28.40, 28.33, 27.57, 24.43, 22.51, 17.73. **HRMS ESI** m/z calculated for: $C_{27}H_{40}N_6O_5$ $[M+H]^+$: 529.3138, measured: 529.3117.

Compound **53**.

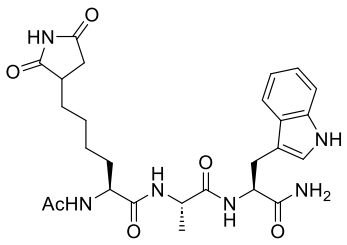

Synthesized according to the method described for **27**. Yield: 8.8 mg (16.7 µmol, 21%). **^{1}H NMR (600 MHz, DMSO-d_6)** δ 11.04 (s, 1H), 10.78 (d, *J* = 2.4 Hz, 1H), 8.07 (dd, *J* = 7.0, 3.5 Hz, 1H), 7.70 (d, *J* = 8.0 Hz, 1H), 7.56 (d, *J* = 7.9 Hz, 1H), 7.28 (s, 1H), 7.11 (d, *J* = 2.3 Hz, 1H), 7.07 – 7.01 (m, 2H), 6.98 – 6.92 (m, 1H), 4.40 (td, *J* = 7.8, 5.4 Hz, 1H), 4.25 – 4.09 (m, 2H), 3.11 (dd, *J* = 14.7, 5.4 Hz, 1H), 2.98 (dd, *J* = 14.7, 7.8 Hz, 1H), 2.79 – 2.65 (m, 2H), 2.34 – 2.24 (m, 1H), 1.84 (s, 3H), 1.64 (td, *J* = 10.0, 4.6 Hz, 1H), 1.61 – 1.50 (m, 1H), 1.41 (dtt, *J* = 27.6, 9.1, 4.7 Hz, 2H), 1.30 – 1.19 (m, 4H), 1.16 (d, *J* = 7.1 Hz, 3H). **^{13}C**

NMR (151 MHz, DMSO) δ 181.65, 178.33, 173.12, 171.89, 171.87, 171.80, 169.47, 135.99, 127.42, 123.46, 120.79, 118.43, 118.20, 111.20, 109.99, 53.17, 52.57, 52.52, 48.53, 40.66, 35.13, 31.62, 30.10, 30.07, 27.55, 25.93, 25.11, 25.06, 22.50, 17.74. **HRMS ESI** m/z calculated for $C_{26}H_{34}N_6O_6$ $[M+H]^+$: 527.2618, measured: 527.2608.

Compound **56.**

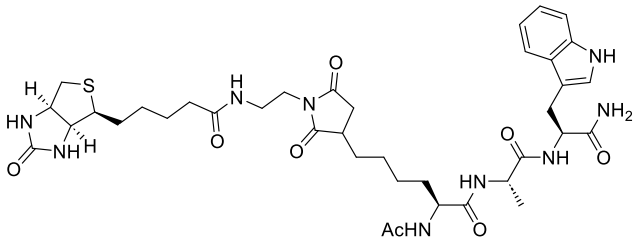

Synthesized according to the method described for **27** on a 17.5 µmol scale. Yield: 2.0 mg (2.5 µmol, 14.4%). **HRMS ESI** m/z calculated for $C_{38}H_{53}N_9O_8S$ $[M+H]^+$: 796.3816, measured: 796.3810.

Compound **61**.

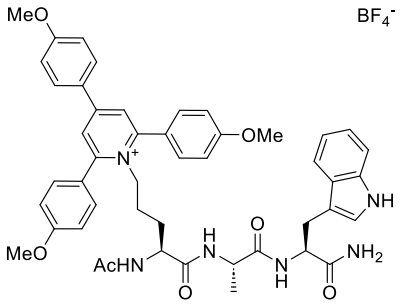

Synthesized according to the method described for **1.** Yield: 76.1 mg (84.7 µmol, 85%). **^{1}H NMR (700 MHz, DMSO-d_6)** δ 10.78 (d, *J* = 2.4 Hz, 1H), 8.25 (s, 2H), 8.21 (d, *J* = 9.0 Hz, 2H), 7.87 (d, *J* = 6.9 Hz, 1H), 7.82 – 7.76 (m, 2H), 7.75 (d, *J* = 8.7 Hz, 4H), 7.55 (d, *J* = 8.0 Hz, 1H), 7.29 (d, *J* = 8.1 Hz, 1H), 7.25 (s, 1H), 7.19 (d, *J* = 8.9 Hz, 4H), 7.11 (d, *J* = 9.0 Hz, 2H), 7.10 (d, *J* = 2.5 Hz, 1H), 7.02 (t, *J* = 7.6 Hz, 1H), 7.00 (s, 1H), 6.92 (t, *J* = 7.4 Hz, 1H), 4.45 – 4.31 (m, 4H), 4.12 (p, *J* = 7.1 Hz, 1H), 3.87 (s, 3H), 3.86 (s, 6H), 3.10 (dd, *J* = 14.6, 5.6 Hz, 1H), 2.97 (dd, *J* = 14.7, 7.8 Hz, 1H), 1.75 (s, 3H), 1.31 (p, 2H), 1.10 (d, *J* = 7.1 Hz, 3H), 1.09 – 1.05 (m, 1H), 0.95 – 0.82 (m, 1H). **^{13}C NMR (176 MHz, DMSO)** δ 173.03, 171.74, 170.81, 169.22, 162.78, 160.88, 155.86, 153.05, 135.91, 130.92, 130.50, 127.30, 125.32, 125.03, 124.53, 123.43, 120.72, 118.35, 118.12, 114.96, 114.42, 111.14, 109.94, 55.42, 54.04, 53.33, 51.40, 48.32, 28.32, 27.45, 25.25, 22.41, 22.33, 17.80, 17.77. **HRMS ESI** m/z calculated for $C_{47}H_{51}N_6O_7^+$ $[M]^+$: 811.3814, measured: 811.3794.

Compound **62**.

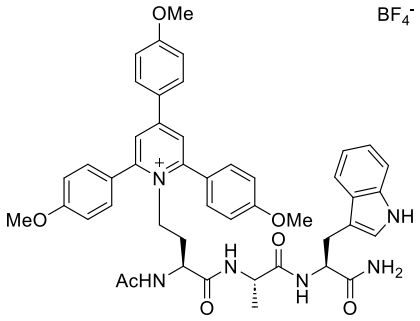

Synthesized according to the method described for **21**. Yield: 46.0 mg (52.0 µmol, 52%). **^{1}H NMR (700 MHz, DMSO-d_6)** δ 10.79 (d, *J* = 2.4 Hz, 1H), 8.29 – 8.21 (m, 4H), 7.85 (d, *J* = 7.2 Hz, 1H), 7.78 – 7.71 (m, 5H), 7.69 (d, *J* = 8.1 Hz, 1H), 7.57 (d, *J* = 7.9 Hz, 1H), 7.31 (s, 2H), 7.29 (d, *J* = 8.0 Hz, 1H), 7.18 (d, *J* = 8.9 Hz, 4H), 7.14 (d, *J* = 9.0 Hz, 2H), 7.08 (d, *J* = 2.4 Hz, 1H), 7.05 – 7.00 (m, 1H), 6.96 – 6.91 (m, 1H), 4.53 – 4.43 (m, 2H), 4.44 – 4.38 (m, 1H), 4.02 (p, *J* = 7.0 Hz, 1H), 3.87 (s, 3H), 3.85 (s, 6H), 3.79 – 3.73 (m, 1H), 3.16 – 3.05 (m, 1H), 2.96 (dd, *J* = 14.8, 8.1 Hz, 1H), 1.73 – 1.64 (m, 1H), 1.58 (s, 3H), 1.53 – 1.45 (m, 1H), 1.05 (d, *J* = 7.1 Hz, 3H). **^{13}C NMR (176 MHz, DMSO)** δ 173.15, 171.38, 169.60, 169.40, 162.79, 160.90, 155.98, 153.13, 135.93, 130.90, 130.52, 127.29, 125.21, 125.07, 124.55, 123.38, 120.73, 118.33, 118.12, 114.98, 114.43, 111.16, 109.93, 55.60, 55.39, 53.21, 51.86, 49.56, 48.36, 31.66, 27.55, 22.28, 17.85. **HRMS ESI** m/z calculated for $C_{46}H_{49}N_6O_7^+$ $[M]^+$: 797.3657, measured: 797.3629

Compound **63**.

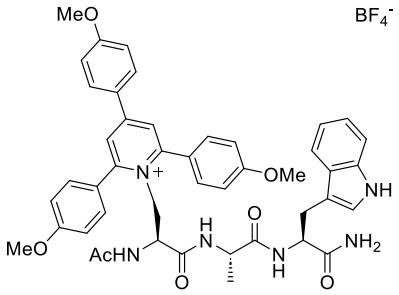

Synthesized according to the method described for **21**. Yield: 39.7 mg (45.6 µmol, 46%). **^{1}H NMR (700 MHz, DMSO-d_6)** δ 10.77 (d, *J* = 2.4 Hz, 1H), 8.24 (d, *J* = 9.0 Hz, 2H), 8.19 (s, 2H), 8.00 (d, *J* = 8.4 Hz, 1H), 7.85 (s, br, 2H), 7.74 (d, *J* = 7.9 Hz, 1H), 7.66 (d, *J* = 7.3 Hz, 1H), 7.55 (d, *J* = 8.0 Hz, 1H), 7.32 (d, *J* = 8.1 Hz, 1H), 7.26 (s, 1H), 7.20 (s, br, 4H), 7.13 (d, *J* = 9.1 Hz, 2H), 7.07 – 7.02 (m, 2H), 6.98 (s, 1H), 6.96 – 6.92 (m, 1H), 5.07 (dd, *J* = 14.5, 4.9 Hz, 1H), 4.71 (dd, *J* = 14.4, 9.4 Hz, 1H), 4.35 (q, 1H), 4.28 – 4.21 (m, 1H), 4.03 (p, *J* = 7.1 Hz, 1H), 3.87 (s, 3H), 3.84 (s, br 6H), 3.03 (dd, *J* = 14.7, 5.9 Hz, 1H), 2.93 – 2.86 (m, 1H), 1.68 (s, 3H), 1.02 (d, *J* = 7.1 Hz, 3H). **^{13}C NMR (176 MHz, DMSO)** δ 172.87, 171.12, 169.42, 166.71, 162.86, 161.06, 156.96, 153.63, 135.93, 131.42, 130.60, 127.33, 125.11, 123.43, 120.73, 118.41,

118.12, 114.94, 114.57, 111.14, 109.82, 55.63, 55.44, 53.15, 50.70, 48.36, 27.55, 22.22, 17.70. **HRMS ESI** m/z calculated for $C_{45}H_{47}N_6O_7^+$: 783.3501, measured: 783.3502.

Compound **64**.

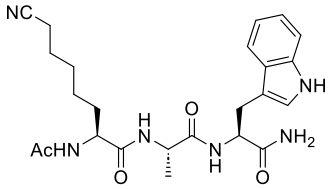

Synthesized according to the method described for **27**. Yield: 13.8 mg (29.5 µmol, 31%). **^{1}H NMR (700 MHz, DMSO-d_6)** δ 10.78 (d, *J* = 2.4 Hz, 1H), 8.08 (d, *J* = 7.0 Hz, 1H), 7.99 (d, *J* = 7.7 Hz, 1H), 7.70 (d, *J* = 8.0 Hz, 1H), 7.56 (d, *J* = 6.9 Hz, 1H), 7.31 (d, *J* = 8.1 Hz, 1H), 7.29 (s, 1H), 7.11 (d, *J* = 2.4 Hz, 1H), 7.07 – 7.02 (m, 2H), 6.99 – 6.94 (m, 1H), 4.43 – 4.37 (m, 1H), 4.24 – 4.14 (m, 2H), 3.12 (dd, *J* = 14.9, 5.5 Hz, 1H), 2.99 (dd, *J* = 14.8, 7.4 Hz, 1H), 2.45 – 2.38 (m, 2H), 1.84 (s, 3H), 1.61 – 1.54 (m, 1H), 1.49 (qd, *J* = 7.1, 3.4 Hz, 2H), 1.46 – 1.36 (m, 1H), 1.34 – 1.22 (m, 4H), 1.17 (d, *J* = 7.1 Hz, 3H). **^{13}C NMR (176 MHz, DMSO)** δ 173.14, 171.87, 171.82, 169.52, 136.01, 127.44, 123.48, 120.81, 120.71, 118.44, 118.22, 111.22, 109.98, 53.18, 52.57, 48.56, 31.52, 27.74, 27.58, 24.59, 24.47, 22.51, 17.75, 16.04. **HRMS ESI** m/z calculated for: $C_{24}H_{32}N_6O_4$ $[M+H]^+$: 469.2563, measured: 469.2556.

Compound **65**.

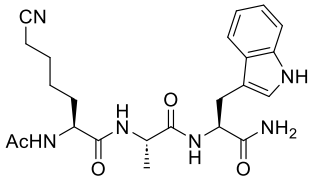

Synthesized according to the method described for **27**. Yield: 9.9 mg (21.8 µmol, 42%). **^{1}H NMR (700 MHz, DMSO-d_6)** δ 10.78 (d, *J* = 2.4 Hz, 1H), 8.11 (d, *J* = 7.1 Hz, 1H), 8.01 (d, *J* = 7.9 Hz, 1H), 7.67 (d, *J* = 8.0 Hz, 1H), 7.57 (d, *J* = 7.9 Hz, 1H), 7.33 – 7.28 (m, 2H), 7.11 (d, *J* = 2.3 Hz, 1H), 7.07 – 7.01 (m, 2H), 6.98 – 6.94 (m, 1H), 4.44 – 4.38 (m, 1H), 4.25 – 4.16 (m, 2H), 3.16 – 3.09 (m, 1H), 2.99 (dd, *J* = 14.4, 7.8 Hz, 1H), 2.46 – 2.36 (m, 2H), 1.84 (s, 3H), 1.62 – 1.54 (m, 1H), 1.54 – 1.47 (m, 2H), 1.47 – 1.38 (m, 1H), 1.37 – 1.28 (m, 2H), 1.17 (d, *J* = 7.1 Hz, 3H). **^{13}C NMR (176 MHz, DMSO)** δ 173.11, 171.74, 171.70, 169.43, 135.98, 127.43, 123.47, 120.79, 120.67, 118.44, 118.20, 111.19, 109.92, 53.07, 52.15, 48.54, 31.03, 27.61, 24.48, 24.45, 22.48, 17.77, 16.00. **HRMS ESI** m/z calculated for: $C_{23}H_{30}N_6O_4$ $[M+H]^+$: 455.2407, measured: 455.2391

Compound **66**.

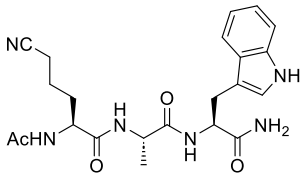

Synthesized according to the method described for **27**. Yield: 4.5 mg (10.2 µmol, 29%). **^{1}H NMR (700 MHz, DMSO-d_6)** δ 10.78 (d, *J* = 2.4 Hz, 1H), 8.12 (d, *J* = 7.0 Hz, 1H), 8.05 (d, *J* = 7.8 Hz, 1H), 7.75 (d, *J* = 8.0 Hz, 1H), 7.57 (d, *J* = 7.9 Hz, 1H), 7.31 (d, *J* = 8.2 Hz, 2H), 7.12 (d, *J* = 2.3 Hz, 1H), 7.07 – 7.02 (m, 2H), 6.96 (t, *J* = 7.4 Hz, 1H), 4.48 – 4.38 (m, 1H), 4.27 – 4.22 (m, 1H), 4.23 – 4.18 (m, 1H), 3.11 (dd, *J* = 14.7, 5.4 Hz, 1H), 2.99 (dd, *J* = 14.7, 7.8 Hz, 1H), 2.45 – 2.41 (m, 2H), 1.85 (s, 3H), 1.73 – 1.62 (m, 1H), 1.59 – 1.49 (m, 3H), 1.17 (d, *J* = 7.1 Hz, 3H). **^{13}C NMR (176 MHz, DMSO) δ** 173.14, 171.73, 171.20, 169.45, 135.98, 127.41, 123.47, 120.79, 120.47, 118.45, 118.20, 111.18, 109.98, 53.14, 51.73, 48.50, 40.02, 39.88, 39.76, 39.64, 39.52, 39.40, 39.28, 39.16, 30.99, 27.58, 22.46, 21.34, 17.79, 15.84. **HRMS ESI** m/z calculated for: $C_{22}H_{28}N_6O_4$ $[M+H]^+$: 441.2250, measured: 441.2241.

Compound **67**.

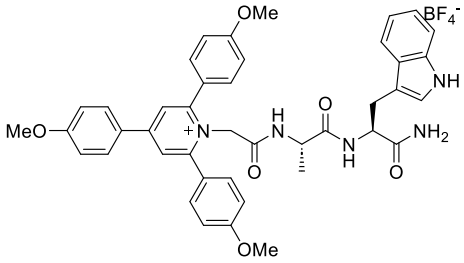

Synthesized according to the method described for **21.** Yield: 59.0 mg (73.8 µmol, 74%). **^{1}H NMR (700 MHz, DMSO-d_6)** δ 10.79 (d, *J* = 2.4 Hz, 1H), 8.32 (s, 2H), 8.27 (d, *J* = 9.0 Hz, 2H), 8.21 (d, *J* = 7.3 Hz, 1H), 8.08 (d, *J* = 8.1 Hz, 1H), 7.59 (d, *J* = 7.8 Hz, 1H), 7.54 (d, *J* = 8.1 Hz, 4H), 7.32 (s, 1H), 7.29 (d, *J* = 8.0 Hz, 1H), 7.18 – 7.10 (m, 6H), 7.08 (d, *J* = 2.4 Hz, 1H), 7.03 (s, 1H), 7.04 – 6.99 (m, 1H), 6.94 – 6.88 (m, 1H), 4.97 (d, *J* = 17.1 Hz, 1H), 4.83 (d, *J* = 17.1 Hz, 1H), 4.44 – 4.36 (m, 1H), 4.15 (p, *J* = 7.0 Hz, 1H), 3.88 (s, br, 3H), 3.81 (s, 6H), 3.10 (dd, *J* = 14.6, 5.5 Hz, 1H), 2.92 (dd, *J* = 14.6, 8.3 Hz, 1H), 0.97 (d, *J* = 6.9 Hz, 3H). **^{13}C NMR (176 MHz, DMSO)** δ 172.99, 170.94, 164.29, 162.91, 160.92, 156.34, 153.78, 135.92, 130.75, 130.66, 127.23, 125.02, 124.74, 123.91, 123.37, 120.73, 118.37, 118.09, 115.01, 114.32, 111.17, 110.05, 56.77, 55.63, 55.43, 55.40, 53.39, 48.45, 27.60, 18.31. **HRMS ESI** m/z calculated for $C_{42}H_{42}N_5O_6^+$ $[M]^+$: 712.3130, measured: 712.3109

Compound **68**.

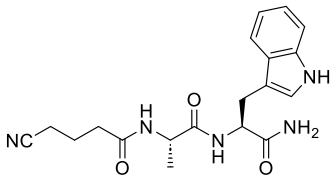

Synthesized according to the method described for **27**. Yield: 4.6 mg (12.5 µmol, 17%). **^{1}H NMR (700 MHz, DMSO-d_6)** δ 10.78 (d, *J* = 2.4 Hz, 1H), 8.12 (d, *J* = 7.0 Hz, 1H), 8.05 (d, *J* = 7.8 Hz, 1H), 7.75 (d, *J* = 8.0 Hz, 1H), 7.57 (d, *J* = 7.9 Hz, 1H), 7.31 (d, *J* = 8.2 Hz, 2H), 7.12 (d, *J* = 2.3 Hz, 1H), 7.07 – 7.02 (m, 2H), 6.96 (t, *J* = 7.4 Hz, 1H), 4.48 – 4.38 (m, 1H), 4.27 – 4.22 (m, 1H), 4.23 – 4.18 (m, 1H), 3.11 (dd, *J* = 14.7, 5.4 Hz, 1H), 2.99 (dd, *J* = 14.7, 7.8 Hz, 1H), 2.45 – 2.41 (m, 2H), 1.85 (s, 3H), 1.73 – 1.62 (m, 1H), 1.59 – 1.49 (m, 3H), 1.17 (d, *J* = 7.1 Hz, 3H).**^{13}C NMR (176 MHz, DMSO) δ** 173.14, 171.73, 171.20, 169.45, 135.98, 127.41, 123.47, 120.79, 120.47, 118.45, 118.20, 111.18, 109.98, 53.14, 51.73, 48.50, 40.02, 39.88, 39.76, 39.64, 39.52, 39.40, 39.28, 39.16, 30.99, 27.58, 22.46, 21.34, 17.79, 15.84. **HRMS ESI** m/z calculated for: $C_{19}H_{23}N_5O_3[M+H]^+$: 370.1879, measured: 370.1874.

Compound **74/76**.

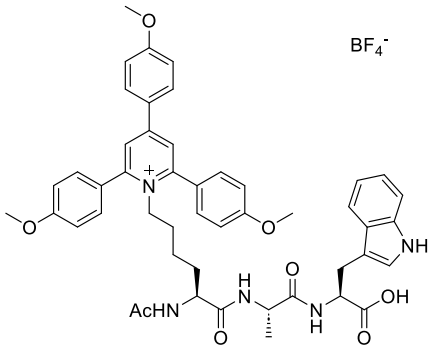

Resins were loaded according to general method **2h**, and the peptides were synthesized according to the method described for **21.** Thereafter, a 100 µmol aliquot was cleaved and deprotected according to general method **2e.** The crude peptide was then purified by general purification method **B** (Wang resin) or **A** (HMPB resin). Yields: a) Wang resin 48.0 mg (53.2 µmol, 53%); b) HMPB resin 64.0 mg (70.4 µmol, 70%). **^{1}H NMR (700 MHz, DMSO-d_6)** δ 10.82 (d, *J* = 2.4 Hz, 1H), 8.27 (s, 2H), 8.24 (d, *J* = 9.0 Hz, 2H), 8.01 (d, *J* = 7.5 Hz, 1H), 7.80 (d, *J* = 7.4 Hz, 1H), 7.76 – 7.71 (m, 5H), 7.49 (d, *J* = 7.8 Hz, 1H), 7.30 (d, *J* = 8.1 Hz, 1H), 7.19 (d, *J* = 8.8 Hz, 4H), 7.15 – 7.11 (m, 3H), 7.03 (t, *J* = 7.5 Hz, 1H), 6.95 (t, *J* = 7.4 Hz, 1H), 4.45 – 4.38 (m, 1H), 4.33 (t, *J* = 7.6 Hz, 2H), 4.22 (p, *J* = 7.1 Hz, 1H), 4.02 – 3.95 (m, 1H), 3.87 (s, 3H), 3.85 (s, 6H), 3.11 (dd, *J* = 14.8, 5.6 Hz, 1H), 3.02 (dd, *J* = 14.7, 7.5 Hz, 1H), 1.73 (s, 3H), 1.41 – 1.24 (m, 2H), 1.14 (d, *J* = 7.0 Hz, 2H), 1.02 – 0.93 (m, 2H), 0.81 – 0.61 (m, 2H). **^{13}C NMR (176 MHz, DMSO)** δ 173.00, 171.97, 170.88, 169.09, 162.78, 160.90, 155.83, 153.06, 135.94, 130.91, 130.50,

127.12, 125.34, 125.03, 124.46, 123.63, 120.79, 118.27, 118.05, 114.97, 114.39, 111.24, 109.41, 55.60, 55.43, 54.11, 52.86, 51.63, 47.73, 30.90, 28.31, 26.89, 22.28, 21.75, 18.03. **HRMS ESI** m/z calculated for $C_{48}H_{52}N_5O_8^+$ $[M]^+$: 826.3810, measured: 826.3794.

Compound **77**.

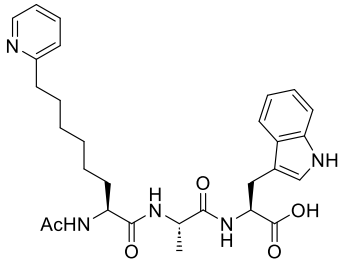

Synthesized according to the method described for **27**. Yield: HMBP resin on 62 µmol scale: (10.7mg, 20.0 µmol; 32%) Wang resin on 100 µmol scale: (11.2 mg, 10.0 µmol, 21%). **^{1}H NMR (700 MHz, DMSO-d_6)** δ 10.84 (d, *J* = 2.4 Hz, 1H), 8.73 (dd, *J* = 5.6, 1.7 Hz, 1H), 8.39 – 8.24 (m, 1H), 8.01 (d, *J* = 7.6 Hz, 1H), 7.95 (dd, *J* = 14.4, 7.8 Hz, 2H), 7.80 (d, *J* = 8.0 Hz, 1H), 7.75 (t, *J* = 6.6 Hz, 1H), 7.51 (d, *J* = 7.0 Hz, 1H), 7.32 (d, *J* = 8.1 Hz, 1H), 7.16 (d, *J* = 2.3 Hz, 1H), 7.05 (ddd, *J* = 8.1, 6.9, 1.2 Hz, 1H), 6.96 (ddd, *J* = 8.0, 6.9, 1.0 Hz, 1H), 4.43 (td, *J* = 7.5, 5.6 Hz, 1H), 4.30 (p, *J* = 7.1 Hz, 1H), 4.21 (td, *J* = 8.4, 5.3 Hz, 1H), 3.14 (dd, *J* = 14.7, 5.6 Hz, 1H), 3.05 (dd, *J* = 14.7, 7.5 Hz, 1H), 2.90 (t, *J* = 7.8 Hz, 2H), 1.82 (s, 3H), 1.70 – 1.61 (m, 2H), 1.61 – 1.52 (m, 1H), 1.43 (qd, *J* = 9.0, 3.3 Hz, 1H), 1.29 – 1.20 (m, 6H), 1.20 (d, *J* = 7.1 Hz, 3H). **^{13}C NMR (176 MHz, DMSO)** δ 173.07, 172.11, 171.45, 169.20, 158.34, 158.15, 136.03, 127.23, 126.04, 123.91, 123.71, 120.87, 118.34, 118.15, 111.34, 109.50, 55.96, 52.95, 52.32, 47.87, 33.56, 31.98, 28.59, 28.28, 28.26, 27.00, 25.06, 22.49, 18.14. **HRMS ESI** m/z calculated for $C_{48}H_{52}N_5O_8^+$ $[M]^+$: 536.2873, measured: 536.2861

Compound **78**.

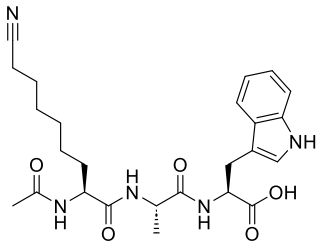

Synthesized according to the method described for **4** with HMBP resin. Yield: 11.0 mg (22.8 µmol, 32%). **^{1}H NMR (500 MHz, DMSO-d_6)** δ 12.67 (s, 1H), 10.86 (d, *J* = 2.5 Hz, 1H), 8.06 – 7.94 (m, 3H), 7.52 (d, *J* = 7.9 Hz, 1H), 7.33 (d, *J* = 8.0 Hz, 1H), 7.17 (d, *J* = 2.5 Hz, 1H), 7.06 (ddd, *J* = 8.1, 6.9, 1.2 Hz, 1H), 7.01 – 6.92 (m, 1H), 4.45 (td, *J* = 7.5, 5.6 Hz, 1H), 4.35 – 4.27 (m, 1H), 4.21 (td, *J* = 8.5, 5.2 Hz, 1H), 2.42 (t, *J* = 7.1 Hz, 2H), 1.64 – 1.40 (m, 4H), 1.34 – 1.21 (m, 6H), 1.20 (d, *J* = 7.2 Hz, 3H). **^{13}C NMR (126 MHz,**

DMSO) δ 173.15, 172.14, 171.55, 169.28, 136.07, 127.27, 123.75, 120.94, 120.78, 118.40, 118.22, 111.38, 109.52, 52.93, 52.38, 47.93, 31.98, 27.95, 27.89, 27.04, 25.06, 24.66, 22.52, 18.17, 16.07. **HRMS ESI** m/z calculated for $C_{48}H_{52}N_5O_8^+$ [M]$^+$: 484.2560, measured: 484.2550

Compound **69**.

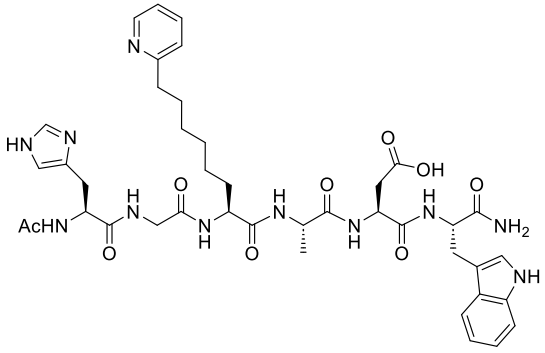

Synthesized according to general method **2a – 2d** and peptide cleavage was carried out according to method **2f** followed by purification using method **D**. Yield: 3.7 mg (4.4 µmol, 4%). **HRMS ESI** m/z calculated for $C_{48}H_{52}N_5O_8^+$ [M+H]$^+$: 844.4106 measured: 844.4084.

Compound **70**.

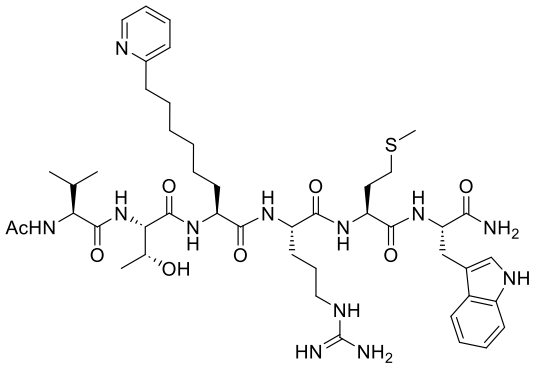

Synthesized according to general method **2a – 2d** and peptide cleavage was carried out according to method **2g** followed by purification using method **D**. Yield: 7.5 mg (7.9 µmol, 8%). **HRMS ESI** m/z calculated for $C_{48}H_{52}N_5O_8^+$ [M+H]$^+$: 951.5239, measured: 951.5220.

Compound **71**.

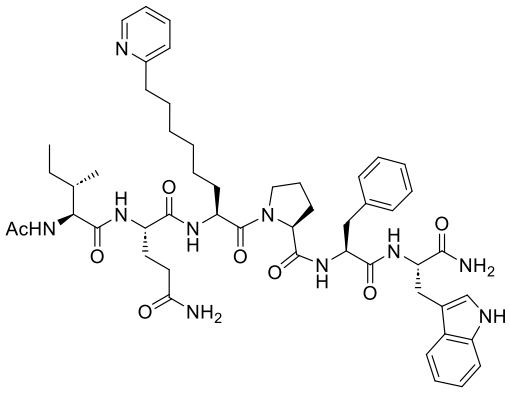

Synthesized according to the method described for **69**. Yield: 12.4 mg (13.4 µmol, 13%). **HRMS ESI** m/z calculated for $C_{48}H_{52}N_5O_8^+$ $[M+H]^+$: 949.5300, measured: 949.5284.

Compound **72**.

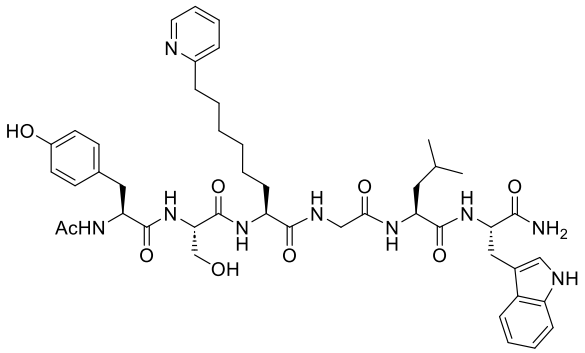

Synthesized according to the method described for **69**. Yield: 11.8 mg (13.4 µmol, 13%). **HRMS ESI** m/z calculated for $C_{48}H_{52}N_5O_8^+$ $[M]^+$: 884.4670, measured: 844.4655.

Compound **73**.

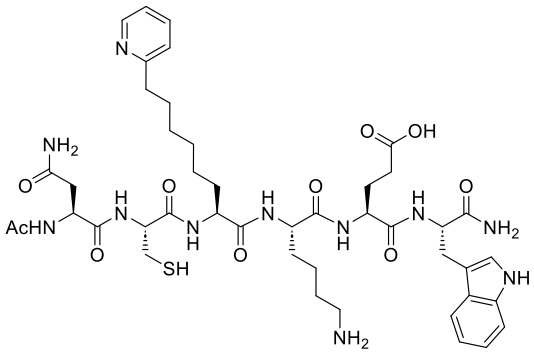

Synthesized according to the method described for **70**. Yield: 8.0 mg (8.5 µmol, 8%). **HRMS ESI** m/z calculated for $C_{48}H_{52}N_5O_8^+$ $[M]^+$: 938.4558, measured: 938.4538.

Compound **82**.

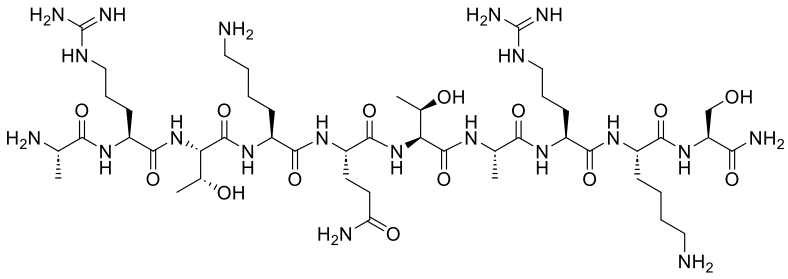

Synthesized according to general method **2a – 2d** and peptide cleavage was carried out according to method **2f** and purification was performed using purification method **E**. Yield: 54.4 mg (47.5 µmol, 48%). **HRMS ESI** m/z calculated for $C_{46}H_{88}N_{20}O_{14}$ $[M+2H]^{2+}$: 573.3473, measured: 573.3467.

Compound **83.**

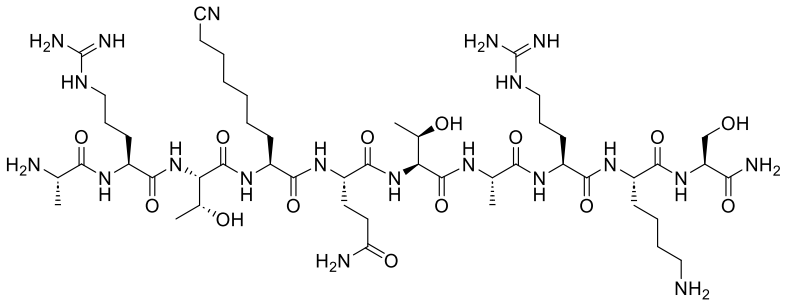

Synthesized according to general method **2a** – **2d** on a 100 µmol scale**.** Peptide cleavage was carried out according to method **2f** and purification was performed using purification method **E**. Yield: 22.0 mg (18.6 µmol, 19%). **HRMS ESI** m/z calculated for $C_{49}H_{90}N_{20}O_{14}$ $[M+2H]^{2+}$: 592.3551, measured: 592.3531.

Compound **84**.

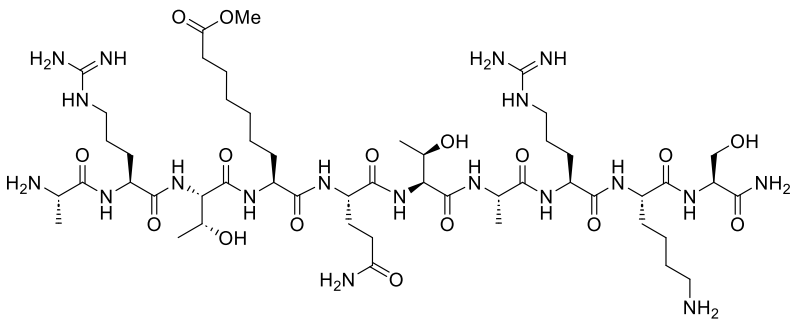

Synthesized according to the method described for **83**. Yield: 16.1 mg (13.2 µmol, 13%). **HRMS ESI** m/z calculated for $C_{50}H_{93}N_{19}O_{16}$ $[M+2H]^{2+}$: 608.8602, measured: 608.8587.

Compound **86**.

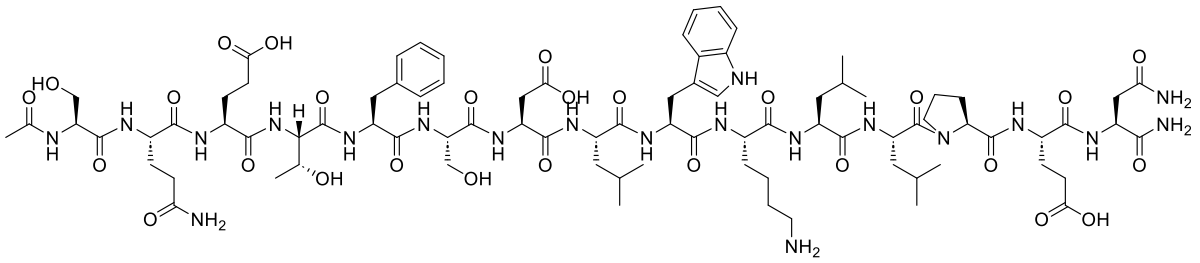

Synthesized according to the method described for **39**. Yield: 46.0 mg (24.9 µmol, 25%)

HRMS ESI m/z calculated for $C_{91}H_{137}N_{21}O_{29}$ $[M+2H]^{2+}$: 924.4629, measured: 924.4594

Compound **87**.

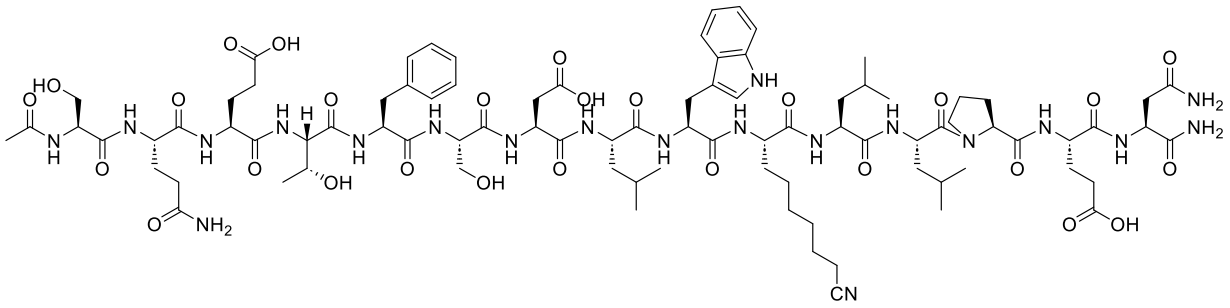

Synthesized according to the method described for **69**. Yield: 16.1 mg (13.2 µmol, 13%). **HRMS ESI** m/z calculated for $C_{87}H_{128}N_{20}O_{27}$ $[M+H]^{+}$: 1885.9336, measured: 1885.9325.

Compound **88**.

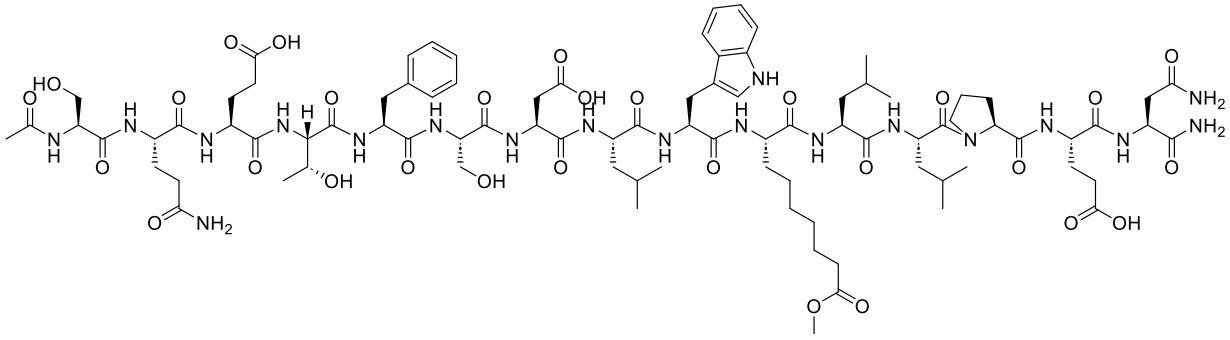

Synthesized according to the method described for **69**. Yield: 16.7 mg (8.7 µmol, 9%). **HRMS ESI** m/z calculated for $C_{91}H_{137}N_{21}O_{29}$ $[M+2H]^{2+}$: 959.9758, measured: 959.9753.

Compound **90**.

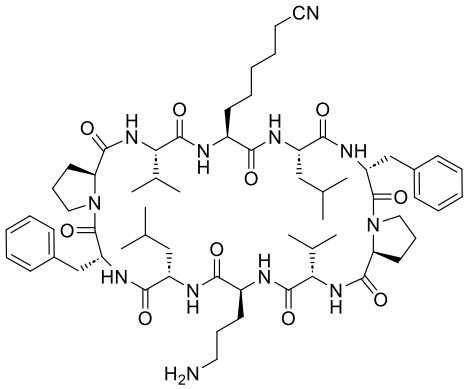

Wang resin loading of Fmoc-dPhe-OH was performed by method **2h** followed by synthesis of the linear peptide with Boc-Pro-OH at the N-terminus according to method **2a** on a 100 µmol scale. Alloc deprotection was carried out using method **2b** and subsequently Katritzky salt synthesis and photochemistry according to methods **2c** and **2d** respectively. Next, the peptide was cleaved using method **2f**. The cleaved IvDde protected peptides were dissolved in a minimum amount of DMF required for dissolution and CH_2Cl_2 (200 ml) followed by the addition of HCTU (2 eq) and DIPEA (4 eq). The solvent was removed in vacuo after stirring overnight. Crude cyclized peptides were taken up in THF and transferred to a 25 mL round bottomed flask followed by treatment with 2% H_2NNH_2/THF (10 mL) at room temperature while stirring. After 16 h, the crude mixture was concentrated in vacuo, dissolved in acetonitrile/water (1:1) and purified by preparative HPLC according to purification method **D**. Yield: 10.0 mg (8.5 µmol, 8%). **HRMS ESI** m/z calculated for $C_{63}H_{94}N_{12}O_{10}$ $[M+H]^+$: 1179.7294, measured: 1179.7300.

Compound **91**.

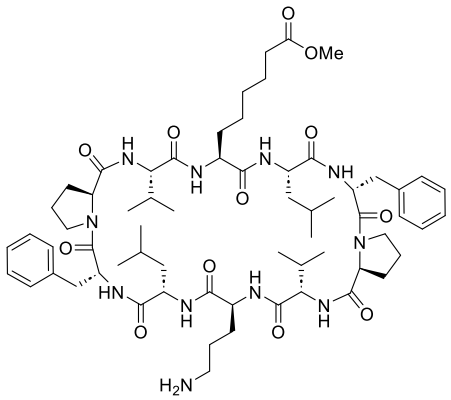

Synthesized according to the method described for **90**. Yield: 8.5 mg (7.0 µmol, 7%). **HRMS ESI** m/z calculated for $C_{64}H_{97}N_{11}O_{12}$ $[M+2H]^{2+}$:606.8738, measured: 606.8766.

5. Bibliography

[1] H. D. Springall, H. D. Law, *Q. Rev. Chem. Soc.* **1956**, *10*, 230–257.

[2] L. Sukmarini, *IOP Conf. Ser. Mater. Sci. Eng.* **2021**, *1011*, 012063.

[3] S. L. Wenski, S. Thiengmag, E. J. N. Helfrich, *Synth. Syst. Biotechnol.* **2022**, *7*, 631–647.

[4] L. Y. Jan, Y. N. Jan, *J. Physiol.* **1982**, *327*, 219–246.

[5] Y. Wang, M. Wang, S. Yin, R. Jang, J. Wang, Z. Xue, T. Xu, *Database J. Biol. Databases Curation* **2015**, *2015*, bav038.

[6] A. M. Flower, R. C. Doebele, T. J. Silhavy, *J. Bacteriol.* **1994**, *176*, 5607–5614.

[7] R. Unger, L. Orci, *The Lancet* **1975**, *305*, 14–16.

[8] S. Cohen, *J. Biol. Chem.* **1962**, *237*, 1555–1562.

[9] C. R. Savage, J. H. Hash, S. Cohen, *J. Biol. Chem.* **1973**, *248*, 7669–7672.

[10] Y. Huan, Q. Kong, H. Mou, H. Yi, *Front. Microbiol.* **2020**, *11*.

[11] S.-C. Yang, C.-H. Lin, C. T. Sung, J.-Y. Fang, *Front. Microbiol.* **2014**, *5*.

[12] G. Wang, X. Li, Z. Wang, *Nucleic Acids Res.* **2016**, *44*, D1087–D1093.

[13] G. S. Dijksteel, M. M. W. Ulrich, E. Middelkoop, B. K. H. L. Boekema, *Front. Microbiol.* **2021**, *12*, 616979.

[14] S. Hartwig, C. Dovengerds, C. Herrmann, B. T. Hovemann, *FEBS J.* **2014**, *281*, 5147–5158.

[15] K. A. J. Bozhüyük, A. Linck, A. Tietze, J. Kranz, F. Wesche, S. Nowak, F. Fleischhacker, Y.-N. Shi, P. Grün, H. B. Bode, *Nat. Chem.* **2019**, *11*, 653–661.

[16] M. A. Fischbach, C. T. Walsh, *Chem. Rev.* **2006**, *106*, 3468–3496.

[17] D. Giordano, D. Coppola, R. Russo, R. Denaro, L. Giuliano, F. M. Lauro, G. di Prisco, C. Verde, in *Adv. Microb. Physiol.* (Ed.: R.K. Poole), Academic Press, **2015**, pp. 357–428.

[18] D. P. Dowling, Y. Kung, A. K. Croft, K. Taghizadeh, W. L. Kelly, C. T. Walsh, C. L. Drennan, *Proc. Natl. Acad. Sci.* **2016**, *113*, 12432–12437.

[19] M. Nourisefat, F. Panahi, A. Khalafi-Nezhad, *Mol. Divers.* **2019**, *23*, 317–331.

[20] L. L. Guan, Y. Sera, K. Adachi, F. Nishida, Y. Shizuri, *Biochem. Biophys. Res. Commun.* **2001**, *283*, 976–981.

[21] J. T. Mhlongo, E. Brasil, B. G. de la Torre, F. Albericio, *Mar. Drugs* **2020**, *18*, 203.

[22] R. Dahiya, S. Dahiya, N. K. Fuloria, S. Kumar, R. Mourya, S. V. Chennupati, S. Jankie, H. Gautam, S. Singh, S. K. Karan, S. Maharaj, S. Fuloria, J. Shrivastava, A. Agarwal, S. Singh, A. Kishor, G. Jadon, A. Sharma, *Mar. Drugs* **2020**, *18*, 329.

[23] H. Luo, S.-Y. Hong, R. M. Sgambelluri, E. Angelos, X. Li, J. D. Walton, *Chem. Biol.* **2014**, *21*, 1610–1617.

[24] Z. Wu, Y. Li, Y. Xu, Y. Zhang, G. Tao, L. Zhang, G. Shi, *ACS Synth. Biol.* **2022**, *11*, 1325–1335.

[25] C. Dennis, J. Webster, *Trans. Br. Mycol. Soc.* **1971**, *57*, 41-IN4.

[26] K. Sikora, M. Jaśkiewicz, D. Neubauer, D. Migoń, W. Kamysz, *Pharmaceuticals* **2020**, *13*, 442.

[27] B. M. Rode, *Peptides* **1999**, *20*, 773–786.

[28] J. C. Charlesworth, B. P. Burns, *Archaea* **2015**, *2015*, e282035.

[29] M. Muttenthaler, G. F. King, D. J. Adams, P. F. Alewood, *Nat. Rev. Drug Discov.* **2021**, *20*, 309–325.

[30] M. W. F. S. Macedo, N. B. da Cunha, J. A. Carneiro, R. A. da Costa, S. A. de Alencar, M. H. Cardoso, O. L. Franco, S. C. Dias, *Front. Mar. Sci.* **2021**, *8*.

[31] D. Smith, A. G. Buddie, R. J. M. Goss, J. Overmann, C. Lepleux, M. Brönstrup, B. Kloareg, T. Meiners, P. Brennecke, A. Ianora, F.-Y. Bouget, P. Gribbon, M. Pina, *World J. Microbiol. Biotechnol.* **2019**, *35*, 107.

[32] S. Jones, J. M. Thornton, *Proc. Natl. Acad. Sci.* **1996**, *93*, 13–20.

[33] M. G. Kann, *Brief. Bioinform.* **2007**, *8*, 333–346.

[34] B. O. Villoutreix, C. Labbé, D. Lagorce, G. Laconde, O. Sperandio, *Curr. Pharm. Des.* **2012**, *18*, 4648–4667.

[35] J. A. Wells, C. L. McClendon, *Nature* **2007**, *450*, 1001–1009.

[36] Y. Qiao, Y. Xiong, H. Gao, X. Zhu, P. Chen, *BMC Bioinformatics* **2018**, *19*, 14.

[37] F. G. Banting, C. H. Best, J. B. Collip, W. R. Campbell, A. A. Fletcher, *Can. Med. Assoc. J.* **1922**, *12*, 141–146.

[38] F. Sanger, H. Tuppy, *Biochem. J.* **1951**, *49*, 481–490.

[39] V. du Vigneaud, C. Ressler, S. Trippett, *J. Biol. Chem.* **1953**, *205*, 949–957.

[40] V. du Vigneaud, C. Ressler, J. M. Swan, C. W. Roberts, P. G. Katsoyannis, *J. Am. Chem. Soc.* **1954**, *76*, 3115–3121.

[41] H. Schwarz, F. M. Bumpus, I. H. Page, *J. Am. Chem. Soc.* **1957**, *79*, 5697–5703.

[42] C. H. Li, J. Meienhofer, E. Schnabel, D. Chung, T.-B. Lo, J. Ramachandran, *J. Am. Chem. Soc.* **1960**, *82*, 5760–5762.

[43] K. Hofmann, H. Yajima, N. Yanaihara, T. Liu, S. Lande, *J. Am. Chem. Soc.* **1961**, *83*, 487–489.

[44] T. O. Alves, C. T. S. D'Almeida, K. A. Scherf, M. S. L. Ferreira, *Front. Plant Sci.* **2019**, *10*.

[45] R. B. Merrifield, in *Hypotens. Pept.* (Eds.: E.G. Erdös, N. Back, F. Sicuteri, A.F. Wilde), Springer, Berlin, Heidelberg, **1966**, pp. 1–13.

[46] M. Goodman, K. C. Stueben, *J. Am. Chem. Soc.* **1959**, *81*, 3980–3983.

[47] G. W. Anderson, F. M. Callahan, *J. Am. Chem. Soc.* **1958**, *80*, 2902–2903.

[48] G. W. Anderson, *Ann. N. Y. Acad. Sci.* **1960**, *88*, 676–688.

[49] R. B. Merrifield, *J. Am. Chem. Soc.* **1963**, *85*, 2149–2154.

[50] R. B. Merrifield, *Biochemistry* **1964**, *3*, 1385–1390.

[51] R. B. Merrifield, J. Morrow. Stewart, Nils. Jernberg, *Anal. Chem.* **1966**, *38*, 1905–1914.

[52] M. W. Pennington, in *Pept. Synth. Protoc.* (Eds.: M.W. Pennington, B.M. Dunn), Humana Press, Totowa, NJ, **1995**, pp. 41–62.

[53] M. Amblard, J.-A. Fehrentz, J. Martinez, G. Subra, *Mol. Biotechnol.* **2006**, *33*, 239–254.

[54] D. Sun, *Molecules* **2022**, *27*, 1012.

[55] W. J. Henzel, J. T. Stults, *Curr. Protoc. Protein Sci.* **2001**, *24*, 11.6.1-11.6.16.

[56] I. Vávra, A. Machová, V. Holecek, J. H. Cort, M. Zaoral, F. Sorm, *The Lancet* **1968**, *291*, 948–952.

[57] J. F. Borel, C. Feurer, H. U. Gubler, H. Stähelin, *Agents Actions* **1976**, *6*, 468–475.

[58] K. Bozovičar, T. Bratkovič, *Int. J. Mol. Sci.* **2019**, *21*, 215.

[59] Á. Furka, F. Sebestyén, M. Asgedom, G. Dibó, *Int. J. Pept. Protein Res.* **1991**, *37*, 487–493.

[60] S. Chen, I. Rentero Rebollo, S. A. Buth, J. Morales-Sanfrutos, J. Touati, P. G. Leiman, C. Heinis, *J. Am. Chem. Soc.* **2013**, *135*, 6562–6569.

[61] E. L. Osher, A. Tavassoli, in *Split Inteins Methods Protoc.* (Ed.: H.D. Mootz), Springer, New York, NY, **2017**, pp. 27–39.

[62] T. Shi, P. E. Polderman, M. Pagès-Gallego, R. M. van Es, H. R. Vos, B. M. T. Burgering, T. B. Dansen, *Antioxidants* **2021**, *10*, 1578.

[63] Z. Wang, T. Rejtar, Z. S. Zhou, B. L. Karger, *Rapid Commun. Mass Spectrom. RCM* **2010**, *24*, 267–275.

[64] B. H. Gless, C. A. Olsen, *J. Org. Chem.* **2018**, *83*, 10525–10534.

[65] M. A. Elsawy, C. Hewage, B. Walker, *J. Pept. Sci.* **2012**, *18*, 302–311.

[66] C. Brieke, M. J. Cryle, *Org. Lett.* **2014**, *16*, 2454–2457.

[67] J. S. Davies, *J. Pept. Sci.* **2003**, *9*, 471–501.

[68] K. L. Zapadka, F. J. Becher, A. L. Gomes dos Santos, S. E. Jackson, *Interface Focus* **2017**, *7*, 20170030.

[69] W. Wang, S. K. Singh, N. Li, M. R. Toler, K. R. King, S. Nema, *Int. J. Pharm.* **2012**, *431*, 1–11.

[70] M. Werle, A. Bernkop-Schnürch, *Amino Acids* **2006**, *30*, 351–367.

[71] G. A. Fleisher, H. R. Butt, N. Goplerud, *J. Clin. Invest.* **1953**, *32*, 674–680.

[72] J. Jyrkäs, A. Tolonen, *J. Pharm. Biomed. Anal.* **2021**, *196*, 113921.

[73] S. C. Penchala, M. R. Miller, A. Pal, J. Dong, N. R. Madadi, J. Xie, H. Joo, J. Tsai, P. Batoon, V. Samoshin, A. Franz, T. Cox, J. Miles, W. K. Chan, M. S. Park, M. M. Alhamadsheh, *Nat. Chem. Biol.* **2015**, *11*, 793–798.

[74] C. A. Lipinski, F. Lombardo, B. W. Dominy, P. J. Feeney, *Adv. Drug Deliv. Rev.* **2001**, *46*, 3–26.

[75] N. Barlow, D. K. Chalmers, B. J. Williams-Noonan, P. E. Thompson, R. S. Norton, *ACS Chem. Biol.* **2020**, *15*, 2070–2078.

[76] S. Gangwar, S. D. S. Jois, T. J. Siahaan, D. G. Vander Velde, V. J. Stella, R. T. Borchardt, *Pharm. Res.* **1996**, *13*, 1657–1662.

[77] D. F. Veber, S. R. Johnson, H.-Y. Cheng, B. R. Smith, K. W. Ward, K. D. Kopple, *J. Med. Chem.* **2002**, *45*, 2615–2623.

[78] B. C. Doak, B. Over, F. Giordanetto, J. Kihlberg, *Chem. Biol.* **2014**, *21*, 1115–1142.

[79] B. C. Doak, J. Zheng, D. Dobritzsch, J. Kihlberg, *J. Med. Chem.* **2016**, *59*, 2312–2327.

[80] P. Matsson, B. C. Doak, B. Over, J. Kihlberg, *Adv. Drug Deliv. Rev.* **2016**, *101*, 42–61.

[81] S. Gomez, P. Gluschankof, A. Lepage, P. Cohen, *Proc. Natl. Acad. Sci. U. S. A.* **1988**, *85*, 5468–5472.

[82] R. Pike, W. McGraw, J. Potempa, J. Travis, *J. Biol. Chem.* **1994**, *269*, 406–411.

[83] R. Yazbeck, S. E. Jaenisch, C. A. Abbott, *Biochem. Pharmacol.* **2021**, *188*, 114517.

[84] A. K. Ghose, V. N. Viswanadhan, J. J. Wendoloski, *J. Comb. Chem.* **1999**, *1*, 55–68.

[85] L. Wang, N. Wang, W. Zhang, X. Cheng, Z. Yan, G. Shao, X. Wang, R. Wang, C. Fu, *Signal Transduct. Target. Ther.* **2022**, *7*, 1–27.

[86] M. Rask-Andersen, S. Masuram, H. B. Schiöth, *Annu. Rev. Pharmacol. Toxicol.* **2014**, *54*, 9–26.

[87] A. P. Crew, K. Raina, H. Dong, Y. Qian, J. Wang, D. Vigil, Y. V. Serebrenik, B. D. Hamman, A. Morgan, C. Ferraro, K. Siu, T. K. Neklesa, J. D. Winkler, K. G. Coleman, C. M. Crews, *J. Med. Chem.* **2018**, *61*, 583–598.

[88] M.-Q. Zhang, B. Wilkinson, *Curr. Opin. Biotechnol.* **2007**, *18*, 478–488.

[89] G. B. Santos, A. Ganesan, F. S. Emery, *ChemMedChem* **2016**, *11*, 2245–2251.

[90] S. A. Waksman, H. B. Woodruff, *Proc. Soc. Exp. Biol. Med.* **1940**, *45*, 609–614.

[91] A. A. Kaspar, J. M. Reichert, *Drug Discov. Today* **2013**, *18*, 807–817.

[92] K. Fosgerau, T. Hoffmann, *Drug Discov. Today* **2015**, *20*, 122–128.

[93] C. Kristensen, T. Kjeldsen, F. C. Wiberg, L. Schäffer, M. Hach, S. Havelund, J. Bass, D. F. Steiner, A. S. Andersen, *J. Biol. Chem.* **1997**, *272*, 12978–12983.

[94] A. Adhikari, B. Raj Bhattarai, A. Aryal, N. Thapa, P. Kc, A. Adhikari, S. Maharjan, P. B. Chanda, B. P. Regmi, N. Parajuli, *RSC Adv.* **2021**, *11*, 38126–38145.

[95] F. Agostini, J.-S. Völler, B. Koksch, C. G. Acevedo-Rocha, V. Kubyshkin, N. Budisa, *Angew. Chem. Int. Ed.* **2017**, *56*, 9680–9703.

[96] J. Michael Conlon, R. Al-Kharrge, E. Ahmed, H. Raza, S. Galadari, E. Condamine, *Peptides* **2007**, *28*, 2075–2080.

[97] A. Bhardwaj, V. Nayan, P. Sharma, S. Kumar, Y. Pal, J. Singh, *Silico Pharmacol.* **2017**, *5*, 5.

[98] Engel J.B, Diedrich K, Honig A, *Lett. Drug Des. Discov.* **2005**, *2*, 533–536.

[99] M. A. T. van de Plassche, T. J. O'Neill, T. Seeholzer, B. Turk, D. Krappmann, S. H. L. Verhelst, *J. Med. Chem.* **2020**, *63*, 3996–4004.

[100] P. G. Dougherty, A. Sahni, D. Pei, *Chem. Rev.* **2019**, *119*, 10241–10287.

[101] H. Shimizu, A. R. Renslo, *ChemMedChem* **2022**, *17*, e202200204.

[102] M. C. Lucana, Y. Arruga, E. Petrachi, A. Roig, R. Lucchi, B. Oller-Salvia, *Pharmaceutics* **2021**, *13*, 2065.

[103] X. Wei, C. Zhan, Q. Shen, W. Fu, C. Xie, J. Gao, C. Peng, P. Zheng, W. Lu, *Angew. Chem. Int. Ed Engl.* **2015**, *54*, 3023–3027.

[104] Z. Li, J. Xie, S. Peng, S. Liu, Y. Wang, W. Lu, J. Shen, C. Li, *Bioconjug. Chem.* **2017**, *28*, 2167–2179.

[105] D. Meister, S. M. Taimoory, J. F. Trant, *Pept. Sci.* **2019**, *111*, e24058.

[106] A. Tapeinou, M.-T. Matsoukas, C. Simal, T. Tselios, *Pept. Sci.* **2015**, *104*, 453–461.

[107] C. K. Wang, D. J. Craik, *Pept. Sci.* **2016**, *106*, 901–909.

[108] T. Rückle, P. de Lavallaz, M. Keller, P. Dumy, M. Mutter, *Tetrahedron* **1999**, *55*, 11281–11288.

[109] C. J. White, A. K. Yudin, *Nat. Chem.* **2011**, *3*, 509–524.

[110] P. 't Hart, L. H. J. Kleijn, G. de Bruin, S. F. Oppedijk, J. Kemmink, N. I. Martin, *Org. Biomol. Chem.* **2014**, *12*, 913–918.

[111] M. Malesevic, U. Strijowski, D. Bächle, N. Sewald, *J. Biotechnol.* **2004**, *112*, 73–77.

[112] M. V. Trivedi, J. S. Laurence, T. J. Siahaan, *Curr. Protein Pept. Sci.* **2009**, *10*, 614–625.

[113] D. S. H. W. Nicol, L. F. Smith, *Nature* **1960**, *187*, 483–485.

[114] P. 't Hart, P. Hommen, A. Noisier, A. Krzyzanowski, D. Schüler, A. T. Porfetye, M. Akbarzadeh, I. R. Vetter, H. Adihou, H. Waldmann, *Angew. Chem. Int. Ed.* **2021**, *60*, 1813–1820.

[115] D. Kobayashi, Y. Kohmura, T. Sugiki, E. Kuraoka, M. Denda, T. Fujiwara, A. Otaka, *Chem. – Eur. J.* **2021**, *27*, 14092–14099.

[116] S. Funakoshi, N. Fujii, K. Akaji, H. Irie, H. Yajima, *Chem. Pharm. Bull. (Tokyo)* **1979**, *27*, 2151–2156.

[117] L. Feni, I. Neundorf, in *Pept. Macrocycles Methods Protoc.* (Eds.: M.B. Coppock, A.J. Winton), Springer US, New York, NY, **2022**, pp. 375–389.

[118] W.-J. Fang, T. F. Murray, J. V. Aldrich, *Med. Chem. Res.* **2021**, *30*, 1397–1407.

[119] Y. S. Chang, B. Graves, V. Guerlavais, C. Tovar, K. Packman, K.-H. To, K. A. Olson, K. Kesavan, P. Gangurde, A. Mukherjee, T. Baker, K. Darlak, C. Elkin, Z. Filipovic, F. Z. Qureshi, H. Cai, P. Berry, E. Feyfant, X. E. Shi, J. Horstick, D. A. Annis, A. M. Manning, N. Fotouhi, H. Nash, L. T. Vassilev, T. K. Sawyer, *Proc. Natl. Acad. Sci.* **2013**, *110*, E3445–E3454.

[120] M. B. Elbaum, M. A. Elkhalifa, G. A. Molander, D. M. Chenoweth, *Org. Lett.* **2022**, *24*, 5176–5180.

[121] D. A. Horton, G. T. Bourne, M. L. Smythe, *J. Comput. Aided Mol. Des.* **2002**, *16*, 415–431.

[122] J. R. Frost, C. C. G. Scully, A. K. Yudin, *Nat. Chem.* **2016**, *8*, 1105–1111.

[123] E. Danelius, V. Poongavanam, S. Peintner, L. H. E. Wieske, M. Erdélyi, J. Kihlberg, *Chem. – Eur. J.* **2020**, *26*, 5231–5244.

[124] P. A. Carrupt, B. Testa, A. Bechalany, N. El Tayar, P. Descas, D. Perrissoud, *J. Med. Chem.* **1991**, *34*, 1272–1275.

[125] C. K. Wang, J. E. Swedberg, P. J. Harvey, Q. Kaas, D. J. Craik, *J. Phys. Chem. B* **2018**, *122*, 2261–2276.

[126] H. Zhang, S. Chen, *RSC Chem. Biol.* **2022**, *3*, 18–31.

[127] G. C. Fu, R. H. Grubbs, *J. Am. Chem. Soc.* **1993**, *115*, 3800–3801.

[128] I. Kabelka, R. Vácha, *Acc. Chem. Res.* **2021**, *54*, 2196–2204.

[129] M. Pelay-Gimeno, A. Glas, O. Koch, T. N. Grossmann, *Angew. Chem. Int. Ed.* **2015**, *54*, 8896–8927.

[130] J. M. David, A. K. Rajasekaran, *J. Kidney Cancer VHL* **2015**, *2*, 15–24.

[131] P. Hosseinzadeh, P. R. Watson, T. W. Craven, X. Li, S. Rettie, F. Pardo-Avila, A. K. Bera, V. K. Mulligan, P. Lu, A. S. Ford, B. D. Weitzner, L. J. Stewart, A. P. Moyer, M. Di Piazza, J. G. Whalen, P. Jr. Greisen, D. W. Christianson, D. Baker, *Nat. Commun.* **2021**, *12*, 3384.

[132] M. B. Zwick, J. Shen, J. K. Scott, *Curr. Opin. Biotechnol.* **1998**, *9*, 427–436.

[133] A. I. Ekanayake, L. Sobze, P. Kelich, J. Youk, N. J. Bennett, R. Mukherjee, A. Bhardwaj, F. Wuest, L. Vukovic, R. Derda, *J. Am. Chem. Soc.* **2021**, *143*, 5497–5507.

[134] A. Tavassoli, *Curr. Opin. Chem. Biol.* **2017**, *38*, 30–35.

[135] E. Miranda, I. K. Nordgren, A. L. Male, C. E. Lawrence, F. Hoakwie, F. Cuda, W. Court, K. R. Fox, P. A. Townsend, G. K. Packham, S. A. Eccles, A. Tavassoli, *J. Am. Chem. Soc.* **2013**, *135*, 10418–10425.

[136] D. J. Craik, D. P. Fairlie, S. Liras, D. Price, *Chem. Biol. Drug Des.* **2013**, *81*, 136–147.

[137] A. D. Frankel, C. O. Pabo, *Cell* **1988**, *55*, 1189–1193.

[138] P. L. McNeil, R. F. Murphy, F. Lanni, D. L. Taylor, *J. Cell Biol.* **1984**, *98*, 1556–1564.

[139] H. Brooks, B. Lebleu, E. Vivès, *Adv. Drug Deliv. Rev.* **2005**, *57*, 559–577.

[140] D. M. Copolovici, K. Langel, E. Eriste, Ü. Langel, *ACS Nano* **2014**, *8*, 1972–1994.

[141] G. Kilic, R. B. Doctor, J. G. Fitz, *J. Biol. Chem.* **2001**, *276*, 26762–26768.

[142] Z. Luo, X.-W. Cao, C. Li, M.-D. Wu, X.-Z. Yang, J. Zhao, F.-J. Wang, *J. Pept. Sci.* **2016**, *22*, 689–699.

[143] K. Sadler, K. D. Eom, J.-L. Yang, Y. Dimitrova, J. P. Tam, *Biochemistry* **2002**, *41*, 14150–14157.

[144] I. Nakase, in *Cell-Penetrating Pept.*, **2023**, pp. 29–44.

[145] E. Savier, L. Simon-Gracia, F. Charlotte, P. Tuffery, T. Teesalu, O. Scatton, A. Rebollo, *Pharmaceutics* **2021**, *13*, 1631.

[146] H. Young Kim, S. Young Yum, G. Jang, D.-R. Ahn, *Sci. Rep.* **2015**, *5*, 11719.

[147] A. El-Sayed, S. Futaki, H. Harashima, *AAPS J.* **2009**, *11*, 13–22.

[148] G. Gajski, V. Garaj-Vrhovac, *Environ. Toxicol. Pharmacol.* **2013**, *36*, 697–705.

[149] M. Akishiba, T. Takeuchi, Y. Kawaguchi, K. Sakamoto, H.-H. Yu, I. Nakase, T. Takatani-Nakase, F. Madani, A. Gräslund, S. Futaki, *Nat. Chem.* **2017**, *9*, 751–761.

[150] A. El-Aneed, *J. Controlled Release* **2004**, *94*, 1–14.

[151] S. R. Schwarze, A. Ho, A. Vocero-Akbani, S. F. Dowdy, *Science* **1999**, *285*, 1569–1572.

[152] E. Vivès, J. Schmidt, A. Pèlegrin, *Biochim. Biophys. Acta BBA - Rev. Cancer* **2008**, *1786*, 126–138.

[153] A. Aubry, B. Vitoux, G. Boussard, M. Marraud, *Int. J. Pept. Protein Res.* **1981**, *18*, 195–202.

[154] D. Roemer, H. H. Buescher, R. C. Hill, J. Pless, W. Bauer, F. Cardinaux, A. Closse, D. Hauser, R. Huguenin, *Nature* **1977**, *268*, 547–549.

[155] R. H. Mazur, P. A. James, D. A. Tyner, E. A. Hallinan, J. H. Sanner, R. Schulze, *J. Med. Chem.* **1980**, *23*, 758–763.

[156] E. Biron, J. Chatterjee, H. Kessler, *J. Pept. Sci.* **2006**, *12*, 213–219.

[157] E. Biron, J. Chatterjee, O. Ovadia, D. Langenegger, J. Brueggen, D. Hoyer, H. A. Schmid, R. Jelinek, C. Gilon, A. Hoffman, H. Kessler, *Angew. Chem. Int. Ed.* **2008**, *47*, 2595–2599.

[158] C. R. Pye, W. M. Hewitt, J. Schwochert, T. D. Haddad, C. E. Townsend, L. Etienne, Y. Lao, C. Limberakis, A. Furukawa, A. M. Mathiowetz, D. A. Price, S. Liras, R. S. Lokey, *J. Med. Chem.* **2017**, *60*, 1665–1672.

[159] O. A. Raevsky, V. Yu. Grigor'ev, D. B. Kireev, N. S. Zefirov, *Quant. Struct.-Act. Relatsh.* **1992**, *11*, 49–63.

[160] G. Bhardwaj, J. O'Connor, S. Rettie, Y.-H. Huang, T. A. Ramelot, V. K. Mulligan, G. G. Alpkilic, J. Palmer, A. K. Bera, M. J. Bick, M. Di Piazza, X. Li, P. Hosseinzadeh, T. W. Craven, R. Tejero, A. Lauko, R. Choi, C. Glynn, L. Dong, R. Griffin, W. C. van Voorhis, J. Rodriguez, L. Stewart, G. T. Montelione, D. Craik, D. Baker, *Cell* **2022**, *185*, 3520-3532.e26.

[161] A. T. Bockus, J. A. Schwochert, C. R. Pye, C. E. Townsend, V. Sok, M. A. Bednarek, R. S. Lokey, *J. Med. Chem.* **2015**, *58*, 7409–7418.

[162] M. R. Naylor, A. M. Ly, M. J. Handford, D. P. Ramos, C. R. Pye, A. Furukawa, V. G. Klein, R. P. Noland, Q. Edmondson, A. C. Turmon, W. M. Hewitt, J. Schwochert, C. E. Townsend, C. N. Kelly, M.-J. Blanco, R. S. Lokey, *J. Med. Chem.* **2018**, *61*, 11169–11182.

[163] M. Fujikawa, K. Nakao, R. Shimizu, M. Akamatsu, *Bioorg. Med. Chem.* **2007**, *15*, 3756–3767.

[164] J. A. Ruell, K. L. Tsinman, A. Avdeef, *Eur. J. Pharm. Sci.* **2003**, *20*, 393–402.

[165] P. Wadhwani, S. Afonin, M. Ieronimo, J. Buerck, A. S. Ulrich, *J. Org. Chem.* **2006**, *71*, 55–61.

[166] C. Toniolo, *CRC Crit. Rev. Biochem.* **1980**, *9*, 1–44.

[167] J. Chatterjee, C. Gilon, A. Hoffman, H. Kessler, *Acc. Chem. Res.* **2008**, *41*, 1331–1342.

[168] J. Urban, T. Vaisar, R. Shen, M. S. Lee, *Int. J. Pept. Protein Res.* **1996**, *47*, 182–189.

[169] H. Wu, G. Mousseau, S. Mediouni, S. T. Valente, T. Kodadek, *Angew. Chem.* **2016**, *128*, 12827–12832.

[170] R. N. Zuckermann, J. M. Kerr, S. B. H. Kent, W. H. Moos, *J. Am. Chem. Soc.* **1992**, *114*, 10646–10647.

[171] J. M. Astle, D. G. Udugamasooriya, J. E. Smallshaw, T. Kodadek, *Int. J. Pept. Res. Ther.* **2008**, *14*, 223–227.

[172] T. J. Sanborn, C. W. Wu, R. N. Zuckermann, A. E. Barron, *Biopolymers* **2002**, *63*, 12–20.

[173] C. Lamers, *Future Drug Discov.* **2022**, *4*, FDD75.

[174] V. K. Mulligan, *Expert Opin. Drug Discov.* **2020**, *15*, 833–852.

[175] W. M. Hewitt, S. S. F. Leung, C. R. Pye, A. R. Ponkey, M. Bednarek, M. P. Jacobson, R. S. Lokey, *J. Am. Chem. Soc.* **2015**, *137*, 715–721.

[176] G. Abbenante, D. P. Fairlie, L. R. Gahan, G. R. Hanson, G. K. Pierens, A. L. van den Brenk, *J. Am. Chem. Soc.* **1996**, *118*, 10384–10388.

[177] I. V. Smolyar, A. K. Yudin, V. G. Nenajdenko, *Chem. Rev.* **2019**, *119*, 10032–10240.

[178] U. Mocek, A. R. Knaggs, R. Tsuchiya, T. Nguyen, J. M. Beale, H. G. Floss, *J. Am. Chem. Soc.* **1993**, *115*, 7557–7568.

[179] W. S. Horne, M. K. Yadav, C. D. Stout, M. R. Ghadiri, *J. Am. Chem. Soc.* **2004**, *126*, 15366–15367.

[180] H. S. Soor, S. D. Appavoo, A. K. Yudin, *Bioorg. Med. Chem.* **2018**, *26*, 2774–2779.

[181] D. S. Nielsen, H. N. Hoang, R.-J. Lohman, F. Diness, D. P. Fairlie, *Org. Lett.* **2012**, *14*, 5720–5723.

[182] A. A. Rzepiela, L. A. Viarengo-Baker, V. Tatarskii, R. Kombarov, A. Whitty, *J. Med. Chem.* **2022**, *65*, 10300–10317.

[183] G. J. Saunders, A. K. Yudin, *Angew. Chem. Int. Ed.* **2022**, *61*, e202206866.

[184] P. Thansandote, R. M. Harris, H. L. Dexter, G. L. Simpson, S. Pal, R. J. Upton, K. Valko, *Bioorg. Med. Chem.* **2015**, *23*, 322–327.

[185] M. Rossi Sebastiano, B. C. Doak, M. Backlund, V. Poongavanam, B. Over, G. Ermondi, G. Caron, P. Matsson, J. Kihlberg, *J. Med. Chem.* **2018**, *61*, 4189–4202.

[186] B. Over, P. Matsson, C. Tyrchan, P. Artursson, B. C. Doak, M. A. Foley, C. Hilgendorf, S. E. Johnston, M. D. Lee, R. J. Lewis, P. McCarren, G. Muncipinto, U. Norinder, M. W. D. Perry, J. R. Duvall, J. Kihlberg, *Nat. Chem. Biol.* **2016**, *12*, 1065–1074.

[187] S. D. Appavoo, T. Kaji, J. R. Frost, C. C. G. Scully, A. K. Yudin, *J. Am. Chem. Soc.* **2018**, *140*, 8763–8770.

[188] E. C. Freeman, L. M. Weiland, W. S. Meng, *J. Biomater. Sci. Polym. Ed.* **2013**, *24*, 398–416.

[189] A. Reinhardt, I. Neundorf, *Int. J. Mol. Sci.* **2016**, *17*, 701.

[190] T. Del'Guidice, J.-P. Lepetit-Stoffaes, L.-J. Bordeleau, J. Roberge, V. Théberge, C. Lauvaux, X. Barbeau, J. Trottier, V. Dave, D.-C. Roy, B. Gaillet, A. Garnier, D. Guay, *PLOS ONE* **2018**, *13*, e0195558.

[191] O. Tietz, F. Cortezon-Tamarit, R. Chalk, S. Able, K. A. Vallis, *Nat. Chem.* **2022**, *14*, 284–293.

[192] Y. Ping, *Nat. Chem.* **2022**, *14*, 250–252.

[193] Y. Sun, S. Y. Lau, Z. W. Lim, S. C. Chang, F. Ghadessy, A. Partridge, A. Miserez, *Nat. Chem.* **2022**, *14*, 274–283.

[194] Z. W. Lim, Y. Ping, A. Miserez, *Bioconjug. Chem.* **2018**, *29*, 2176–2180.

[195] J. A. Rothwell, A. J. Day, M. R. A. Morgan, *J. Agric. Food Chem.* **2005**, *53*, 4355–4360.

[196] A. Alex, in *Absorpt. Drug Dev.*, **2012**, pp. 251–318.

[197] M. Kansy, F. Senner, K. Gubernator, *J. Med. Chem.* **1998**, *41*, 1007–1010.

[198] S. Otasevic, T. Vojinovic, *Prog. Nutr.* **2020**, *22*, e2020035–e2020035.

[199] K. Lanevskij, R. Didziapetris, *J. Pharm. Sci.* **2019**, *108*, 78–86.

[200] H. Yu, Q. Wang, Y. Sun, M. Shen, H. Li, Y. Duan, *PLOS ONE* **2015**, *10*, e0116502.

[201] F. J. Sharom, *J. Membr. Biol.* **1997**, *160*, 161–175.

[202] P. V. Balimane, Y.-H. Han, S. Chong, *AAPS J.* **2006**, *8*, E1-13.

[203] H. Lennernäs, K. Palm, U. Fagerholm, P. Artursson, *Int. J. Pharm.* **1996**, *127*, 103–107.

[204] W. S. Putnam, L. Pan, K. Tsutsui, L. Takahashi, L. Z. Benet, *Pharm. Res.* **2002**, *19*, 27–33.

[205] C. Pidgeon, S. Ong, H. Liu, X. Qiu, M. Pidgeon, A. H. Dantzig, J. Munroe, W. J. Hornback, J. S. Kasher, *J. Med. Chem.* **1995**, *38*, 590–594.

[206] A. Tsantili-Kakoulidou, *Expert Opin. Drug Discov.* **2020**, *15*, 273–276.

[207] L. Grumetto, G. Russo, F. Barbato, *Int. J. Pharm.* **2016**, *500*, 275–290.

[208] L. Grumetto, G. Russo, F. Barbato, *Mol. Pharm.* **2016**, *13*, 2808–2816.

[209] K. Valko, C. M. Du, C. D. Bevan, D. P. Reynolds, M. H. Abraham, *J. Pharm. Sci.* **2000**, *89*, 1085–1096.

[210] E. Krause, M. Dathe, T. Wieprecht, M. Bienert, *J. Chromatogr. A* **1999**, *849*, 125–133.

[211] Y. Iwakuma, H. Okamoto, R. Hamaguchi, Y. Kuroda, *Chromatographia* **2019**, *82*, 1311–1320.

[212] Y. Iwakuma, H. Okamoto, R. Hamaguchi, Y. Kuroda, *Chromatographia* **2023**, *86*, 43–54.

[213] K. Ciura, N. Ptaszyńska, H. Kapica, M. Pastewska, A. Łęgowska, K. Rolka, W. Kamysz, W. Sawicki, K. E. Greber, *Antibiotics* **2021**, *10*, 1237.

[214] M. J. Winningham, D. Y. Sogah, *J. Am. Chem. Soc.* **1994**, *116*, 11173–11174.

[215] D. Lee, S. Lee, J. Choi, Y.-K. Song, M. J. Kim, D.-S. Shin, M. A. Bae, Y.-C. Kim, C.-J. Park, K.-R. Lee, J.-H. Choi, J. Seo, *J. Med. Chem.* **2021**, *64*, 8272–8286.

[216] C. Bonnel, B. Legrand, J.-L. Bantignies, H. Petitjean, J. Martinez, N. Masurier, L. T. Maillard, *Org. Biomol. Chem.* **2016**, *14*, 8664–8669.

[217] L. T. Taylor, *J. Supercrit. Fluids* **2009**, *47*, 566–573.

[218] G. H. Goetz, W. Farrell, M. Shalaeva, S. Sciabola, D. Anderson, J. Yan, L. Philippe, M. J. Shapiro, *J. Med. Chem.* **2014**, *57*, 2920–2929.

[219] G. H. Goetz, L. Philippe, M. J. Shapiro, *ACS Med. Chem. Lett.* **2014**, *5*, 1167–1172.

[220] J. Wencel-Delord, F. Glorius, *Nat. Chem.* **2013**, *5*, 369–375.

[221] J. Börgel, T. Ritter, *Chem* **2020**, *6*, 1877–1887.

[222] B.-B. Zhan, M.-X. Jiang, B.-F. Shi, *Chem. Commun.* **2020**, *56*, 13950–13958.

[223] J. N. deGruyter, L. R. Malins, P. S. Baran, *Biochemistry* **2017**, *56*, 3863–3873.

[224] C. Nájera, J. M. Sansano, *Chem. Rev.* **2007**, *107*, 4584–4671.

[225] W. Wang, M. M. Lorion, J. Shah, A. R. Kapdi, L. Ackermann, *Angew. Chem. Int. Ed.* **2018**, *57*, 14700–14717.

[226] R. G. Bergman, *Nature* **2007**, *446*, 391–393.

[227] S. A. Byrne, M. J. Bedding, L. Corcilius, D. J. Ford, Y. Zhong, C. Franck, M. Larance, J. P. Mackay, R. J. Payne, *Chem. Sci.* **n.d.**, *12*, 14159–14166.

[228] J. Alam, T. H. Keller, T.-P. Loh, *J. Am. Chem. Soc.* **2010**, *132*, 9546–9548.

[229] A. Abbas, B. Xing, T.-P. Loh, *Angew. Chem. Int. Ed.* **2014**, *53*, 7491–7494.

[230] J. M. J. M. Ravasco, H. Faustino, A. Trindade, P. M. P. Gois, *Chem. – Eur. J.* **2019**, *25*, 43–59.

[231] A. F. M. Noisier, J. García, I. A. Ionuţ, F. Albericio, *Angew. Chem. Int. Ed.* **2017**, *56*, 314–318.

[232] A. Shatskiy, M. D. Kärkäs, *Synlett* **2022**, *33*, 109–115.

[233] S. J. McCarver, J. X. Qiao, J. Carpenter, R. M. Borzilleri, M. A. Poss, M. D. Eastgate, M. M. Miller, D. W. C. MacMillan, *Angew. Chem. Int. Ed.* **2017**, *56*, 728–732.

[234] Y. Hosono, J. Morimoto, S. Sando, *Org. Biomol. Chem.* **2021**, *19*, 10326–10331.

[235] L. Otvos, J. D. Wade, *Front. Chem.* **2014**, *2*.

[236] S. Kubik, R. Goddard, *J. Org. Chem.* **1999**, *64*, 9475–9486.

[237] T. Katoh, H. Suga, *J. Am. Chem. Soc.* **2022**, *144*, 2069–2072.

[238] Tourwé, D.; Van Hemel, J.; Piron, J., in *Methods Org. Chem.*, Georg Thieme Verlag KG, Stuttgart, **2004**, pp. 606–608.

[239] A. D. de Araujo, H. N. Hoang, J. Lim, J. Y. W. Mak, D. P. Fairlie, *Angew. Chem. Int. Ed.* **2022**, *61*, e202203995.

[240] J. A. Shadish, C. A. DeForest, *Matter* **2020**, *2*, 50–77.

[241] C. Cai, F. Wang, X. Xiao, W. Sheng, S. Liu, J. Chen, J. Zheng, R. Xie, Z. Bai, H. Wang, *Chem. Commun.* **2022**, *58*, 4861–4864.

[242] A. Petrou, M. Fesatidou, A. Geronikaki, *Mol. Basel Switz.* **2021**, *26*, 3166.

[243] T. R. White, C. M. Renzelman, A. C. Rand, T. Rezai, C. M. McEwen, V. M. Gelev, R. A. Turner, R. G. Linington, S. S. F. Leung, A. S. Kalgutkar, J. N. Bauman, Y. Zhang, S. Liras, D. A. Price, A. M. Mathiowetz, M. P. Jacobson, R. S. Lokey, *Nat. Chem. Biol.* **2011**, *7*, 810–817.

[244] C. Li, S. Wainhaus, A. S. Uss, K.-C. Cheng, in *Drug Absorpt. Stud. Situ Vitro Silico Models* (Eds.: C. Ehrhardt, K.-J. Kim), Springer US, Boston, MA, **2008**, pp. 418–429.

[245] Y. Hamuro, S. J. Geib, A. D. Hamilton, *Angew. Chem. Int. Ed. Engl.* **1994**, *33*, 446–448.

[246] B. Brzezinski, G. Zundel, R. Krämer, *Chem. Phys. Lett.* **1986**, *124*, 395–400.

[247] G. Caron, J. Kihlberg, G. Ermondi, *Med. Res. Rev.* **2019**, *39*, 1707–1729.

[248] D. S. Dalisay, E. W. Rogers, A. S. Edison, T. F. Molinski, *J. Nat. Prod.* **2009**, *72*, 732–738.

[249] H. Wahyudi, W. Tantisantisom, X. Liu, D. M. Ramsey, E. K. Singh, S. R. McAlpine, *J. Org. Chem.* **2012**, *77*, 10596–10616.

[250] D. S. Nielsen, N. E. Shepherd, W. Xu, A. J. Lucke, M. J. Stoermer, D. P. Fairlie, *Chem. Rev.* **2017**, *117*, 8094–8128.

[251] T. R. White, C. M. Renzelman, A. C. Rand, T. Rezai, C. M. McEwen, V. M. Gelev, R. A. Turner, R. G. Linington, S. S. F. Leung, A. S. Kalgutkar, J. N. Bauman, Y. Zhang, S. Liras, D. A. Price, A. M. Mathiowetz, M. P. Jacobson, R. S. Lokey, *Nat. Chem. Biol.* **2011**, *7*, 810–817.

[252] *Eur. J. Org. Chem.* **2020**, *2020*, 3796–3807.

[253] T. Zimmermann, S. B. Christensen, H. Franzyk, *Mol. J. Synth. Chem. Nat. Prod. Chem.* **2018**, *23*, 1463.

[254] D. T. Nguyen, T. T. Le, A. J. Rice, G. A. Hudson, W. A. van der Donk, D. A. Mitchell, *J. Am. Chem. Soc.* **2022**, *144*, 11263–11269.

[255] B. A. Hopkins, H. Lee, S. Ha, L. Nogle, B. Sauvagnat, S. McMinn, G. F. Smith, N. Sciammetta, *ACS Med. Chem. Lett.* **2019**, *10*, 874–879.

[256] E. Frérot, J. Coste, A. Pantaloni, M.-N. Dufour, P. Jouin, *Tetrahedron* **1991**, *47*, 259–270.

[257] A. El-Faham, F. Albericio, *J. Pept. Sci.* **2010**, *16*, 6–9.

[258] G. Bellavance, P. Dubé, B. Nguyen, *Synlett* **2012**, *2012*, 569–574.

[259] F. Damkaci, A. Alawaed, E. Vik, *Tetrahedron Lett.* **2016**, *57*, 2197–2200.

[260] F.-T. Wu, N.-N. Yan, P. Liu, J.-W. Xie, Y. Liu, B. Dai, *Tetrahedron Lett.* **2014**, *55*, 3249–3251.

[261] H. P. Kokatla, P. F. Thomson, S. Bae, V. R. Doddi, M. K. Lakshman, *J. Org. Chem.* **2011**, *76*, 7842–7848.

[262] S. Deuri, P. Phukan, *Comput. Theor. Chem.* **2012**, *980*, 49–55.

[263] H. Behera, V. Ramkumar, N. Madhavan, *Org. Biomol. Chem.* **2017**, *15*, 4937–4940.

[264] P. Devi, S. M. Barry, K. M. Houlihan, M. J. Murphy, P. Turner, P. Jensen, P. J. Rutledge, *Sci. Rep.* **2015**, *5*, 9950.

[265] X. Zeng, D. Coquière, A. Alenda, E. Garrier, T. Prangé, Y. Li, O. Reinaud, I. Jabin, *Chem. – Eur. J.* **2006**, *12*, 6393–6402.

[266] G. V. Sagar Reddy, G. V. Rao, R. V. K. Subramanyam, D. S. Iyengar, *Synth. Commun.* **2000**, *30*, 2233–2237.

[267] G. V. Kulkarni, A. Ray, C. C. Patel, *J. Mol. Struct.* **1981**, *71*, 253–262.

[268] P. G. Nantermet, C. S. Burgey, K. A. Robinson, J. M. Pellicore, C. L. Newton, J. Z. Deng, H. G. Selnick, S. D. Lewis, B. J. Lucas, J. A. Krueger, C. Miller-Stein, R. B. White, B. Wong, D. R. McMasters, A. A. Wallace, J. J. Lynch, Y. Yan, Z. Chen, L. Kuo, S. J. Gardell, J. A. Shafer, J. P. Vacca, T. A. Lyle, *Bioorg. Med. Chem. Lett.* **2005**, *15*, 2771–2775.

[269] F. D. Bobbink, S. Das, P. J. Dyson, *Nat. Protoc.* **2017**, *12*, 417–428.

[270] E. A. Englund, H. N. Gopi, D. H. Appella, *Org. Lett.* **2004**, *6*, 213–215.

[271] M. H. Abraham, R. J. Abraham, A. Aghamohammadi, K. Afarinkia, X. Liu, *J. Mol. Liq.* **2020**, *315*, 113730.

[272] I. Dzidic, *J. Am. Chem. Soc.* **1972**, *94*, 8333–8335.

[273] M. Vilches-Herrera, S. Werkmeister, K. Junge, A. Börner, M. Beller, *Catal. Sci. Technol.* **2014**, *4*, 629–632.

[274] N. Kühl, M. M. Leuthold, M. A. M. Behnam, C. D. Klein, *J. Med. Chem.* **2021**, *64*, 4567–4587.

[275] D. S. Nielsen, H. N. Hoang, R.-J. Lohman, T. A. Hill, A. J. Lucke, D. J. Craik, D. J. Edmonds, D. A. Griffith, C. J. Rotter, R. B. Ruggeri, D. A. Price, S. Liras, D. P. Fairlie, *Angew. Chem. Int. Ed.* **2014**, *53*, 12059–12063.

[276] C. K. Wang, S. E. Northfield, B. Colless, S. Chaousis, I. Hamernig, R.-J. Lohman, D. S. Nielsen, C. I. Schroeder, S. Liras, D. A. Price, D. P. Fairlie, D. J. Craik, *Proc. Natl. Acad. Sci.* **2014**, *111*, 17504–17509.

[277] T. Cierpicki, J. Otlewski, *J. Biomol. NMR* **2001**, *21*, 249–261.

[278] G. Gramse, A. Dols-Perez, M. A. Edwards, L. Fumagalli, G. Gomila, *Biophys. J.* **2013**, *104*, 1257–1262.

[279] K. Palm, P. Stenberg, K. Luthman, P. Artursson1, *Pharm. Res.* **1997**, *14*, 568–571.

[280] T. R. Oppewal, I. D. Jansen, J. Hekelaar, C. Mayer, *J. Am. Chem. Soc.* **2022**, *144*, 3644–3652.

[281] C. T. Walsh, S. Garneau-Tsodikova, G. J. Gatto Jr., *Angew. Chem. Int. Ed.* **2005**, *44*, 7342–7372.

[282] E. M. Sletten, C. R. Bertozzi, *Angew. Chem. Int. Ed.* **2009**, *48*, 6974–6998.

[283] A. Beck, L. Goetsch, C. Dumontet, N. Corvaïa, *Nat. Rev. Drug Discov.* **2017**, *16*, 315–337.

[284] M. A. T. Blaskovich, *J. Med. Chem.* **2016**, *59*, 10807–10836.

[285] X. Qi, S. Jambu, Y. Ji, K. M. Belyk, N. R. Panigrahi, P. S. Arora, N. A. Strotman, T. Diao, *Angew. Chem. Int. Ed.* **2022**, *61*, e202213315.

[286] S. Sen, J. Das, D. Maiti, *Tetrahedron Chem* **2022**, *1*, 100005.

[287] M. Limbach, M. Löweneck, J. V. Schreiber, J. Frackenpohl, D. Seebach, A. Billich, *Helv. Chim. Acta* **2006**, *89*, 1427–1441.

[288] S. W. Kim, S. Y. Ahn, J. S. Koh, J. H. Lee, S. Ro, H. Y. Cho, *Tetrahedron Lett.* **1997**, *38*, 4603–4606.

[289] S. B. Blakey, D. W. C. MacMillan, *J. Am. Chem. Soc.* **2003**, *125*, 6046–6047.

[290] D. Alberico, M. E. Scott, M. Lautens, *Chem. Rev.* **2007**, *107*, 174–238.

[291] J. Das, S. Guin, D. Maiti, *Chem. Sci.* **2020**, *11*, 10887–10909.

[292] A. F. M. Noisier, M. A. Brimble, *Chem. Rev.* **2014**, *114*, 8775–8806.

[293] M. Brylinski, *Chem. Biol. Drug Des.* **2018**, *91*, 380–390.

[294] R. Sharma, U. Sharma, *Catal. Rev.* **2018**, *60*, 497–565.

[295] S. Miller, J. Janin, A. M. Lesk, C. Chothia, *J. Mol. Biol.* **1987**, *196*, 641–656.

[296] J. P. Tam, Q. Yu, Z. Miao, *Pept. Sci.* **1999**, *51*, 311–332.

[297] M. J. Lopez, S. S. Mohiuddin, in *StatPearls*, StatPearls Publishing, Treasure Island (FL), **2022**.

[298] M. Schelhaas, H. Waldmann, *Angew. Chem. Int. Ed. Engl.* **1996**, *35*, 2056–2083.

[299] F. Lovering, J. Bikker, C. Humblet, *J. Med. Chem.* **2009**, *52*, 6752–6756.

[300] S. J. Blanksby, G. B. Ellison, *Acc. Chem. Res.* **2003**, *36*, 255–263.

[301] C.-Y. (Dennis) Huang, A. G. Doyle, *J. Am. Chem. Soc.* **2012**, *134*, 9541–9544.

[302] K. R. Buszek, N. Brown, *Org. Lett.* **2007**, *9*, 707–710.

[303] J. B. Bapat, R. J. Blade, A. J. Boulton, J. Epsztajn, A. R. Katritzky, J. Lewis, P. Molina-Buendia, P.-L. Nie, C. A. Ramsden, *Tetrahedron Lett.* **1976**, *17*, 2691–2694.

[304] C. H. Basch, J. Liao, J. Xu, J. J. Piane, M. P. Watson, *J. Am. Chem. Soc.* **2017**, *139*, 5313–5316.

[305] F. J. R. Klauck, M. J. James, F. Glorius, *Angew. Chem. Int. Ed.* **2017**, *56*, 12336–12339.

[306] J. Hu, G. Wang, S. Li, Z. Shi, *Angew. Chem. Int. Ed.* **2018**, *57*, 15227–15231.

[307] M. Ociepa, J. Turkowska, D. Gryko, *ACS Catal.* **2018**, *8*, 11362–11367.

[308] T. Qin, J. Cornella, C. Li, L. R. Malins, J. T. Edwards, S. Kawamura, B. D. Maxwell, M. D. Eastgate, P. S. Baran, *Science* **2016**, *352*, 801–805.

[309] J. Openy, G. Amrahova, J.-Y. Chang, A. Noisier, P. 't Hart, *Chem. – Eur. J.* **2022**, *28*, e202201121.

[310] M. Elkhalifa, M. B. Elbaum, D. M. Chenoweth, G. A. Molander, *Org. Lett.* **2021**, *23*, 8219–8223.

[311] F. J. R. Klauck, H. Yoon, M. J. James, M. Lautens, F. Glorius, *ACS Catal.* **2019**, *9*, 236–241.

[312] A. M. Yousif, S. Colarusso, E. Bianchi, *Eur. J. Org. Chem.* **n.d.**, *n/a*, e202201274.

[313] T. Qin, L. R. Malins, J. T. Edwards, R. R. Merchant, A. J. E. Novak, J. Z. Zhong, R. B. Mills, M. Yan, C. Yuan, M. D. Eastgate, P. S. Baran, *Angew. Chem. Int. Ed.* **2017**, *56*, 260–265.

[314] J. C. Twitty, Y. Hong, B. Garcia, S. Tsang, J. Liao, D. Schultz, A. Dion, D. Kalyani, M. Watson, **2022**, DOI 10.26434/chemrxiv-2022-k3j3f.

[315] M. Wang, C. Wang, Y. Huo, X. Dang, H. Xue, L. Liu, H. Chai, X. Xie, Z. Li, D. Lu, Z. Xu, *Nat. Commun.* **2021**, *12*, 6873.

[316] R. Martin-Montero, V. R. Yatham, H. Yin, J. Davies, R. Martin, *Org. Lett.* **2019**, *21*, 2947–2951.

[317] J. Diccianni, Q. Lin, T. Diao, *Acc. Chem. Res.* **2020**, *53*, 906–919.

[318] S. Ni, C.-X. Li, Y. Mao, J. Han, Y. Wang, H. Yan, Y. Pan, *Sci. Adv.* **2019**, *5*, eaaw9516.

[319] R. Beugelmans, L. Neuville, M. Bois-Choussy, J. Chastanet, J. Zhu, *Tetrahedron Lett.* **1995**, *36*, 3129–3132.

[320] A. R. Katritzky, S. S. Thind, *J. Chem. Soc. Perkin 1* **1980**, *0*, 1895–1900.

[321] J. Liao, C. H. Basch, M. E. Hoerrner, M. R. Talley, B. P. Boscoe, J. W. Tucker, M. R. Garnsey, M. P. Watson, *Org. Lett.* **2019**, *21*, 2941–2946.

[322] J. Wu, L. He, A. Noble, V. K. Aggarwal, *J. Am. Chem. Soc.* **2018**, *140*, 10700–10704.

[323] Y. Ma, Y. Pang, S. Chabbra, E. J. Reijerse, A. Schnegg, J. Niski, M. Leutzsch, J. Cornella, *Chem. – Eur. J.* **2020**, *26*, 3738–3743.

[324] D. J. Charboneau, H. Huang, E. L. Barth, C. C. Germe, N. Hazari, B. Q. Mercado, M. R. Uehling, S. L. Zultanski, *J. Am. Chem. Soc.* **2021**, *143*, 21024–21036.

[325] S. Zalipsky, J. L. Chang, F. Albericio, G. Barany, *React. Polym.* **1994**, *22*, 243–258.

[326] J. Wu, P. S. Grant, X. Li, A. Noble, V. K. Aggarwal, *Angew. Chem. Int. Ed.* **2019**, *58*, 5697–5701.

[327] W. G. Lesniak, A. Jyoti, M. K. Mishra, N. Louissaint, R. Romero, D. C. Chugani, S. Kannan, R. M. Kannan, *Anal. Biochem.* **2013**, *443*, 222–231.

[328] S. Verlinden, N. Geudens, K. Van holsbeeck, M. Mannes, J. C. Martins, G. Verniest, S. Ballet, *J. Pept. Sci.* **2019**, *25*, e3194.

[329] M. W. Rathke, P. J. Cowan, *J. Org. Chem.* **1985**, *50*, 2622–2624.

[330] B. Bacsa, K. Horváti, S. Bõsze, F. Andreae, C. O. Kappe, *J. Org. Chem.* **2008**, *73*, 7532–7542.

[331] M. Amblard, J.-A. Fehrentz, J. Martinez, G. Subra, in *Pept. Synth. Appl.* (Ed.: J. Howl), Humana Press, Totowa, NJ, **2005**, pp. 3–24.

[332] M. Waliczek, M. Kijewska, M. Rudowska, B. Setner, P. Stefanowicz, Z. Szewczuk, *Sci. Rep.* **2016**, *6*, 37720.

[333] F. Lin, Y. Feng, X. Liu, L. Wang, Z.-Q. Yu, Y. Liu, *Mater. Chem. Front.* **2020**, *4*, 1492–1499.

[334] D. C. Miller, J. M. Ganley, A. J. Musacchio, T. C. Sherwood, W. R. Ewing, R. R. Knowles, *J. Am. Chem. Soc.* **2019**, *141*, 16590–16594.

[335] G. Proietti, Y. Wang, G. Rainone, J. Mecinović, *Sci. Rep.* **2020**, *10*, 13046.

[336] Y. Yamazaki, J. Naganuma, H. Gotoh, *Sci. Rep.* **2019**, *9*, 20339.

[337] A. Boto, C. C. González, D. Hernández, I. Romero-Estudillo, C. J. Saavedra, *Org. Chem. Front.* **2021**, *8*, 6720–6759.

[338] A. Isidro-Llobet, M. Álvarez, F. Albericio, *Chem. Rev.* **2009**, *109*, 2455–2504.

[339] A. F. M. Noisier, M. J. Johansson, L. Knerr, M. A. Hayes, W. J. Drury III, E. Valeur, L. R. Malins, R. Gopalakrishnan, *Angew. Chem. Int. Ed.* **2019**, *58*, 19096–19102.

[340] C. Schöneich, D. Pogocki, G. L. Hug, K. Bobrowski, *J. Am. Chem. Soc.* **2003**, *125*, 13700–13713.

[341] A. R. Mitchell, *Pept. Sci.* **2008**, *90*, 215–233.

[342] S. S. Wang, *J. Am. Chem. Soc.* **1973**, *95*, 1328–1333.

[343] T. Kassem, D. Sabatino, X. Jia, X. X. Zhu, W. D. Lubell, *Int. J. Pept. Res. Ther.* **2009**, *15*, 211–218.

[344] M. H. A. Somehsaraie, V. F. Vavsari, M. Kamangar, S. Balalaie, *Iran. J. Pharm. Res.* **2022**, *21*, DOI 10.5812/ijpr-123879.

[345] B. E. Collins, C. B. Greer, B. C. Coleman, J. D. Sweatt, *Epigenetics Chromatin* **2019**, *12*, 7.

[346] F. Lan, R. E. Collins, R. De Cegli, R. Alpatov, J. R. Horton, X. Shi, O. Gozani, X. Cheng, Y. Shi, *Nature* **2007**, *448*, 718–722.

[347] G. M. Popowicz, A. Czarna, U. Rothweiler, A. Szwagierczak, M. Krajewski, L. Weber, T. A. Holak, *Cell Cycle Georget. Tex* **2007**, *6*, 2386–2392.

[348] W. C. Chan, B. W. Bycroft, D. J. Evans, P. D. White, *J. Chem. Soc. Chem. Commun.* **1995**, 2209–2210.

[349] C. Bleiholder, S. Suhai, A. G. Harrison, B. Paizs, *J. Am. Soc. Mass Spectrom.* **2011**, *22*, 1032–1039.

[350] K. A. Ogawa, A. E. Goetz, A. J. Boydston, *J. Am. Chem. Soc.* **2015**, *137*, 1400–1403.

[351] Y. Ma, Y. Pang, S. Chabbra, E. J. Reijerse, A. Schnegg, J. Niski, M. Leutzsch, J. Cornella, *Chem. - Eur. J.* **2020**, *26*, 3738–3743.

[352] E. Tatunashvili, B. Chan, P. E. Nashar, C. S. P. McErlean, *Org. Biomol. Chem.* **2020**, *18*, 1812–1819.

6. Appendix

6.1. Supplementary Spectral data

6.1.1. Chapter 2

4a ^{1}H NMR

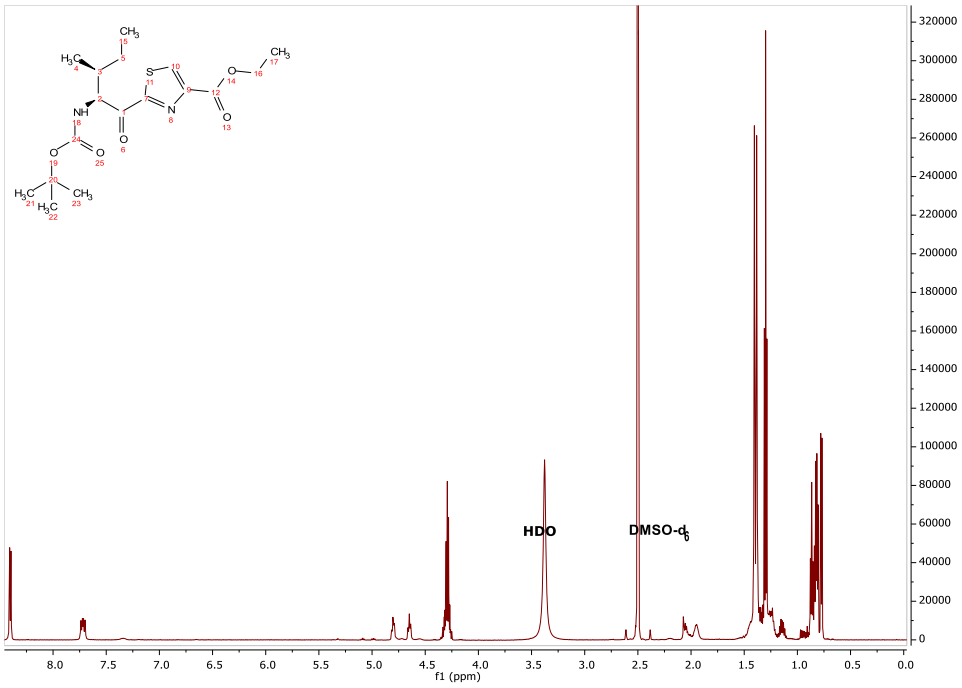

4a ^{13}C NMR

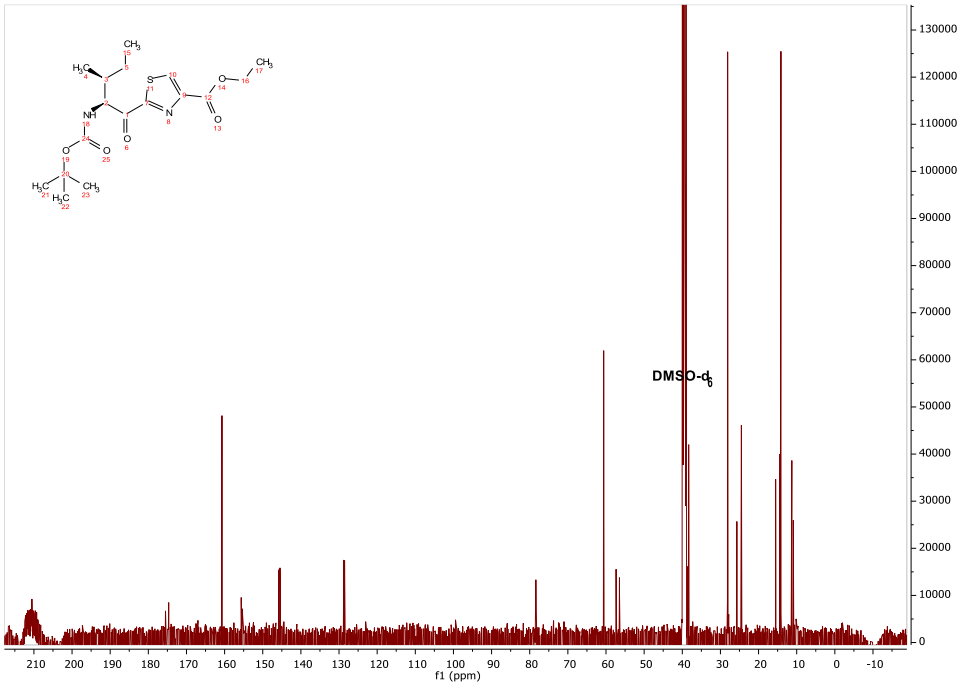

4b ^{1}H NMR

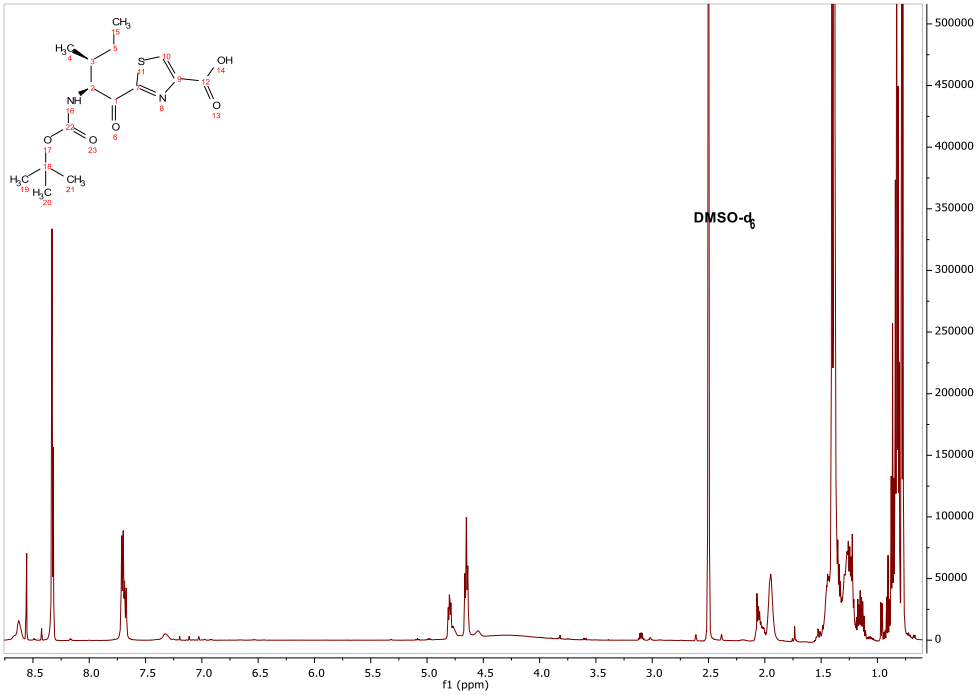

4b ^{13}C NMR

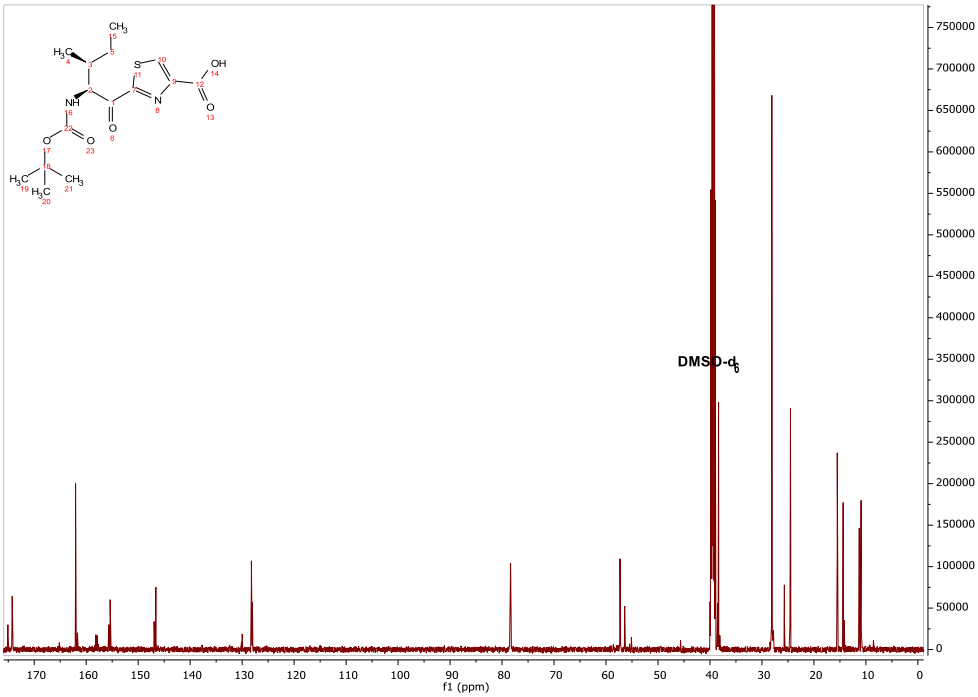

15 ^{1}H NMR

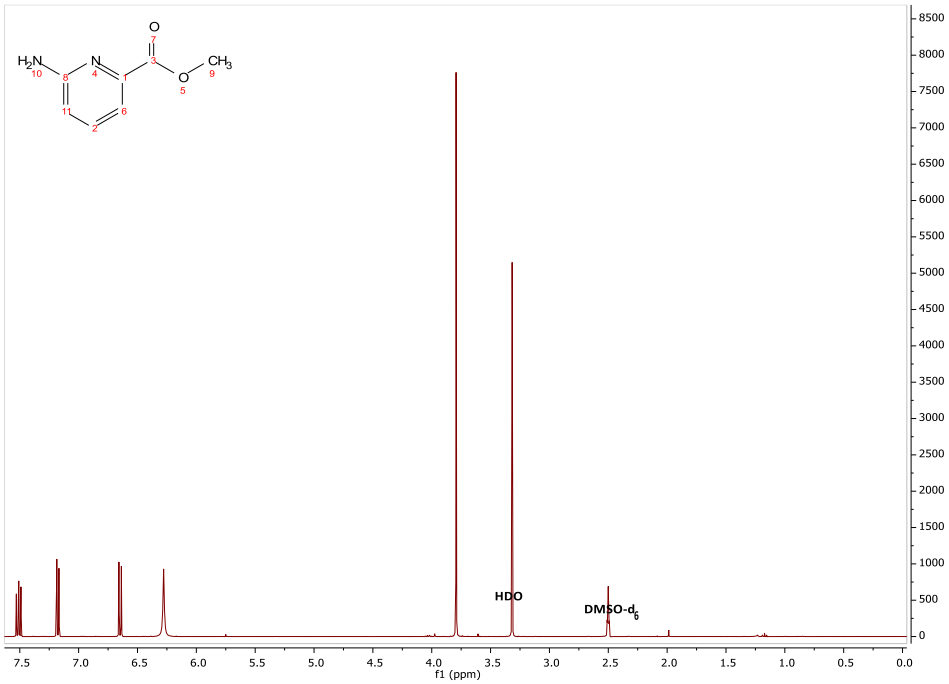

15 ^{13}C NMR

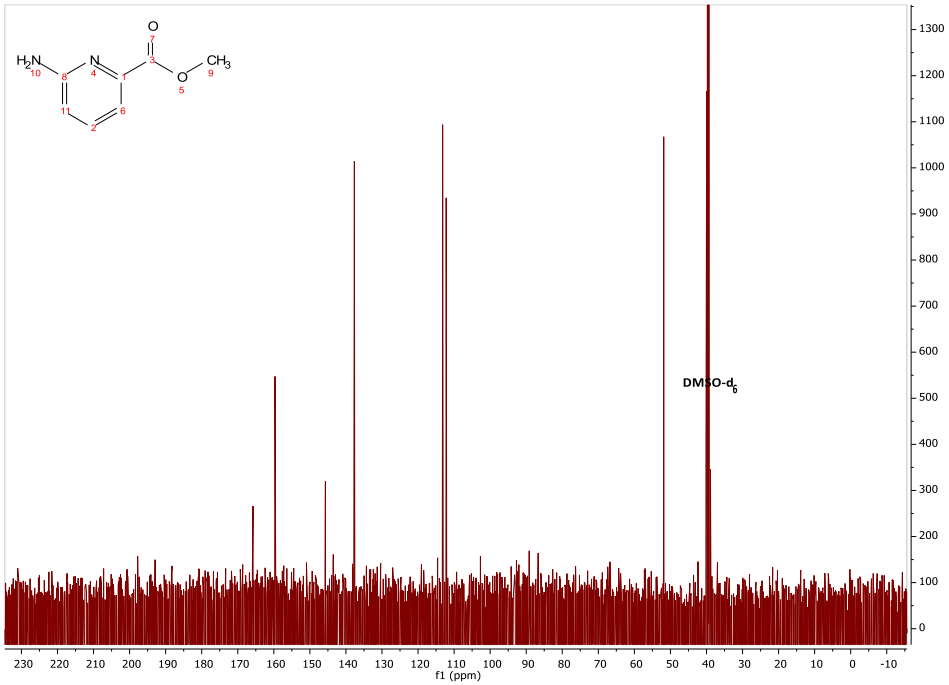

16 ^{1}H NMR

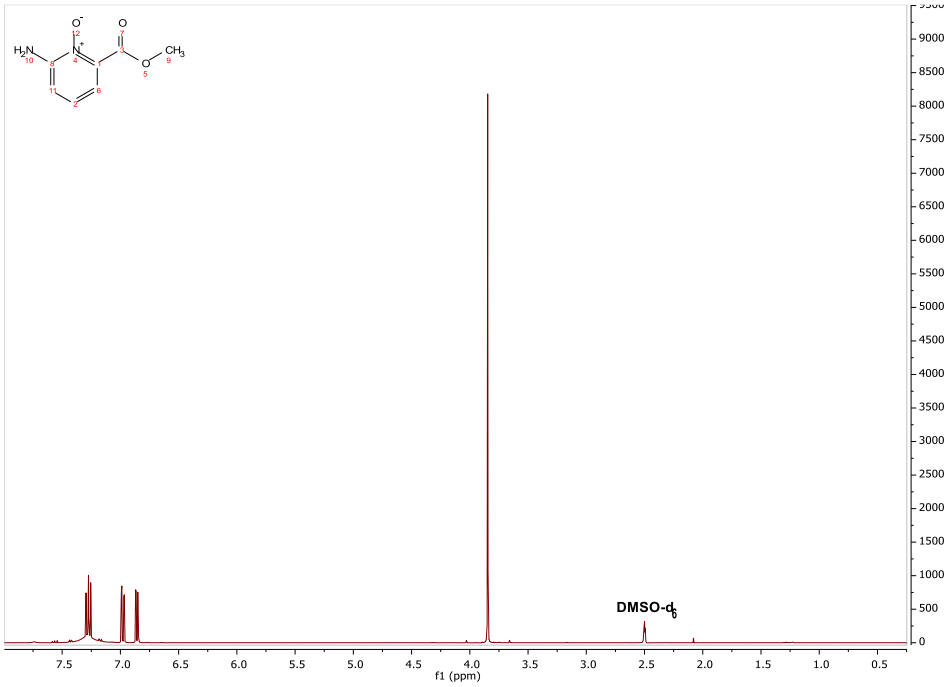

16 ^{13}C NMR

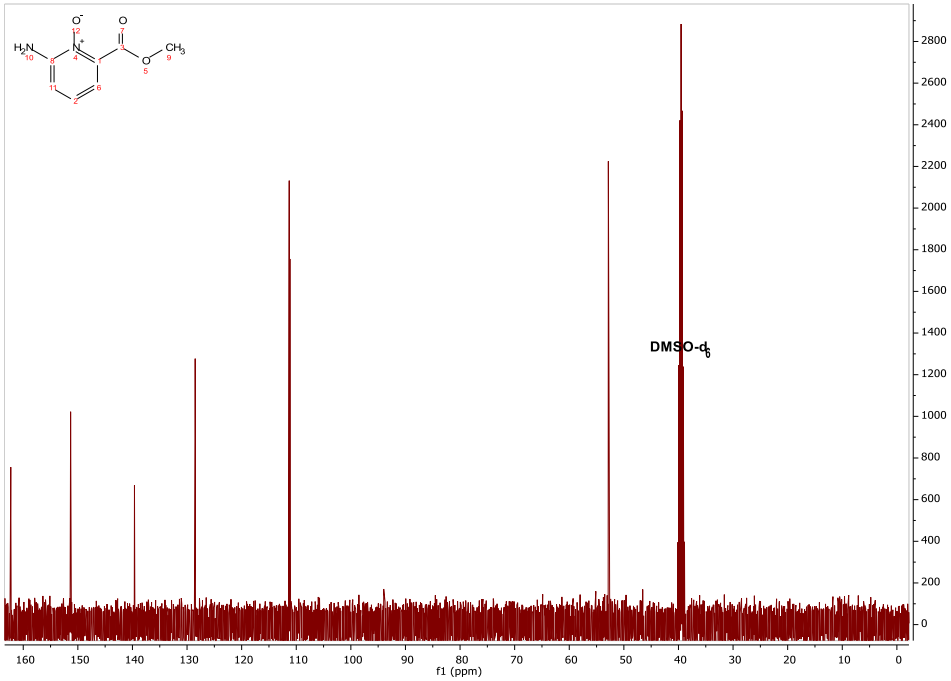

17 ^{1}H NMR

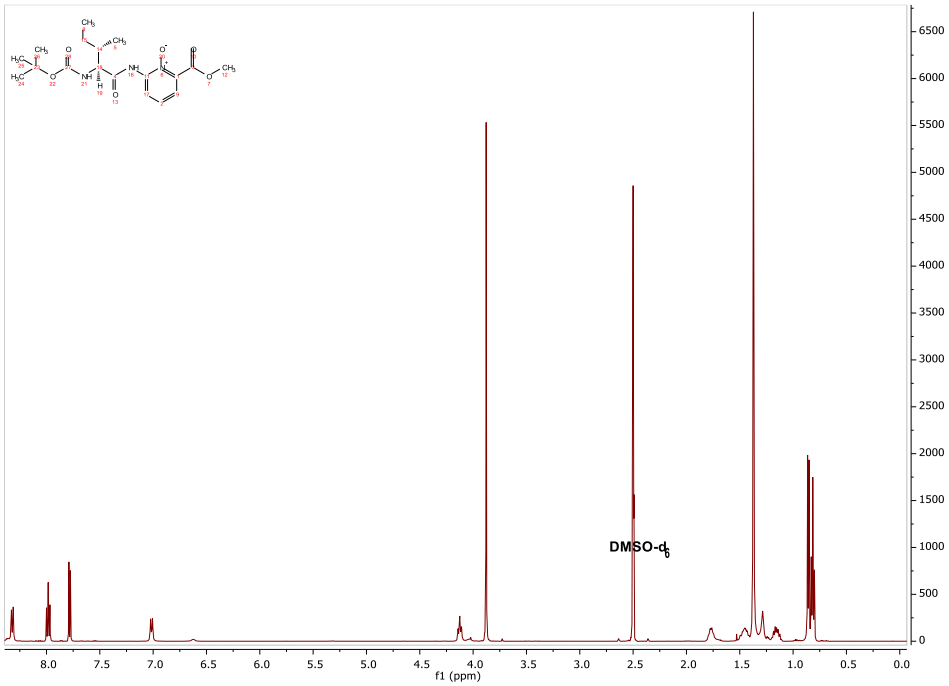

17 ^{13}C NMR

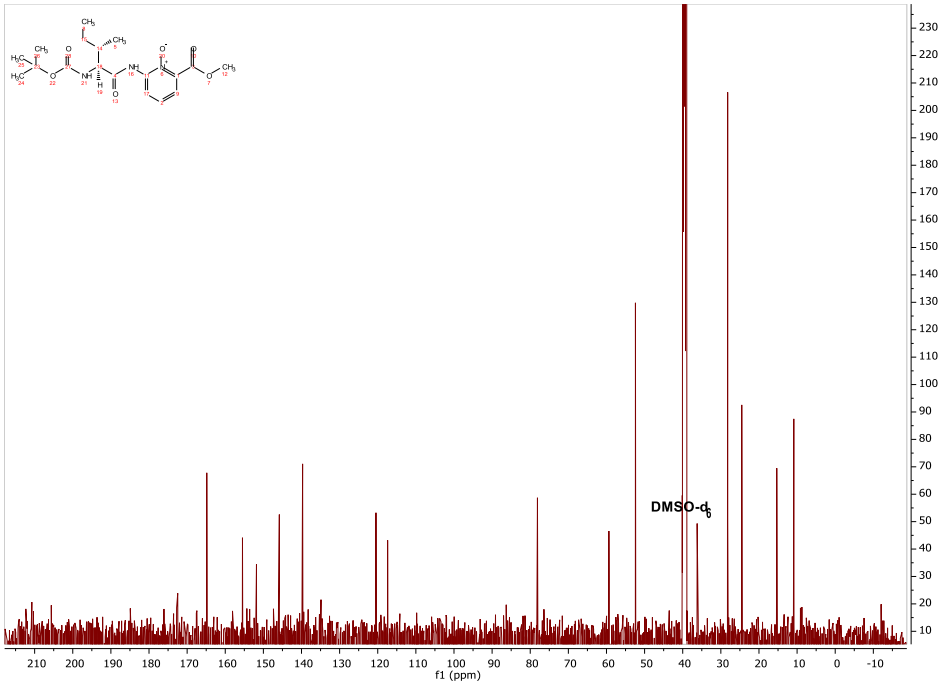

18 ^{1}H NMR

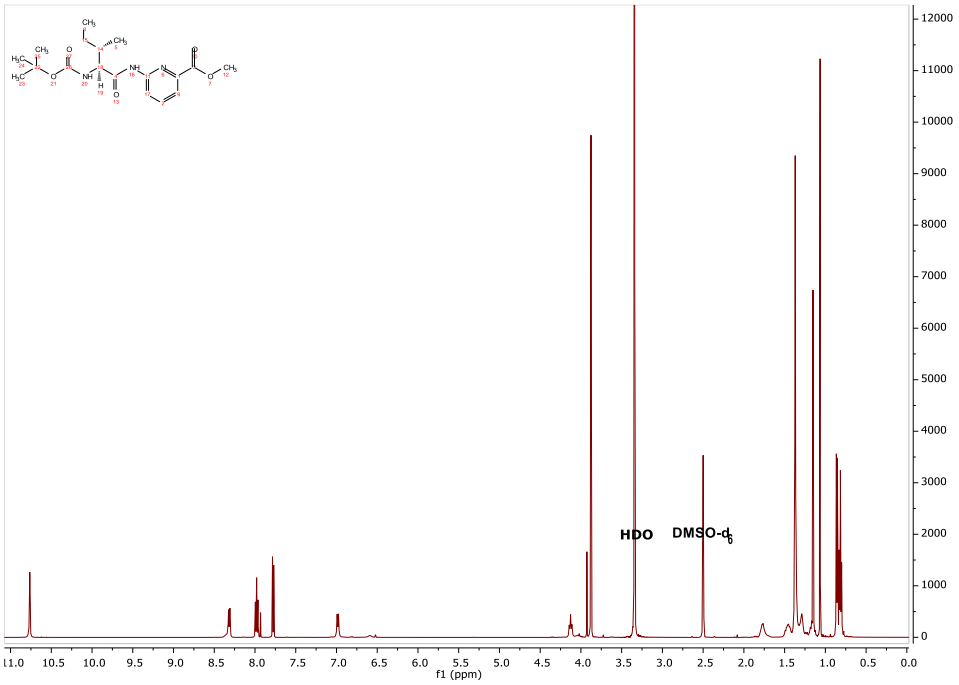

18 ^{13}C NMR

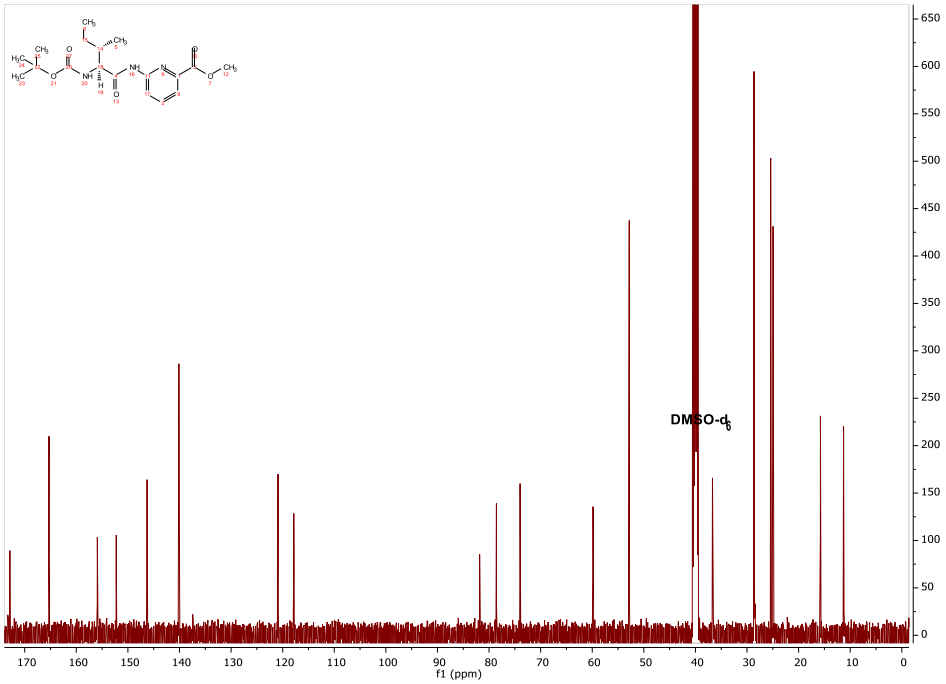

19 ^{1}H NMR

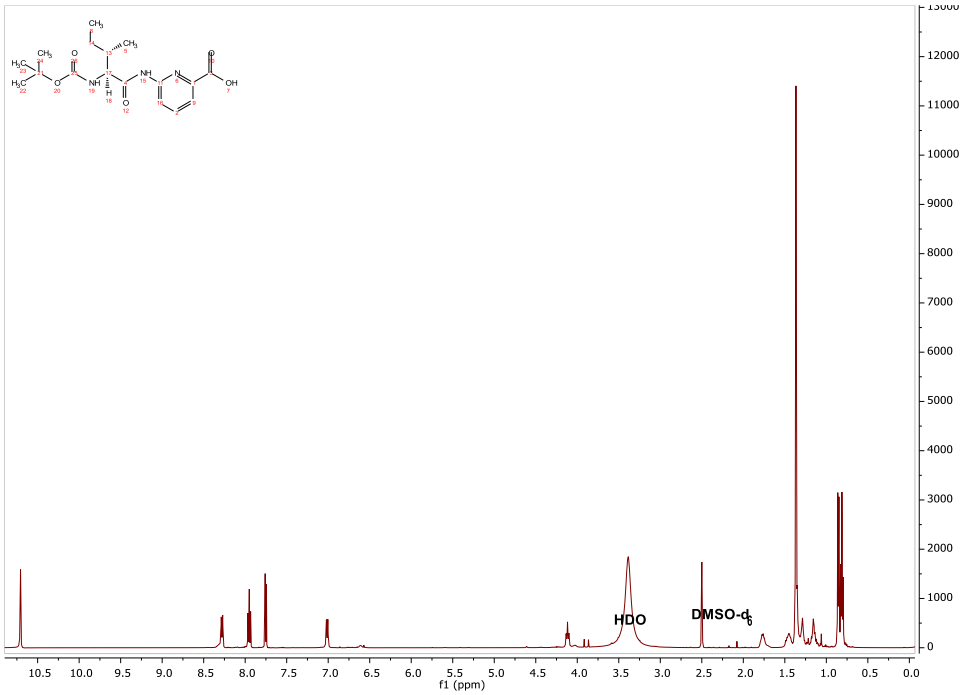

19 ^{13}C NMR

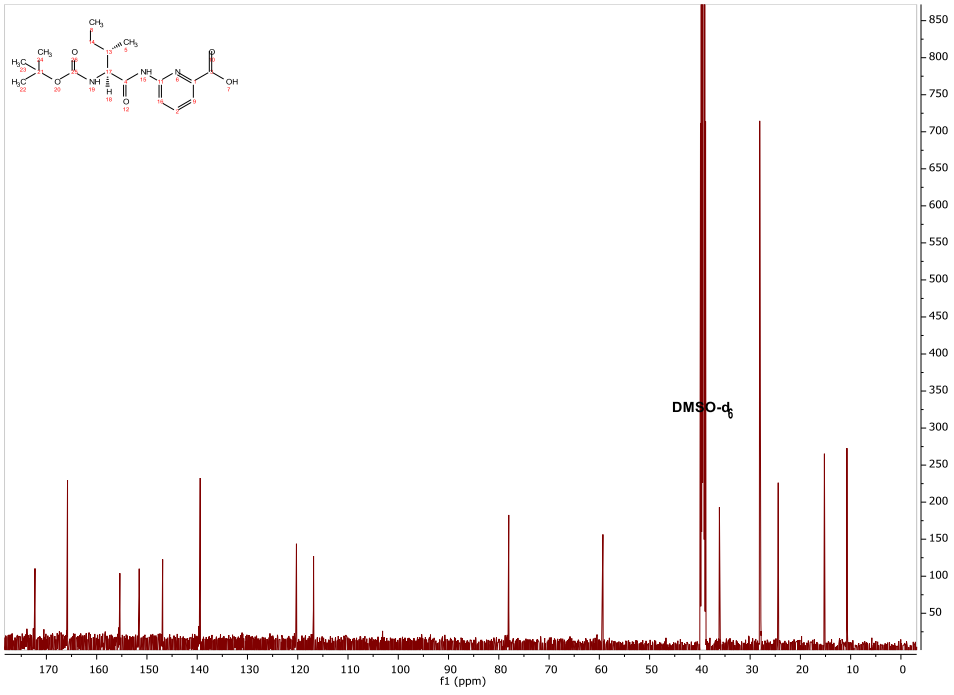

20 ^{1}H NMR

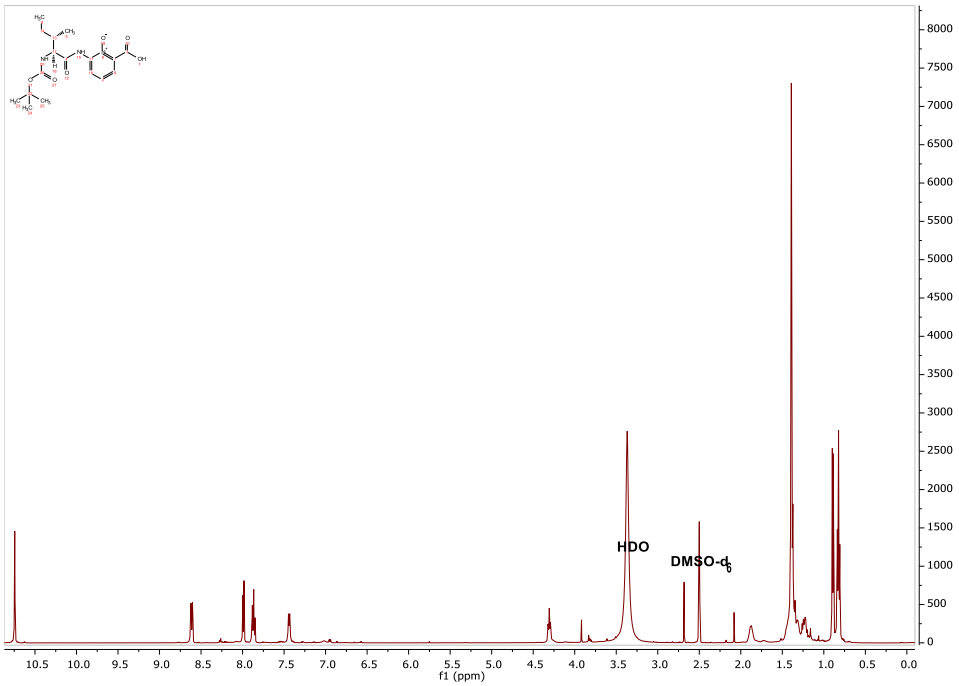

20 ^{13}C NMR

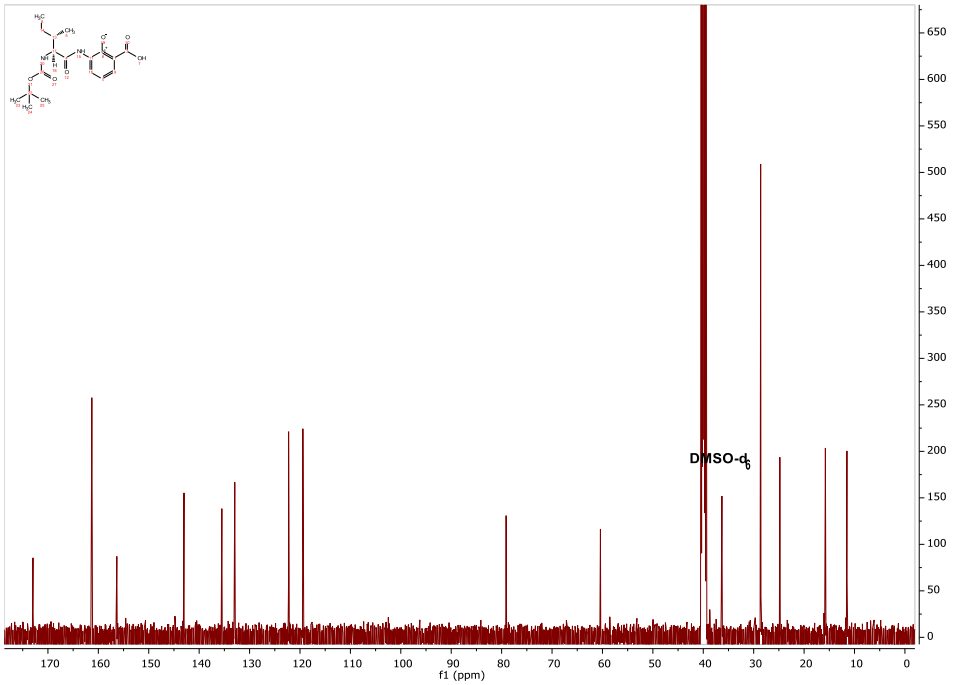

24 ^{1}H NMR

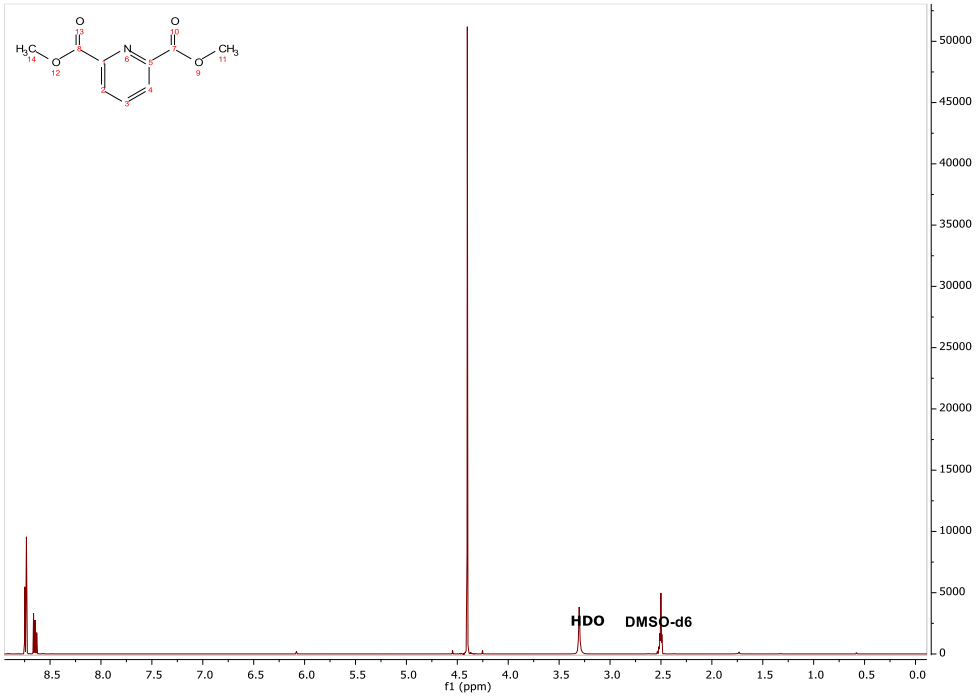

24 ^{13}C NMR

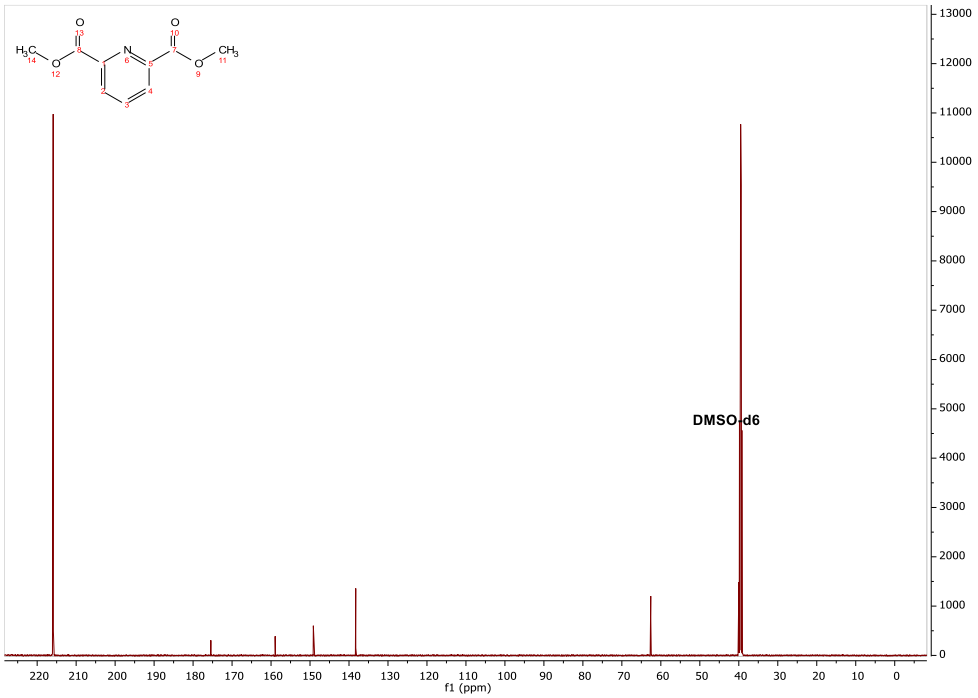

25 ^{1}H NMR

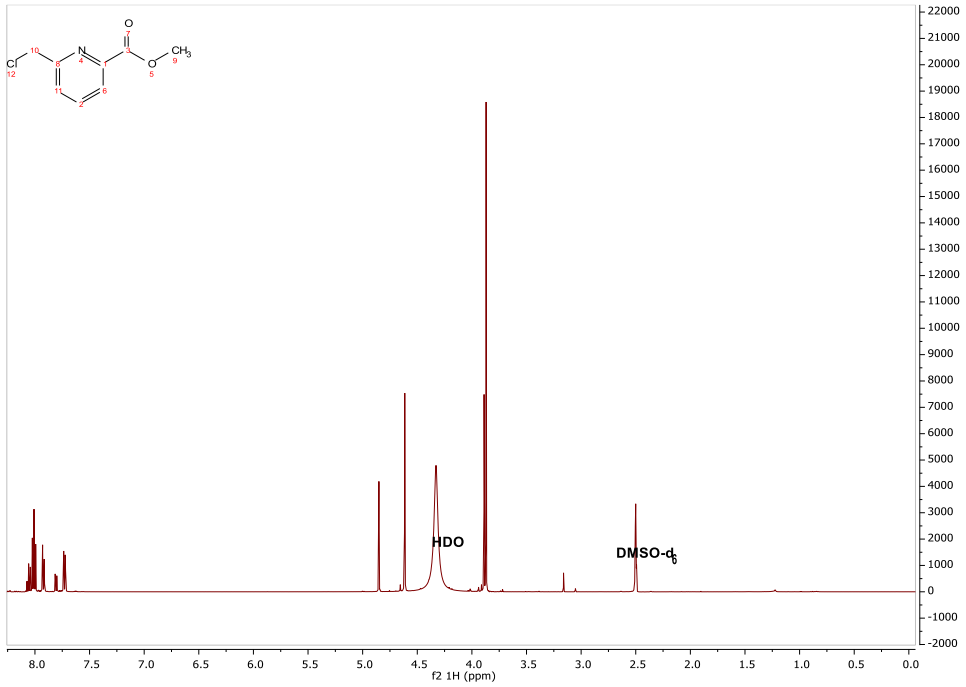

25 ^{13}C NMR

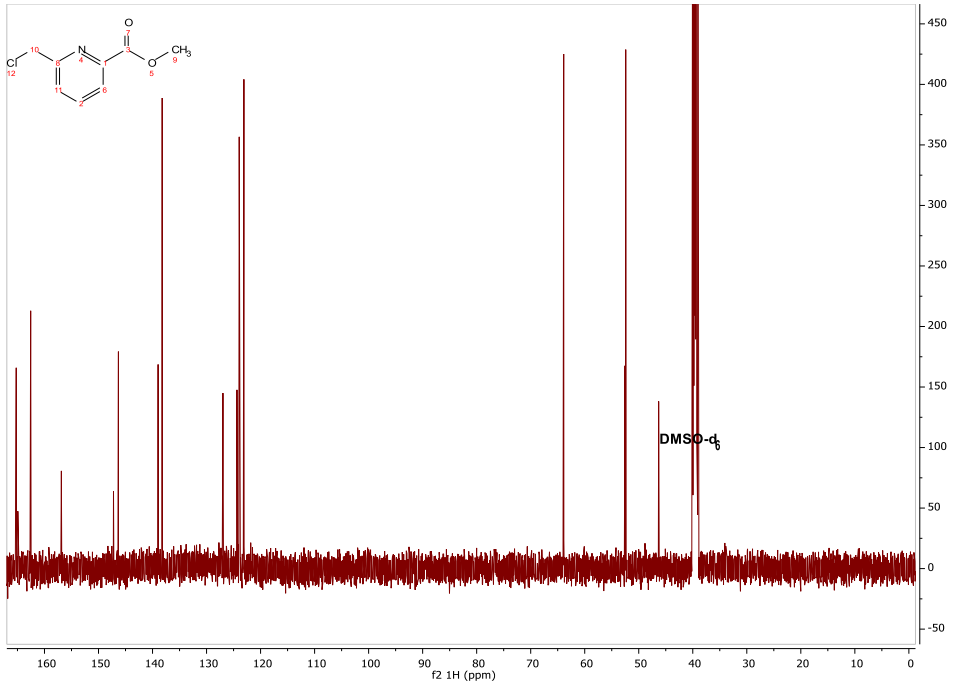

26 ^{1}H NMR

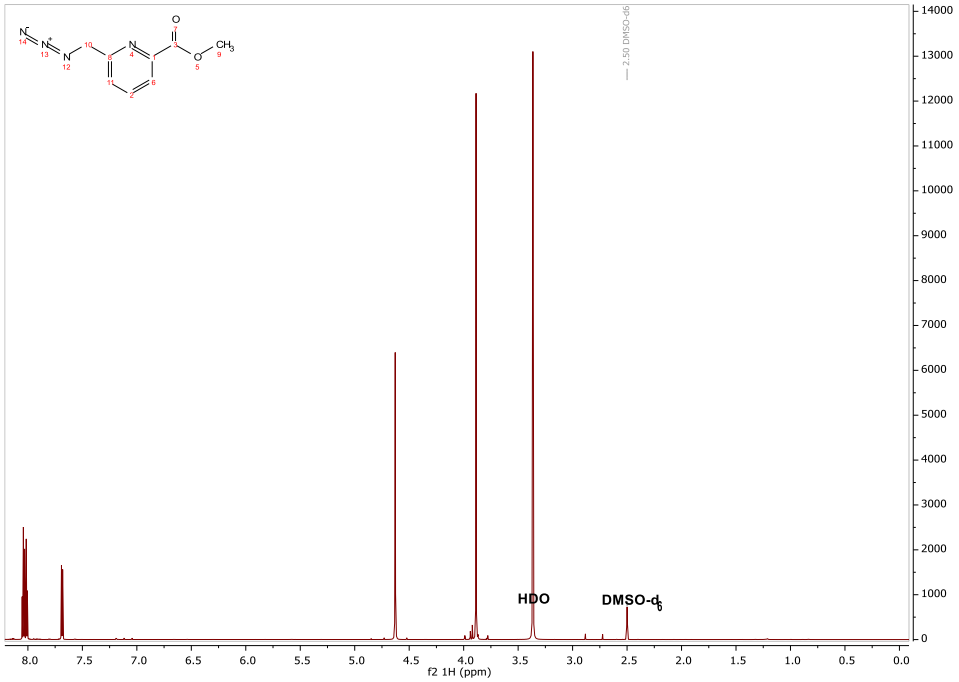

26 ^{13}C NMR

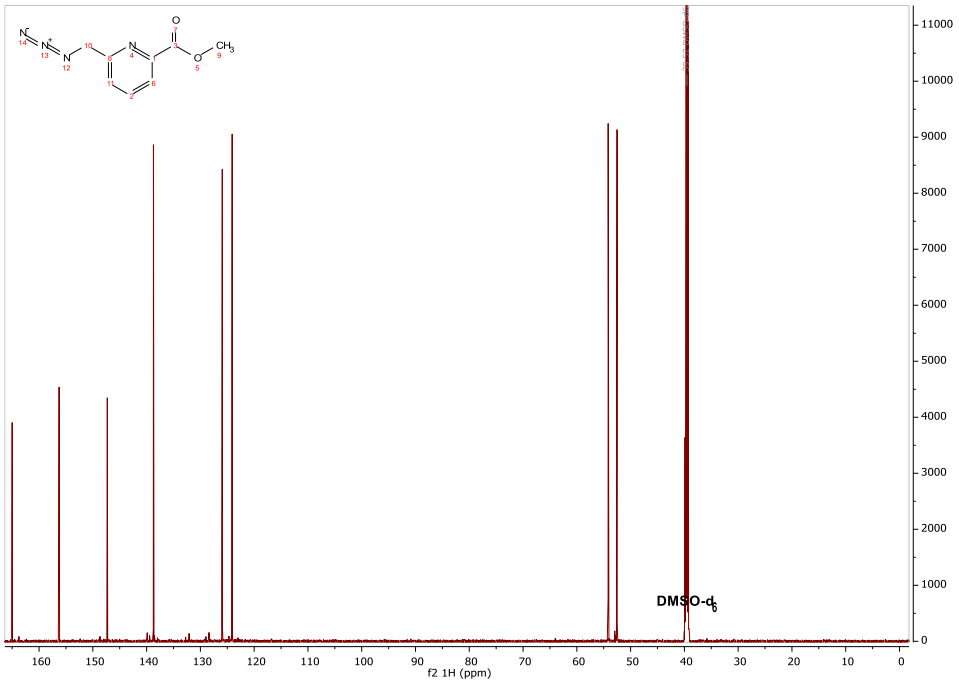

27 ^{1}H NMR

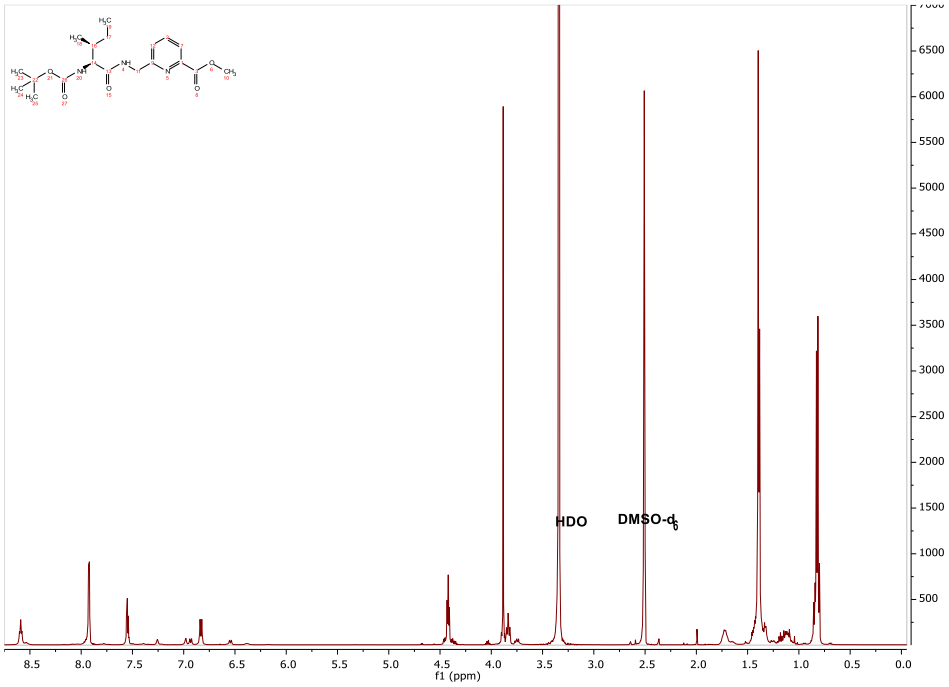

27 ^{13}C NMR

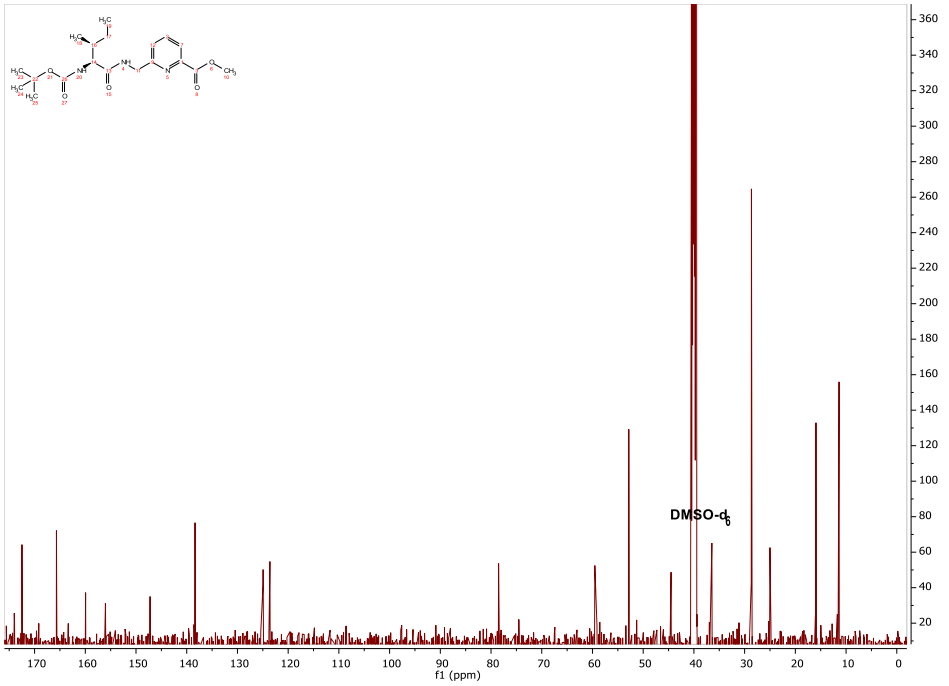

28 ^{1}H NMR

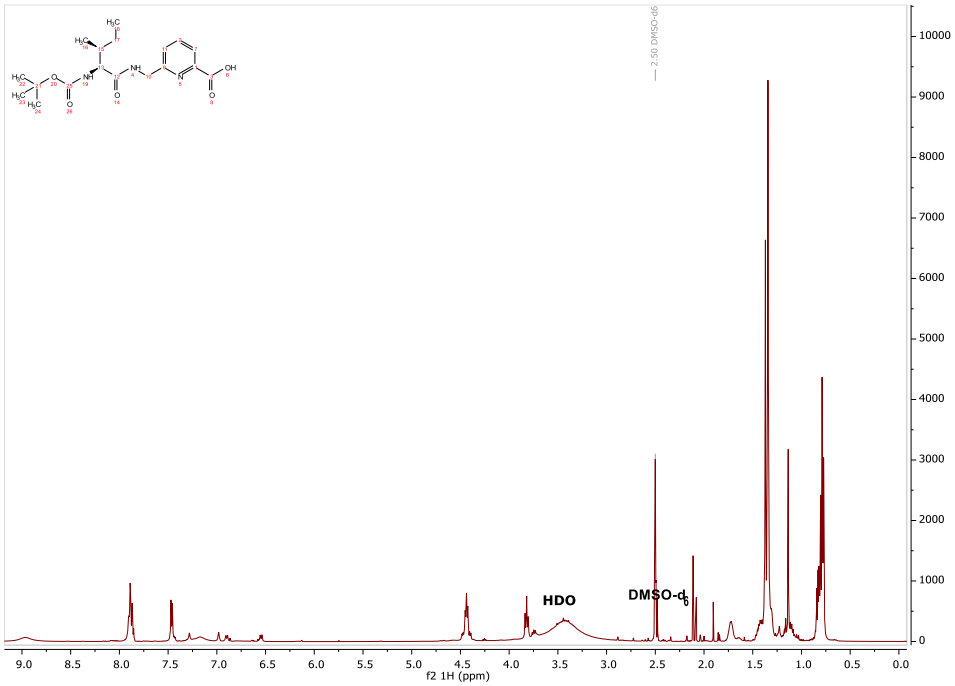

28 ^{13}C NMR

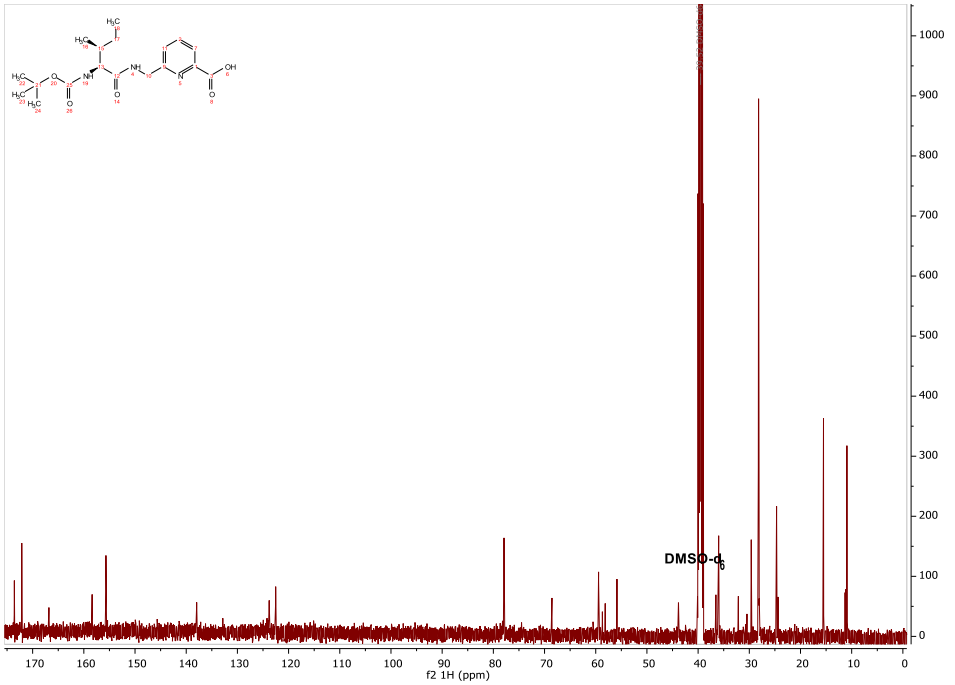

29 ^{1}H NMR

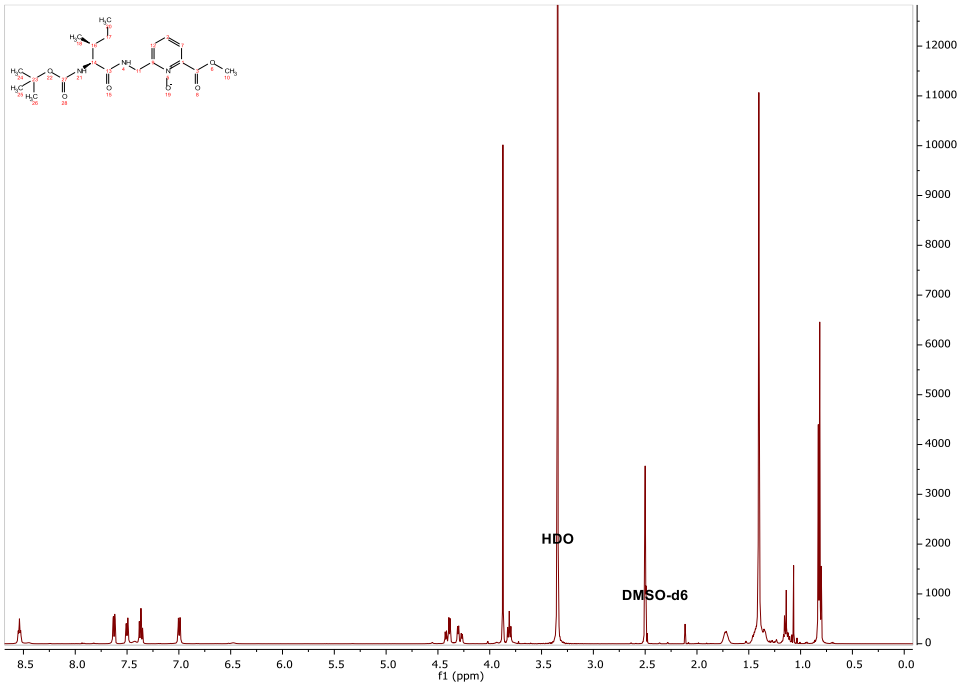

29 ^{13}C NMR

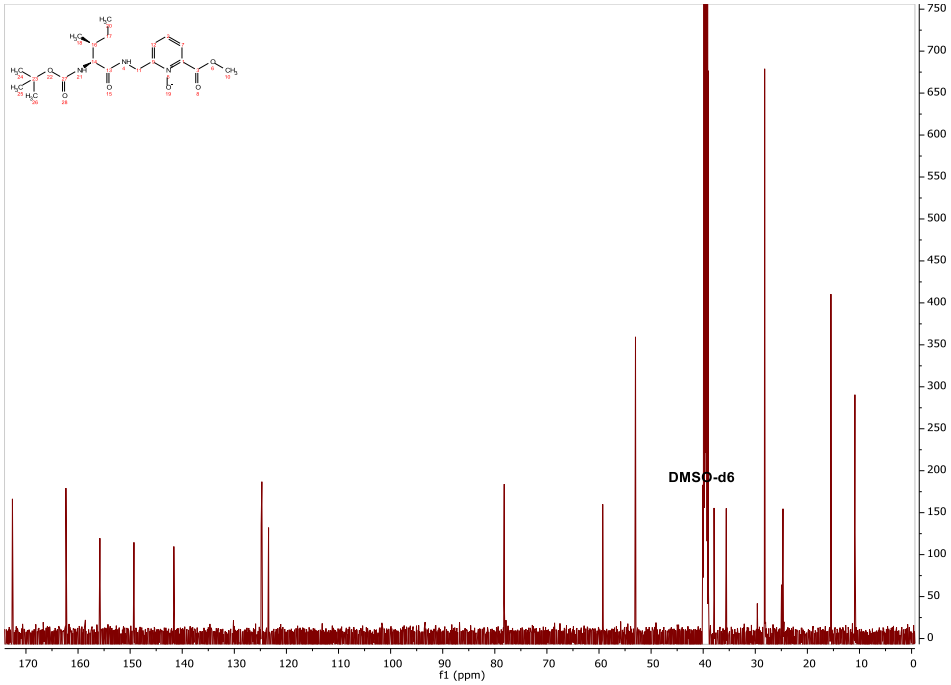

30 ^{1}H NMR

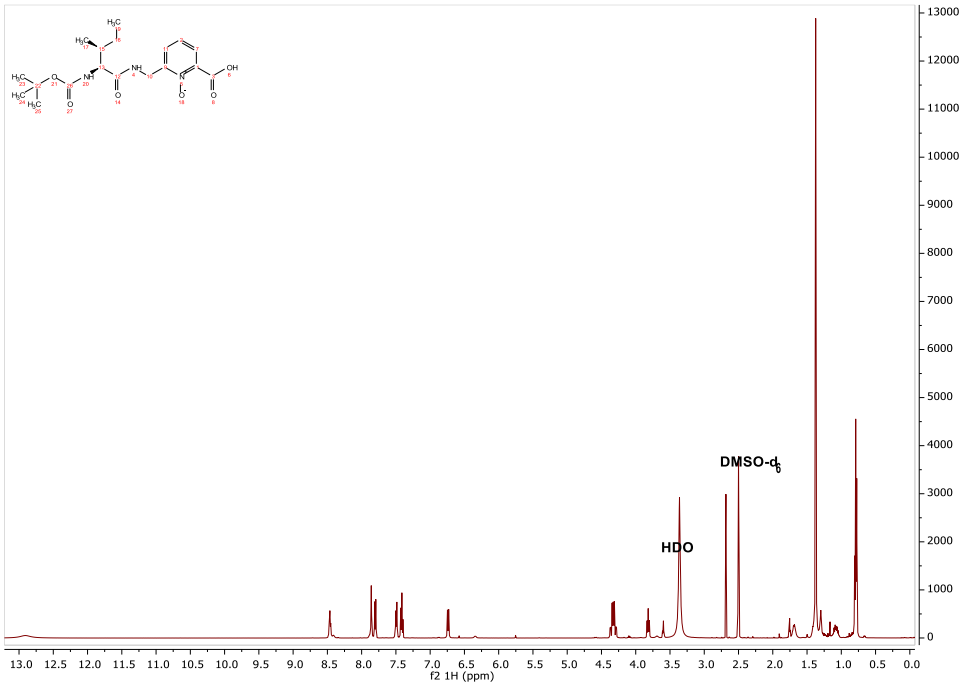

30 ^{13}C NMR

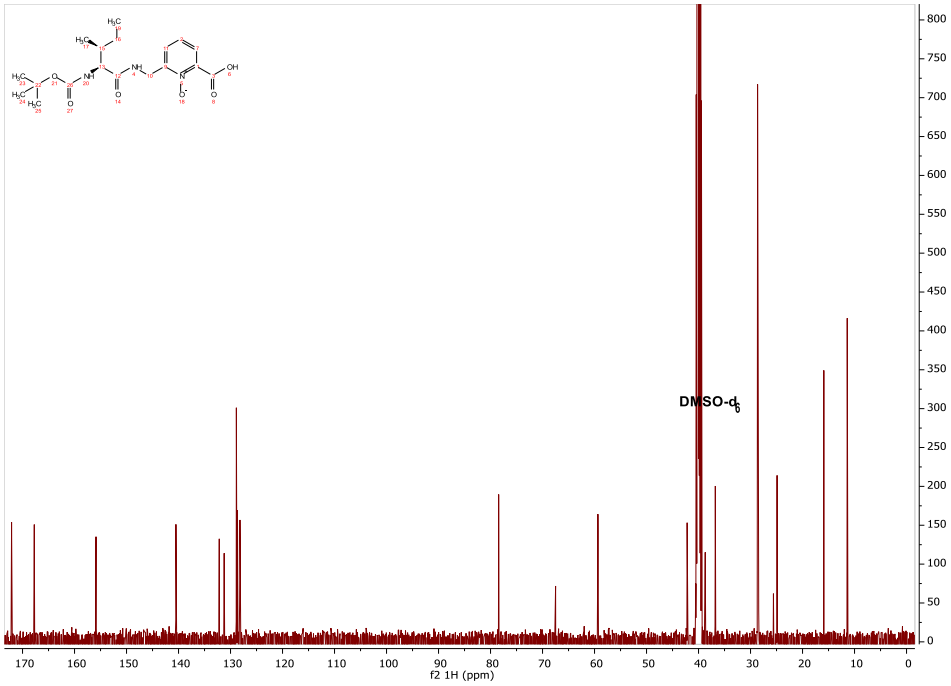

34 ^{1}H NMR

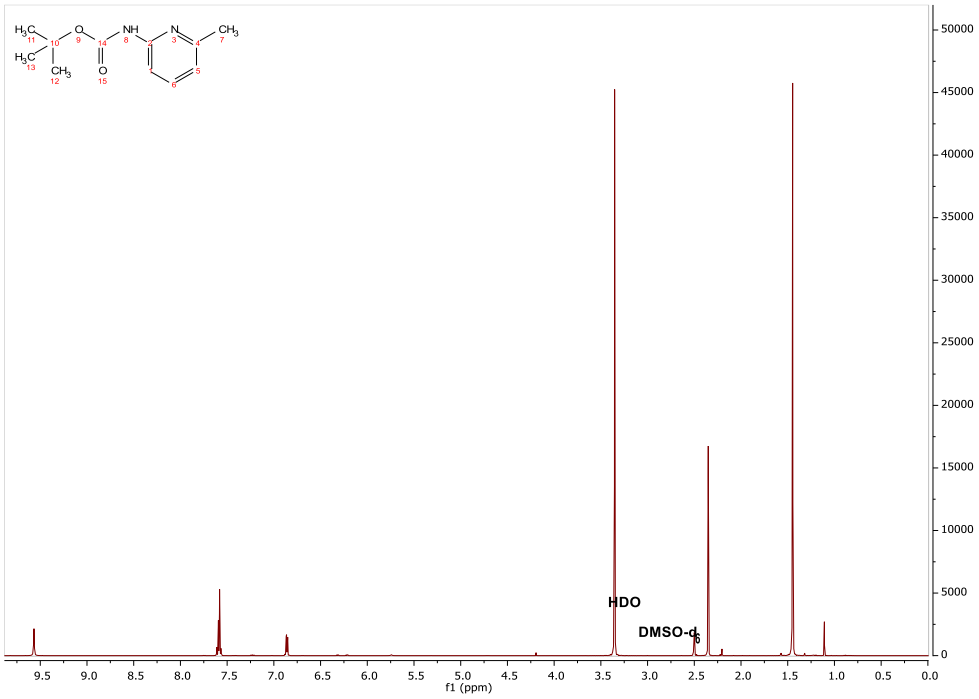

34 ^{13}C NMR

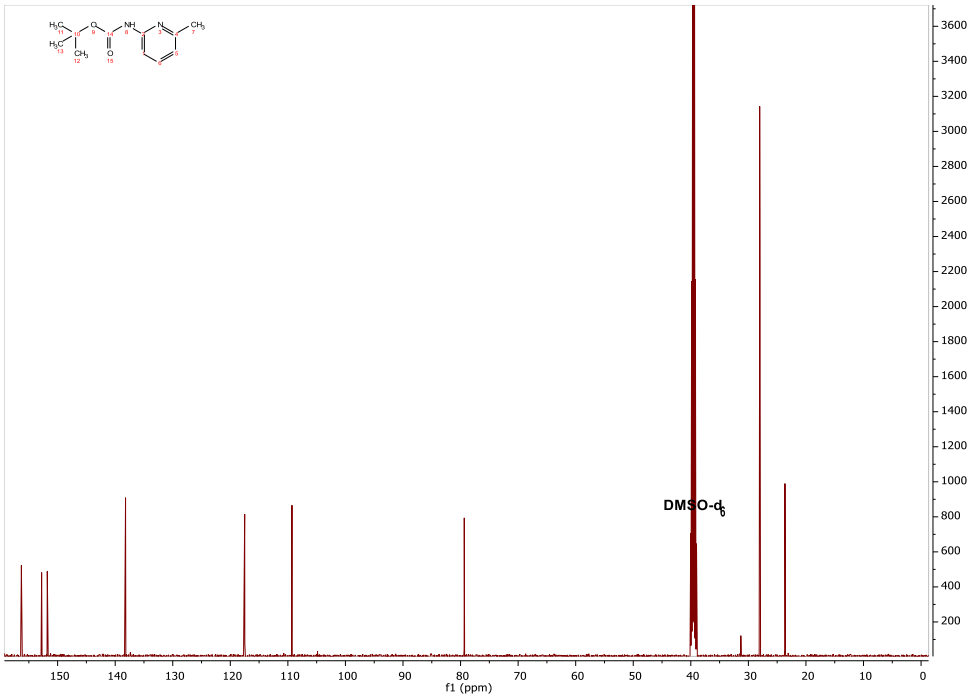

35 ^{1}H NMR

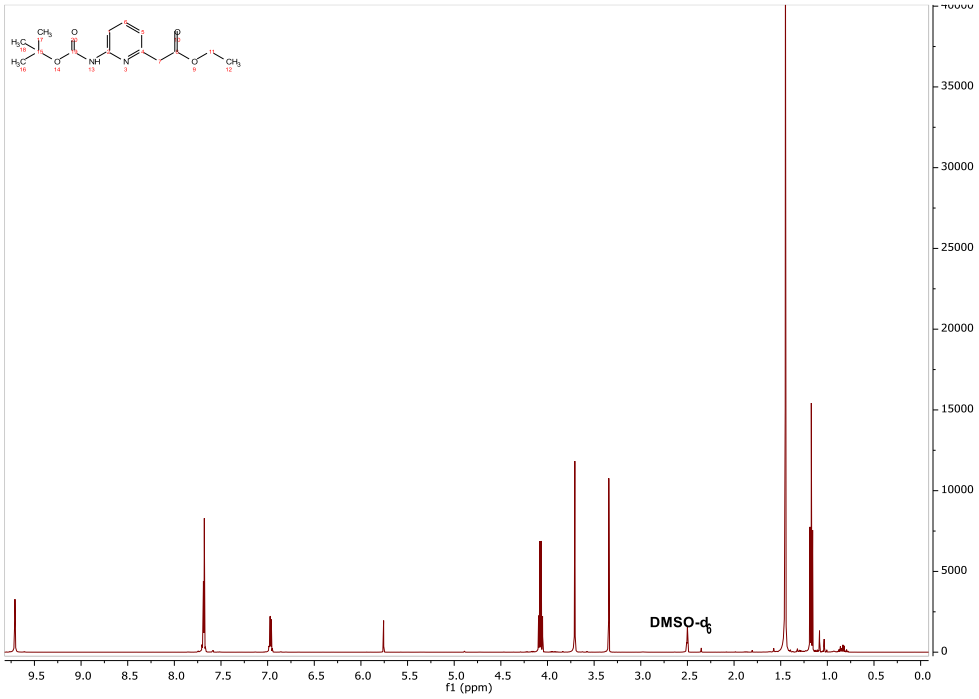

35 ^{13}C NMR

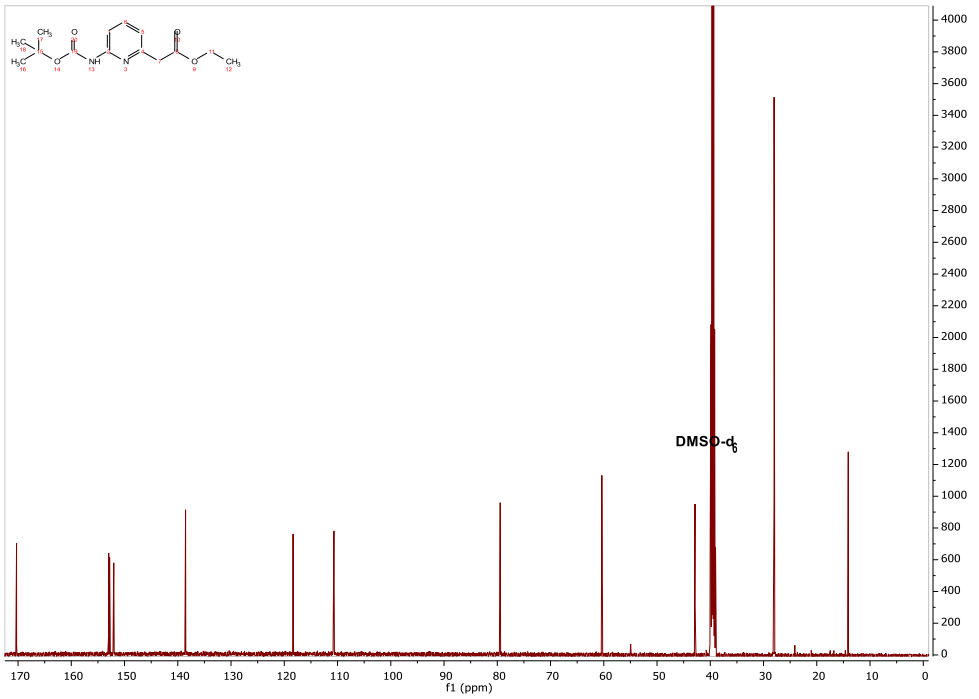

36 ^{1}H NMR

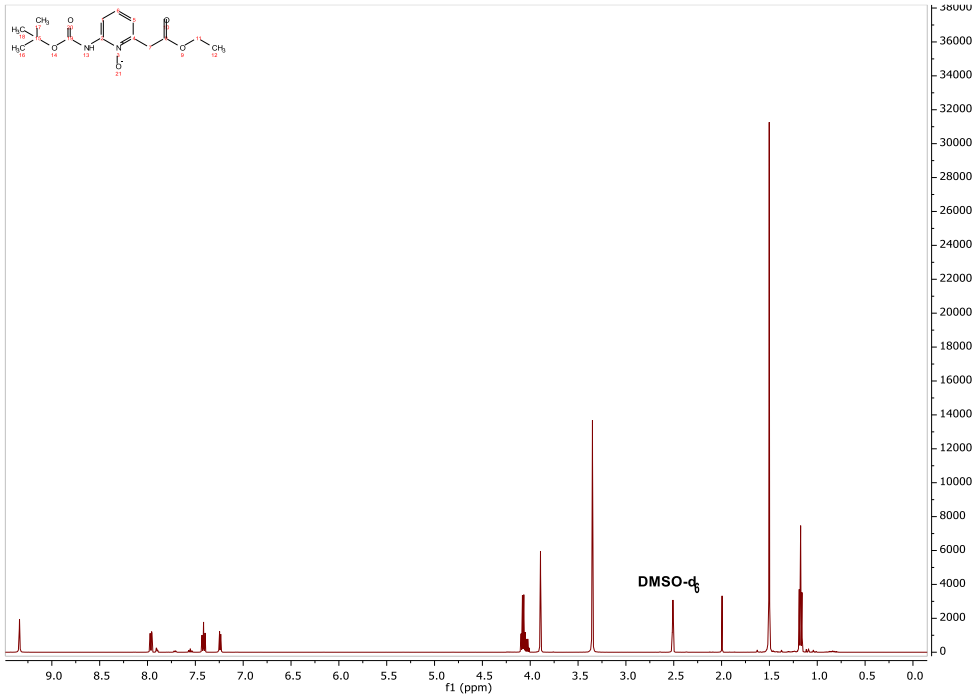

36 ^{13}C NMR

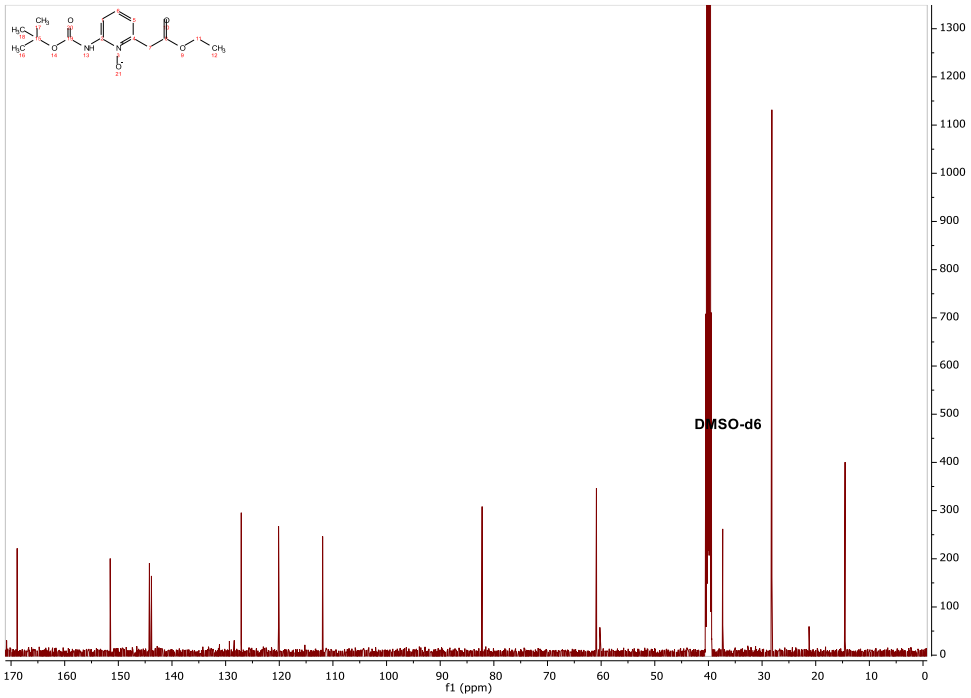

37 ^{1}H NMR

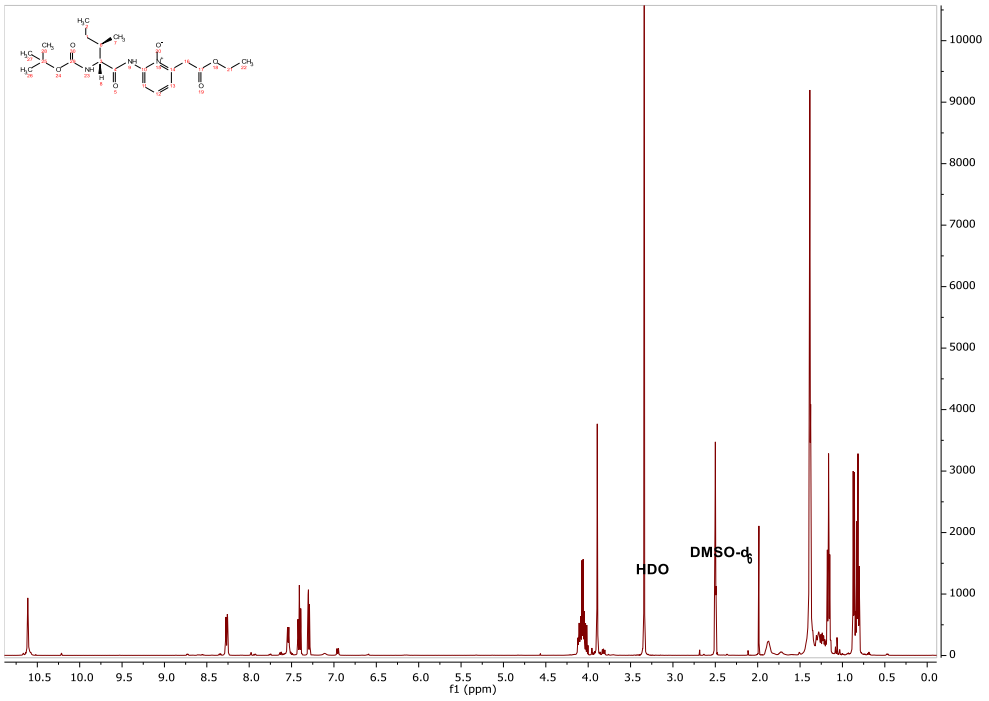

37 ^{13}C NMR

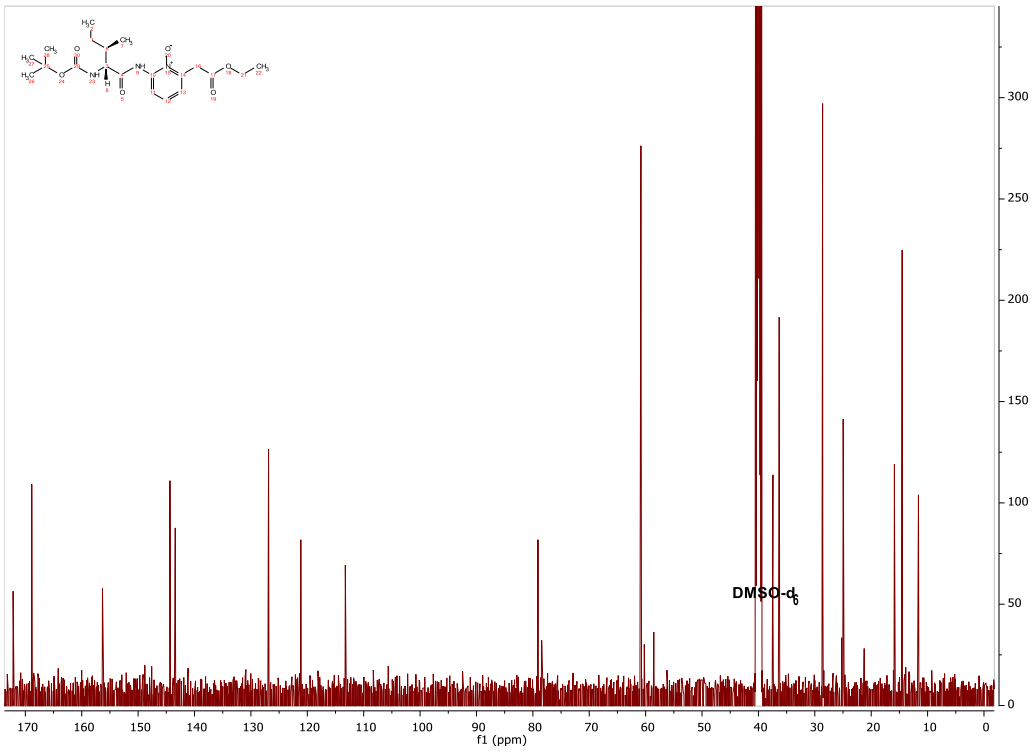

38 ^{1}H NMR

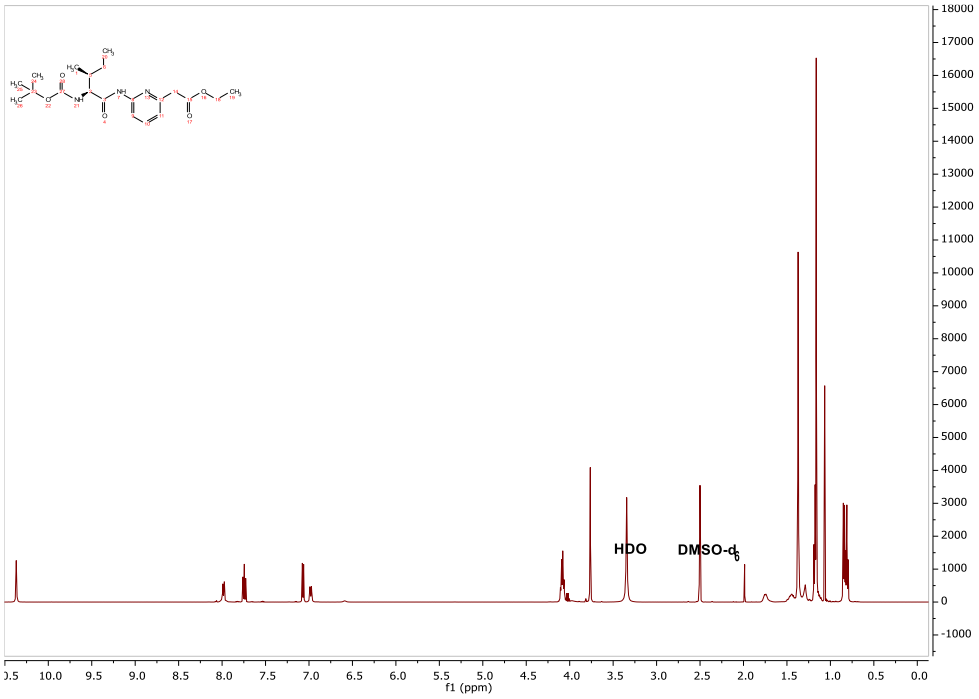

38 ^{13}C NMR

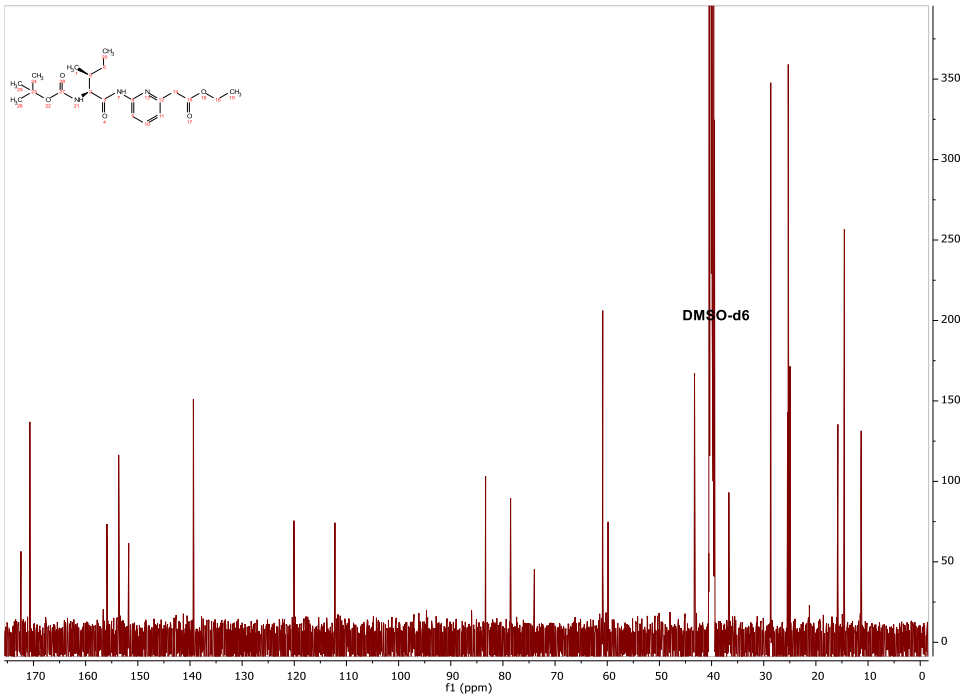

39 ^{1}H NMR

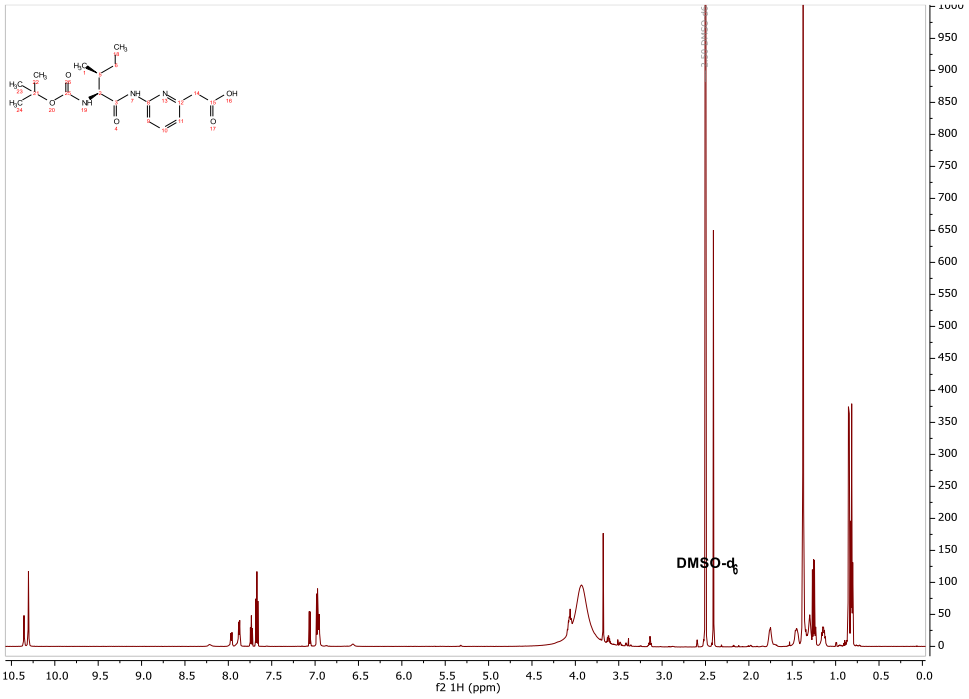

39 ^{13}C NMR

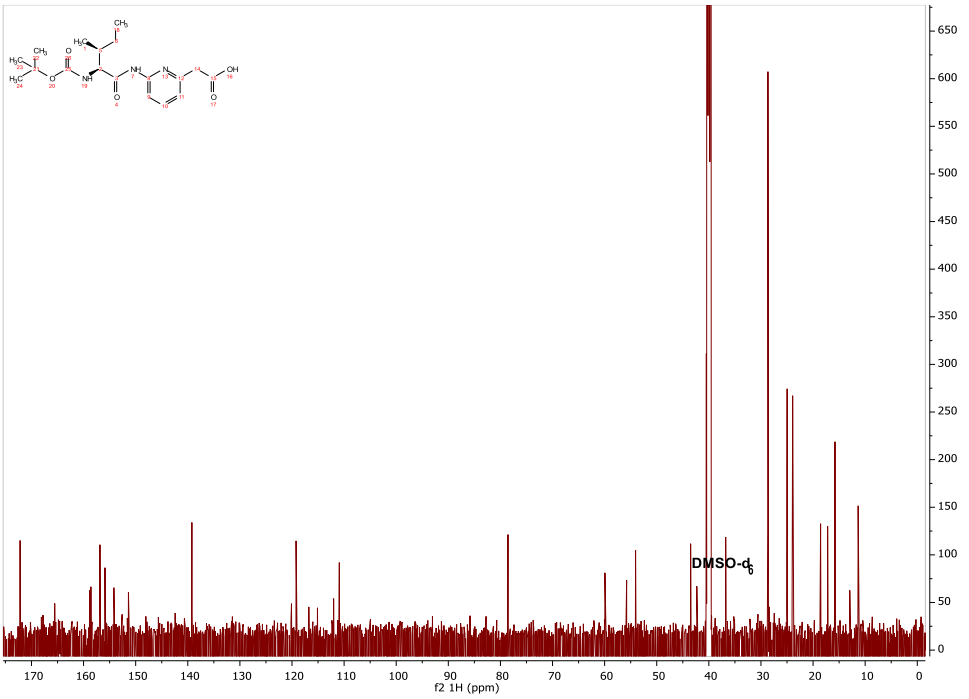

40 ^{1}H NMR

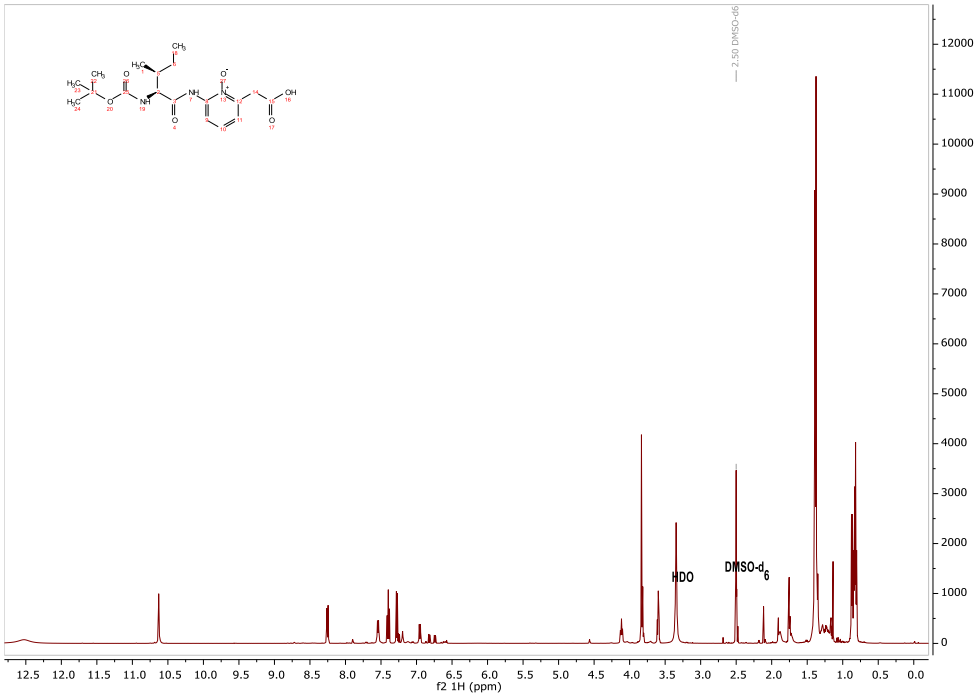

40 ^{13}C NMR

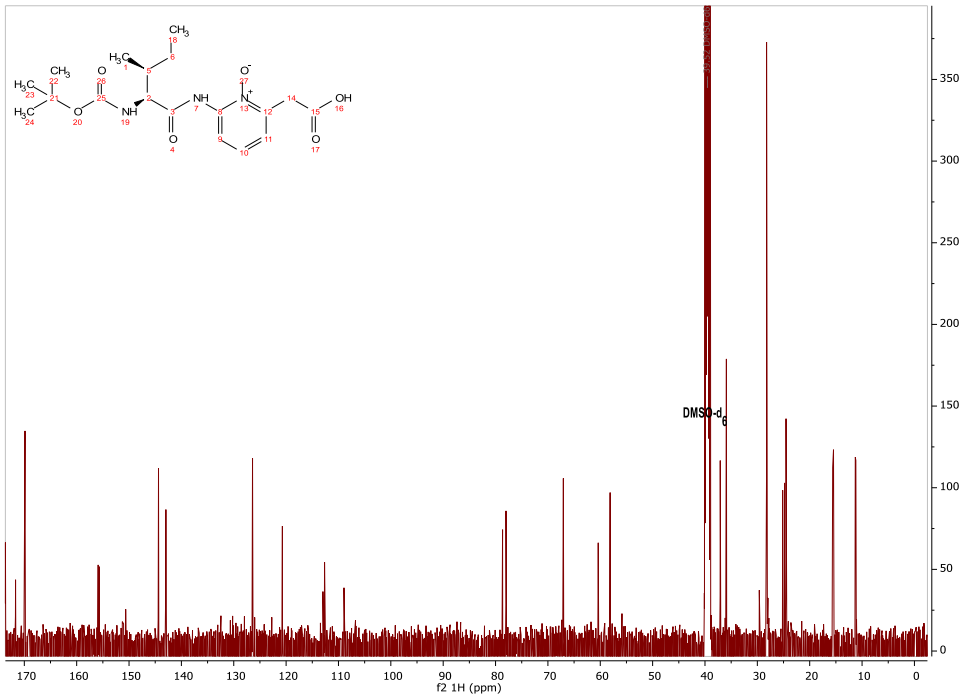

44 ^{1}H NMR

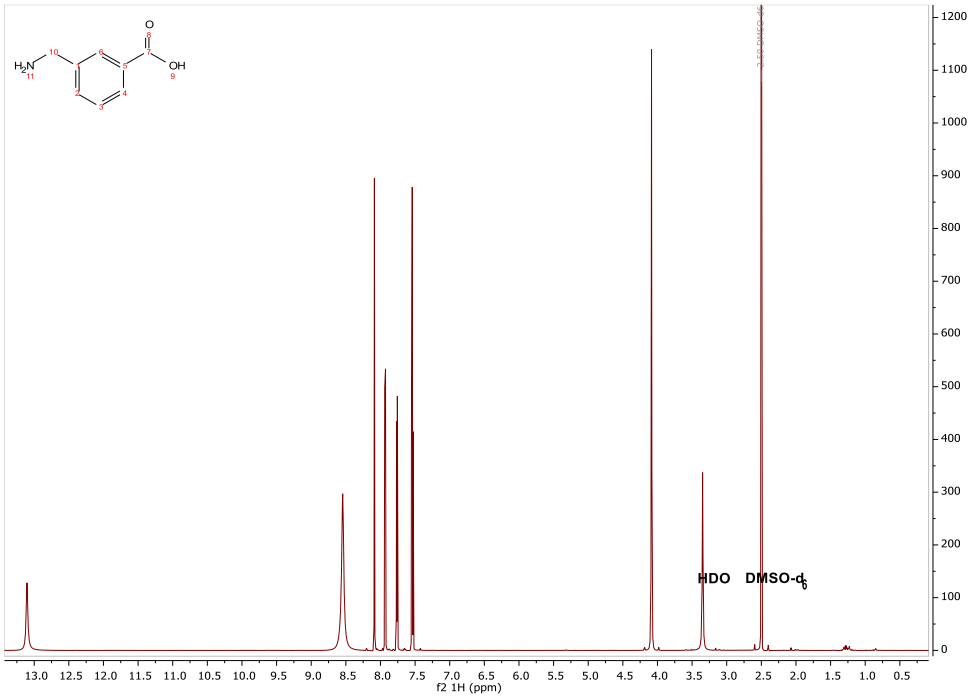

44 ^{13}C NMR

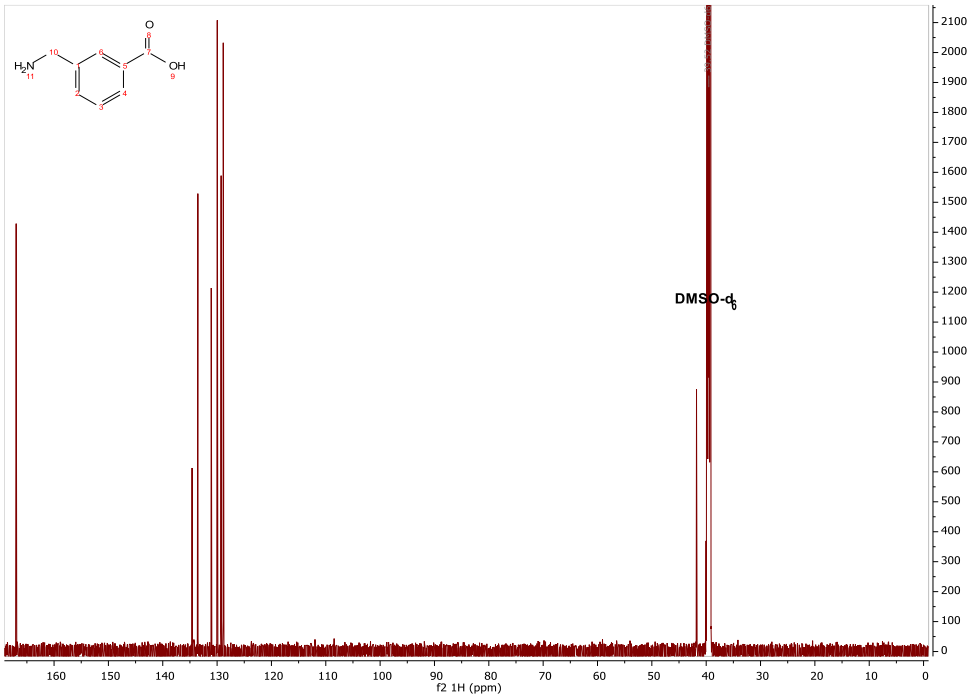

47 ^{1}H NMR

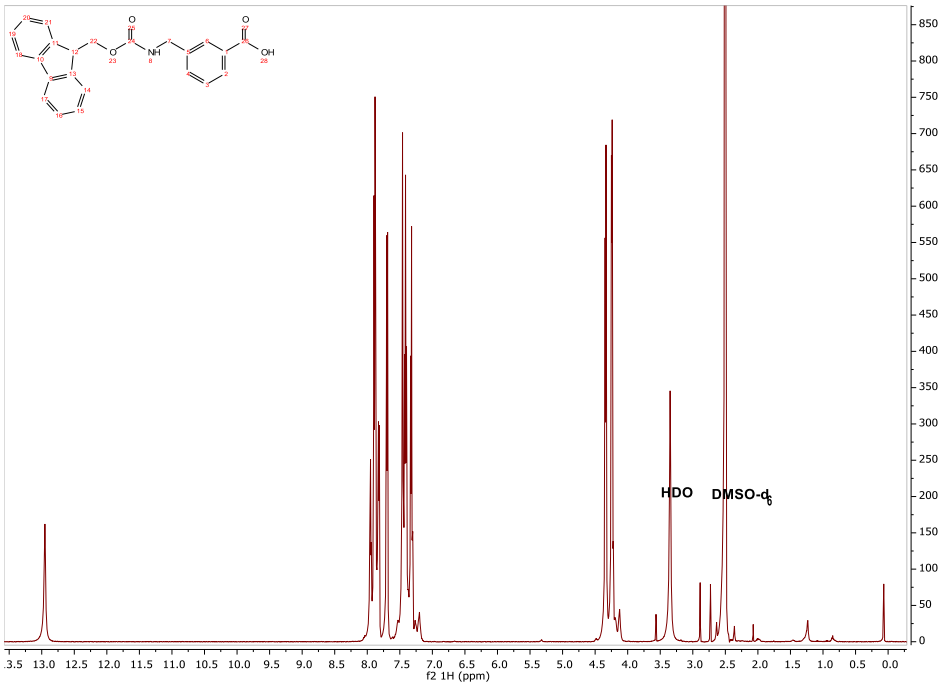

47 ^{13}C NMR

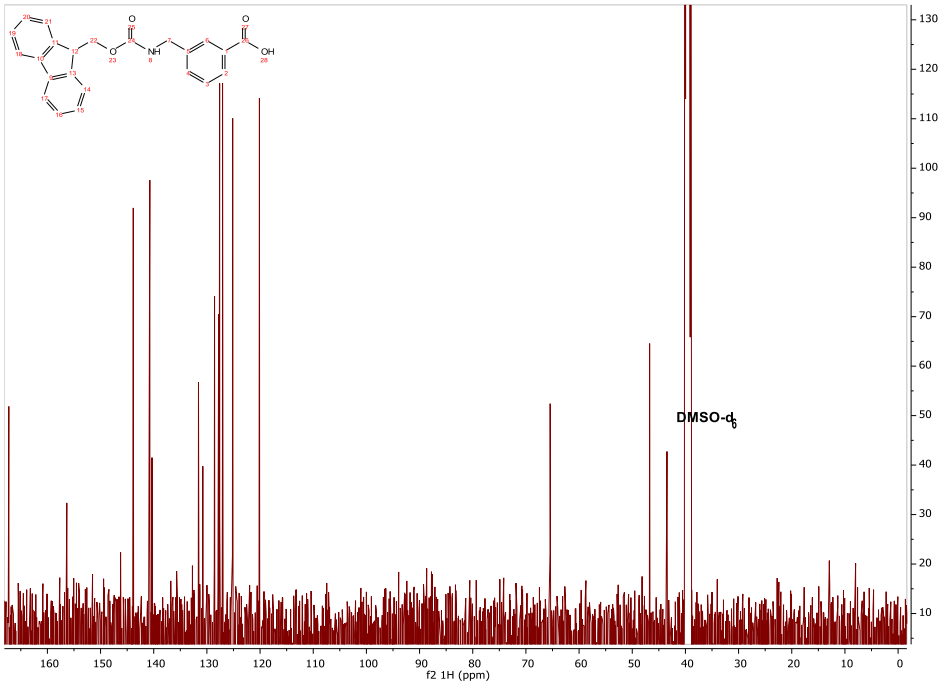

48 ^{1}H NMR

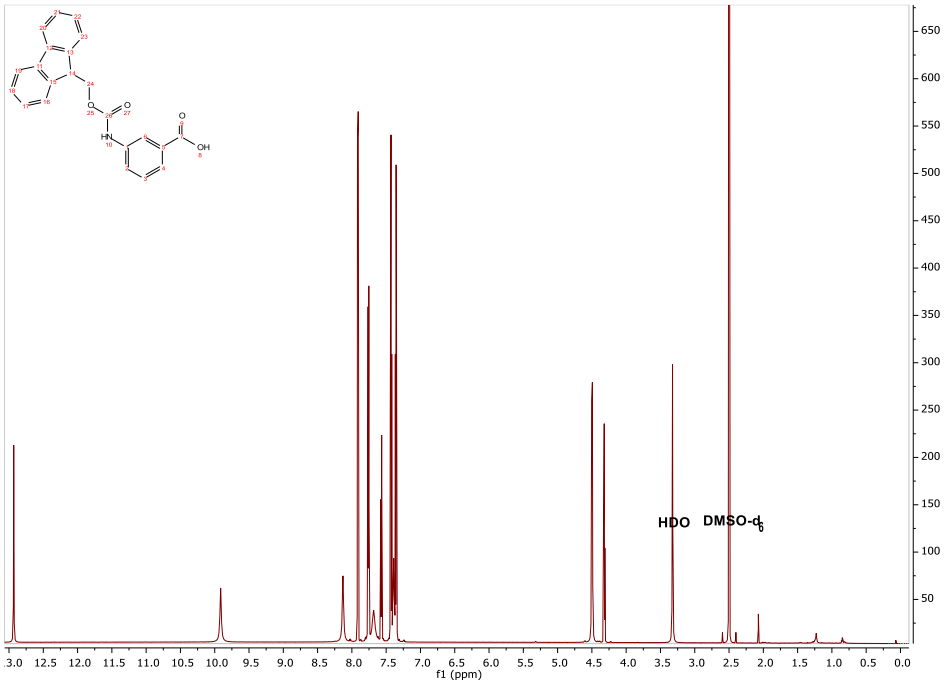

48 ^{13}C NMR

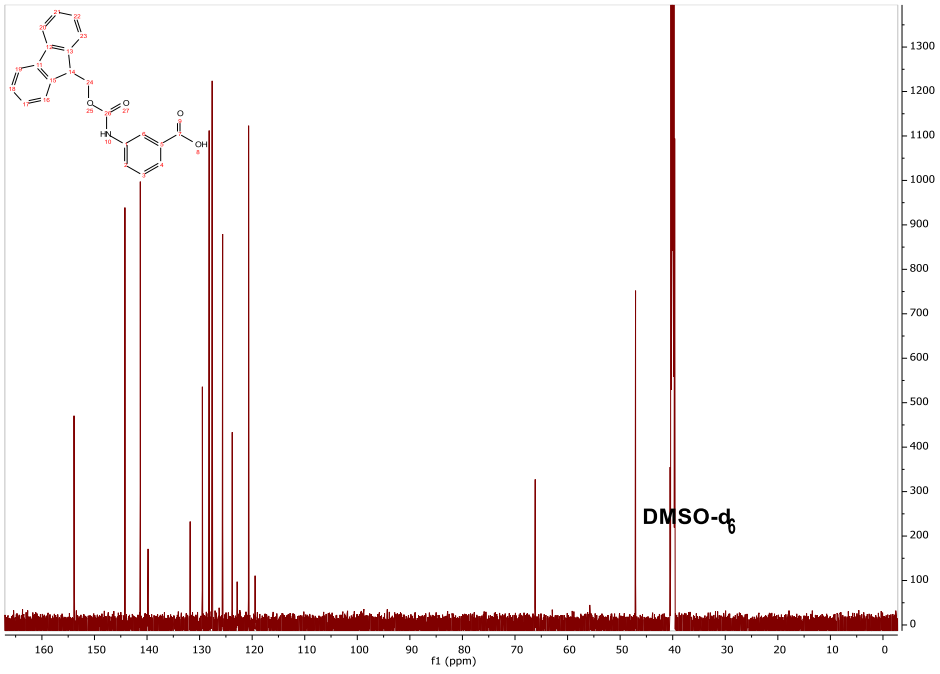

49 ^{1}H NMR

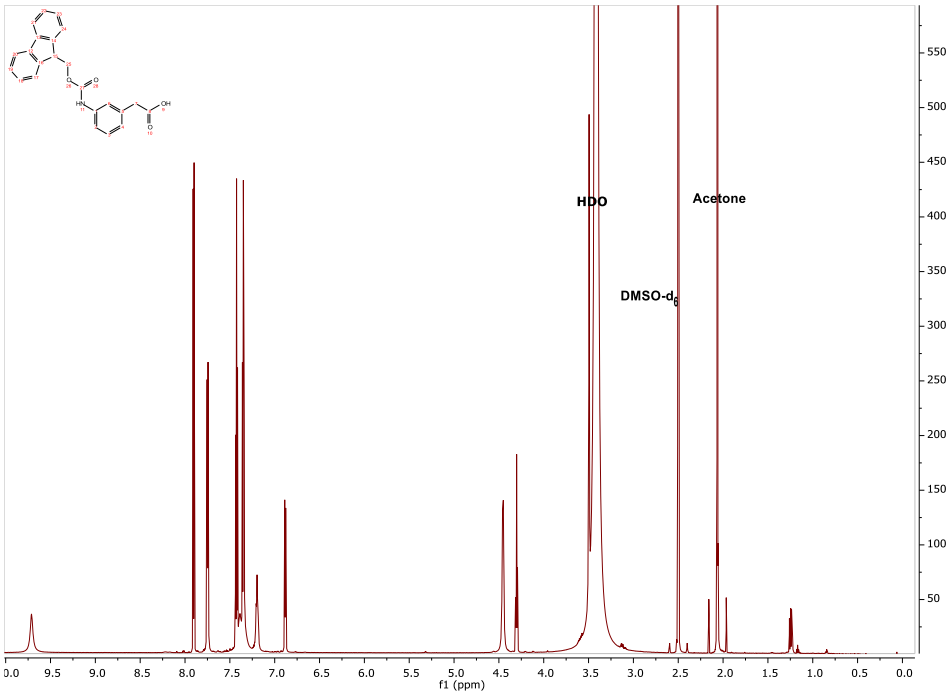

49 ^{13}C NMR

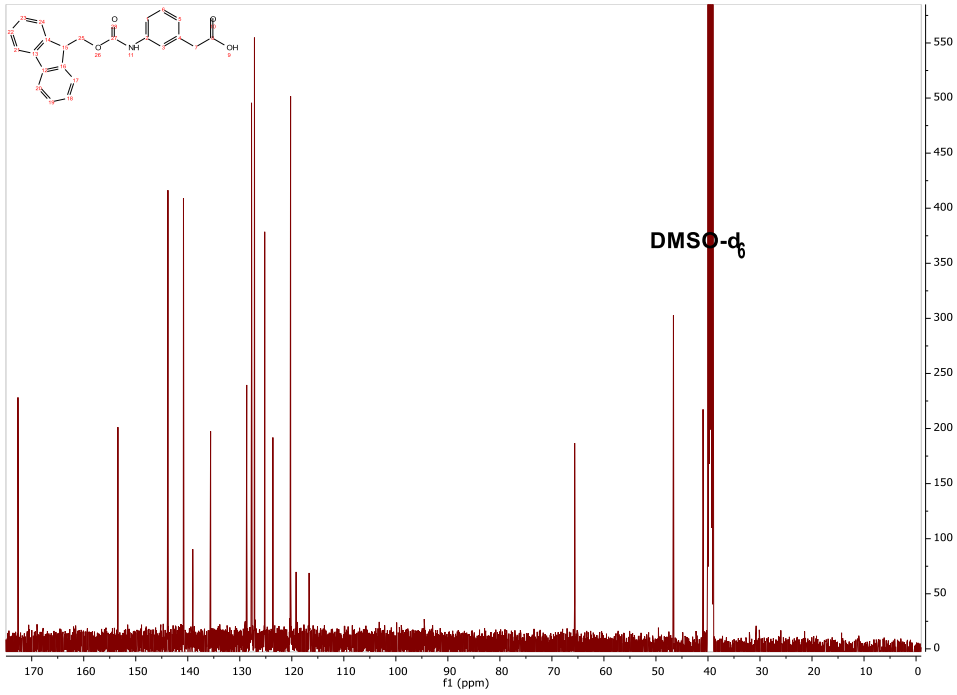

Compound **1** ^{1}H NMR (DMSO-d_6)

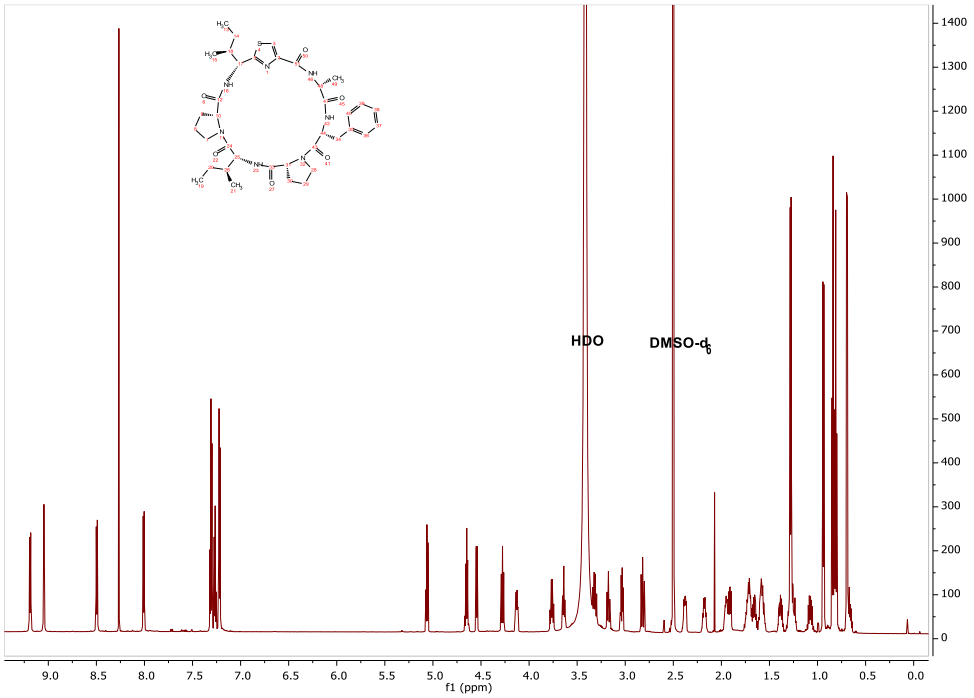

Compound **1** ^{13}C NMR (DMSO-d_6)

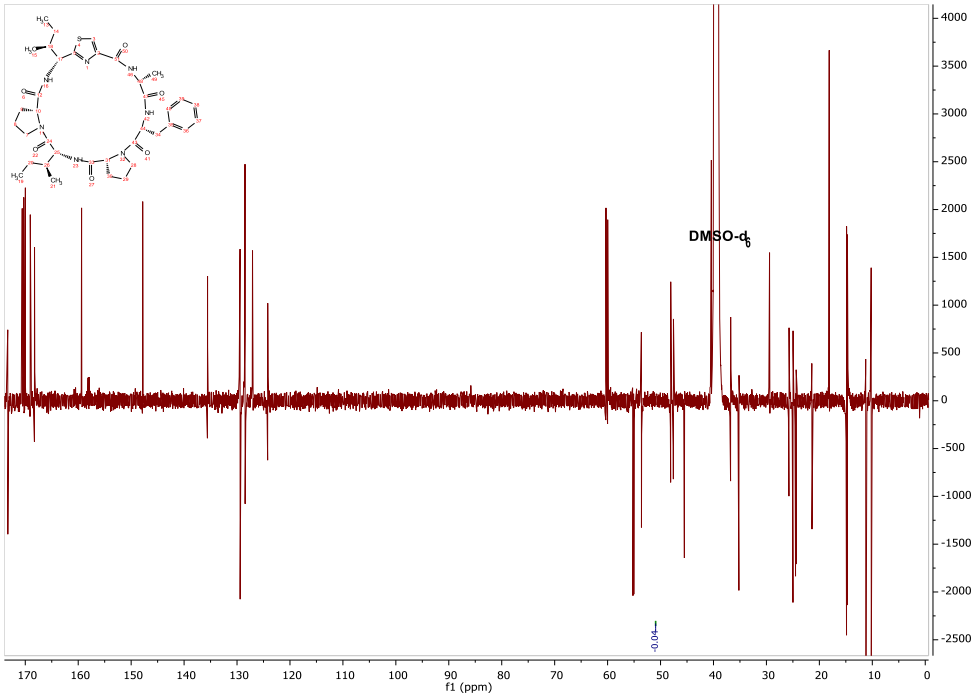

Compound **1** ^{1}H NMR ($CDCl_3$)

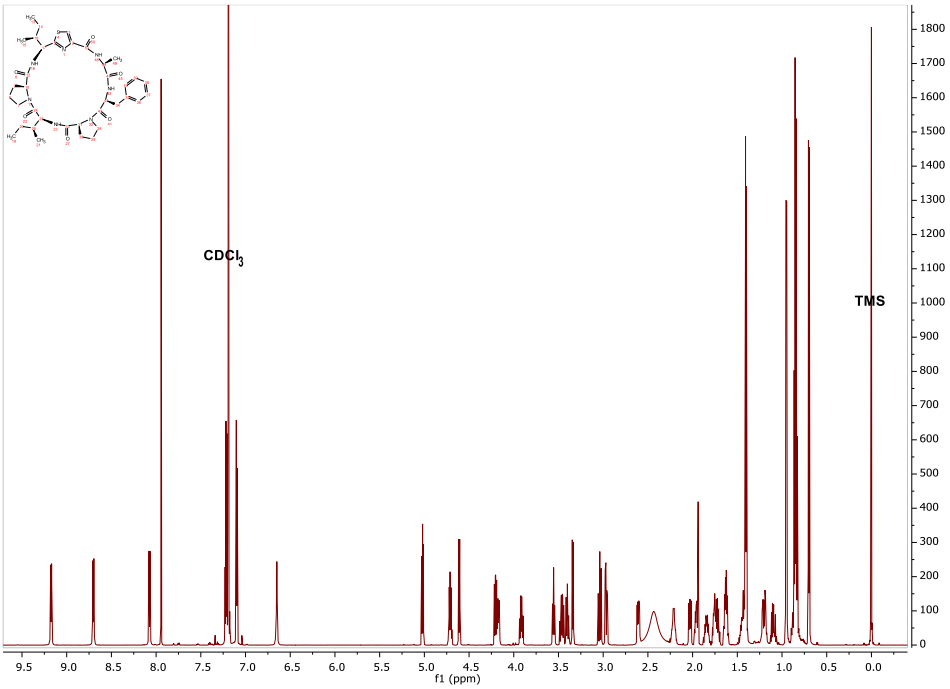

Compound **1** ^{13}C NMR ($CDCl_3$)

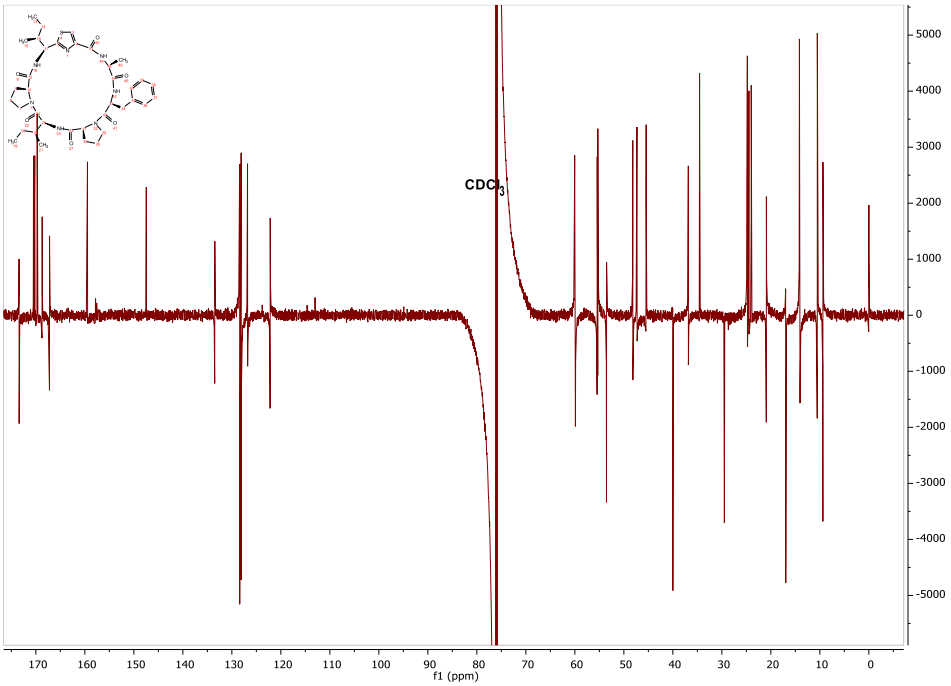

Compound **1** ^{1}H NMR (DMSO-d_6)

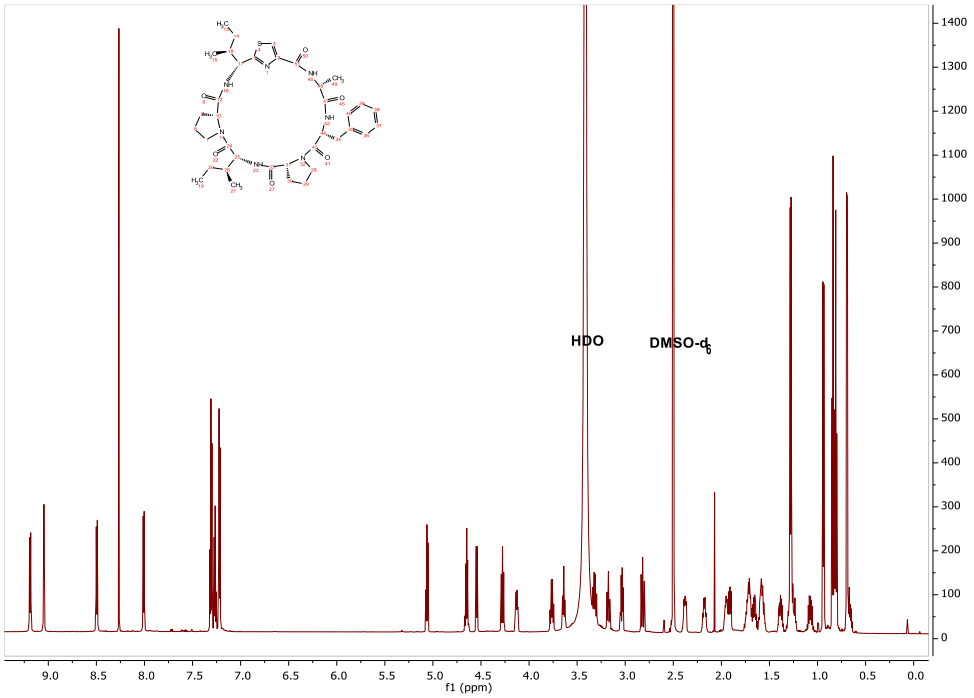

Compound **1** ^{13}C NMR (DMSO-d_6)

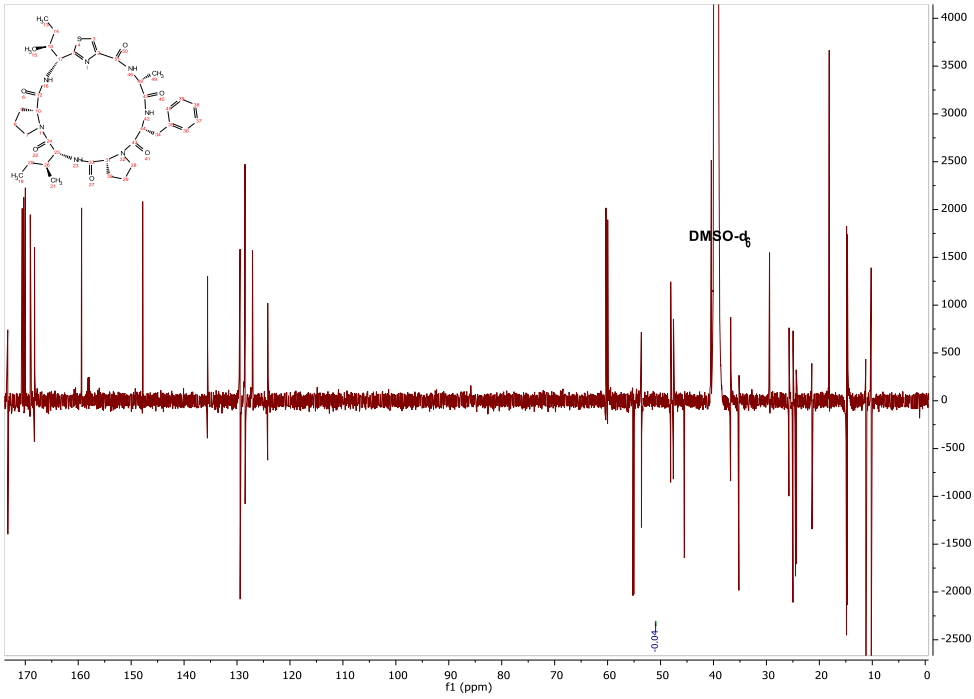

Compound **2** ^{1}H NMR

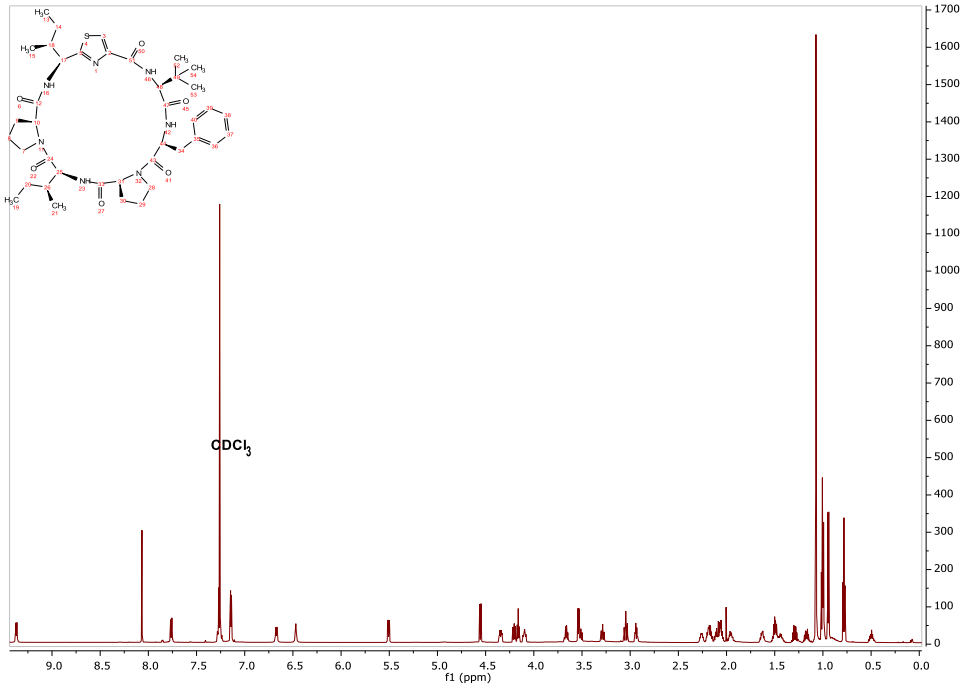

Compound **2** ^{13}C NMR

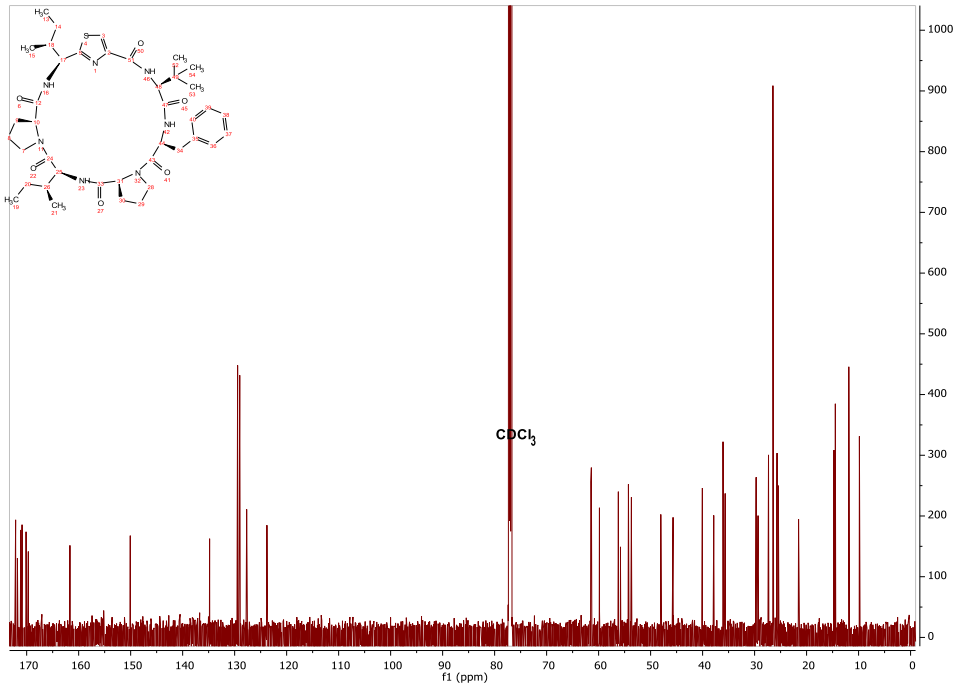

Compound **3** NMR Spectrum (HSQC cutout not showing aromatic proton shifts)

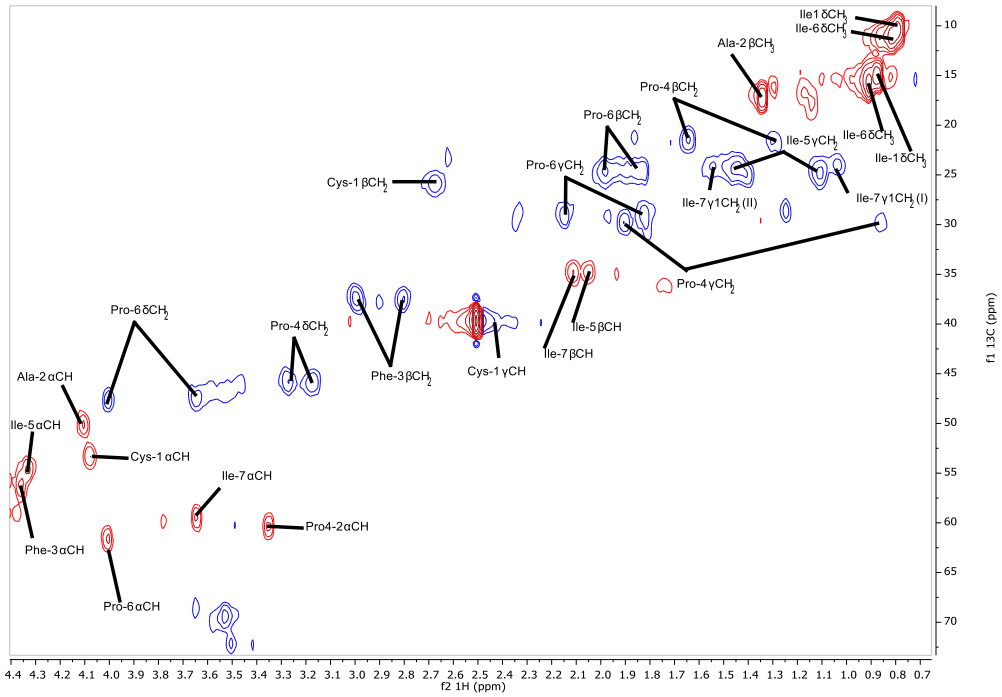

Compound **21** ^{1}H NMR (DMSO-d_6)

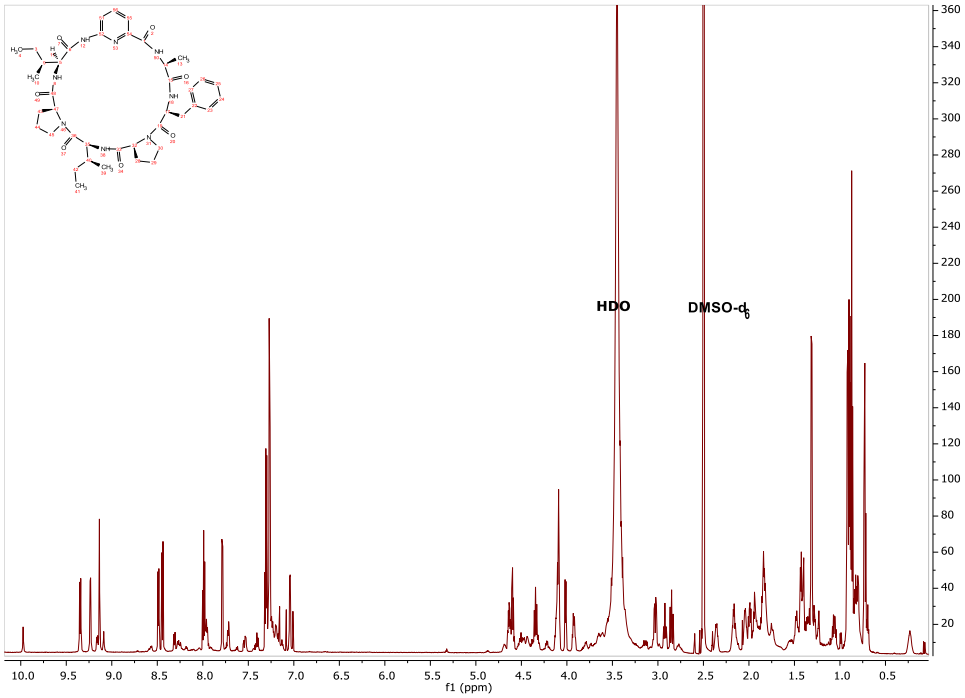

Compound **21** ^{13}C NMR (DMSO-d_6)

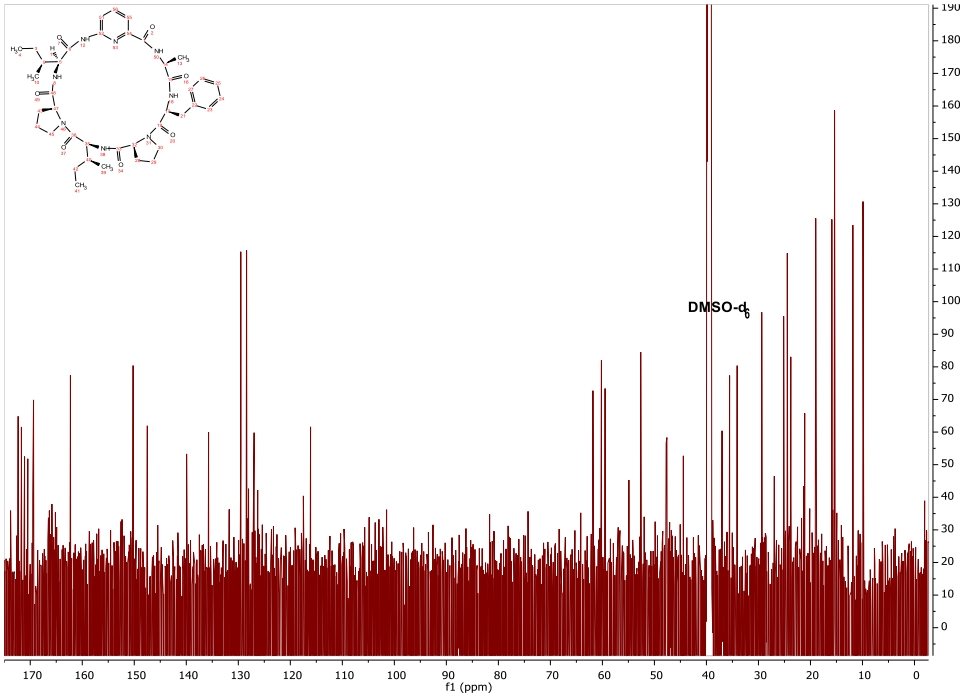

Compound **21** ^{1}H NMR ($CDCl_3$)

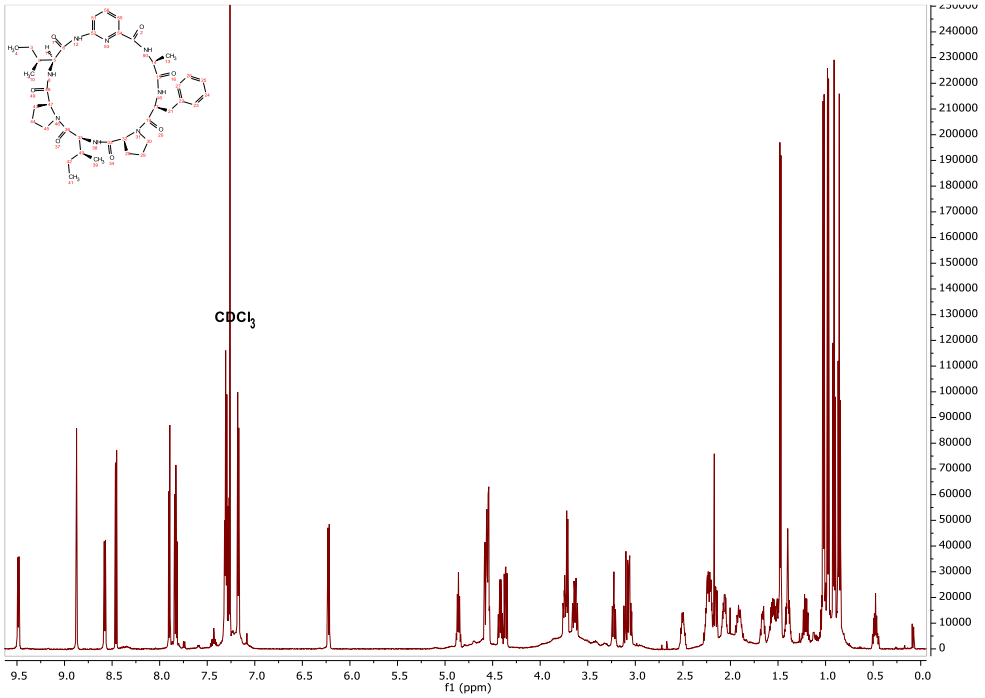

Compound **21** ^{13}C NMR Spectrum ($CDCl_3$)

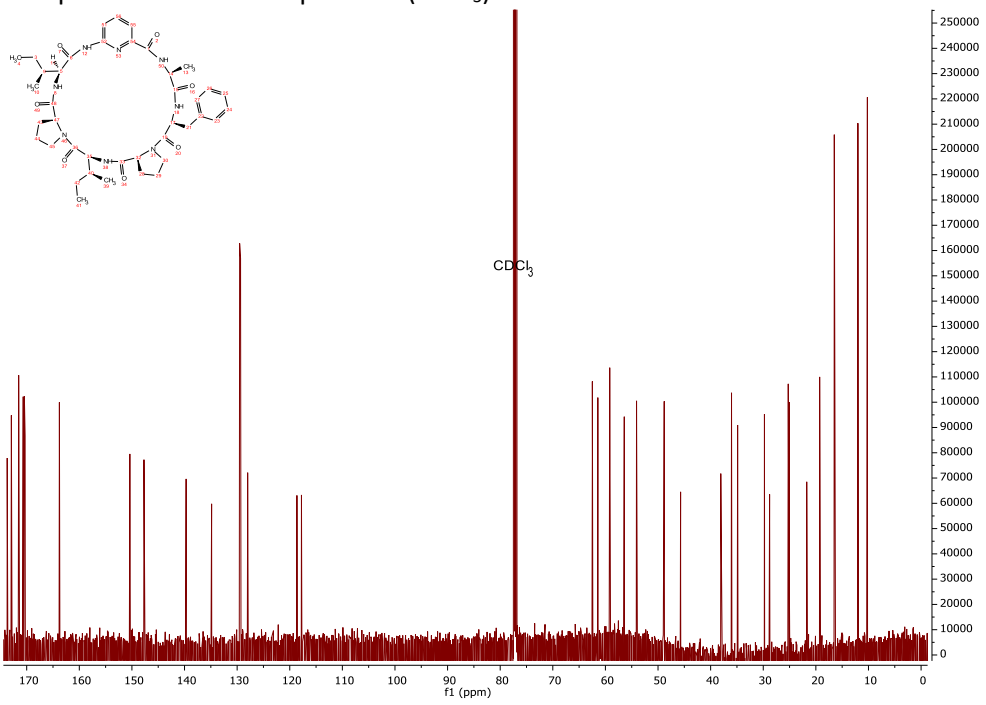

Compound **22** ^{1}H NMR (DMSO-d_6)

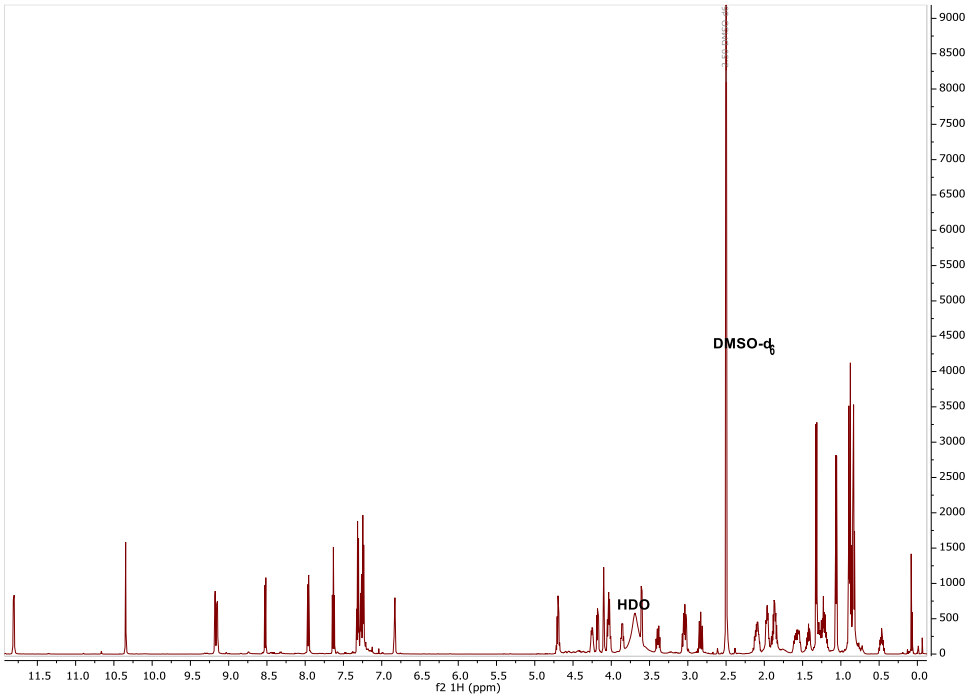

Compound **22** ^{13}C NMR Spectrum (DMSO-d_6)

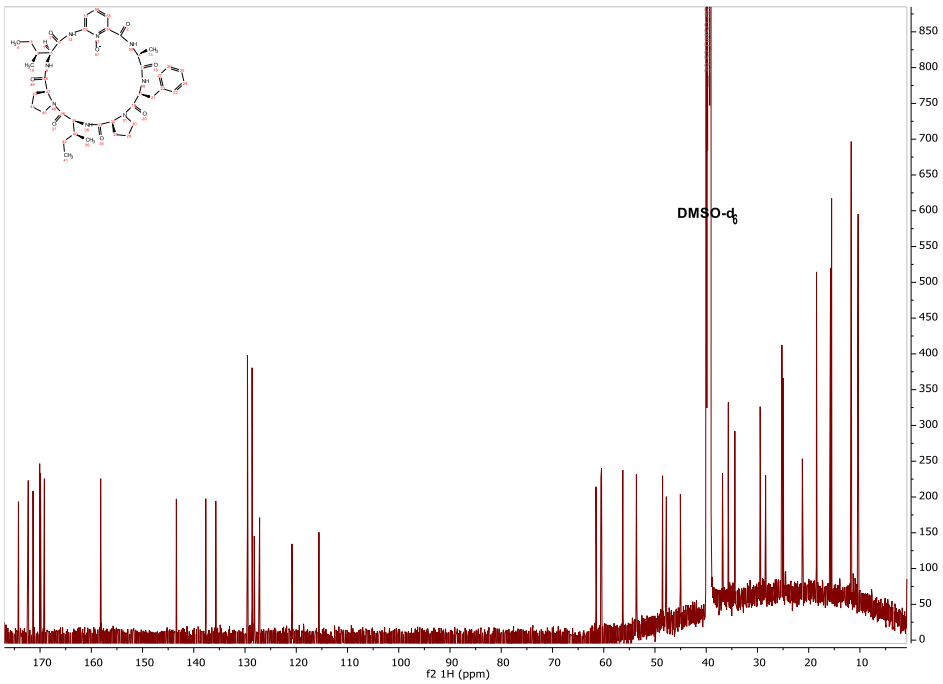

Compound **22** ^{1}H NMR ($CDCl_3$)

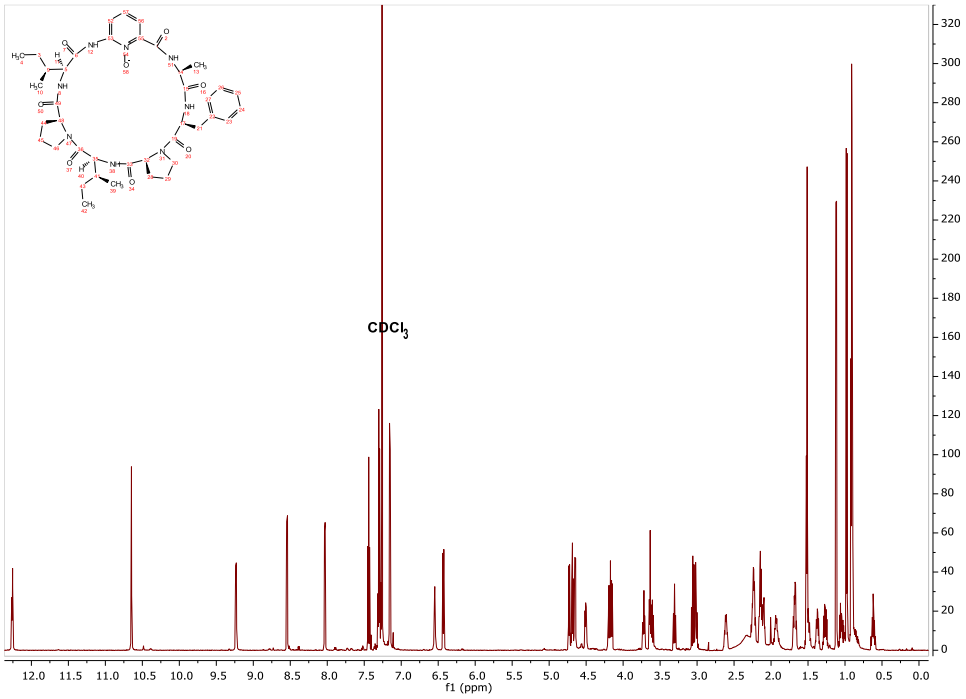

Compound **22** ^{13}C NMR ($CDCl_3$)

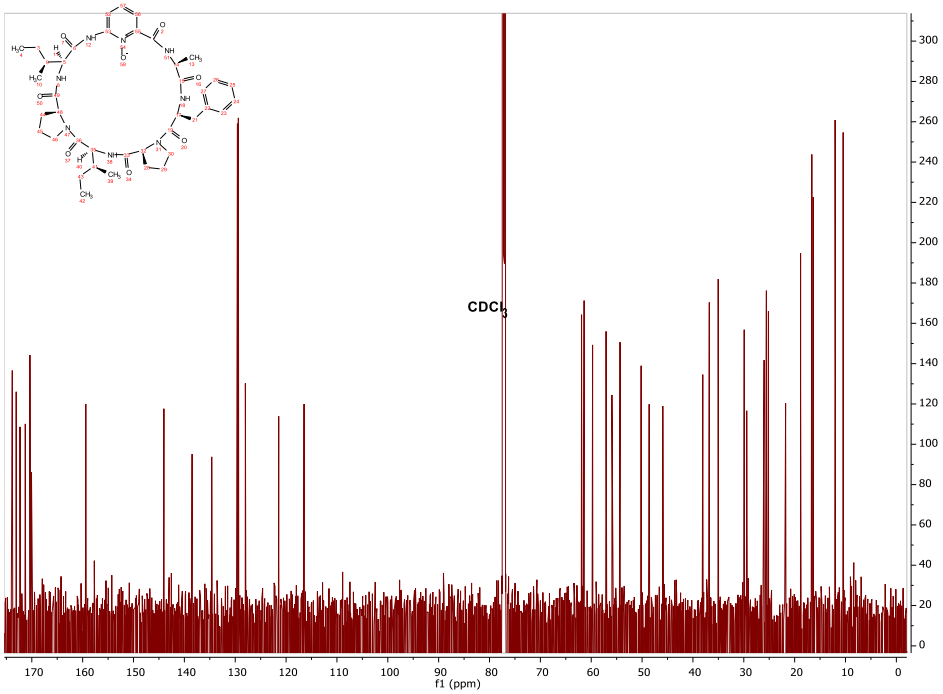

Compound **50** ^{1}H NMR (DMSO-d_6)

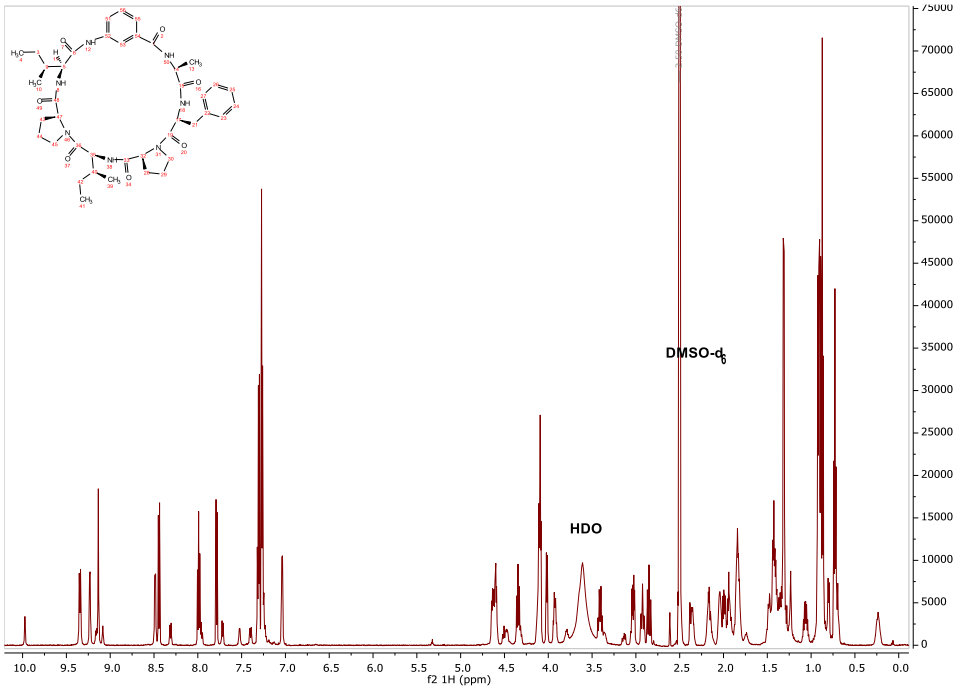

Compound **50** ^{13}C NMR (DMSO-d_6)

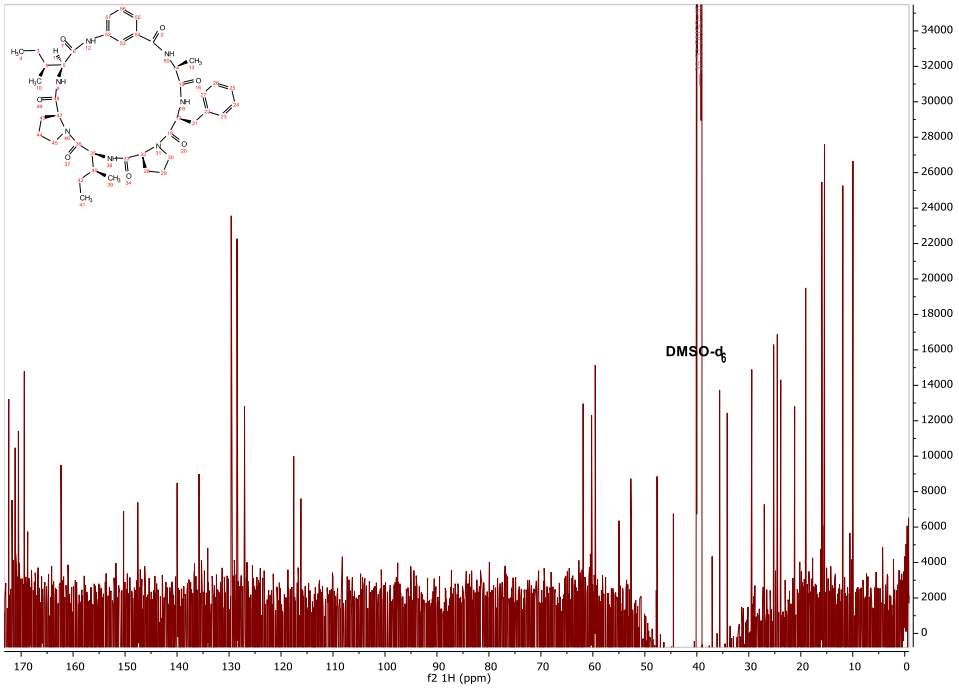

Compound **31** ^{1}H NMR

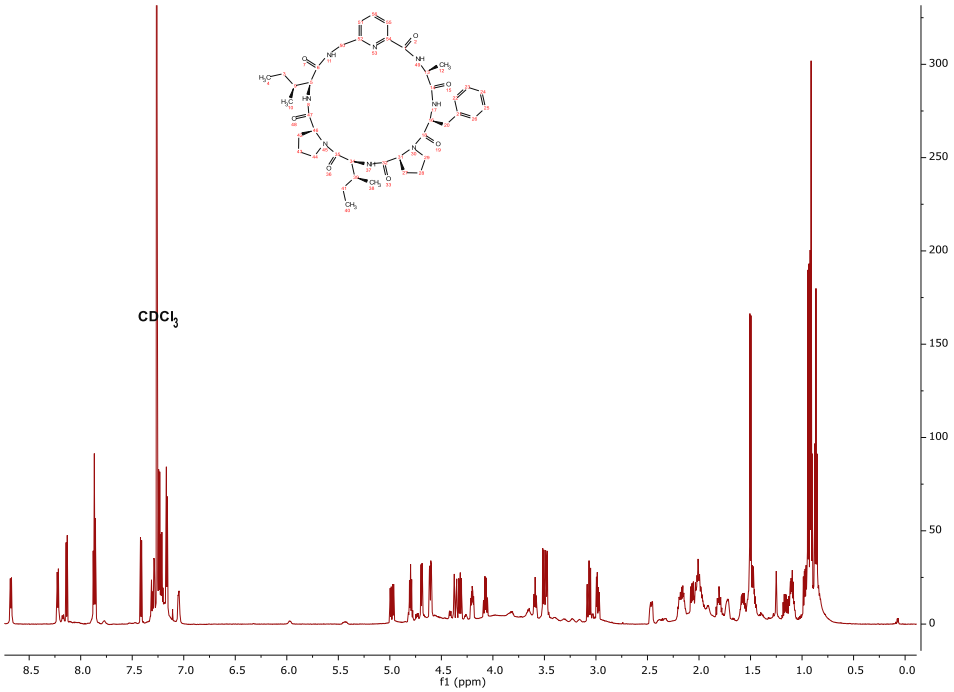

Compound **31** ^{13}C NMR

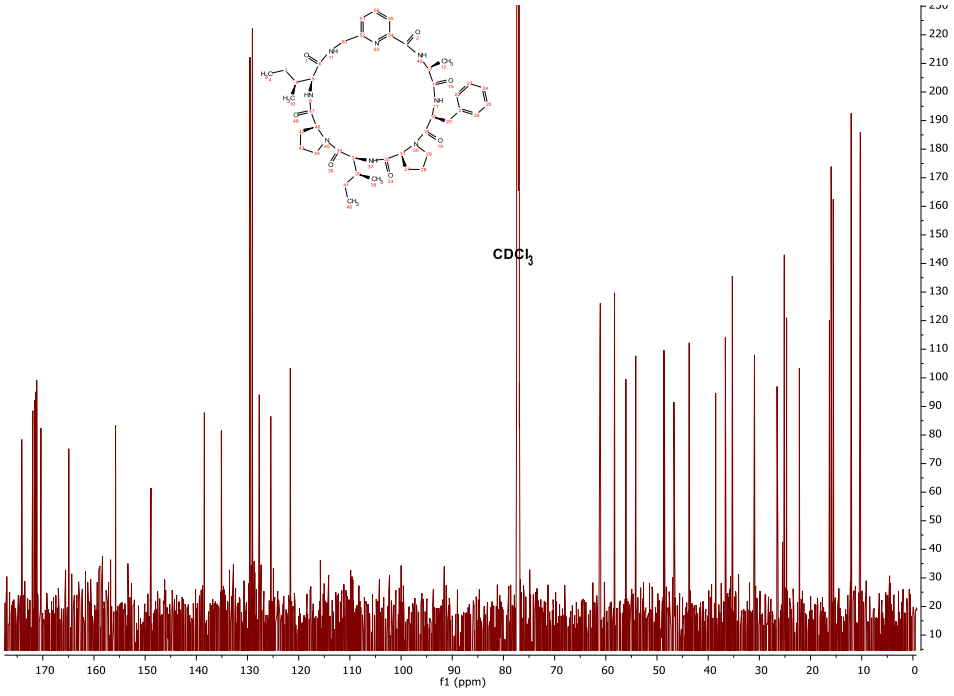

Compound **32** ^{1}H NMR

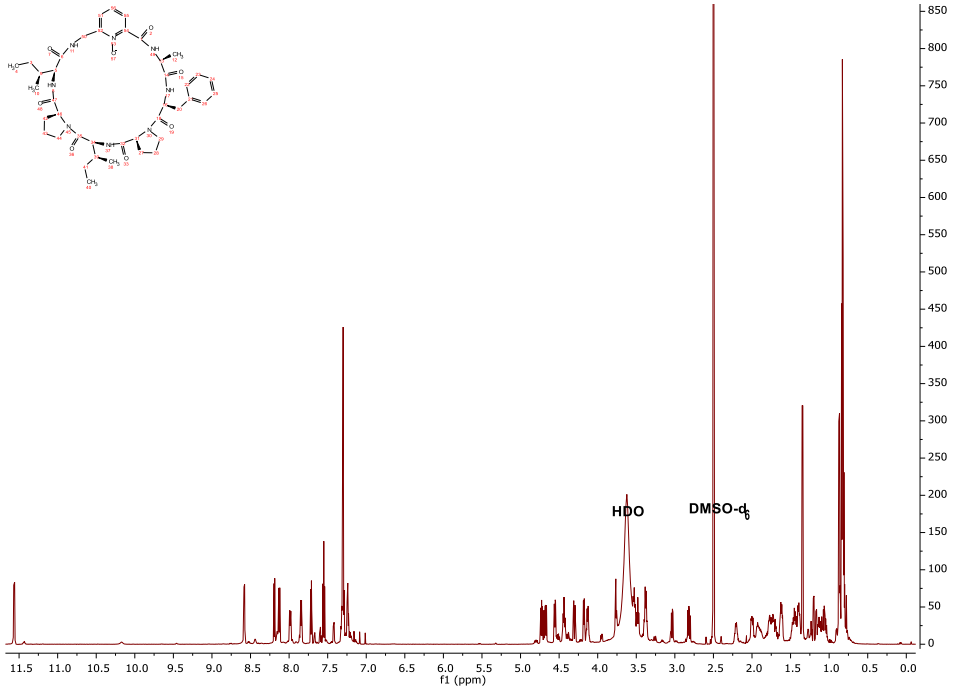

Compound **32** ^{13}C NMR

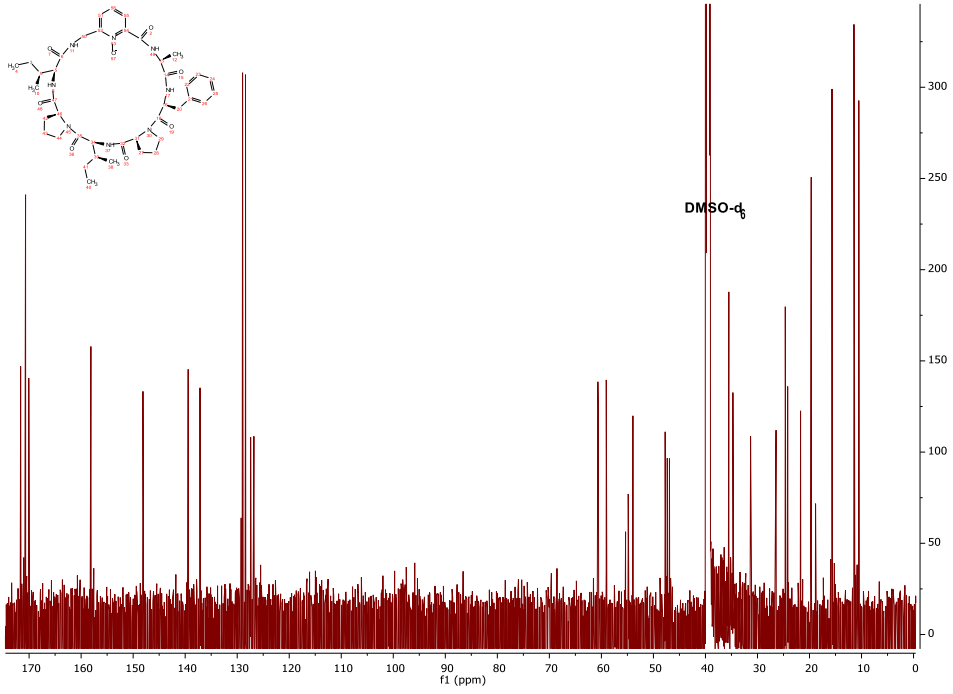

Compound **51** ^{1}H NMR

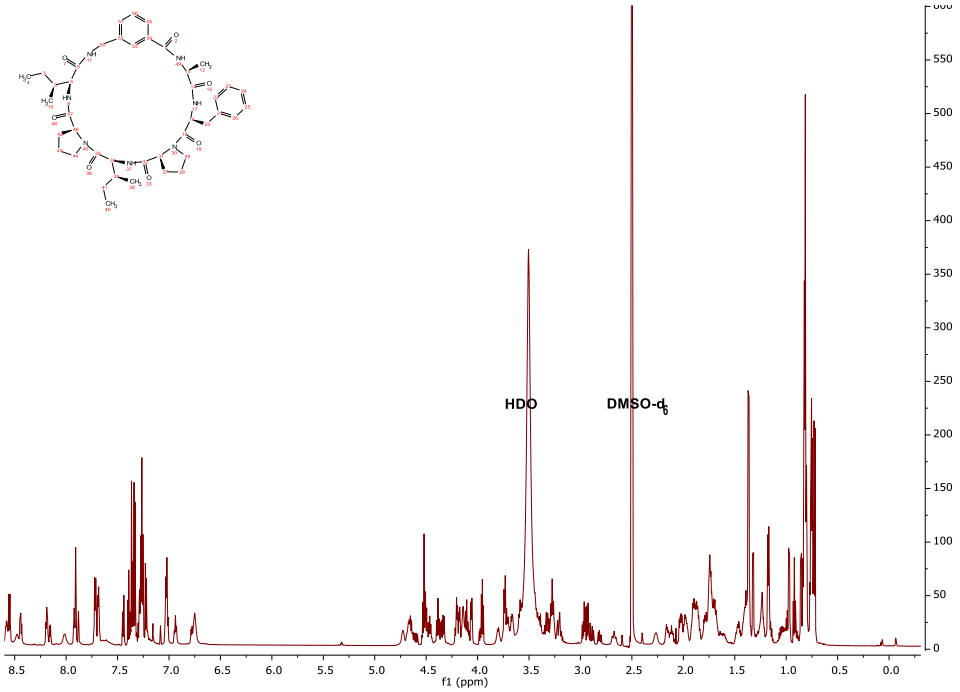

Compound **51** ^{13}C NMR

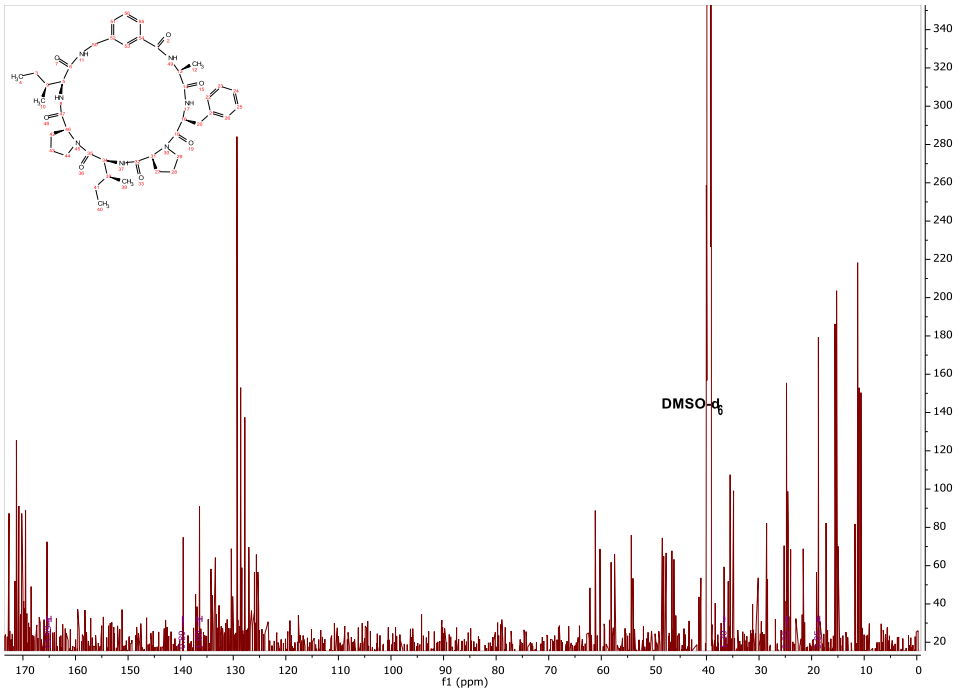

Compound **41** NMR Spectrum (HSQC cutout not showing aromatic proton shifts) in DMSO-D_6

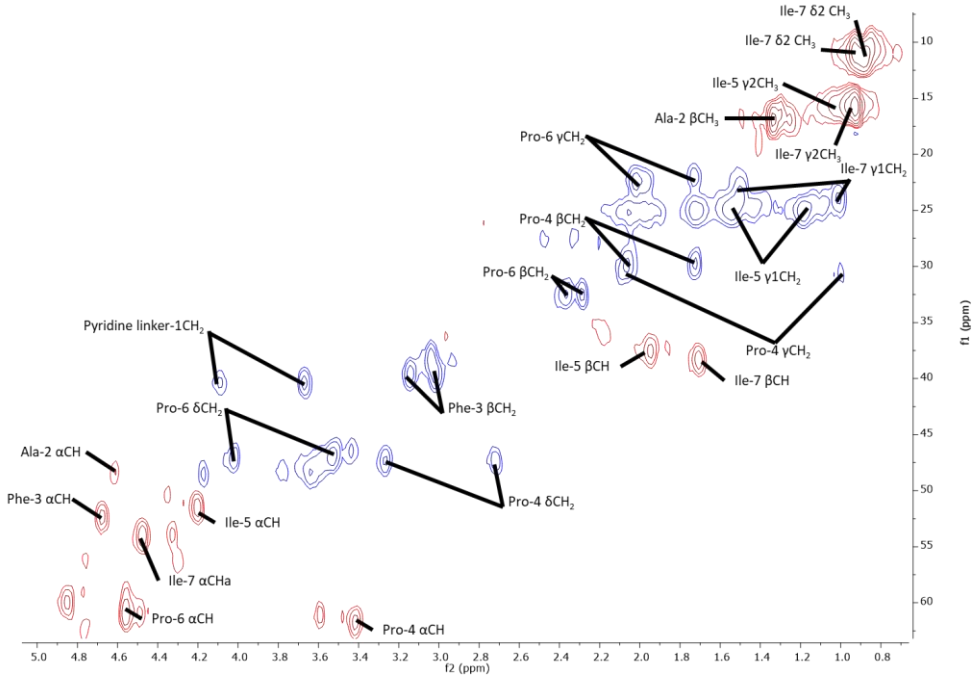

Compound **42** ^{1}H NMR

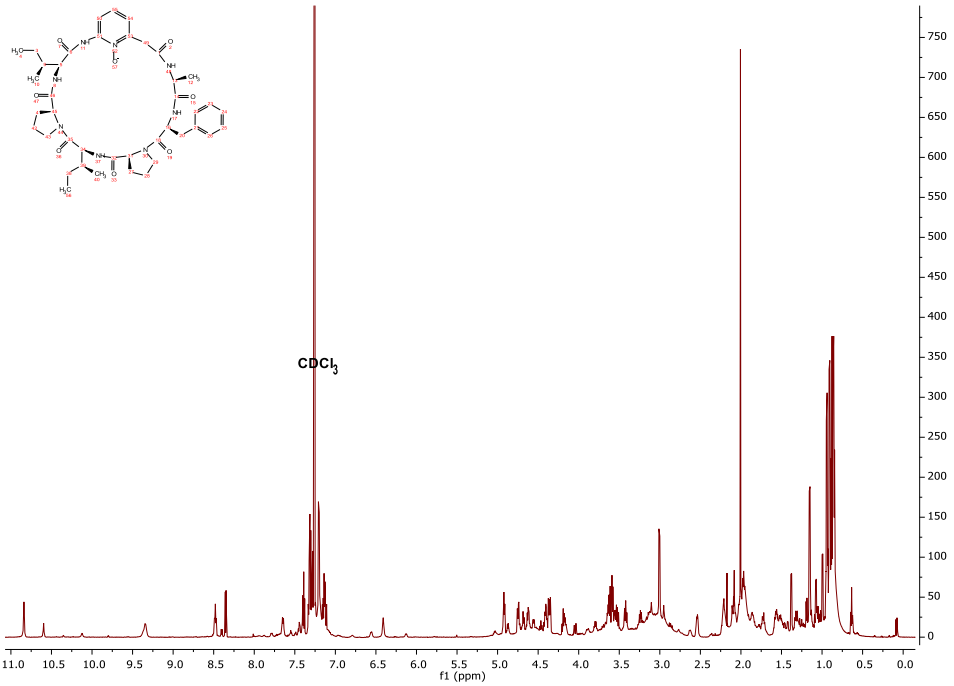

Compound **42** ^{13}C NMR

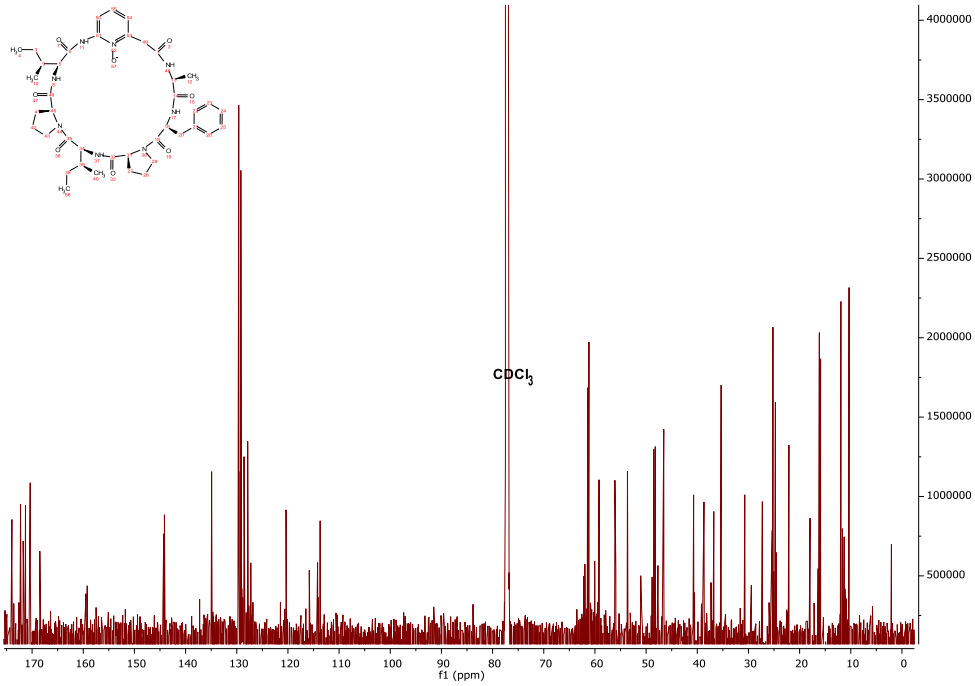

Compound **52** NMR Spectrum (HSQC cutout not showing aromatic proton shifts) in $CDCl_3$

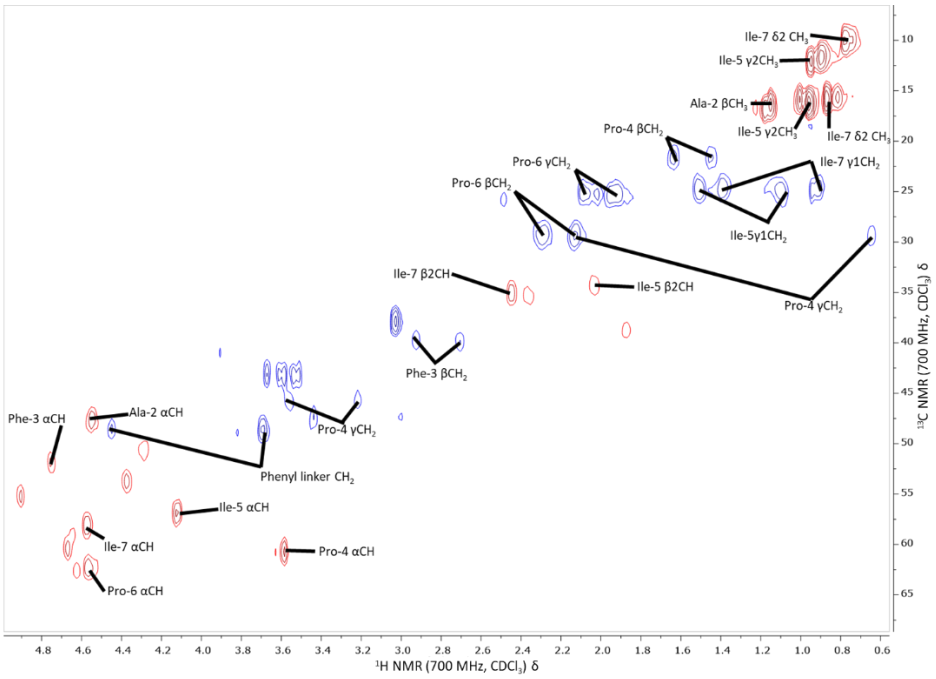

6.1.2. Chapter 3

NMR spectra

5 ^{1}H NMR

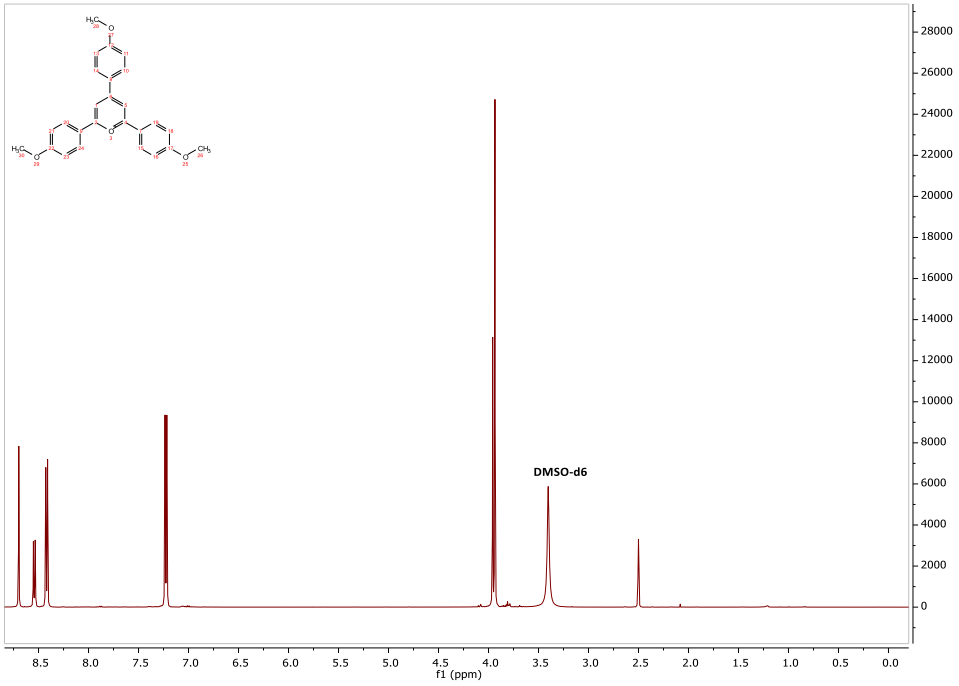

5 ^{13}C NMR

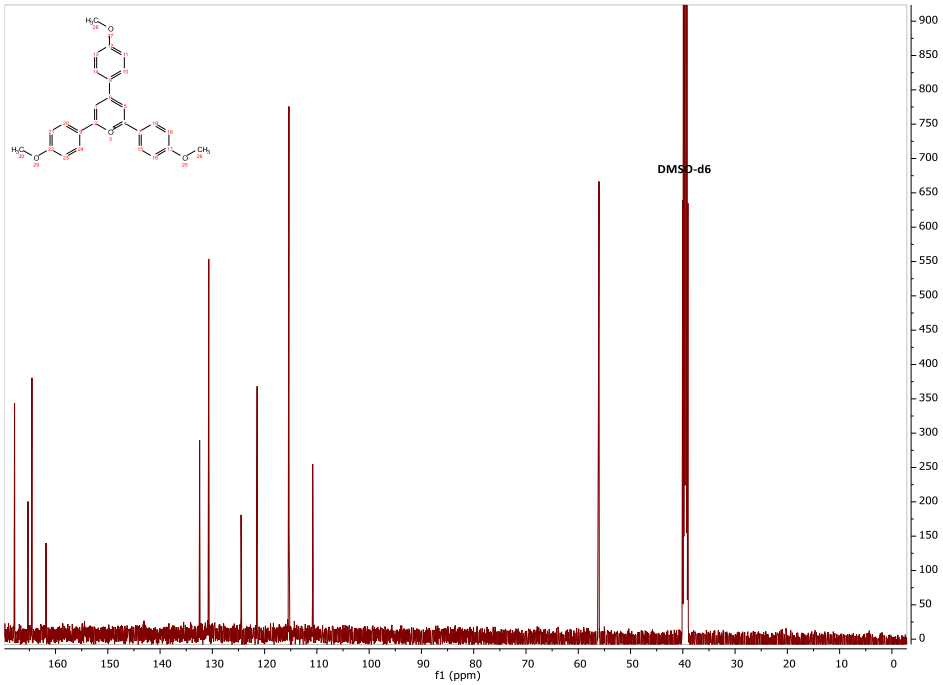

7 ^{1}H NMR

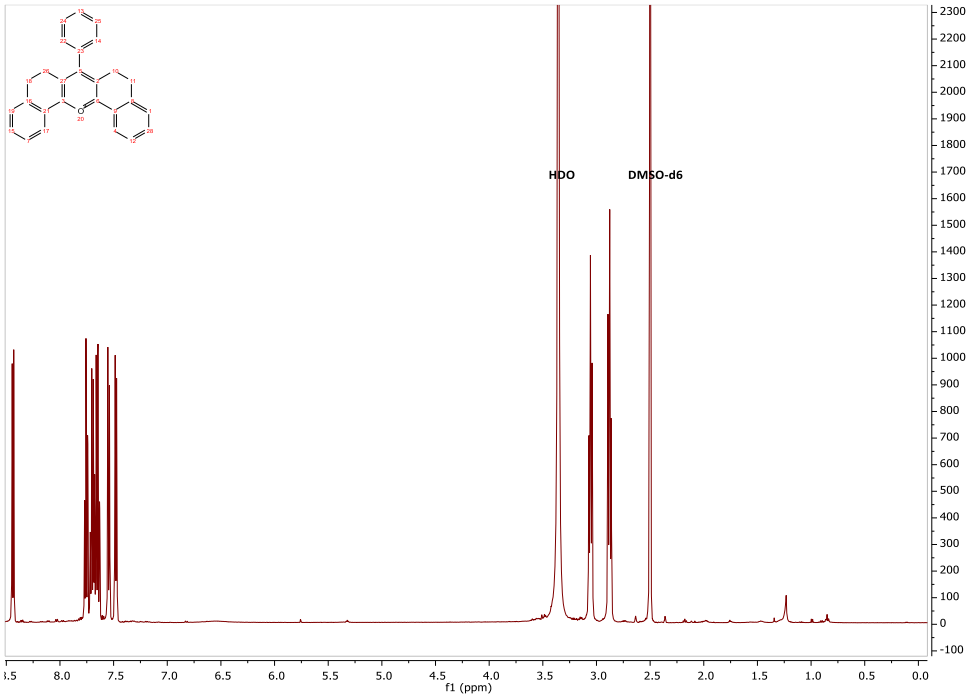

7 ^{13}C NMR

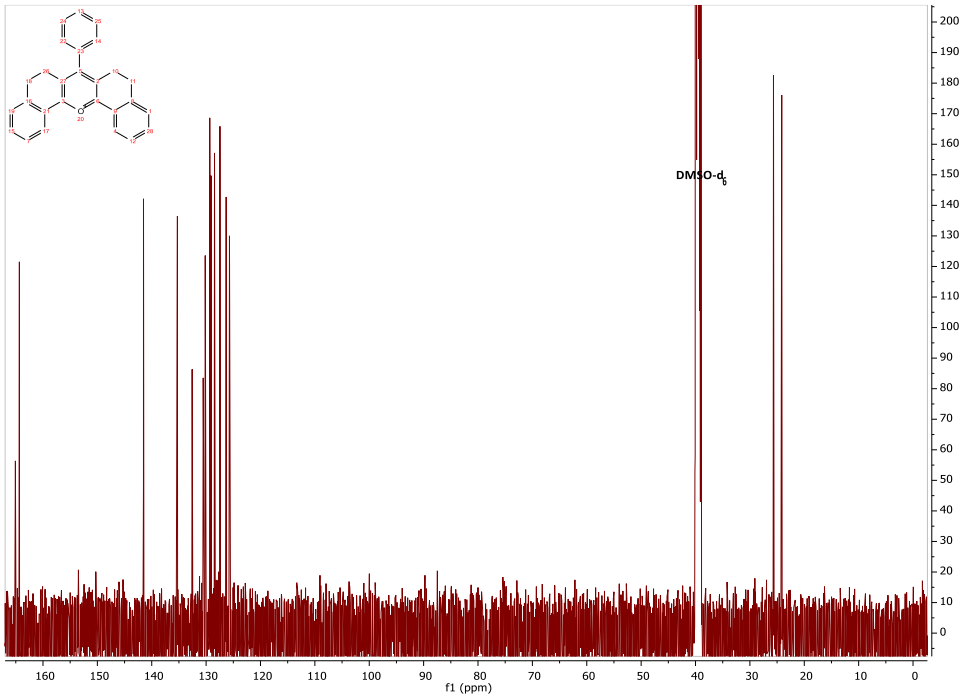

9 ^{1}H NMR

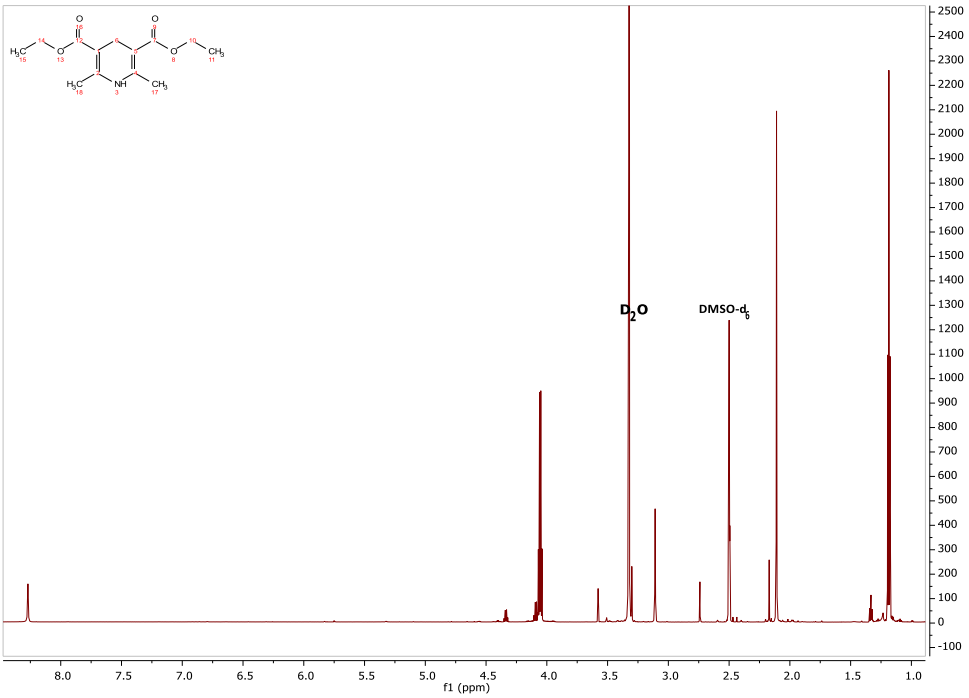

9 ^{13}C NMR

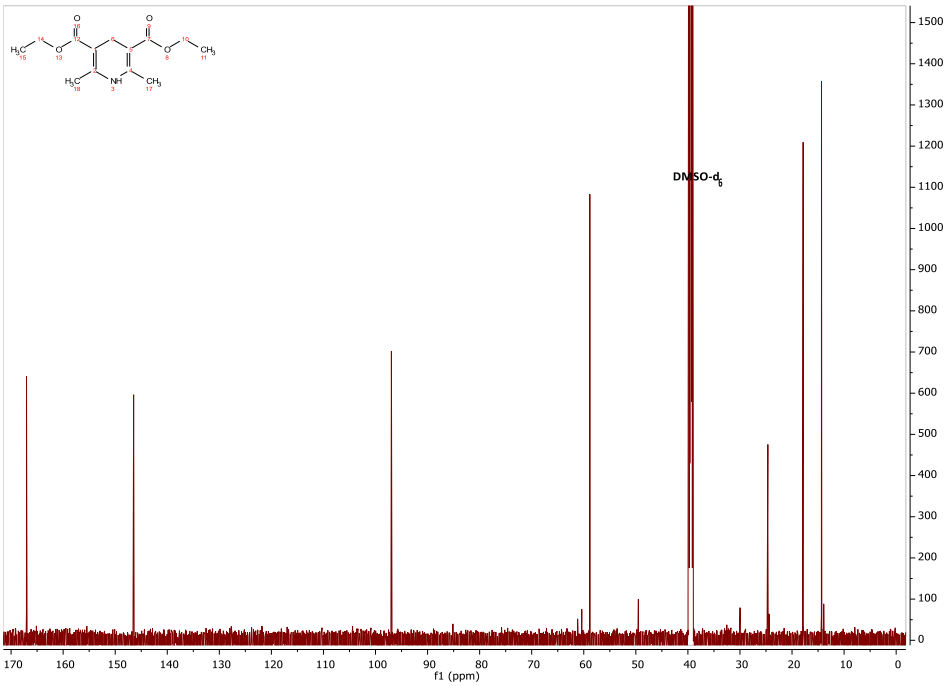

28 ^{1}H NMR

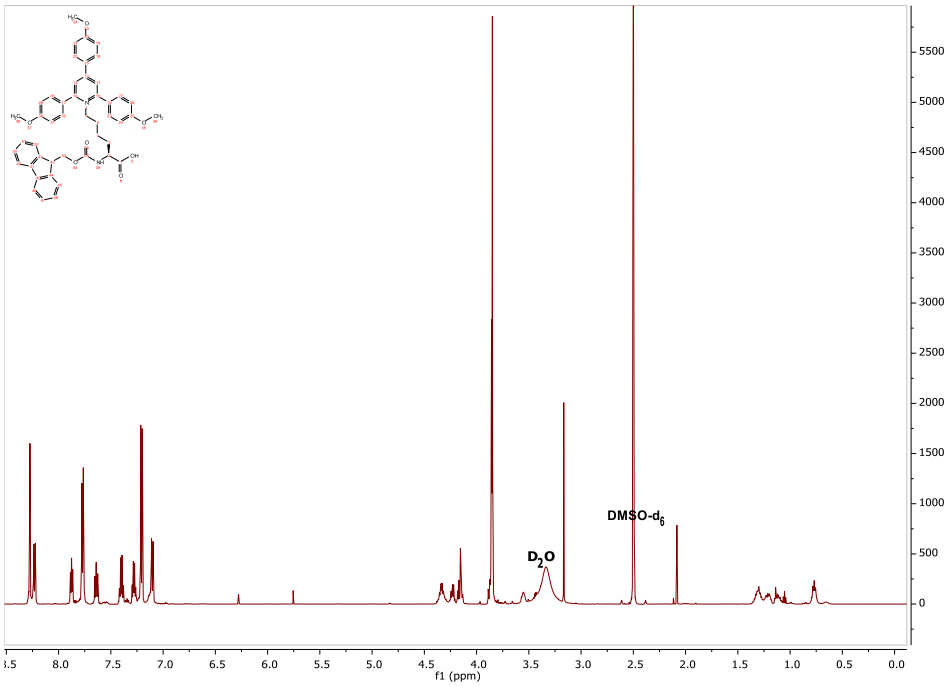

28 ^{13}C NMR

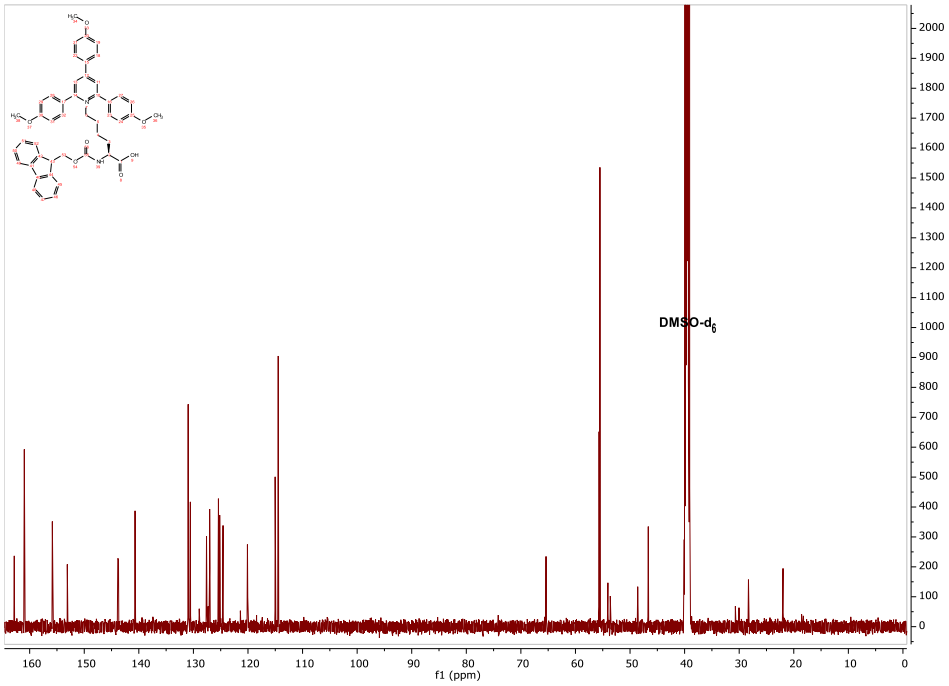

29 ^{1}H NMR

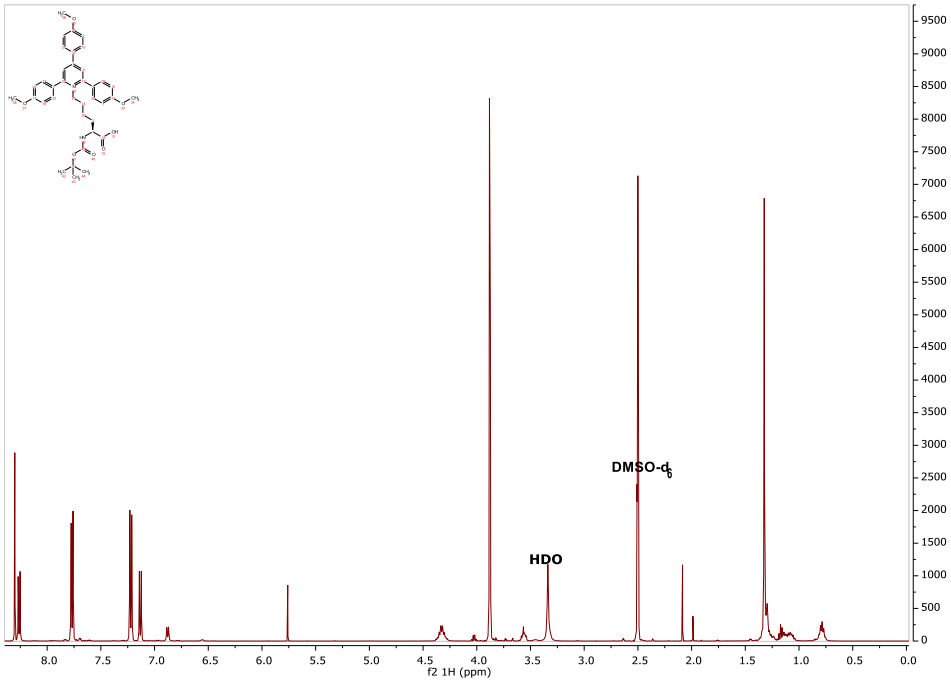

29 ^{13}C NMR

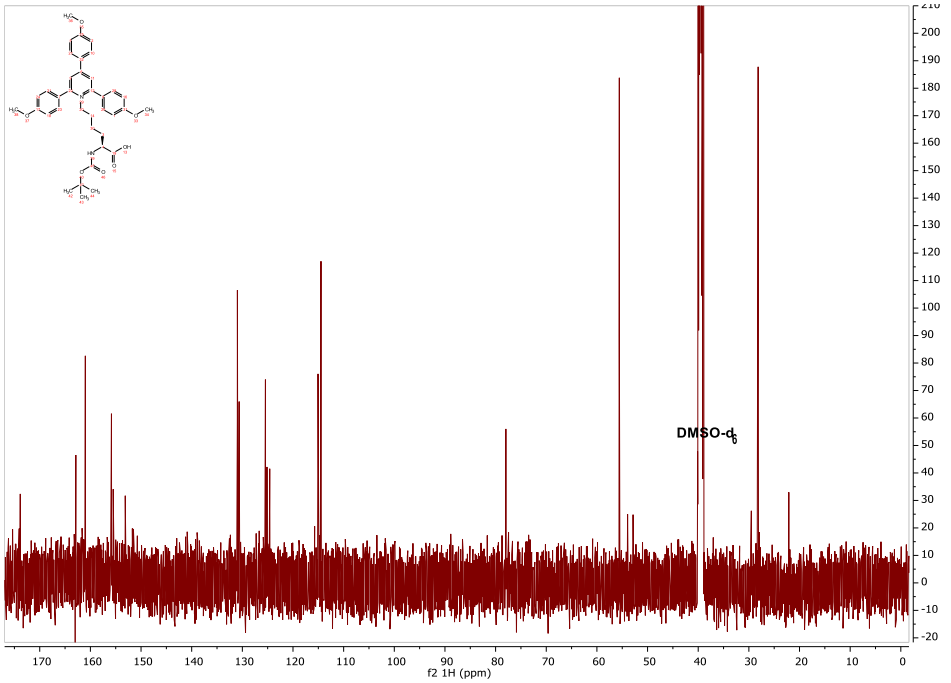

30 ^{1}H NMR

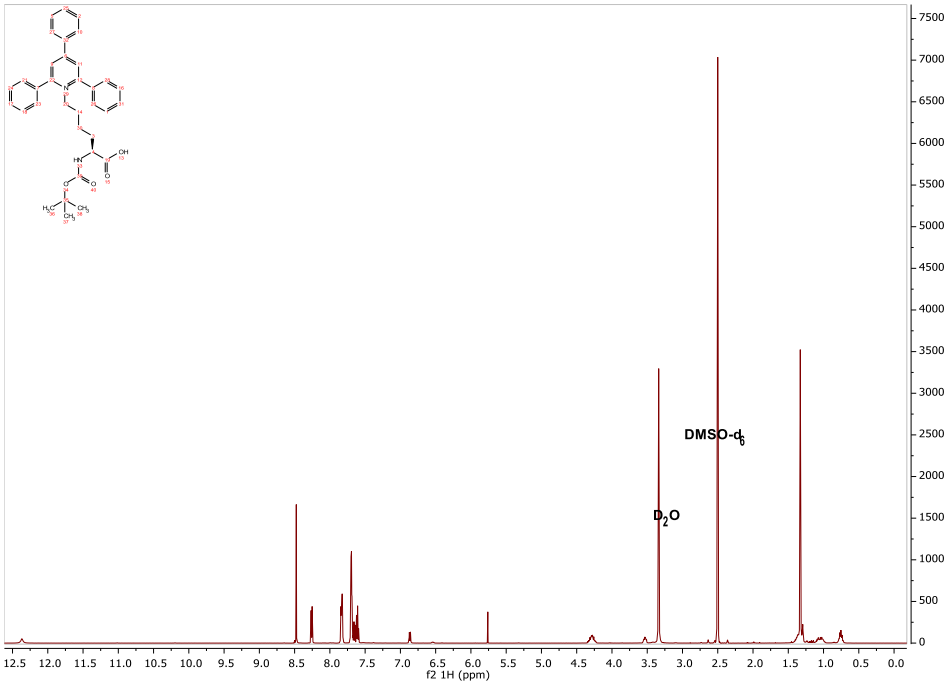

30 ^{13}C NMR

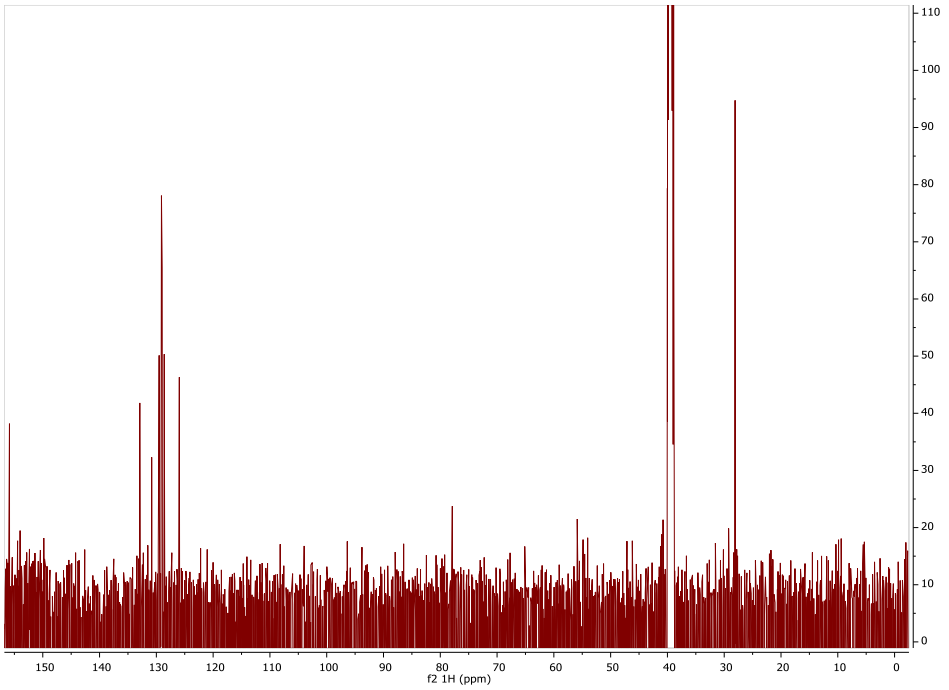

31 ^{1}H NMR

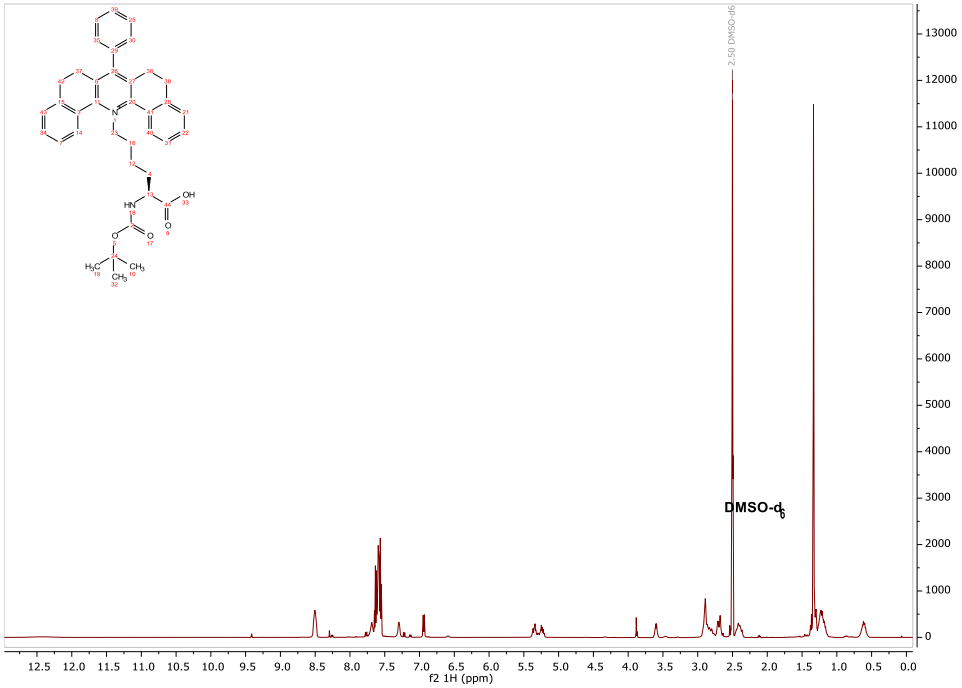

31 ^{13}C NMR

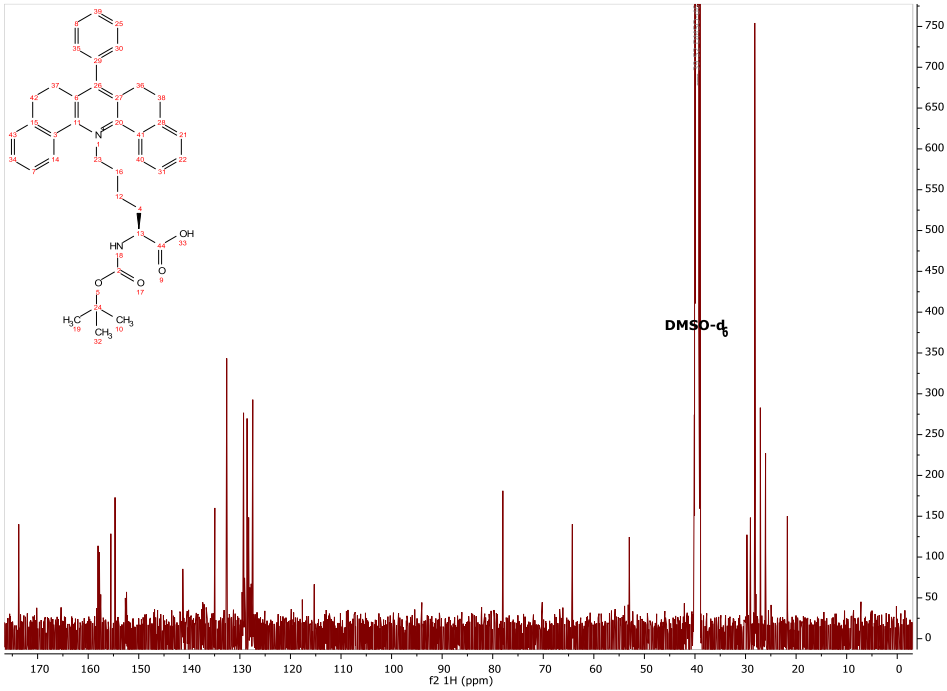

18 ^{1}H NMR

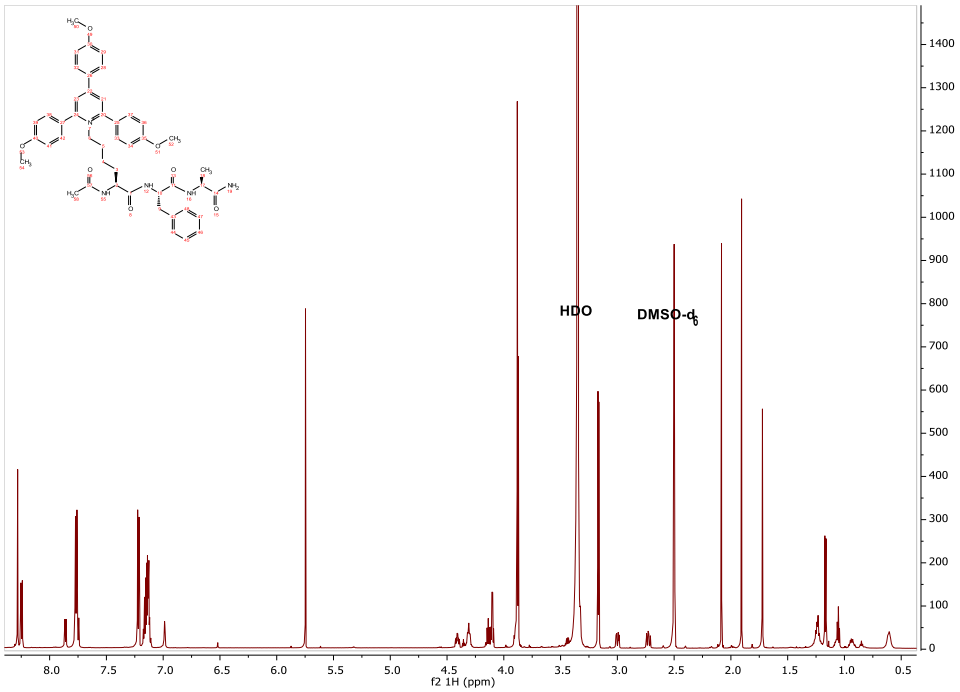

18 ^{13}C NMR

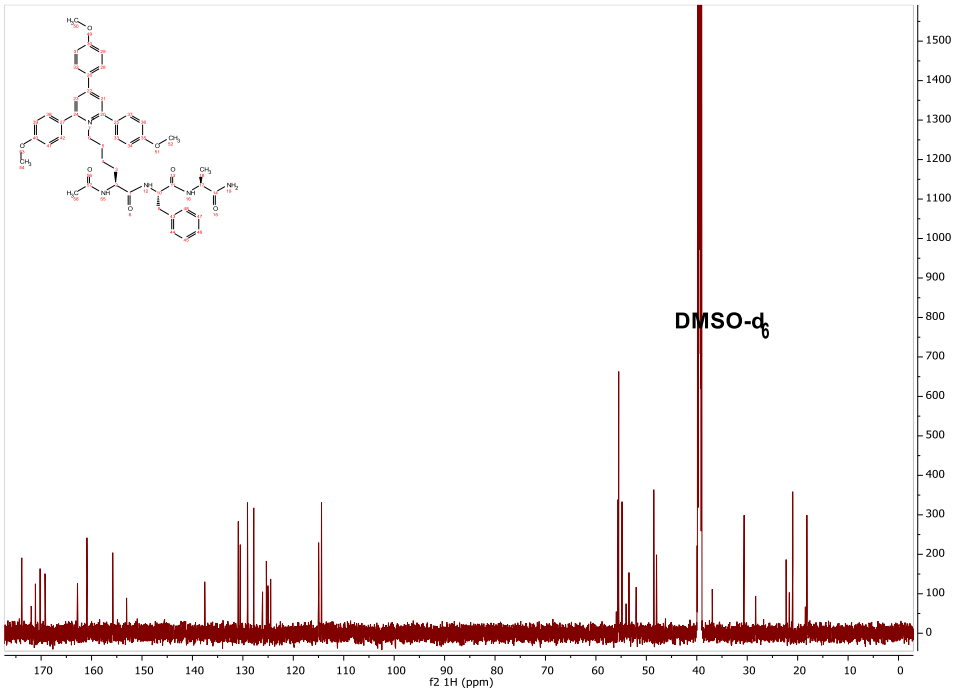

19 ^{1}H NMR

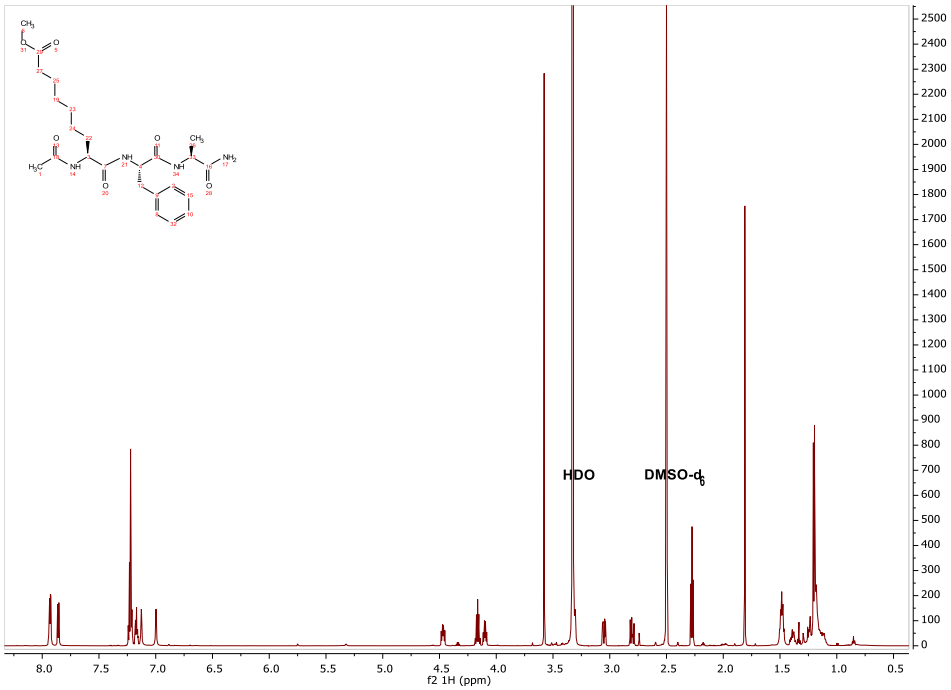

19 ^{13}C NMR

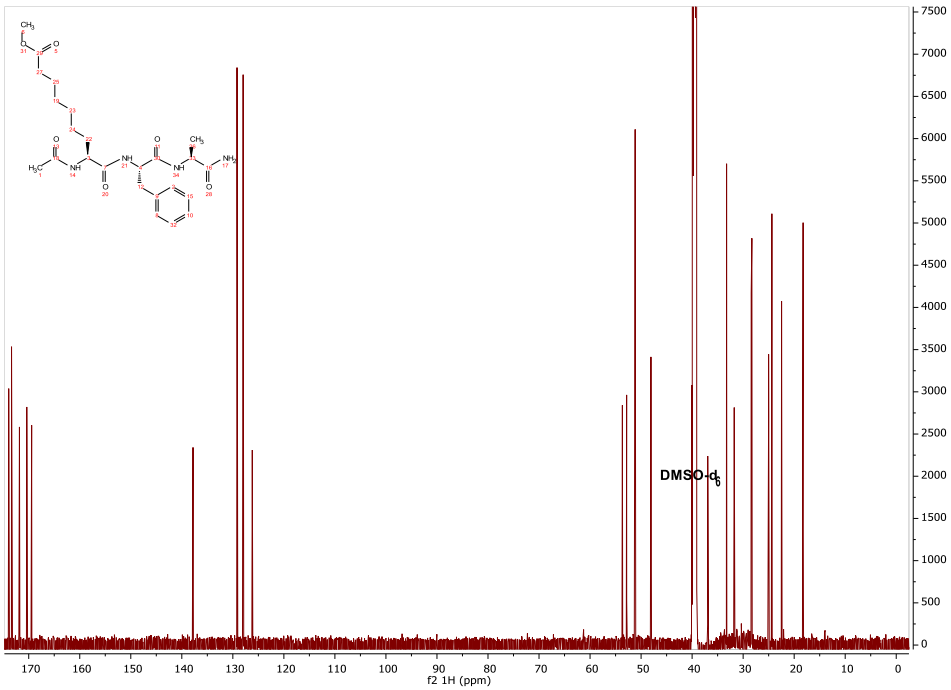

21 ^{1}H NMR

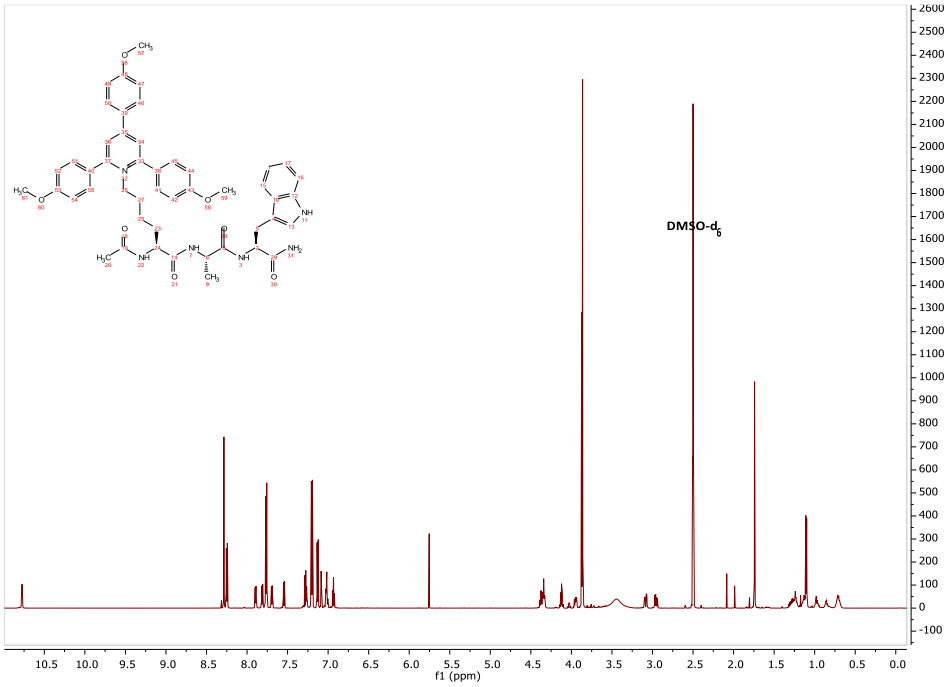

21 ^{13}C NMR

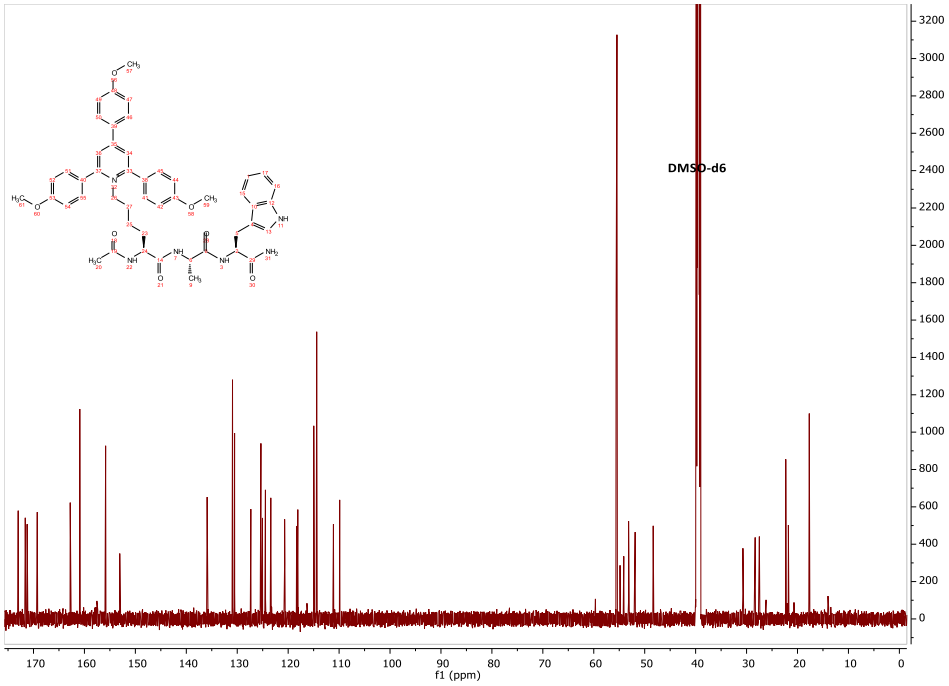

22 ^{1}H NMR

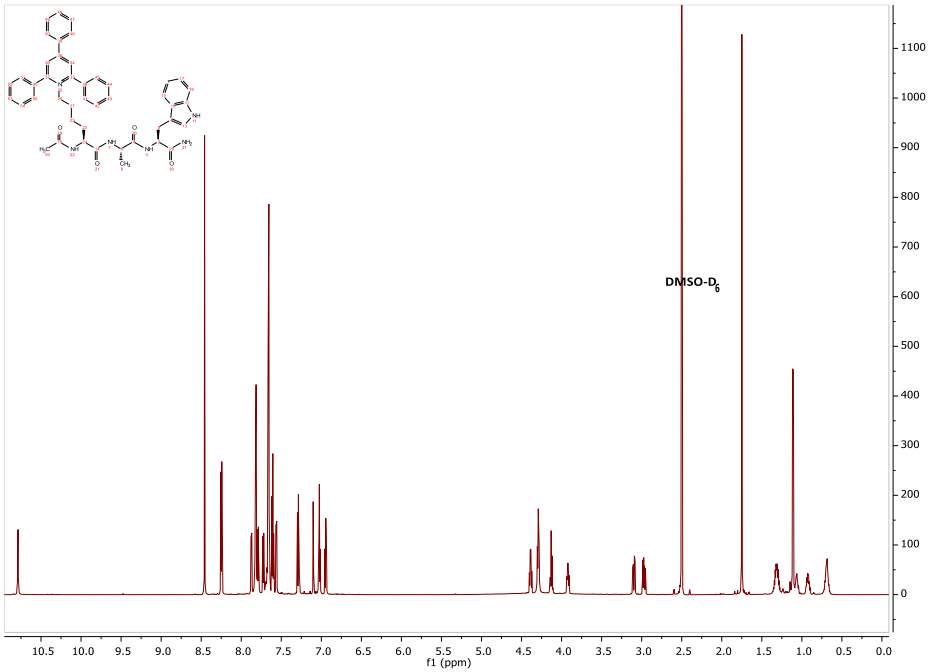

22 ^{13}C NMR

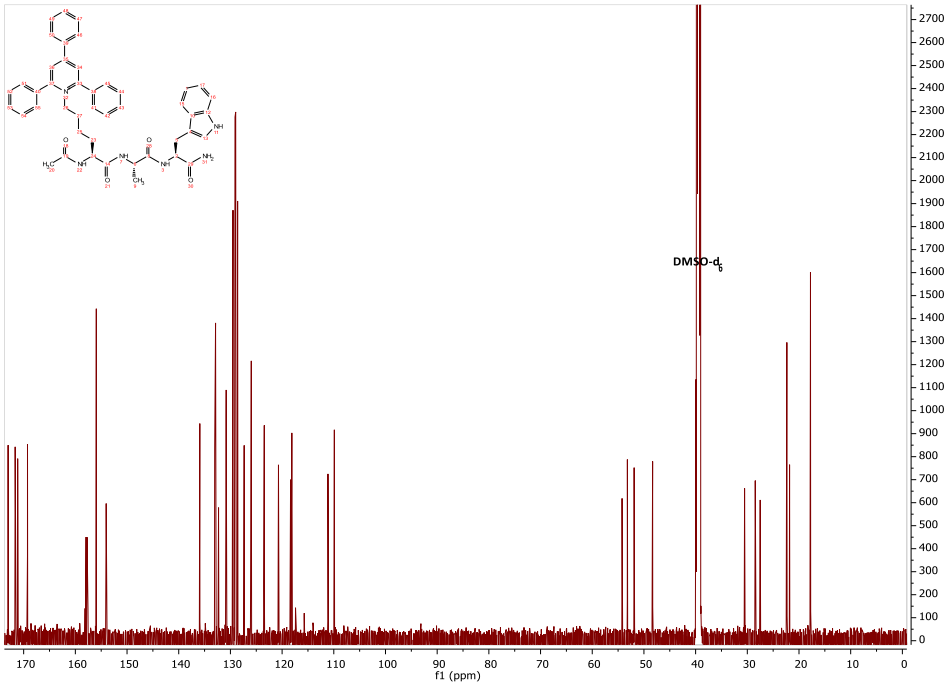

23 ^{1}H NMR

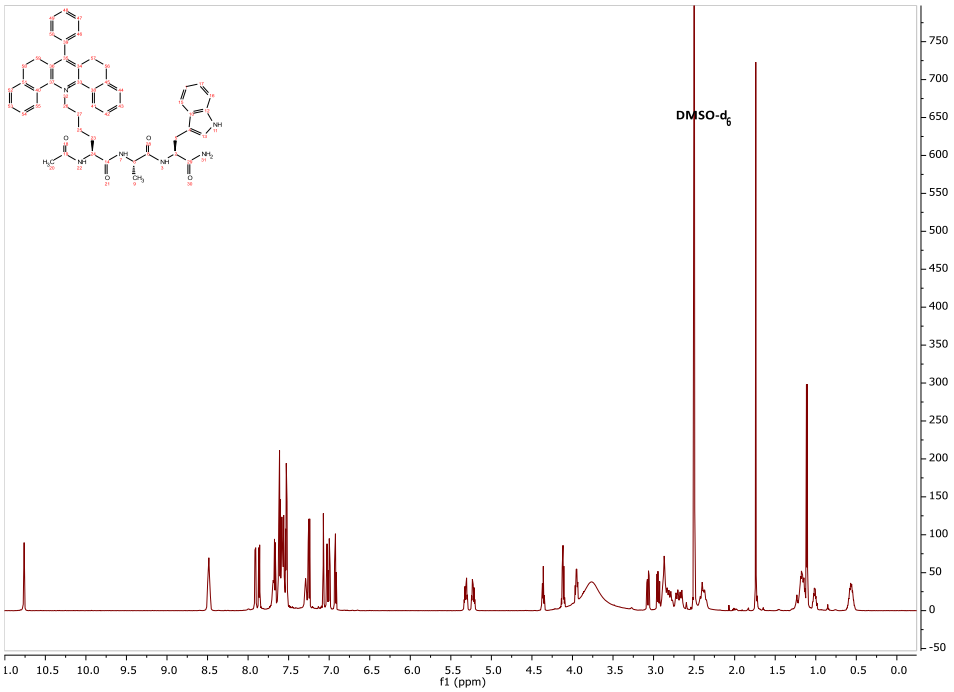

23 ^{13}C NMR

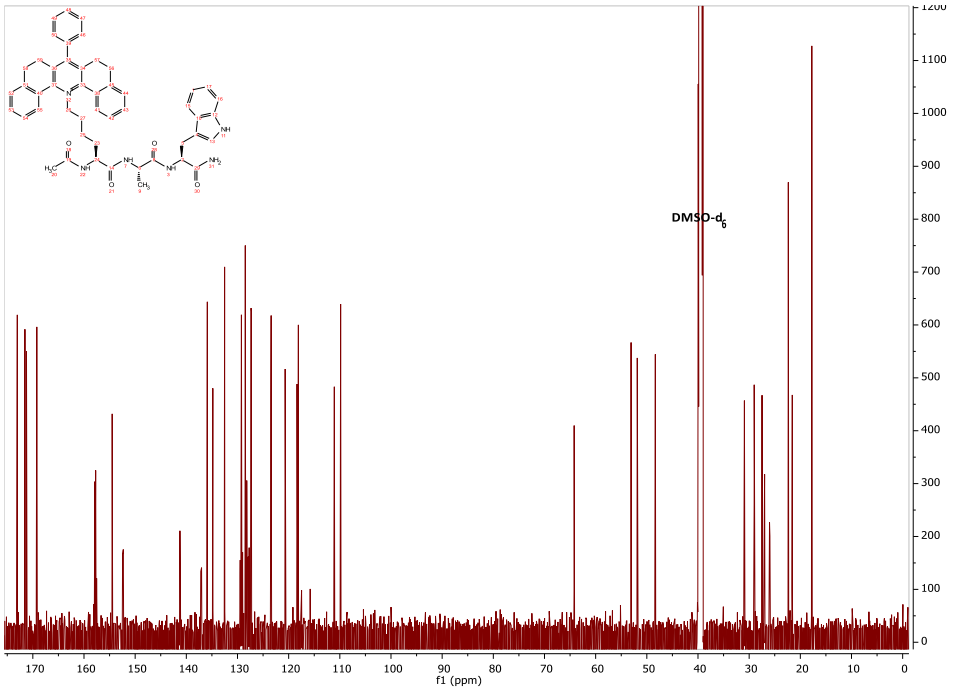

27 ^{1}H NMR

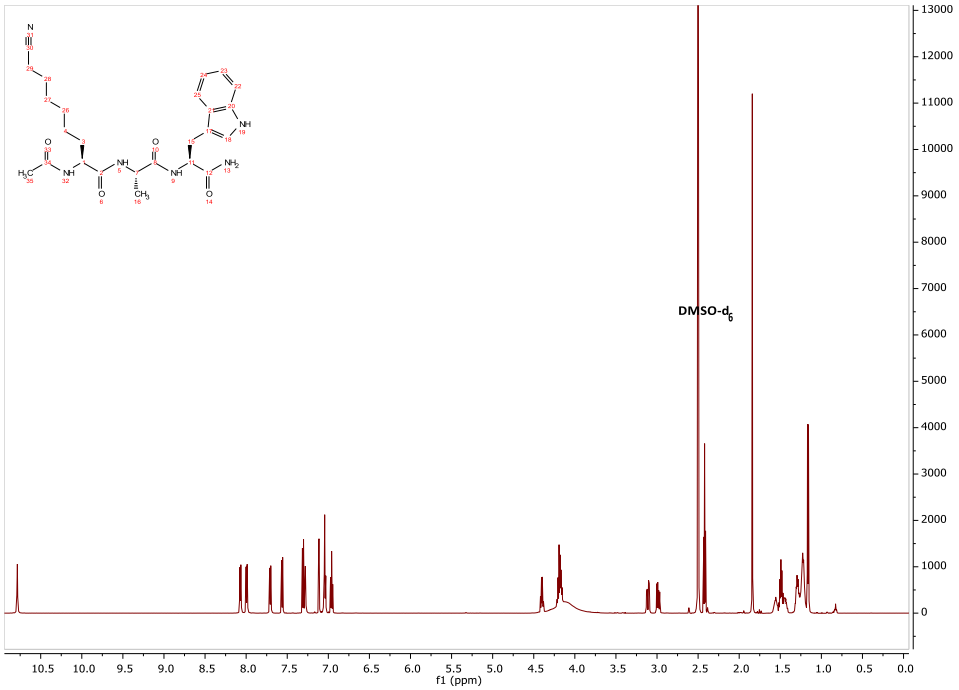

27 ^{13}C NMR

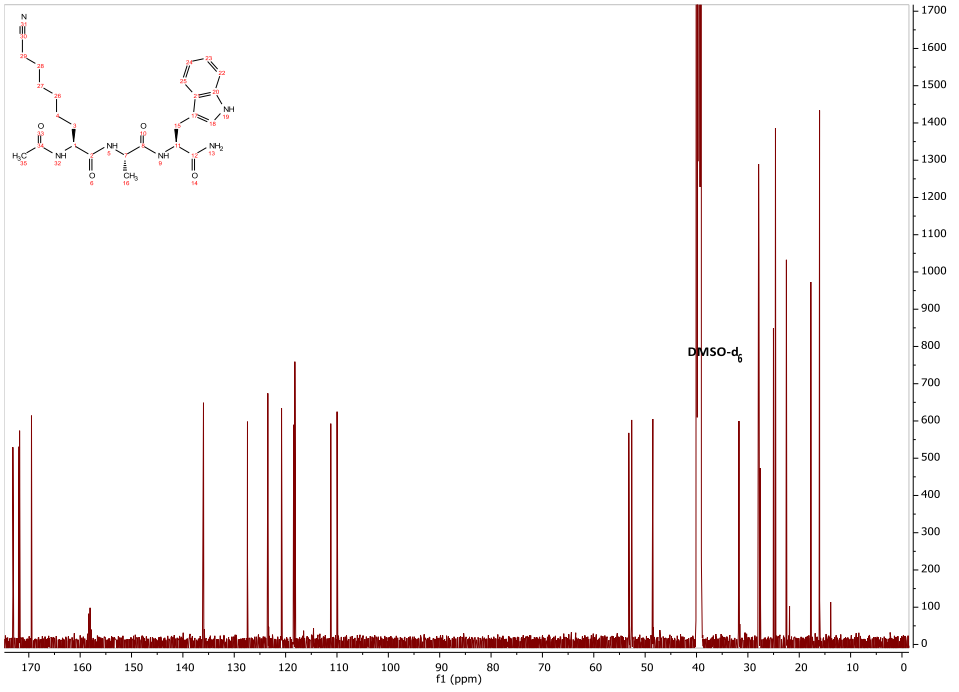

33 ^{1}H NMR

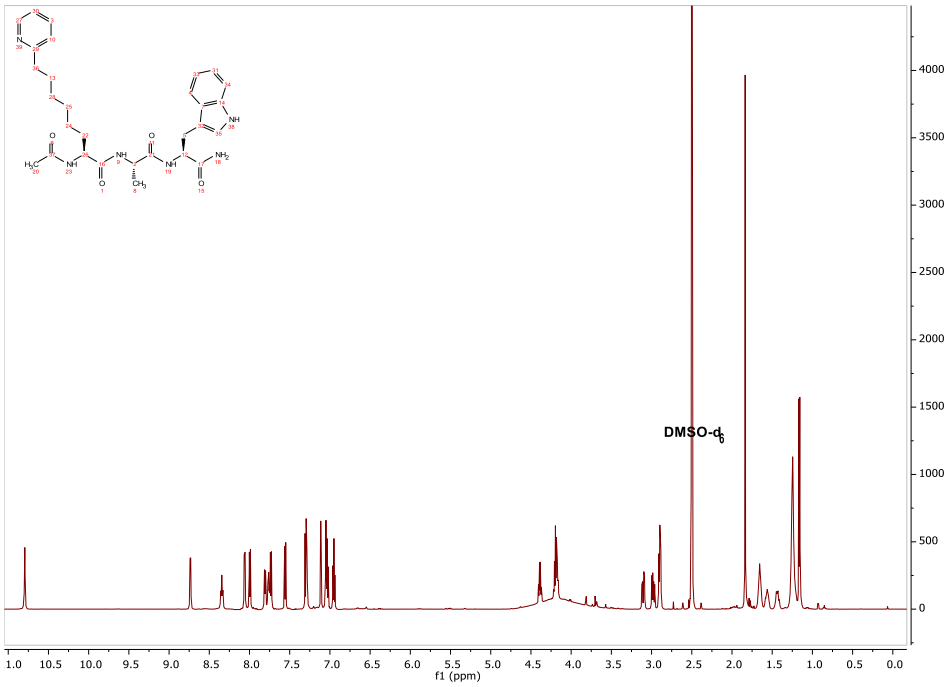

33 ^{13}C NMR

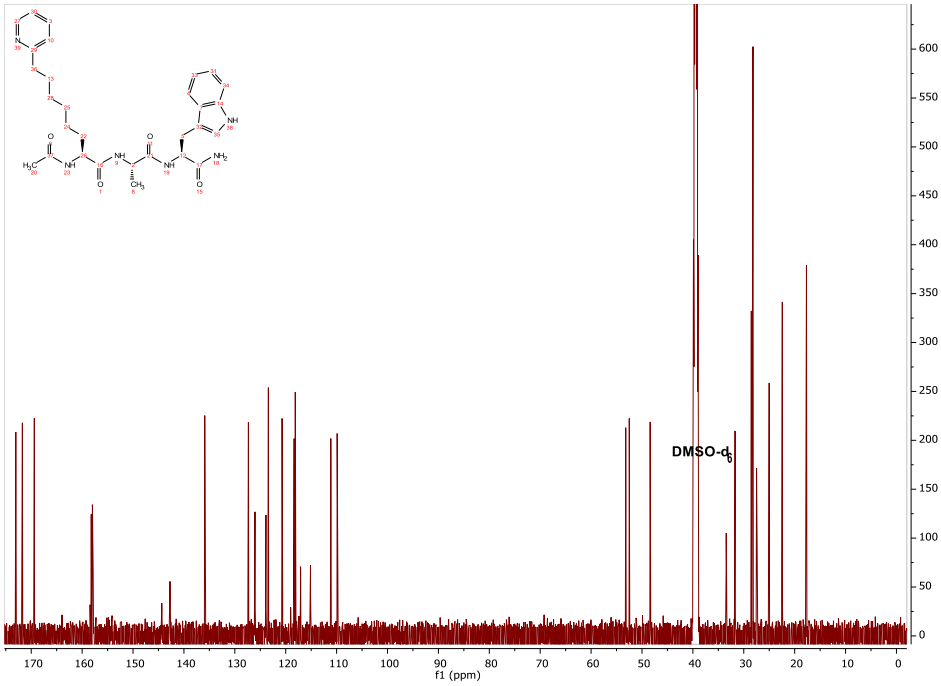

34 ^{1}H NMR

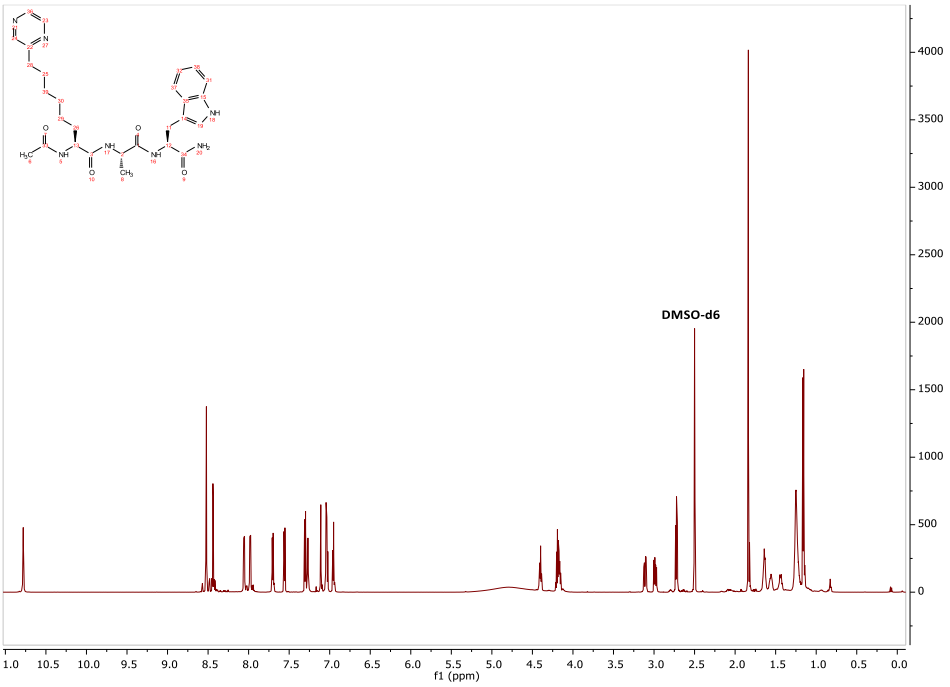

34 ^{13}C NMR

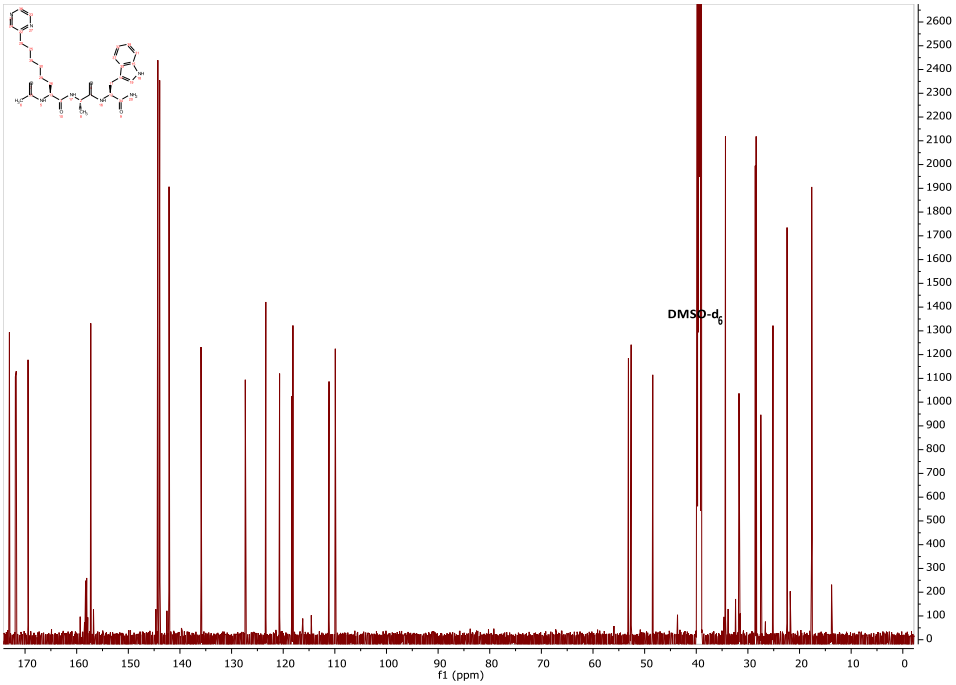

35 ^{1}H NMR

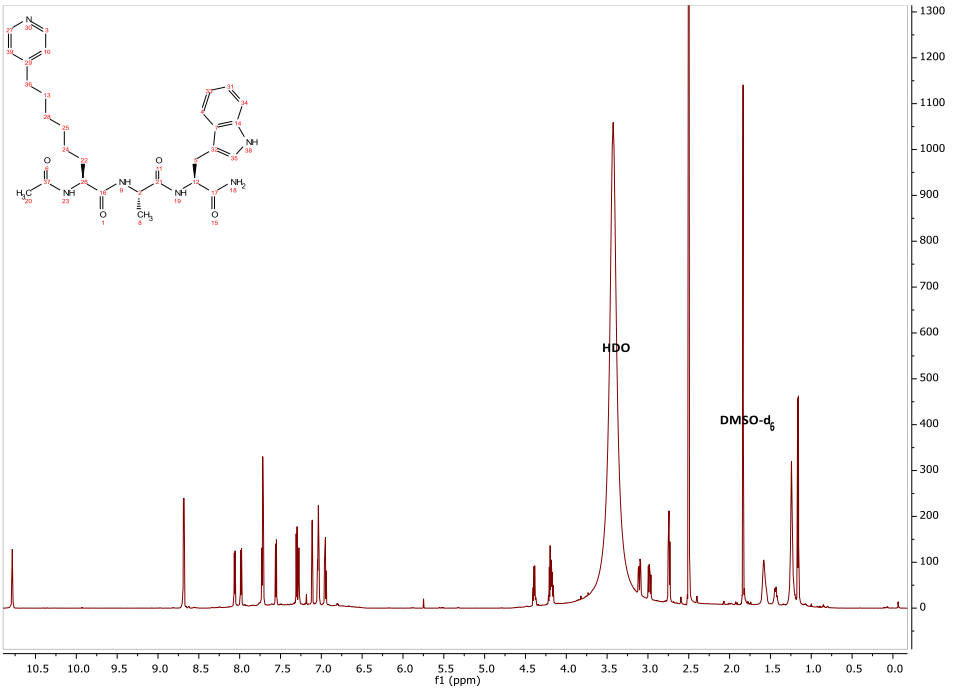

35 ^{13}C NMR

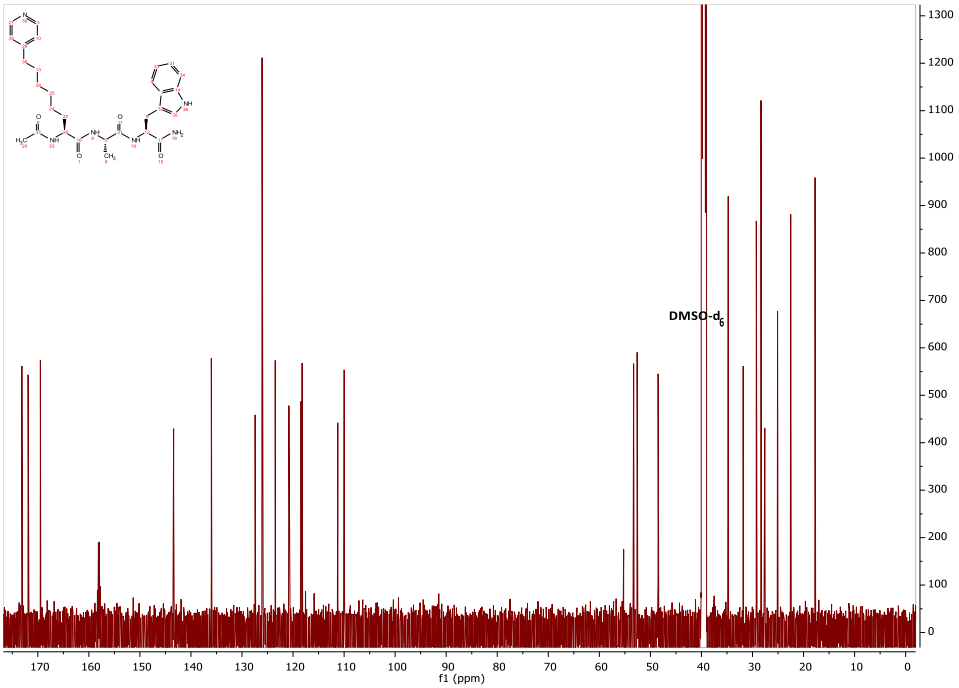

36 ^{1}H NMR

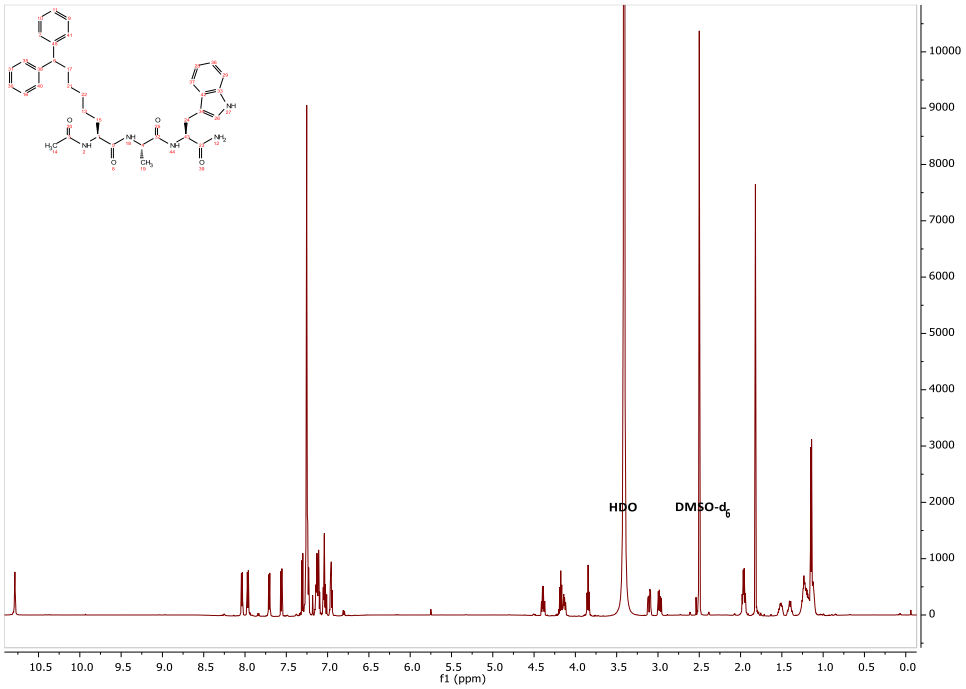

36 ^{13}C NMR

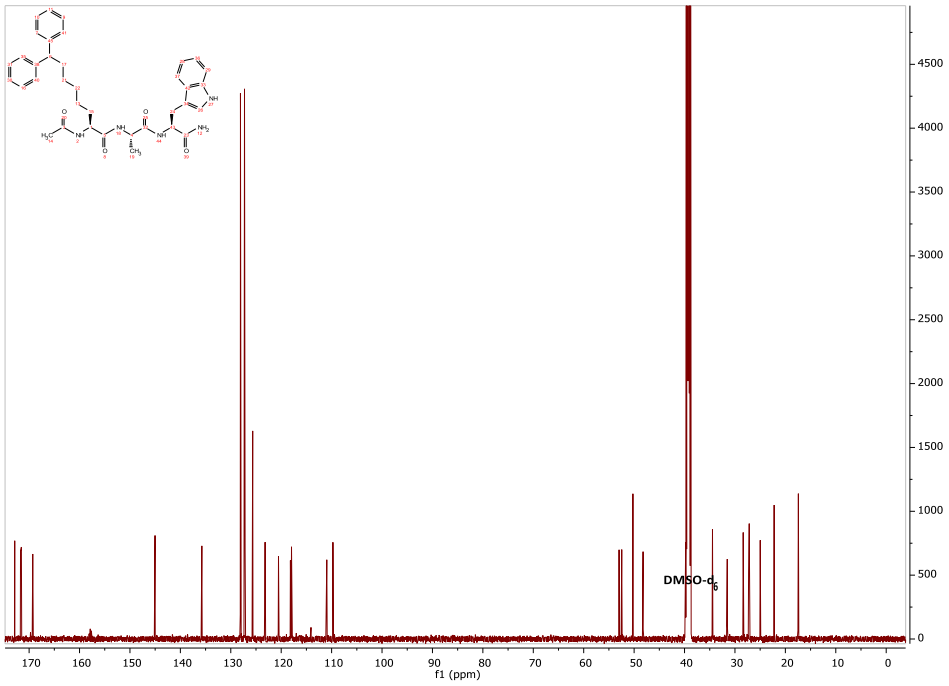

40 ^{1}H NMR

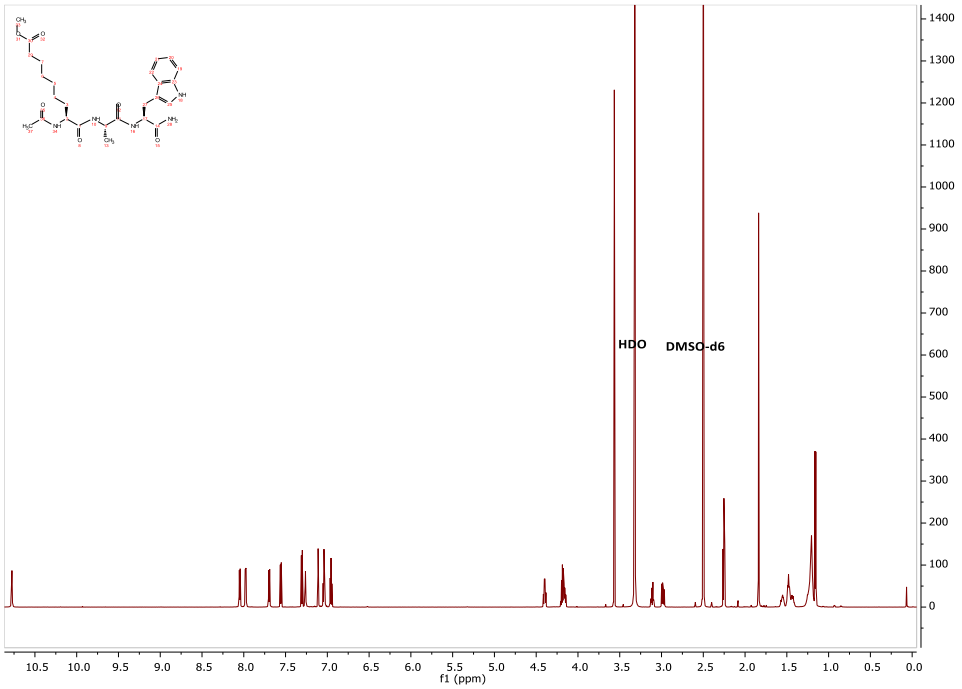

40 ^{13}C NMR

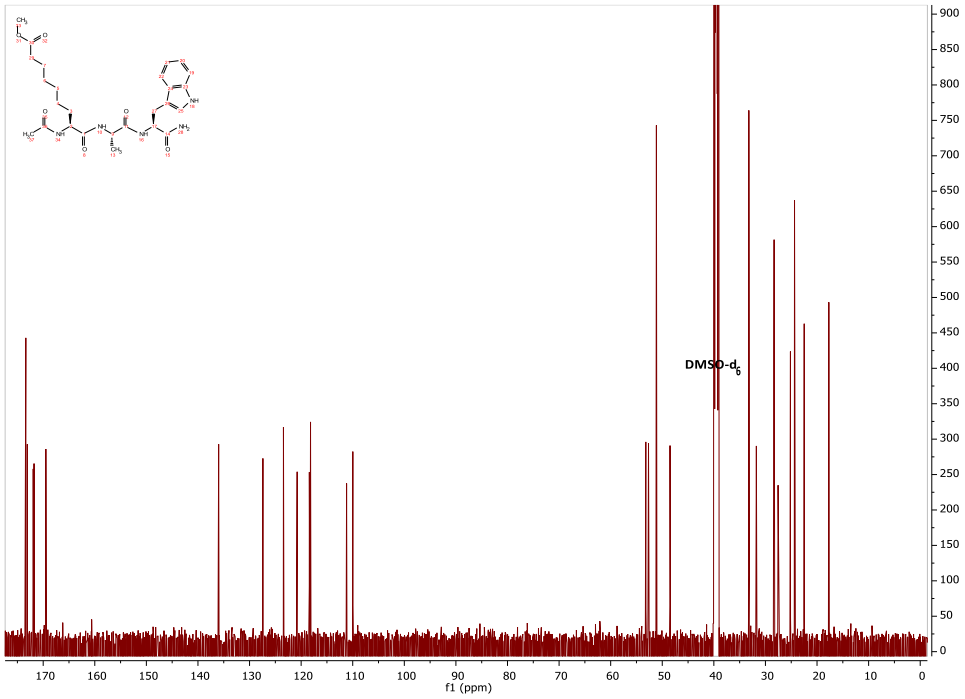

41 ^{1}H NMR

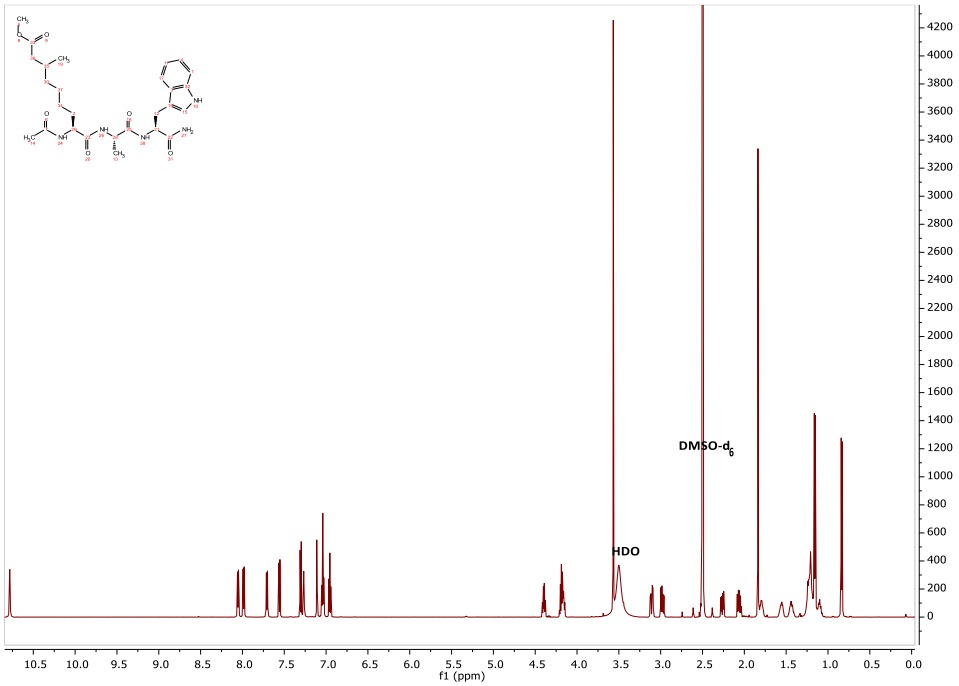

41 ^{13}C NMR

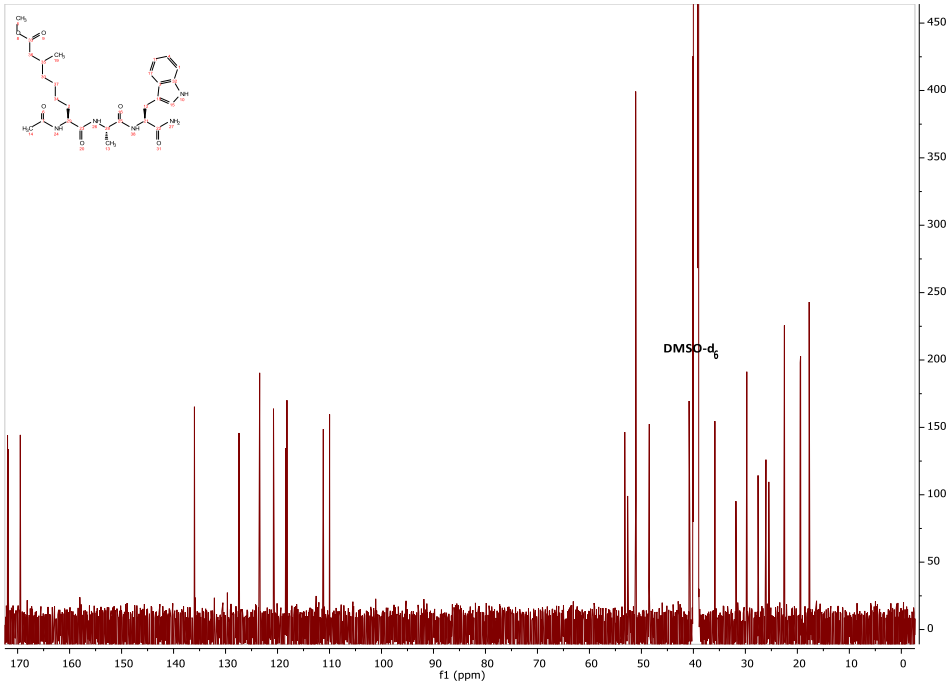

43 ^{1}H NMR

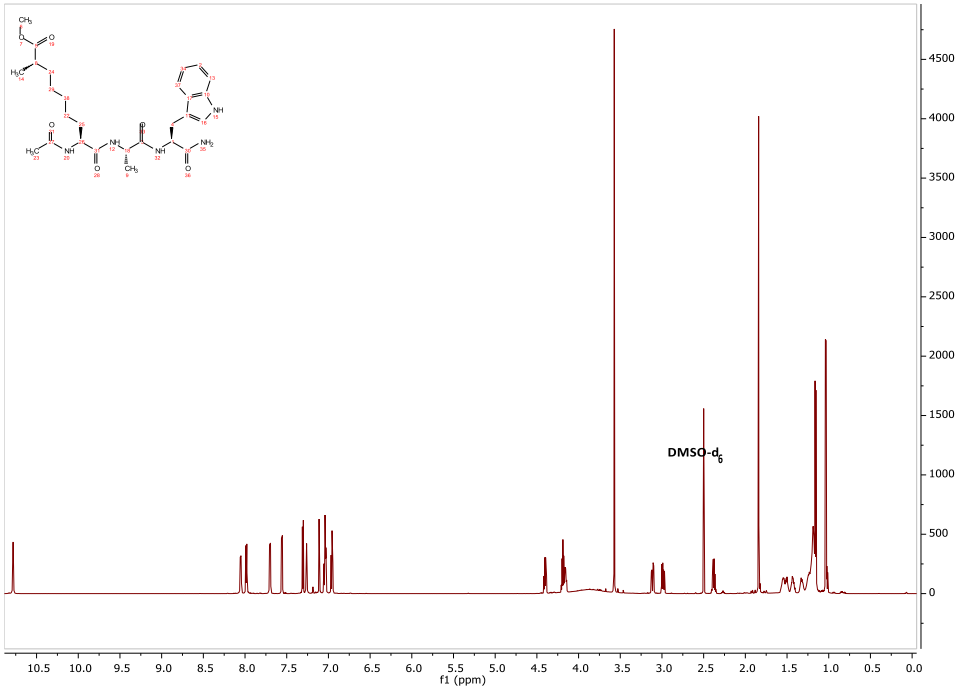

43 ^{13}C NMR

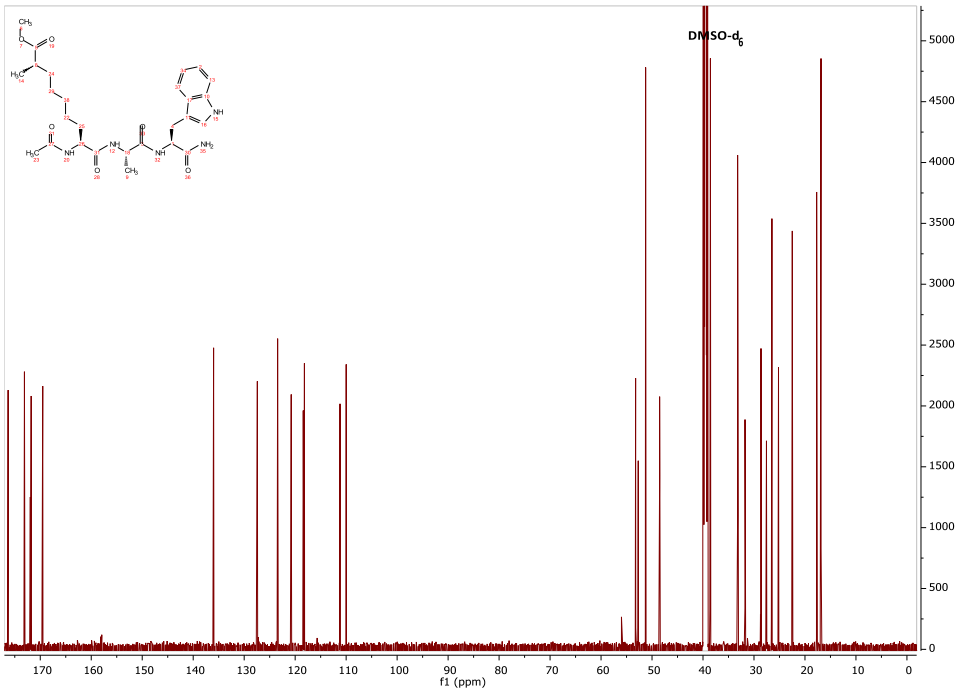

44 ^{1}H NMR

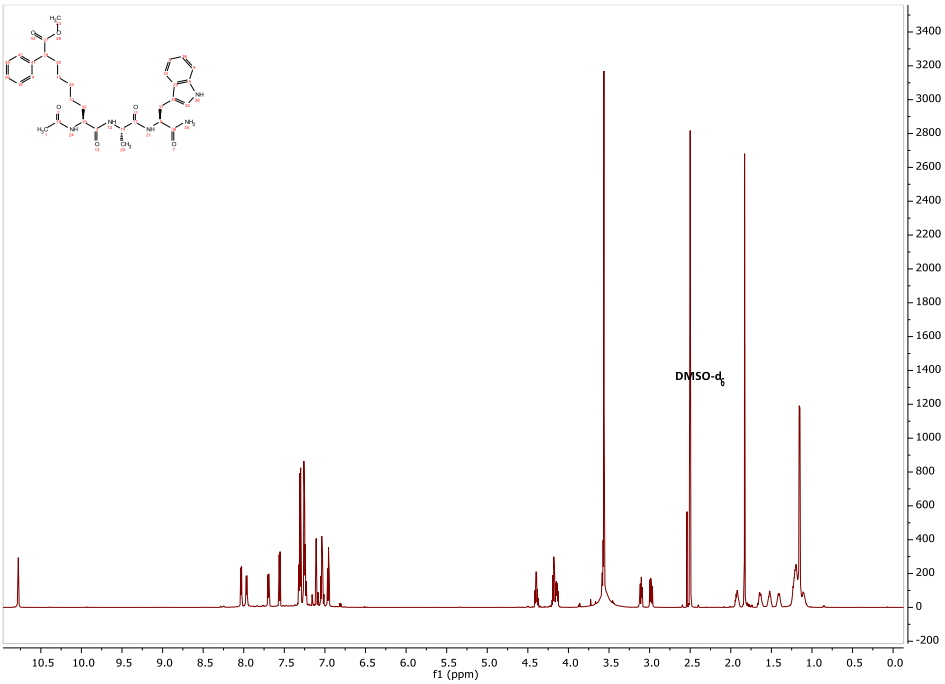

44 ^{13}C NMR

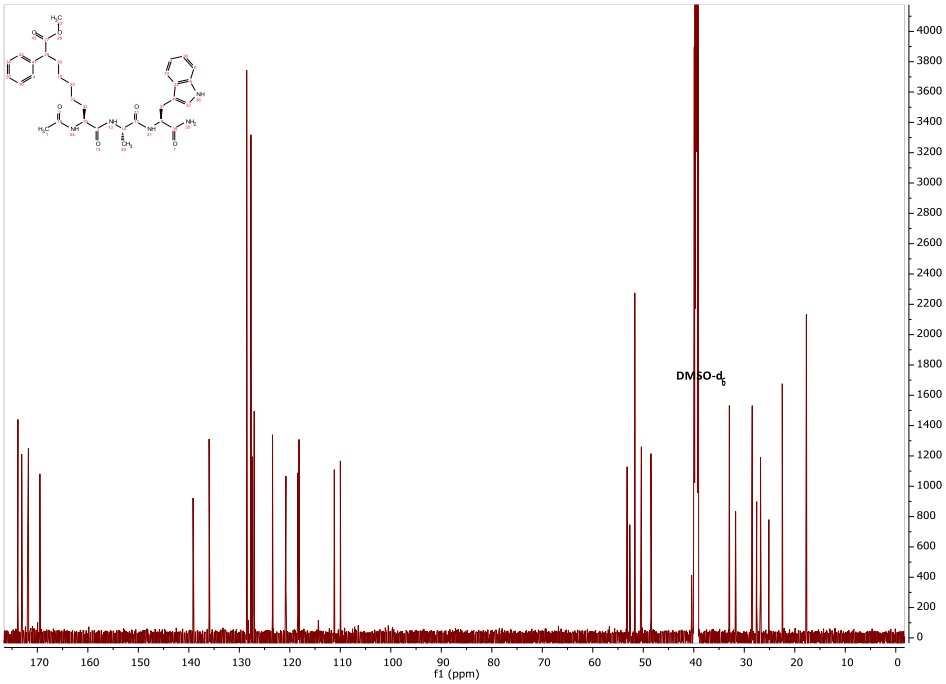

45 ^{1}H NMR

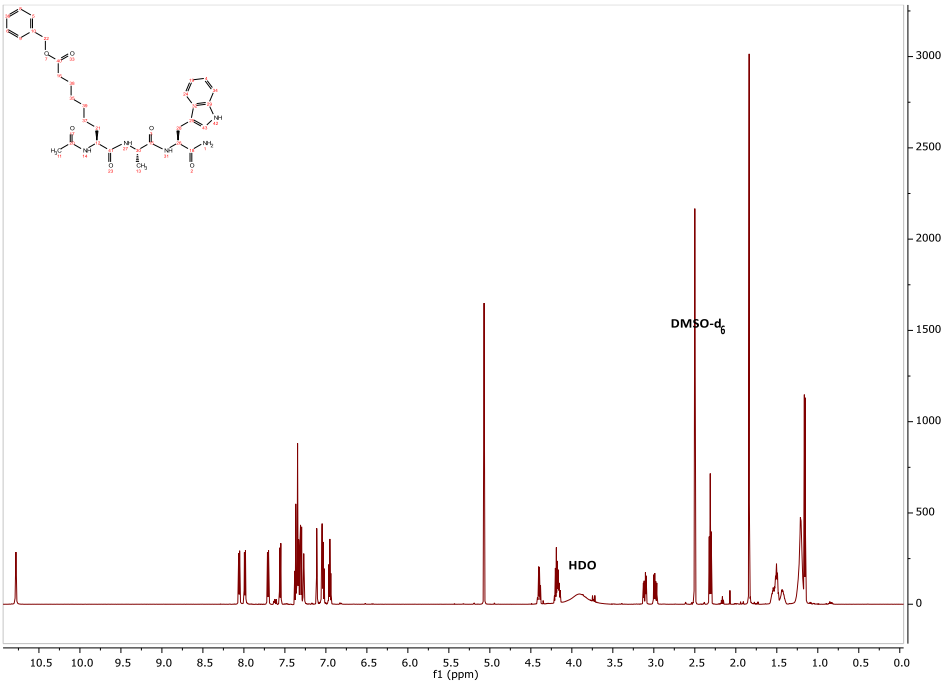

45 ^{13}C NMR

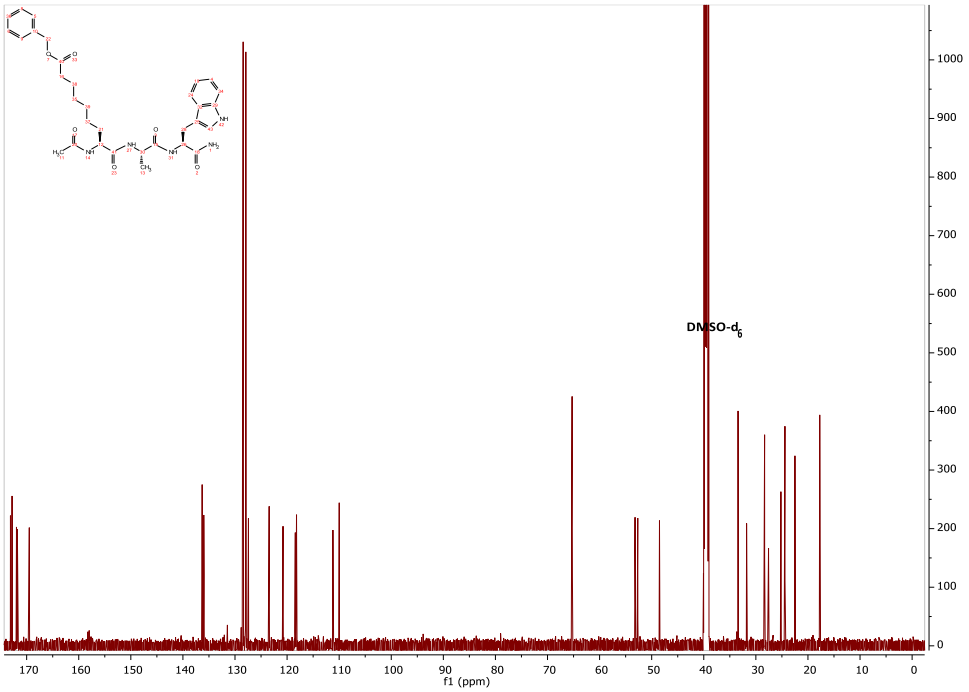

46 ^{1}H NMR

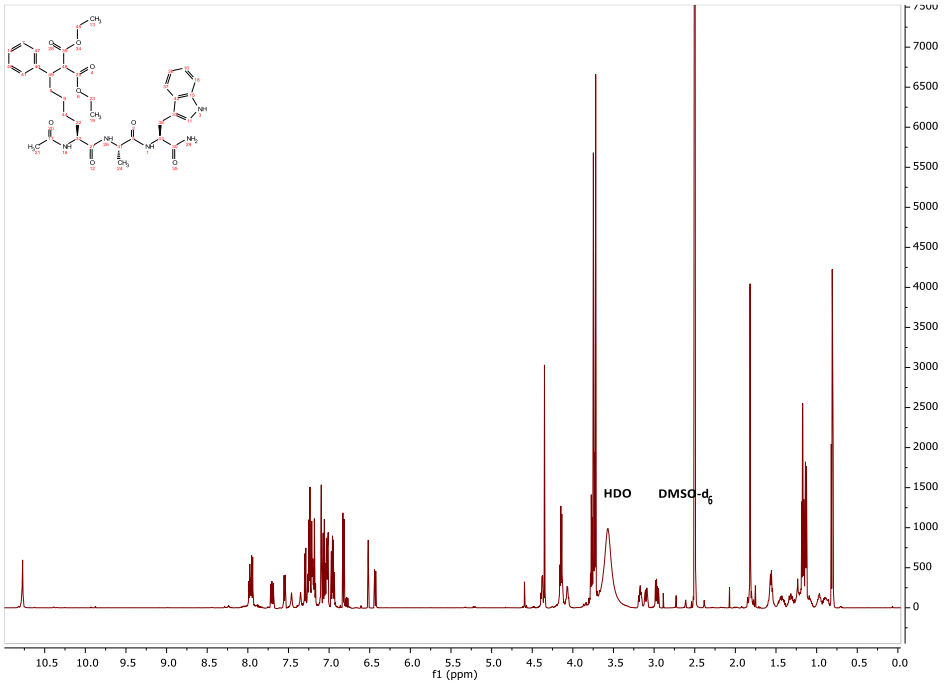

46 ^{13}C NMR

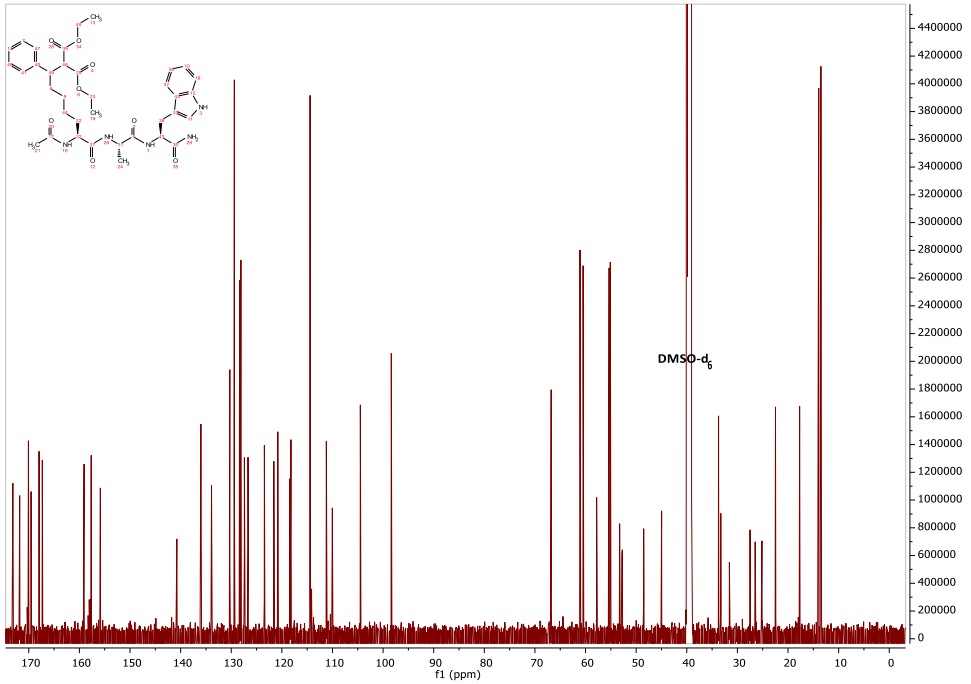

47 ^{1}H NMR

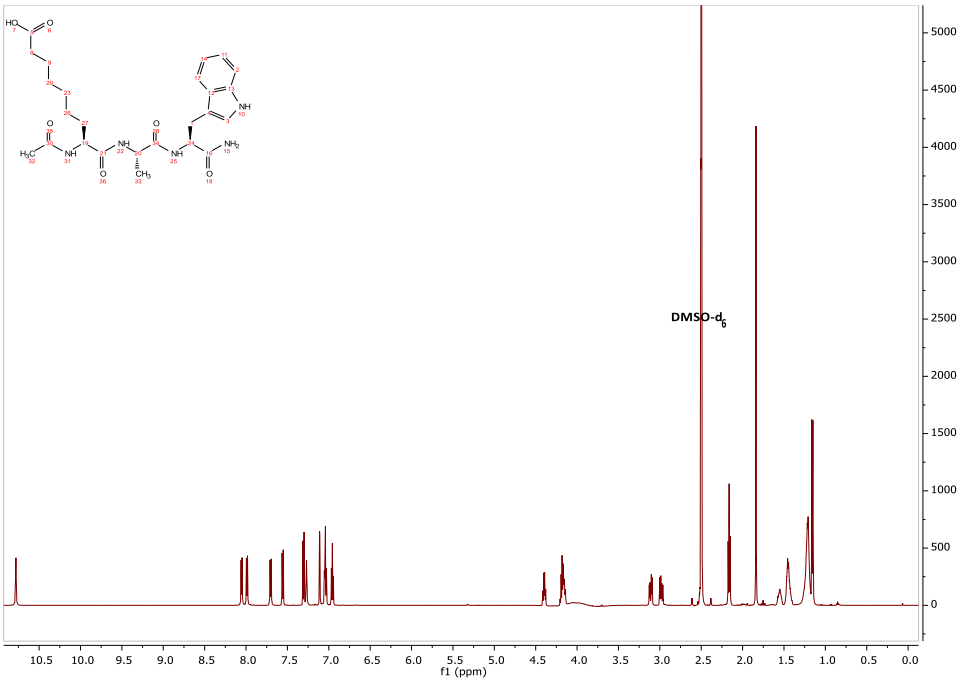

47 ^{13}C NMR

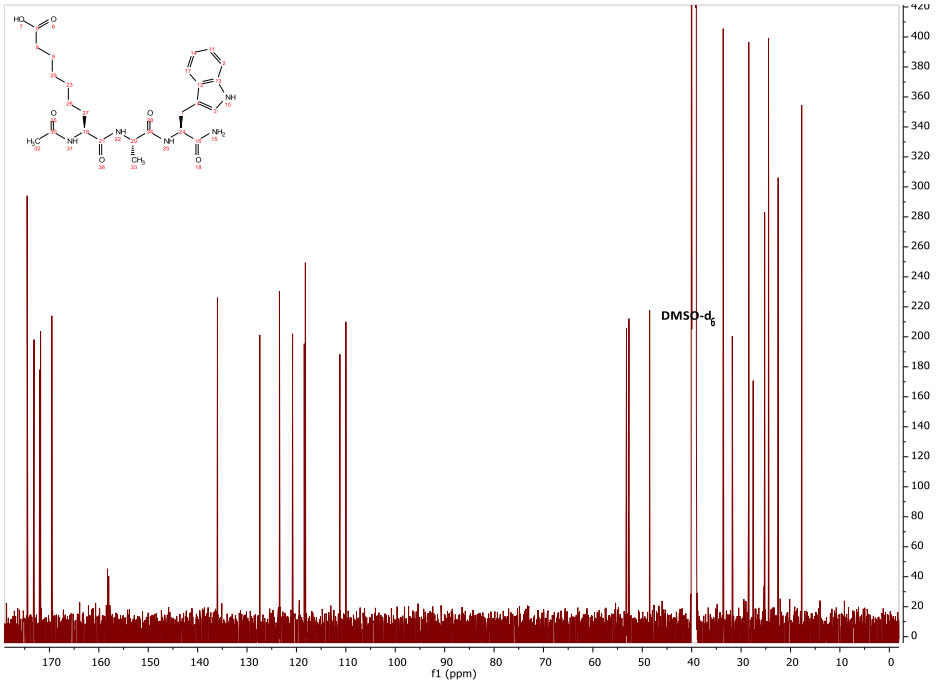

48 ^{1}H NMR

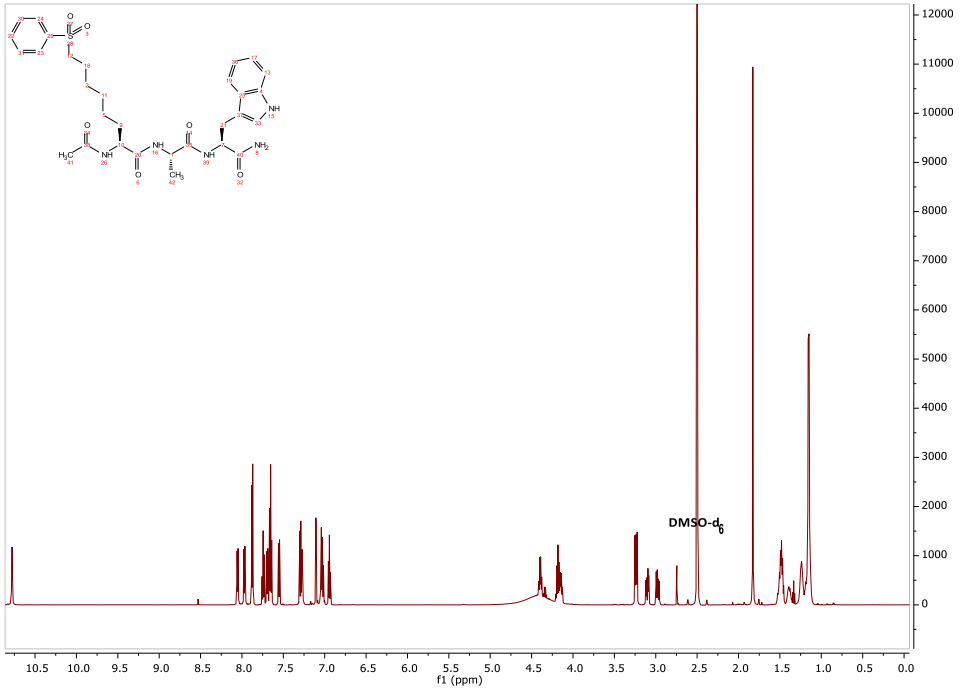

48 ^{13}C NMR

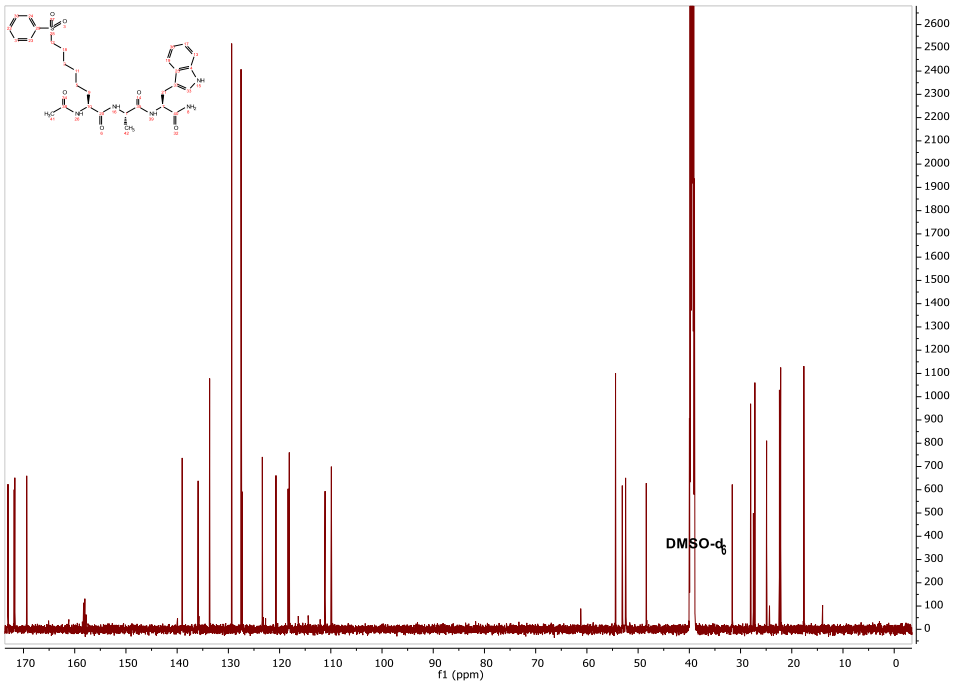

49 ^{1}H NMR

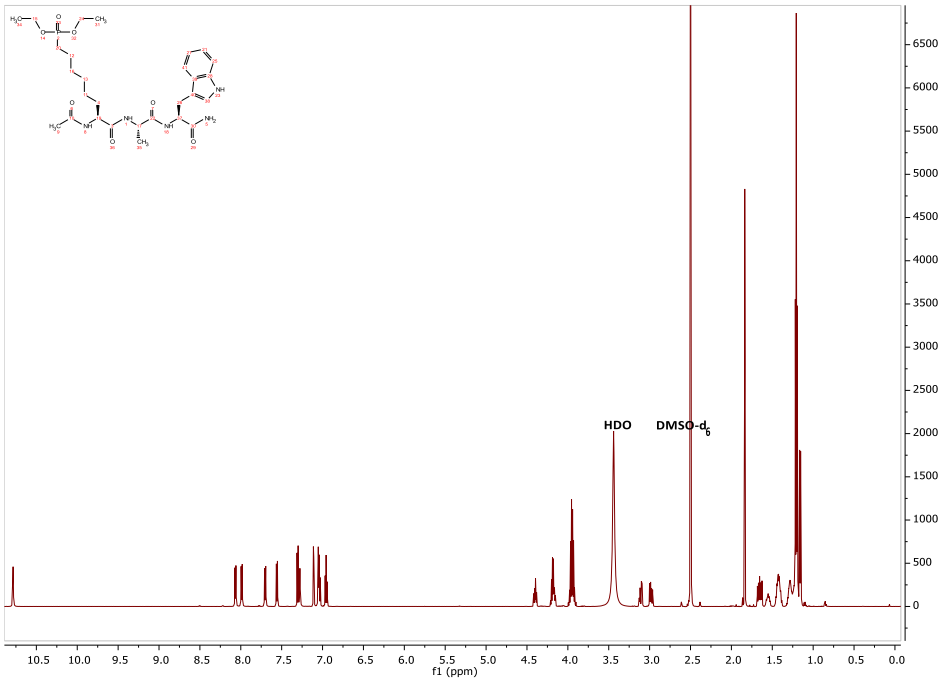

49 ^{13}C NMR

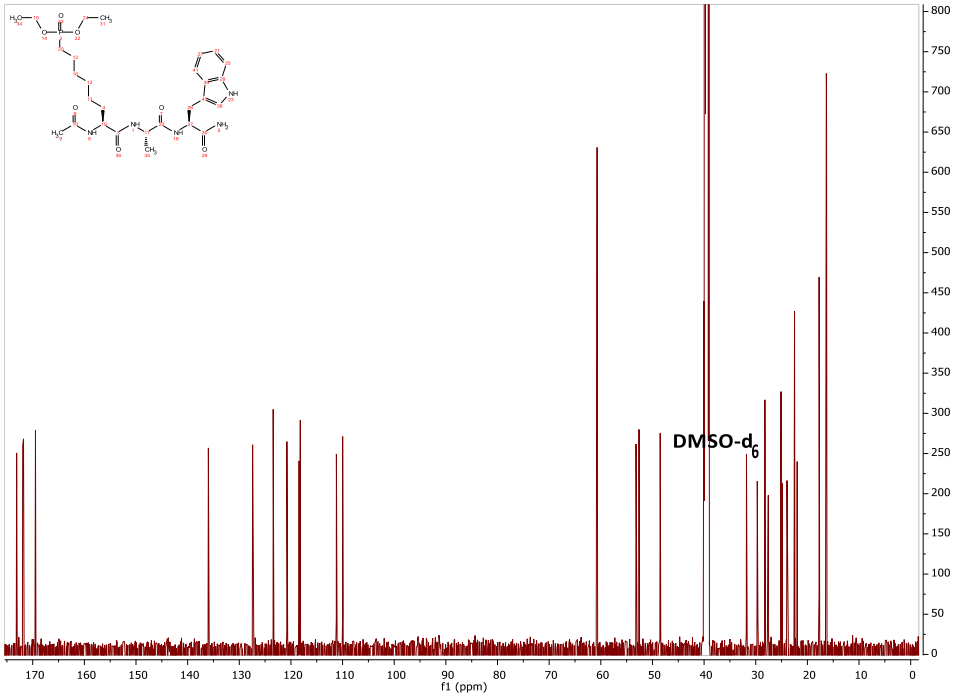

50 ^{1}H NMR

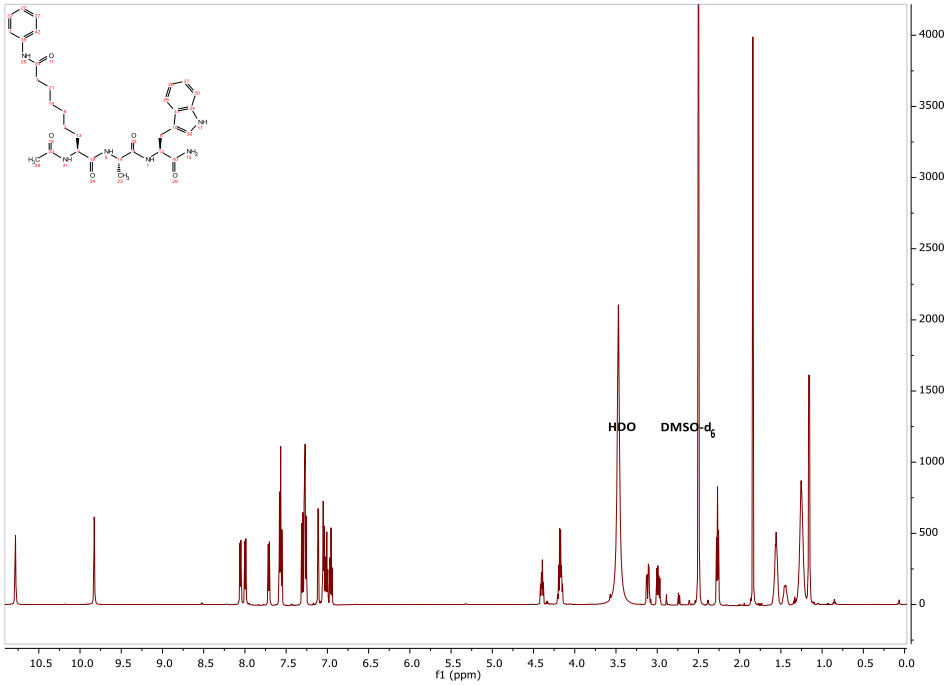

50 ^{13}C NMR

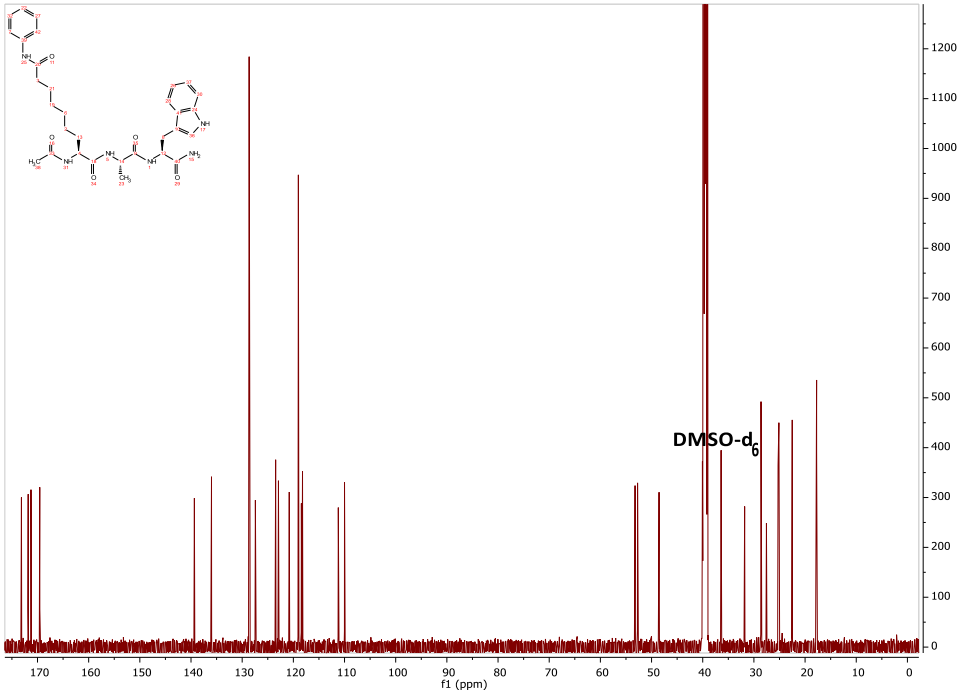

51 ^{1}H NMR

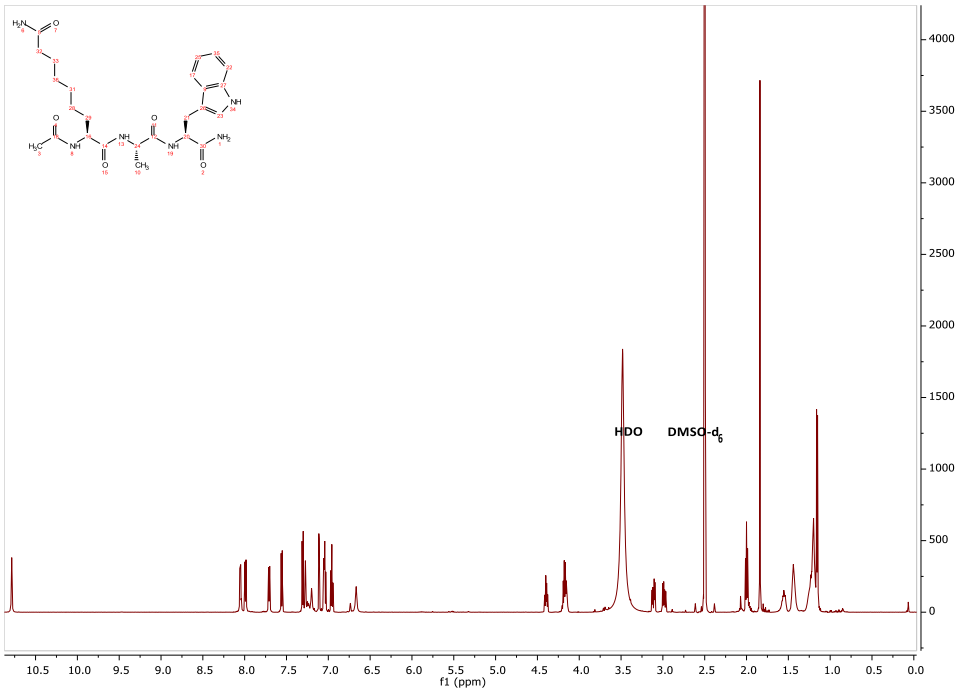

51 ^{13}C NMR

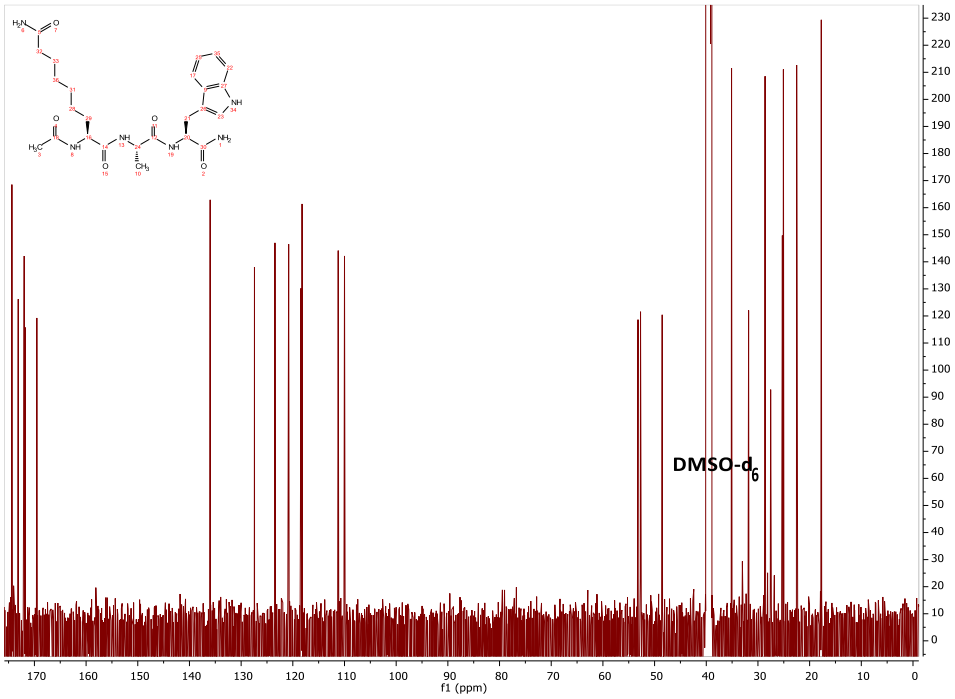

52 ^{1}H NMR

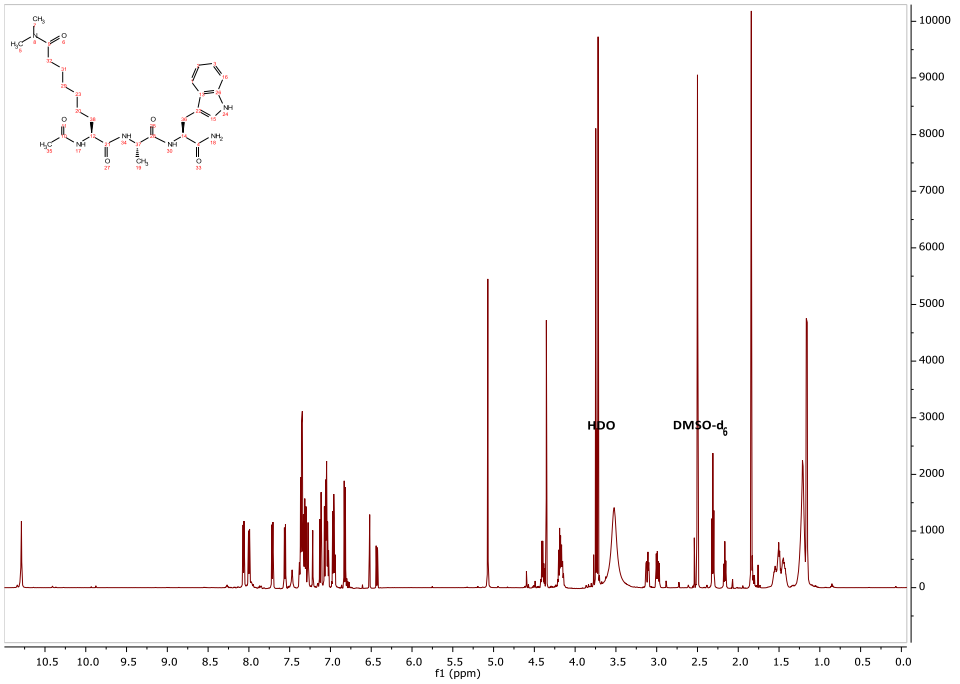

52 ^{13}C NMR

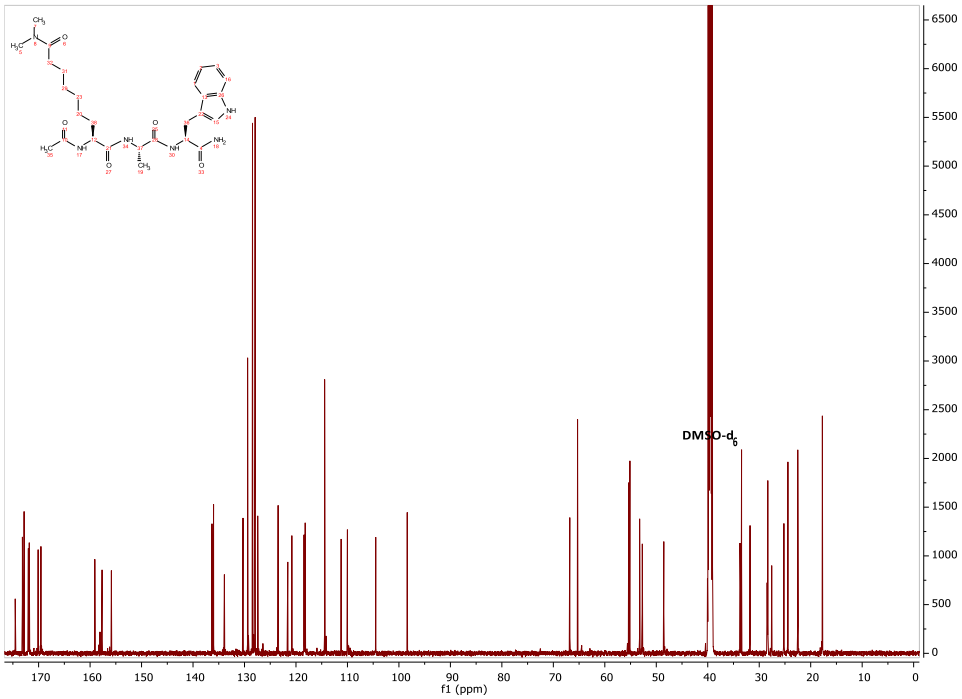

53 ^{1}H NMR

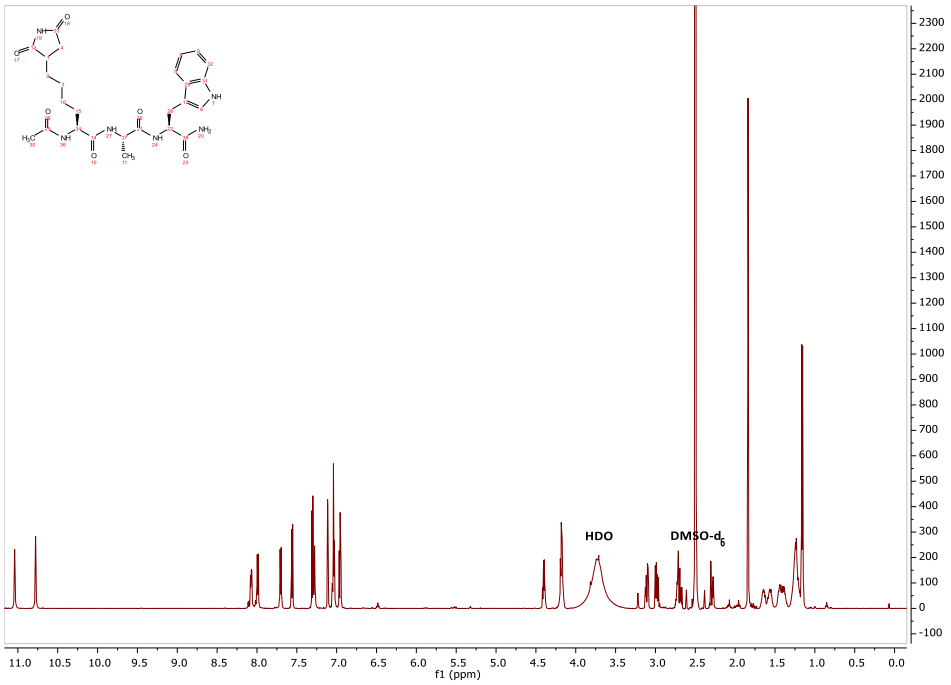

53 ^{13}C NMR

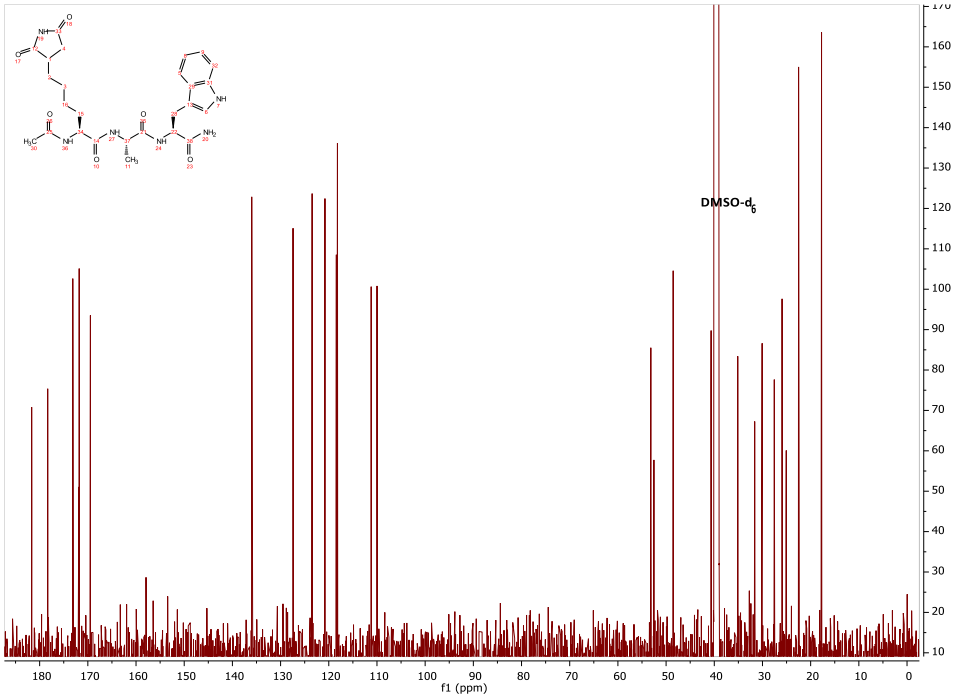

61 ^{1}H NMR

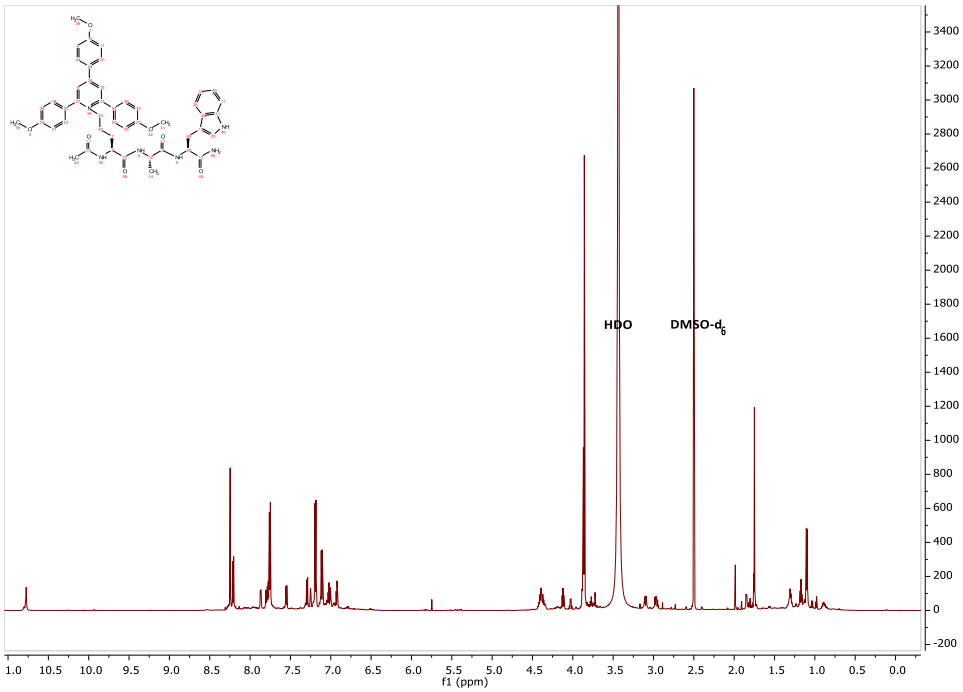

61 ^{13}C NMR

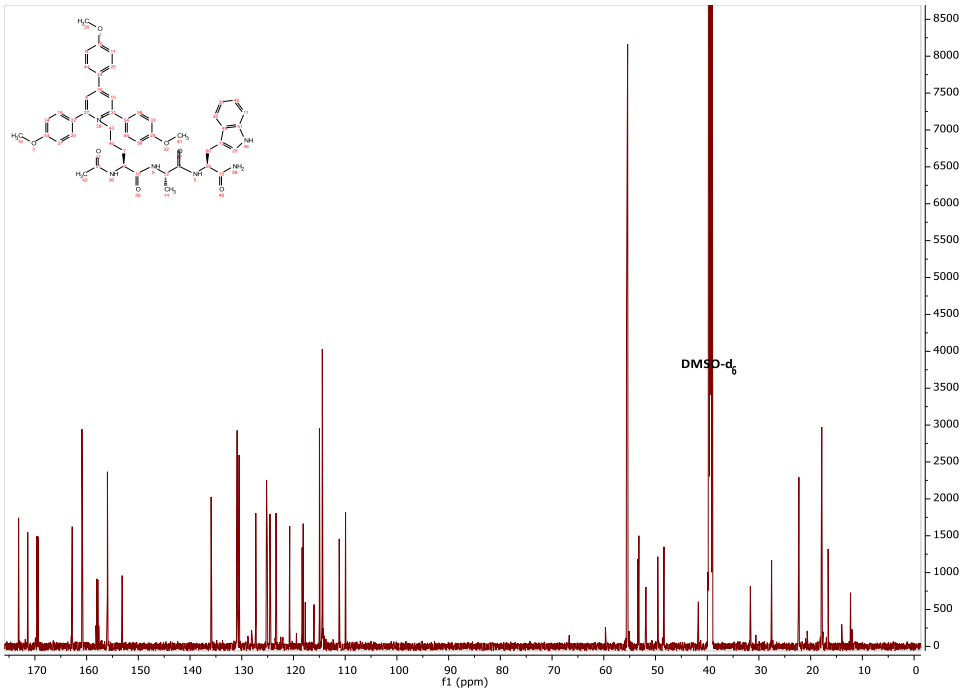

62 ^{1}H NMR

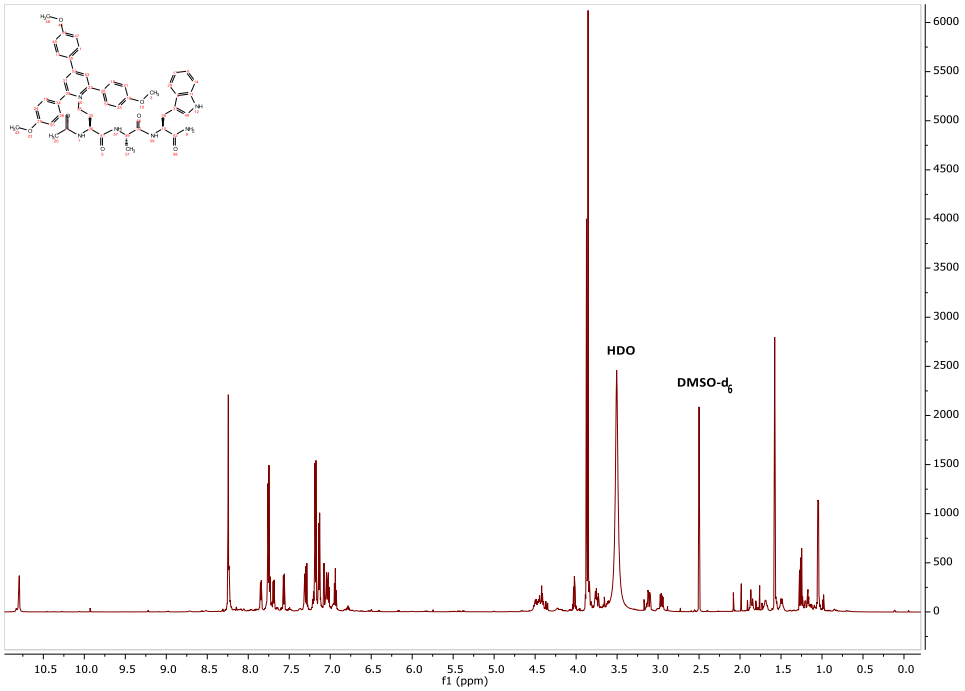

62 ^{13}C NMR

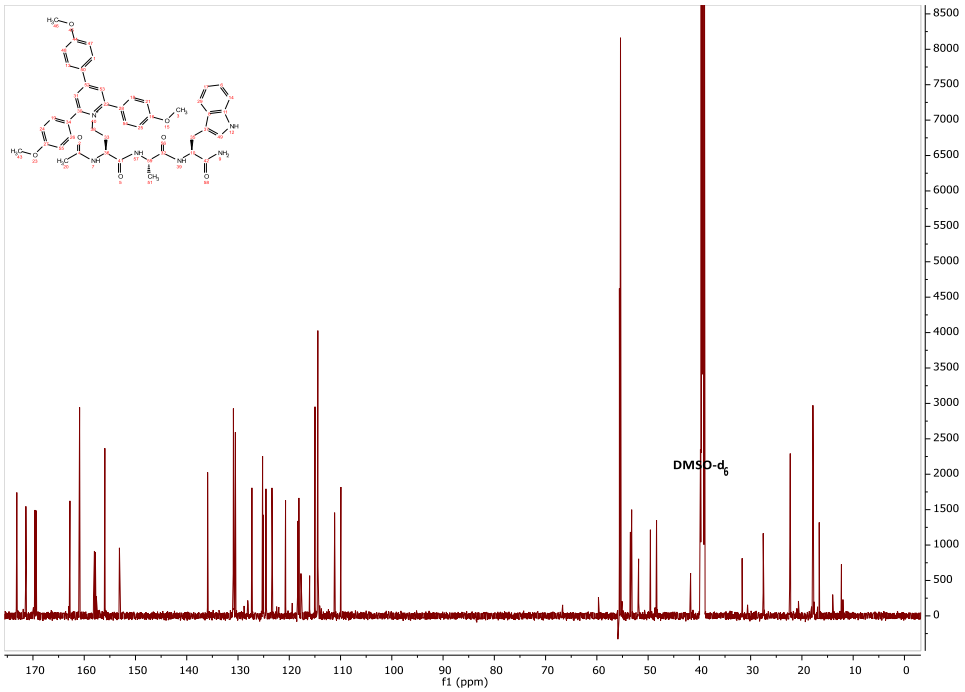

63 ^{1}H NMR

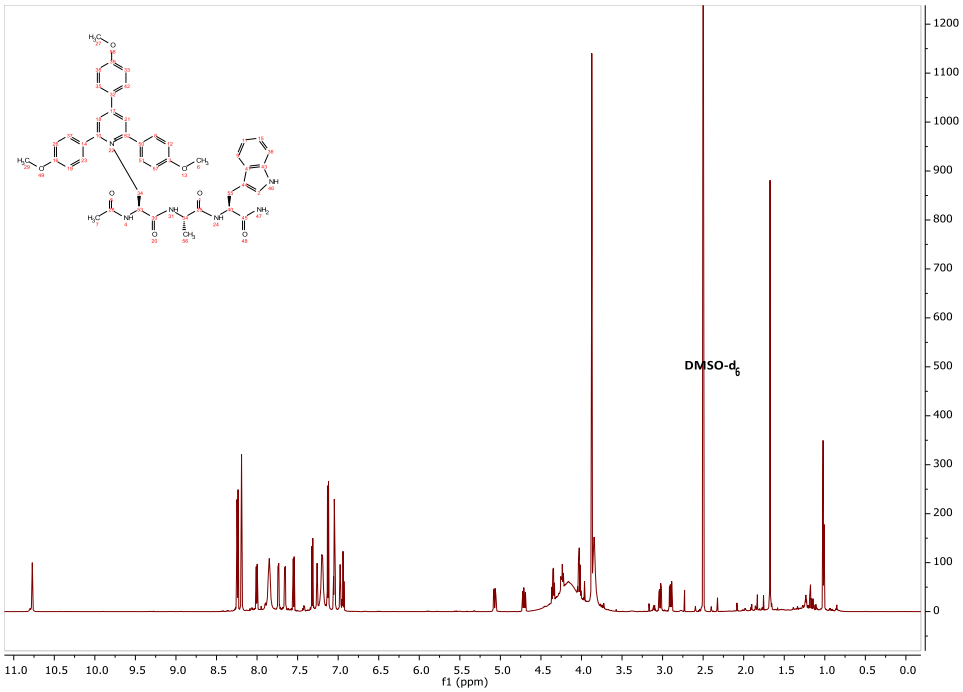

63 ^{13}C NMR

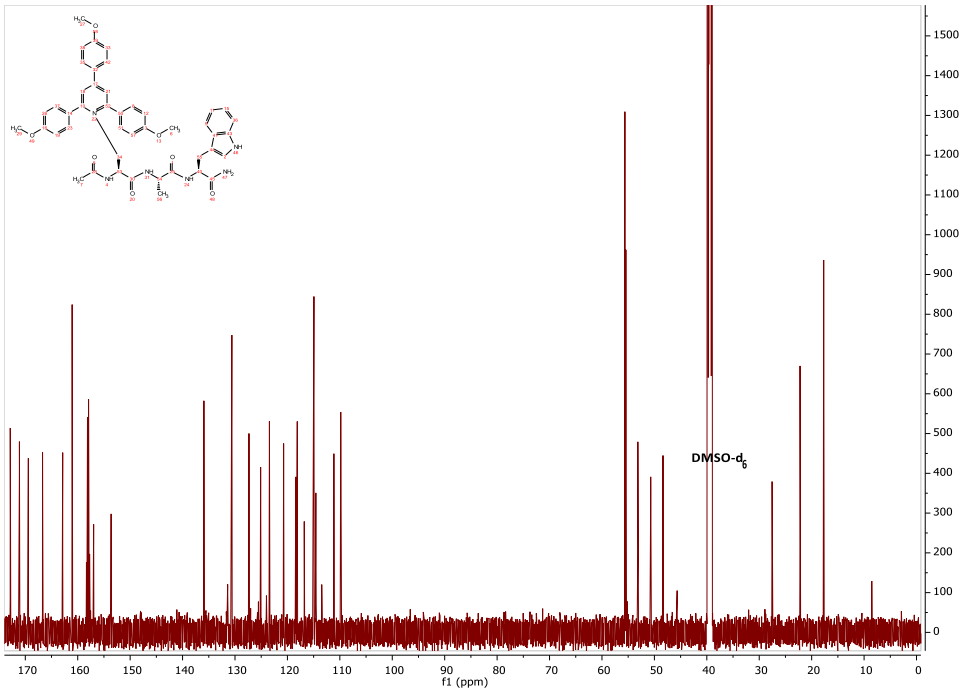

64 ^{1}H NMR

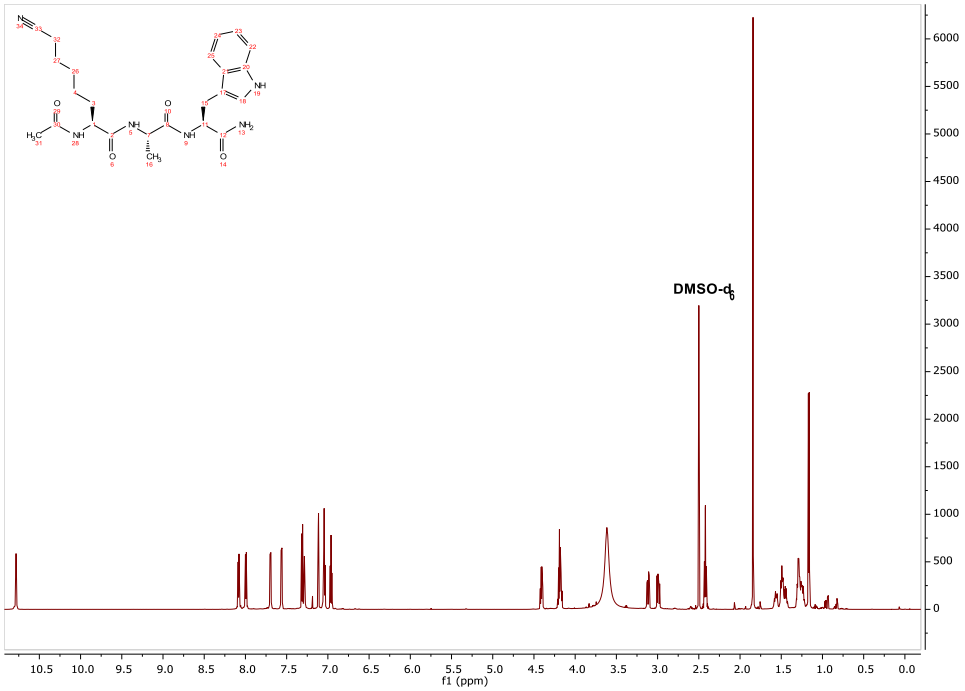

64 ^{13}C NMR

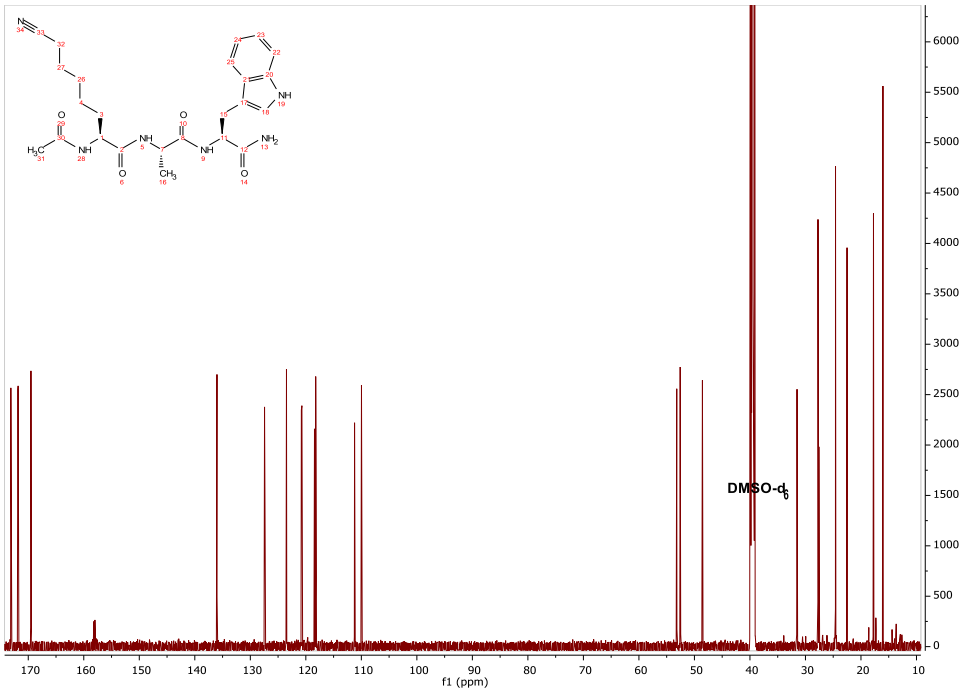

65 ^{1}H NMR

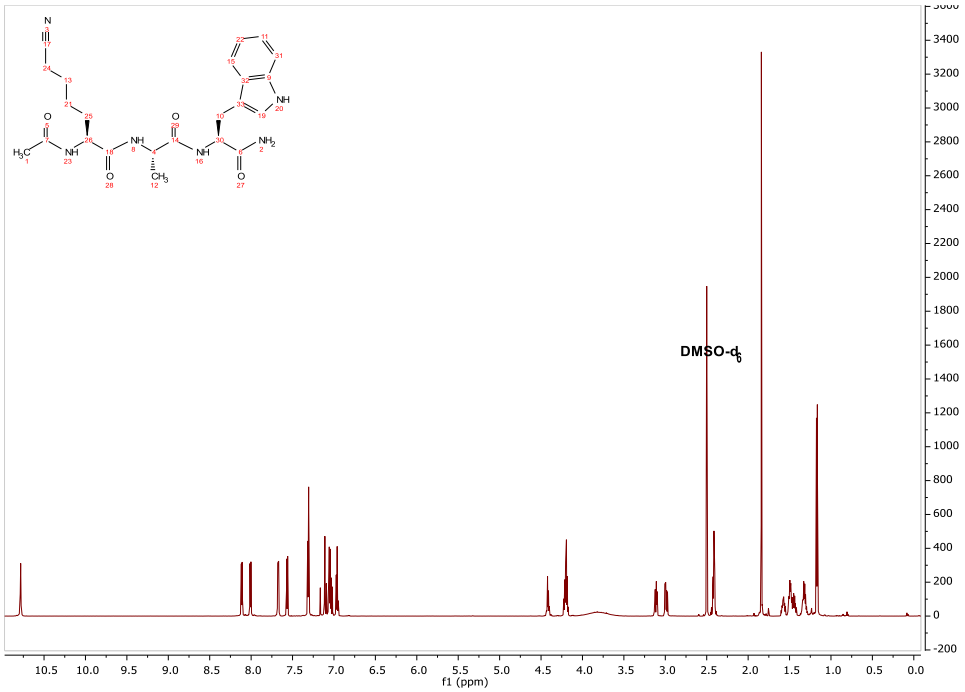

65 ^{13}C NMR

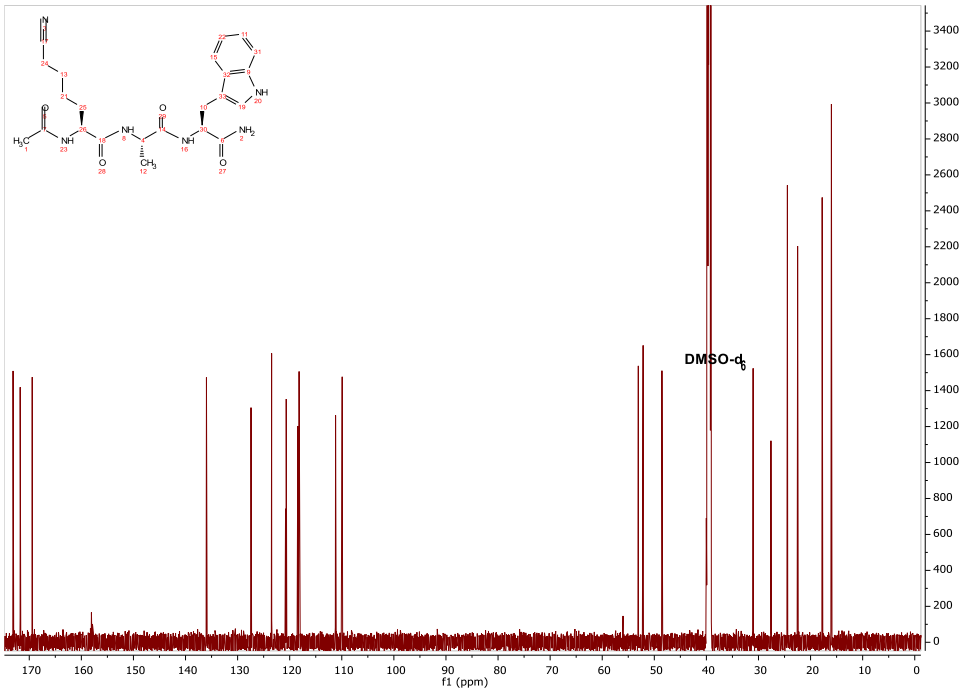

66 ^{1}H NMR

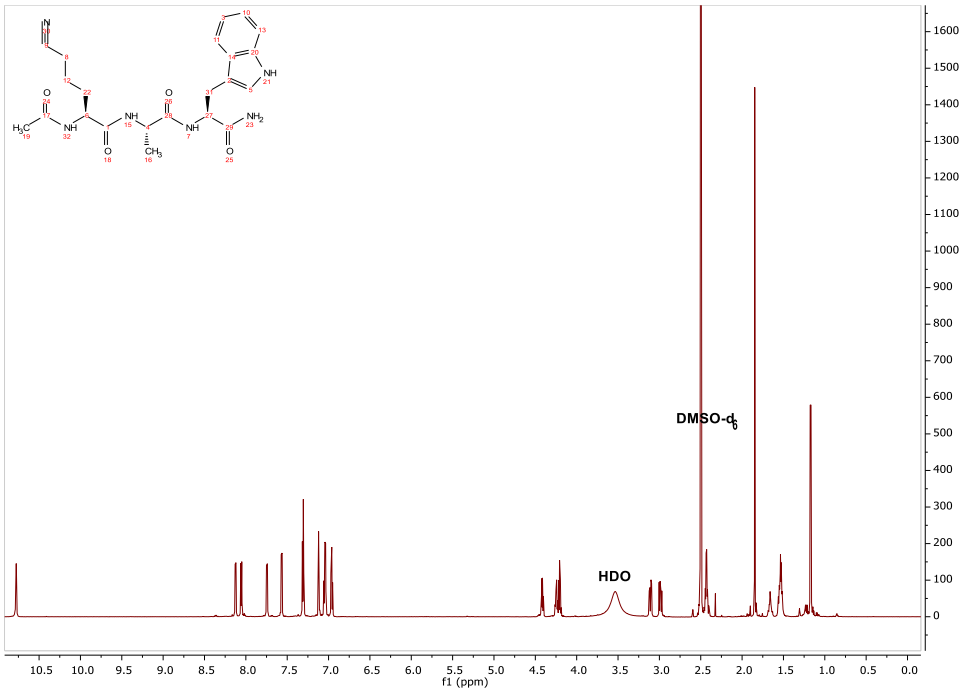

66 ^{13}C NMR

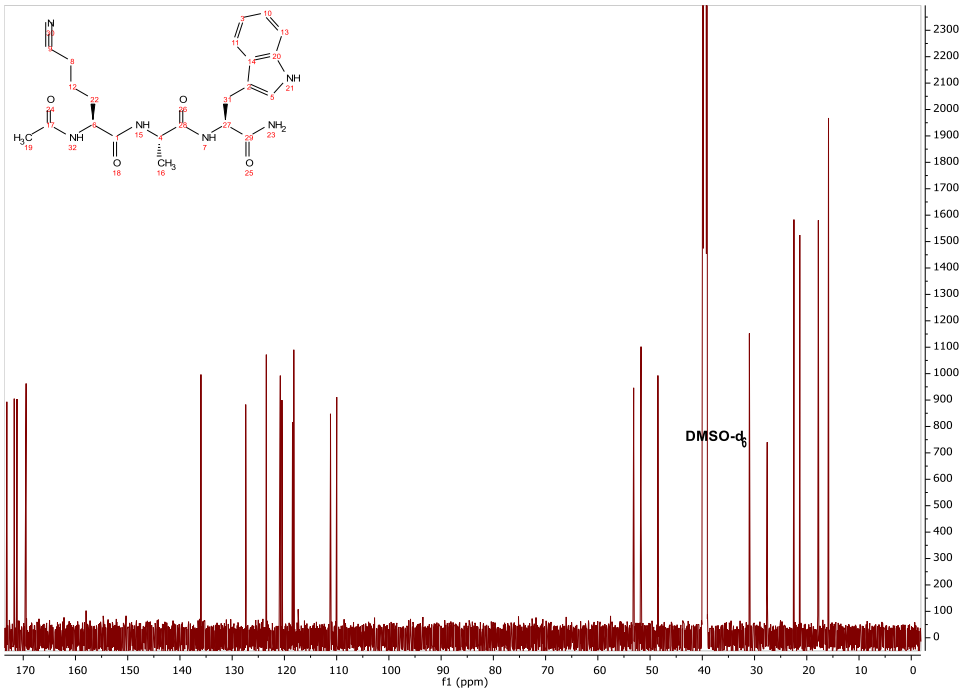

67 ^{1}H NMR

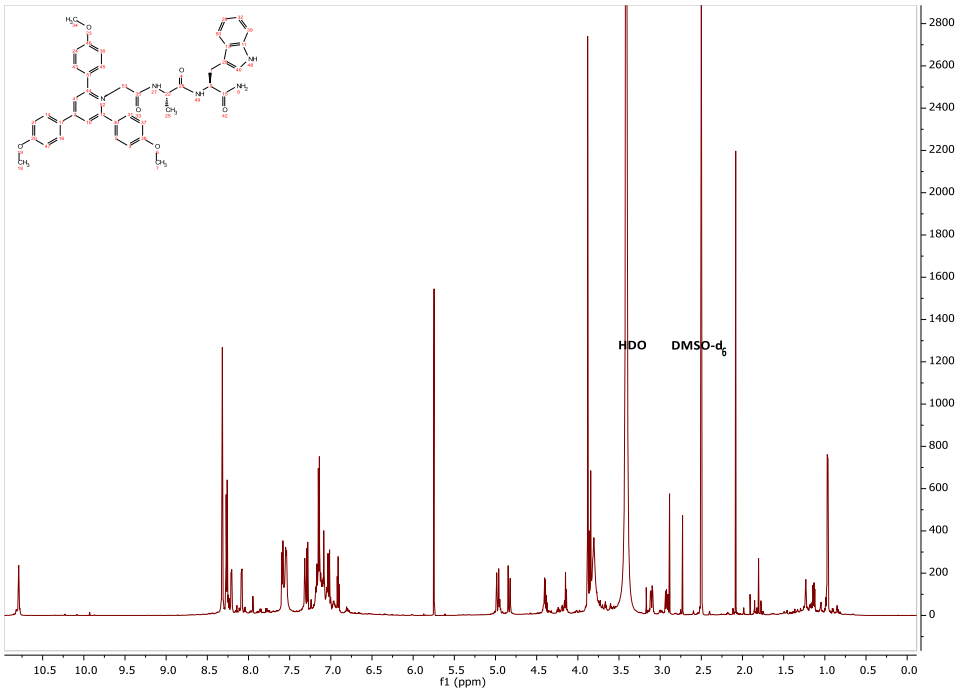

67 ^{13}C NMR

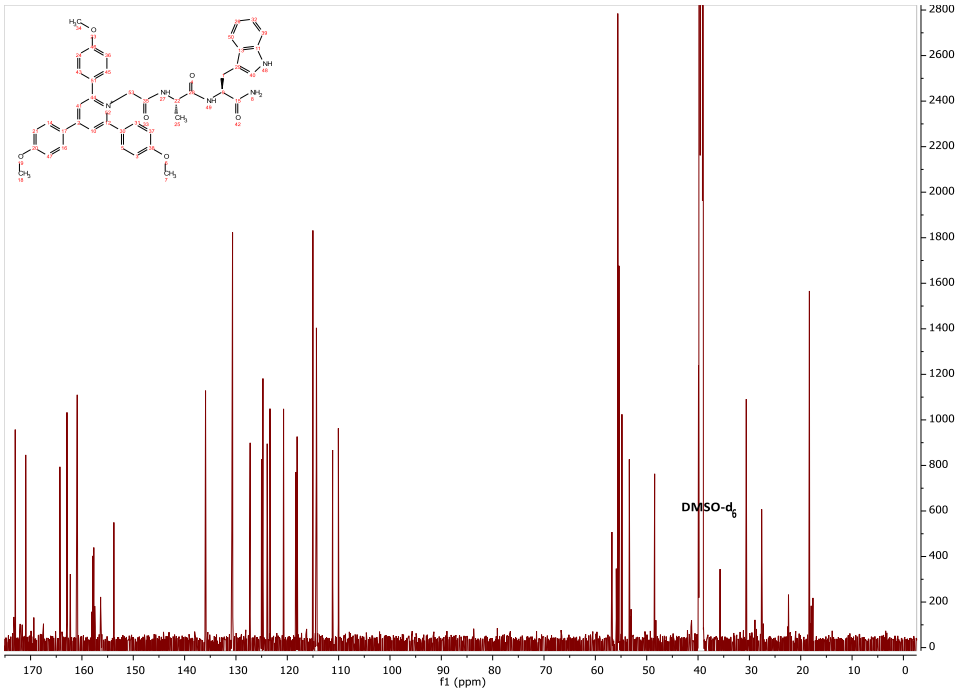

68 ^{1}H NMR

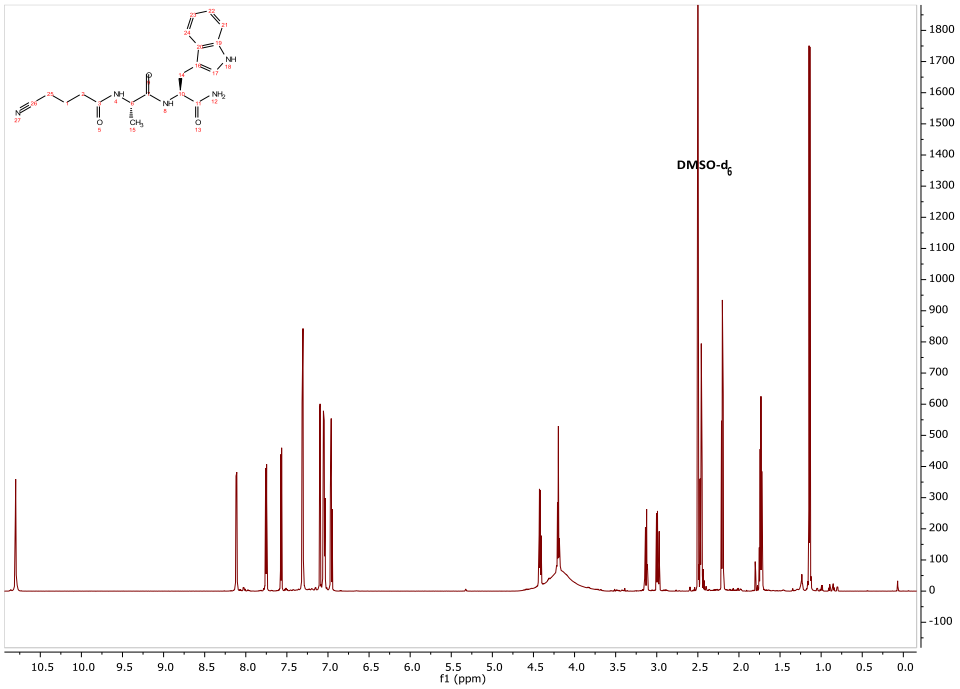

68 ^{13}C NMR

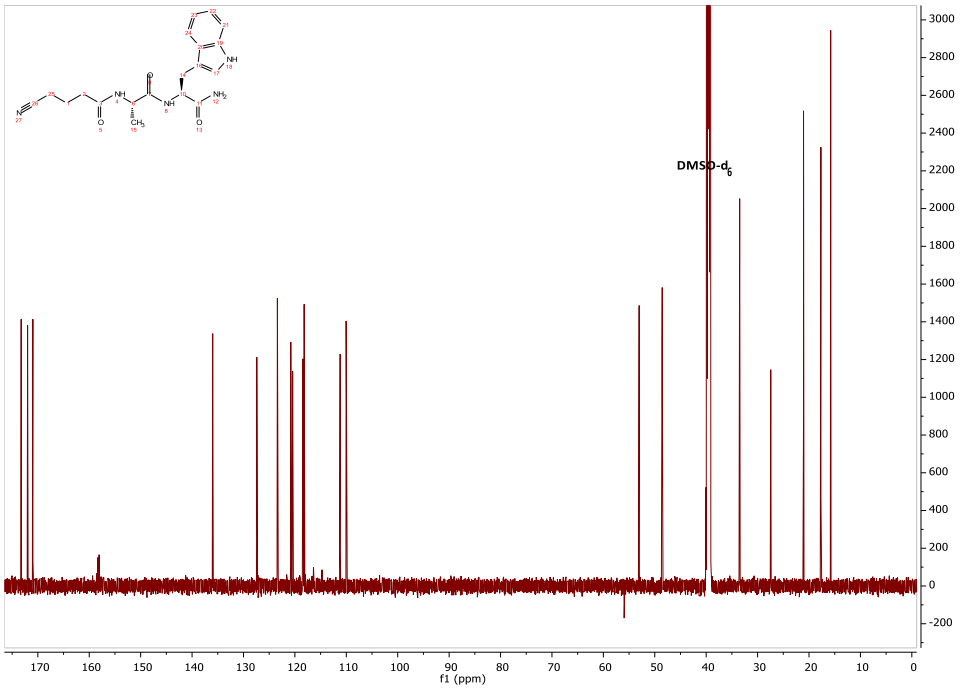

74/76 ^{1}H NMR

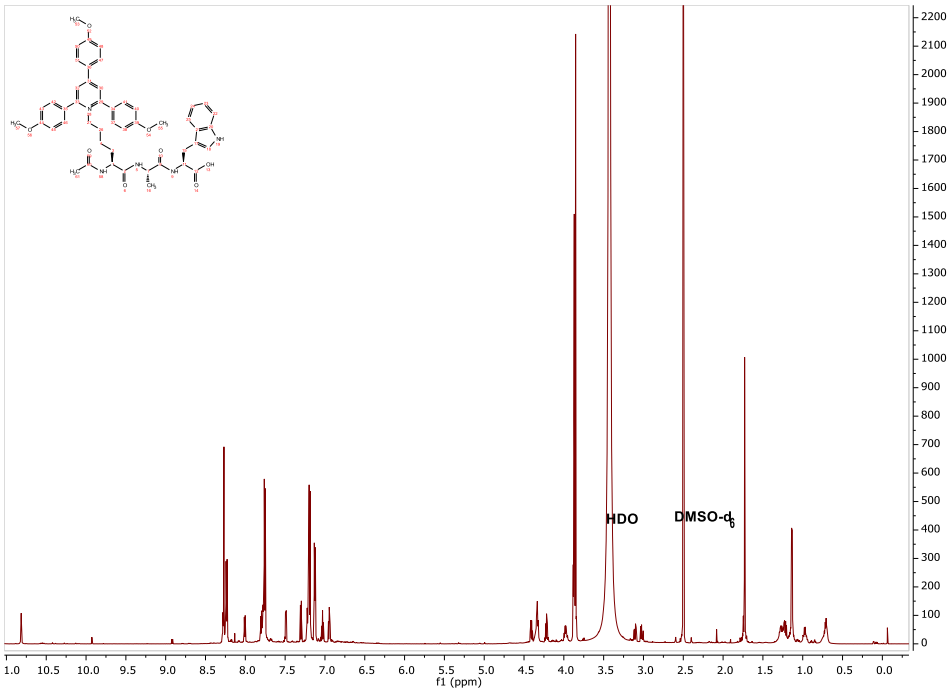

74/76 ^{13}C NMR

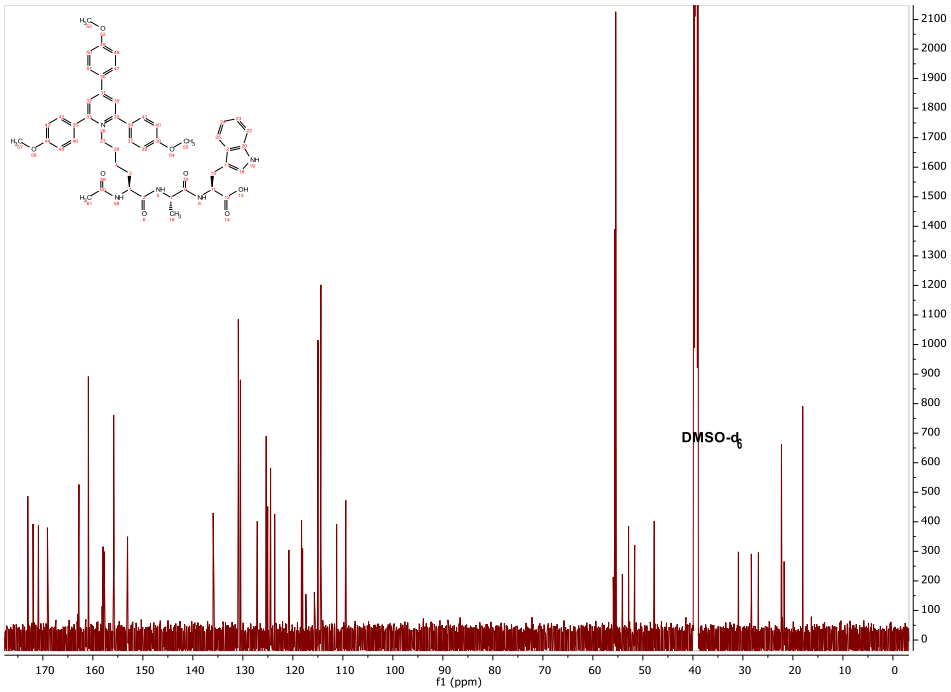

77 ^{1}H NMR

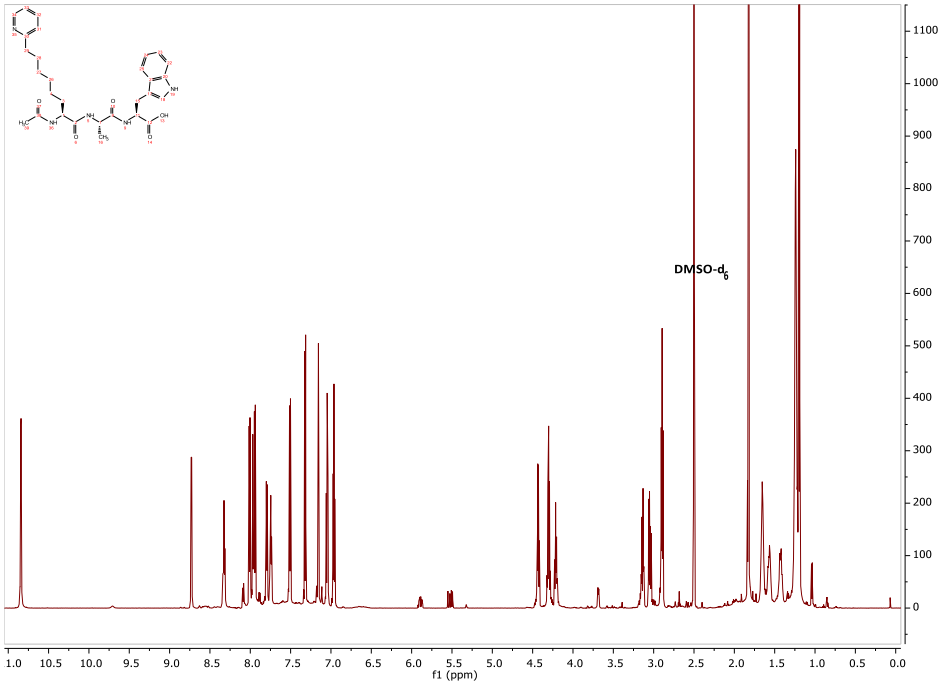

77 ^{13}C NMR

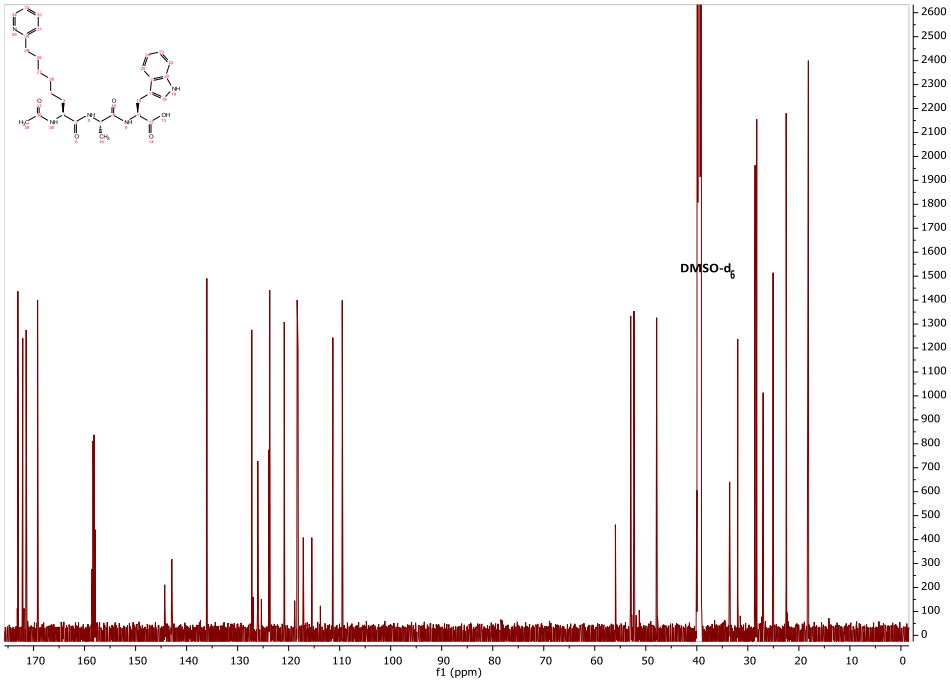

78 ^{1}H NMR

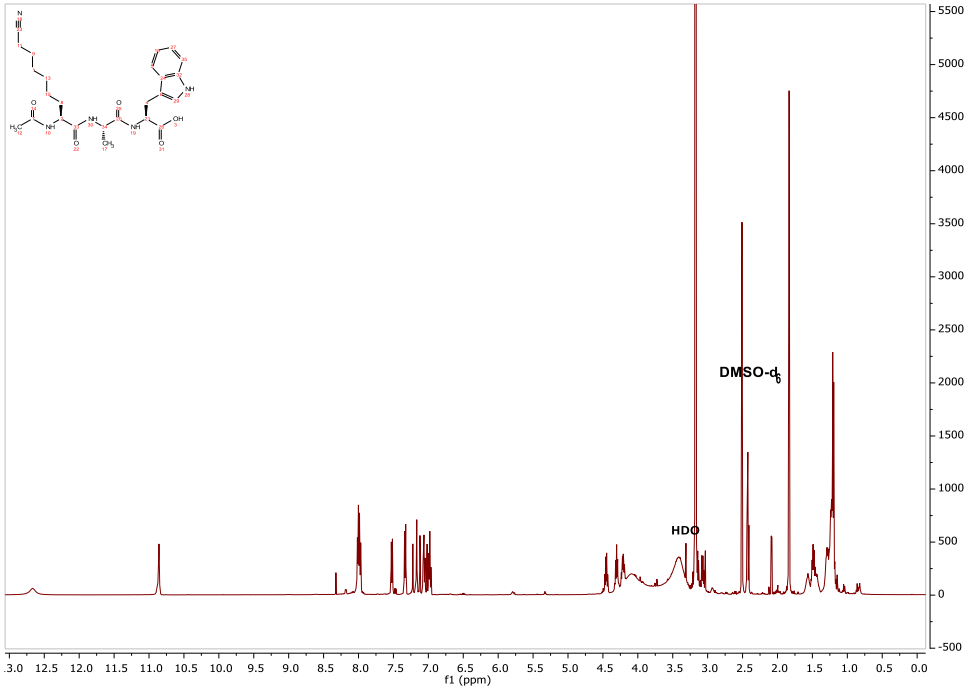

78 ^{13}C NMR

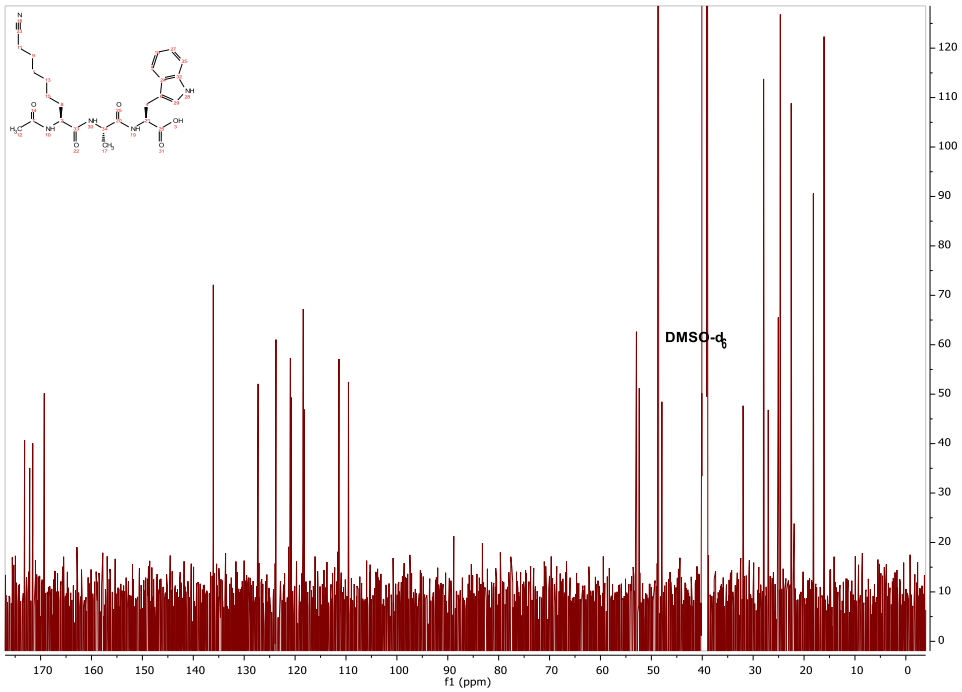

HPLC traces

Compound **56**

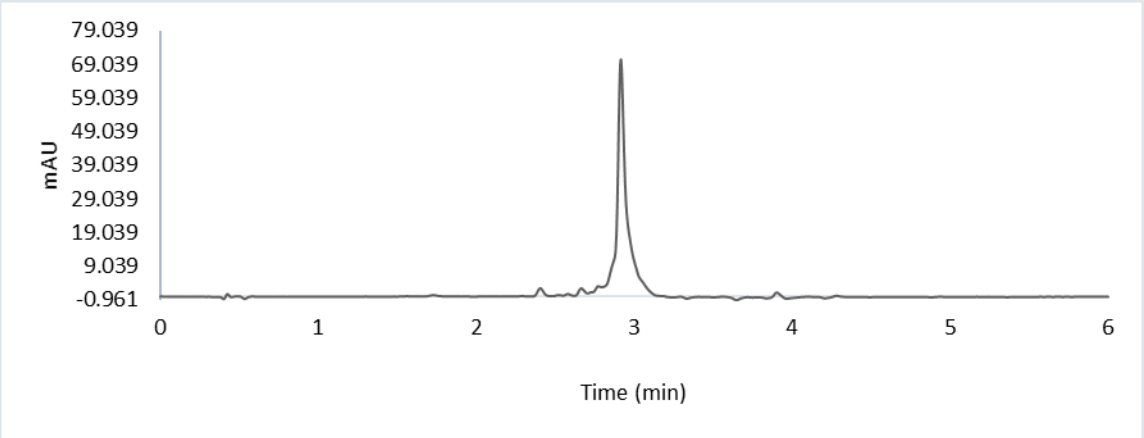

Compound **69**

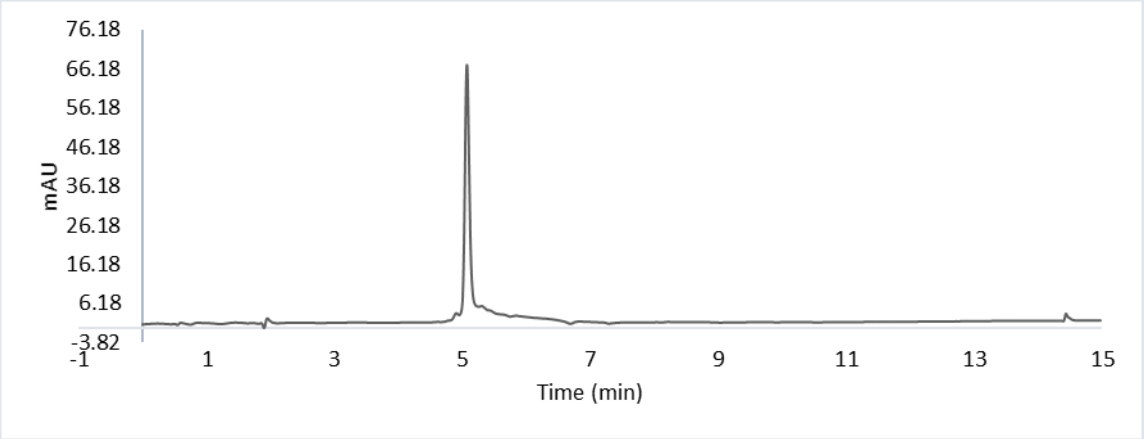

Compound **70**

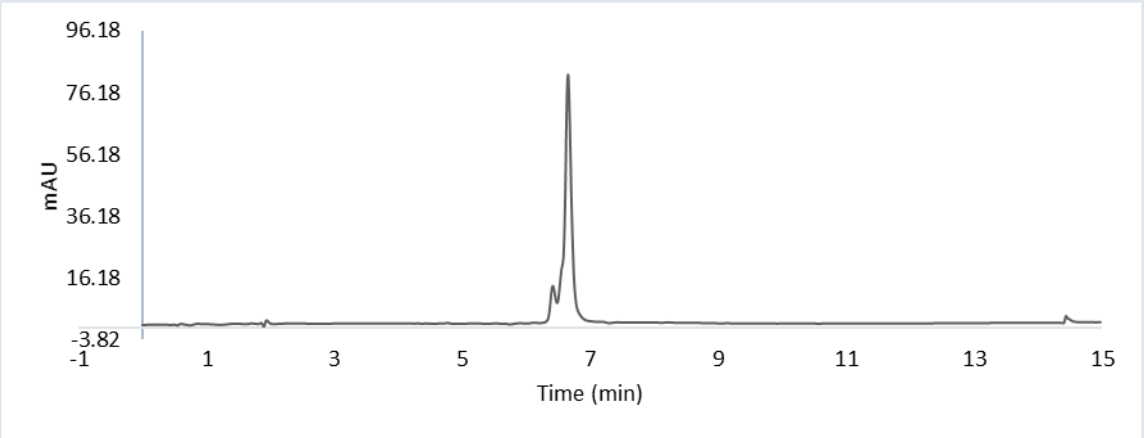

Compound **71**

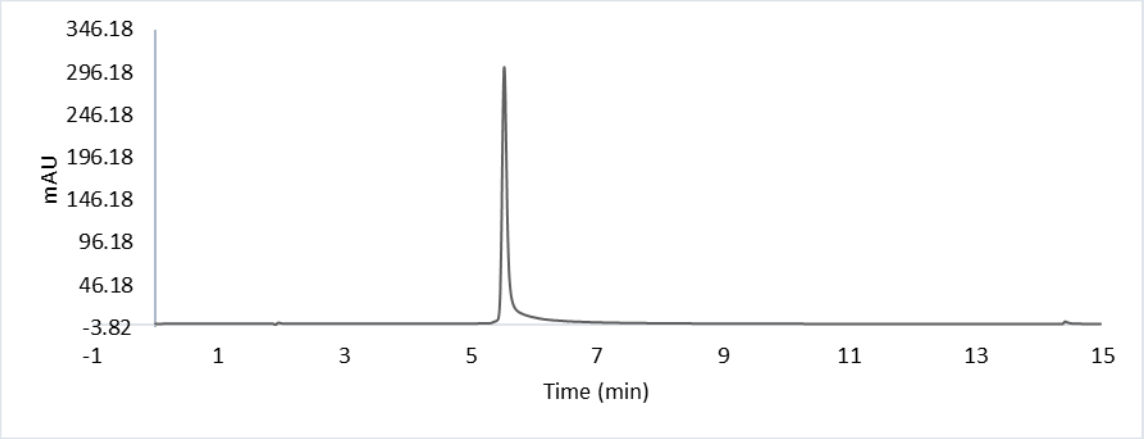

Compound **72**

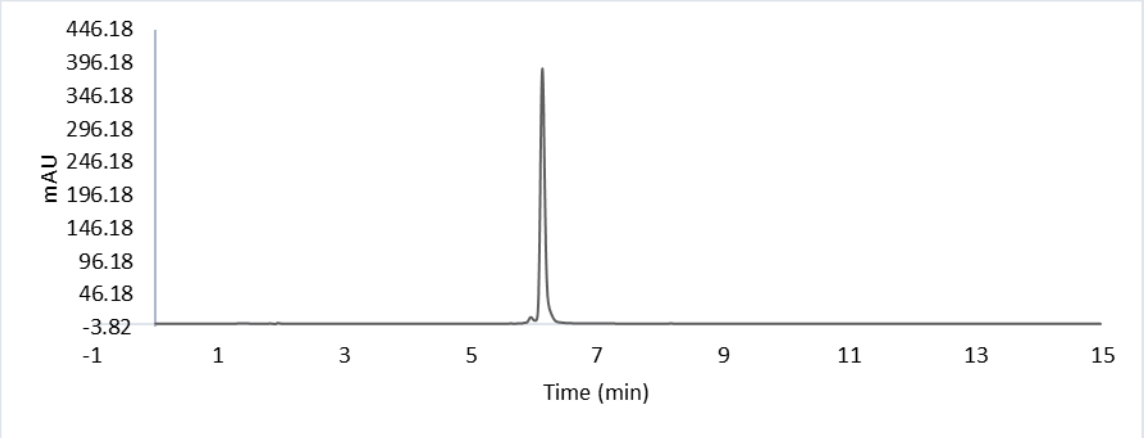

Compound **73**

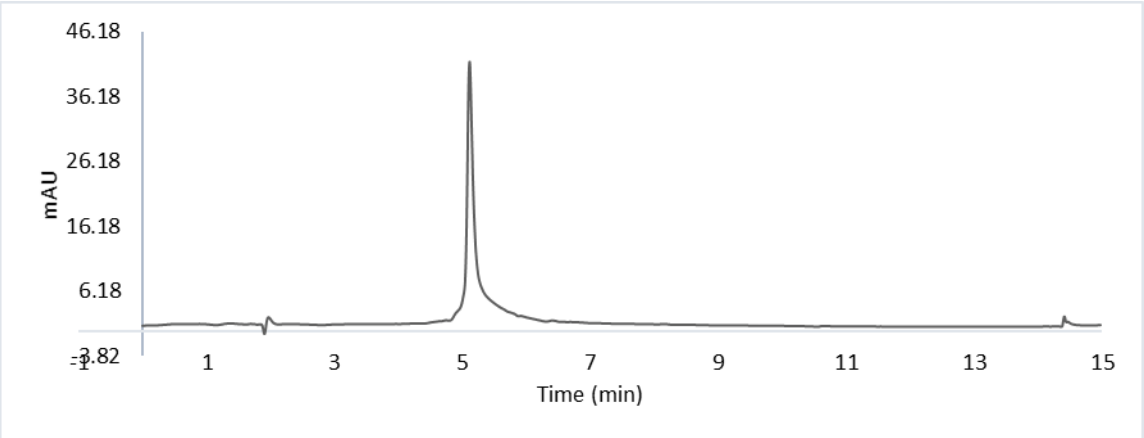

Compound **82**

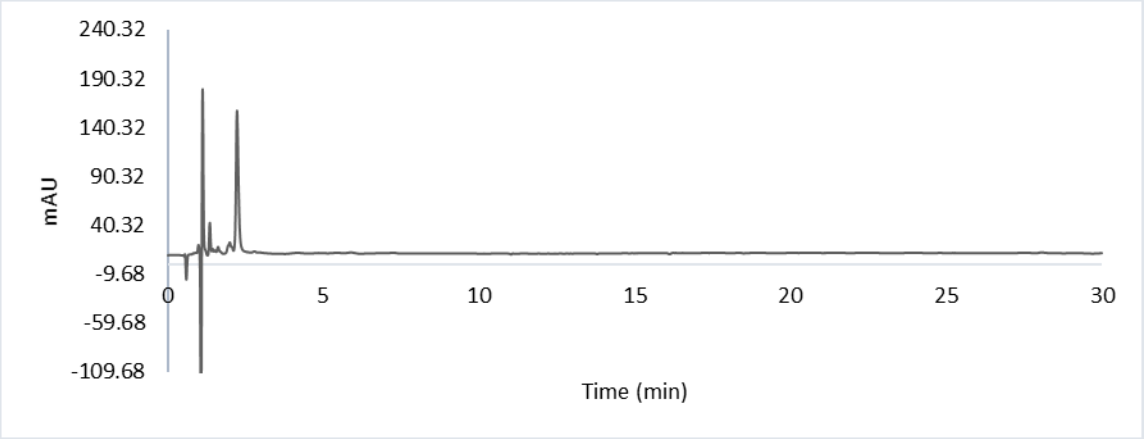

Compound **83**

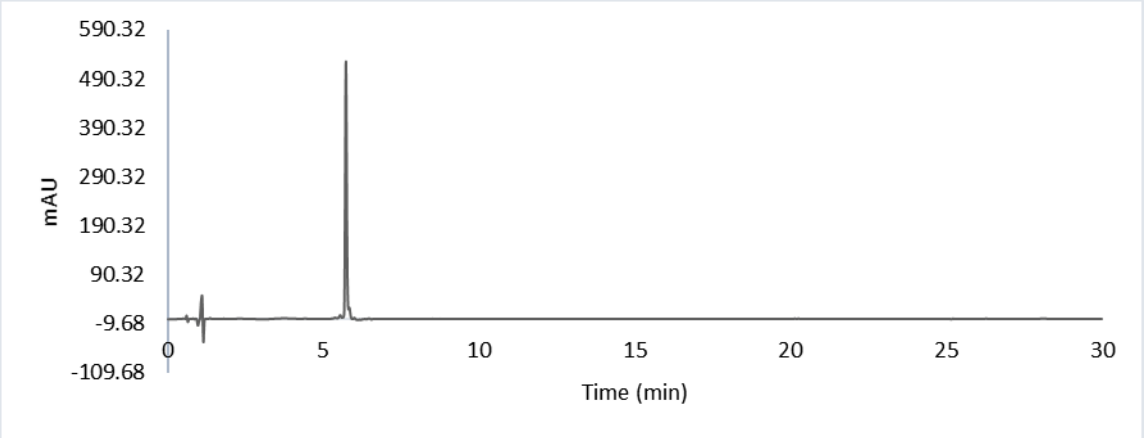

Compound **84**

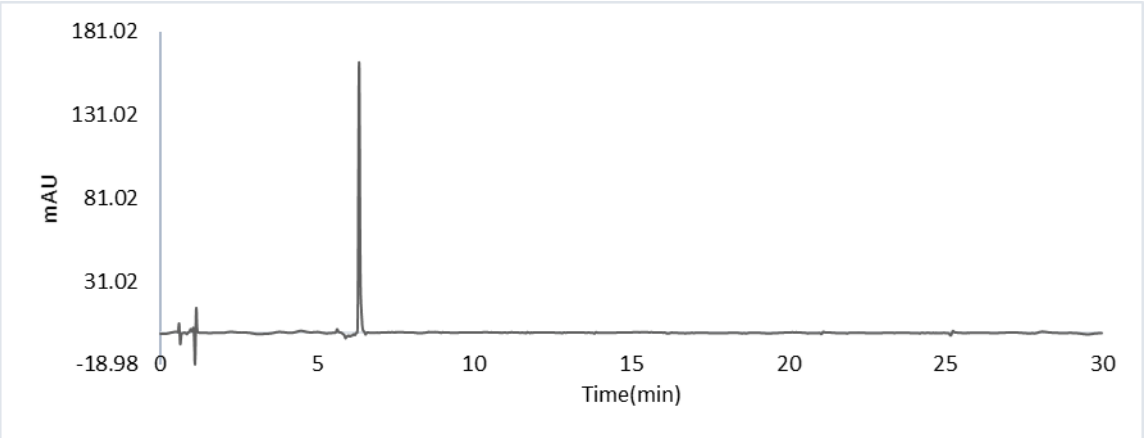

Compound **86**

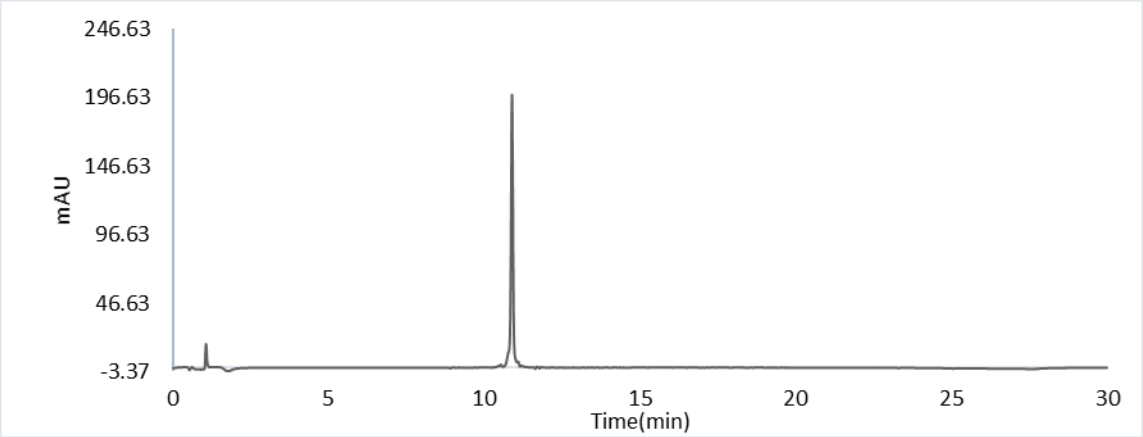

Compound **87**

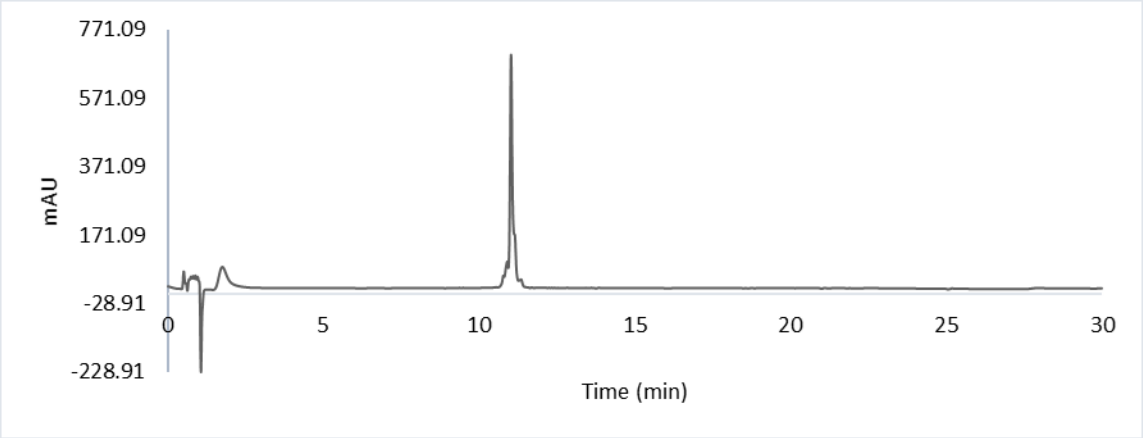

Compound **88**

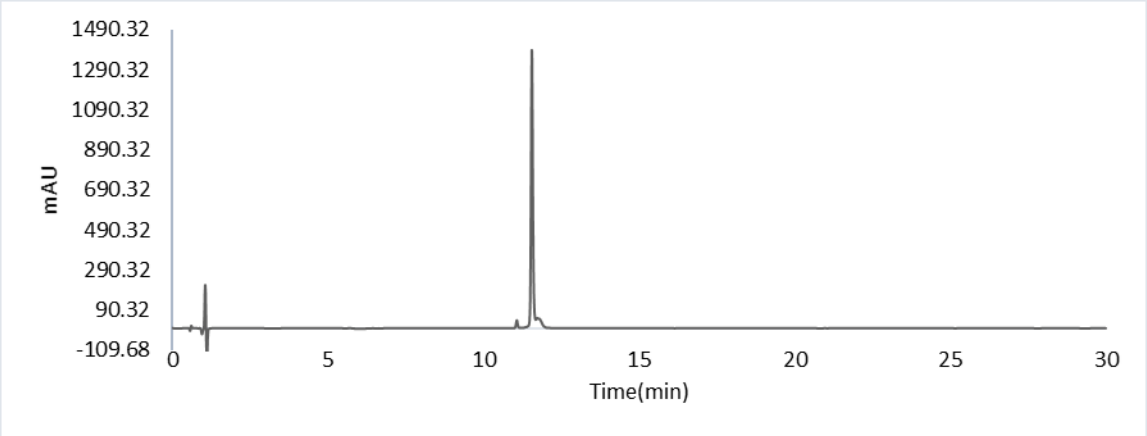

Compound **90**

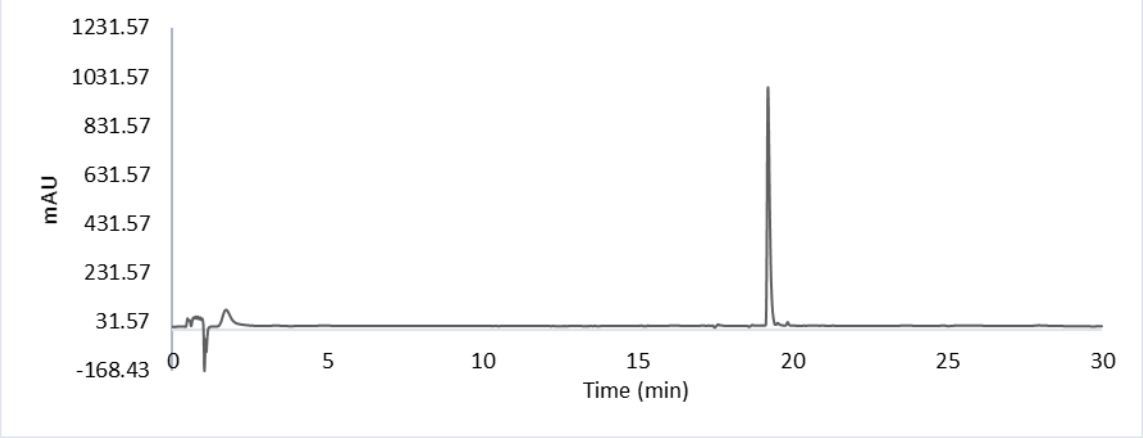

Compound **91**